Studies of the Formation of Homogeneous Mixed Silicon-Titanium/Zirconium Oxides by the Sol-Gel Route

A thesis submitted in partial fulfilment for
the degree of Doctor of Philosophy

by

Melanie Hudson

Department of Chemistry
Brunel University
Uxbridge
Middlesex.

October 1994

Abstract

This thesis is concerned with the preparation of mixed silicon-titanium oxides (TiO_2=4·1-21·9wt%) and silicon-zirconium oxides (ZrO_2=4·1-22·1wt%) by the sol-gel route. Methods of preparing homogeneous SiO_2-TiO_2 gels and SiO_2-ZrO_2 gels have been explored.

In this work bis(acetylacetonato)titanium diisopropoxide or bis(acetylacetonato)zirconium dipropoxide and tetraethyl orthosilicate (TEOS) have been hydrolysed simultaneously in iso-propanol to form homogeneous gels. Using these systems, the effects of the reaction conditions, amount of titania/zirconia present in the gel, drying conditions and thermal treatment of the dry gels on the bulk and structural properties have been investigated by a variety of experimental methods including X-ray diffraction, mid- and near-infrared spectroscopy and gas adsorption techniques.

For SiO_2-TiO_2 powders and monoliths, and SiO_2-ZrO_2 monoliths, thermal treatment has been found to significantly reduce the surface area (from 750-1·0m^2g^{-1}), pore volume (from 0·56-0·001cm^3g^{-1}) and relative number of silanol groups on the surface of the sample above 700°C. Average pore diameters remain constant at temperatures below 900°C (*ca* 54-21Å for monoliths), although the micropore volume does decrease (0·04-0·0cm^3g^{-1}) suggesting that smaller pores are destroyed by the heating process. For SiO_2-TiO_2 powders, the average pore diameter was *ca* 10Å larger than for the corresponding monolith suggesting that small pores are destroyed during powdering. At 1100°C, gas adsorption data indicate that the samples are fully densified. This is supported by NIR spectra which detect no silanol groups on the surface of the sample.

Structural changes arising from compositional changes and differing thermal treatment regimes have been monitored using mid-infrared spectroscopy and X-ray diffraction. With increasing temperature the silica matrix strengthens and titanium/zirconium are incorporated into the matrix. Monolithic SiO_2-TiO_2 gels (TiO_2=6·34 weight%) remained amorphous at 1100°C, whereas powders began to exhibit diffraction patterns predominantly from anatase at 700°C. Anatase crystallite sizes have been calculated using the Scherrer equation and have been found to be between 16·3 and 5·4nm. Monolithic SiO_2-ZrO_2 gels containing 4·1 and 4·9 weight% zirconia were found to be amorphous after treatment at 1100°C. Increasing the zirconia content to 6·4 and 22·1 weight% resulted in gels that were amorphous up to 900°C. Further treatment at 1100°C, resulted in tetragonal zirconia and some cristobalite being formed. Crystallite sizes have been calculated as being between 2·7 and 1·6nm for tetragonal zirconia and from 4·1 to 2·8nm for cristobalite.

Increasing the levels of titania/zirconia in the sample resulted in higher relative levels of hydrogen-bonded silanol groups. On hydration, the increased levels of titania/zirconia resulted in no observable free silanol groups on the surface suggesting that the surface becomes more hydrophilic as the amount of titania/zirconia present in the sample increases. This suggests that water becomes more tightly bound to Ti-OH /Zr-OH groups on the surface and within the pores, resulting in fewer free silanol type groups.

A double alkoxide bis(acetylacetonato)titanium di(triethoxysilane) [$Ti(acac)_2(OSi(OC_2H_5)_3)_2$] has also been synthesised and characterised. Mixed SiO_2-TiO_2 gels have also been prepared by the simultaneous hydrolysis of $Ti(acac)_2(OSi(OC_2H_5)_3)_2$ and TEOS under acidic conditions in ethanol. The effects of reaction conditions and thermal treatment of the dry gels have been investigated.

Increasing the treatment temperature of the samples resulted in the progressive decrease in surface area (533-3·0m^2g^{-1}), pore volume (0·18-0·003cm^3g^{-1}), micropore volume (0·06-0·00cm^3g^{-1}) and relative number of silanol groups on the surface. However, the average pore diameter remained constant at temperatures up to 700°C. Changes in pore volume (0·07-0·005cm^3g^{-1}), surface area (300-3·0m^2g^{-1}) and average pore diameter (26·9-91·9Å) were largest at 900°C, and the samples were found to be almost completely dense. This was confirmed by the absence of observable silanol groups by NIR spectroscopy.

After heating at temperatures up to 900°C, the samples were found to be amorphous by XRD. However increasing the temperature to 1100°C resulted in the formation of some crystalline anatase. The anatase crystal sizes have been calculated as being from 16·3 to 10·8nm in diameter.

NIR studies of silica-zirconia and silica-titania gels (prepared by both methods), indicate that decreasing the amount of acid used in the hydrolysis reaction resulted in higher relative levels of hydrogen bonded silanol species. Similarly, decreasing the amount of acid increased the micropore volume and decreased the mesoporosity of the resulting samples.

Generally, decreasing the amount of acid used for the hydrolysis for silica-zirconia and silica-titania gels (prepared by both methods), results in a decrease in the overall surface area and pore volume of the resulting material. The resulting isotherms indicate that the samples became less mesoporous as the amount of acid used in the hydrolysis reaction decreased. This was accompanied by an increase in the micropore volume.

For SiO_2-TiO_2 monoliths prepared from a double alkoxide and SiO_2-ZrO_2 monoliths the resulting pore structure is more rigid and composed of smaller pores than that of SiO_2-TiO_2 powders and monoliths prepared from bis(acetylacetonato)titanium diisopropoxide.

Contents

'There is an art, or rather, a knack to flying. The knack lies in learning how to throw yourself at the ground and miss.
The first part is easy.
All it requires is simply the ability to throw yourself forward with all your weight, and the willingness not to mind that it's going to hurt.
That is, it's going to hurt if you fail to miss the ground.'

Life, The Universe and Everything - Douglas Adams

Acknowledgements

I would like to thank my supervisor Dr. C.C. Harrison for her constant support, guidance and good humour throughout my 3 years 'under her wing'. Thanks are also due to Dr. S.L.W. McWhinnie for his supervision in Dr. Harrison's absence. I wish to thank
Dr. A. Minihan and Dr. A. Lovell as representatives for Unilever/Crosfields for co-funding this work in conjunction with the Science and Engineering Research Council.
My thanks go to Simon Aulton, Dr. Neil Loton, Carolynn Peacock, James McGiveron and Dr. Yun Lu for making my time at Brunel enjoyable.
I owe thanks to the glassblowers, Jeff Bridge and Richard Coffey for constructing my vacuum line. Without which, monitoring of the surface by near-infrared spectroscopy would have been impossible. Thanks are also due to Frank Coates whose ability for fixing pieces of equipment that seemed like lost causes continues to astound me.
Thanks are also due to Roger Corbally who taught me how to use the multinuclear Jeol 200FX NMR.
I would like to thank Dr. P.G. Harrison, Nottingham University, for helping with mass spectrometry. Also to the new and relocated members of Dr. C.C. Harrison's group at The Nottingham Trent University for putting up with me during my visits.
My cordial thanks go to all the remaining technicians for helping me obtain raw materials and equipment and to Neil Taylor the chief technician.
I would like also like to take this opportunity to thank my parents for their continued support and backing. My final debt is to Matt who has suffered the highs and lows of this project, and without his encouragement this thesis may never have seen the light of day.

Chapter 1: Introduction

1.1 Introduction

This thesis is concerned with the preparation and characterisation of mixed silicon-titanium oxides and silicon-zirconium oxides by the sol-gel route.

The formation of porous or dense glasses and ceramics by the sol-gel route is not fully understood, but the reaction initially involves hydrolysis and polymerisation reactions in the solution phase. Evolution of gel structure is governed by the variation of hydrolysis rate, polymerisation rate, concentration, precursor functionality, pH, and the use of catalysts. Theoretically, from the methods used for sol-gel preparations the resulting products should be very homogeneous. Assuming that typical sol-gel solutions contain all the components mixed at or near the molecular level and that this state can be maintained during the polymerisation, then the resulting product should be homogeneous. The majority of early sol-gel work was successfully aimed at obtaining homogeneous products.

Although the most common sol-gels are those containing silicon, a wide variety of compounds have been prepared from non silicates. In each case, the polymerisation of both inorganic precursors in an aqueous environment and metal organic precursors in a variety of mixed solvents leads to the formation of sol-gels.

1.2 Preparation of Silica in Aqueous Environments

In the 1850's, Mendeleyev discovered that hydrolysis of silicon tetrachloride [$SiCl_4$] yielded silicic acid [$Si(OH)_4$] which undergoes repeated condensation reactions to form high molecular weight polysiloxanes. The polymerisation of silicic acid was originally assumed to be an aggregation process or a polymerisation by which smaller molecular units link together into larger units. These discrete particles undergo nucleation and growth prior to the start of the aggregation process.

Compared to transition metals, silicon is generally less electropositive *ie* silicon has a smaller partial positive charge.

$$\delta\ (Si) \text{ in } Si(OC_2H_5)_4 = +0{\cdot}32$$
$$\delta\ (Ti) \text{ in } Ti(OC_2H_5)_4 = +0{\cdot}63$$
$$\delta\ (Zr) \text{ in } Zr(OC_2H_5)_4 = +0{\cdot}65$$

The reduced partial positive charge makes silicon less susceptible to nucleophilic reagents and thus causes the kinetics of hydrolysis and condensation to be much slower than those observed in transition metal systems.

Due to its small ionic radius, silicon is hydrolysed even in dilute acid and $Si(OH)_4$ (pK_a 9·9) is the predominant mononuclear solution species below pH 7. Above pH 7, further hydrolysis leads to anionic species:

$$Si(OH)_{4\,(aq)} \rightarrow SiO_x(OH)_{4-x}^{x-} \qquad 1.1$$

where $SiO(OH)_3^-$ [x=1 in equation 1.1] is the predominant mononuclear species. Because $SiO(OH)_3^-$ is a very weak acid (pK_a 18), $SiO_2(OH)_2^{2-}$ is observed in appreciable quantities

only at a pH>12.

Figure 1.1: Distribution of aqueous silicate species at 25°C. ionic strength I=3M[1].

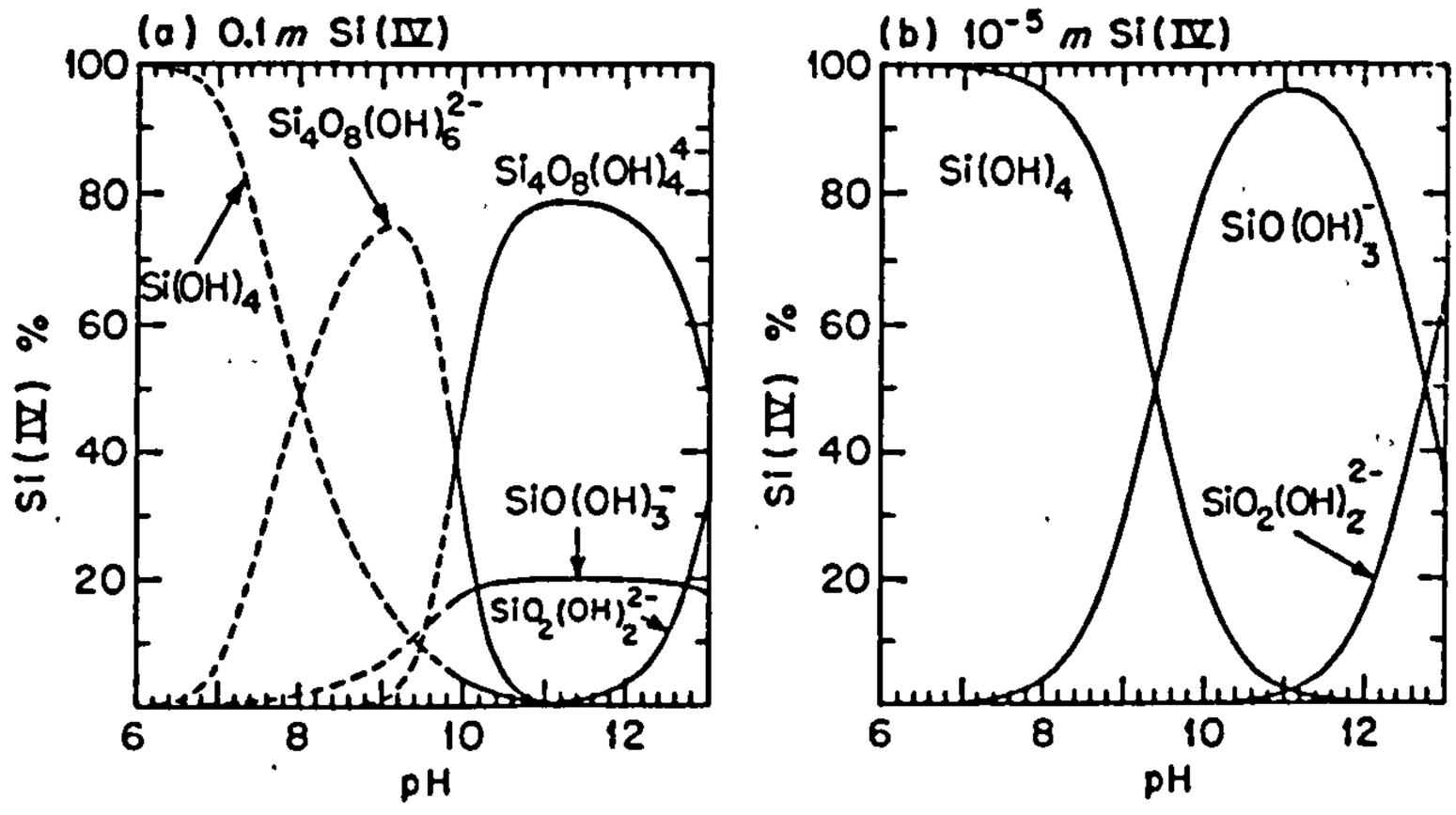

The results shown in figure 1.1 were obtained by making potentiometric measurements with a hydrogen electrode. The data obtained for an ionic strength of 3M were explained by Lagerström[2] who assumed an equilibrium existed between the mononuclear species $Si(OH)_4$, $SiO(OH)_3^-$, $SiO_2(OH)_2^{2-}$, and in addition $Si_2O_3(OH)_4^{2-}$ and $Si_4O_8(OH)_4^{4-}$. At an ionic strength of 0·5M, Lagerström explained his results in terms of the species $Si(OH)_4$, $SiO(OH)_3^-$, $SiO_2(OH)_2^{2-}$, and $Si_4O_6(OH)_6^{2-}$. From the results of Lagerström the formation of polynuclear aqueous silicate species depends on the ionic strength of the solution.

Silicic acid itself is prepared by hydrolysing an ester such as tetraethyl orthosilicate (TEOS), this is a stepwise process but can be simplified as in equation 1.2.

$$Si(OC_2H_5)_{4\,(aq)} \rightarrow SiO_x(OH)_{4-x}^{x-} \qquad 1.2$$

It has been postulated by Iler[3] that the polymerisation of silicic acid occurs in one of two ways. Either the monomers and other small primary particles aggregate or individual particles increase in size and decrease in number. Since silicic acid solutions gradually increase in viscosity and finally gel in a similar way to organic gels, before 1979, most people believed that $Si(OH)_4$ polymerised into siloxane chains which branched and cross-linked like many organic polymers[3]. In reality there is no relation or analogy between silicic acid polymerised in an aqueous system and condensation type organic polymers. Carman recognised that silicic acid actually polymerises into discrete particles that in turn aggregate into chains and networks[4]. Polymerisation occurs in three recognised stages:

1) polymerisation of monomer to form particles

2) growth of particles

3) linking of particles together into branched chains, then networks, finally extending throughout the liquid medium, thickening it to a gel.

Further experimental data has confirmed Carman's ideas.

The initial formation of particles by the condensation of silanol groups

$$-SiOH + HOSi- \rightarrow -SiOSi- + H_2O \qquad \textbf{1.3}$$

has been studied using potentiometric methods, trimethylsilation, molybdic acid reagent and ^{29}Si Nuclear Magnetic Resonance (NMR) spectroscopy. The results from the potentiometric experiments have been explained using cyclic tetramers, $Si_4O_6(OH)_6^{2-}$ and $Si_4O_8(OH)_4^{4-}$ along with the mononuclear species $Si(OH)_4$, $SiO(OH)_3^-$ and $SiO_2(OH)_2^{2-}$. Using ^{29}Si NMR and spin-perturbation techniques, Knight *et al*[5-7] have positively identified at least twelve species in moderately concentrated potassium silicate solutions, isotopically enriched to 95% in ^{29}Si. Such solutions are composed of a variety of cyclic and cage anions in dynamic equilibrium, the distribution of which depends on external solution conditions such as concentration, pH and the nature of the counterion. The results of two-dimensional ^{29}Si-NMR exchange spectroscopy (EXSY) experiments provide evidence of at least six single-step exchange processes. The $\mathbf{Q^n}$ notation denotes a ^{29}Si nucleus with a $Si(OSi)_n(OX)_{4-n}$ local environment, *ie.* n oxygen bridges to neighbouring silicon nuclei. The remaining (4-n) coordination sites are occupied either by hydroxyl groups (X=H) or by bridges to other metal centres (X=M). Therefore, a large $\mathbf{Q^4}$ percentage indicates a high degree of cross-linking in the silica domains.

Four of the silicate species observed by Knight *et al* are intermolecular, involving the monomeric anion, $\mathbf{Q^0}$, the formation and dissociation of the linear dimer, $\mathbf{Q^1_2}$; the formation and dissociation of the linear trimer, $\mathbf{Q^1_2Q^2}$; the formation and dissociation of the linear tetramer, $\mathbf{Q^1_2Q^2_2}$; and the formation and dissociation of the substituted cyclic trimer, $\mathbf{Q^1Q^3Q^2_2}$. The remaining two are intramolecular and consist of ring opening/ring closing reactions of the cyclic trimer, $\mathbf{Q^2_3}$ and an internal rearrangement of the bicyclic pentamer, $\mathbf{Q^2Q^3_2Q^2_2}$. These results agree with Iler's opinion that condensation occurs in a manner that maximises the number of Si-O-Si bonds and minimises the number of terminal hydroxyl groups through internal condensation. Therefore, rings are rapidly formed to which monomers quickly add to create three dimensional particles. These particles condense to the most compact state leaving hydroxyl groups on the outside. The particles serve as nuclei with further growth proceeding *via* an Ostwald ripening mechanism. In this mechanism particles grow in size and decrease in number as highly soluble small particles dissolve and then reprecipitate on larger, less soluble nuclei. Particle growth stops when the difference in solubility between the smallest and the largest particles becomes only a few parts per million.

1.2.1 pH Dependence

The polymerisation process is divided into three approximate pH domains[3]:

< pH 2

pH 2-7

> pH 7

The boundary at pH 2 arises because the point of zero charge (PZC), where the surface

charge is zero, and the isoelectric point (IEP), where the electrical mobility of the silica particles is zero, both occur in the range pH 1-3. A boundary appears at pH 7 because both the silica solubility and dissolution rates are maximised, and the silica particles are appreciably ionised above pH 7 enabling particle growth to occur without aggregation or gelation.

1.2.1.1 pH 2-7

Gelation times decrease steadily between pH 2 and pH 6, and it is generally assumed that above the IEP the condensation rate is proportional to the concentration of hydroxyl ions.

$$\equiv SiOH + OH^- \rightarrow \equiv SiO^- + H_2O \qquad \text{fast} \qquad \textbf{1.4}$$

$$\equiv SiO^- + HOSi \equiv \rightarrow \equiv SiOSi \equiv + OH^- \qquad \text{slow} \qquad \textbf{1.5}$$

This enables:

(i) the following of the progressive polymerisation of monomers

(ii) the observation of the initial formation of three dimensional condensed silica polymers or nuclei particles.

Iler states that monomeric $Si(OH)_4$ has a pK_a around 9·9, and that the pK_a of the dimer is reported to be higher but is likely to be lower than that of the monomer. This is because higher polymerised species have a much lower pK_a, approaching 6·7, and are more highly ionised than the dimer or monomer. The implication of this is that the greater the number of siloxane linkages and the fewer OH groups on a silicon atom, the stronger the acidity.

Polymerisation involves intermediate ionisation to hydrated forms of $\equiv SiO^-$ at less than pH 2, or to $\equiv SiOH_2^+$ above pH 2. The key point is that condensation involves the reaction of either the anion or cation with a non ionised silanol group:

$$\equiv SiO^- + HOSi \equiv \rightarrow \equiv SiOSi \equiv + OH^- \qquad \textbf{1.6}$$

Therefore at low pH where $Si(OH)_4$ is only very slightly ionized and no polymeric species are present, siloxane bond formation is minimal and dimerisation is slow. Similarly, if the dimer is a stronger acid than the monomer then the main reaction is with the ionised dimer:

$$(HO)_3SiOSi(OH)_2O^- + Si(OH)_4 \rightarrow (OH)_3SiOSi(OH)_2OSi(OH)_3 + OH^- \qquad \textbf{1.7}$$

However, the existence of a linear trimer is simply as a transition state and concentration is believed to be low. On formation, the dimer may be ionised and combine with its own ionised species to form a linear tetramer. The short distance between silanol end groups in a given linear polymer and the low concentration of the monomer ensures that ring closure is rapid. These cyclic products are mainly tetramers because bond angles make ring closure of the linear trimer unlikely. Once the predominant species are cyclic then there is a preferential reaction between the monomeric and dimeric species, and the polymeric more highly ionised cyclic species. This reaction occurs simultaneously with the condensation of adjacent silanol groups on the polymers where further cyclisation is possible. The resulting

species, being a more compact three dimensional species, is more highly ionised and any remaining monomer and dimer react preferentially and build up to give larger spherical particles. These almost spherical polymers undergo internal condensation and rearrangement to a more compact state of colloidal particles with a SiO_2 core and surface SiOH groups.

Figure 1.2: Conceivable steps in the polymerisation of silica to cyclic species.

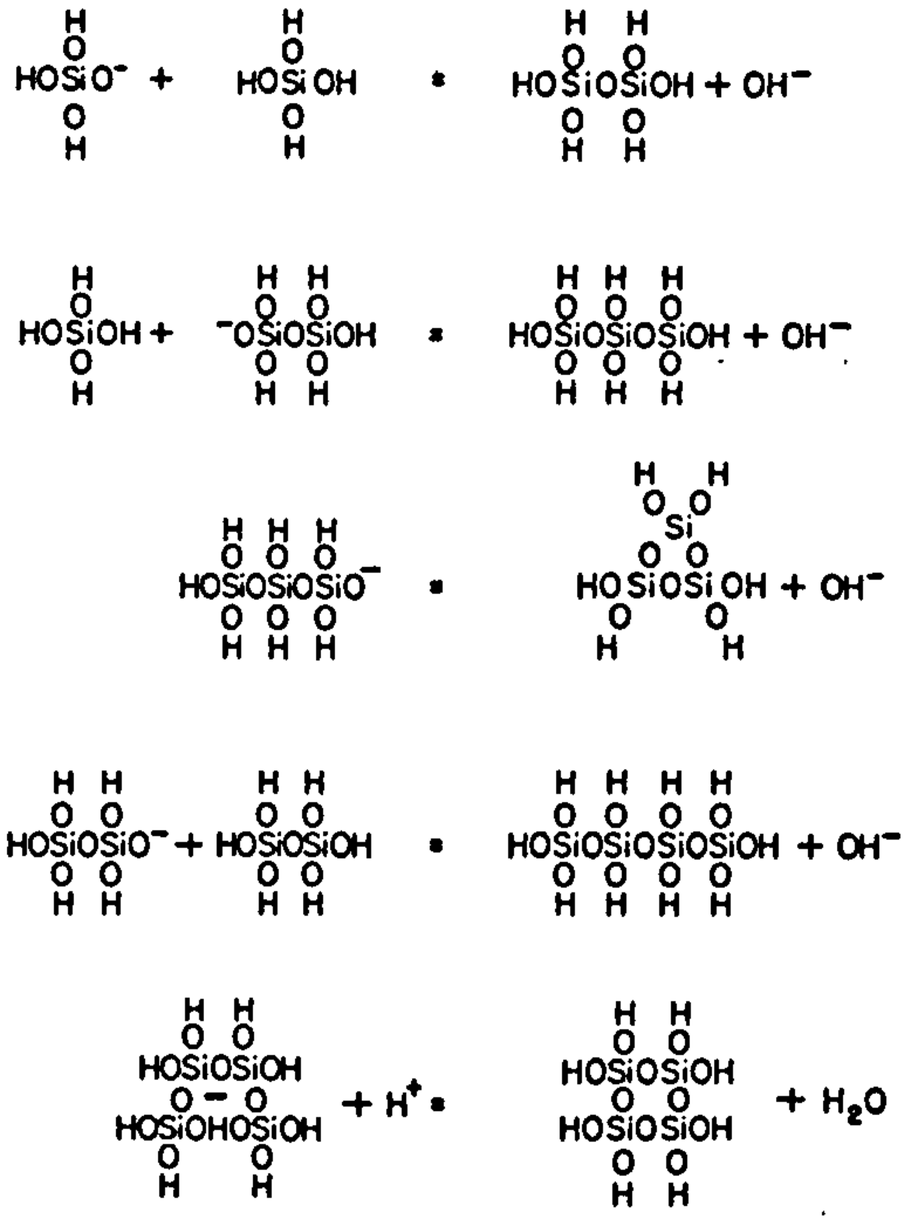

1.2.1.2 > pH 7

Above pH 7 the polymerisation occurs by the same nucleophilic mechanism. But, because all the condensed species are more likely to be ionised, and hence repel each other, particle growth is primarily by the addition of monomers to more highly condensed particles rather than by particle aggregation. Once pH 12 is exceeded, the majority of the silanols are deprotonated making the primary building blocks cyclic trimers and tetramers. Cyclic trimers are stable in this pH range because the planar, cyclic configuration permits the greatest separation of charge between the deprotonated sites[8]. Because there is a greater size dependence of solubility and the greater solubility of silica above pH 7, the growth of the primary particles continues by Ostwald ripening. Overall, particle growth is rapid and is highly dependent on the temperature. A higher temperature leads to the formation of larger particles because of the increase in the solubility of silica. The rate of particle growth depends on the distribution of particle sizes, since growth occurs by the more soluble smaller particles dissolving and the silica being deposited on larger ones.

Therefore, when very small individual silica particles are introduced into the same solution

as larger ones, especially at pH 9-10 where the dissolution and deposition is catalysed by hydroxyl ions, the small particles dissolve and the larger ones grow.

1.2.1.3 < pH 2

Below pH 2, the rate of polymerisation is proportional to the concentration of H^+ [3]. It was proposed by Iler *et al* that the mechanism of acid-catalysed polymerisation involves a siliconium ion intermediate, $\equiv Si^+$:

$$\equiv SiOH + H_3O^+ \rightarrow \equiv Si^+ + 2H_2O \qquad \textbf{1.8}$$

$$\equiv Si^+ + HOSi \rightarrow \equiv Si - O - Si \equiv + H^+ \qquad \textbf{1.9}$$

However, from alkoxide polymerisation it seems that condensation is more likely to proceed *via* an associative $\equiv SiOHR(OH_2)^+$ intermediate, see section 1.3.1.1.

In this situation, the solubility of silica below pH 2 is quite low and at acidities between pH 0-2 the silicate species should not be highly ionised. Consequently it is likely that the formation and aggregation of primary particles are simultaneous and Ostwald ripening contributes very little to particle growth once they exceed 2nm diameter.

1.3 Non Aqueous Environments: Hydrolysis and Condensation of Silicon Alkoxides

Silicate gels are commonly synthesised by the hydrolysis of monomeric, tetrafunctional alkoxides using a catalyst of either a mineral acid or base. The polymerisation is described by the following equations:

$$\equiv SiOR + H_2O \rightarrow \equiv SiOH + ROH \qquad \textbf{1.10}$$

Where the forward reaction is hydrolysis and the reverse is esterification.

$$\equiv SiOR + HOSi \equiv \rightarrow \equiv SiOSi \equiv + ROH \qquad \textbf{1.11}$$

The forward reaction is alcohol condensation and the reverse is alcoholysis.

$$\equiv SiOH + HOSi \equiv \rightarrow \equiv SiOSi \equiv + H_2O \qquad \textbf{1.12}$$

Here the forward reaction is water condensation and the reverse is hydrolysis.

A hydrolysis reaction 1.10 results in the replacement of the alkoxide groups (OR) with hydroxyl groups (OH). The resulting condensation of the silanol groups produces siloxane bonds (Si-O-Si) and either water or alcohol. Generally, these condensation reactions will have begun before the hydrolysis of $Si(OR)_4$ is completed. The immiscibility of alkoxysilanes and water indicates the need for a mutual solvent[9], this is because the alcohol produced from the hydrolysis is not sufficient to homogenise the system.

Variation of the H_2O:Si molar ratio (r) from values less than 1 to greater than 50, and the use of different concentrations of acids and bases from less than 0.01M[11] to 7M[12] changes the properties of the end product. Theoretically, an r value of 2 is sufficient for the complete hydrolysis and condensation of the alkoxide to yield anhydrous silica:

$$n\,Si(OR)_4 + 2n\,H_2O \rightarrow n\,SiO_2 + 4n\,ROH \qquad \textbf{1.13}$$

But, even when excess water (r>2) is used, the reaction does not go to completion and results in a series of intermediate species $[SiO_x(OH)_y(OR)_z]_n$ (where 2x+y+z=4) being formed. The use of ^{29}Si NMR to follow the reaction of an acid-catalysed silicate solution

revealed a distribution of Q^0 to Q^4 species over a period of 14 days.

Figure 1.3: ^{29}Si NMR spectra of acid catalysed TEOS (r=2) after a)3 hours, b)3 days, c)14 days. Chemical shift,δ, in ppm,relative to TMS[10].

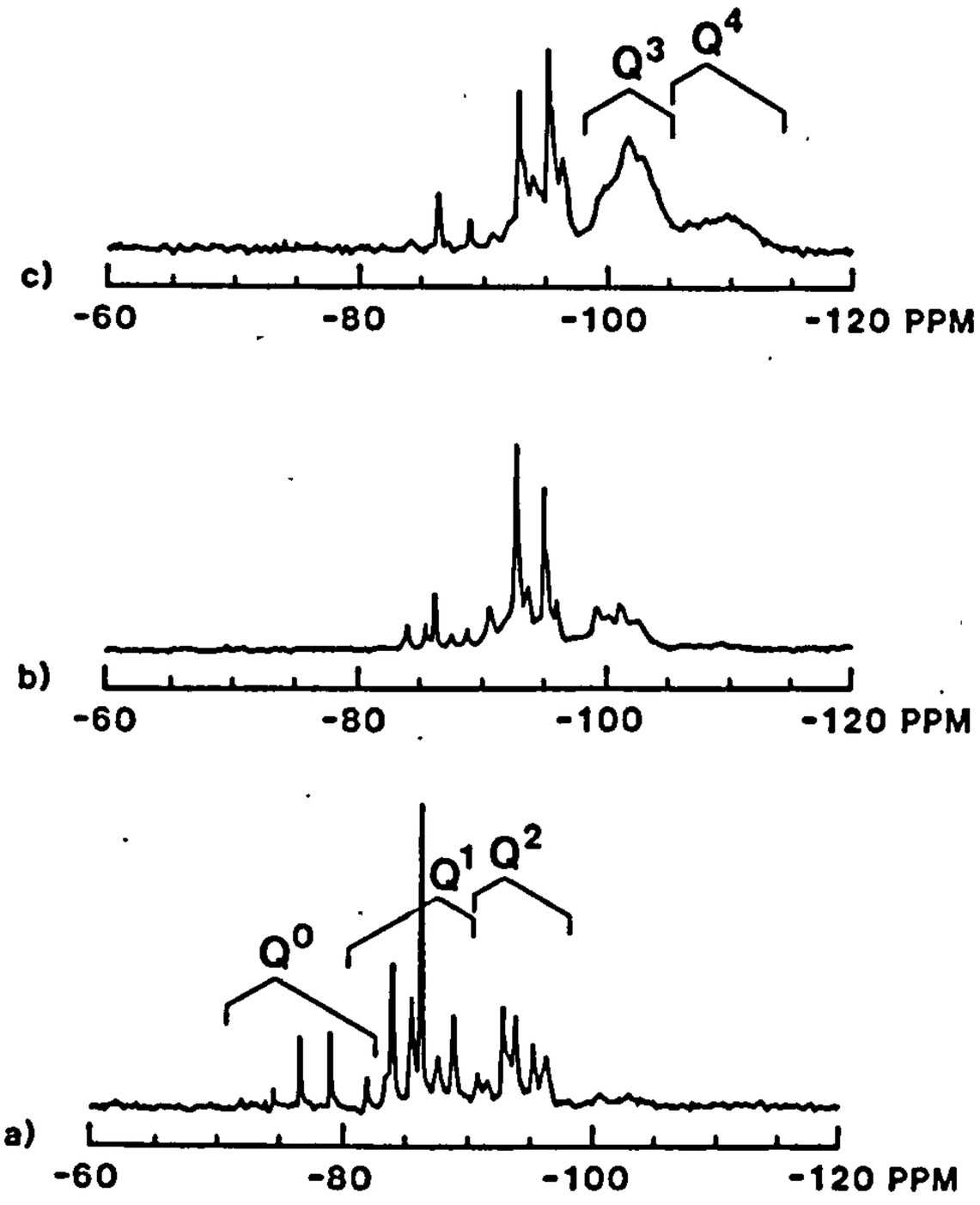

The evolution of silicate species is shown in figure 1.3, clearly the reaction to form anhydrous silica has not gone to completion as shown by the presence of Q^1 and Q^2 species as well as the expected Q^3 and Q^4 species after 14 days.

From *in situ* SAXS studies[11,13,14], Schaefer, Keefer and others showed that varying the hydrolysis and condensation conditions affects the structures of sol-gel silicates. Acid catalysed hydrolysis with low H_2O:Si ratios results in weakly bonded polymerised sols, whereas base catalysis with a large H_2O:Si ratio forms highly condensed particulate sols. Therefore sol-gel silicates evolve sequentially from successive hydrolysis and condensation reactions. Any structural variations result from changes in the sequencing of the three basic reactions shown in equations 1.10, 1.11 and 1.12; this sequence can be changed by varying the physical and chemical factors involved under different processing conditions.

1.3.1 Hydrolysis

The hydrolysis of tetraalkoxysilanes (eg TEOS) occurs by nucleophilic attack of the oxygen in water on the silicon atom. This has been confirmed by the use of isotopically labelled water with TEOS; the resulting alcohol was found to be unlabelled in both acid and base catalysed systems:

$$SiOR + H^{18}OH \rightarrow Si{-}^{18}OH + ROH \qquad 1.14$$

Hydrolysis of tetraalkoxysilanes is made easier by the use of a solvent such as alcohol, dioxane, acetone or THF in which both the tetraalkoxysilane and water are miscible. Addition of solvents is beneficial in promoting the hydrolysis of silanes with bulky alkoxy ligands. However, they may also promote esterification or depolymerisation reactions, the reverse reactions of equations 1.10 and 1.11.

Alcohol exchange reactions occur readily with metal alkoxide precursors:

$$M(OR)_z + xR'OH \rightarrow M(OR)_{z-x}(OR')_x + xROH$$

as a result alcohol exchange is a common method of alkoxide synthesis[15]. Exchange is facilitated when $\delta(M) \geq 1$ and when R′ is less sterically bulky than R. Alcohol exchange rates decrease as MeOH>EtOH>Pr^{i}OH>Bu^{t}OH[16]. However, since hydrolysis rates decrease with steric bulk of the alkoxy ligands, chemical modification normally involves exchange of a bulky ligand for a less bulky one.

1.3.1.1 Catalysts

The use of catalysts such as mineral acids, ammonia, acetic acid, potassium hydroxide, amines, potassium fluoride and hydrofluoric acid is widespread. From the literature the general consensus of opinion is that mineral acids are more effective as catalysts than an equivalent concentration of base. However, the increasing acidity of silanol groups and the possible neutralisation of the catalyst as hydrolysis and condensation proceeds, and the generation of unhydrolysed monomers *via* base-catalysed alcoholic or hydrolytic depolymerisation processes have not generally been considered. These unhydrolysed monomers persist past the gel point and result in an "inverted" molecular weight distribution, in which both high and low molecular weight species are maximised with respect to intermediate molecular weight species.

The hydrolysis of TEOS under both acidic and basic conditions in several cosolvents: ethanol, methanol and dioxane has been investigated by Aelion *et al*[17]. The final extent of the hydrolysis reaction can be determined by distillation of the ethanol produced. Similarly the consumption of water by the hydrolysis pathway and its production by condensation can be monitored by Karl Fischer titration. Unfortunately, quantitative information is unreliable because some silanol groups are consumed by the Karl Fischer reagent. Aelion *et al* observed that the rate and extent of hydrolysis was most influenced by the strength and concentration of the acid or base catalyst. They discovered that temperature and solvent were secondary factors and concluded that the reaction was first order with respect to acid

concentration. Although general acid catalysis cannot be ruled out, the hydrolysis reaction mechanisms that have been postulated involve hydrogen ions implying specific acid catalysis.

Hydrolysis of TEOS in basic media was also found to occur as a function of the catalyst concentration[17]. Under these conditions the order of reaction was determined by comparison of the times required to achieve a specified degree of hydrolysis. In very dilute solutions in sodium hydroxide, the reaction was found to be first order, but as the concentration of TEOS was increased, the reaction no longer followed a simple order but became complicated by secondary reactions. The use of weaker bases such as ammonium hydroxide and pyridine, as catalysts only produced measurable speeds of reaction when they were present in large concentrations. Overall hydrolysis kinetics were more strongly affected by the nature of the solvent.

Different catalysts affect the overall hydrolysis and condensation of TEOS in ethanol (when r=4) differently[18], table 1.1 illustrates that not only the hydronium ion and hydroxyl ion affect the gel times but also the conjugate base, notably F^-. Many of the properties of HF catalysed gels are similar to base-catalysed gels which implies that the similarity in size of OH^- and F^- enables F^- to increase the coordination of silicon above four.

Table 1.1: Gel Times and Solution pH for TEOS Systems Employing Different Catalysts[18].

Catalyst	Concentration (mol:TEOS)	Initial pH of Solution	Gelation Time (h)
HF	0·05	1·90	12
HCl	0·05	0·05[a]	92
HNO_3	0·05	0·05[a]	100
H_2SO_4	0·05	0·05[a]	106
HOAc	0·05	3·70	72
NH_4OH	0·05	9·95	107
No Catalyst	---	5·00	1000

[a] Between 0·01 and 0·05

A mechanism for the action of F^- was proposed by Corriu[19] in which the first step is the fast reversible formation of a pentavalent intermediate, this increases the length of and weakens the surrounding Si-OR bonds.

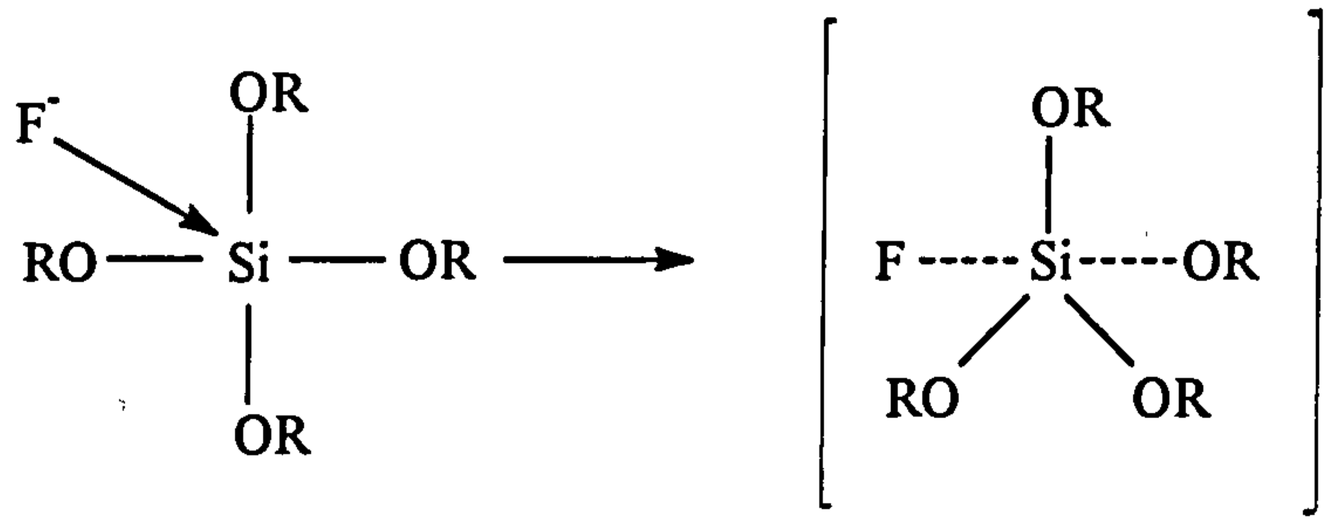

The rate determining step is the nucleophilic attack of water leading to nucleophilic substitution by proton transfer and loss of ROH.

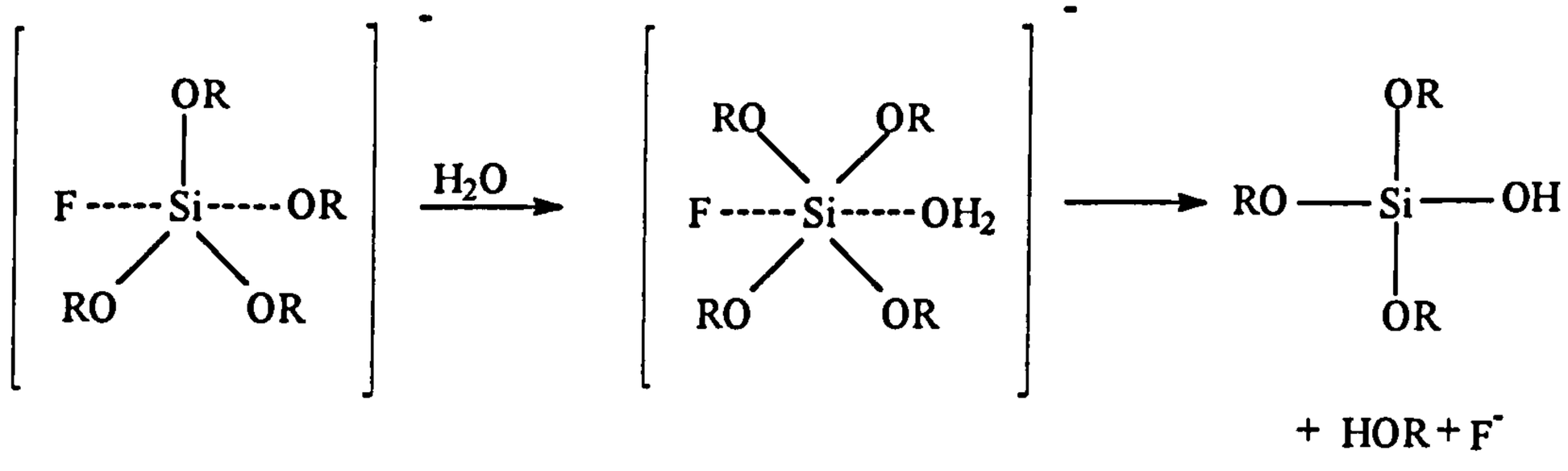

1.3.1.2 Steric and Inductive Effects

Steric factors in TEOS and related alkoxides have a large effect on the hydrolytic stability of the compounds. Any branching or extension of the alkyl chain length reduces the rate of hydrolysis[17].

Table 1.2: Rate Constant k for Acid Hydrolysis of Tetraalkoxysilanes $(RO)_4Si$ @20°C

R	k 10^2 (l $mol^{-1}s^{-1}[H^+]^{-1}$)
C_2H_5	5.1
C_4H_9	1.9
C_6H_{13}	0.83
$(CH_3)_2CH(CH_2)_3CH(CH_3)CH_2$	0.30

Inductive effects result in alterations to the hydrolysis rate. Under acidic conditions the rate of hydrolysis decreases with each subsequent hydrolysis step (electron withdrawing), but under basic conditions, the increased electron withdrawing capabilities of OH and AcOH compared to OR may result in a condition in which each subsequent hydrolysis step gets faster as hydrolysis and condensation proceed.

1.3.1.3 Solvent Effects

Originally, solvents were introduced into the system to prevent liquid-liquid phase separation during the first stages of the hydrolysis reaction and control the concentrations of silicate and water that influence the gelation kinetics. Now, other solvents are added as drying control chemical additives (DCCA) to act as cosolvents with alcohol and enable the fast drying of a monolithic gel without cracking[20].

The nature and characteristics of the solvent used affect its solvating power; the most important of these characteristics are:

1) polarity
2) dipole moment
3) availability of labile protons

Polarity of the solvent is important in determining its solvating ability for polar or nonpolar species. Solvents such as water, alcohol and formamide which are polar are used to solvate polar, tetrafunctional silicate species used in sol-gel processing. For incompletely hydrolysed systems, less polar solvents such as dioxane or tetrahydrofuran (THF) are used.

Availability of protic solvents *ie* those which have labile protons determines the strength of solvation of anions or cations through hydrogen bonding. If solvent molecules hydrogen bond to hydroxyl or hydronium ions then any catalytic activity under basic or acidic conditions respectively is reduced.

The availability of labile protons also influences the extent of the reverse reactions, reesterification (reverse of equation 1.10) or siloxane bond alcoholysis or hydrolysis (reverse of equations 1.11 and 1.12). Solvents that are aprotic do not participate in reverse reactions like reesterification or hydrolysis, due to the lack of sufficiently electrophilic protons and the inability to be deprotonated to form the strong nucleophiles required for these reactions.

Addition of cosolvents (eg formamide) as DCCAs to influence the structure or drying behaviour of the gel network has been studied using ^{29}Si NMR and Raman spectroscopy. The effects of formamide on the hydrolysis of TMOS in methanol under neutral conditions have been studied by Jonas[21], Artaki *et al* [22], and Orcel and Hench[23]. By using a cosolvent such as formamide instead of pure methanol, a reduction in the hydrolysis rate constant was observed, whereas the condensation-rate constant was increased. Similarly, under acidic conditions, Hench[24] observed that use of 50% methanol and 50% formamide as the solvent increased hydrolysis and reduced condensation rates.

For neutral conditions, the effects of formamide can be explained by hydrogen bonding and solvent viscosity[22,23]. Since both methanol and formamide can act as donors or acceptors in hydrogen bonding, from the higher values of dielectric constant, ε at 25°C and dipole moment, μ exhibited by formamide the hydrogen bonds formed are expected to be stronger. The high viscosity of formamide may reduce the ability of molecules to reorient to achieve

the maximum charge separation needed for rapid hydrolysis.

1.3.2 Condensation

The polymerisation of alkoxides to form siloxane bonds occurs either *via* an alcohol condensation (equation 1.11) or water condensation (equation 1.12) reaction.

At concentrations less than about 100 ppm as SiO_2, monosilicic acid is soluble and stable in H_2O at 25°C. When a monomer solution, $Si(OH)_4$, is formed at a concentration greater than 100-200 ppm as SiO_2, the monomer polymerises by condensation to form dimer and higher polymeric species. Condensation polymerisation itself occurs *via* an ionic mechanism in which the rate of polymerisation is proportional to the concentration of OH^- at >pH 2 and below pH 2 to H^+ ion.

Polymerisation of silicic acid occurs in a manner that results in a maximum number of siloxane bonds and a minimum number of uncondensed SiOH groups. In the early stages of polymerisation, condensation quickly results in ring structures *ie* cyclic tetramers are produced. Further addition of monomer results in addition to these cyclic structures and linking of the cyclic polymer to form larger three-dimensional structures. These three-dimensional structures undergo internal condensation to form a compact molecule with SiOH groups on the outside. These are the units that develop into larger particles by the mechanism described in 1.2.1.2.

Condensation of aqueous silicates at pH 7-12 has been studied using ^{29}Si NMR techniques[25]. The results obtained indicate that condensation products are typically monomer, dimer, linear trimer, cyclic trimer, cyclic tetramer and higher-order rings. To achieve this the condensation reaction requires both depolymerisation and the availability of monomer which is in solution equilibrium with the oligomeric species and can also be generated by depolymerisation [reverse of equations 1.11 and 1.12].

In the usual alcohol-water systems that are used the depolymerisation rate is lower than in an aqueous medium especially at pH 2-7. Under these conditions, Iler[3] suggested that where the depolymerisation reaction is least likely to occur, condensation is irreversible and once they have been formed the siloxane bonds can not be hydrolysed. Here the condensation process may resemble the classical polycondensation of a polyfunctional organic monomer resulting in a three dimensional network. Because silica is insoluble under these conditions the condensation polymer of siloxane chains will not rearrange into particles. This implies that the structure of a product from a sol-gel process may range from a molecular network to a colloidal particle depending on the conditions.

1.3.2.1 Catalysts

The condensation of silanols can proceed thermally without the use of a catalyst. Observation of the average condensation rate (1/gel time) for TEOS hydrolysed with solutions of various acids[26] (figure 1.4) shows that the overall condensation rate reaches a minimum at pH 1·5 and is maximized at intermediate pH.

Figure 1.4: Average condensation rates (1/gel times) for TEOS hydrolysed with solutions of various acids: (HOAc) acetic acid; (p-TSA) p-toluenesulphonic acid; (TFA) tri-fluoroacetic acid.

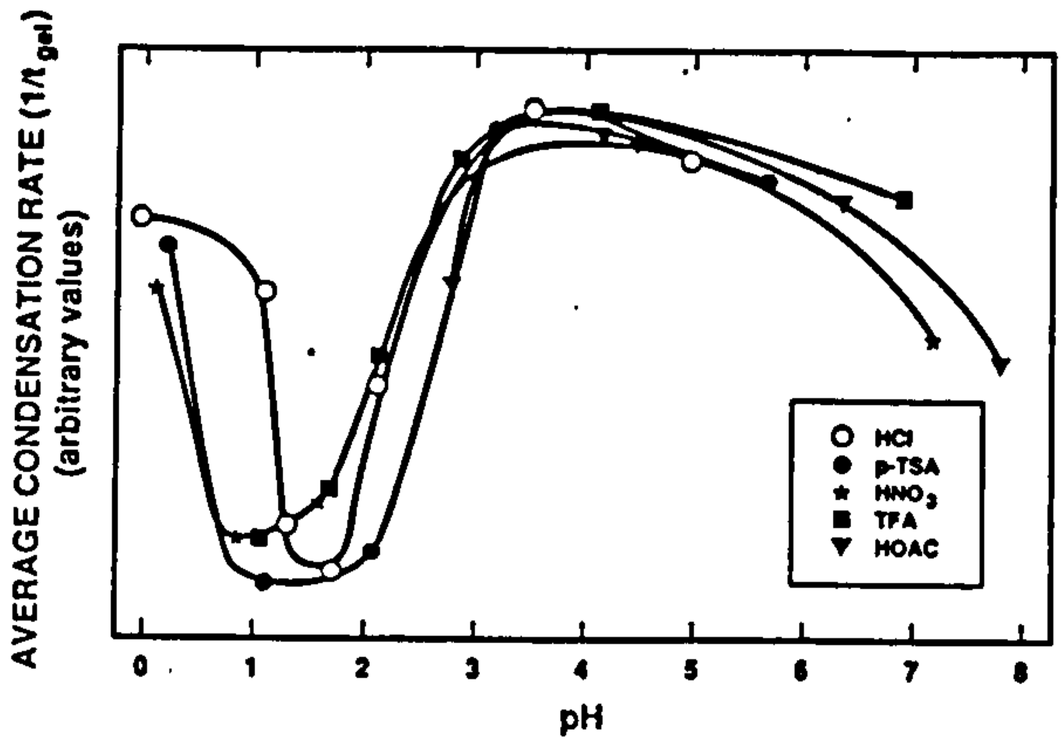

Under basic conditions, a stable (nongelling) system results. From the pH-dependence of the condensation mechanism for acid and base catalysis it has been postulated that the minimum at approximately pH 2 is consistent with the isoelectric point of silica. At a lower pH than the IEP, *ie* < pH 2, any surface silanol groups are protonated. At pH values higher than that of the IEP surface silanols are deprotonated.

The use of HF as a catalyst below pH 2 has been observed by Iler[3] who found that the polymerisation rate is proportional to the concentration of H^+ and F^-. From these results a condensation mechanism involving a bimolecular intermediate in which the coordination of one silicon is increased from four to five or six by the fluoride ion has been proposed. This is similar to the case of the hydroxyl ion. Other mechanisms have been proposed, in one such mechanism the F^- displaces an OH^-, causing localised attractions to other silanol species and hence resulting in an increase in the condensation rate[27]. Since F^- is more electron withdrawing than OH^- it can also be argued that F^- substitution for OH^- reduces the electron density on silicon, making it more susceptible to nucleophilic attack. The latter argument is consistent with the ideas of Corriu *et al* [19].

1.3.2.2 Steric and Inductive Effects

As mentioned previously (section 1.3), condensation can occur by two different reactions (1.11 and 1.12) between different solution species, *ie* monomers, dimers and oligomers, that have been hydrolysed to different extents. The presence of the variety of solution species and the variety of condensation rates makes it difficult to draw any conclusions about steric and inductive effects. This accounts for the comparative lack of information on steric and inductive effects for tetraalkoxides. In these compounds we expect the substituents to increase steric crowding in the transition state and reduce the condensation rate. Increasing the number of silanols on the silicon atom, increases the silanol activity and can be explained

by steric and inductive effects.

Acid and base catalysed condensation mechanisms involve both protonated and deprotonated silanols respectively. The substituents present on the silicon influence the acidity of the silanols involved in condensation. Electron withdrawing groups such as -OH or -OSi, increase the acidity of the silanol and the IEP and minimum condensation rate are at approximately pH 2.

Although inductive effects are important, in acid catalysed condensation reactions, steric effects predominate over inductive effects. Therefore, for the tetrafunctional alkoxide precursors used, the inductive effects resulting from longer chain alkyl substituents are not particularly significant.

1.3.2.3 Solvent Effects

Because the condensation mechanism is highly pH dependent as mentioned in (Section 1.3.1.3), protic solvents form hydrogen bonds with nucleophilic deprotonated silanols and aprotic solvents hydrogen bond to electrophilic protonated silanols. Therefore, protic solvents slow down base catalysed condensation and increase the rate of acid catalysed condensation, whereas aprotic solvents have the reverse effect.

Using an aprotic solvent, such as dioxane, under base catalysed conditions (pH> 2·5) Artaki *et al* [28] suggested that the solvent can not hydrogen bond to the SiO^- nucleophile. Also, because it is nonpolar it does not stabilise the reactants with respect to the activated complex. This should result in a significant enhancement of the condensation rate and result in an efficient reaction to form large, compact spherical particles. Similarly, polar aprotic solvents, dimethylformamide and acetonitrile, do not form hydrogen bonds with the silicate nucleophile. But, because of their polarity, anionic reactants are stabilised with respect to the activated complex and reduce the rate of the condensation reaction.

Protic solvents such as methanol and formamide can hydrogen bond to SiO^-, making it less nucleophilic. From experimental work Artaki *et al* [28] suggest that because formamide has a larger dipole moment (3·7) than methanol (1·7), it forms stronger hydrogen bonds to the reactant species. Formamide should therefore contribute more extensive shielding around the silicon than methanol, thus preventing efficient condensation. But from the results obtained by Artaki *et al* it appears that more extensive condensation is achieved in the formamide system. This has been explained by the partial hydrolysis of formamide to formic acid and ammonia. The presence of ammonia should increase the condensation rate by acting as a catalyst for silanol condensation at a pH> 2·5.

Solvents used in sol-gel processing also have the ability to promote depolymerisation. Nucleophiles, such as OH^-, are involved in the base catalysed hydrolysis of siloxane bonds (reverse 1.12), aprotic solvents can not hydrogen bond to OH^- thus making it a stronger nucleophile. This promotes restructuring and results in a greater condensed species.

1.4 Effect of the Environment on Titanium and Zirconium Alkoxides

1.4.1 Physical Properties

The size and electropositive nature of the central metal atom both influence the volatility and degree of polymerisation of the resulting alkoxides. This is illustrated in table 1.3.

Table 1.3: Physical Properties of Metal Ethoxides

	$Si(OC_2H_5)_4$	$Ti(OC_2H_5)_4$	$Zr(OC_2H_5)_4$	$Hf(OC_2H_5)_4$	$Th(OC_2H_5)_4$
Electronegativity	1·74	1·32	1·22	1·23	1·11
Covalent radius(Å)	1·11	1·32	1·45	1·44	1·55
Boiling point (°C/mm)	166/760	103/0·1	190/0·1	178/0·1	300/0·1
Degree of polymerisation	1·0	2·4	3·6	3·6	6·0

The above table shows that as atomic size increases within the same group, the degree of polymerisation of the alkoxide increases yet the volatility decreases.

Increased chain branching of the alkyl group not only decreases the degree of polymerisation (due to steric hindrance) but also the electron releasing tendency (+I effect) which makes the metal-oxygen-carbon bond less polar and increases the volatility of the alkoxide derivative.

Table 1.4 shows that both boiling point and degree of polymerisation decrease with increased akyl chain branching. It is also clear that the values for the zirconium alkoxides are greater than those for the corresponding titanium alkoxide. The higher degree of polymerisation of zirconium alkoxides compared to those of the titanium analogues may be attributed to the greater atomic radius of zirconium and its tendency to achieve a higher coordination number.

Table 1.4: Comparison of Titanium and Zirconium Alkoxides[29,30,31,32]

R	Boiling point (°C/mm)		Degree of polymerisation	
	$Ti(OR)_4$	$Zr(OR)_4$	$Ti(OR)_4$	$Zr(OR)_4$
C_2H_5	103/0·1	180/0·1	2·4	3·6
$CH_3(CH_2)_3$	142/0·1	243/0·1	---------	3·4
$CH_2(CH_2)_7$	214/0·1	---------	1·4	3·4
$(CH_3)_2CH$	49/0·1	160/0·1	1·4	3·0
$(C_2H_5)_2CH$	112/0·1	181/0·1	1·0	2·0
$(C_3H_7^n)_2CH$	156/0·1	163/0·1	1·0	1·0
$(CH_3)_3C$	94/5	89/5	1·0	1·0
$C_2H_5(CH_3)_2C$	143/5·0	139/5	1·0	1·0
$CH_3(CH_2)_4$	175/0·8	256/0·01	1·4	3·2
$(CH_3)_2CH(CH_2)_2$	148/0·1	247/0·1	1·2	3·3
$(CH_3C_2H_5)CHCH_2$	154/0·5	238/0·1	1·1	3·7
$(CH_3)_3CCH_2$	105/0·05	188/0·2	1·3	2·4
$(C_2H_5)_2CH$	112/0·05	178/0·05	1·0	2·0
$(CH_3C_3H_7^n)CH$	135/1	175/0·05	1·0	2·0
$(CH_3C_3H_7^i)CH$	131/0·5	156/0·01	1·0	2·0
$(CH_3)_2C_2H_5C$	98/0·1	95/0·1	1·0	1·0

1.4.2 Structure

Wright and Williams[33] carried out a deatiled X-ray crystal study for titanium tetramethoxide and confirmed a structure, figure 1.5, in which each unit is centrosymmetric and the titanium atoms are octahedrally coordinated in a group of four edge sharing octahedra.

Solid crystalline titanium tetraethoxide was found to be tetrameric. The proposed structure, figure 1.6, has each titanium atom octahedrally surrounded by ethoxy groups and the Ti_4O_{16} framework is similar to that of the methoxide. However, in solution and in the liquid state titanium tetraethoxide is trimeric. The most probable structure in solution is that suggested by Russo and Nelson[34] on the basis of light scattering and Raman spectra, see figure 1.7. This structure is also supported by both infrared and ^1H NMR spectroscopic data. At room temperature (or higher) the ^1H NMR spectrum contains only one quartet due to CH_2 protons and one triplet due to CH_3 protons. This has been attributed to rapid intramolecular exchange of bridging and terminal ethoxide groups[35].

Figure 1.5: Structure of $[Ti(OMe)_4]_4$

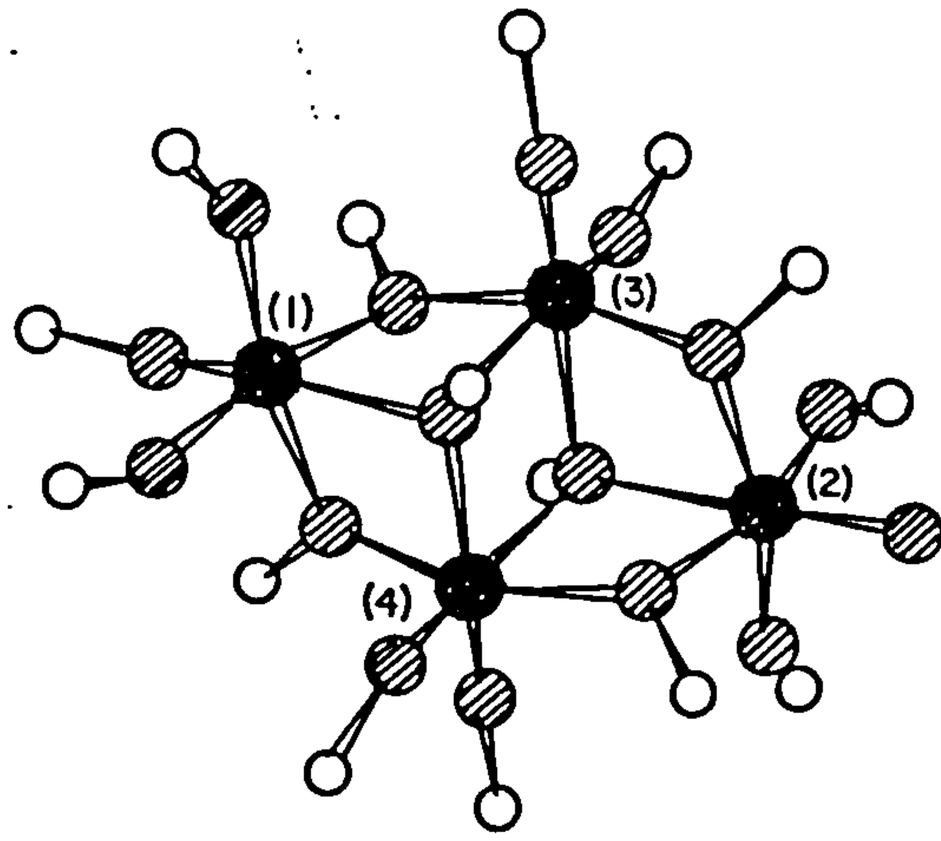

Figure 1.6: Stucture of Solid $Ti(OEt)_4$

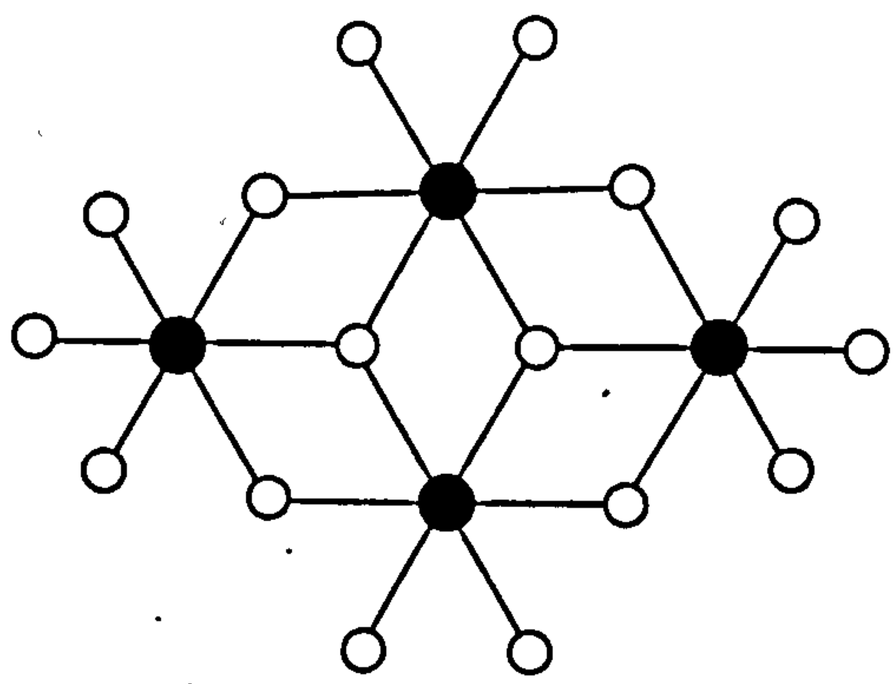

Figure 1.7: Structure of $Ti_3(OEt)_{12}$

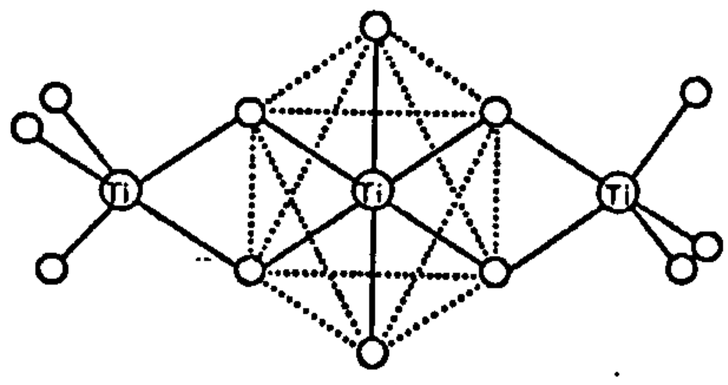

Trimeric straight chain alkoxides like ethoxide, n-propoxide and n-butoxide show a constant chemical shift over a range of temperatures up to 160°C. At a low temperature, less than -20°C, a new sharp peak was observed in the ethoxide which increased the likelihood of tetrameric species being present. Both $Ti(O^iPr)_4$ and $Ti(O^iBu)_4$ are monomeric at room

temperature, but exhibit temperature and concentration dependent behaviour. The spectra of these derivatives exhibit no splitting even at -50°C suggesting that the exchange of terminal and bridging alkoxy groups is very fast and the solution is a mixture of monomer, dimer and trimer.

1.4.3 Alkoxide Hydrolysis

Since transition metals are more electropositive than silicon, hydrolysis of transition metal alkoxides is much easier.

$$\delta \text{ (Si) in } Si(OC_2H_5)_4 = +0{\cdot}32$$

$$\delta \text{ (Ti) in } Ti(OC_2H_5)_4 = +0{\cdot}63$$

$$\delta \text{ (Zr) in } Zr(OC_2H_5)_4 = +0{\cdot}65$$

The reduced partial positive charge makes silicon less susceptible to nucleophilic reagents and thus causes the kinetics of hydrolysis and condensation to be very slow. Conversely, transition metal alkoxides react vigorously and a strongly exothermic reaction results.

On hydrolysis of the transition metal alkoxide, coordination expansion of the metal readily occurs. Therefore, hydrolysis rates are higher than for $Si(OR)_4$ where the fourfold coordination of silicon is already satisfied.

It is observed that alkoxy bridges are more stable toward hydrolysis than associated solvent molecules and in some cases terminal alkoxy ligands. Therefore, starting from a particular alkoxide, the kinetics and resulting structure can be controlled by appropriate choice of solvent. Partial hydrolysis of $Zr(O^nPr)_4$ dissolved in the polar, protic solvent (contains labile proton *ie.* alcohol and water) n-propanol results in a precipitate, whereas homogeneous gels are obtained by hydrolyis of $Zr(O^nPr)_4$, dissolved in nonpolar, aprotic solvents, such as cyclohexane[36]. These differences mirror the influence of molecular complexity on the hydrolysis kinetics: alkoxy-bridging occurs in cyclohexane allowing controlled hydrolysis, whereas alcohol association (rather than alkoxy bridging) occurs preferentially in n-propanol resulting in rapid hydrolysis and formation of a highly condensed product.

A similar difference is observed for titanium alkoxides: $Ti(OEt)_4$ dissolved in ethanol exhibits an oligomeric structure and hydrolysis results in precipitation of monosized particles. However, $Ti(O^iPr)_4$ in iso-propanol is monomeric and hydrolysis results in rapid precipitation of a polydispersed product[37,38].

1.5 Multicomponent Silicates

The preparation of multicomponent glasses by the sol-gel process is an established technique and on densification gives a glass more homogeneous than glasses prepared by a more conventional method. The prime objectives in all preparations of multicomponent oxide compositions is to initially have a solution of all components as soluble precursors; mixing can then be considered to be on a molecular level and if this can be maintained throughout the conversion then a homogeneous product should result. Such preparations highlight the problems arising from the different hydrolysis and condensation rates of the

components. Less electropositive elements have a smaller partial positive charge thus making them less susceptible to nucleophilic reagents and slowing the kinetics of hydrolysis and condensation.

There are a number of different types of precursor that can be used. These should be soluble in organic solvents and simply converted to the relevant oxide preferably by hydrolysis but alternatively by chemical reaction or thermal or oxidative decomposition. A variety of synthetic strategies are used in multicomponent synthesis. For an aqueous system coprecipitation is the commonly used technique. In alkoxide systems there are three general approaches:

1) hydrolysis of mixed alkoxide precursors

2) sequential addition of alkoxides to partially hydrolysed precursors.

3) synthesis of a single alkoxide containing all species in the correct molar ratios.

1.5.1 Alkoxide Methods

Metal alkoxides are probably the best starting materials for sol-gel preparations. With the exception of silicon and phosphorus, all metal alkoxides are rapidly hydrolysed to the hydroxide or oxide. However the method of hydrolysis can be varied and often depends on the final use of the product. As mentioned previously, (section 1.3.1.1), silicon alkoxides require either an acid or base catalyst for hydrolysis.

The easiest method of preparing multicomponent systems is that of making a solution of all the components as alkoxide precursors in a suitable organic solvent before reacting the solution with water to form an oxide mix. For example a basic three component system might be: SiO_2 - TiO_2 - ZrO_2

$$M(OR)_a + M'(OR)_b + M''(OR)_c + x\,H_2O \rightarrow MO_{a/2} + M'O_{b/2} + M''O_{c/2} + y\,ROH$$

This method is widely used but is more complicated than the simple hydrolysis shown above. The first stage of the reaction is hydrolysis of the alkoxide groups to hydroxide groups and their subsequently condensation to form M-O-M linkages. The products can contain one or more metal atoms in the same molecule depending on the relative reaction rates of the hydrolysis and condensation for the component metal alkoxides.

Any variation in reaction rates especially in the initial hydrolysis may lead to inhomogeneities in the final product. When alkoxide hydrolysis is rapid, for instance when there is an excess of liquid water, the hydrolysis rate of silicon alkoxides is still very slow so that they may remain substantially unreacted even when all the other components in the mixture have been precipitated as oxides. The resulting product may contain gross inhomogeneities.

This is achieved by carrying out the hydrolysis very slowly. This is achieved by making the alkoxide mixture up in a suitable solvent and then exposing it to either bulk atmospheric moisture or wet alcohol containing an acid or basic catalyst. In each case the initial polymerised products are soluble, gradually the viscosity increases and gelation eventually

occurs.

Problems arising due to variable hydrolysis rates can be avoided by partially hydrolysing the silicon alkoxide with an equimolar amount of water using an acid catalyst, this results in a trialkoxysilanol which stays in solution:

$$(RO)_4 Si + H_2O \rightarrow (RO)_3 SiOH + ROH$$

The next stage is the addition of other alkoxides which then react to form soluble metallosiloxane derivatives:

$$(RO)_3 SiOH + M(OR')_x \rightarrow (RO)_3 Si - O - M(OR')_{x-1} + R'OH$$

This method was popularised by Yoldas[39,40], here the alkoxides are added in the sequence, least reactive precursor first and a partial hydrolysis step is performed after each addition. The homogeneity of the product depends on the size of the polymeric species to which the last component is added.

1.6 SiO_2-TiO_2 System

These systems are technologically important in the low temperature formation of refractory, ultralow thermal expansion glasses (about 8 mole % TiO_2) and graded refractive index optics. The overall homogeneity of sol-gel processed TiO_2-SiO_2 compositions has been considered by Yoldas[41] and Basil and Lin[42,43].

1.6.1 Preparation

Yoldas suggested that the addition of $Ti(OR)_4$ to partially hydrolysed silicon alkoxides should result in homogeneous glasses. In his investigations Yoldas prepared monolithic materials from TEOS and titanium ethoxide (TET). Soluble polymerisable species were formed by the controlled partial hydrolysis of the alkoxides[41]. Due to the slow hydrolysis of TEOS in comparison with TET, the hydrolysis of a mixture of these alkoxides results in preferential hydrolysis of TET and segregation. It is therefore necessary to form polymerisable species from at least one of the alkoxides separately before reacting with each other.

The TEOS was initially hydrolysed in ethanol, of molar volume greater than or equal to that of TEOS. A controlled amount of water was added gradually into the solution, so that hydrolysis was unable to reach completion, along with a small amount of mineral acid as a catalyst. Yoldas found that hydrolysis took place at most temperatures; but, refluxing or maintaining the mixture at 50-60°C for several hours gave a suitable rate of hydrolysis. However, even in an excess of water TEOS does not completely hydrolyse to an "OR" free complex[31].

For glasses including titania, TEOS is partially hydrolysed with 1 mole water in ethanol at the above temperature. On cooling to room temperature, the TET was added with stirring to the solution.

$$(EtO)_3 SiOH + Ti(OEt)_4 \rightarrow (EtO)_3 Si - O - Ti(OEt)_3 + EtOH \qquad \text{fast}$$

The subsequent dimerisation reaction is highly exothermic, and on ageing, further polymerisation reactions with other silanols will occur. However, such reactions are governed by variation in the rate of hydrolysis of the alkoxide groups in the mixed alkoxides.

$$(EtO)_3SiOH + Ti(OEt)_4 \rightarrow (EtO)_3SiOTi(OEt)_2OSi(OEt)_3 + EtOH$$

Any reactions with species containing titanium occur at a much greater rate than any self-condensation reactions, resulting in Si-O-Ti bonding. Further polymerisation and cross-linking to form a stiff clear single phase only occurs on the introduction of more water.

The prehydrolysis of the less reactive silicon alkoxide before addition of the titanium alkoxide is by far the most common method of preparing SiO_2-TiO_2 oxide gels[41,44-51].

By partially hydrolysing TEOS before the addition of $Ti(OEt)_4$, Yoldas[41] found that the as prepared gels were amorphous by x-ray diffraction (XRD), but at elevated temperatures the anatase form of titania tended to crystallize instead of the expected rutile phase. It is also reported that the temperature at which crystallinity occurs decreases as the concentration of titania in the glass increases[41,44-50].

Ramirez-del-Solar *et al* [49,50] partially hydrolysed TEOS, using HCl as the hydrolysis catalyst. The silicate solution was cooled to 0°C before the addition of $Ti(OBu)_4$ (TiO_2= 1-10wt%) modified with acetic acid, and the effects of ultrasonic and classical methods on the resulting structures were compared. They found that the sintering temperature was always lower in sonogels than in the classic gels, and that anatase was again the preferred phase.

Cogliati *et al* [51] prepared gels containing up to 30% titania from prehydrolysed tetramethyl orthosilicate (TMOS) and either titanium alkoxides or titanium tetrachloride ($TiCl_4$). They compared the structures of an aerogel and a xerogel at 300°C, both containing 15 mole % titania, using XRD. Using titanium propoxide, the xerogel was amorphous but the aerogel exhibited crystallinity due to anatase. By comparing the relative magnitudes of the broad amorphous peak to the heights of the largest peaks in the x-ray diffraction patterns obtained, they determined the amorphous content of the gels. The amorphous content of aerogels prepared from $TiCl_4$ remained constant up to 15 mol% TiO_2, whereas that of the alkoxide gels did not, making $TiCl_4$ a more desirable starting material.

Best and Condrate[52] partially hydrolysed TEOS in a mixture of ethanol and propan-2-ol (IPA) before the addition of $Ti(O^iPr)_4$ and acetylacetone to control the reaction kinetics. Thermal treatment of gels containing greater than 20 mol % TiO_2 to temperatures of 700°C or above resulted in the formation of anatase.

Researchers have also successfully prepared SiO_2-TiO_2 oxides by the simultaneous hydrolysis of both the silicon and titanium precursors. Nakabayashi[53] hydrolysed a mixture of TEOS and $Ti(O^iPr)_4$ in IPA with excess water at 80°C before drying the resulting precipitates in an oven at 110°C, followed by calcination at 500°C for 3 hours. The resulting gels were amorphous by XRD.

Stakheev *et al*[54] prepared TiO_2-SiO_2 samples by homogeneous precipitation from a solution of TEOS and titanium nitrate at 120°C, initially at pH=1 and then to pH=11 with nitric acid and ammonia respectively. Calcination at 500°C for hours resulted in amorphous samples at less than 10 weight % titania. Unfortunately nothing has been reported about treatment at higher temperatures.

Mobilio *et al*[55] dissolved TEOS and titanium n-butoxide in ethanol and n-butanol with small amounts of acetylacetone, the resulting solution was stirred and heated under reflux at 80°C for 2 hours before being cooled and gelled. Samples containing titania at 4·5, 10 and 19 weight % were amorphous on heating to 700°C. Increasing the amount of titania to 19 weight % resulted in anatase being well established at 1000°C whereas the other two samples were amorphous at 1200°C. Morikawa *et al*[56] carried out a similar hydrolysis in ethanol, adding a mixture of water and acetic acid in ethanol dropwise to the alkoxides.

Abe *et al* have prepared mixed silicon-titanium oxides containing 5-50 mol% TiO_2 from bis-acetylacetonato titanium diisopropoxide [$Ti(acac)_2(O^iPr)_2$] in alcohol using a variety of silicon precursors. They used a variety of precursors including, prehydrolysed TEOS[57], $Si(OH)_2(O^tBu)_2$[58] and silicic acid[59-62]. Amorphous gels have been prepared with less than 20 mol% titania using $Ti(acac)_2(O^iPr)_2$, however using the corresponding ethyl acetoacetonate complex amorphous monolithic gels with titania contents up to 94 mol% have been prepared at room temperature.

Wokaun *et al*[63] prepared mixed oxides by completely hydrolysing the silicon and titanium alkoxide precursors before mixing. These were amorphous at 120°C but some dried at 600°C contained TiO_2 detected by Raman spectroscopy. However, they found that prehydrolysis of TEOS before the addition of the titanium alkoxide resulted in mixed oxides that contained no crystalline domains.

The cohydrolysis of an organic-substituted alkoxysilane, $R_nSi(OR')_{4-n}$ (where n=1,2 or 3; R and R'=organic groups),with a titanium alkoxide modifies the resulting structure due to the different properties and molecular structure of the silicate[64,65]. Livage and coworkers[64] used diethoxy dimethylsilane (DEDMS) to make gels that began to segregate anatase at Ti:Si molar ratios of 50:50.

The use of atmospheric moisture[66] to hydrolyse a mixture of TEOS and $Ti(O^iPr)_4$ formed gels containing greater than 14 weight % titania having titanium occupying the interstitial sites and as a result anatase was precipitated at 900°C.

1.6.1.1 Catalytic Effect of Titanium Alkoxides on the Hydrolysis of Silicon Alkoxides

Because $Ti(OR)_4$ catalyses silanol condensation reactions, Basil and Lin[42,43] studied Yoldas's hypothesis by observing the effect of the addition of TET from 1-50 mole % (on theoretical silicon concentration) on partially hydrolysed TEOS solutions. A ^{29}Si NMR study of these solutions containing TEOS, H_2O, HNO_3 and ethanol (1:1:0.006:4.5 (molar ratios)), which had been reacted for 2 hours prior to the addition of TET. From the results obtained, Basil

and Lin concluded that with 0·025 equivalents of TET approximately 62% of the silanols were removed, and with 10% TET no silanols were detected. This was accompanied by the production of high molecular weight, fully condensed silicon ethoxides; such as $Si_2O(OEt)_6$, the linear trimer and tetramer. They found no evidence for reactions between singly hydrolysed silicate monomers and TET to form a product containing $(EtO)_3SiOTi\equiv$ groups. On addition to a partially hydrolysed solution, any TET added is only incorporated into oligomers containing a Si:Ti ratio around 10:1. This is not the expected result of 1:1 condensation products, if the heterocondensation rate is much greater than the rate of silicate homocondensation. Therefore the method of preparation of TiO_2-SiO_2 gels from alkoxides has a great effect on the product homogeneity.

1.7 Structural Evolution and Characterisation

For all types of gels the receding liquid during the final stages of drying exposes an interconnected porous network within the gel that completely surrounds the solid or skeletal phase. The average dimensions of the pores and the thickness of the skeleton depend upon the structure that exists at the gel point and the extent of the collapse or distortion of this structure that results from drying[67]. Dried gels are distinguished from other porous, ceramic green bodies by their enormous surface areas and small pore sizes, a result of the molecular- to colloidal-scale structures that form as products of hydrolysis and condensation during gelation, aging and drying.

1.7.1 Structural Evolution

Surface tension forces created in a gel during solvent removal causes the network to fold as the coordination of the particles is increased[3]. Porosity develops when the gel network becomes strong enough, due to cross linking or neck formation, to resist the compressive forces of surface tension. Therefore, the dried xerogel structure (which comprises both the skeletal and porous phases) will be a contracted and distorted version of the structure originally formed in solution.

Figure 1.8: Schematic representation of weakly cross-linked acid-catalysed gel (A), dessicated gel (B), and TEM micrograph of xerogel prepared by two-step acid-catalysed hydrolysis of TEOS (r=5)followed by drying at 50°C, bar =25nm (C)[68]

(A) (B) (C)

1.7.2 Characterisation of Dried Gels

1.7.2.1 Gas Adsorption[69]

Gas adsorption-desorption isotherms, typically those of nitrogen, are used for the quantitative determination of surface area, pore size distribution, and pore volume. The shapes of the resulting isotherms can be used not only to determine the size of the pores but also their shape.

1.7.2.2 Nuclear Magnetic Resonance (NMR) Spectroscopic Studies

NMR studies of dried gels had previously been limited mainly to silicate and aluminate systems.

Figure 1.9: ^{29}Si MAS NMR spectra of a) xerogel prepared by single-step hydrolysis of TMOS (r=4) with no added catalyst followed by gelation at 40°C and drying at 60°C for 8 hours[70]; b) xerogel as in a after drying open for 11 months at 25°C[70]; c) xerogel prepared by a two-step acid-base-catalysed hydrolysis of TEOS (r=3.8) followed by drying at 50°C for over one-year[71]; d) ν-SiO_2 prepared by sintering the xerogel in c at 1100°C for one hour[71].
(The proportions of Q^1 to Q^4 species present are indicated on the individual spectra.)

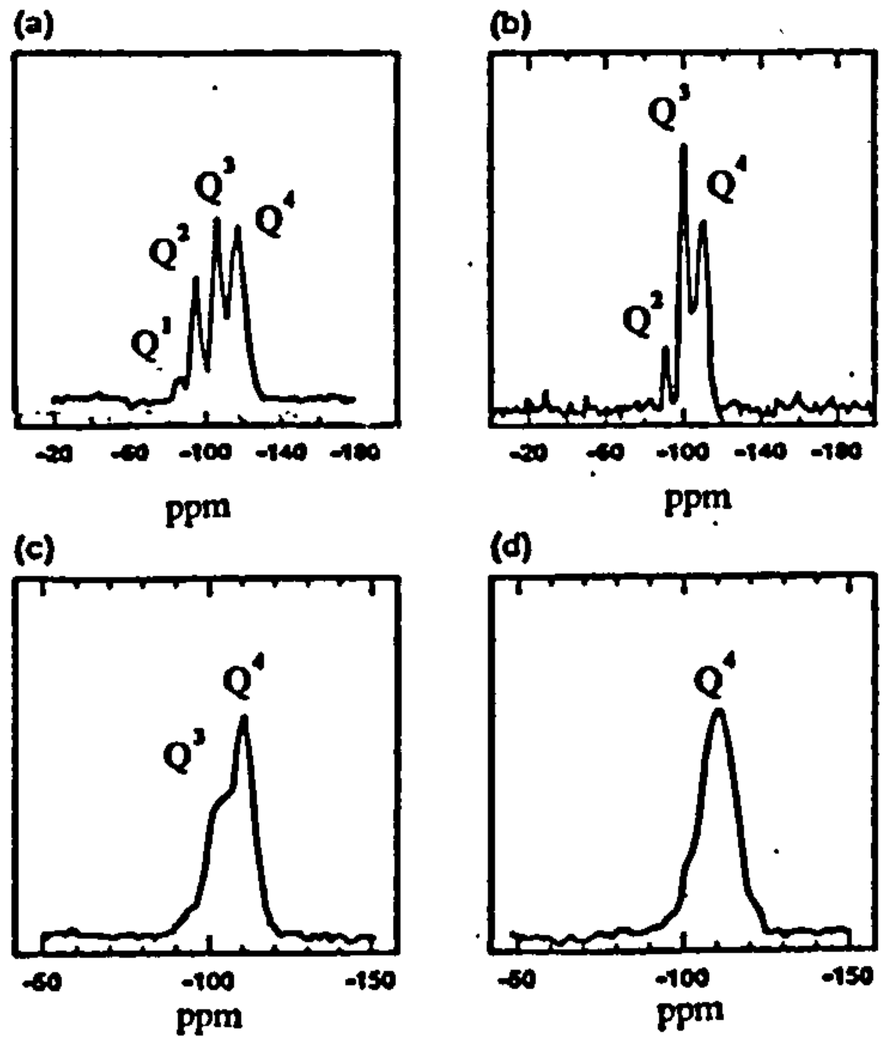

In silicate systems[70,71], it was concluded that the xerogels are weakly condensed compared to fully dense, vitreous silica, which exhibits only a Q^4 resonance in the ^{29}Si magic angle spinning (MAS) spectrum (see figure 1.9d). However, more extensive drying increases the extent of condensation seen by the reduced intensity of the Q^1 resonance and an increase in the intensity of the Q^3 resonance, see figure 1.9 a+b. Using and acid-base synthesis resulted in a more highly condensed structure shown by the greater relative intensity ratio, Q^4/Q^3, in figure 1.9c compared to figures 1.9 a+b.

NMR experiments have been used to obtain additional information on the influence of the drying temperature mainly on a two-stage hydrolysis of gels where both TEOS and $Ti(O^iPr)_4$ were hydrolysed in acid[63]. The Q^n notation denotes a ^{29}Si nucleus with a

$Si(OSi)_n(OX)_{4-n}$ local environment, *ie.* n oxygen bridges to neighbouring silicon nuclei. The remaining (4-n) coordination sites are occupied either by hydroxyl groups (X=H) or by bridges to Ti^{IV} centres (X=Ti). Therefore, a large $\mathbf{Q^4}$ percentage indicates a high degree of cross-linking in the silica domains. The $\mathbf{Q^2}$ and $\mathbf{Q^3}$ signals contain contributions from incompletely cross-linked sites at the surface of a cluster, and from regions where covalent bonds between silica and titania centres exist.

Schraml-Marth *et al* [63] found that separate TiO_2 and SiO_2 domains prevail in single-stage hydrolysed gels, whereas in the two-stage hydrolysed samples the existence of silica sites with a directly bound $O\text{-}Ti^{IV}$ ligand is inferred from lineshape analysis.

An increase in cross-linking as a result of high temperature drying has been observed in the $\mathbf{Q^4}$ sites about 35% at 120°C to 90% at 600°C. If wet gels prepared by a two-stage hydrolysis are redispersed in base then there is an increase in the fractions of $\mathbf{Q^2}$ and $\mathbf{Q^3}$ sites, as compared to samples not subjected to redispersion. These results suggest the formation of Si-O-Ti linkages as a consequence of redispersion.

1.7.2.3 Raman and Infrared Spectroscopic Investigations

Due to the selection rules, Raman and infrared (IR) investigations are complementary in nature, providing molecular-scale information on the xerogel framework.

Best and Condrate[52] used Raman spectroscopy to investigate SiO_2-TiO_2 glasses containing up to 65 mol% TiO_2. Raman spectra obtained after heat treatments at 500 and 700°C are shown in figures 1.10 (a) and (b).

Figure 1.10: Raman spectra of a series of binary gels of composition $xTiO_2$-$(1-x)SiO_2$: (A) x=3·3; (B) x=6·3; (C) x=11·2; (D) x=20·1; (E) x=29·6; (F) x=36·8; (G) x=43·1; (H) x=50·2; (I) x=65·4. Figure a) after heating to 500°C; b) after heating to 700°C[52].

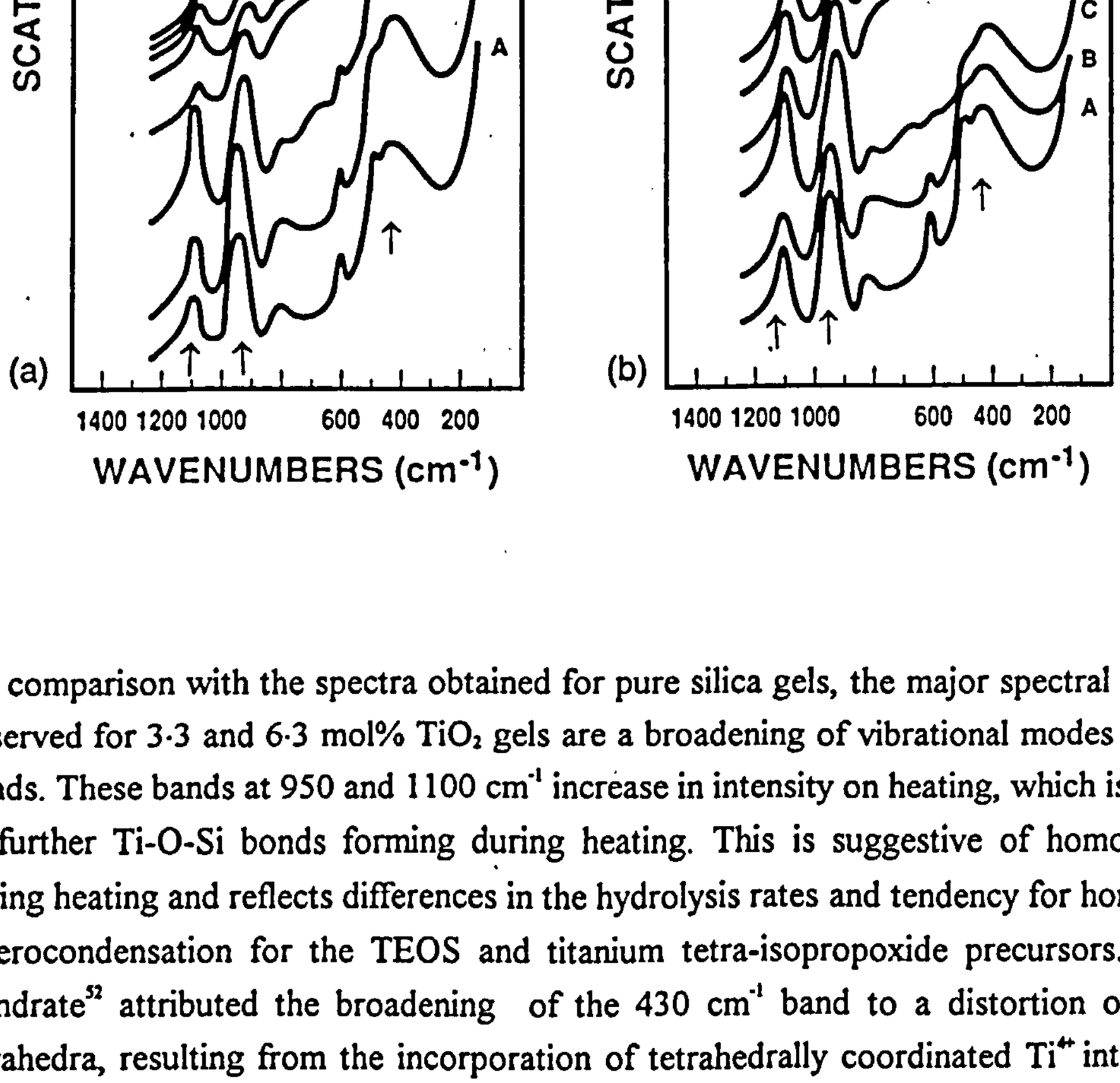

On comparison with the spectra obtained for pure silica gels, the major spectral differences observed for 3·3 and 6·3 mol% TiO_2 gels are a broadening of vibrational modes of Si-O-Ti bonds. These bands at 950 and 1100 cm^{-1} increase in intensity on heating, which is indicative of further Ti-O-Si bonds forming during heating. This is suggestive of homogenization during heating and reflects differences in the hydrolysis rates and tendency for homo- versus heterocondensation for the TEOS and titanium tetra-isopropoxide precursors. Best and Condrate[52] attributed the broadening of the 430 cm^{-1} band to a distortion of the SiO_4 tetrahedra, resulting from the incorporation of tetrahedrally coordinated Ti^{4+} into the SiO_2 network. Hence the ordering of the tetrahedral environment around the Ti is apparently

accomplished by a distortion of the Si environment[55].

Increasing the titania content to 11·2 mol% results in further broadening of the 430 cm^{-1} band, consistent with greater incorporation of Ti in tetrahedral sites in SiO_2 network. But, a band appears at 665 cm^{-1} associated with octahedrally coordinated Ti. However, Emili *et al*[55] observed octahedrally coordinated Ti by XANES and EXAFS only after heating to 1200°C. This discrepancy can be explained either by a greater sensitivity in the Raman experiment or actual differences that exist due to the original gel synthesis conditions. Unfortunately XRD data are not included to determine whether or not the appearance of octahedrally coordinated Ti is accompanied by the crystallisation of anatase.

Increasing the TiO_2 concentration above 11·2 mol% causes a progressive decrease in the 952 and 1100 cm^{-1} bands due to Si-O-Ti bonding. This suggests that the titanate species associate preferentially with themselves rather than silicate species. This has been interpreted as evidence for phase separation preceding the crystallisation of anatase at 700°C[52]. In spectra D to I of figure 1.10b where the TiO_2 concentration was greater than 20·1 mol%, bands in the region 300-700cm^{-1} attributed to crystalline titania were observed. Densification occurs by continued condensation reactions, and the IR spectra[72] indicate a progressive increase in both the relative intensity of the 735 cm^{-1} band, attributed to the asymmetric stretching vibrations of Ti-O for a Ti containing group in a tetrahedral environment, and the frequency of the asymmetric Si-O stretching vibration at 1080 cm^{-1}.

Similar IR and Raman investigations by Perry *et al* [73] concluded that the IR spectra were very similar in shape and behaviour to those of silica-only samples. However, the peak positions were found to have shifted by *ca.* 5cm^{-1} and the band width was greater than for the corresponding silica-only sample. They concluded that this was because the silica network was more open and disordered in the presence of low levels of titanium. The Raman spectra exhibited differences similar to those observed in the IR although band broadenings, up to 615°C, were less marked. The presence of titanium resulted in an increase in the significance of the band at *ca.* 970 cm^{-1}. This was assigned as being predominantly due to SiOH and TiOH stretching vibrations, the high intensity being explained by the larger polarizability change associated with the Ti-O bond. At temperatures greater than 615°C water loss occurred resulting in the formation of Si-O-Ti bonds, this is accompanied by a decrease in Raman intensity and the appearance of Si-O-Ti features at 945 and 1110cm^{-1}. From this it was concluded that full incorporation of titanium atoms into the silica framework occurs only at elevated temperatures.

1.7.2.4 Near Infrared Spectroscopy

Major NIR spectral features (1200-2500nm)[74-81]

λ /nm	Assignment	
2200	H-bonded Si-OH	ν_{OH}(SiOH,H)
2190	Combination stretching-bending of vicinal free SiO-H	ν_{OH}(SiOH,F)+ν_s(Si-O-Si)
1890	Combination stretching-bending of H-bonded water	ν_{OH}(H_2O,H)+ν(H_2O,M) or $2\nu_{OH}$(Si-OH,F)+ν_s(Si-O-Si)
1940		ν_{OH}(H_2O,P)+ν(H_2O,P)
1450	First harmonic of mutually H-bonded SiO-H	$2\nu_{OH}$(H_2O,P)
1400		ν_{OH}(H_2O,M)(SiOH,H)
1365	First overtone of vicinal free SiO-H	$2\nu_{OH}$(SiOH,F)

H= H-bonded; M= monomer; P= polymer; F= free

Studies in both the first (1200-2500nm) and second (900-1350nm) overtone regions, by Perry and Li[72] enabled the identification of both free silanol species and isolated water molecules as well as partly and fully hydrogen bonded species. The addition of titanium leads to a reduction in free silanol levels and an increase in hydrogen bonded silanol groups on a dehydrated surface. On comparison with a silica only sample, they observed that the peak at approximately 1370nm decreased in intensity and a shoulder appeared around 1400nm as the level of titanium was increased. They concluded that the addition of titanium results in materials that are more hydrophilic than for similar silica samples.

1.8 Summary

From the literature, it is obvious that sol-gel processing is complicated and that the initial chemical reactions involved in the polymerisation process are affected by a number of factors. Generally, these include pH dependence, the mechanism of hydrolysis and condensation, the necessity of a catalyst to increase the rate of reaction and the effect of solvent on the kinetics.

In the case of multicomponent silicate systems, such as SiO_2-TiO_2 and SiO_2-ZrO_2, problems arise due to the faster hydrolysis rates of titanium and zirconium alkoxides compared to silicon alkoxides. Therefore, hydrolysis of a mixture of these more reactive alkoxides results in preferential hydrolysis of the titanium or zirconium alkoxide and segregation of the oxide phase. In the literature, this problem has been overcome by either forming a solution of partially hydrolysed silicon alkoxide before reacting the precusors with each other, or by controlling the reactivity of the titanium or zirconium alkoxides through chelation of the

metal ion. The most common method in the literature[41,44-51] is the prehydrolysis of the less reactive silicon alkoxide before addition of the titanium alkoxide. A less common method found in the literature is the hydrolysis of bis(acetylacetonato) titanium diisopropoxide $[Ti(acac)_2(O^iPr)_2]$ in alcohol together with a variety of silicon precursors. The silicon precursors which have been studied include prehydrolysed TEOS[57], $Si(OH)_2(O^tBu)_2$[58] and silicic acid[59-62] all of which contain hydroxyl groups which are highly reactive towards condensation reactions.

The first stage of the current research programme was to develop and explore different routes to homogeneous SiO_2-TiO_2 gels and SiO_2-ZrO_2 gels. In this work bis(acetylacetonato) titanium diisopropoxide (or bis(acetylacetonato) zirconium dipropoxide) and TEOS have been simultaneously hydrolysed under acidic conditions in iso-propanol to form homogeneous gels.

Using the above systems, the effects of the reaction conditions, amount of titania/zirconia present in the gel, drying conditions and thermal treatment of the dry gels, on the bulk and structural properties of the gels have been investigated.

In this work, mixed SiO_2-TiO_2 gels have also been prepared by the simultaneous hydrolysis of bis(acetylacetonato) titanium di(triethoxysilane) $[Ti(acac)_2(OSi(OC_2H_5)_3)_2]$ and TEOS under acidic conditions in ethanol. The effects of the reaction conditions and thermal treatment of the dry gels on the bulk and structural properties of the gels have been investigated.

1.9 References

1 C.F. Baes and R.E. Mesmer, *The Hydrolysis of Cations* (Wiley, New York, 1976)

2 G. Lagerström, *Acta Chemica Scan.* **13** (1959) 722-736

3 R.K. Iler, in *The Chemistry of Silica* p.172-311 (Wiley, 1979)

4 P.C. Carman, *Trans. Faraday Soc.* **36** (1940) 964-973

5 C.T.G. Knight, R.J. Kirkpatrick and E. Oldfield, *J. Mag. Reson.* **78** (1988) 31-40

6 C.T.G. Knight, R.J. Kirkpatrick and E. Oldfield, *J. Am. Chem. Soc.* **108** (1986) 30-33

7 R.K. Harris, C.T.G. Knight and W.E. Hull, in *Soluble Silicates* p.79-93, ed. J.R. Falcone Jr. (Am. Chem. Soc., 1982)

8 L.S. Dent-Glasser and E.E. Lachowski, *J. Chem. Soc. Dalton Trans.* **393** (1980) 399-402

9 D. Avrir and V.R. Kaufman, *J. Non Crystalline Solids* **92** (1987) 180-182

10 C.J. Brinker and G.W. Scherer, in *Sol-gel Science: the physics and chemistry of sol-gel processing* p.111 (Academic Press, 1990)

11 C.J. Brinker, K.D. Keefer, D.W. Schaefer and C.S. Ashley, *J. Non Crystalline Solids* **48** (1982) 47-64

12 W. Stober, A. Fink and E. Bohn, *J. Colloid & Interface Science* **26** (1968) 62-69

13 D.W. Schaefer, J.E. Martin and K.D. Keefer,in *Physics of Finely Divided Matter* p. 31, eds. N. Bocarra and M. Daoud (Springer-Verlag, 1985)

14 D.W. Schaefer and K.D. Keefer, in *Fractals in Physics* p. 39-45, eds. L. Pietronero and E. Tosatti (North-Holland, 1986)

15 D.C. Bradley, R.C. Mehrotra and D.P. Gaur, *Metal Alkoxides* (Academic Press, London, 1978)

16 J. Livage, M. Henry and C. Sanchez, *Sol-Gel Chemistry of Transition Metal Oxides* in *Progress in Solid State Chemistry* **18** (1988) 259-342

17 R. Aelion, A. Loebel and F. Eirich, *J. Am. Chem. Soc.* **72** (1950) 5705-5712

18 E.J.A Pope and J.D. Mackenzie, *J. Non Crystalline Solids* **87** (1986) 185-198

19 R.J.P. Corriu, D. LeClercq, A. Vioux, M. Paultre and J. Phalippou, in *Ultrastructure Processing of Advanced Ceramics* p113-126, eds. J.D. Mackenzie and D.R. Ulrich (Wiley, New York, 1988)

20 L.L. Hench, G. Orcel and J.L. Nogues, in *Better Ceramics Though Chemistry 2* p.35-47, eds. C.J. Brinker, D.E. Clark and D.R. Ulrich (Mat. Res. Soc., Pittsburgh, 1986)

21 J. Jonas, in *Science of Ceramic Chemical Processing* p 65-72, eds. L.L. Hench and D.R. Ulrich (Wiley, New York, 1986)

22 I. Artaki, M. Bradley, T.W. Zerda, J. Jonas, G. Orcel and L.L. Hench, in *Science of Ceramic Chemical Processing* p 73-80, eds. L.L. Hench and D.R. Ulrich (Wiley, New York, 1986)

23 G. Orcel and L.L. Hench, *J. Non Crystalline Solids* **79** (1986) 177-194

24 L.L. Hench, in *Science of Ceramic Chemical Processing* p.52-64, eds. L.L. Hench and D.R. Ulrich (Wiley, New York, 1986)

25 V.G. Engelhardt, W. Altenburg, D. Hoebbel and W.Z. Wieker, *Z. Anorg. Allg. Chem.* **428** (1977) 43-52

26 B.K. Coltrain, S.M. Melpolder and J.M. Salva, in U*ltrastructure Processing of Advanced Materials* p.69-76, eds D.R. Uhlmann and D.R. Ulrich (Wiley, New York, 1992)

27 E.M. Rabinovich and D.L. Wood , in *Better Ceramics Through Chemistry 2* p.251-268, eds. C.J. Brinker, D.E. Clark and D.R. Ulrich (Mat. Res. Soc., Pittsburgh,1986)

28 I. Artaki, T.W. Zerda and J. Jonas, *J. Non Crystalline Solids* **81** (1986) 381-395

29 D.C. Bradley, R.C. Mehrotra and W. Wardlow, *J. Chem. Soc.* (1952) 5020-5023

30 D.C. Bradley, R.C. Mehrotra and W. Wardlow, *J. Chem. Soc.* (1952) 2027-2032

31 D.C. Bradley, R.C. Mehrotra and W. Wardlow, *J. Chem. Soc.* (1952) 4204-4209

32 D.C. Bradley, R.C. Mehrotra and W. Wardlow, *J. Chem. Soc.* (1952) 2025-2030

33 D.A. Wright and D.A. Williams, *Acta. Cryst. Sect.B* **24** (1968) 1107-1114

34 W.R. Russo and W.H. Nelson, *J. Am. Chem. Soc.* **92** (1970) 1521-1526

35 D.C. Bradley and C.E. Holloway, *J. Chem. Soc. (A)* (1968) 1316-1319

36 D. Kundu and D. Ganguli, *J. Mat. Sci. Lett.* **5** (1986) 293-295

37 E.A. Barringer and H.K. Bowen, *Langmuir* **1** (1985) 414-419

38 E.A. Barringer and H.K. Bowen, *Langmuir* **1** (1985) 420-428

39 B.E. Yoldas, *J. Mat. Sci.* **12** (1977) 1203-1208

40 B.E. Yoldas, *J. Mat. Sci.* **14** (1979), 1843-1849

41 B.E. Yoldas, *J. Non Crystalline Solids* **38,39** (1980) 81-86

42 J.D. Basil and C. C. Lin, in *Ultrastructure Processing of Advanced Ceramics* p. 783-794, eds. J.D. Mackenzie and D.R. Ulrich (Wiley, New York, 1988)

43 J.D. Basil and C. C. Lin, in *Better Ceramics Through Chemistry 3* p. 49-55, eds. C.J. Brinker, D.E. Clark and D.R. Ulrich (Mat. Res. Soc., Pittsburgh, 1988)

44 Y-C Cheng and L.L. Hench, in *Better Ceramics Through Chemistry 3* p. 593-596, eds. C.J. Brinker, D.E. Clark and D.R. Ulrich (Mat. Res. Soc., Pittsburgh, 1988)

45 J. Cheng and D. Wang, *J. Non Crystalline Solids* **100** (1988) 288-291

46 L. Yuan and G. Yao, *J. Non Crystalline Solids* **100** (1988) 309-315

47 I.M. Niranda Salvado and J.M. Fernandez Navarro, *J. Non Crystalline Solids* **147,148** (1992) 256-261

48 L. Armelao, P. Colombo, G. Granozzi and M. Guglielmi, *J. Non Crystalline Solids* **139** (1992) 198-204

49 M. Ramirez-del-Solar, L. Esquivias, A.F. Craievich and J. Zarzycki, *J. Non Crystalline Solids* **147,148** (1992) 206-212

50 M. Ramirez-del-Solar, N. de la Rosa-Fox, L. Esquivias and J. Zarzycki, *J. Non Crystalline Solids* **121** (1992) 84-89

51 G. Cogliati, M. Guglielmi, T.M. Che and T.J. Clark, in *Better Ceramics Through Chemistry 4* p. 329-334, eds. B.J. Zelinski, C.J. Brinker, D.E. Clark and D.R. Ulrich (Mat. Res. Soc., Pittsburgh, 1990)

52 M.F. Best and R.A. Condrate Sr., *J. Mat. Sci. Lett.* **4** (1985) 994-998

53 H. Nakabayashi, *Bull. Chem. Soc. Jpn.* **65** (1992) 914-916

54 A. Yu. Stakheev, E.S. Shpiro and J. Apijak, *J. Phys. Chem.* **97** (1993) 5668-5672

55 M. Emili, L. Incoccia, S. Mobilio, G. Fagherazzi and M. Guglielmi, *J. Non Crystalline Solids* **74** (1985) 129-145

56 H. Morikawa, T. Osuka, F. Marumo, A. Yasumori, M. Yamane and M. Momura, *J. Non Crystalline Solids* **82** (1986) 97-102

57 T. Gunji, Y. Nagao, T. Misono and Y. Abe, *Nippon Seramikkusu Kyokai Gakujutsu Ronbunshi* **99**, 2 (1991) 178-179

58 Y. Abe, T. Gunji, Y. Kimata, M. Kuramata, A. Kasgoz and T. Misono, *J. Non*

Crystalline Solids **121** (1990) 21-25

59 T. Gunji, Y. Nagao, T. Misono and Y. Abe, *J. Polymer Sci. Part A: Polymer Chem.* **30** (1992) 371-377

60 T. Gunji, Y. Nagao, T. Misono and Y. Abe, *J. Polymer Sci. Part A: Polymer Chem.* **29** (1991) 941-947

61 Y. Abe, N. Sugimoto, Y. Nagao and T. Misono, *J. Non Crystalline Solids* **104** (1988) 164-169

62 T. Gunji, Y. Nagao, T. Misono and Y. Abe, *J. Non Crystalline Solids* **107** (1989) 149-154

63 M. Schraml-Marth, K.L. Walther, A. Wokaun, B.E. Handy and A. Baiker, *J. Non Crystalline Solids* **143** (1992) 93-111

64 S. Dire, F. Babonneau, G. Carturas and J. Livage, *J. Non Crsytalline Solids* **147,148** (1992) 62-66

65 L. Lan, G. Gnappi and A. Montenero, *J. Mat. Sci.* **28** (1993) 2119-2123

66 C.J.R. Gonzalez-Oliver, P.F. James and H. Rawson, *J. Non Crystalline Solids* **48** (1982) 129-152

67 G.W. Scherer, *J. Non Crystalline Solids* **100** (1988) 77-92

68 C.J. Brinker, W.D. Drotning and G.W. Scherer, in *Better Ceramics Through Chemistry* p.25-32, eds. C.J. Brinker, D.E. Clark and D.R. Ulrich (Elsevier, North-Holland, New York, 1984)

69 S.J. Gregg and K.S.W. Sing, *Adsorption, Surface Area and Porosity* (Academic Press, London, 1982)

70 W.G. Klemperer, V.V. Mainz and D.M. Millar, in *Better Ceramics Through Chemistry 2* p.15-26, eds. C.J. Brinker, D.E. Clark and D.R. Ulrich (Mat. Res. Soc., Pittsburgh Pa., 1986)

71 C.J. Brinker, R.J. Kirkpatrick, D.R. Tallant, B.C. Bunker and B. Montez, *J. Non Crystalline Solids* **99** (1988) 418-428

72 T. Hayashi, T. Yamada and H. Saito, *J. Mat. Sci.* **18** (1983) 3137-3142

73 C.C. Perry, X. Li and D.N. Waters, *Spectrochimica Acta* **47A**, 9/10 (1991) 1487-1494

74 K. Buijs and G.R. Choppin, *J. Chem. Phys.* **39** (1963) 2035-2041; 2042-2050

75 C.C. Perry and X. Li, *J. Chem. Soc. Faraday Trans.* **87**,5 (1991) 761-766

76 C.C. Perry and X. Li, *J. Chem. Soc. Faraday Trans.* **87**,24 (1991) 3857-3862

77 J.H. Anderson and K.A. Wickersheim, *Surface Sci.* **2** (1964) 252-260

78 M.R. Basila, *App. Spec. Rev.* **1** (1968) 289-372

79 A.V. Kiselev, *Dis. Faraday Soc.* **52** (1971) 14-32

80 D.F. Mifel, V.B. Kazarsky and V.M. Andreev, *Surface Sci.* **72** (1978) 342-356

81 F. Orgaz and H. Rawson, *J. Non Crystalline Solids* **82** (1986) 57-68

82 C.C. Perry and X. Li, in *Chemical Processing of Advanced Materials*, p.131-141 eds. L.L. Hench and J.K. West (Wiley, New York, 1992)

Chapter 2: Experimental Methods

2.1 Infrared Spectroscopy[1,2,3,4]

The infrared region extends over the region 12800 to 10cm^{-1} wavenumbers or wavelengths of 0·78 to 1000μm, and is divided into three regions, see table 2.1.

Table 2.1

Region	Wavelength Range (λ), μm	Wavenumber Range (ν), cm^{-1}	Origin of Infrared Band
Near	0·78 - 2·5	12800 - 4000	overtone and combination vibrations
Middle	2·5 - 50	4000 - 200	fundamental vibrations
Far	50 - 1000	200 - 10	rotation and some vibrations and torsions

Analytical applications are found in the mid-infrared section from 4000-400cm^{-1} or wavelengths of 2·5-25μm.

2.1.1 Theory

Absorption of infrared radiation is largely restricted to molecules in which small energy differences exist between several vibrational and rotational states. For a molecule to absorb infrared radiation it must undergo a net change in dipole moment as a consequence of its vibrational motion. Only then can the alternating electrical field of the radiation interact with the molecule and cause changes in the amplitude of one of its motions. A dipole moment is determined by the magnitude of the charge difference and the distance between the two charge centres. If the frequency of the radiation matches a natural vibrational frequency of the molecule, then a net transfer of energy occurs that results in a change in the amplitude of the molecular vibration, and absorption of radiation is the consequence. Molecular vibrations fall into three basic categories: stretching , bending (see figure 2.1) and torsion (which is neither stretching and bending).

Figure 2.1: Infrared Stretching and Bending Vibrations

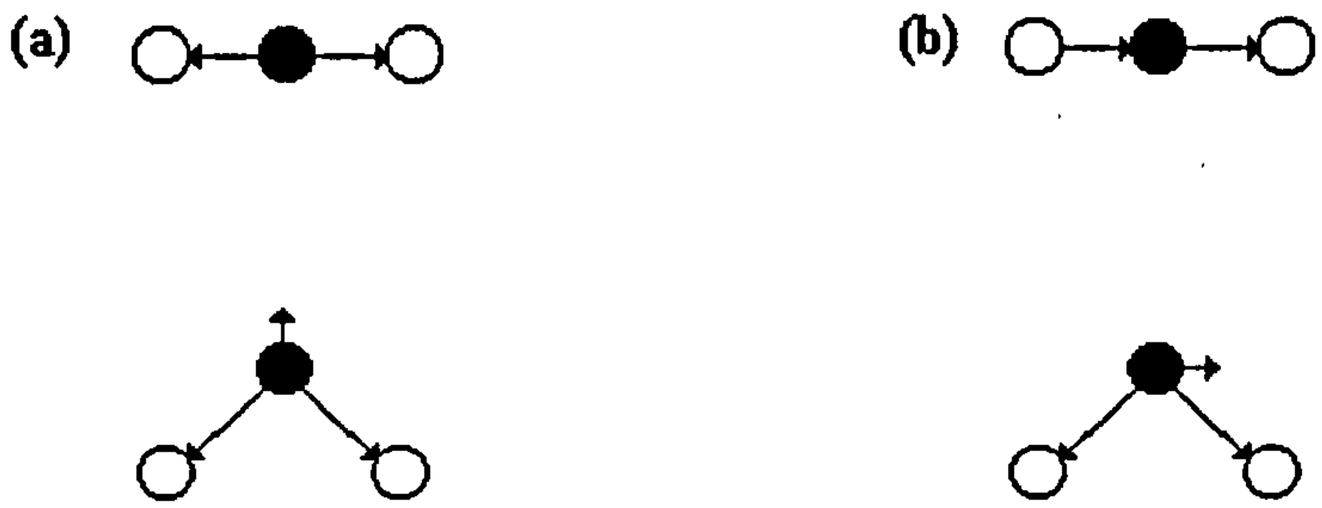

Stretching vibrations (a) symmetric; (b) asymmetric

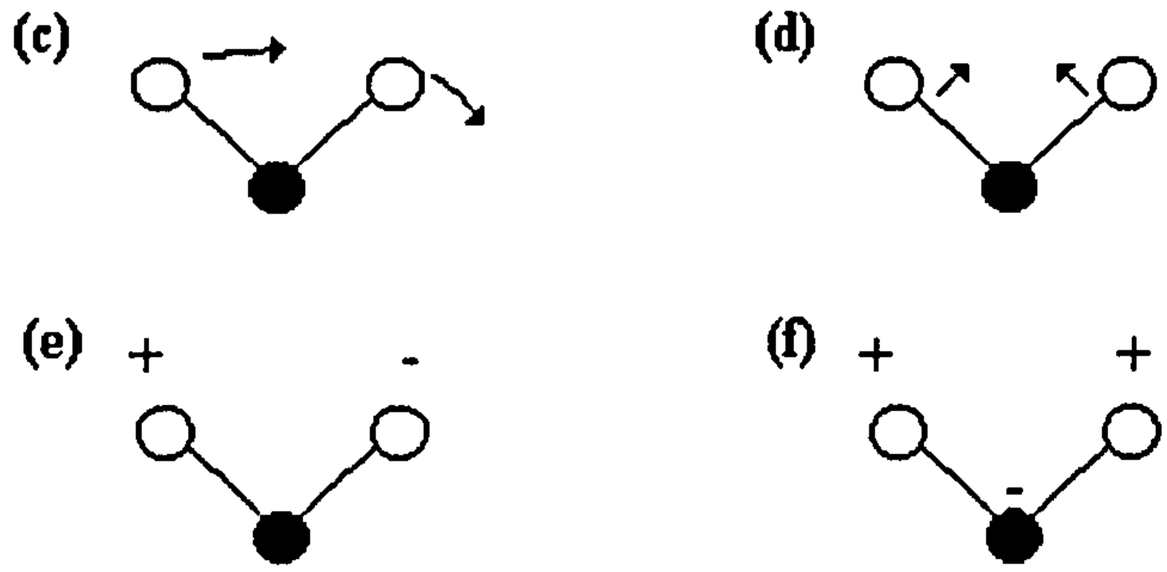

Bending vibrations (c) in-plane rocking; (d) in-plane scissoring; (e) out-of-plane twisting; (f) out-of-plane wagging.

Where + = motion out-of-page; - = motion into page.

Stretching vibrations involve a continuous change in the interatomic distance along the bond between two atoms. These coupled vibrations can be either symmetric *ie.* in different directions or asymmetric, in the same direction. Bending vibrations are characterised by a change in the angle between two bonds and these can be one of four types: scissoring, rocking, wagging and twisting.

2.1.2 Instrumentation: Fourier Transform Infrared Spectrometer

Any structural changes in the samples prepared have been studied in the IR fundamental region (4000-400cm^{-1}) on a Perkin-Elmer 1710 spectrometer under computer control using the Perkin-Elmer Infrared Data Manager (IRDM).

Figure 2.2: Michelson Interferometer

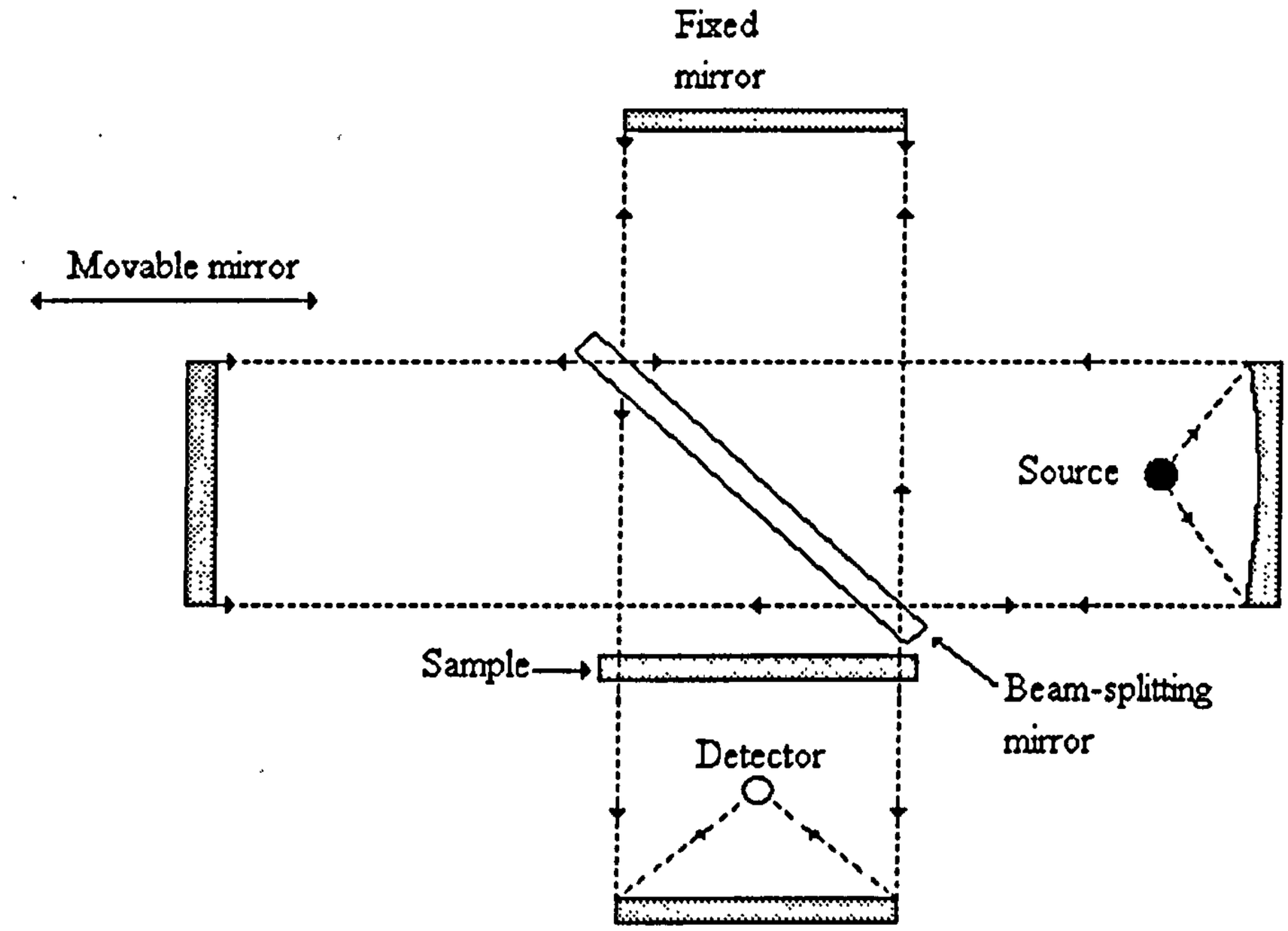

A beam of radiation from a source is collimated and the resultant beam "impinges" on the beamsplitter which transmits approximately half of the radiation to a moving mirror, and reflects the other half to a fixed mirror. After reflection, the beams recombine at the beamsplitter, the intensity of the light depends on the differences in the path lengths of the divided light beams. Constructive interference occurs when the light paths are the same. The interferometer is scanned by moving the mirror at a constant velocity, this causes the intensity of the radiation at any wavelength to fluctuate in a regular sinsusoidal manner. For an infrared source, the emerging beam is a complex combination of frequencies which after passage through the sample are focused onto the detector. The interferogram is measured by recording the detector signal as a function of the path difference between the two beams. The signal has to be sampled at precise intervals corresponding to equal steps in path difference. This is achieved by using a helium neon laser as a reference. The normal frequency spectrum is constructed from the interferogram by applying a Fourier transformation.

Generally, a well-designed interferometer has several basic advantages over a classical dispersive instrument. These are:

(i) Fellgett (or Multiplex) Advantage Since all frequencies are measured simultaneously in an interferometer, a complete spectrum can be very rapidly obtained. Therefore, the same spectral signal-to-noise ratio can be obtained in a fraction of the time taken for a single scan of a dispersive spectrometer.

(ii) Jacquinot (or Throughput) Advantage The energy throughput of an interferometer is much larger than for a dispersion instrument because there are no slits to limit the incoming energy.

(iii) Connes Advantage The frequency scale of an interferometer is derived from a helium neon laser that acts as an internal reference for each scan. As a result, the frequency calibration of interferometers is much more accurate and has much better long term stability

(iv) Because of the way in which the interferometer modulates each frequency, there is no direct equivalent of the stray light found in dispersive spectrometers.

(v) Resolution is constant at all wavelengths whereas in a dispersive instrument the resolution varies because of the slit.

(vi) There are no discontinuities in the spectrum because there are no grating or filter changes.

(vii) Data can be easily manipulated by computer.

2.1.3 Experimental

Typically samples were analysed as potassium bromide discs containing 0·5mg of sample in 100mg of potassium bromide. Transmittance data was acquired on a Perkin-Elmer 1710 spectrometer under computer control using the Perkin-Elmer Infrared Data Manager (IRDM) using the following conditions:

scans=20

resolution = $4cm^{-1}$

frequency range= $4000\text{-}400cm^{-1}$.

Once spectra were obtained they were converted to absorbance using IRDM.

2.2 Ultraviolet / Visible / Near Infrared Spectroscopy

2.2.1 Near Infrared (NIR) Spectroscopy[5,6]

Absorption bands in the spectral region 780-2500nm, are due to overtones and combinations of the fundamental mid-infrared vibrational bands. The most prominent bands are those related to O-H, C-H and N-H groups.

If a bond obeys Hooke's law (see figure 2.3) then:

$$f = -k\left(r - r_{eq}\right) \qquad \textbf{2.1}$$

where:

f = restoring force

k = force constant

r = internuclear distance

r_{eq} = equilibrium internuclear distance

Equation 2.1 implies the following form for the potential energy V:

$$V = \tfrac{1}{2}k\left(r - r_{eq}\right)^2 \qquad \textbf{2.2}$$

Figure 2.3: Ideal Harmonic Oscillator

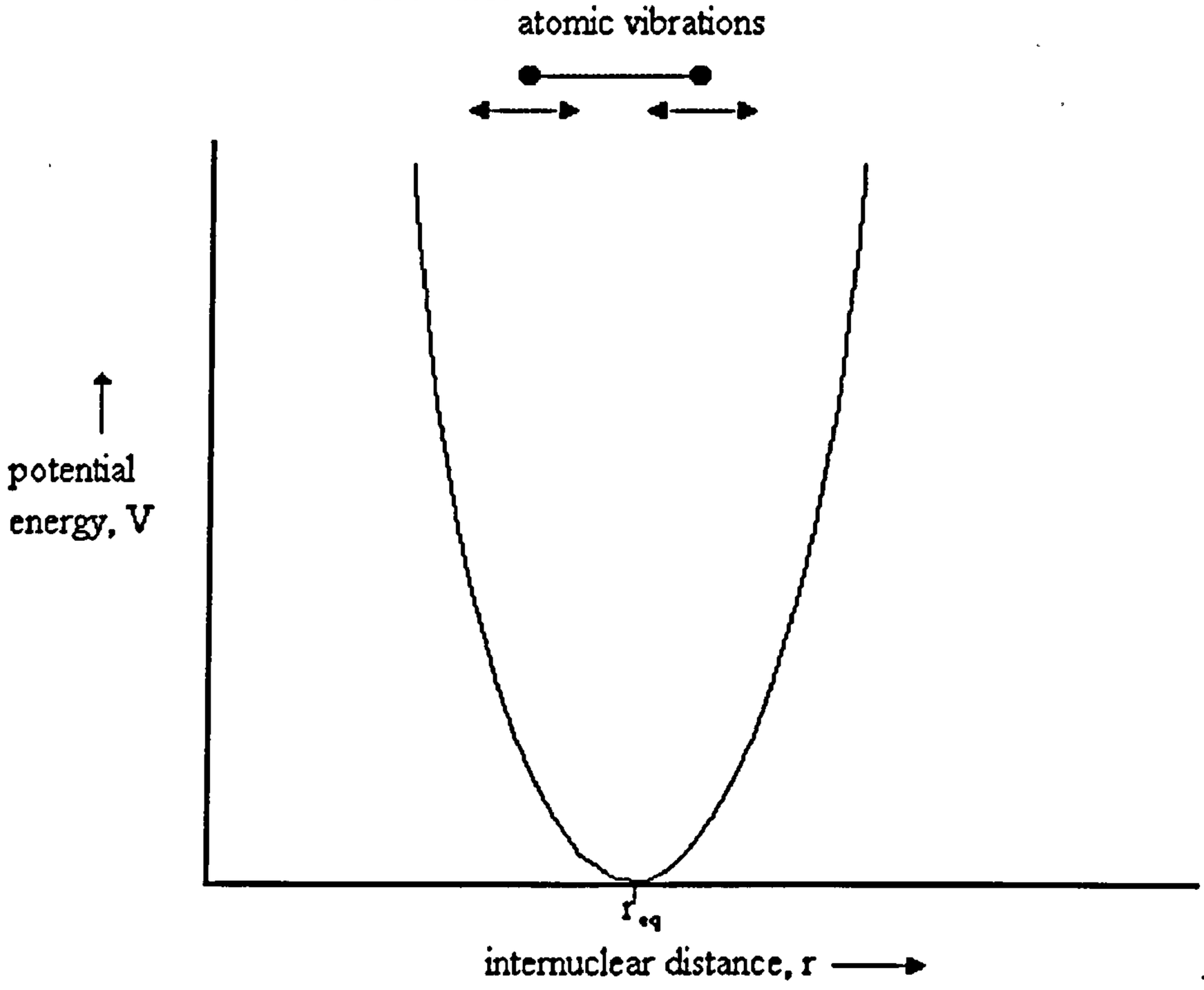

The quantum mechanical expression for vibrational energy implies that the energy E is restricted to specific levels according to:

$$E = \frac{h}{2\pi}\sqrt{\frac{f}{\mu}}\left(\upsilon + \tfrac{1}{2}\right) \qquad \textbf{2.3}$$

υ = vibrational quantum number

μ = reduced mass

but the frequency of vibration of the oscillator is

$$\nu = \frac{1}{2\pi}\sqrt{\frac{f}{\mu}}$$

and energy is

$$E = h\nu\left(\upsilon + \tfrac{1}{2}\right) \qquad \textbf{2.4}$$

Therefore only discrete energy levels are allowed. The separation of these levels is:

$$\Delta E = h\nu$$

In the ideal case, quantum mechanical selection rules[6] forbid transitions between states separated by greater than one energy level. Therefore only the fundamental vibration would be observed and therefore no near infrared spectrum.

However, real bonds do not accurately obey Hooke's law. For example, in the limit of large *r*, the bond will break and the molecule dissociate into atoms. For small deviations from equilibrium the bond is assumed to be perfectly elastic, for larger deviations a more complex model must be followed (see figure 2.4).

The Morse function is a good approximation to the curve

$$E = D_{eq}\left[1-\exp\left\{a\left(r_{eq}-r\right)\right\}\right]^2 \qquad \textbf{2.5}$$

where:

a = constant for a particular molecule

D_{eq}=dissociation equilibrium.

Therefore for an anharmonic oscillator the energy levels are expressed as[7]:

$$E = \left(\upsilon + \tfrac{1}{2}\right)hc\bar{\nu} - \left(\upsilon + \tfrac{1}{2}\right)^2 hc\bar{\nu}x \qquad \textbf{2.6}$$

where:

x =anharmonicity constant ≈+0·01

c=speed of light

Figure 2.4: Morse Curve for Large Deviations from Equilibrium

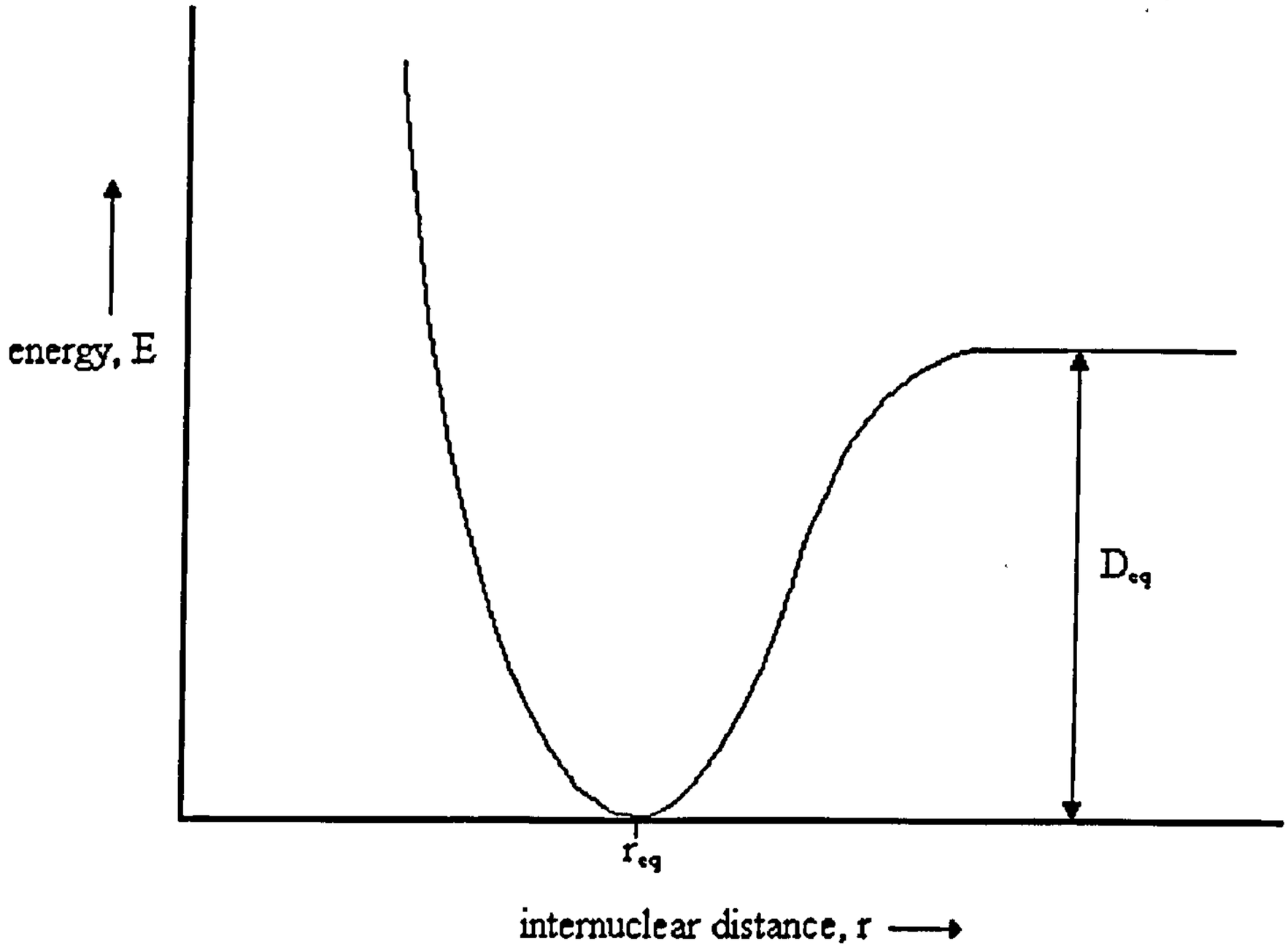

A direct result of the anharmonicity of molecular vibrations is that transitions separated by more than one energy level are allowed, and hence overtone absorption bands occur. Since the anharmonicity constant, *x*, is always positive, the vibrational energy levels slowly converge with increasing vibrational quantum number. Therefore overtones do not occur at precisely two or three times the fundamental frequency, but differ slightly, according to the

anharmonicity constant. From equation 2.6 the general formula for the separation of energy levels v and v-1 is derived as:

$$\Delta E = E_v - E_{v-1} = (1 - 2vx)h\nu \qquad 2.7$$

However, the complexity of the NIR region is increased by the presence of both simple overtones and combination bands. For silica, such bands usually involve fundamentals or overtones of the O-H stretch as well as some deformation modes.

2.2.2 Ultraviolet and Visible (UV/Vis) Absorbance Spectroscopy[8,9]

This covers the spectral region from 180 to 780nm in the electromagnetic spectrum. Absorbance generally arises from the electronic transitions of bonding electrons from the ground to the excited state. There are three types of electronic transition by which absorbing species are categorised. These include transitions involving:

(1) π, σ and n electrons

(2) d and f electrons

(3) charge transfer electrons

2.2.2.1 π, σ and n Electrons

Absorbing species containing π, σ and n electrons include organic molecules and ions as well as a number of inorganic anions. There are four possible types of transition:

(1) $\sigma \rightarrow \sigma^*$ which correspond to radiant frequencies in the vacuum UV region.

(2) $n \rightarrow \sigma^*$ these transitions are usually found in saturated compounds containing atoms with unshared electron pairs (non bonding electrons) and are caused by radiation between 150 and 250nm, with most absorbance peaks occurring at less than 200nm.

(3) & (4) $n \rightarrow \pi^*$ and $\pi \rightarrow \pi^*$ transitions occur in the region 200 to 700nm. Both require the presence of an unsaturated functional group to provide orbitals.

2.2.2.2 d and f Electrons

These are most common for complexes in the first and second row transition metal series, and are due to electronic transitions between the new energy levels. These arise from an interaction of the electronic field from the nearest ligands, with the free ion energy levels. Different types of new energy levels arise from variations in the symmetry of the ligand field. The energy difference between two sets of split levels is Δ which is a semi-empirical parameter measuring the ligand strength. The larger the value of Δ, the larger the ligand splitting and the greater the ligand strength. Therefore bands are often broad and are strongly influenced by chemical factors, see table 2.2.

Table 2.2:

(a) Crystal Field Splittings by Various Ligands for Cr^{III} (d^3) [10]

	Absorbance Peak /cm^{-1}	Δ_o/ $kJmol^{-1}$
$[Cr^{III}Cl_6]^{3-}$	13640	163
$[Cr^{III}(H_2O)_6]^{3+}$	17830	213
$[Cr^{III}(NH_3)_6]^{3+}$	21680	259
$[Cr^{III}(CN)_6]^{3-}$	26280	314

(b) Crystal Field Splittings for One Group of Elements[10]

	Absorbance Peak /cm^{-1}	Δ_o/ $kJmol^{-1}$
$[Co(NH_3)_6]^{3+}$	23000	275
$[Rh(NH_3)_6]^{3+}$	34000	406
$[Ir(NH_3)_6]^{3+}$	41000	490

Where $1kJmol^{-1} \equiv 83{\cdot}7cm^{-1}$

For lanthanide and actinide ions, the absorption results from electronic transitions of 4f and 5f electrons. The screening of such inner orbitals by electrons occupying outer orbitals from the external environment results in narrow bands that are largely unaffected by the nature of the ligand field.

2.2.2.3 Charge Transfer Electrons

These transitions occur mainly in inorganic complexes. In order for a complex to exhibit a charge transfer spectrum, it is essential for one component to have electron-donor and the other electron-acceptor properties. Therefore, absorbance of radiation involves transfer of an electron from the donor to an orbital associated with the acceptor.

2.2.3 UV/Vis/NIR Spectra of Transition Metal Doped Gels

2.2.3.1 Theory

2.2.3.1 Crystal Field Theory

The crystal field theory assumes that the coordinate bond consists entirely of the electrostatic attraction between a transition metal cation and a ligand. This results in the splitting of the previously degenerate d-orbitals of the metal into two sets:

$$t_{2g} = d_{xy}, d_{yz}, d_{xz}$$

$$e_g = d_{x^2-y^2}, d_{z^2}$$

the separation of which is Δ or 10Dq.

Therefore, in an octahedral complex $d_{x^2-y^2}$ and d_{z^2}, which point at the ligands are more strongly affected than d_{xy}, d_{xz} and d_{yz} which point between the ligands (figure 2.5).

In a tetrahedral field (figure 2.6), the electrons in the t_2 orbitals are more strongly repelled

Figure 2.5: Energy Levels of d-orbitals in an Octahedral Field

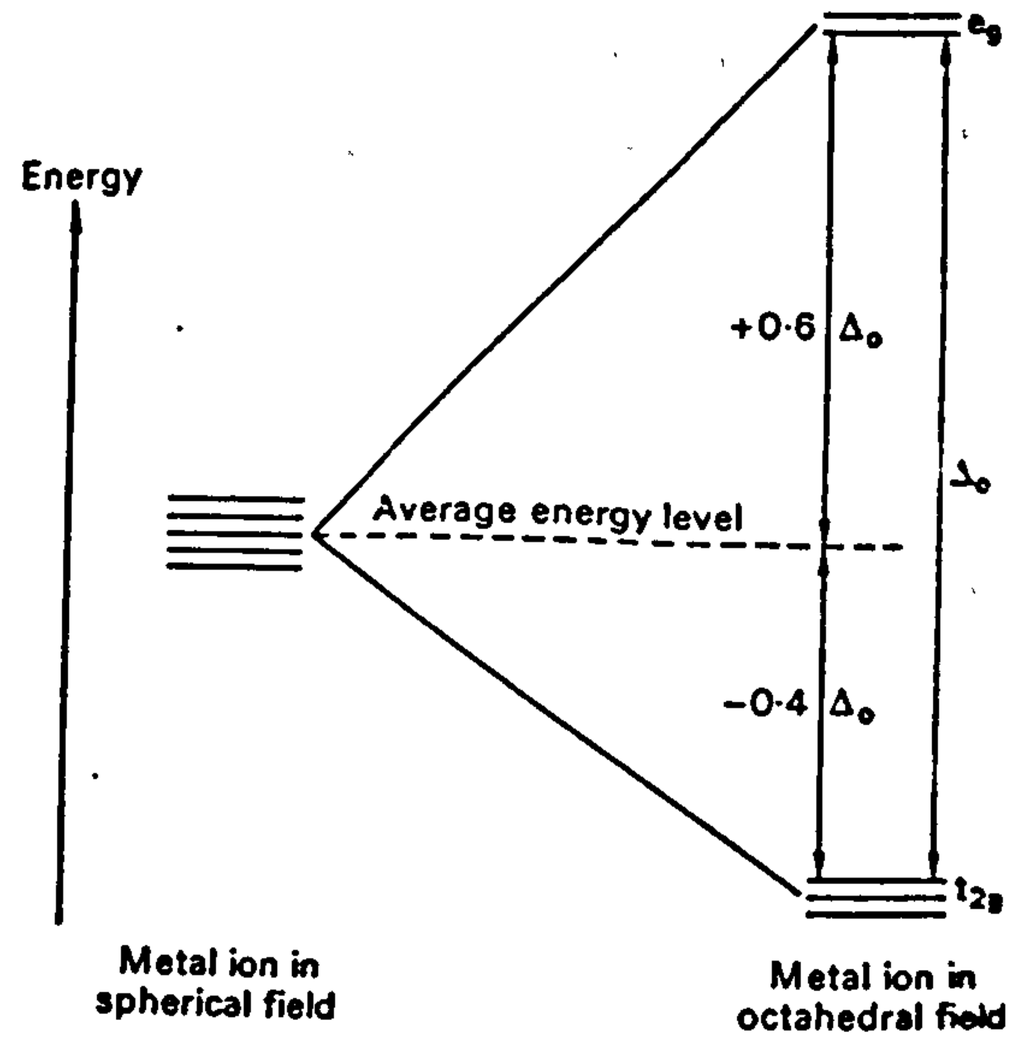

Figure 2.6: Energy Levels of d-orbitals in an Tetrahedral Field

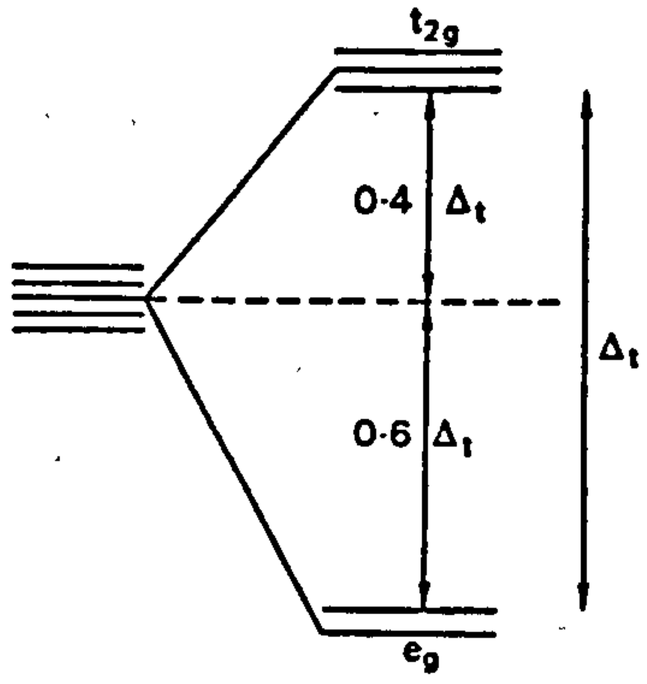

than those in the e orbitals.

2.2.3.2 Transition Metal Spectra[11,12]

The crystal field theory also allows the interpretation of the spectra of transition metal complexes. Such complexes are coloured if an internal energy change of energy ΔE, which is in the visible region, occurs when exposed to a quantum of visible light. The energy values ΔE correspond to the frequency range of visible light that result in electronic transitions.

For a high spin d^7 system, such as cobalt(II), the spectroscopic ground term is ^4F. The ground term describes the lowest energy electronic arrangement of the atom, it is the action of the crystal field on the ground term of the isolated transition metal ion (free ion) which is responsible for the observed spectrum. In the ground term the number 4 is the "spin multiplicity" 2S+1 where S is equal to ½ × number of unpaired spin electrons. The letter term comes from a value of L which is derived from the vectoral sum of the angular momentum associated with the orbital quantum number, l. The value of L is derived in the same manner that the orbital symbols arise from the value of the orbital quantum number. Therefore, S, P, D, F etc, correspond to L= 0, 1, 2, 3 etc.

The crystal field raises the degeneracy of both the atomic orbitals and the orbitals of the ground term and produces a number of component terms. The resulting Tanabe-Sugano diagram is shown in figure 2.7[13].

The P term is the excited state of the ground term, F. The component terms are denoted as follows:

A orbitally non-degenerate

E doubly degenerate

T triply degenerate

The octahedral crystal field environment of the d^7 ion gives rise to a splitting of the spectroscopic ground term (figure 2.8a). This splitting results in 3 spin allowed bands which appear in the spectrum (see figure 2.9).

ν_1 $^4T_{2g}(F)$----$^4T_{1g}(F)$

ν_2 $^4A_{2g}(F)$----$^4T_{1g}(F)$

ν_3 $^4T_{1g}(P)$----$^4T_{1g}(F)$

The ν_1 transition appears as a band in the near infrared; and another band appears in the visible often with a shoulder on the low energy side. This weak shoulder is attributed to the usually very weak ν_2 transition, formally 2 electron, from $t^5_{2g}e^2_g$ to $t^3_{2g}e^4_g$. The ν_3 transition appears as a broad band in the visible region at *ca* 500nm.

In tetrahedral d^7 complexes, the splitting of the free ion, ground F term in the crystal field is shown in figure 2.8b.

ν_1 $^4T_2(F)$----$^4A_2(F)$

ν_2 $^4T_1(F)$----$^4A_2(F)$

ν_3 $^4T_1(P)$----$^4A_2(F)$

Figure 2.7: Tanabe-Sugano Diagram for Co(II) a d^7 ion

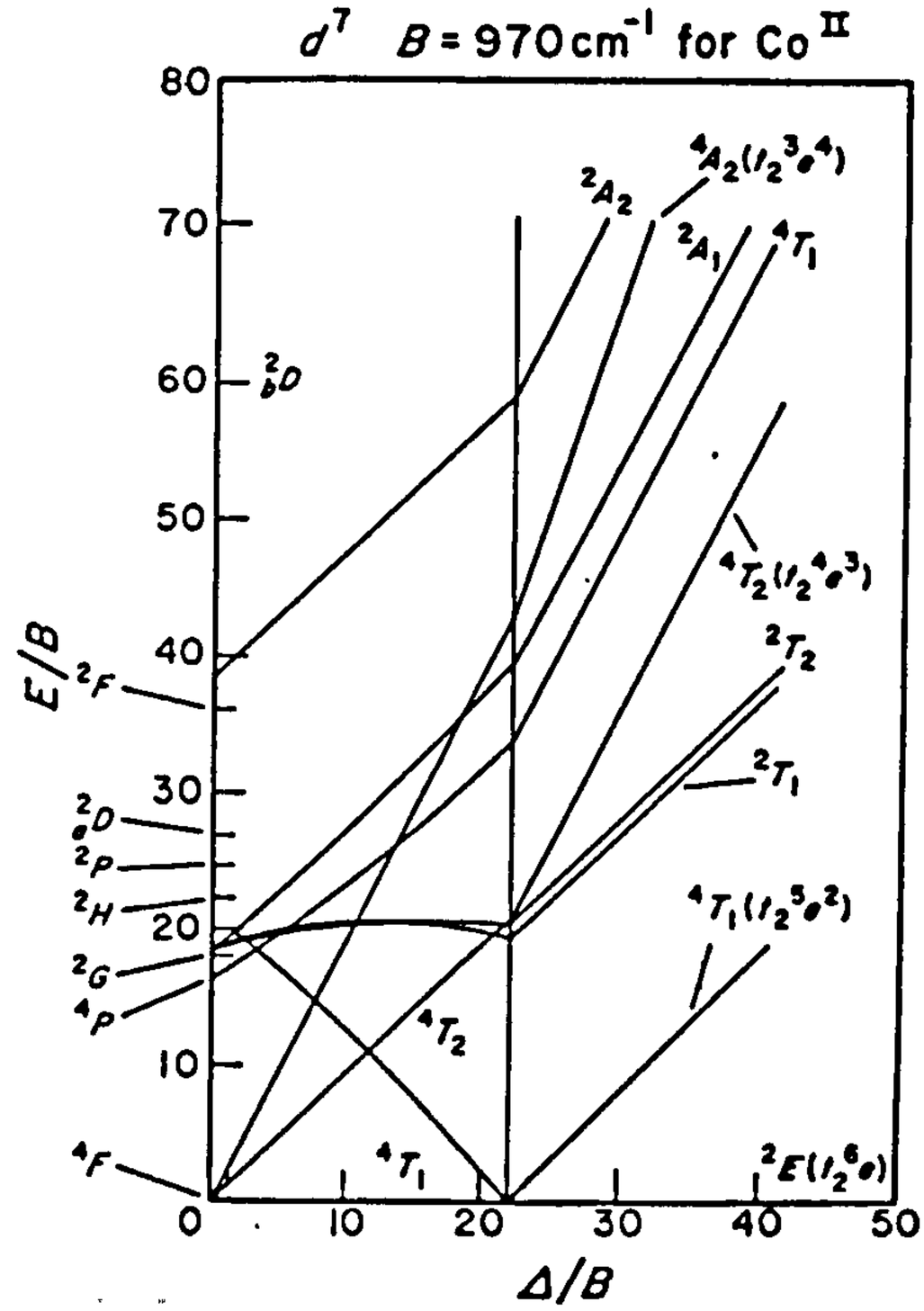

Figure 2.8: Splitting of the Spectroscopic Ground Term, F in (a) octahedral crystal field; (b) tetrahedral crystal field

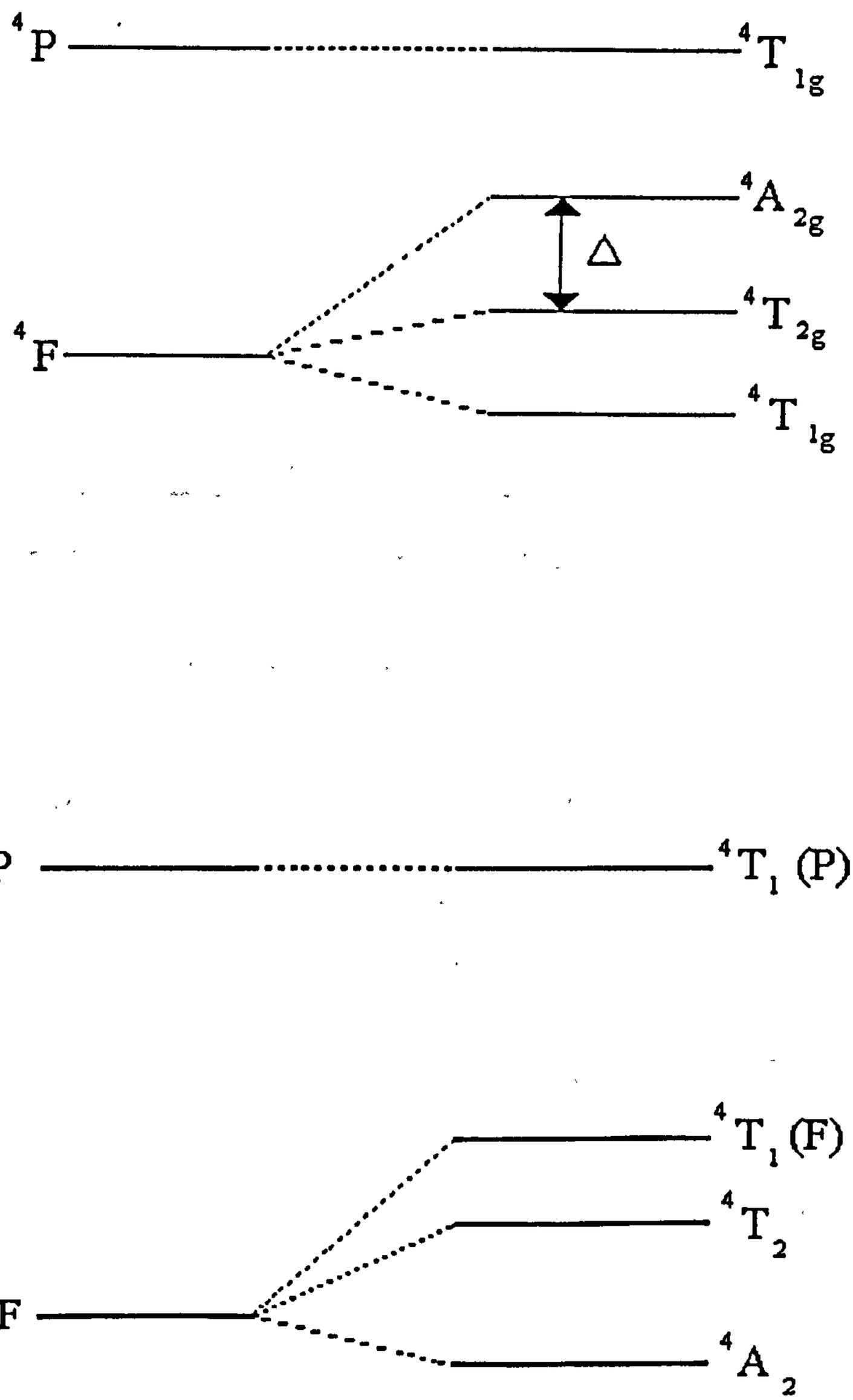

Figure 2.9: The Absorption Spectra of Octahedral $CoCl_2$ at Room Temperature (---) and -253°C (—)

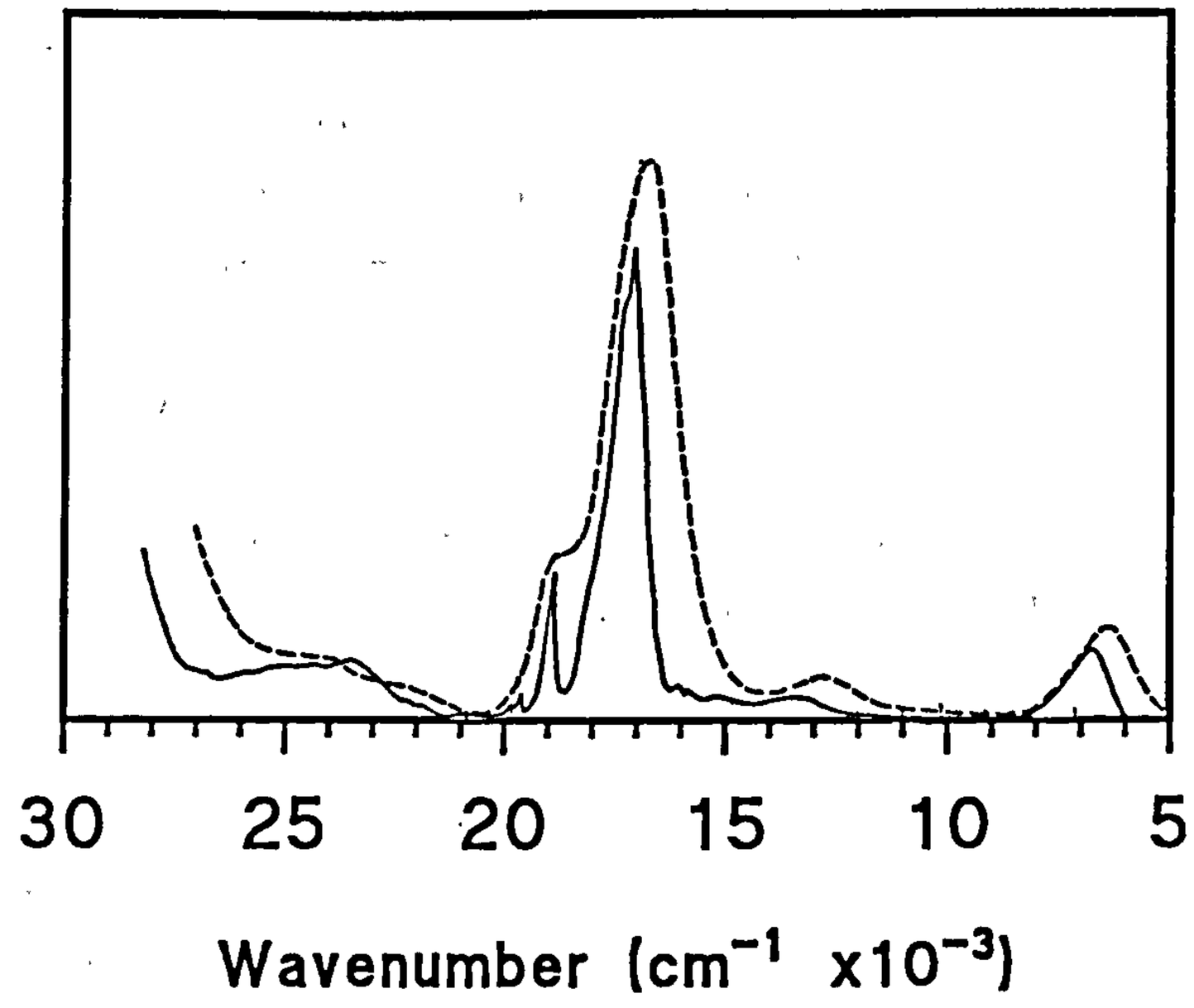

Figure 2.10: The Visible Spectra of (a) $[Co(H_2O)_6]^{2+}$; (b) $[CoCl_4]^{2-}$

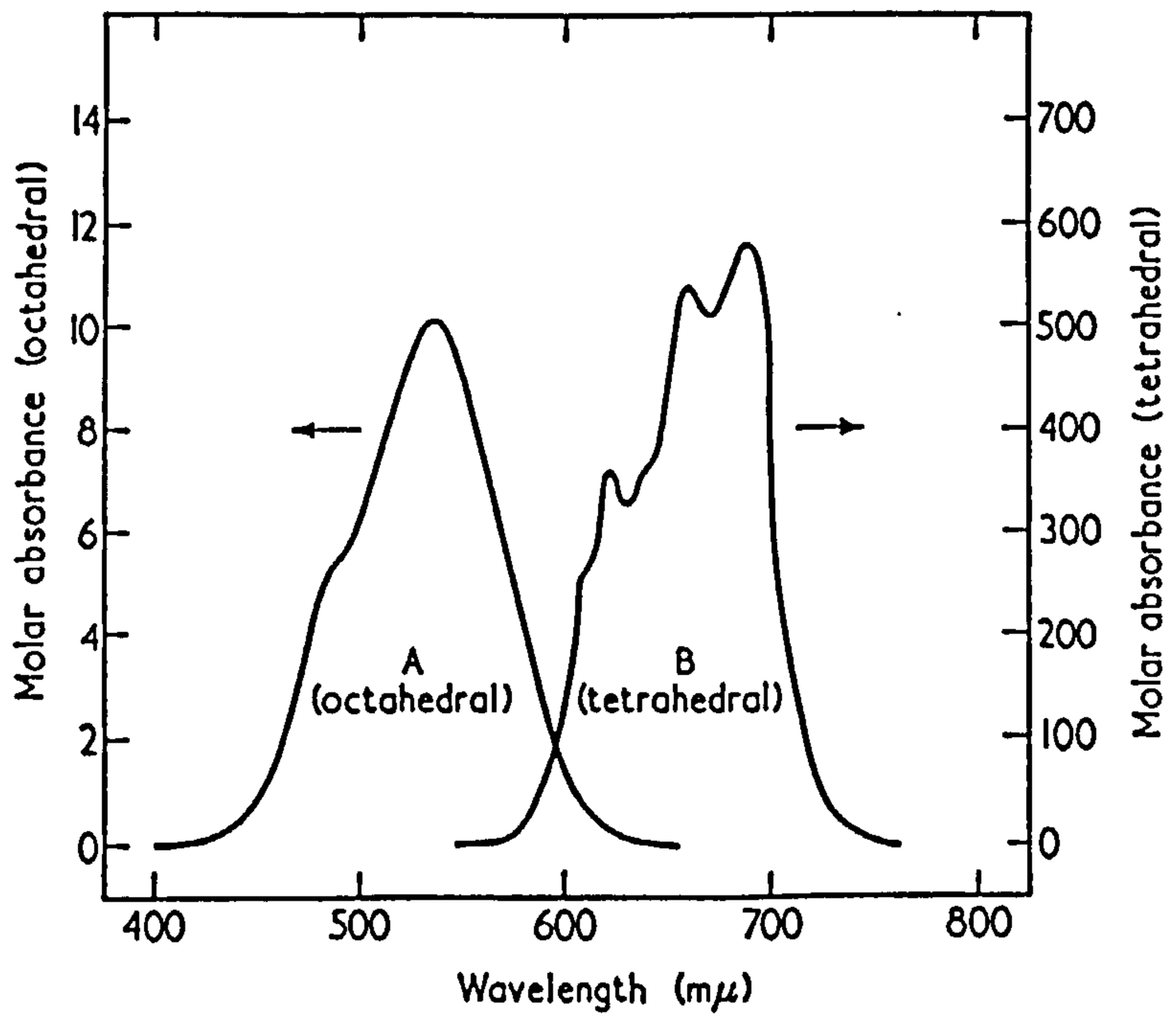

Again the ν_1 band lies in the near infrared between 3300 and 2000nm.
In the case of cobalt(II) complexes containing simple ligands, tetrahedral cobalt has a structured peak in the visible region. The fine structure arises because a number of transitions to doublet excited states occur in the same region and acquire some intensity by means of spin-orbit coupling. The blue colour which frequently arises for tetrahedral cobalt is due to the ν_3 transition which usually occurs between 666 and 500nm (see figure 2.10). The frequently observed pink colour of octahedral cobalt can be attributed to the weak ν_2 transition.

2.2.4 Instrumentation[1]

Because of the similarity in the optical elements, the NIR region is traditionally accessed on the same instrument as the UV-Vis region. In this case, a Perkin-Elmer Lambda 9 UV-Vis-NIR spectrophotometer has been used. This is a double beam, double monochromator grating instrument with two radiation sources and two detector systems.
The UV region uses a deuterium lamp as the source, whereas the visible/NIR source is a halogen lamp. Similarly, the UV/Vis region uses a photomultiplier detector while a PbS detector is used in the NIR range.
The instrument allows either transmittance or reflectance spectra to be recorded over a range of wavelengths from 185 to 3200nm. In the reflection mode, a 60mm integrating sphere attachment replaces the usual detector, see figure 2.11. This comprises of a sphere internally coated with $BaSO_4$ containing a side-on photomultiplier and a PbS cell.

Figure 2.11: Integrating Sphere Attachment

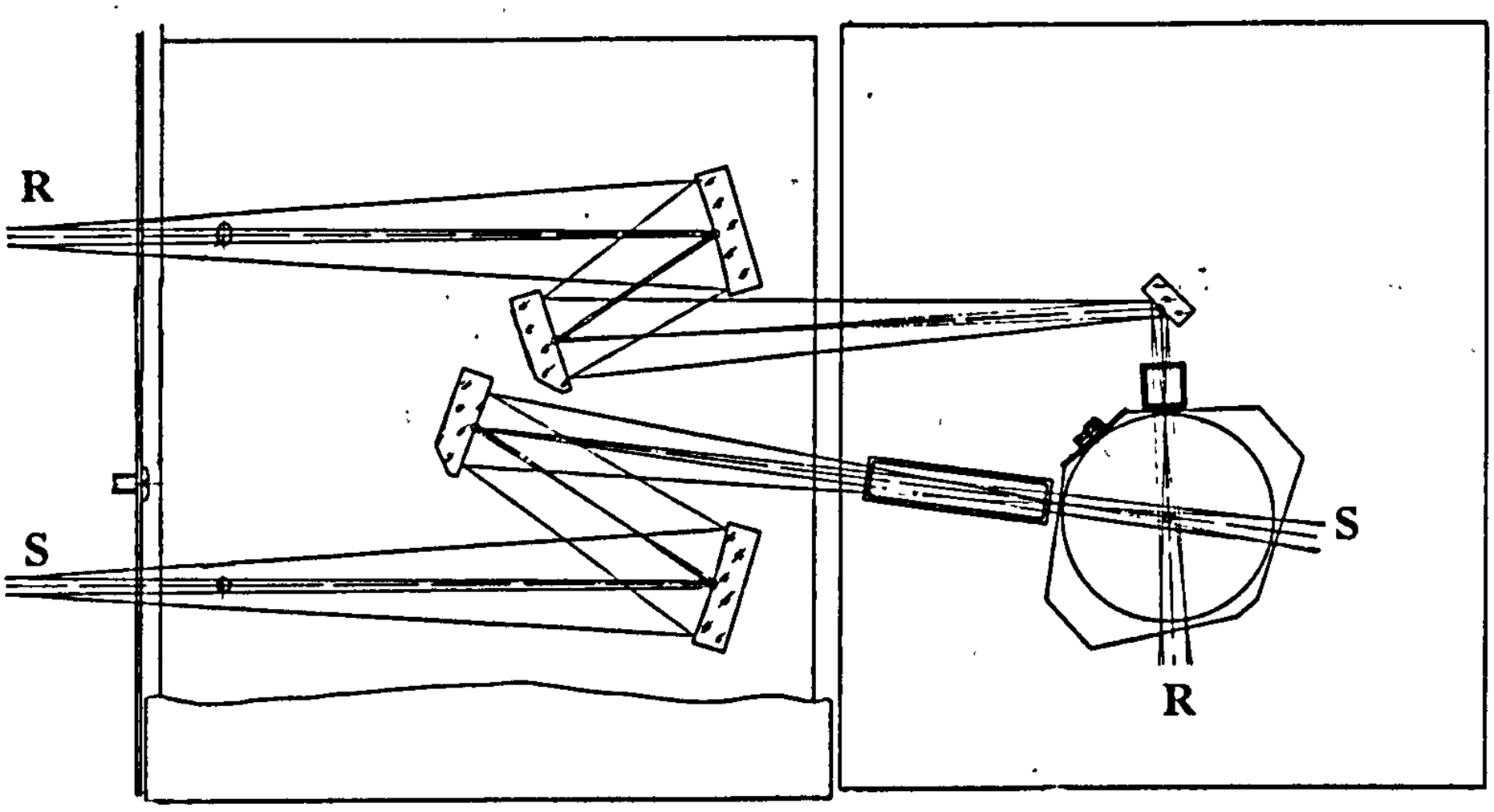

R=reference; S=sample

2.2.5 Experimental

2.2.5.1 Near Infrared Region

Samples were pressed into 20mm self-supporting discs and then dehydrated *in vacuo* on an outgassing rig equipped with both rotary and diffusion pumps. Reflectance spectra were recorded over the 900-2500nm region, using an integrating sphere on a Perkin-Elmer Lambda 9 UV-VIS-NIR spectrophotometer controlled by Perkin-Elmer Computerised Spectroscopy Software (PECSS) at a scan speed of 240nm per minute.

2.2.5.2 Ultraviolet/Visible Region

Reflectance visible spectroscopy (350 to 800nm) of the ground samples in the form of self-supporting discs were obtained using the blank gel as the reference. Spectra were obtained for dehydrated samples immediately on removal from the oven.

2.3 Nuclear Magnetic Resonance (NMR) Spectroscopy

Multinuclear nuclear magnetic resonance spectroscopy has been used in the identification of compounds and to monitor the reactions occurring in the sol-gel process.

2.3.1 Theory[1,5,14-17]

All nuclei rotate about an axis and therefore exhibit a nuclear spin. The maximum spin component for a particular nucleus is its spin quantum number I; and it is found that a nucleus will then have $(2I+1)$ discrete states. The component of angular momentum for these states in any chosen direction, **I**, is given by:

$$\mathbf{I} = \sqrt{I(I+1)}\left(\frac{h}{2\pi}\right)$$

where

h=Planck's constant

which is often simplified to:

$$\mathbf{I} = I\frac{h}{2\pi}$$

Such a charged particle spinning about an axis constitutes a circular current which in turn produces a magnetic dipole. The resulting magnetic dipole μ is oriented along the axis of spin and has a value that is characteristic for each type of nucleus. The size of the dipole for a point charge can be shown to be:

$$\mu = \frac{q}{2m}\mathbf{I} = q\frac{\sqrt{I(I+1)}}{2m}\frac{h}{2\pi} = \frac{qh}{4\pi m}\sqrt{I(I+1)} \qquad \mathbf{2.8}$$

where q and m are the charge and mass of the particle. In reality electrons and nuclei are not point charges, and equation 2.8 is modified by the inclusion of a numerical factor G:

$$\mu = \frac{Gqh}{4\pi m}\sqrt{I(I+1)} \qquad [JT^{-1}]$$

Nuclear dipoles are expressed in terms of a nuclear magneton β_N, which is defined in terms of the mass and charge of the proton:

$$\beta_N = \frac{eh}{4m_p\pi} = 5{\cdot}050 \text{ x } 10^{-27} \text{ JT}^{-1}$$

where m_p is the protonic mass.

Therefore, a nucleus of mass M and charge pe (where p is the number of protons) is described by equation 2.9:

$$\mu = \frac{Gpe}{2M}\sqrt{I(I+1)}\frac{h}{2\pi} = \frac{Gm_pp}{M}\beta_N\sqrt{I(I+1)} \qquad \mathbf{2.9}$$

$$\mu = g\beta_N\sqrt{I(I+1)} \qquad \mathbf{2.10}$$

in which the factor

$$g = \frac{Gm_pp}{M}$$

is characteristic of each nucleus.

2.3.1.1 Energy Levels in a Magnetic Field

When a particle possessing a magnetic moment is brought into an external magnetic field it orientates so that the magnetic moment and spin axis take up one of certain fixed directions with respect to the field. The potential energy of the particle depends upon the orientation of the dipole with respect to the field. The energy (or alignment) of the nucleus is limited to (2I+1) discrete values. The potential energy of a magnet in a field is given by the relationship.

$$E = m\mu_z B_z$$

and

$$\mu_z = g\beta_N I_z$$

where μ_z is the component of the magnetic moment in the direction of an external field of strength B_z.

The number of possible energy levels is limited by the quantum character of the nucleus, see figure 2.12.

Figure 2.12: Magnetic Moment and Energy Levels for a Proton with Spin Quantum Number, I=½

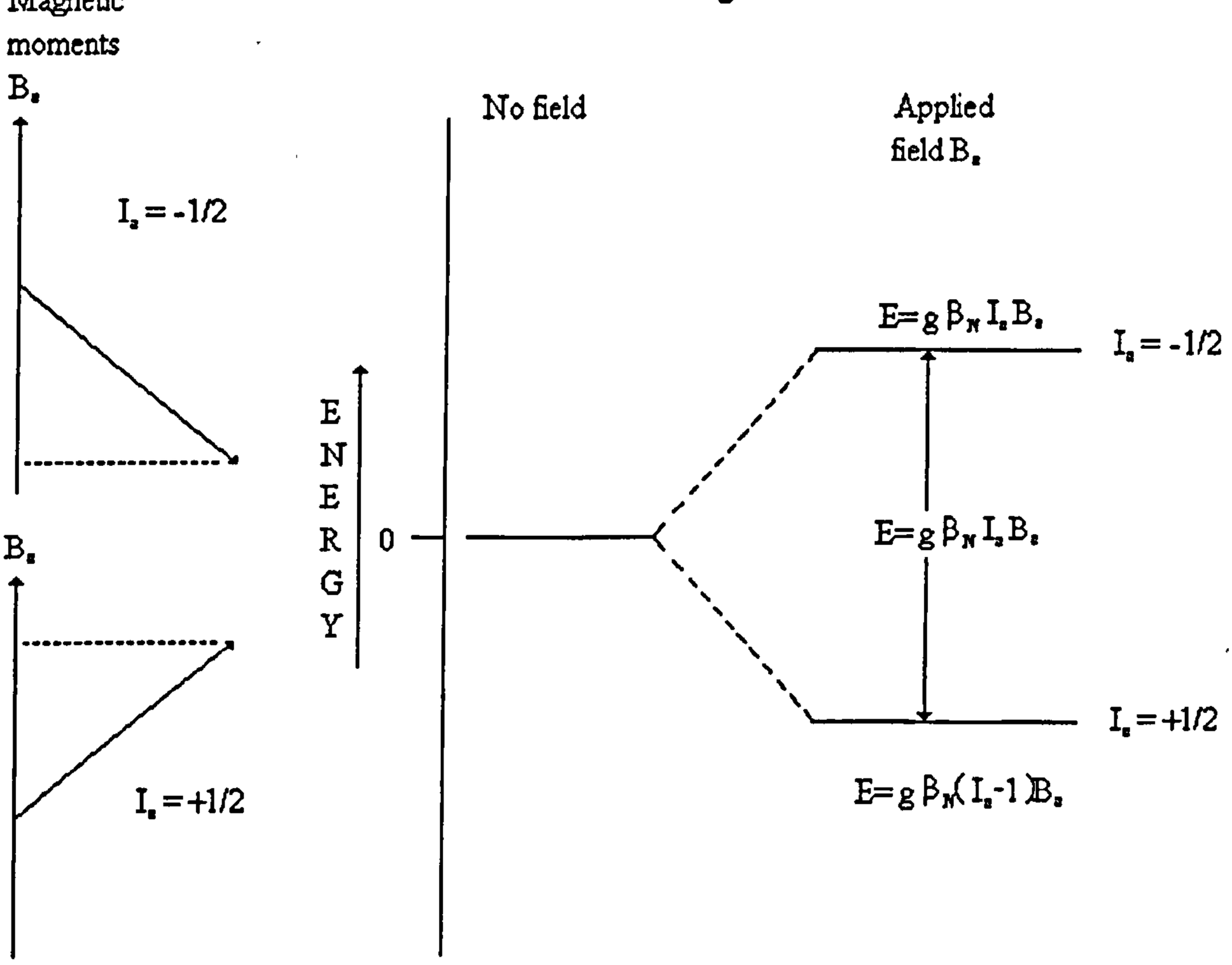

In the particular case of ^{29}Si the g value is negative (-1·11), as a result μ_z has a sign opposite from I_z and the order of labelling of the energy levels in figure 2.12 is reversed.

In general, the energy difference between two levels is given by

$$\Delta E = \mu_z B_z = g\beta_N B_z$$

2.3.1.2 Distribution of Particles Between Magnetic Quantum States

In the absence of a magnetic field, the energies of the magnetic quantum states are identical. Therefore, a large number of protons will contain an identical number of nuclei with m=+½ and m=-½. However, in a magnetic field, the nuclei tend to orient themselves so that the lower energy state (m=+½) predominates. Classical theory states that at a temperature T K the ratio of the population of such levels will be given by:

$$\frac{N_j}{N_o} = \exp\frac{-\Delta E}{kT}$$

where

ΔE=energy level separation

N_j = number of protons in the higher energy state

N_O = number of protons in the lower energy state

k = Boltzmann constant

This ratio is almost equal to unity and spins are almost equally distributed between the (2I+1) energy levels.

2.3.1.3 The Larmor Precession

This considers the nature of the interaction between radiation and the particle spins which can give rise to transitions between these levels.

The dipole moment of a spinning nucleus is given by equation 2.10, and the vector represented by μ can only be oriented so its components are integral or half-integral. If I is integral or half-integral in a reference, the vector arrow can never be exactly in the field direction. This is illustrated in figure 2.13 for a particle with spin ½. For such a particle:

$$\mu = g\beta_N \sqrt{3/4}$$

and

$$\mu_z = \pm 1/2\, g\beta_N$$

Hence, whichever energy state a spinning nucleus or electron is in, it will always lie more or less across the field and will therefore be under the influence of a couple tending to turn it into the field direction. The axis of the rotating particle precesses, or moves in a circular path around the magnetic field. This is the Larmor precession which is similar to a gyroscope and is illustrated in figure 2.13.

The precessional or Larmor frequency, ω, is given by:

$$\omega = \frac{\mu B_z}{2\pi \mathbf{I}}$$

where **I**=component of angular momentum.

Therefore:

$$\omega = \frac{g\beta_N \sqrt{I(I+1)}}{\sqrt{I(I+1)}\frac{h}{2\pi}}\frac{B_z}{2\pi} = \frac{g\beta_N B_z}{h} \qquad \text{[Hz]}$$

which is the same as the frequency separation between energy levels.

Therefore, this is a mechanism by which particle spins can interact with a beam of electromagnetic radiation. If the beam has the same frequency as that of the precessing particle, it can interact with the particle and energy can be exchanged; but if any other frequency, there will be no interaction. For the nucleus this is known as *nuclear magnetic resonance (NMR)*.

Figure 2.13: Precession of a Rotating Particle in a Magnetic Field

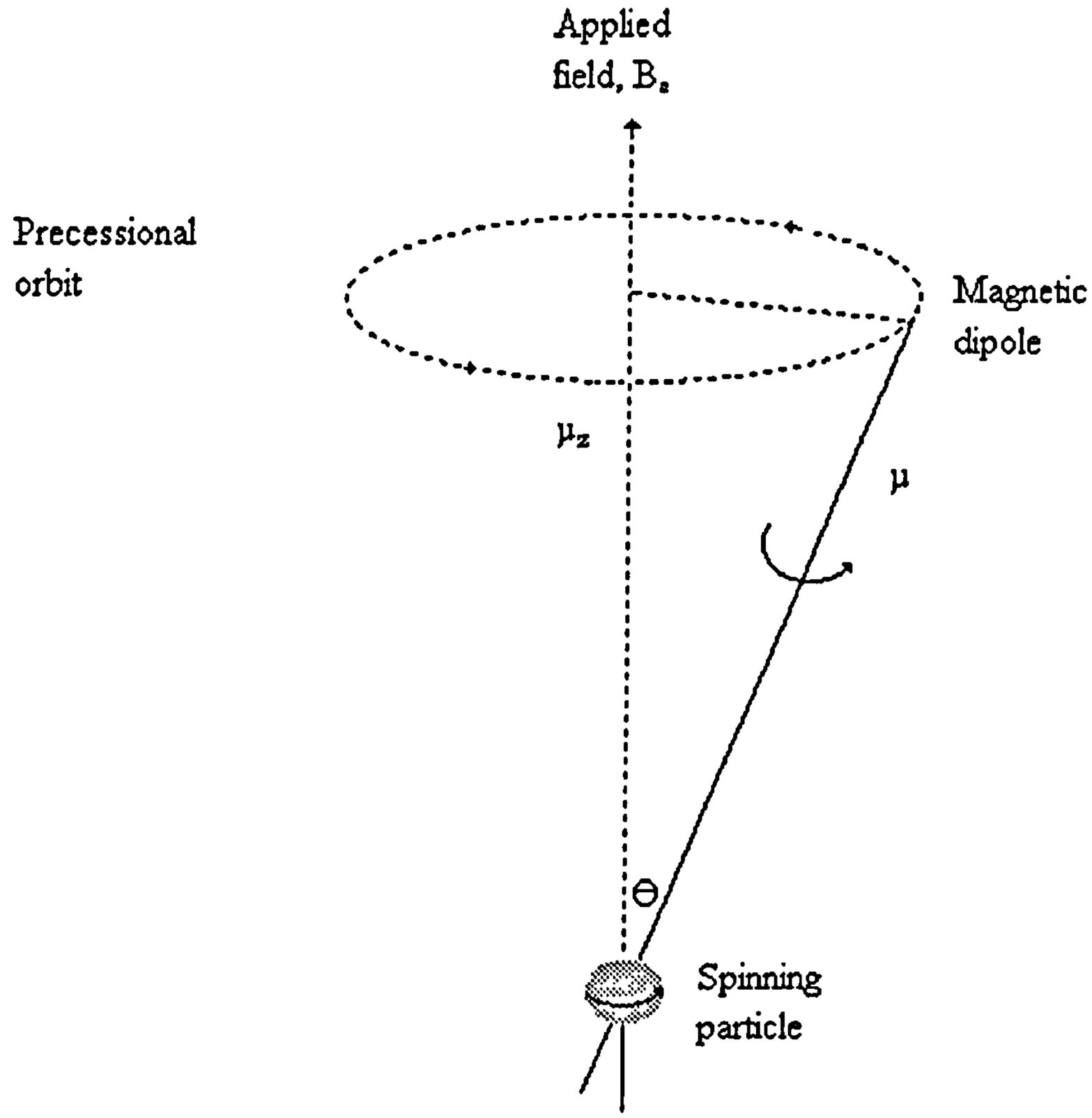

There is a choice of two experimental arrangements:

(i) application of a fixed magnetic field to a set of identical nuclei so that their Larmor frequencies are identical. If the frequency of the radiation beam is then swept over a

range of frequencies including the Larmor frequency, resonance absorption will occur at precisely that frequency.

(ii) similarly if the nuclei are bathed in radiation at a fixed frequency and the applied field swept over a range until absorption occurs.

If the character of NMR spectra was determined solely by nuclear properties, only single absorption lines would be observed for each isotope. However, the frequency of radiation that is absorbed by a given nucleus is weakly influenced by the chemical environment in which it exists. There are two such effects: chemical shift and spin-spin coupling.

In the case of chemical shift, differences occur in the absorption frequency of the proton depending on the group to which the hydrogen atom is bonded. Spin-spin coupling occurs because the effective field around one nucleus is further enhanced or reduced by local fields generated by the hydrogen nuclei bonded to an adjacent atom. The multiplicity is equal to:

$Multiplicity = n+1$

where:

n= number of adjacent protons.

2.3.2 Instrumentation: Fourier Transform Nuclear Magnetic Resonance Spectrometer

In pulsed NMR, the sample is periodically irradiated with brief, highly intense pulses of radio-frequency radiation, following which the free induction decay signal (FID), a characteristic radio-frequency emission signal stimulated by the irradiation is recorded as a function of time.

The NMR experiments were performed on a Jeol FX200 FT NMR spectrometer capable of multinuclear analysis.

2.3.3 Experimental

2.3.3.1 ^{1}H NMR of the Hydrolysis Reaction

The reaction mixture was made up comprising of bis(acetylacetonato) titanium diisopropoxide and tetraethyl orthosilicate (TEOS) in the required ratio, the alcohol normally used in the reaction was replaced with t-butanol and the acid was replaced with a mixture of deuterium chloride and deuterium oxide.

The probe was cooled to -30°C with liquid nitrogen, and all spectra acquired at this temperature in d_6-acetone, at 199·5MHz under the following conditions:

pulse width= 10μs

pulse delay= 1s

scans=32

frequency range= 0-9ppm.

The reaction was monitored over a period of 1 hour and the relative amounts of TEOS monitored by comparison of the integrals of the methylene peaks in the TEOS before hydrolysis and at the reaction time.

2.3.3.2 General ^{1}H NMR Spectra

For chemical identification the probe was maintained at 30°C and spectra acquired as a 5%v/v solution of sample in deuterated chloroform ($CDCl_3$), at 199·5MHz under the following conditions:

pulse width= 10μs

pulse delay= 1s

scans=32

frequency range= 0-9ppm.

2.3.3.3 ^{13}C NMR Spectra

Both coupled and decoupled spectra were obtained for 20%v/v solutions of Si/Ti double alkoxide in $CDCl_3$ at 50°C and 50·1MHz. The conditions applied were as follows:

pulse width= 10μs

pulse delay= 3s

scans=8000

frequency range= 0-230ppm.

2.3.3.4 ^{29}Si NMR Spectra

Spectra were obtained for 20%v/v solutions of Si/Ti double alkoxide and chromium acetylacetonate in d_6-acetone at 27°C and 39·6MHz. Chromium acetylacetonate was added to aid the relaxation of the molecule after irradiation and thus cut down acquisition times. The following conditions were used:

pulse width= 20μs

pulse delay= 3s

scans=512

frequency range= 0 to -150ppm.

2.4 X-Ray Diffraction (XRD)

2.4.1 Theory[6]

When x-rays are scattered by the ordered environment in a crystal, interference (both constructive and destructive) takes place among the scattered rays because the distances between the scattering centres are of the same order of magnitude as the wavelength of the radiation. Diffraction is the result.

When a X-ray beam strikes a crystal surface at some angle, a portion of the beam penetrates to the second layer of atoms where again a fraction is scattered, and the remainder passes on to the third layer etc. (figure 2.14)

The requirements for X-ray diffraction are:

(1) the spacing between layers of atoms must be roughly the same as the wavelength of the radiation.

(2) the scattering centres must be spatially distributed in a highly regular way.

Bragg treated the diffraction of X-rays by crystals, as in figure 2.14. Here, a narrow beam strikes the crystal surface at an angle; scattering occurs as a result of interaction of the radiation with atoms located at O,P and R.

Figure 2.14: Diffraction of X-rays by a Crystal

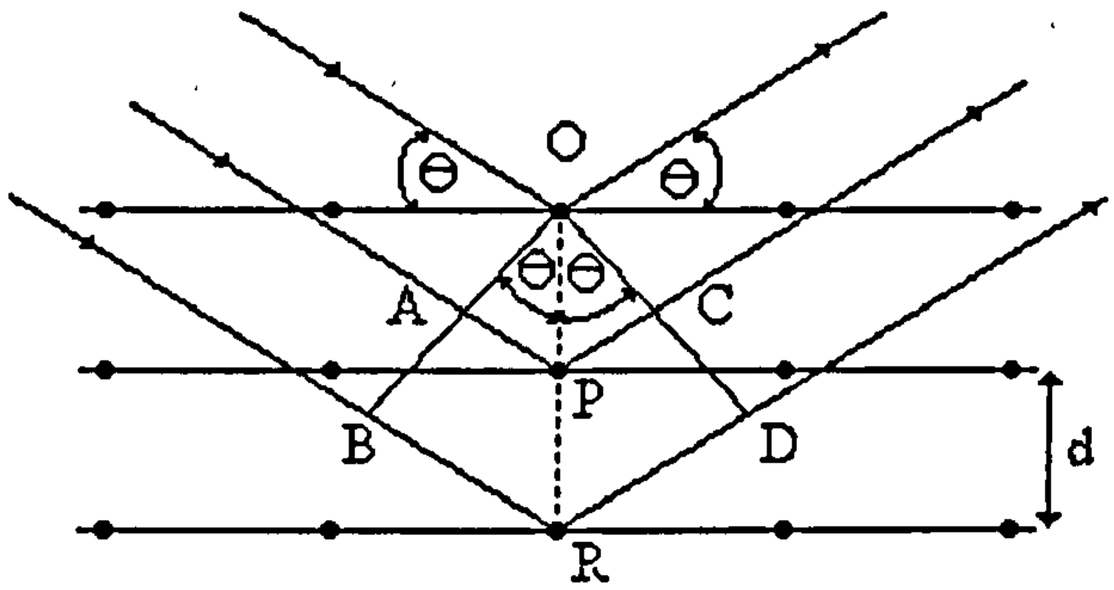

If the distance:

$$AP + PC = n\lambda$$

when:

n=integer

then the scattered radiation will be in phase at OCD, and the crystal will appear to reflect the X-radiation. But it is readily seen that:

$$AP = PC = d \sin\theta$$

where d is the interplanar distance of the crystal. Therefore, the conditions for constructive interference of the beam at an angle θ are:

$$n\lambda = 2d \sin\theta \qquad \textbf{2.11}$$

From the Bragg equation (2.11), it is obvious that X-rays appear to be reflected from the crystal only if the angle of incidence satisfies the condition that

$$\sin\theta = \frac{n\lambda}{2d}$$

At any other angle destructive interference occurs.

2.4.1.1 Crystal Size

The *Scherrer equation* (2.12) has been used to calculate the average particle size of the crystals from the peak width at half height.

$$\beta = \frac{k\lambda}{\bar{d}\cos\theta} \qquad \textbf{2.12}$$

$\bar{d}$ =average particle size

β=peak width (radians)

λ=1·5418 Å

θ=diffracted angle

k=0.9

If the average crystal size is less than 2000Å then peak broadening can occur. The lower limit of detection occurs when the peaks become so broad that they disappear into the background radiation. For very small particle sizes it is best to use low angle peaks if possible because, for a given crystal thickness, the broadening increases with angle.

2.4.2 X-Ray Spectrometer

The powder X-ray diffraction method is useful in qualitative phase analysis because every crystalline material has its own characteristic powder pattern. The resulting powder patterns have two characteristic features:

the *d*-spacings of the lines

the intensities of the lines.

X-ray diffraction peaks from crystalline material are considered detectable if the reflections have an intensity three times the square root of the background intensity. X-ray diffraction was carried out on samples using a Philips PW1729 X-ray generator of monochromatic Cu K_α=1·5418Å radiation equipped with a PW1710 diffractometer control unit.

A X-ray monochromator consists of a pair of beam collimators, which produce a parallel beam of radiation, and a dispersing element (figure 2.15). The dispersing element is a single crystal mounted on a goniometer that enables variation and precise determination of the angle θ between the crystal face and the collimated incident beam.

Figure 2.15:X-ray Monochromator and Detector

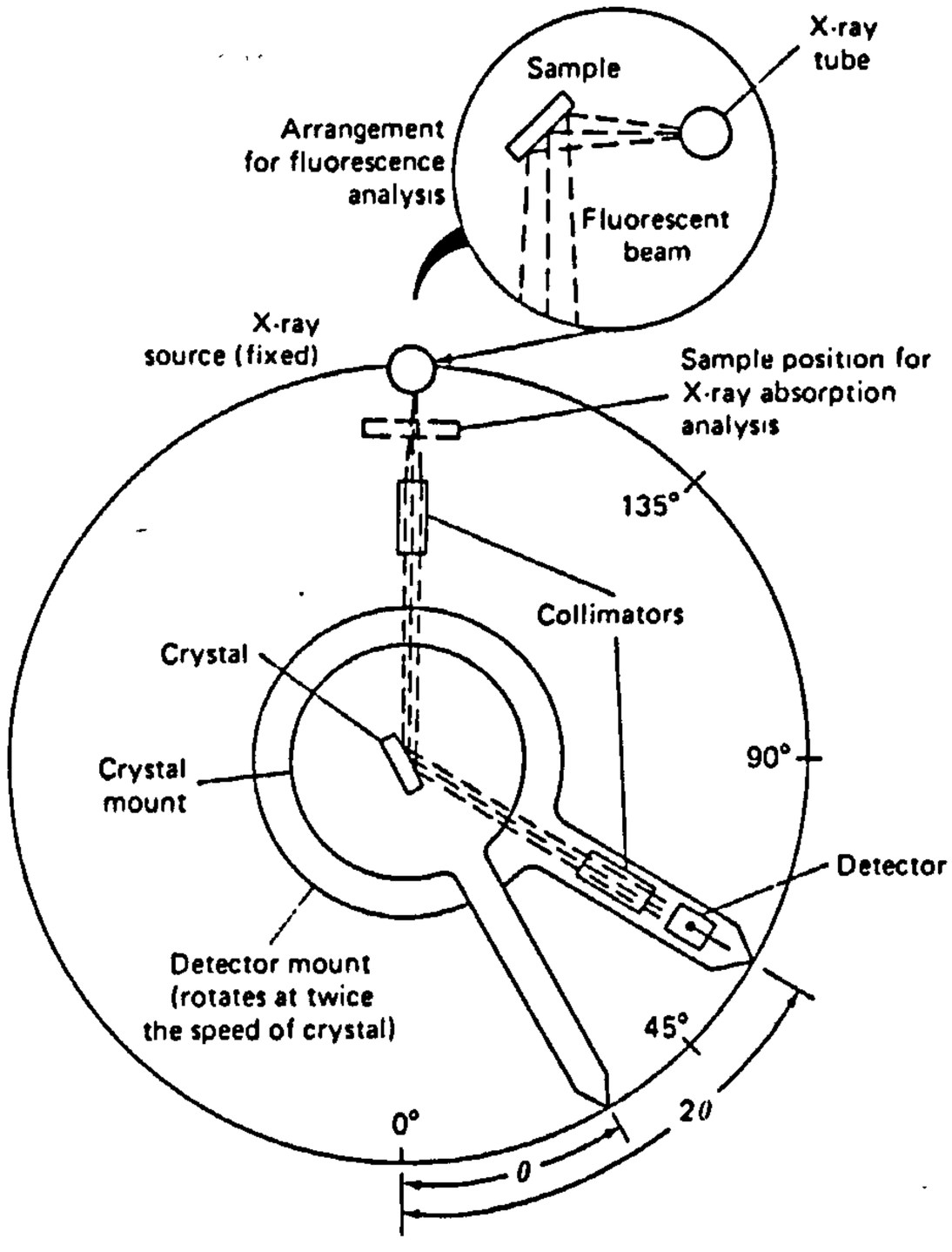

From the Bragg equation, it is obvious that only a few wavelengths are diffracted at any given angle. Therefore, a X-ray monochromator only diffracts a particular wavelength when the goniometer is set at the correct angle. To obtain a spectrum, the exit beam collimator and the detector must be mounted on a second table that rotates at twice the speed of the first. Therefore, as the crystal rotates through an angle θ , the detector simultaneously moves through an angle 2θ.

2.4.3 Experimental

The sample was ground and mounted on a glass sample holder using petroleum jelly. The sample was then scanned over the range 20-80° of 2θ at a speed of 0·02 $°2\theta s^{-1}$ and recorded at a chart speed of $2mms^{-1}$.

2.5 Gas Adsorption

Gas adsorption occurs whenever an adsorbable gas is brought into contact with the surface of a porous solid. Both the surface area and pore volume (porosity) of a solid play complementary roles in the adsorption phenomena. The amount of gas taken up by a solid is proportional to the mass *m* of sample, the temperature *T*, the pressure *p* of the vapour, and depends on the natures of both the solid and gas. At constant temperature, the *adsorption isotherm* is the relationship between the amount of gas adsorbed and the pressure of the gas. Most isotherms that arise from physisorption can be assigned to the five classes I to V of the Brunauer, Emmett and Teller (BET) classification. The most common of which are types I, II and IV isotherms which are found in microporous, nonporous or macroporous solids, respectively. Types III and V isotherms are characteristic of weak gas-solid interactions, the Type III isotherm being given by a nonporous or macroporous solid and the Type V isotherm by a mesoporous or microporous solid. For completeness, the stepped isotherm, Type VI, although rare is also included in the classification. These are shown in Figure 2.16[18].

Figure 2.16: Classification of Physisorption Isotherms[18]

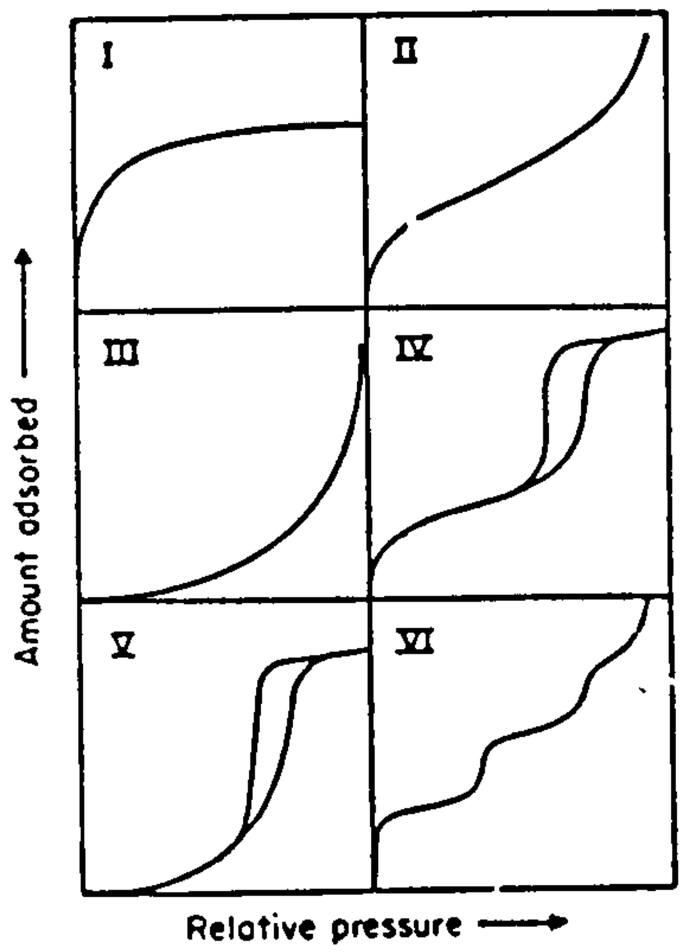

2.5.1 Theory

2.5.1.1 Surface Area Determination

The Brunauer-Emmett-Teller (BET) gas adsorption method[19] is the commonest standard procedure for the determination of the surface area of finely divided and porous materials. The BET equation is usually applied in the linear form

$$\frac{p}{n(p^\circ - p)} = \frac{1}{n_m C} + \frac{(C-1)p}{n_m C p^\circ} \qquad 2.13$$

where:

n = the amount of gas adsorbed at relative pressure p/p°

n_m = monolayer volume

C = constant.

However,

$$C = e^{(q_1 - q_L)/RT}$$

where

(q_1-q_L) =net heat of adsorption

q_L=molar heat of condensation

Therefore the BET equation requires a linear relationship between p/n(p°-p) and p/p°, this is the BET plot. The linear region is usually found between p/p° = 0·05 and 0·30, once this has been determined, the BET area can be calculated from the monolayer volume using the following equations.

$$A_s(BET) = n_m L a_m$$

and

$$a_s(BET) = \frac{A_s(BET)}{m}$$

where:

$A_s(BET)$ = total area

$a_s(BET)$ = specific area

L = Avogadro constant

a_m = molecular cross-sectional area [$a_m(N_2)$ = 16·2 Å^2 at 77K].

In the case of less porous or more coarsely crystalline solids of lower adsorptive capacity, none of the recognised nitrogen adsorption methods is sensitive enough. The usefulness of the BET method[19] and the Harkins and Jura "relative" method[20] have been limited by the need for a large correction for unadsorbed nitrogen gas up to fairly high relative pressures. This is due to the high saturation pressure of nitrogen, approximately one atmosphere at liquid nitrogen temperature.

However, by performing adsorptions at temperatures well below the boiling point of the vapour being adsorbed the saturation pressure becomes low. In the case of krypton vapour, the saturation pressure is about 2mmHg at liquid nitrogen temperatures, this is low enough to make krypton suitable for the accurate measurement of surface area. Beebe *et al*[21] successfully used krypton to measure the specific surface area of a number of samples from 0·02-120 m^2g^{-1} *via* the BET method.

2.5.1.2 Determination of the Properties of Porous Materials

The pore sizes within a solid are classified on the basis that each size range corresponds to characteristic adsorption effects which manifest in the isotherm. Pores have been classified, as in table 2.3 below, according to their average width[22].

Table 2.3

	Pore Width
Micropores	Less than 2 nm
Mesopores	Between 2 and 50 nm
Macropores	Greater than 50 nm

The porosity of a material is therefore an important factor in determining the nature of the isotherm. *Porosity* is defined as the ratio of the volume of accessible open pores to the total volume of the solid[23]. However, the total pore volume, V_p, is frequently calculated from the amount of vapour adsorbed in the region of the isotherm in which the relative pressure is close to unity (figure 2.17) by assuming that the pores are then filled with condensed adsorptives in the normal liquid state. In fact the value of pore volume is calculated from the amount of nitrogen adsorbed (STP) at $p/p^\circ \approx 0{\cdot}95$ using

$$V_p = 0{\cdot}00156\ V_{0{\cdot}95}$$

where 0·00156 is a conversion coefficient between nitrogen at STP and liquid nitrogen at 77K.

Figure 2.17: Typical Physisorption Isotherm[18]

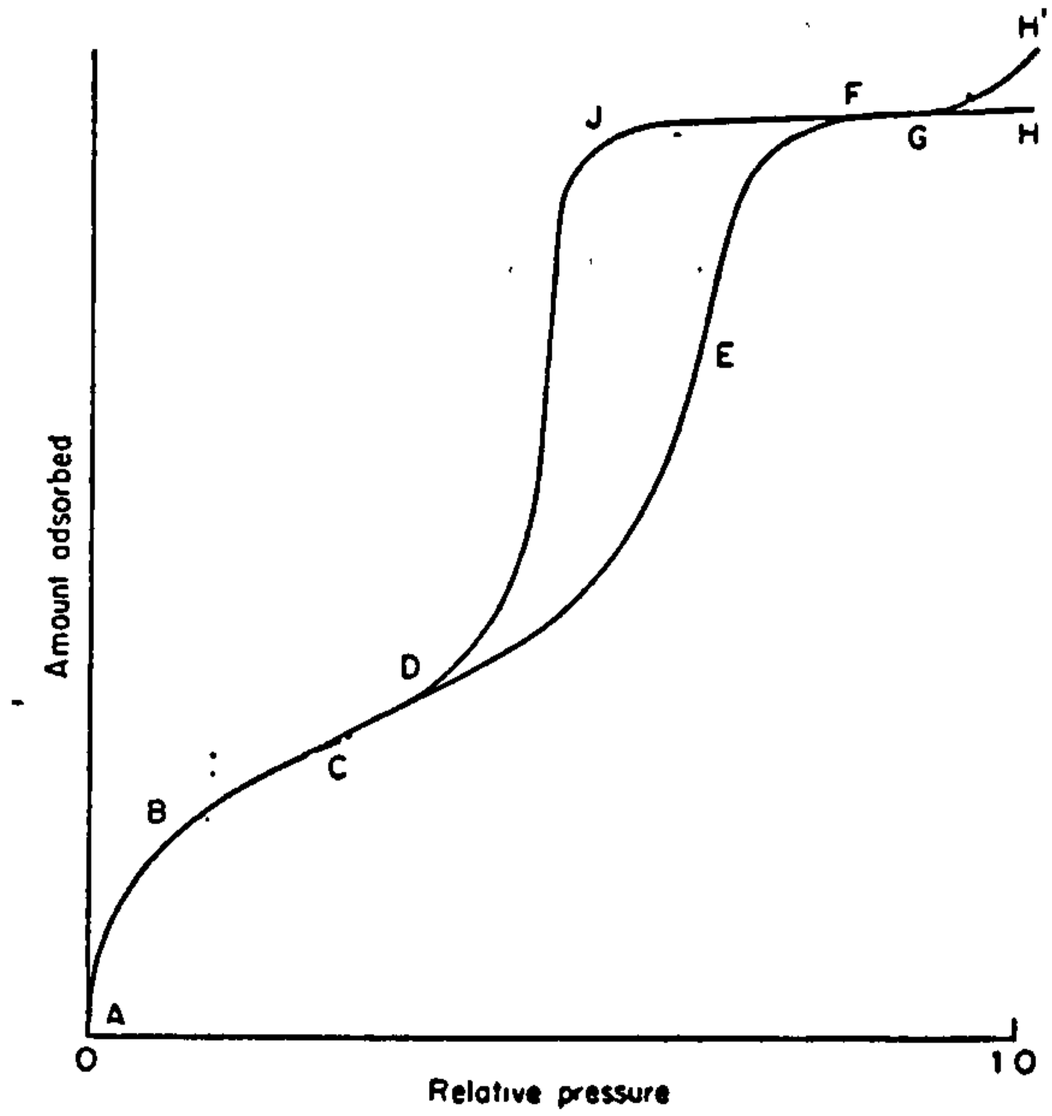

The mean pore size was calculated assuming that the sample under investigation contained cylindrical pores.

$$r_p = 2V_p A_s^{-1} \times 10^4$$

where

r_p= mean pore radius Å

V_p= pore volume cm^3

A_s= BET surface area m^2

Barrett, Joyner and Halenda[26] developed a method for estimating the volume and area of porous adsorbents. Originally developed to deal with relatively coarsely porous adsorbents exhibiting a wide range of pore sizes, the method has since been found to be applicable to porous solids of any nature.

By assuming that equilibrium between the gas and adsorbed phases during desorption is determined by two mechanisms:

1) physical adsorption on the pore walls (which would occur to the same extent whether the area involved was made up of walls of pores or a flat surface impenetrable to nitrogen)

2) capillary condensation in the intercapillary volume

it is possible to analyse the relationship between nitrogen desorption isotherms at liquid nitrogen temperatures and the distribution of pore volume and area with respect to pore

radius* . Results from the BJH method are typically plotted as dV/dlog(D) pore size distributions when:

$$dV/d\log(D) = \frac{\text{Incremental Pore Volume}}{\log\left(\frac{\text{diameter } a}{\text{diameter } b}\right)}$$

where a and b are average pore diameters and $a>b$.

Reasonable agreement with the BET area has been achieved from the distribution curves but since the BET area is calculated from the low pressure part of the isotherm and the BJH method primarily involves the high pressure portion there are some inevitable discrepancies.

The α_s-method of Sing, is a modification of the t-method which accounts for the process of micropore filling and under certain conditions enables an assessment of the micropore volume. In this modification t, the statistical multilayer thickness for the adsorption of nitrogen on a nonporous reference solid is replaced by α_s where:

$$\alpha_s = \frac{V}{V_{0.4}}$$

and $V_{0.4}$= amount adsorbed at $p/p^0 = 0{\cdot}4$.

Therefore the reduced standard isotherm on the nonporous reference solid is arrived at empirically and not *via* the monolayer volume.

Assigning α_s an arbitrary value *ie.* $\alpha_s = 1$, at $p/p^0 = 0{\cdot}4$ may be justified with nitrogen isotherms at 77K, since monolayer coverage and micropore filling occur at $p/p^0 < 0{\cdot}4$, whereas any hysteresis loop (associated with capillary condensation) is located at $p/p^0 > 0.4$. Greater precision is achieved by locating $\alpha_s = 1$ in the middle range of the isotherm as opposed to at $p/p^0 = 0{\cdot}1$ (especially if C is low)[24].

2.5.1.3 The Type IV Isotherm

The investigation of the pore structure of mesoporous solids is inextricably linked with the interpretation of the Type IV isotherm. Therefore the mesopore size range is generally accepted as the pore size range that results in a Type IV isotherm.

The most significant feature of any Type IV isotherm is its hysteresis loop; the exact shape of which varies from one adsorption system to another.

To facilitate interpretation of such isotherms, Zsigmondy proposed a model based on the Kelvin equation. This assumed that along the initial part of the isotherm (ABC in fig. 2.17), adsorption is restricted to a thin layer on the walls, until at D (the start of the hysteresis loop) capillary condensation in the finest pores begins. Progressively increasing the pressure

---

* All such calculations are based on a desorption model irrespective of whether adsorption or desorption data is under investigation.

results in the filling of wider and wider pores until at the saturation pressure the entire system is full of condensate.

In the reverse of this process, evaporation, problems arising from nucleation do not arise. This is because the liquid phase is already present and spontaneous evaporation will occur as soon as the pressure is low enough. Since evaporation and condensation are not always the exact reverse of each other hysteresis can result.

De Boer[24] proposed the original classification of five types of hysteresis loop (see fig. 2.18), although in practice classification assignment is never as clear cut.

Type A (H1): Both adsorption and desorption branches are steep at intermediate relative pressures.

Type B (H3): The adsorption branch is steep at saturation pressure, the desorption branch is steep at intermediate relative pressures.

Type C: The adsorption branch is steep at intermediate relative pressures, the desorption branch is sloping.

Type D: The adsorption branch is steep at saturation pressure, the desorption branch is sloping.

Type E (H2): The adsorption branch has a sloping character, the desorption branch is steep at intermediate relative pressures.

In practice, Types C and D hardly ever occur so are omitted in a revised classification.

Type A (H1) hysteresis loops can be given by a number of pore types (see figure 2.19) each of which has a different effect on the width of the loop itself.

(i) Narrow loop given by tubular capillaries either open at both ends or with slightly widened parts.

(ii) A very narrow loop is given by wide-necked ink-bottles and tubular capillaries either with rectangular cross-section or with one narrowed part.

(iii) Wide loops arise from ink-bottles with narrow and short necks and capillaries open at both ends with wide parts and narrow short necks.

Hysteresis loops of type B (H3) classification can be attributed to open slit-shaped capillaries with parallel walls and capillaries with very wide bodies and narrow short necks (figure 2.20).

Type E (H2) hysteresis loops are wider than types A (H1) and B (H3) and arise from the following pore shapes (see figure 2.21):

(i) tubular or ink-bottle capillaries with short necks and wide sloping bodies

(ii) tubular capillaries with wider parts of varying widths.

Figure 2.18: Classification of Hysteresis Loops[26]

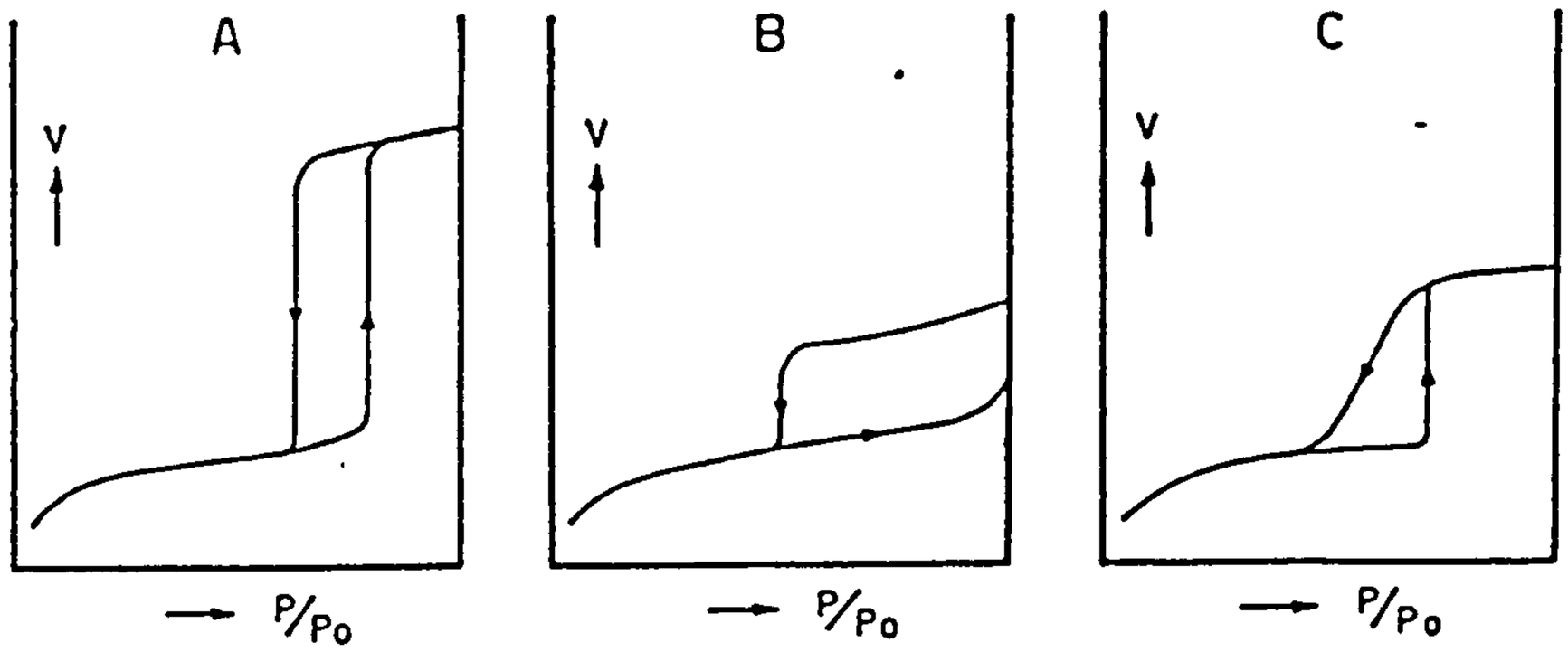

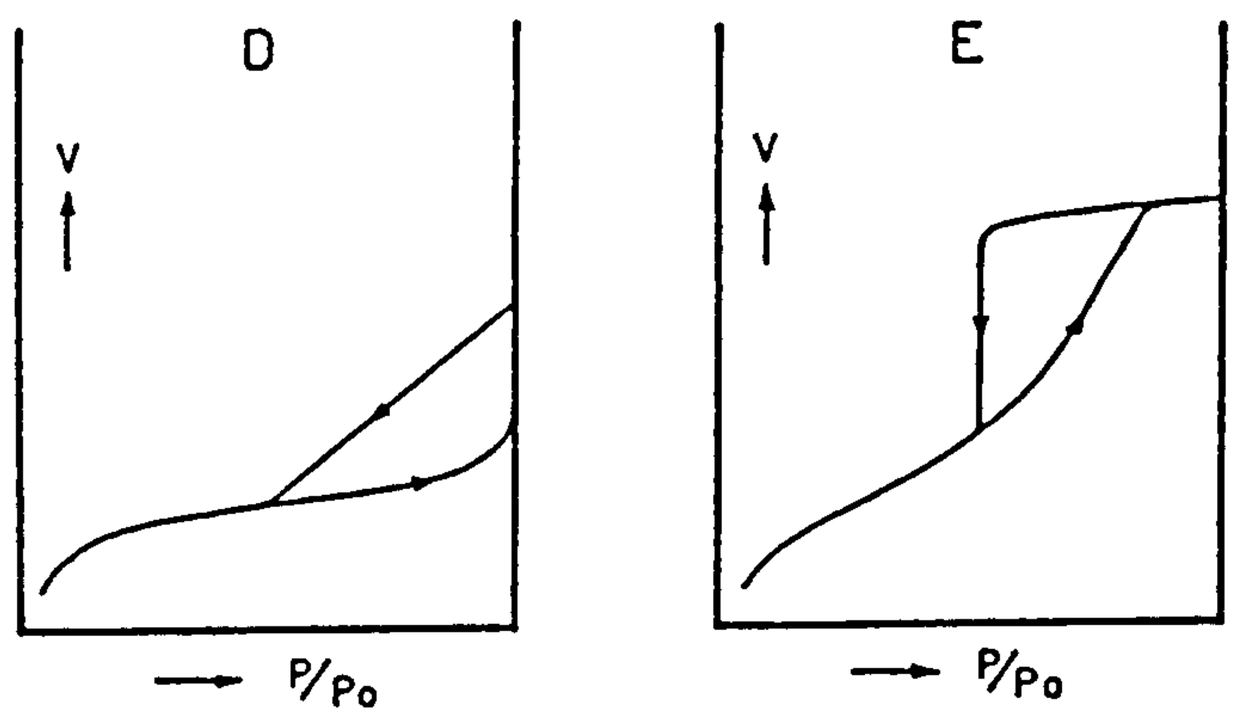

Old Classification	New Classification
Type A	H1
Type B	H3
Type E	H2

* Types C & D rarely occur so are omitted in the revised classification.

Figure 2.19: Pore Types that give rise to Hysteresis Loop type A(H1)[26]

(i) tubular capillaries

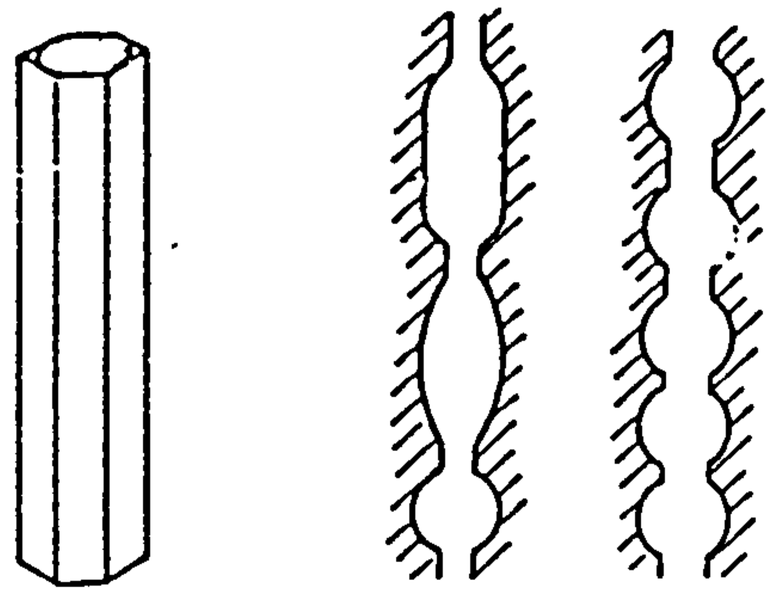

(ii) & (iii) wide-necked "ink" bottles and tubular capillaries with narrowed sections of rectangular cross-section area

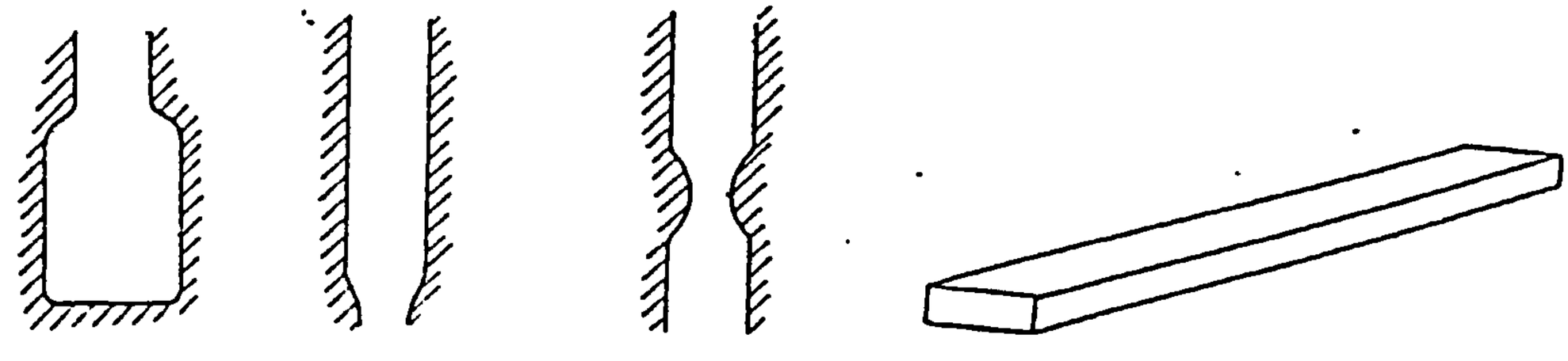

Figure 2.20: Pore Types that give rise to Hysteresis Loops of Type B (H3)[26]

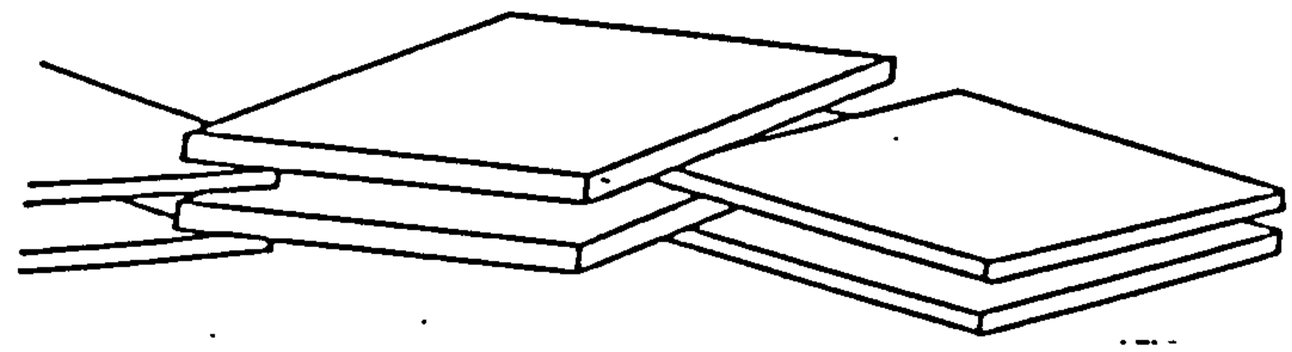

Figure 2.21: Pore Types that give rise to Hysteresis Loops of Type E (H2)[26]

(i)

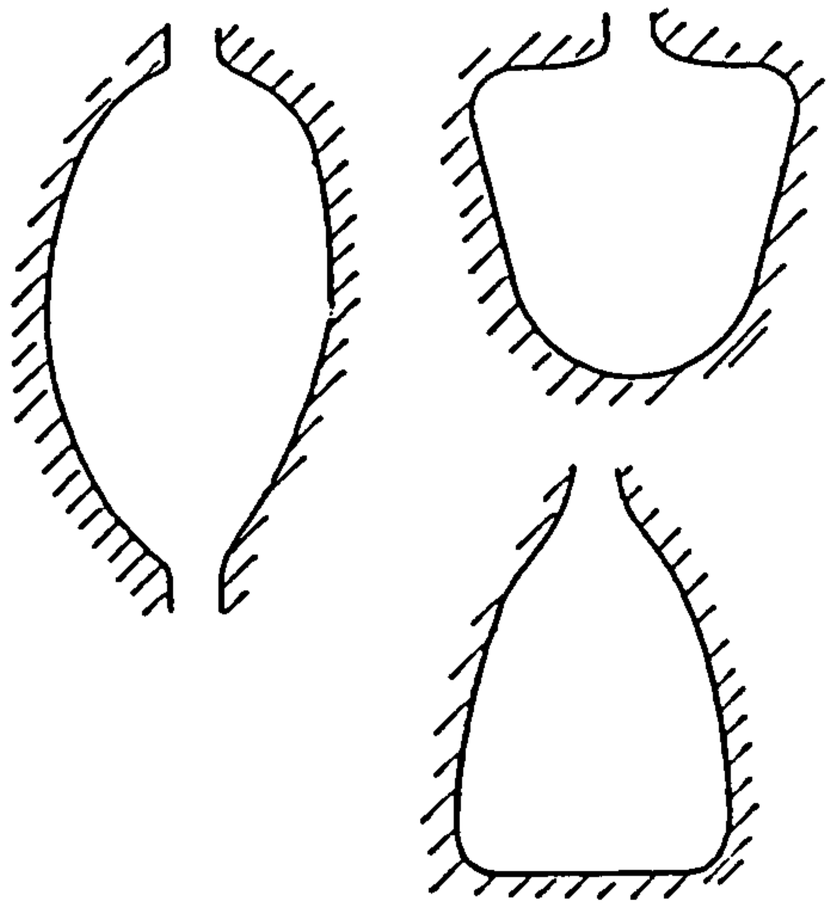

(ii)

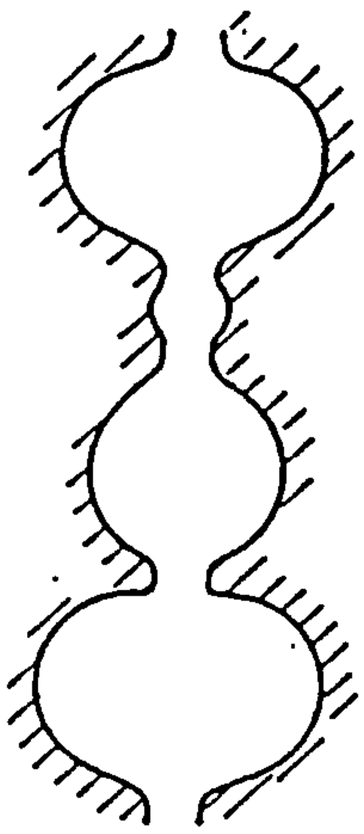

2.5.2 Instrumentation

There are two techniques available for the determination of gas adsorption isotherms: volumetric and gravimetric. Volumetric methods are generally preferred particularly when significant accuracy is required at high relative pressure. For the evaluation of both the surface area and the pore size distribution of a solid from a single isotherm, nitrogen adsorption at 77K (the boiling point of nitrogen at ambient atmospheric pressure) is the most suitable.

A typical schematic volumetric N_2 adsorption experiment is detailed in Figure 2.22, based on a Micromeritics ASAP 2000. In the experiment, the burette containing the sample has a limited volume and is maintained at a constant temperature of 77K. A known amount of pure N_2 is introduced into the burette *via* a series of valves. As adsorption occurs, the pressure in the burette drops until equilibrium is reached at a pressure previously specified

in the method, and it is this variable that is measured. The adsorption isotherm is constructed a point at a time by the successive additions of aliquots of N_2 and application of the gas laws.

Figure 2.22: Schematic of Micromeritics ASAP 2000

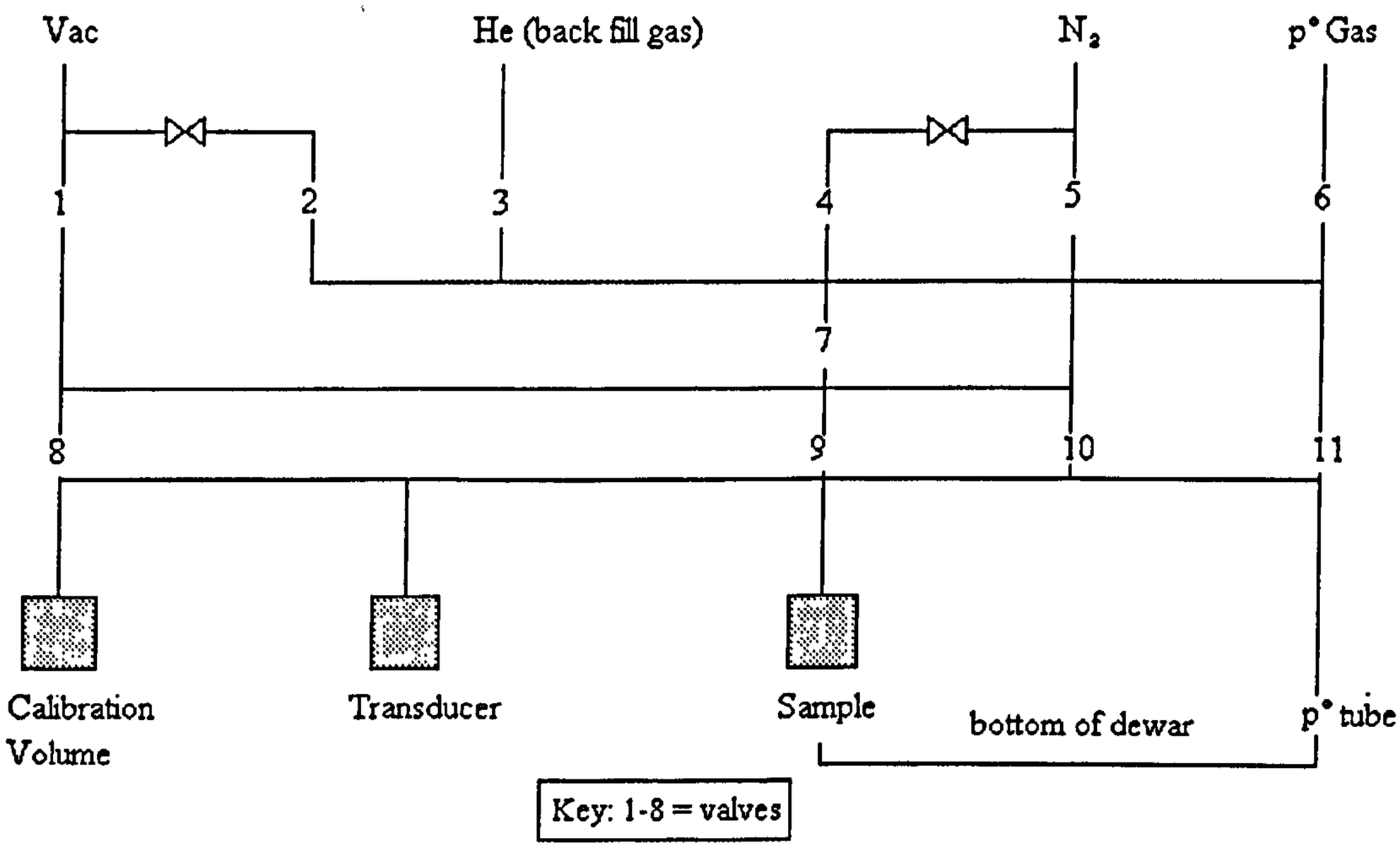

At intervals throughout the experiment the value of p^o is measured by filling the p^o tube, which is in the dewar, with nitrogen.

The helium is a safety measure and is used as a backfill gas to fill the sample tube before and after the experiment so tubes are not handled under vacuum.

2.5.3 Experimental

For nitrogen adsorption, about 0·2g of sample was outgassed at 30°C for 10 to 12 hours on one of the degas ports of the Micromeritics ASAP 2000.

Because krypton adsorption is a highly sensitive technique which measures very small changes in the sample pressure, outgassing conditions on the degas ports needed to be more severe, 250°C for 12 hours, to ensure both the complete degassing of the sample and the accuracy of the results.

Gas adsorption isotherms were obtained volumetrically using a Micromeritics ASAP 2000. The isotherm, surface area, pore volume and pore size information were automatically obtained using the instrument operating software. The values used for surface area were obtained from the BET[18] method, whereas the BJH[23] method was used to calculate the pore volume and average pore diameter of the sample. For micropores, the α_s-method was used and raw data was processed using a program called "FAWLTY" available in the department. This program uses Fransil-I, a nonporous hydroxylated silica with BET nitrogen surface area of 38.7 m^2g^{-1} as a reference[27].

2.6 Thermal Methods

2.6.1 Theory

Thermal methods of analysis are techniques based upon the measurement of the dynamic relationship between the temperature and properties of the system such as mass, heat of reaction or volume. These can be used to identify reactions and phase transformations that occur on heating.

2.6.1.1 Differential Thermal Analysis (DTA)

Differential thermal analysis (DTA) is a technique of recording the difference in temperature between a substance and a reference material (*ie* alumina) as the two specimens are subjected to identical temperature regimes in an environment heated or cooled at a controlled rate. This results in a DTA curve which, provided the sample is thermally active in the temperature range used, shows a series of peaks, the position of which are determined by the chemical composition and crystal structure of the substance. The area of DTA peaks is related to the energy change involved in the reaction occurring[1,,28,29].

Generally, phase transitions, dehydration, reduction, and some decomposition reactions produce endothermic effects, whereas crystallisation, oxidation, and some decomposition reactions produce exothermic effects.

The temperature changes that occur during these physical or chemical changes are detected by a differential method, see figure 2.23[28].

Figure 2.23: Basic DTA system[28]

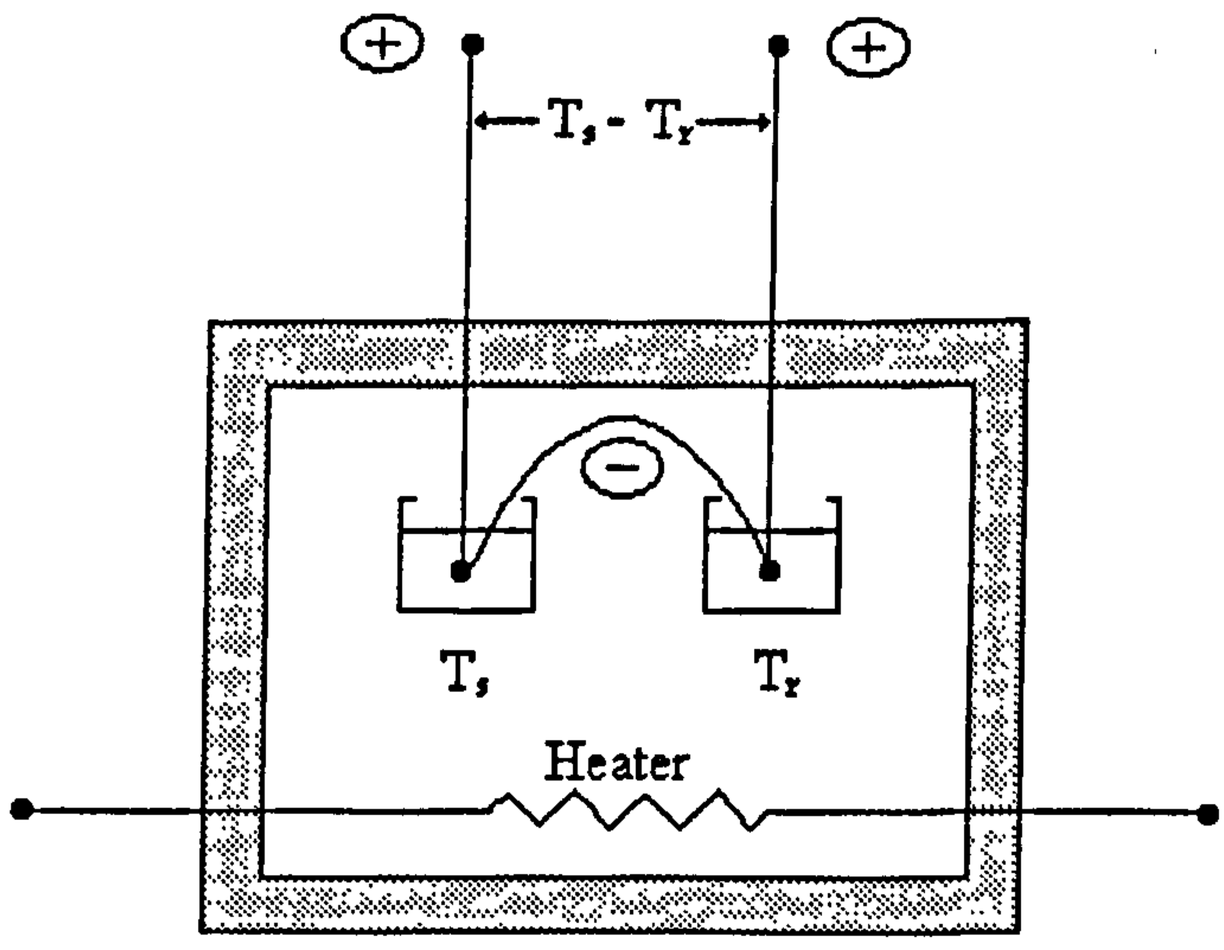

T_s=sample temperature

T_r=reference temperature

Since T_s and T_r are the sample and reference temperatures respectively, then the difference, T_s-T_r, is the recorded differential value. One advantage of the resulting DTA curve is that all energy changes in the sample during heating are detected, provided that the sensitivity

(voltage amplification) is adequate. The area under the resulting peaks is proportional to the enthalpic change (±ΔH) and sample mass.

In the generalised DTA curve (figure 2.24) A is the pre-transition base line, B is the post-transition base line, T_i the procedural initial deviation temperature which can be detected by the instrument, ΔT_{min} is the minimum peak temperature, and T_f is the final temperature of the peak. On the temperature axis, T_n is the temperature of the reference (T_r), sample (T_s), or furnace (T_e=external). The differential temperature, T_s-T_r or ΔT is plotted on the y-axis.

Figure 2.24: Generalised DTA curve[28]

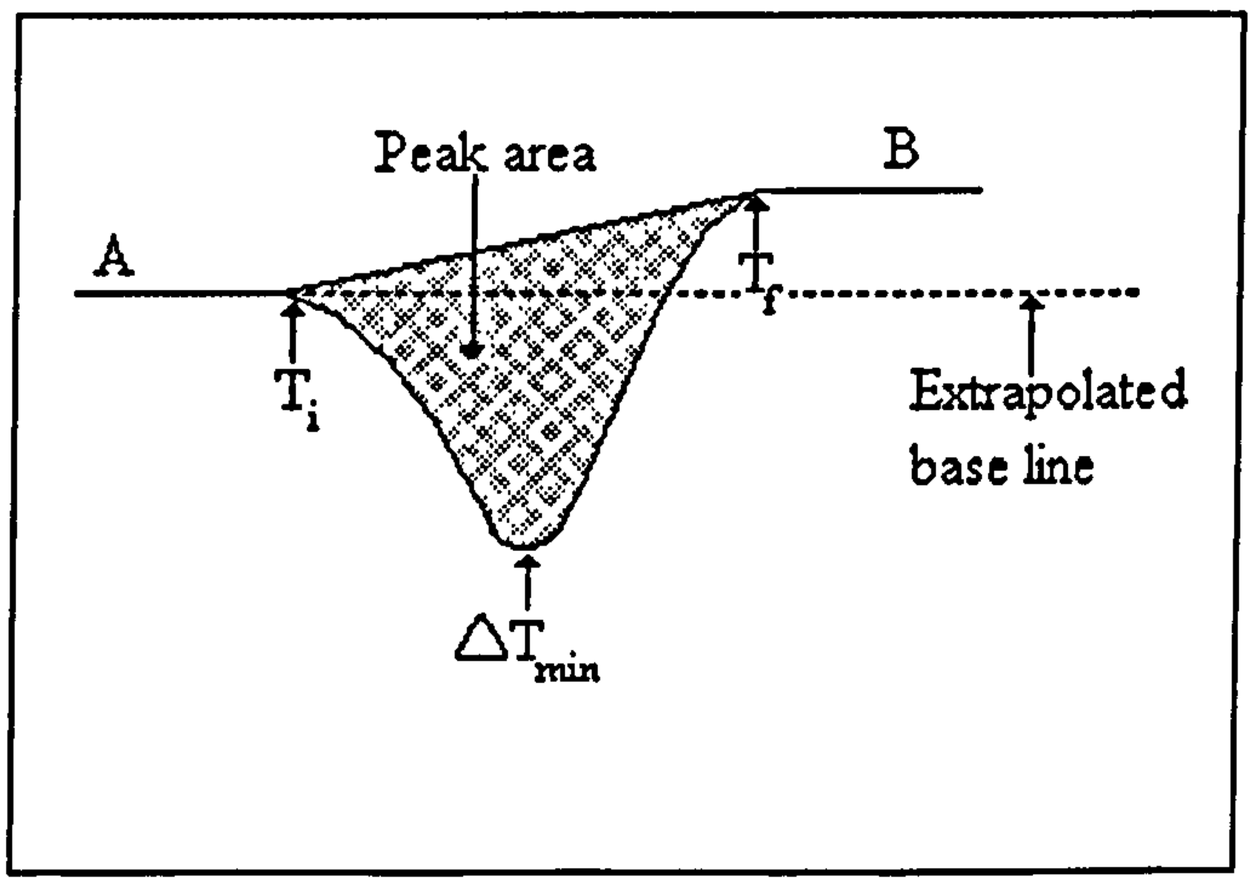

From the resulting DTA curve it is possible to determine both the energy and temperature involved in a transition. Combination with thermogravimetric analysis, TGA, yields information on whether a mass loss is involved with the energy change.

2.6.1.2 Thermal Gravimetric Analysis (TGA)

In a thermogravimetric analysis (TGA), the mass of sample is continuously recorded as its temperature is linearly increased over the range of the analysis. The resulting plot of mass as a function of temperature (thermogram) provides both qualitative and quantitative information on the thermal stability and composition of the initial, intermediate and final compounds. The characteristics of a single-stage mass loss curve are shown in figure 2.25[28]. There are two temperatures that are characteristic of any single-stage non-isothermal reaction: T_i, the initial temperature, which is the temperature at which the cumulative mass-change reaches a magnitude that can be detected by the thermobalance; and T_f, the final temperature, which is the temperature at which the cumulative mass-change first reaches its maximum value, corresponding to complete reaction. Although T_i may be the lowest temperature that a change in mass may be detected, it is neither a transition temperature nor a true decomposition temperature below which the reaction rate becomes zero. At a linear heating rate, T_f must be greater than T_i, and the difference T_f-T_i, is the reaction interval.

Figure 2.25: Characteristics of a Single-Stage Thermogravimetric Curve[28]

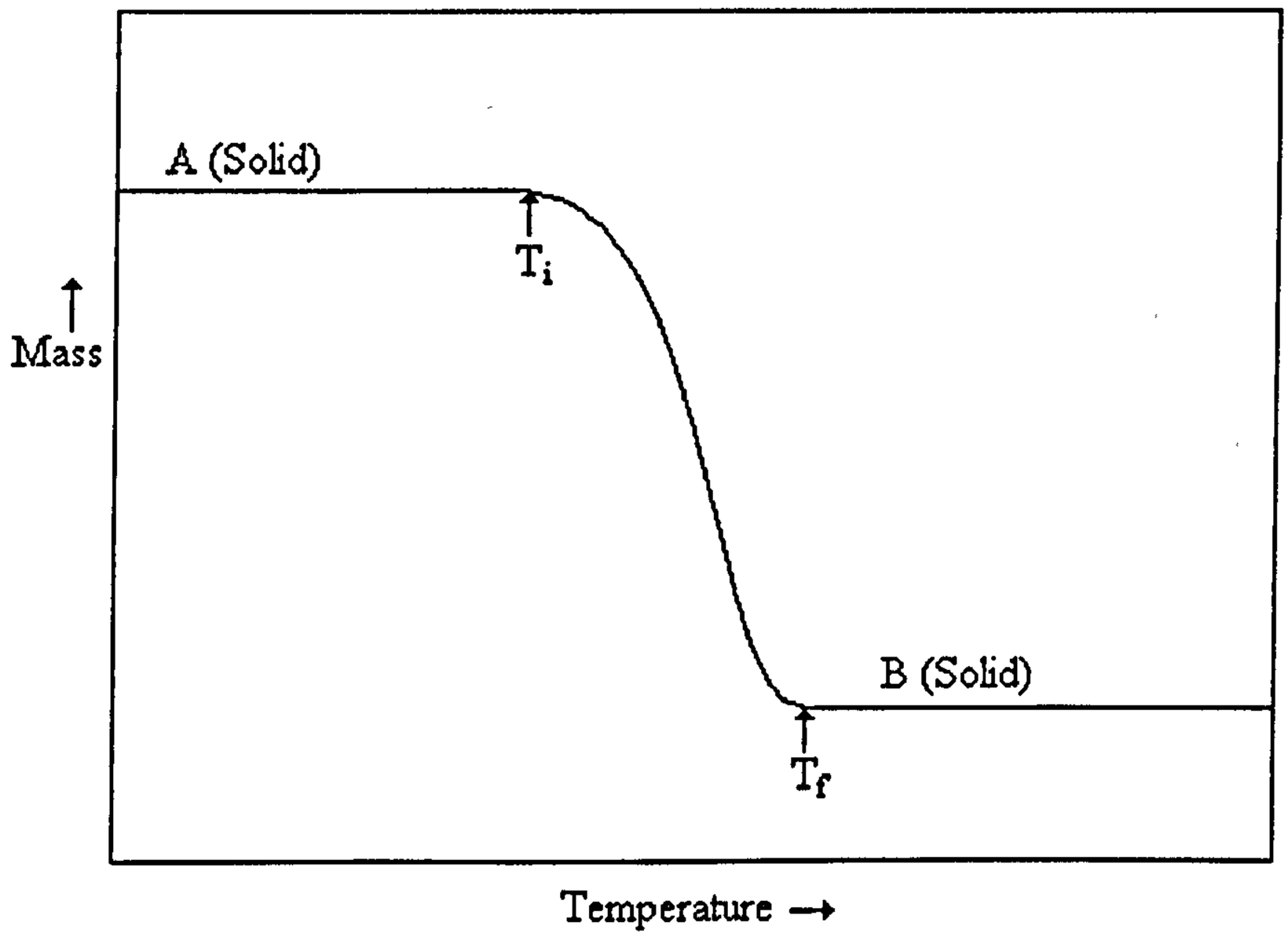

$$A\ (Solid) \longrightarrow B\ (Solid) + C\ (Gas)$$

The thermal stability of a sample is defined as its ability to maintain its properties as unchanged as possible on heating. Practically, thermal stability must be defined in terms of the environment imposed on the material.

2.6.2 Instrumentation and Experimental

Thermal analysis was carried out on a Stanton-Redcroft STA 780 series instrument capable of simultaneously measuring the thermogravimetric (TG) and differential thermal analysis (DTA) curves up to 1000°C. This uses a Pt v. 13% Rh-Pt flat plate thermocouple system to measure both ΔT and T. The sample, about 30mg, and reference (α-alumina) were placed in Pt-Rh sample holders and heated in a furnace from 20-970°C at 10°C/min under a flowing nitrogen atmosphere.

2.7 References

1 D.A. Skoog, in *Principles of Instrumental Analysis*, 3rd edition (Saunders College Publishing, 1985)

2 N.B. Colthup, L.H. Daly and S.E. Wiberly, *Introduction to Infrared and Raman Spectroscopy* (Academic Press, New York, 1975)

3 K. Nakamishi and P.H. Solomon, *Infrared Absorption Spectroscopy*, 2nd edition (Holden-Day, San Francisco, 1977)

4 A.L. Smith, *Applied Infrared Spectroscopy* (Wiley, New York, 1979)

5 C.N. Banwell, in *Fundamentals of Molecular Spectroscopy*, 3rd edition (McGraw-Hill, London, 1983)

6 K.B. Whetsel, *App. Spec. Rev.* **2** (1968) 1-67

7 L.G. Weyer, *ibid* **21** (1985) 1-43

8 H.H. Jaff and M. Orchin, in *Theory and Applications of Ultraviolet Spectroscopy* (Wiley, New York, 1962)

9 C.N.R. Rao, *Ultraviolet and Visible Spectroscopy: Chemical Applications* (Butterworths, London, 1975)

10 J.D. Lee, *Concise Inorganic Chemistry*, 3rd edition (Van Nostrand, England, 1977)

11 A.B.P. Lever, in *Inorganic Electronic Spectroscopy* p.479 (Elsevier, Amsterdam, 1984)

12 R.L. Carlin, in *Transition Metal Chemistry, Vol.1*, (Edward Arnold Ltd., 1965)

13 F.A. Cotton and G. Wilkinson, in *Advanced Inorganic Chemistry*, 3rd edition p. 1117 (Wiley, New York, 1972)

14 J.W. Akitt, in *NMR and Chemistry: An Introduction to the Fourier Transform-multinuclear era*, 2nd edition (Chapman and Hall, New York, 1983)

15 E.D. Becker, in *High Resolution NMR: Theory and Chemical Applications* (Academic Press, London, 1980)

16 M.L. Martin, J.-J. Delpuech and G.J. Martin, in *Practical NMR Spectroscopy* (Heyden, London, 1980)

17 E.D. Becker and T.C. Farrar, *Science* **178** (1972) 361-368

18 S.J. Gregg and K.S.W. Sing, *Adsorption, Surface Area and Porosity* (Academic Press, London, 1982)

19 S. Brunauer, P.H. Emmett and E. Teller, *J. Am. Chem. Soc.* **60** (1938) 309-319

20 W.D. Harkins and G. Jura, *J. Am. Chem. Soc.* **66** (1944) 1362; **66** (1944) 1366-1373

21 R.A. Beebe, J.B. Beckwith and J.M. Honig, *J. Am. Chem. Soc.* **67** (1945) 1554-1558

22 M.M. Dubinin, *Chem. Rev.* **60** (1960) 235-241

23 K.S.W. Sing, in *Characterisation of Powder Surfaces*, eds. G.D. Parfitt and K.S.W. Sing (Academic Press, London and New York, 1976)

24 E.P. Barrett, L.G. Joyner and P.P. Halenda, *J. Am. Chem. Soc.* **73** (1951) 373-380

25 K.S.W. Sing, in *Principles and Applications of Pore Structural Characterisation* p.1, eds. J.M. Haynes and P. Rossi-Doria (Arrowsmith, Bristol, 1985)

26 J.H. De Boer, in *The Structure and Properties of Porous Materials* p 68, eds. D.H. Everett and F.S. Stone (Butterworths, London, 1958)

27 M.R. Bhambhani, P.A. Cutting, K.S.W. Sing and D.H. Turk, *J. Colloid Interface Sci.* **38**,1 (1972) 109-117

28 W.W. Wendlandt, in *Thermal Methods of Analysis*, 2nd edition (Wiley-Interscience, New York, 1974)

29 R.C. Mackenzie, in *Differential Thermal Analysis Vol.1 Fundamental Aspects*, ed. R.C. Mackenzie (Academic Press, London, 1970)

Chapter 3: Sample Preparation

This chapter contains information on the preparation of the mixed oxide gels investigated in this thesis. The synthesis and structural characterisation of the starting materials has been included where appropriate.

3.1 Preparation of SiO_2-TiO_2 Gels

The reactivity of titanium alkoxides is high compared to that of silicon alkoxides and the difference in reactivity makes the products of the sol-gel reaction inhomogeneous. It is therefore necessary to form polymerisable species from at least one of the alkoxides separately before reacting with each other. Alternatively, it is possible to reduce the reactivity of titanium alkoxides through chelation of the metal ion and the pH of the hydrolysis water used in the subsequent hydrolysis and condensation reaction pathway.

Previous work by Aizawa *et al*[1] has used acetylacetone (acac), glycols, mono-methyl maleate, di-butyl phosphate and combinations of these ligands, to form titanium chelates.

La Course and Kim[2], using acac as a complexing ligand for titanium, found that the infrared spectra of a bis(acetylacetonato) titanium diisopropoxide and tetraethyl orthosilicate (TEOS) sol contained no peaks arising from the iso-propoxy groups indicating the almost immediate hydrolysis of the isopropoxide groups on the chelate, this suggests that the overall slower reaction is due to a reduction in the condensation rate. The two isopropoxide groups on the bis(acetylacetonato) titanium diisopropoxide are easily hydrolysable whereas the acetylacetonate groups are quite stable in water and are slowly removed during the condensation processes.

As discussed in section 1.6.1, Abe *et al* have prepared mixed silicon-titanium oxides from bis(acetylacetonato) titanium diisopropoxide and a variety of silicon precursors including, prehydrolysed TEOS[3], $Si(OH)_2(O^tBu)_2$[4] and silicic acid[5-8]. All of these precursors contain hydroxyl groups which are highly reactive to condensation. By forming bis(acetylacetonato) titanium diisopropoxide, the need for prehydrolysis of TEOS is eliminated and the simultaneous hydrolysis of the titanium chelate and silicon alkoxide to form homogeneous gels becomes possible. This method is used in the preparation of SiO_2-TiO_2 and SiO_2-ZrO_2 gels described in this and subsequent chapters.

3.1.1 Preparation of bis(acetylacetonato) titanium diisopropoxide

Bis(acetylacetonato) titanium diisopropoxide $[Ti(acac)_2(O^iPr)_2]$ has been successfully prepared by mixing titanium iso-propoxide [ex-Aldrich, 97%] (1 mole) with acetylacetone [ex-Aldrich, 98%] (2 mole) at room temperature. The resulting mixture was stirred until the evolution of heat had ceased and the resulting golden solution had returned to room temperature.

$$Ti(O^i\,Pr)_4 + 2acac \rightarrow Ti(O^i\,Pr)_2(acac)_2 + 2\,Pr^iOH$$

The solvent produced in the reaction was not removed. The structure of the titanium complex was confirmed by both proton nuclear magnetic resonance (NMR) and infrared

spectroscopy. The NMR spectra were recorded in d_6-acetone at 21°C and -30°C (figure 3.1), and the chemical shift values and peak assignments are detailed in table 3.1. The infrared spectrum of a thin film of the titanium complex between sodium chloride plates clearly shows peaks due to both the alkoxy and acac groups, see figure 3.2.

Table 3.1: Proton Chemical Shift Values and Assignments for $Ti(acac)_2(O^iPr)_2$ (relative to TMS)

	Assignment	**Chemical Shift/ ppm**	**Multiplicity**
diketonate	CH_3-	1·98	doublet
	-CH=	5·53	
alkoxide	CH_3-	1·19	doublet
	>CH-	4·81	septet

Bradley and Holloway[9,10] used proton NMR to determine whether the *trans*- or *cis*- isomer is more stable. They determined that on cooling the resonances due to the acac-methyl protons separated into two separate signals of equal intensity.

The results obtained suggest that at 21°C (figure 3.1a), $Ti(acac)_2(O^iPr)_2$ is already exhibiting splitting of the acac-methyl protons due to the *cis*- isomer. On cooling to -30°C the splitting of the doublet was more pronounced (figure 3.1b), confirming the presence of the *cis*-isomer.

Figure 3.3: The Structure of *cis*-bis(acetylacetonato) titanium diisopropoxide

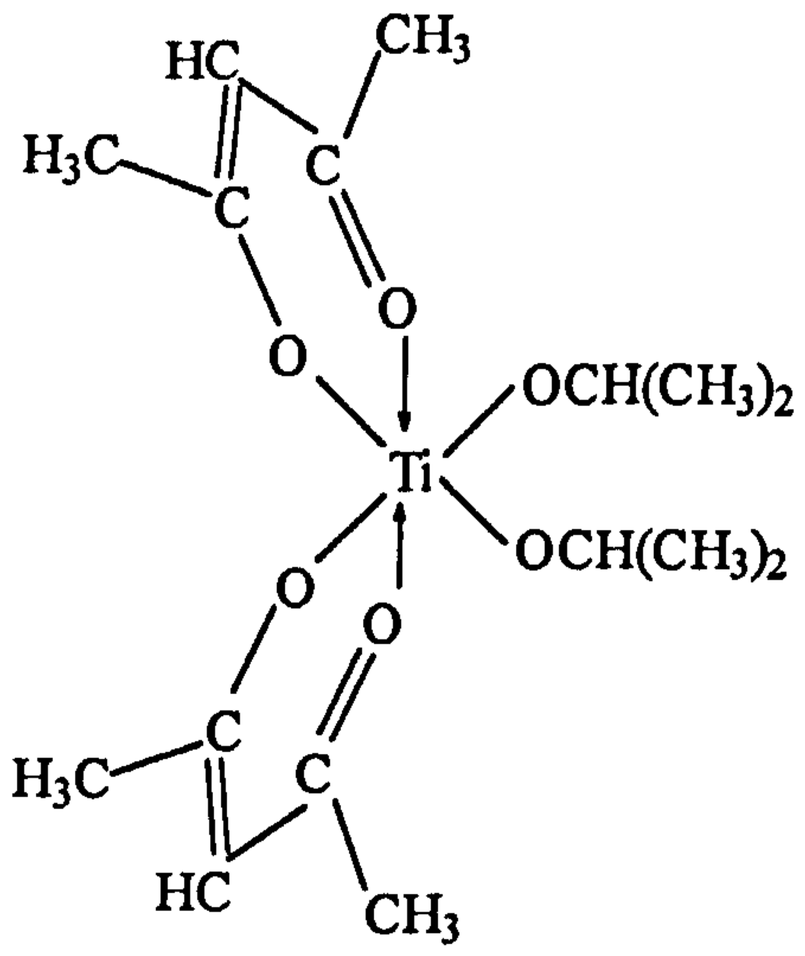

Figure 3.1: ^{1}H NMR Spectra of $Ti(acac)_2(O^iPr)_2$ at (a) 21°C; (b) -30°C

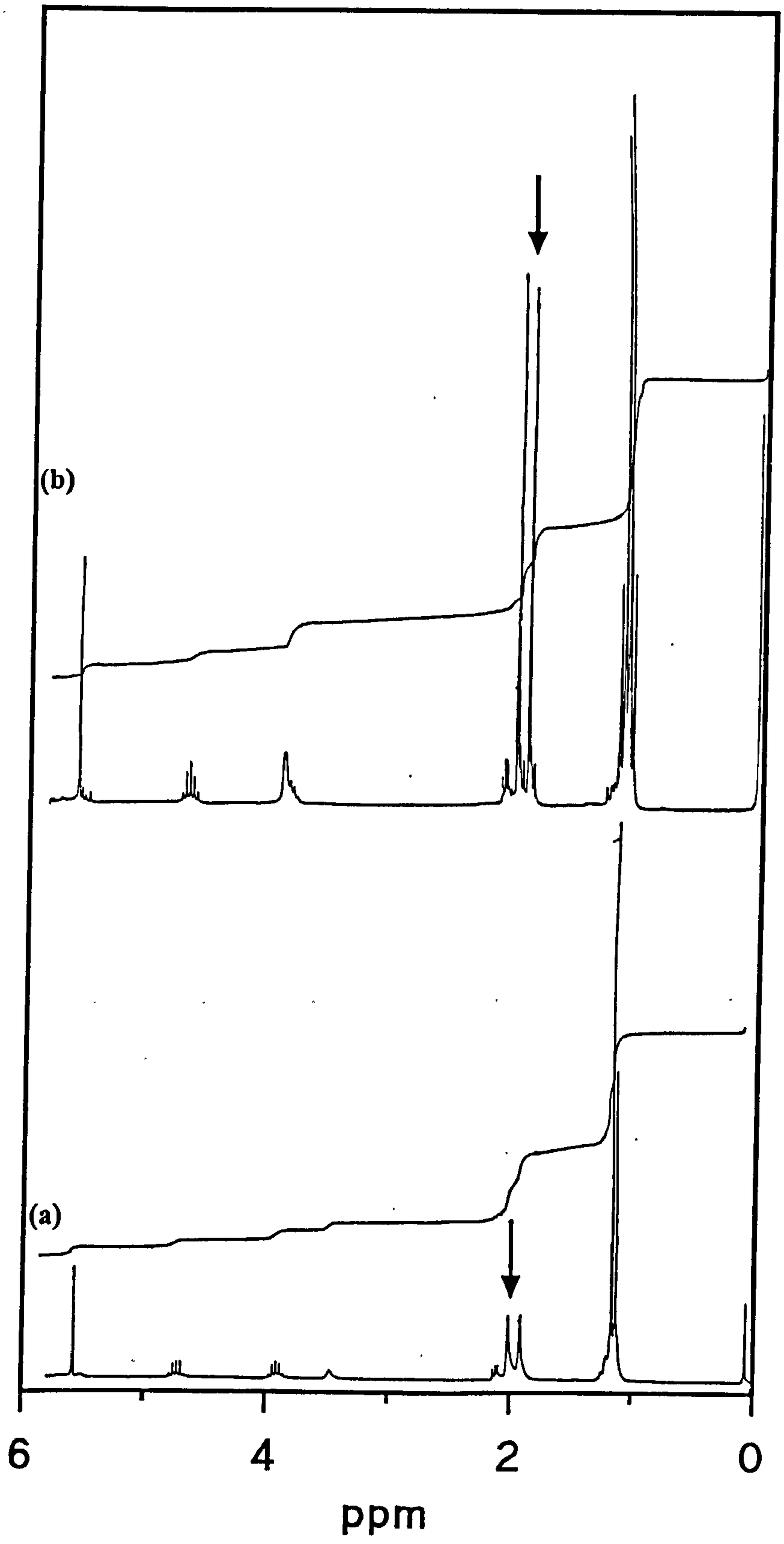

Figure 3.2: Mid-Infrared Spectrum of $Ti(acac)_2(O^iPr)_2$ between NaCl Plates

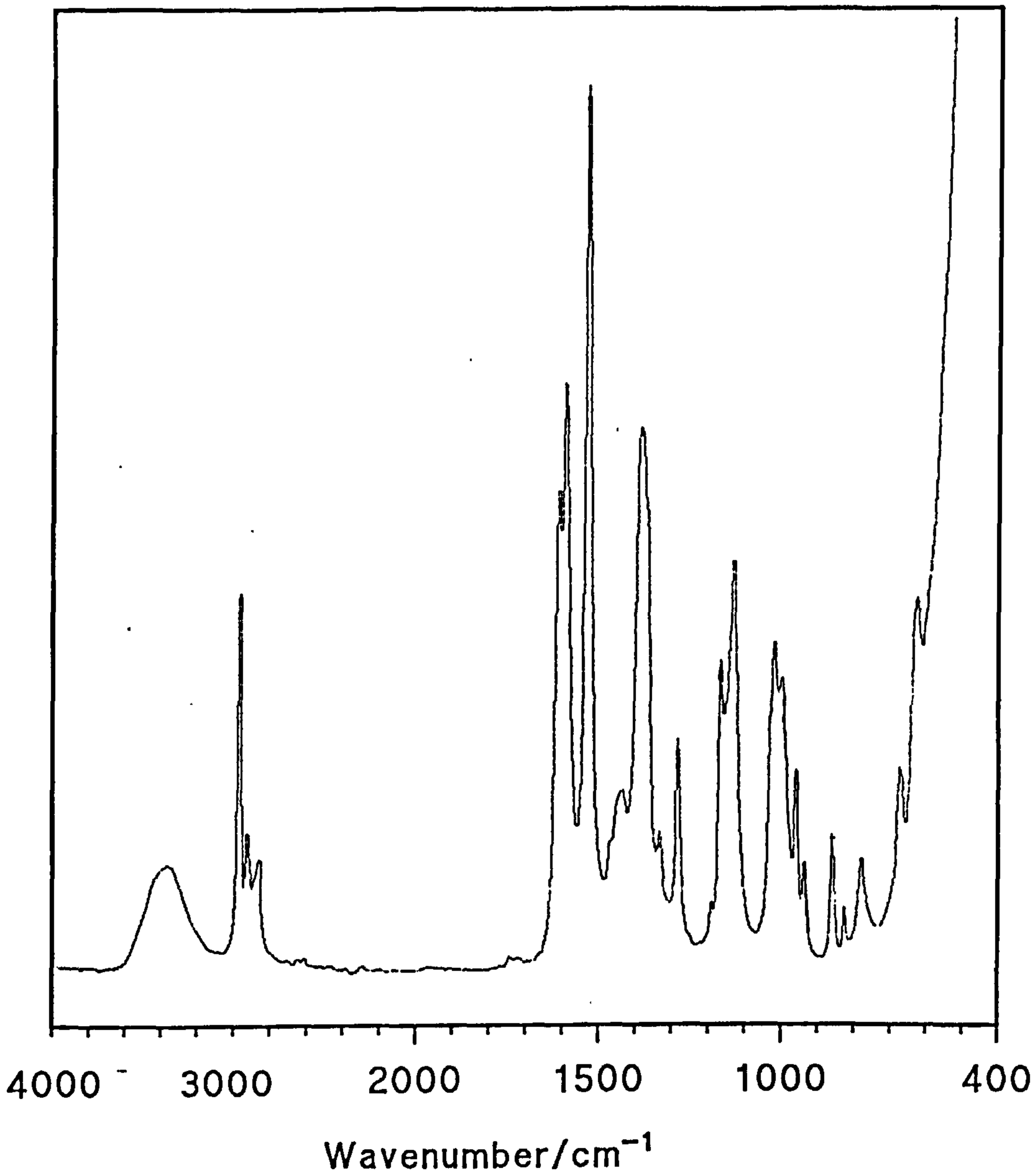

Assignment	Wavenumber/ cm^{-1}
ν_s(C=O)	1608 vs; 1585 vs
ν_{as}(C=C)	1525 vs
$\delta(CH_3)$	1385 s
δ(C-H)	1190 w; 1025
ν(Ti-O^{i}Pr)	613 m
ν(Ti-O)	437 m

3.1.2 Preparation of SiO_2-TiO_2 Gels

Tetraethyl orthosilicate [TEOS] [ex-Aldrich, 99%] (0·0372 mole) and enough bis(acetylacetonato) titanium isopropoxide [$Ti(acac)_2(O^iPr)_2$] to give the required TiO_2 weight % content, were mixed together for 15 minutes, to obtain an even distribution. To this was rapidly added a mixture of the required amount of hydrochloric acid (HCl) in iso-propyl alcohol (IPA) dried over molecular sieve and the resulting solution stirred for 2 hours before being covered with Nesco™ film and left to gel at room temperature. In the case of monoliths, on gelation the resulting gels were slowly dried in an oven at 40°C until no further solvent loss was observed. However, for powders the gel was allowed to dry rapidly after gelation. This caused the gel to crack and after further drying the small pieces of gel were gradually broken until a powder was formed.

Bulk properties of these gels were studied after thermal treatment in a muffle furnace at 120, 300, 500, 700, 900 and 1100°C for 12 hours.

3.1.3 A ^{1}H NMR Study of the Hydrolysis Reaction

The hydrolysis of tetraethyl orthosilicate (TEOS) has been extensively studied to elucidate the extent of the hydrolysis reactions occurring in solution[11,12]. Comparison of the ^{1}H NMR spectra of TEOS and ethanol indicate the difference in the chemical shift of the respective methylene protons with respect to tetramethyl silane.

	ppm
-C<u>H</u>$_2$-OSi	3·8
-C<u>H</u>$_2$-OH	3·6

Therefore, the extent of hydrolysis is readily quantified by integrating the peaks centred at 3·6 and 3·8ppm respectively.

A mixture of TEOS and bis(acetylacetonato) titanium diisopropoxide in the following molar ratio:

$$\text{TEOS: } Ti(acac)_2(O^iPr)_2 = 19:1$$

equivalent to a titania content of 6·34 wt%, was hydrolysed *in situ*. The experiments were carried out under the conditions detailed in section 2.3.3.1.

3.1.3.1 Results and Discussion

Initially the experiments were carried out at 20°C, after 90 seconds the ^{1}H NMR spectrum showed a peak centred at 3·6ppm due to the ethanol methylene protons as well as a very small peak at 3·8ppm. After 2 minutes the spectrum showed a peak centred at 3·6ppm due to the ethanol methylene protons. When the experiment was performed at -30°C, the complete conversion of TEOS to ethanol took 64 minutes. Comparison of the times taken for the complete conversion of TEOS to ethanol suggests that 2 minutes at 20°C is equivalent to approximately 64 minutes at -30°C.

After 10 minutes at -30°C (equivalent to approximately 19 seconds at 20°C), the spectrum showed a peak centred at 3·6ppm due to the ethanol methylene protons as well as a very

small peak at 3·8ppm. Measurement of the integrals indicated that up to 90% of the TEOS had already been converted to ethanol. After 64 minutes at -30°C (the equivalent of approximately two minutes at 20°C), the hydrolysis was complete with the conversion of 100% of TEOS to ethanol, see figure 3.4.

Figure 3.4: Monitoring the Extent of Hydrolysis of TEOS using ^1H NMR Spectra acquired after (a) 0 mins; (b) 19 secs; (c) 2 mins.

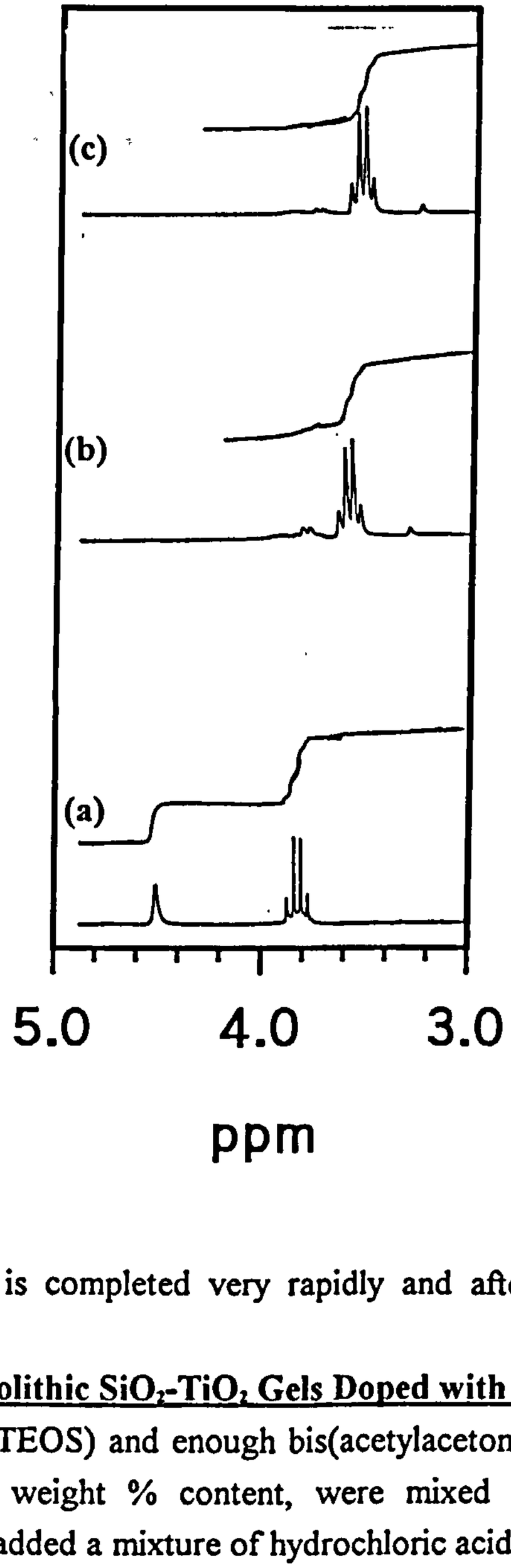

The hydrolysis reaction is completed very rapidly and after two minutes condensation reactions predominate.

3.2 Preparation of Monolithic SiO_2-TiO_2 Gels Doped with Cobalt (II)

Tetraethyl orthosilicate (TEOS) and enough bis(acetylacetonato) titanium isopropoxide to give the required TiO_2 weight % content, were mixed together to obtain an even distribution. To this was added a mixture of hydrochloric acid in 15ml of iso-propyl alcohol

(IPA) (dried over molecular sieve) and the resulting solution stirred for 1 hour. To this solution was added 1ml of:

0·1M $CoCl_2$ [ex-Sigma] in IPA

dry IPA for the blank

and the resulting solution stirred for a further hour before being left to gel at room temperature. On gelation all gels were yellow in colour but the doped ones became green on drying.

3.3 Preparation of SiO_2-ZrO_2 Gels

Gels were prepared by the simultaneous hydrolysis of tetraethyl orthosilicate (TEOS) [ex-Aldrich, 99%] and bis(acetylacetonato) zirconium dipropoxide.

3.3.1 Preparation of bis(acetylacetonato) zirconium dipropoxide [$Zr(acac)_2(O^nPr)_2$]

$$Zr(O^n\mathrm{Pr})_4 + 2acac \rightarrow Zr(acac)_2(O^n\mathrm{Pr})_2 + 2\,\mathrm{Pr}^nOH$$

The acetylacetone [ex-Aldrich, 98%] was rapidly added to the zirconium propoxide [ex-Fluka, ≈70% in propanol] with stirring at room temperature. The initially clear solution gradually formed a cream coloured solid on stirring. The solid was filtered *in vacuo* to remove the solvent produced in the reaction.

Both proton NMR (figure 3.5) and infrared spectroscopy (figure 3.6) have been used to identify the product formed.

Figure 3.5: ^{1}H NMR Spectrum of $Zr(acac)_2(O^nPr)_2$

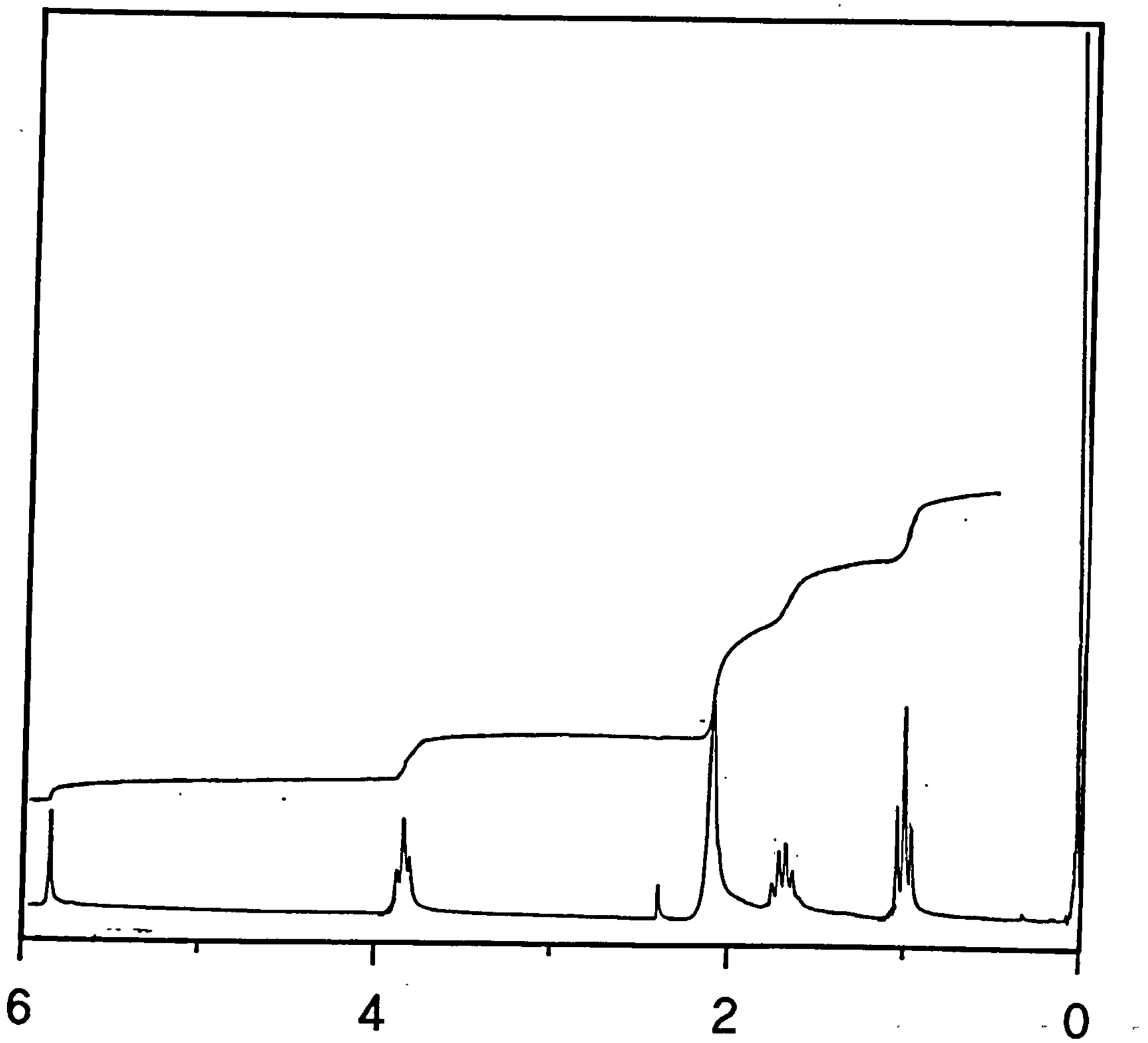

	Assignment	Chemical Shift/ ppm
diketonate	CH_3-	2
	-CH=	5·6
Zr alkoxide	$OC\underline{H}_2CH_2CH_3$	3·8
	$OCH_2C\underline{H}_2CH_3$	1·6
	$OCH_2CH_2C\underline{H}_3$	1·2

Figure 3.6: Mid-Infrared Spectrum of $Zr(acac)_2(O^nPr)_2$

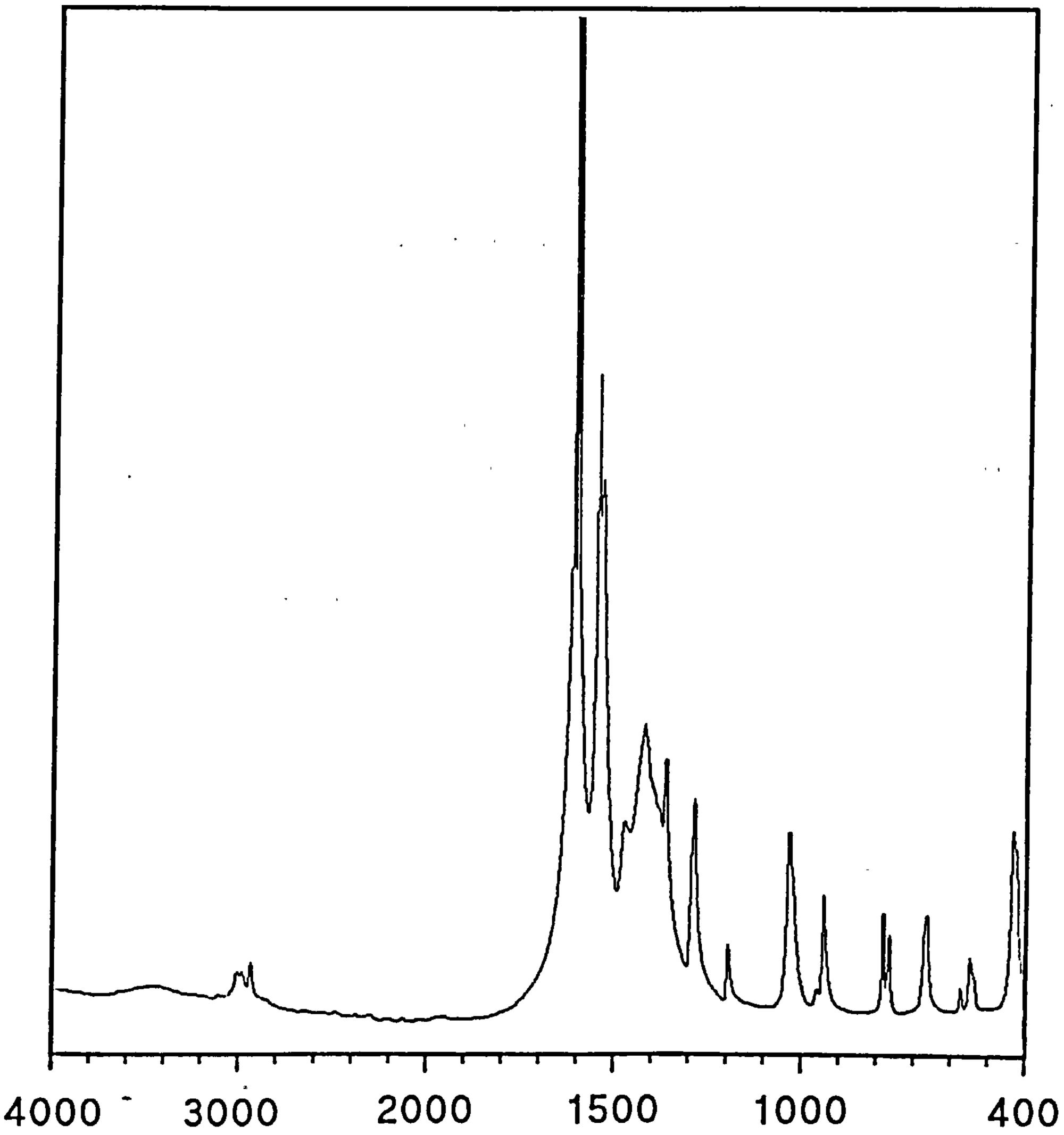

Assignment	Wavenumber/ cm^{-1}
ν_s(C=O)	1608 vs; 1585 vs
ν_{as}(C=C)	1525 vs
$\delta(CH_3)$	1385 s
δ(C-H)	1190 w; 1025
ν(Zr-O^{n}Pr)	613 m
ν(Zr-O)	437 m

3.3.2 Preparation of SiO_2-ZrO_2 Gels

Tetraethyl orthosilicate [TEOS] (0·0372 mole) and enough bis(acetylacetonato) zirconium dipropoxide [$Zr(O^nPr)_2(acac)_2$] to give the required ZrO_2 weight % content, were mixed together until the zirconium complex had dissolved and an even distribution was obtained. To this was added a mixture of the required amount of hydrochloric acid (HCl) in ethanol and the resulting solution stirred for two hours before being covered with Nesco™ film and left to gel at room temperature. On gelation the resulting monolithic gels were oven dried at 40°C until no further solvent loss was observed.

Bulk properties of these gels were studied after thermal treatment of monolithic pieces in a muffle furnace at 120, 300, 500, 700, 900 and 1100°C for 12 hours.

3.3.3 A ^{1}H NMR Study of the Hydrolysis Reaction

The reaction of tetraethyl orthosilicate (TEOS) has been extensively studied to elucidate the extent of the hydrolysis and condensation reactions occurring in solution[11,12]. Comparison of the ^{1}H NMR spectra of TEOS and ethanol indicate the difference in the chemical shift of the respective methylene protons with respect to tetramethyl silane.

	ppm
-C<u>H</u>$_2$-OSi	3·8
-C<u>H</u>$_2$-OH	3·6

Therefore, the extent of hydrolysis is readily quantified by integrating the peaks centred at 3·6 and 3·8ppm respectively.

A mixture of TEOS and bis(acetylacetonato) zirconium dipropoxide in the following molar ratio:

$$TEOS: Zr(acac)_2(O^nPr)_2 = 19:1$$

equivalent to a zirconia content of 6·4 wt%, was hydrolysed *in situ*. The experiments were carried out under the conditions detailed in section 2.3.3.1.

3.3.3.1 Results and Discussion

Using the same comparison and conversions discussed in section 3.1.3.1, the following results were obtained.

After 10 minutes at -30°C (equivalent to 20 seconds at 20°C), the ^{1}H NMR spectrum showed a peak centred at 3·6ppm due to the ethanol methylene protons as well as a very small peak at 3·8ppm. Measurement of the integrals indicated that up to 90% of the TEOS had already been converted to ethanol. After 1 hour at -30°C (the equivalent of two minutes at 20°C), the hydrolysis was complete with conversion of 100% of the TEOS to ethanol, see figure 3.7.

Figure 3.7: Monitoring the Extent of Hydrolysis of TEOS using ^{1}H NMR. Spectra acquired after (a) 0 mins; (b) 19 secs; (c) 2 mins.

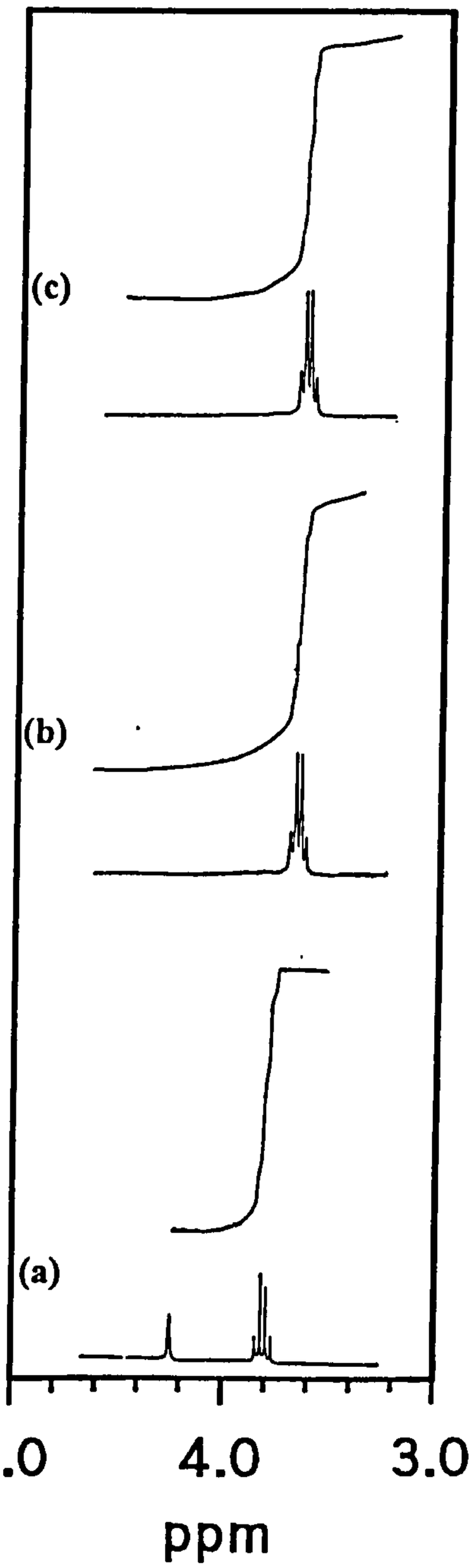

The hydrolysis reaction is completed very rapidly and after two minutes condensation reactions predominate.

3.4 Preparation of Mixed SiO_2-TiO_2 Gels from a Double Alkoxide Precursor

3.4.1 Preparation of Double Alkoxide

A mixture of chlorotriethoxysilane [ex-Fluorochem, 95%] (2 mole) and bis(acetylacetonato) titanium diisopropoxide (1 mole) in toluene was heated under reflux for four hours[13] to form a dark golden solution. The solvent was then removed by distillation *in vacuo* to form a dark red/brown liquid.

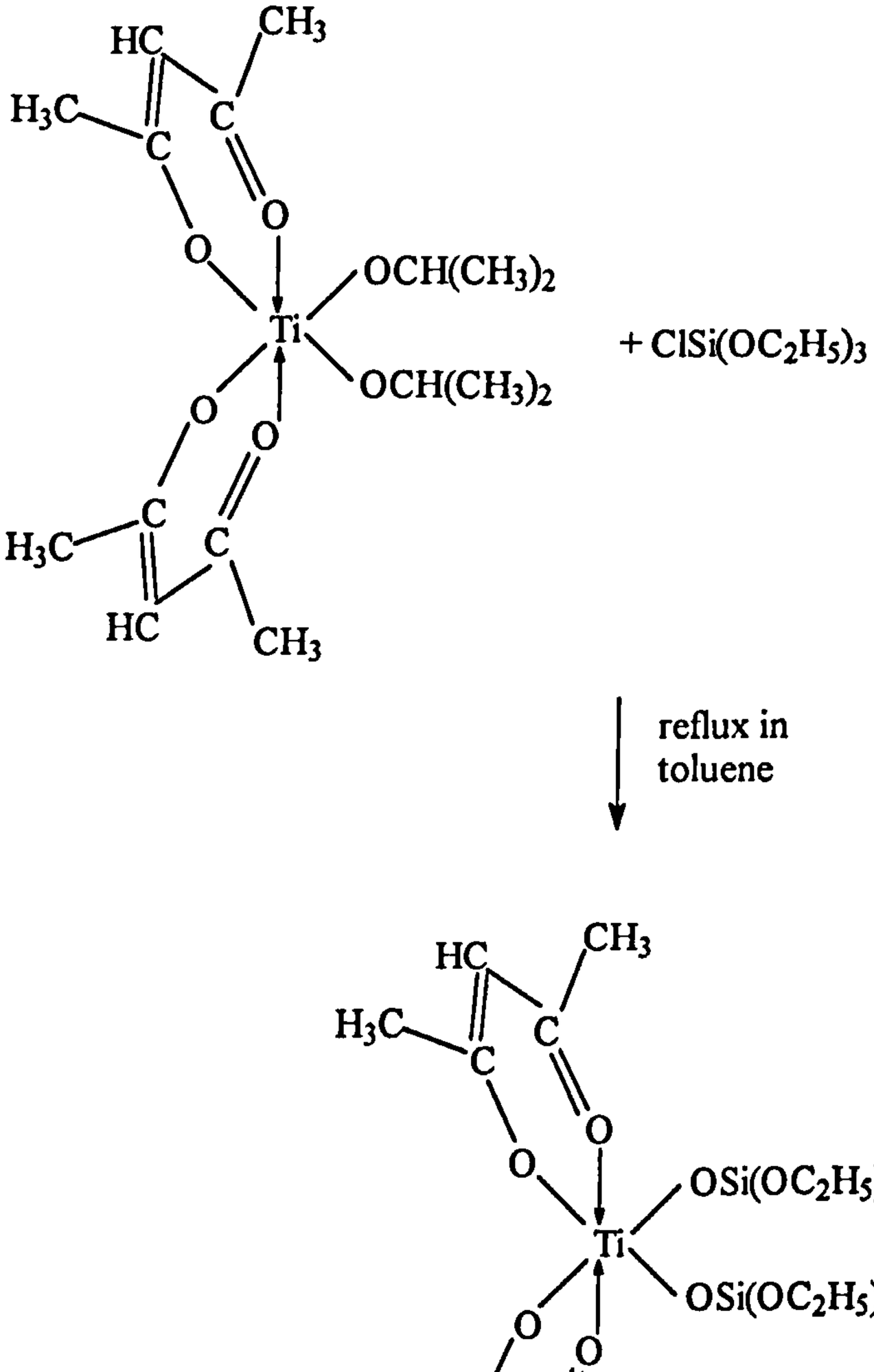

3.4.2 Characterisation of Double Alkoxide

The structure of the double alkoxide has been confirmed using ^{1}H, ^{13}C and ^{29}Si NMR spectroscopy, alongside mass spectrometry, infrared spectroscopy and elemental analysis.

3.4.2.1 ^{1}H NMR Spectroscopy

The proton NMR spectrum were recorded in d_6-acetone at both 29°C and -32°C, see figure 3.8, and the chemical shift values and peak assignments are shown in table 3.2.

Table 3.2: Proton Chemical Shift Values and Assignments of $Ti(acac)_2(OSi(OEt)_3)_2$ (relative to TMS)

	Assignment	Chemical Shift/ ppm	Multiplicity at 29°C	Multiplicity at -32°C	Peak Height Ratio
diketonate	CH_3-	2		doublet	5
	-CH=	5·6			1
Ti alkoxide	CH_3-	1·2	doublet	doublet	* 11
	>CH-	4·8	septet	septet	
Si alkoxide	$OC\underline{H}_2CH_3$	3·8	quartet	quartet	2
	$OCH_2C\underline{H}_3$	1·2	triplet	triplet	* 11
Toluene	C_6H_5	7	> quartet	> quartet	1·5

* Impossible to distinguish fully between peaks due to the different methyl protons so value given is the combined value for both types.

An additional multiplet at 7ppm was also observed due to some toluene remaining in the sample after distillation.

Cooling to -32°C caused the formation of a doublet at 2ppm due to the *cis*- arrangement of the methyl protons on the acetylacetonate groups[9,10].

Figure 3.8: ^{1}H NMR Spectra in d_6-acetone of Double Alkoxide at (a) 29°C; (b) -32°C

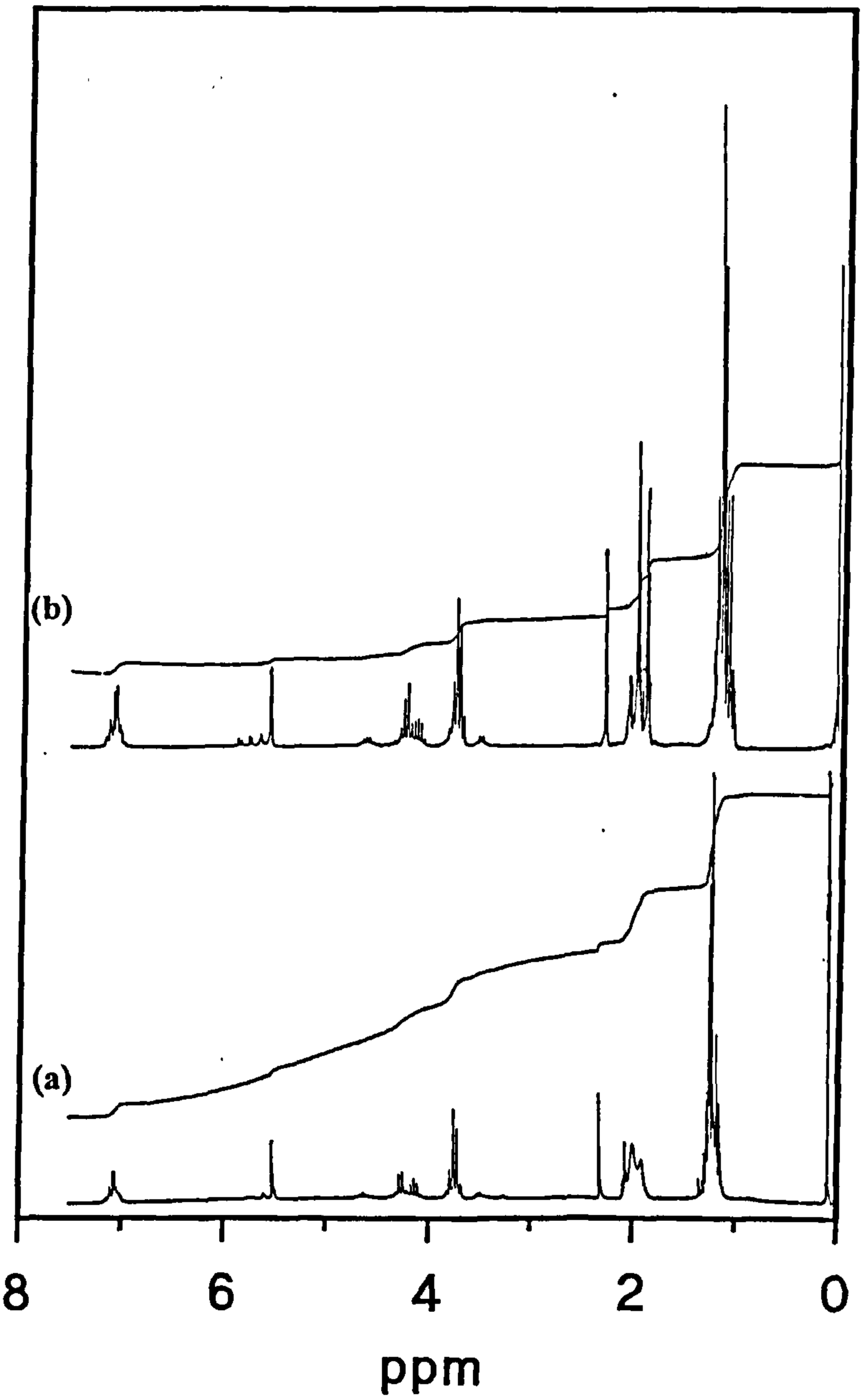

3.4.2.2 ^{13}C NMR Spectroscopy

Further confirmation of the structure was obtained from ^{13}C NMR spectra, see figure 3.10, run in deuterated chloroform under the conditions detailed in section 2.3.3.3. Peaks arising from bis(acetylacetonato) titanium di(triethoxysilane) are detailed in figure 3.9 and table 3.3.

Figure 3.9: ^{13}C NMR Peak Assignments

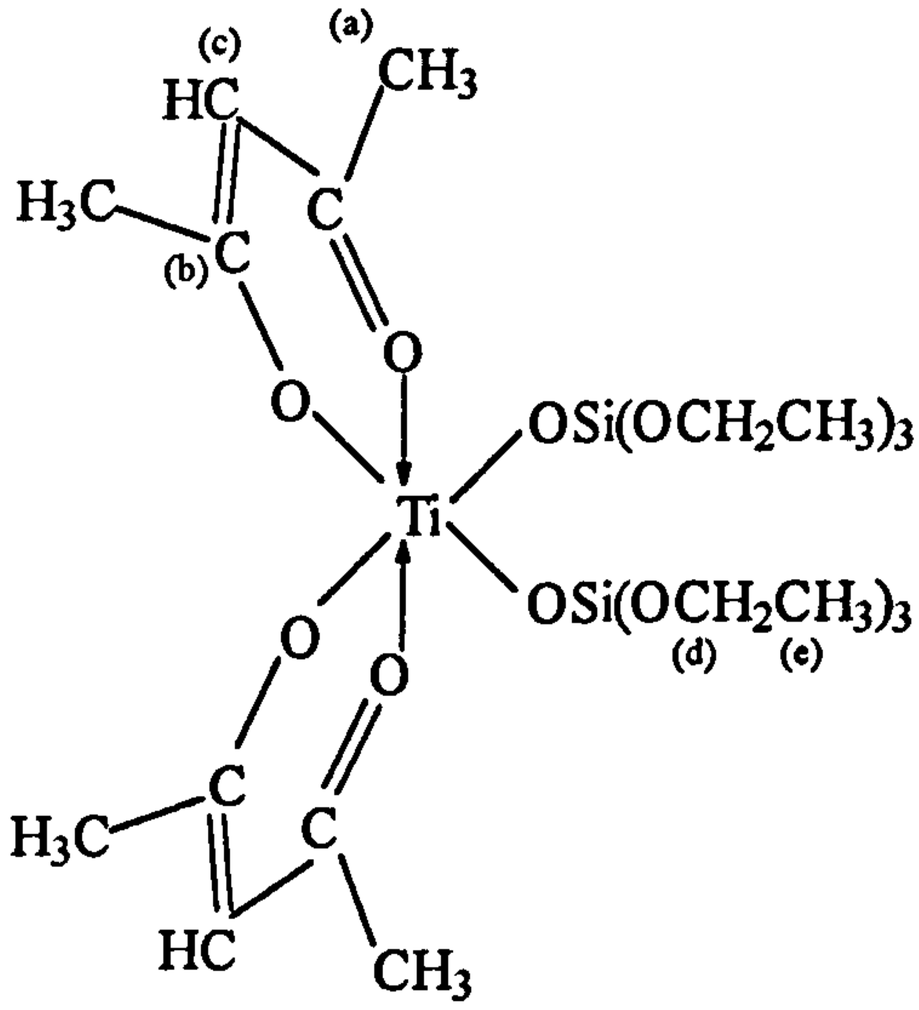

Figure 3.10: ^{13}C NMR Spectra in $CDCl_3$ of Double Alkoxide (a) coupled (NOE); (b) decoupled

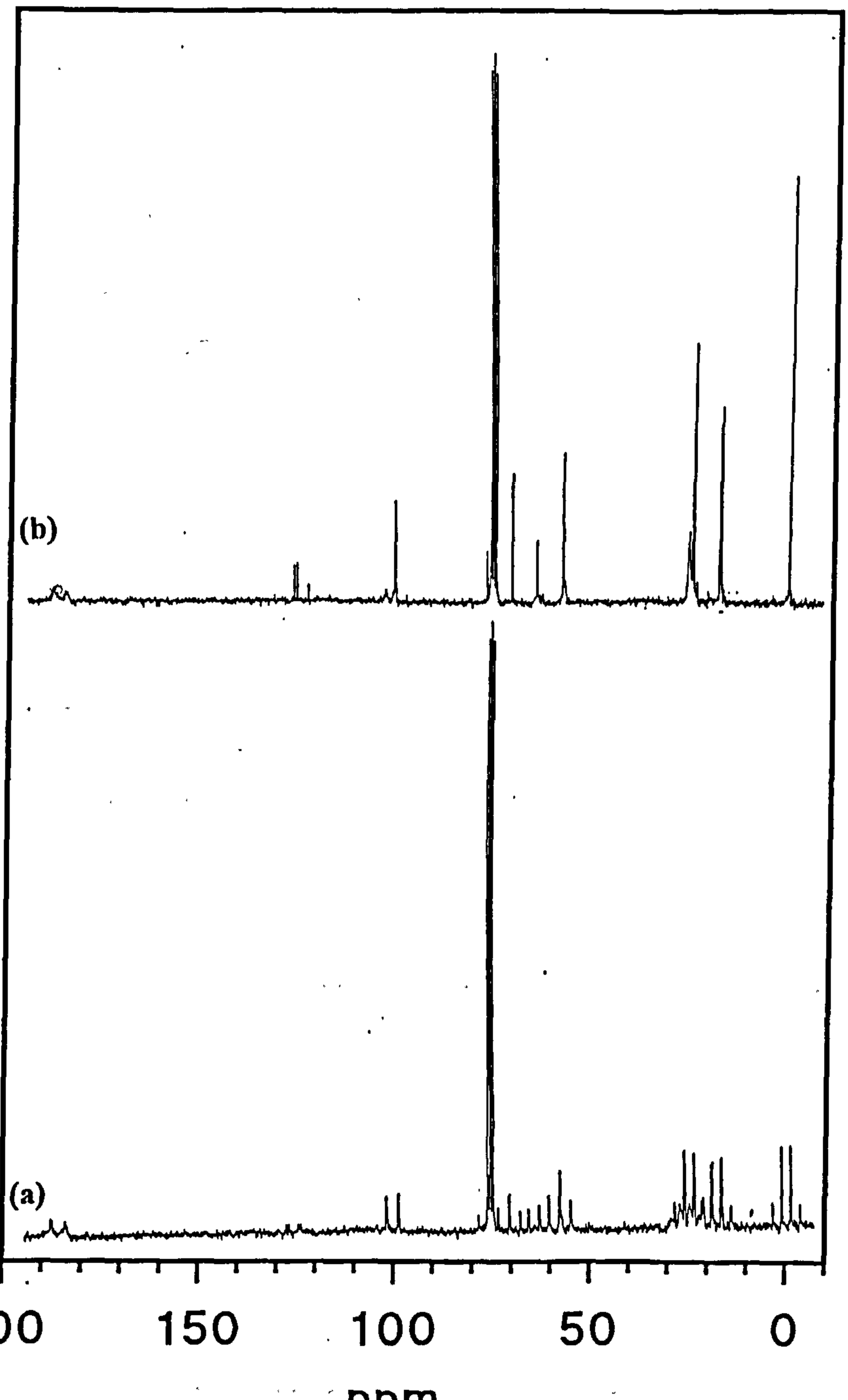

Table 3.3: ^{13}C NMR Assignments for $Ti(acac)_2(OSi(OC_2H_5)_3)_2$

Carbon	Chemical Shift/ ppm
a	25·2
b	approx. 187
c	102·7
d	59
e	18

Three groups of peaks were observed as well as those due to the $Ti(acac)_2(OSi(OC_2H_5)_3)_2$ and have been assigned as below:

(i) the three peaks between 76 and 77ppm arise from the carbon atom in deuterated chloroform.

(ii) the single peak at 78·7ppm is due to -$\underline{C}H(CH_3)_3$ from $Ti(acac)_2(OCH(CH_3)_3)_2$

(iii) peaks between 125 and 137ppm which are due to the various carbon atoms in toluene.

3.4.2.3 ^{29}Si NMR Spectroscopy

The acquisition of ^{29}Si NMR spectra was carried out under the conditions described in section 2.3.3.4. In the resulting spectrum (figure 3.11) the silicon atoms present are attached to a combination of ethoxy and hydroxy groups $(C_2H_5O)_{3-x}(OH)_x\underline{Si}$-O-Si, where x=0,1,2,3. There is also a contribution to the spectrum arising from a combination of dimeric and trimeric siloxane species suggesting that some polymerisation of the hydrolysed siloxane species has already occurred.

Figure 3.11: ^{29}Si NMR Spectrum of Double Alkoxide

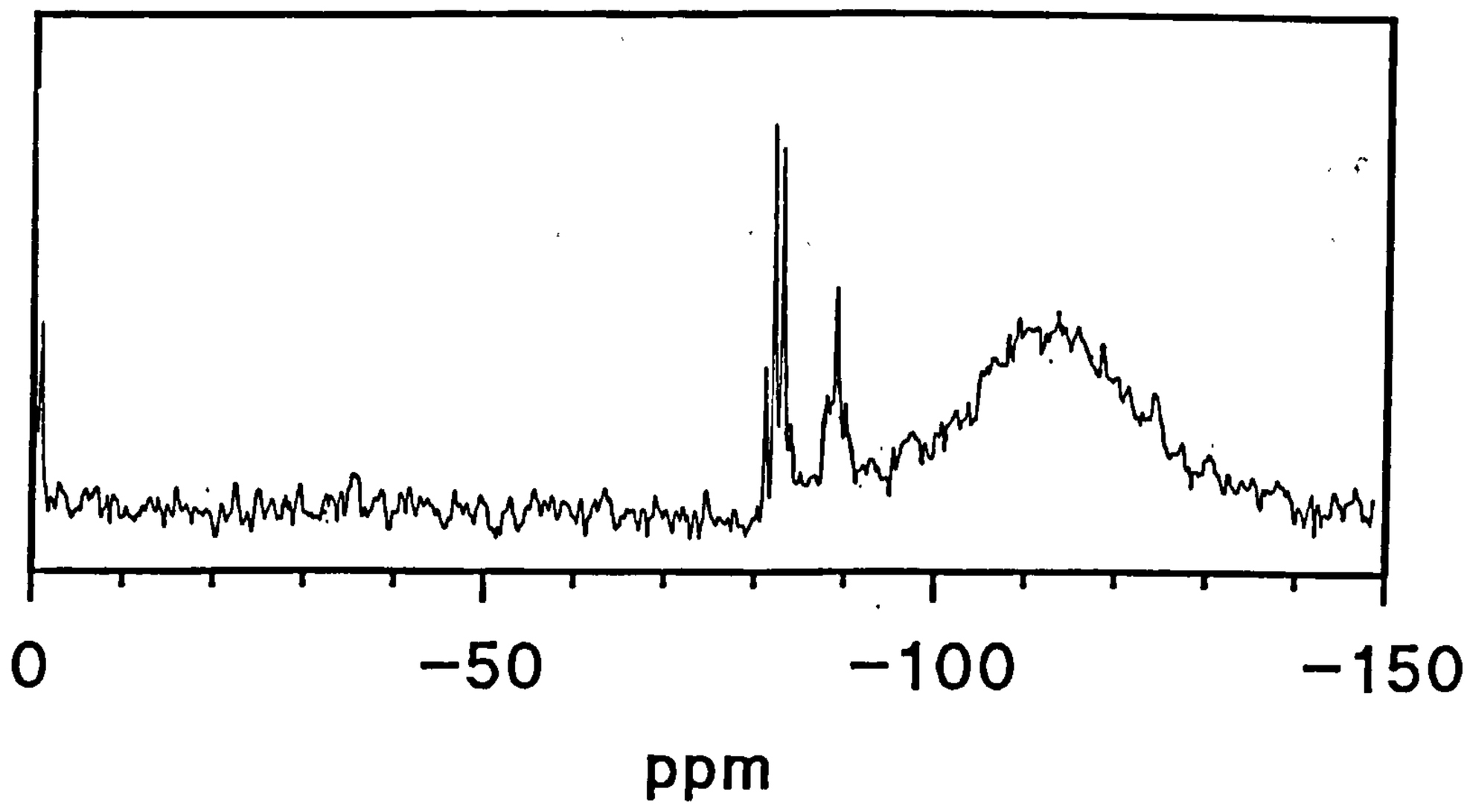

3.4.2.4 Mass Spectrometry

The mass spectrum of the double alkoxide is shown in figure 3.12 and clearly has peaks due to both the bis(acetylacetonato) titanium diisopropoxide and the siloxane groups, indicating the presence of both types of fragment in the final product. The principal fragments detected are detailed below:

m/e 79	$Si(OH)_3^+$	m/e 91	$C_7H_7^+$
m/e 95	$OSi(OH)_3^+$	m/e 107	$Si(OC_2H_5)(OH)_2^+$
m/e 123	$OSi(OC_2H_5)(OH)_2^+$	m/e 135	$Si(OC_2H_5)_2(OH)^+$
m/e 143	$TiOSi(OH)_3^+$	m/e 159	$OTiOSi(OH)_3^+$
m/e 163	$(acac)TiO^+$	m/e 171	$TiOSi(OC_2H_5)(OH)_2^+$
m/e 242	$(acac)TiOSi(OH)_3^+$		
m/e 246	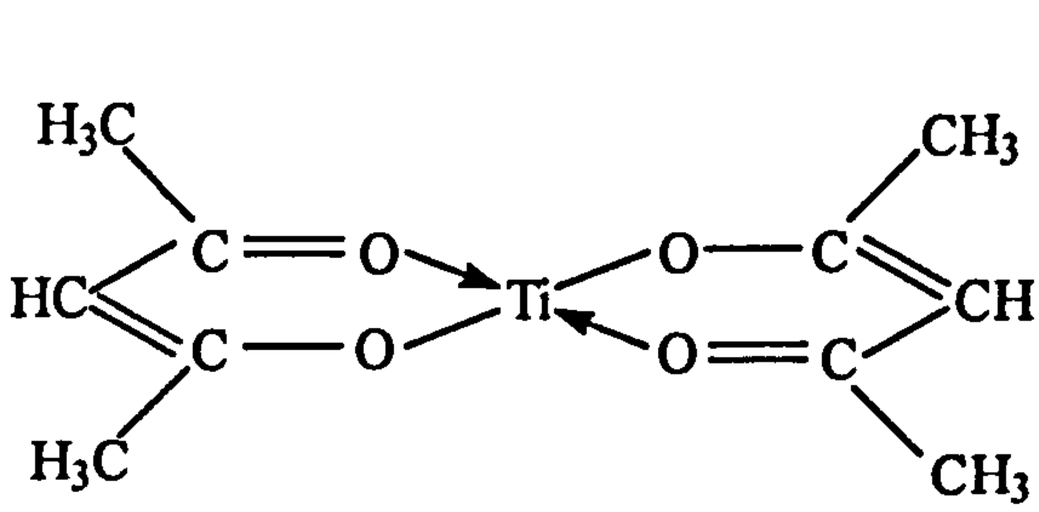		
m/e 263	$Ti(acac)_2(OH)^+$	m/e 280	$Ti(acac)_2(OH)_2^+$
m/e 305	$Ti(acac)_2(O^iPr)^+$	m/e 364	$Ti(acac)_2(O^iPr)_2^+$
m/e 341	$Ti(acac)_2OSi(OH)_3^+$	m/e 324	$Ti(acac)_2OSi(OH)_2^+$
m/e 307	$Ti(acac)_2OSi(OH)^+$	m/e 290	$Ti(acac)_2OSi^+$
m/e 369	$Ti(acac)_2OSi(OC_2H_5)(OH)_2^+$		

The absence of higher molecular weight fragments suggests that the molecular ion readily fragments into more stable species.

Since both silicon and titanium have more than one isotope it was expected that fragments due to Si/Ti species would be observed between m/e 74-80. The most intense of these peaks m/e 76 was calculated to be 10 x intensity of the peak with the second highest intensity. However due to the intensity differences, no isotope pattern was observed for the double alkoxide.

Figure 3.12: Mass Spectrum of Double Alkoxide

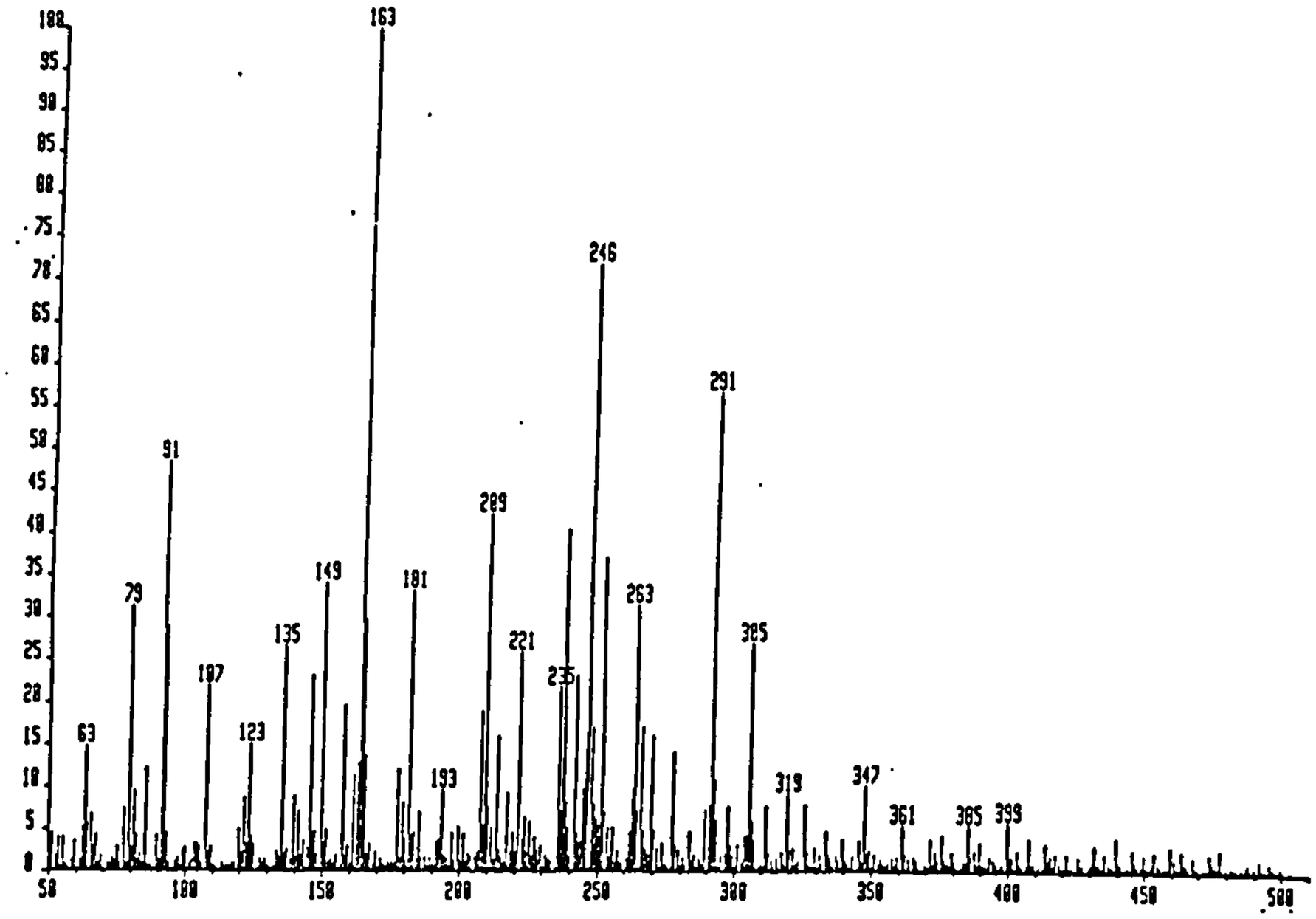

3.4.2.5 Infrared Spectroscopy

The infrared spectrum of a thin film of double alkoxide between sodium chloride plates (see figure 3.13) clearly shows peaks arising from both the acetylacetonate and triethoxy silicate structures. In addition to these bands, an additional band at 1050cm^{-1} was observed due to the antisymmetric stretching vibrations of Si-O-Ti bonds[14].

Figure 3.13: Mid-Infrared Spectrum of Double Alkoxide between NaCl Plates

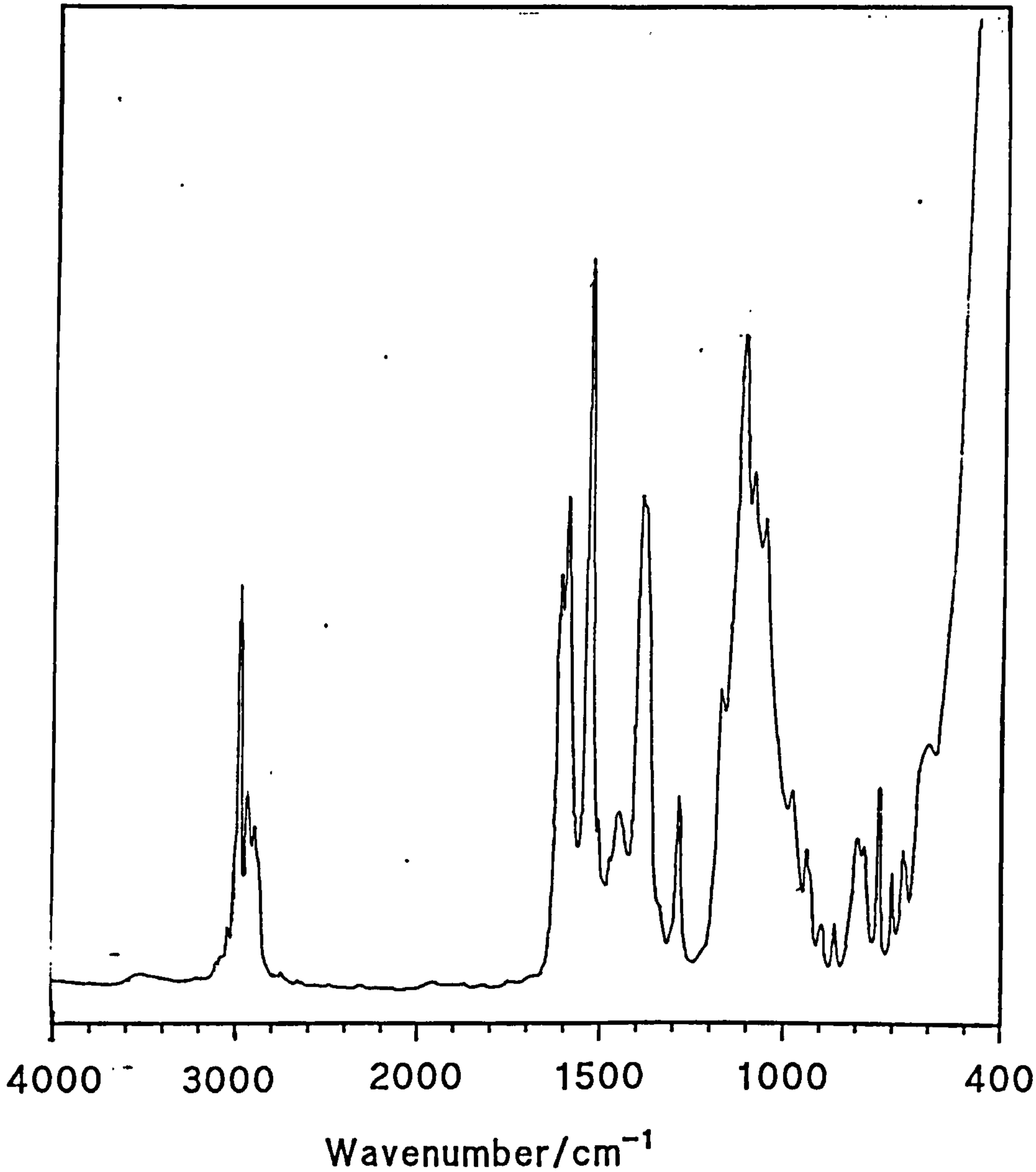

Assignment	Wavenumber/ cm^{-1}
ν_s(C=O)	1606 vs; 1585 vs
ν_{as}(C=C)	1526 vs
$\delta(CH_3)$	1382 s
δ(C-H)	1165 w
ν_{as}(Si-O)	1110 vs
ν_{as}(Si-O)	1083 vs
ν_{as}(Si-O-Ti)	1050 s
ν(Si-O)	971

3.4.2.6 Elemental Analysis

The elemental composition of the double alkoxide $Ti(acac)_2(OSi(OC_2H_5)_3)_2$ has been determined by:

(i) elemental analysis for carbon and hydrogen

(ii) atomic absorption spectroscopy for titanium content

(iii) molybdenum blue method for the determination of silicon.

The theoretical and actual compositions of the double alkoxide are detailed in table 3.4.

Table 3.4: Elemental Composition of $Ti(acac)_2(OSi(OC_2H_5)_3)_2$

Molecular Formula=$TiSi_2O_{12}C_{22}H_{44}$ Molecular Weight=604			
	Elemental Composition/ %		
	Theoretical	**Actual**	**Theoretical Including Toluene contribution**
C	43·7	54·47	48·29
H	7·3	8·265	7·42
Si	9·3	6·3	8·38
Ti	7·95	5·2	7·18
O	31·8		28·73

The elemental analysis revealed some discrepancies between the actual and theoretical values for both the silicon and titanium contents. After distillation some toluene remained in the sample, the effect on the values obtained by elemental analysis can be determined from peak ratios in both the mass and ^1H NMR spectra.

The ratio of the peak intensities in the mass spectrum at m/e 91 (tropylium ion, from toluene) and m/e 246 ($Ti(acac)_2$) [ratio=1·5] is equal to the ratio of the actual and theoretical percentages of titanium [ratio=1·5], determined by elemental analysis. The ratio of the theoretical and actual percentages for silicon [ratio=1·5] is identical to that for titanium. Therefore the presence of toluene accounts for the lower values obtained for the amount of silicon and titanium in the compound. The same results can also be obtained from a comparison of the peak intensities in the ^1H NMR spectrum, arising from toluene and the double alkoxide.

Therefore the molecular formula of the double alkoxide can be calculated as $TiSi_2O_{12}C_{22}H_{44}.(C_6H_5CH_3)_{0·7}$.

3.4.3 Preparation of Monolithic Mixed SiO_2-TiO_2 Gels from the Double Alkoxide

The double alkoxide [$Ti(acac)_2(OSi(OC_2H_5)_3)_2$] and enough tetraethyl orthosilicate [TEOS] to give the theoretical required TiO_2 weight % content, were mixed together for 15 minutes, to obtain an even distribution. To this was rapidly added a mixture of the required amount

of hydrochloric acid (HCl) in ethanol and the resulting solution stirred for 2 hours before being covered with Nesco™ film and left to gel at room temperature. On gelation the resulting gels were slowly dried in an oven at 40°C until no further solvent loss was observed.

Bulk properties of these gels were studied after thermal treatment of monolithic pieces in a muffle furnace at 120, 300, 500, 700, 900 and 1100°C for 12 hours.

3.5 References

1 M. Aizawa, Y. Nasaka and N. Fujii, *J. Non Crystalline Solids* **128** (1991) 77-85

2 W.C. La Course and S. Kim, in *Science of Ceramic Chemical Processing* p.304-310 eds. L.L. Hench and D.R. Ulrich (Wiley, New York, 1986)

3 T. Gunji, Y. Nagao, T. Misono and Y. Abe, *Nippon Seramikkusu Kyokai Gakujutsu Ronbunshi* **99**, 2 (1991) 178-179

4 Y. Abe, T. Gunji, Y. Kimata, M. Kuramata, A. Kasgoz and T. Misono, *J. Non Crystalline Solids* **121** (1990) 21-25

5 T. Gunji, Y. Nagao, T. Misono and Y. Abe, *J. Polymer Sci. Part A: Polymer Chem.* **30** (1992) 371-377

6 T. Gunji, Y. Nagao, T. Misono and Y. Abe, *J. Polymer Sci. Part A: Polymer Chem.* **29** (1991) 941-947

7 Y. Abe, N. Sugimoto, Y. Nagao and T. Misono, *J. Non Crystalline Solids* **104** (1988) 164-169

8 T. Gunji, Y. Nagao, T. Misono and Y. Abe, *J. Non Crystalline Solids* **107** (1989) 149-154

9 D.C. Bradley and C.E. Holloway, *Chem. Comm.* **13** (1965) 284

10 D.C. Bradley and C.E. Holloway, *J. Chem. Soc. (A)* (1969) 282-285

11 C.J. Brinker, K.D. Keefer, D.W. Schaefer, R.A. Assink, B.D. Kay and C.S. Ashley, *J. Non Crystalline Solids* **63** (1984) 45-59

12 R.A. Assink and B.D. Kay, in *Better Ceramics Through Chemistry* p. 301-306 (North-Holland, New York, 1984)

13 R.C. Mehrotra, private communication

14 M.F. Best and R.A. Condrate Sr., *J. Mat. Sci. Lett.* 4(1985) 994-998

Chapter 4: Mixed SiO_2-TiO_2 Gels

4.1 Introduction

The results of an investigation into the effects of reaction conditions, the amount of titania (weight %) present in the gel, the drying conditions (monolith or powder) and thermal treatment on the structure adopted by the gel are presented in this chapter.

4.2 X-ray Diffraction

4.2.1 Introduction

X-ray diffraction has been performed to determine the crystalline nature of mixed silicon-titanium oxides at a number of temperatures (see section 2.4.3). Once crystallinity was observed then the size of the crystallites was calculated using the Scherrer equation (equation 2.12).

4.2.2 Results

4.2.2.1 Powder Samples

The X-ray diffraction pattern obtained from a mixture of anatase:rutile (1:1), it was found that the height of the anatase peak at 24-25° was 1·5 times greater than the height of the corresponding rutile peak at 26-27°, see figure 4.1c. Taking this into account it is possible to compare peak heights and determine whether anatase or rutile is the predominant crystalline phase.

The resulting X-ray diffraction data are presented in table 4.1 and selected traces are shown in figure 4.2 and appendix I.

Table 4.1: X-ray Diffraction Results

TiO_2 (weight %)	Temperature/ °C					
(0·045 mole)	120	300	500	700	900	1100
4·1	X	X	X	X	A	A≈R
4·9	X	X	X	X	A>R	A>R
6·1	X	X	X	X	X	A
6·34	X	X	X	R	A>R	A>R
21·9	R	R	R	R	R	R
(0·030 mole)						
6·34	X	X	R	R	A<R	A<R

X=amorphous; A=anatase (figure 4.1a); R=rutile(figure 4.1b).

Samples with contents of titanium dioxide (weight %) of 4·1 to 6·34 prepared using acid concentrations of 0·045mole HCl, were found to be amorphous at temperatures up to 500°C. On heating to 700°C, the low titania content samples (*ie* those up to 6·1 wt%) remained amorphous. However, a sample containing titania (weight %) of 6·34 prepared

using 0·045 mole HCl, was found to contain some crystalline rutile.

Figure 4.1: X-ray Diffraction Patterns Obtained for (a) anatase; (b) rutile; (c) mixture of anatase:rutile (1:1)

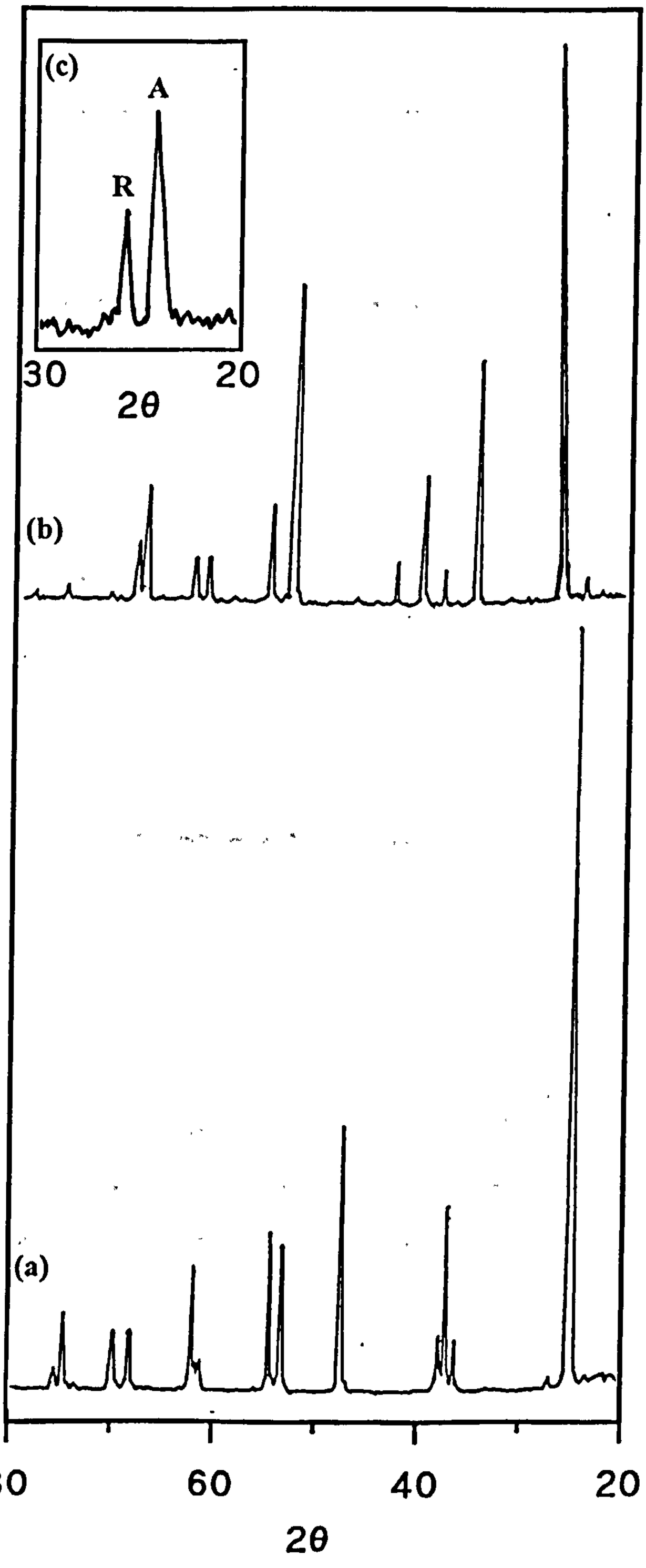

Figure 4.2: X-ray Diffraction Patterns Obtained for a Powder Containing TiO_2=6·34 wt%; HCl=0·045 mole heated at (a) 500°C; (b) 700°C; (c) 900°C; (d) 1100°C
[A=anatase; R=rutile]

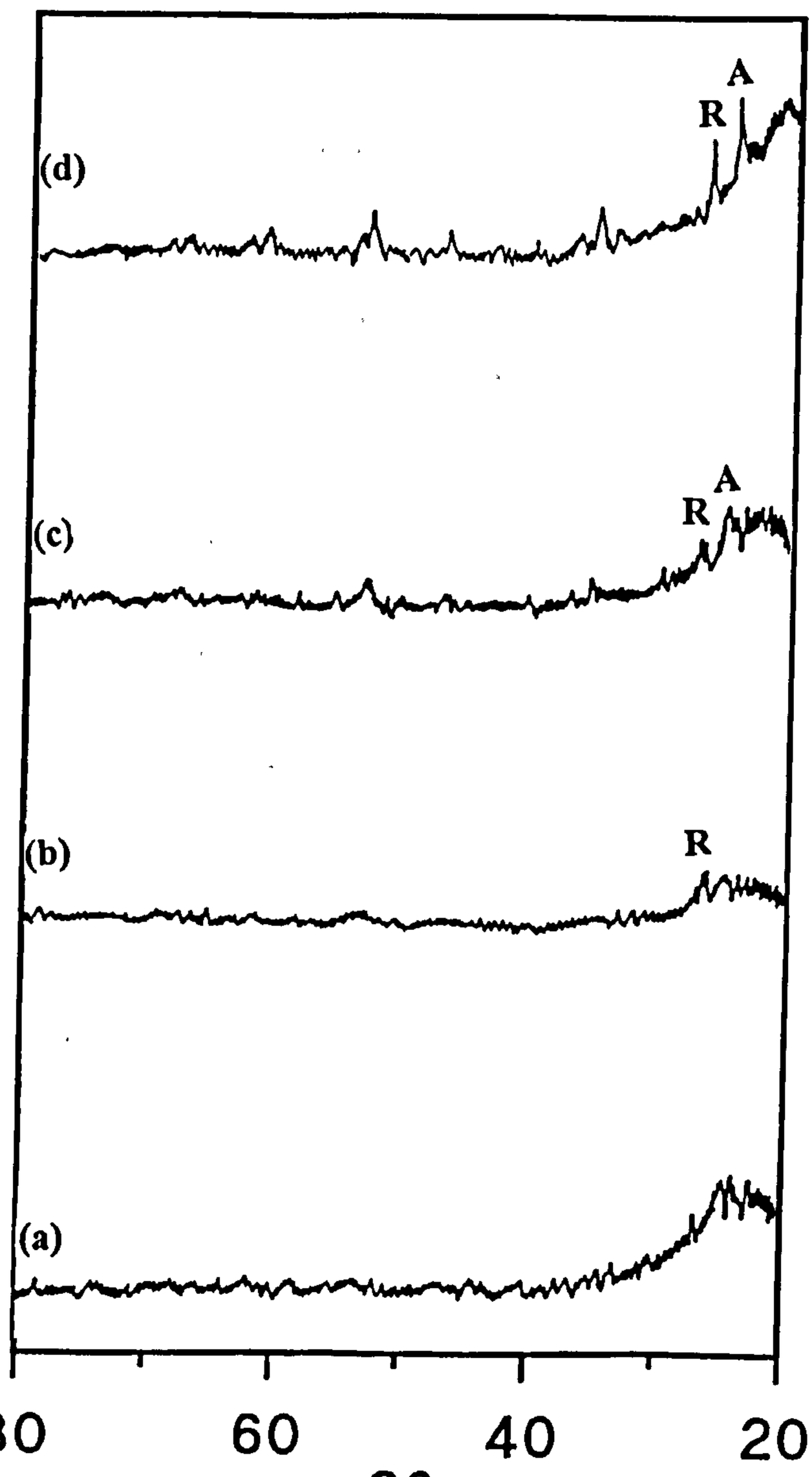

Further heating to 900 and 1100°C resulted in peaks beginning to appear due to anatase, which are more intense than those of rutile. At 900°C all samples except the one containing 6·1 wt% of TiO_2 exhibited some degree of crystallinity the major phase of which is anatase. However, at 1100°C the 6·1 wt% sample began to exhibit signs of crystalline anatase. For the 4·1 wt% titania sample, heating to 900°C resulted in diffraction peaks due to anatase. Further heating to 1100°C enabled diffraction patterns corresponding to an equal amount of rutile to be observed alongside those from anatase. Increasing the titania level to 4·9 wt% and heating to both 900 and 1100°C resulted in diffraction patterns due to both anatase and rutile in the sample, where the pattern from the former is predominant.

However by increasing the titania content to 21·9 wt%, crystallinity due to rutile was exhibited at 120°C. The intensity of rutile peaks and hence the extent of crystallinity was observed to increase with temperature.

For comparison, lowering the concentration of the acid catalyst used to 0·030 mole (HCl) in a sample containing 6·34 wt% titania was investigated. Thermal treatment resulted in crystalline rutile being observed at 500°C and increasing in abundance as the thermal treatment temperature was increased. At temperatures of 900 and 1100°C the formation of anatase was also observed but rutile remained the predominant phase.

Crystallite sizes have been calculated using the Scherrer equation, from the major rutile peak at 26-27° and the major anatase peak at 24-25° (see figure 4.2 and figures in appendix I). These are detailed in table 4.2.

Table 4.2: Average Anatase and Rutile Crystallite Sizes as Calculated from the Rutile and Anatase Peaks at 26-27° and 24-25° 2θ Respectively.

Sample/TiO_2 weight %		**Average Particle Size /nm**	
	°C	**Rutile**	**Anatase**
4·1	900	X	8·1
	1100	10·9	8·1
4·9	900	16·4	5·4
	1100	16·4	16·3
6·1	1100	10·9	8·1
6·34	500	8·1	X
	700	8·1	X
	900	8·2	8·1
	1100	16·3	16·3
21·9	120	5·4	X
	300	5·4	X
	500	5·4	X
	700	8·1	X
	900	16·4	X
	1100	16·4	X
***6·34 (0·030 mole HCl)**	500	4·1	X
	700	10·9	X
	900	8·2	8·1
	1100	10·9	8·1

All contain 0·045 mole HCl except *.

4.2.2.2 Monolithic Gels

Samples with titanium dioxide content of 6·34 weight % (from $Ti(acac)_2(O^iPr)_2$) prepared using different water and acid concentrations as detailed in table 4.3.

Table 4.3: Hydrolysis Acid and Water Contents for Investigated Mixed SiO_2-TiO_2 Gels Containing 6·34 weight % Titania.

Amount (mole)	
HCl	**H_2O**
$2{\cdot}5 \times 10^{-3}$	0·273
5×10^{-3}	0·547
$7{\cdot}5 \times 10^{-3}$	0·821
0·015	0·252
0·030	0·505
0·045	0·757

The gels were dried at 40°C as monoliths until no further moisture loss was observed. Pieces of gel were heated at 1100°C for 16 hours in a muffle furnace, cooled and then ground. X-ray diffraction revealed all six samples to be amorphous after heating at 1100°C.

4.2.3 Discussion

For powdered samples, lowering the concentration of the acid catalyst used to 0·030 mole (HCl) in a sample containing 6·34 wt% titania was investigated. Thermal treatment resulted in crystalline rutile being observed at 500°C and increasing in abundance as the thermal treatment temperature was increased. At temperatures of 900 and 1100°C rutile remained the predominant phase but the formation of anatase was also observed. For the powdered sample containing 0·045 mole (HCl), crystalline rutile was not observed until the thermal treatment temperature was increased to 700°C. In samples prepared using the higher acid concentration, crystalline anatase was found to be the predominant phase. At the stage at which the majority of diffraction peaks become clear enough to accurately measure their positions, the temperature is as high as 900°C. At temperatures as high as this titania should be in the rutile phase[1].

After thermal treatment, the structure of a series of monolithic gels with decreasing acid content was investigated by X-ray diffraction. The X-ray diffraction results revealed all six monolithic samples to be amorphous after heating at 1100°C. Similarly, grinding the monolith before heating to 1100°C for 16 hours results in powders that are amorphous by X-ray diffraction. This is in contrast to the results previously obtained where gels made with 0·045 mole and 0·030 mole HCl and dried as powders, started to exhibit signs of crystallinity at temperatures as low as 500°C.

The effect of temperature on titania has been studied by Lottici *et al*[1] who found that the transformation from anatase to rutile started at temperatures greater than 750°C. However, the diffraction pattern obtained for the 21·9 wt% sample is clearly due to rutile even at 120°C. Therefore, the crystalline nature of titania within the sample must be determined by

the surrounding silica matrix.

Sintering of a gel is a densification process driven by interfacial energy. Material within the sample moves *via* viscous flow or diffusion in a manner which eliminates porosity and hence reduces the solid/vapour interfacial area. In a gel the area is large and hence the driving force is large enough to produce sintering at low temperatures, where the transport processes are relatively slow. However, the kinetics of gel densification are complicated by dehydration and structural relaxation. This results in faster heating permitting complete densification at a lower temperature. In a crystalline gel, densification is hindered by grain growth and phase transformations[2].

The complete drying of gels as monoliths under normal conditions results in xerogels. Xerogels often contain significant amounts of residual organic and hydroxyl (OH) groups bound to the network. If very small pores are present in the gel then such groups can be difficult to remove. The structure of silica gel made from TEOS has been shown to depend on solution pH during both the hydrolysis and condensation reactions[3]. Base-catalysed systems produce gels that are granular in texture and retain less organic material. In this case, acid-catalysis has been used which generally results in a finer, denser structure that is not particulate. Acidic conditions promote the growth of comparatively linear, lightly cross-linked polymers. These polymers entangle early in the growth process, but a gel does not form until a sufficient density of cross-links forms[4,5]. The alkoxide completely hydrolyses[6] before condensation but because of re-esterification during drying, a large number of chemically bound alkoxy groups are found. On heating the gel, alkoxy and hydroxy groups are removed by condensation reactions which result in weight loss. In a monolith, these reactions produce new cross-links and stiffen the structure. Further heating results in densification *via* viscous flow and structural relaxation, as no crystallinity was detected by X-ray diffraction.

When gels are broken up into pieces after gelation and subsequently to powders before being completely dried, some of the cross-links formed at the gel point are broken resulting in re-esterification. Drying in this manner probably results in the formation of regions of inhomogeneity which exist within a non-crystalline polymeric matrix containing chemically bound organics. On heating a powder, some of the alkoxy groups are removed by condensation and form new cross-links within the bulk and some form cross-links with the regions of inhomogeneity.

On initial heating, material moves within these regions of inhomogeneity by diffusion processes from the convex surfaces of the particles to the concave surfaces, and causes the filling of the necks between particles. This results in the region consisting of much larger particles which are more likely to be detected by X-ray diffraction. Further heating causes more growth and hence an increase in the crystallinity observed by X-ray diffraction. This is not possible in a monolith as cross-links are formed within the amorphous bulk.

As the thermal treatment temperature was increased, the intensity and sharpness of the resulting diffraction peaks also increased. This was accompanied by an increase in crystallite size, as calculated from the Scherrer equation. From table 4.2, it can be concluded that increasing the concentration of titania in the gel had no effect on the size of the resulting crystals.

4.3 The Effect of Temperature on the IR Spectra of Silica-Titania Gels of Different Titania Contents

The IR fundamental region (4000-400 cm^{-1}) has been used to investigate any structural changes that may occur within the bulk of the mixed silica-titania gel. as a function of temperature. The gels investigated are detailed in table 4.4.

Table 4.4: Effect of Thermal Treatment on Powdered SiO_2-TiO_2 Samples of Varying TiO_2 content (weight %)

Amount of TiO_2 (weight %)	**Amount of Acid used in Hydrolysis (mole)**
4·1	0·045
4·9	0·045
6·1	0·045
6·34	0·045
6·34	0·030
21·9	0·045

For comparison, the IR spectra of mixes of SiO_2 and TiO_2 at different ratios were recorded to determine any differences in the mid-infrared spectra between mixed oxide gels and oxide mixes.

There are six main vibrational bands of interest in the region studied, the assignments of which are detailed in table 4.5.

Table 4.5: Mid-infrared Absorbance Spectral Assignments

Assignment	Wavenumber/cm^{-1}
ν_{as}(Si-O-Si), LO[7]	1200-1250
ν_{as}(Si-O-Si), TO[7] ν_{as}(Si-O-Ti)*[10]	1024-1100
[a]ν(SiOH, Si-O^-)[8] [b]ν(TiOH, Ti-O^-)[9,12] ν_{as}(Si-O-Ti)**[10]	931-964
ν_s(Si-O-Si)[8]	790-800
ν_s(Ti-O)[9]	550-600
δ(Si-O-Si), o.p[11]	451-468

* Partial contribution to observed band at > 1000°C.

** Major contribution to band at > 1000°C.

[a] ν(SiOH, Si-O^-)=960cm^{-1}; [b] ν(TiOH, Ti-O^-)=970cm^{-1}

4.3.1 Results and Discussion

4.3.1.1 Mixtures of SiO_2 and TiO_2

For titania contents up to 50%, the resulting spectra possess a very weak shoulder at *ca.* 960cm^{-1} attributable to Si-OH stretching vibrations[8]. Increasing the titania content to 50% results in an increase in the intensity of the shoulder at *ca.* 960cm^{-1} as the contributions to the band of the stretching vibrations of Ti-OH[9,12] become more significant, see figure 4.3.

The spectrum of silica only (figure 4.3), reveals a small shoulder at *ca.* 550cm^{-1}. For samples containing titania this has been attributed to symmetric stretching vibrations of Ti-O[9]. As the amount of titania in the mixture was increased, the intensity and width of the shoulder increased.

Therefore, the spectra of oxide mixtures are different from those of mixed oxide gels.

4.3.1.2 Mixed SiO_2-TiO_2 Gels

The spectra obtained for a sample containing a titania concentration of 4·1 weight %, treated at various temperatures (see section 3.1.2) are shown in figure 4.4 (spectra of other titania contents are shown in appendix I).

Figure 4.3: Mid-infrared Spectra of Mixes of Silica and Titania (a) SiO_2; (b) SiO_2:TiO_2=96:4; (c) SiO_2:TiO_2=90:10; (d) SiO_2:TiO_2=50:50; (e) TiO_2 (anatase)

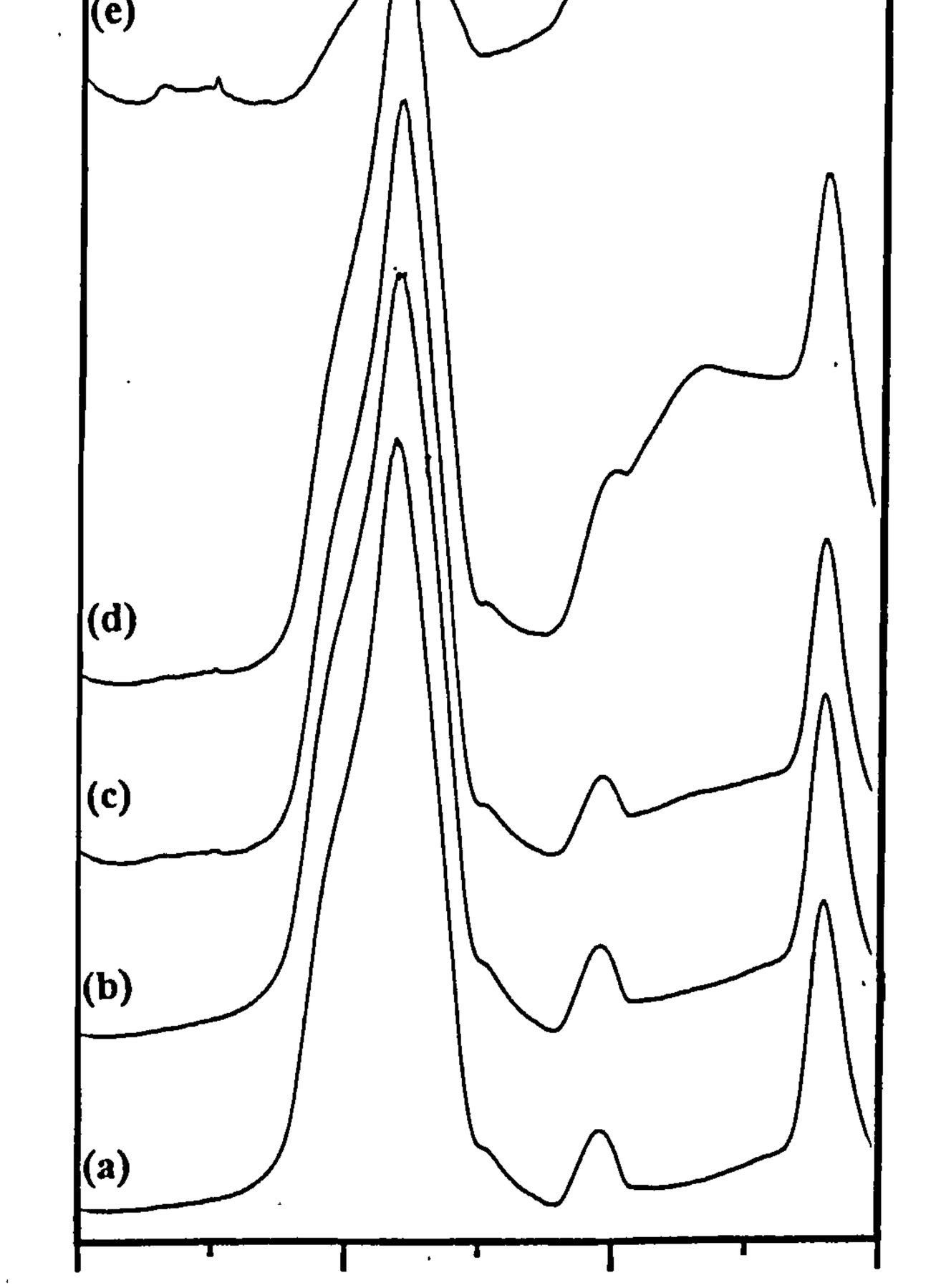

Figure 4.4: Mid-infrared Spectra of a Sample Containing 4·1 weight % Titania Treated at Different Temperatures (a) 120°C; (b) 300°C; (c) 500°C; (d) 700°C; (e) 900°C; (f) 1100°C

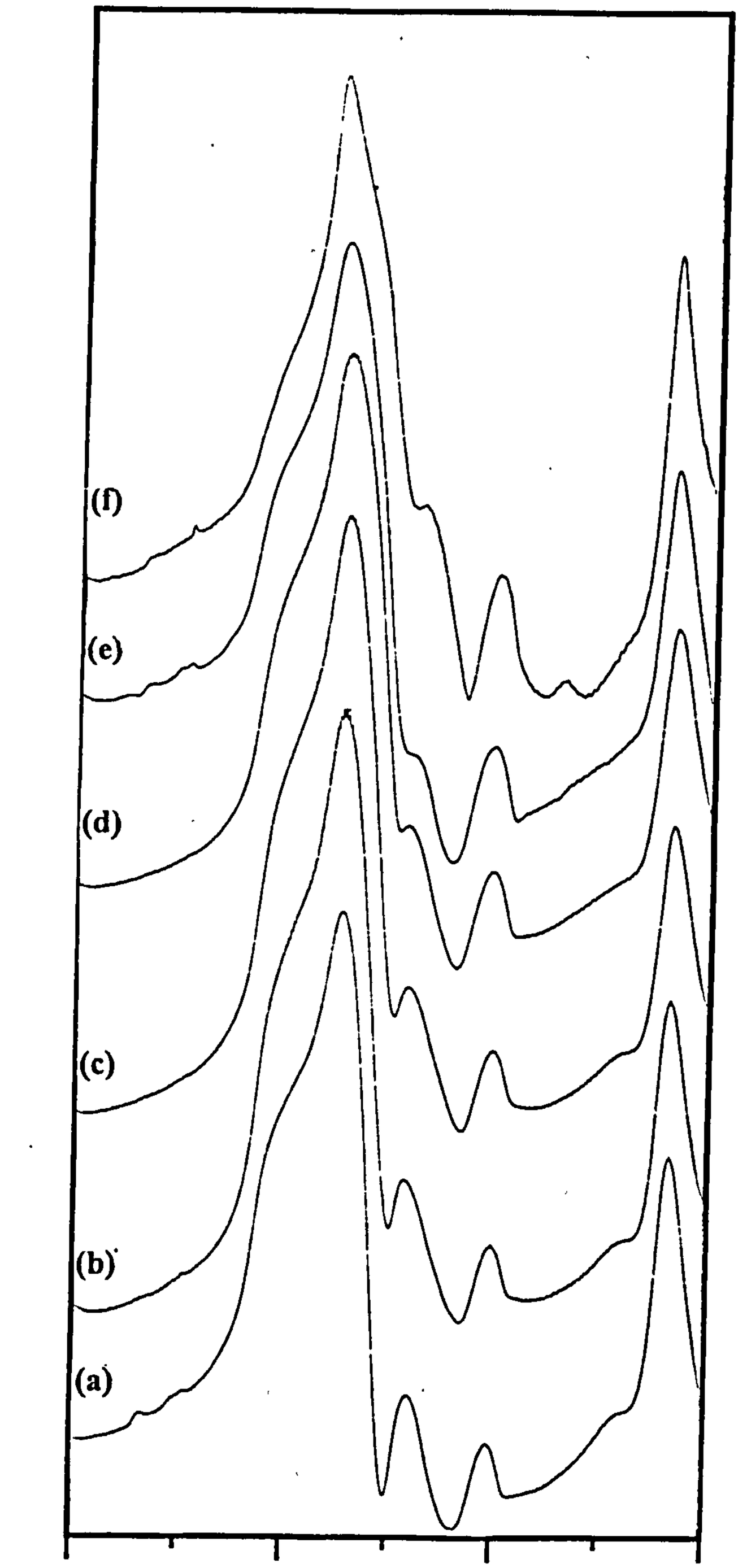

The most intense band, at *ca* 1100 cm^{-1} is asymmetric and possesses a weak shoulder at 1200 cm^{-1} that is present for all treatment temperatures. These two bands are associated with the transverse optical (TO) and longitudinal optical (LO) modes of the antisymmetric Si-O-Si stretching vibration[11] respectively. The band at *ca* 1100 cm^{-1} shifts to a higher wavenumber as the temperature increases above 900°C suggesting a strengthening of the Si-O bonds, this is shown in figure 4.5. Increasing the concentration of titania in the sample has no effect on the position of the transverse optical mode of the antisymmetric stretching band of Si-O-Si. As for the sample containing 4·1 weight % titania, increasing the temperature above 900°C causes the band to shift to a higher wavenumber (see figure 4.5) indicating that the amount of titania present in the sample has no effect on the temperature at which the shift occurs. Therefore, the inclusion of titania in the sample has no effect on the silica matrix.

Figure 4.5: Position of the Antisymmetric O-Si-O Stretching Vibration Near 1100cm^{-1} of Gels Containing Varying Amounts of Titania

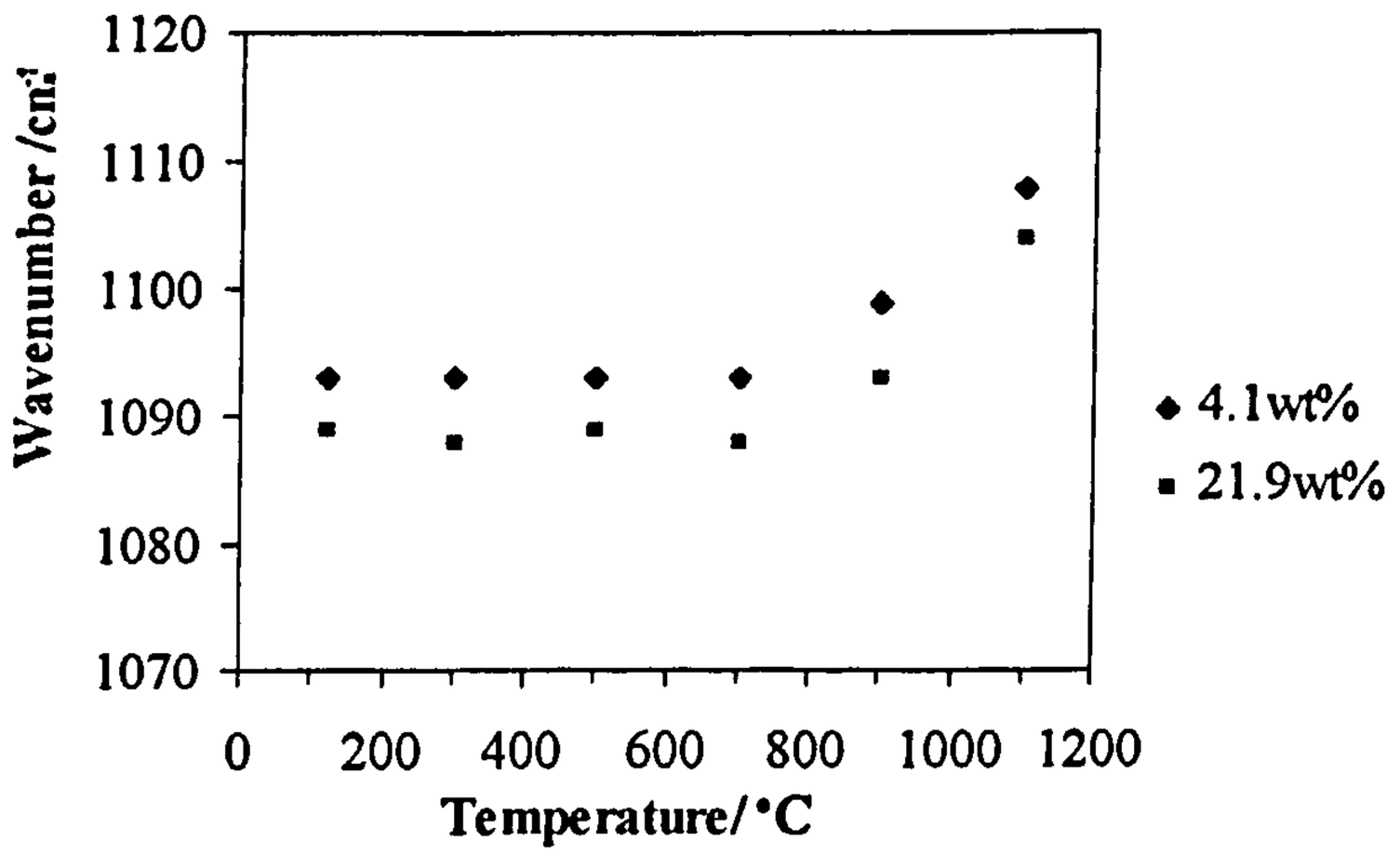

For thermal treatment temperatures less than 1000°C, the band at *ca* 960 cm^{-1} arises from Si-OH and Ti-OH stretching vibrations[8,9,12]. For all titania contents, the relative intensity of the peak decreases as the treatment temperature is increased up to 900°C that is consistent with the removal of SiOH/TiOH from the surface (see figure 4.4 and appendix I). However, increasing the treatment temperature to 1100°C results in an increase in the relative intensity of this band. This is due to an increase in the overall concentration of Si-O-Ti bonds, compared to SiOH/TiOH bonds, that are present in the gel in the latter stages of densification. Therefore, the full incorporation of titanium atoms into the silica framework only occurs at elevated temperatures.

The band at *ca* 800 cm^{-1} has been assigned to a network Si-O-Si symmetric bond stretching vibration[8]. From figure 4.4 and appendix I, it can be seen that increasing the thermal treatment temperature had no effect on either the intensity or position of the peak. Similarly, increasing the concentration of titania in the sample had no effect on either the intensity or

position of the peak. Therefore, the inclusion of titania in the sample has no effect on the behaviour of the silica matrix.

The peak between 466 and 461 cm^{-1} has been assigned to the out-of-plane bending vibrations of network Si-O-Si[11]. For all titania contents, this band remains unchanged in both position and intensity at temperatures up to and including 900°C (see figure 4.4 and appendix I). However, treatment at 1100°C resulted in an increase in the intensity of the peak relative to the 1100 cm^{-1} peak, and a shift to 470 cm^{-1} as the Si-O bonds strengthen. This is consistent with the behaviour of a silica only matrix.

For all titania contents, at temperatures of 900°C and above, there is evidence in the spectra of all the samples studied of a shoulder appearing at *ca* 550 cm^{-1} (see figure 4.4 and appendix I). This band is attributable to the symmetric stretching vibrations of the Ti-O bond[9] and arises due to the formation of titanium dioxide in the bulk gel.

In contrast to the XRD data (see section 4.2) for the titania 21·9 wt% sample which indicates the presence of titania at temperatures as low as 120°C, spectral features from Ti-O bonds are only visible in the IR spectra at temperatures greater than 900°C. The intensity of fundamental vibrational absorption bands is proportional to the square of the rate of change of the dipole moment with respect to the displacement of atoms. When the magnitude of the change in dipole moment is quite small, the absorption bands produced are weak. The small change in dipole moment of the Ti-O bond in comparison with that of the Si-O bond, results in weak bands which increase in intensity as Ti-O and Ti-O-Si bonding become more extensive.

4.3.1.2.1 Fourier Self-Deconvolution

The spectra discussed in section 4.3.1.2, were manipulated using Fourier self-deconvolution and derivative methods. The deconvolution results obtained indicated that the main region of interest was that between 920 and 1250cm^{-1}, from table 4.5 it is obvious that the original spectra usually contain more than one peak within this spectral envelope.

On deconvolution, the band at 1200cm^{-1} previously assigned to the longitudinal optical mode of the antisymmetric Si-O-Si stretching vibration, split into two peaks at *ca* 1230cm^{-1} and *ca* 1170cm^{-1} . The peak at *ca* 1230cm^{-1} can be attributed as the longitudinal optical mode of antisymmetric Si-O-Si stretching vibrations and that at 1170cm^{-1} to antisymmetric stretching vibrations of Si-O within a different framework.

The peak at approximately 1100cm^{-1} split into a further two peaks centred at *ca* 1090cm^{-1} and *ca* 1040cm^{-1}. The higher wavenumber peak has been assigned as the transverse optical mode of antisymmetric Si-O-Si stretching vibrations and the peak at *ca* 1040cm^{-1} to the antisymmetric stretching vibrations of Si-O-Ti bonds.

At thermal treatment temperatures of 900°C or less, the spectra of the sample containing 4·1 weight % titania show that the relative intensity of the band at *ca* 1230cm^{-1} was greater than the band at 1170cm^{-1} (see figure 4.6). Further heating of the sample to 1100°C caused

Figure 4.6: Spectra Resulting from Fourier Self-Deconvolution for a Sample Containing TiO_2=4·1 weight % and Treated at 700°C (a) second derivative; (b) first derivative; (c) Fourier self-deconvolution; (d) original spectrum

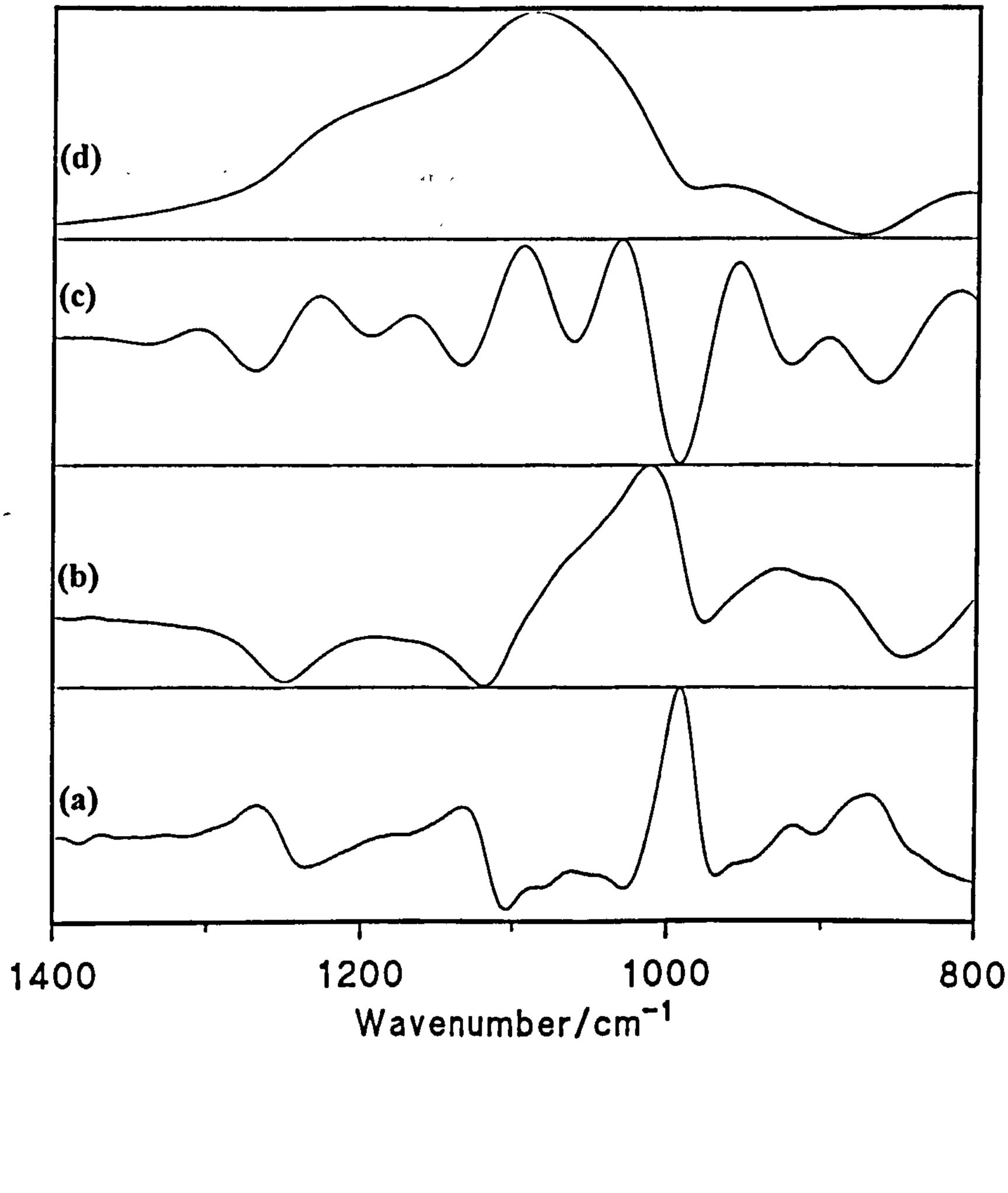

the relative intensity of the band at *ca* 1170cm^{-1} to be greater than that of the band at *ca* 1230cm^{-1}. Varying the amount of titania in the sample had no effect on the resulting spectra. The band at *ca* 1090cm^{-1}, assigned to the transverse optical mode of antisymmetric Si-O-Si stretching vibrations had a lower relative intensity on comparison with the band at *ca* 1040cm^{-1}. Increasing the temperature to 1100°C resulted in the band at *ca* 1090cm^{-1} shifting to a higher wavenumber (1110cm^{-1}) this has been attributed to a strengthening of the Si-O bonds. Increasing the concentration of titania in the sample has no effect on the position of the transverse optical mode of the antisymmetric stretching band of Si-O-Si. Any small variation in the intensity of the bands is difficult to quantify since differences may occur as a result of the data manipulation process.

4.4 The Effect Of Temperature and the Amount of Acid used in Hydrolysis on the Near Infrared (NIR) Spectra of Silica-Titania Gels of Varying Titania Content in the First Overtone Region (1200-2500nm)

4.4.1 Introduction

This section contains data obtained for a series of spectroscopic studies in the first overtone region of the near-infrared (1200-2500nm). Samples were prepared and reflectance spectra recorded as detailed in section 2.2.5. The results obtained have been used to determine how the surface changes with heat-treatment.

The spectral region contains three sets of bands at *ca* 2200, 1900 and 1400nm. These have respectively been assigned as combination stretching vibrations for SiOH with a contribution from the bulk matrix, the combination of stretching and deformation vibrations for water, and the first overtones of the stretching modes of SiOH and H_2O[14,15]. These are detailed more extensively in table 4.6.

Table 4.6: Major NIR spectral features (1200-2500nm)

λ /nm	Assignment	
2200	Combination of H-bonded SiOH	ν_{OH}(SiOH,H)[15]
2190	Combination stretching-bending of Si-O-Si with vicinal free SiO-H	ν_{OH}(SiOH,F)+ν_s(Si-O-Si)[14]
1940	Combination stretching-bending of polymerically H-bonded water	ν_{OH}(H_2O,P)+ν(H_2O,P)[14]
1890	Combination stretching-bending of monomerically H-bonded water and stretching-bending of Si-O-Si with vicinal free Si-OH	ν_{OH}(H_2O,M)+ν(H_2O,M)[15] or 2ν_{OH}(Si-OH,F)+ν_s(Si-O-Si)[14]
1450	First overtone of polymerically H-bonded water	2ν_{OH}(H_2O,P)[16,17]
1400	First overtone H-bonded water on Si-OH	2ν_{OH}(H_2O,M)(SiOH,H)[15,17]
1365	First overtone of vicinal free SiO-H	2ν_{OH}(SiOH,F)[13]

H= H-bonded; M= monomer; P= polymer; F= free

4.4.2 Results and Discussion

The most prominent absorptions occur at 1370 and 2200nm. For low temperature samples, the sharp peak at 1370nm has been assigned as the first overtone of the fundamental OH stretch of free silanol groups[13]. The peak at 2200nm is more perturbed and more intense and has been attributed[14,18] to a combination of the fundamental OH stretching of free silanol groups with the fundamental symmetric stretching of the silica network at 800cm^{-1}. However, this is not the peak assignment given by others[15-17,19,20] who have assigned the 2200nm band to the combination of stretching and deformation vibrations of -SiOH groups. The perturbation imposed on these silanol groups is from the silica network rather than from hydrogen bonding between silanol groups and water molecules, as these absorptions are not affected by the hydration process[14,18]. These results support the assignments of Perry and Li[14,18]. Extended dehydration at room temperature resulted in sharper bands at both 1370 and 2200nm thus implying that the majority of silanol groups are free and little perturbed. However, even after such evacuation, some water molecules remain on the surface trapped within the pores of the gel; the asymmetry of the silanol bands on the high wavelength side being indicative of the presence of hydrogen bonded silanol groups.

The band at 1900nm arises from the combination of stretching and deformation modes of water, and the shoulder at 1400nm from a combination of symmetric and antisymmetric

stretching vibrations. Such absorptions arise from isolated water molecules hydrogen bonded to silanol groups. The presence of shoulders on the major peaks at 1940 and 1450nm is indicative of water molecules hydrogen bonded to one another.

4.4.2.1 Effect of Thermal Treatment on Powders

Generally, from the spectra obtained (see figure 4.7 and appendix I), the overall effect of increasing the thermal treatment temperature is that a systematic reduction in intensity for all three bands occurs corresponding to the dehydroxylation process below:

$$Si-OH+HO-Si \rightarrow Si-O-Si+H_2O$$

Surface dehydroxylation will naturally start at low temperatures with the removal of monomerically bound water (1400nm). From figure 4.7 it can be seen that a significant reduction in the relative number of free SiOH groups is only visible at temperatures of 700°C or greater.

The sharp peak at 1375nm is attributable to both vicinal free OH groups and isolated free OH groups. The free SiOH band, at 1370nm, moves progressively to a lower wavelength by approximately 5nm as the temperature increases to 1100°C. This happens for all titania contents and continues until the band is no longer visible (1100°C), see figure 4.7. Perry and Li[14] found that for silica a similar shift to shorter wavelengths of the maximum to 1362nm occurred at 1000°C. This has been attributed to the consolidation of the silica network and the strengthening and/or shortening of the O-H bond of the silanol group.

The inability of these vicinal and free silanol groups to interact results in the vibrations of the atoms in these groups being unperturbed. Although this band is sharp there is a slight asymmetry on the high wavelength side that appears as a shoulder at approximately 1400nm. This is attributable to the presence of perturbed or hydrogen bonded silanol groups. Both vicinal and geminal silanol groups are possible but cannot be observed separately by IR spectroscopy unlike ^{29}Si nuclear magnetic resonance (NMR) spectroscopy[21-23]. However, Wood *et al*[24] assigned a peak at 1362nm to vicinal free OH groups and a shoulder at 1369nm due to isolated free OH groups. Isolated free OH groups should be much less susceptible to dehydroxylation at low treatment temperatures than vicinal OH groups in which new siloxane bonds are formed inside particles instead of between particles. If Wood *et al*[24] are correct then in the early stages of dehydroxylation, the absorption arising from isolated OH groups should become more pronounced and increase in relative intensity with respect to the band arising from vicinal OH groups. However in these samples a shoulder at 1369nm is not observed at low temperatures, although at 900°C a peak is observed at this wavelength (see figure 4.7). Therefore, the surface of the low temperature gel consists of vicinal OH groups, whereas that of the high temperature gel consists of free silanol groups.

Figure 4.7: Effect of Thermal Treatment Temperature on the Near Infrared (NIR) Spectra of a Sample Containing TiO_2=6·34 weight % [Hydrolysis Acid =0·045 mole]
(a) 120°C; (b) 300°C; (c) 500°C; (d) 700°C; (e) 900°C; (f) 1100°C

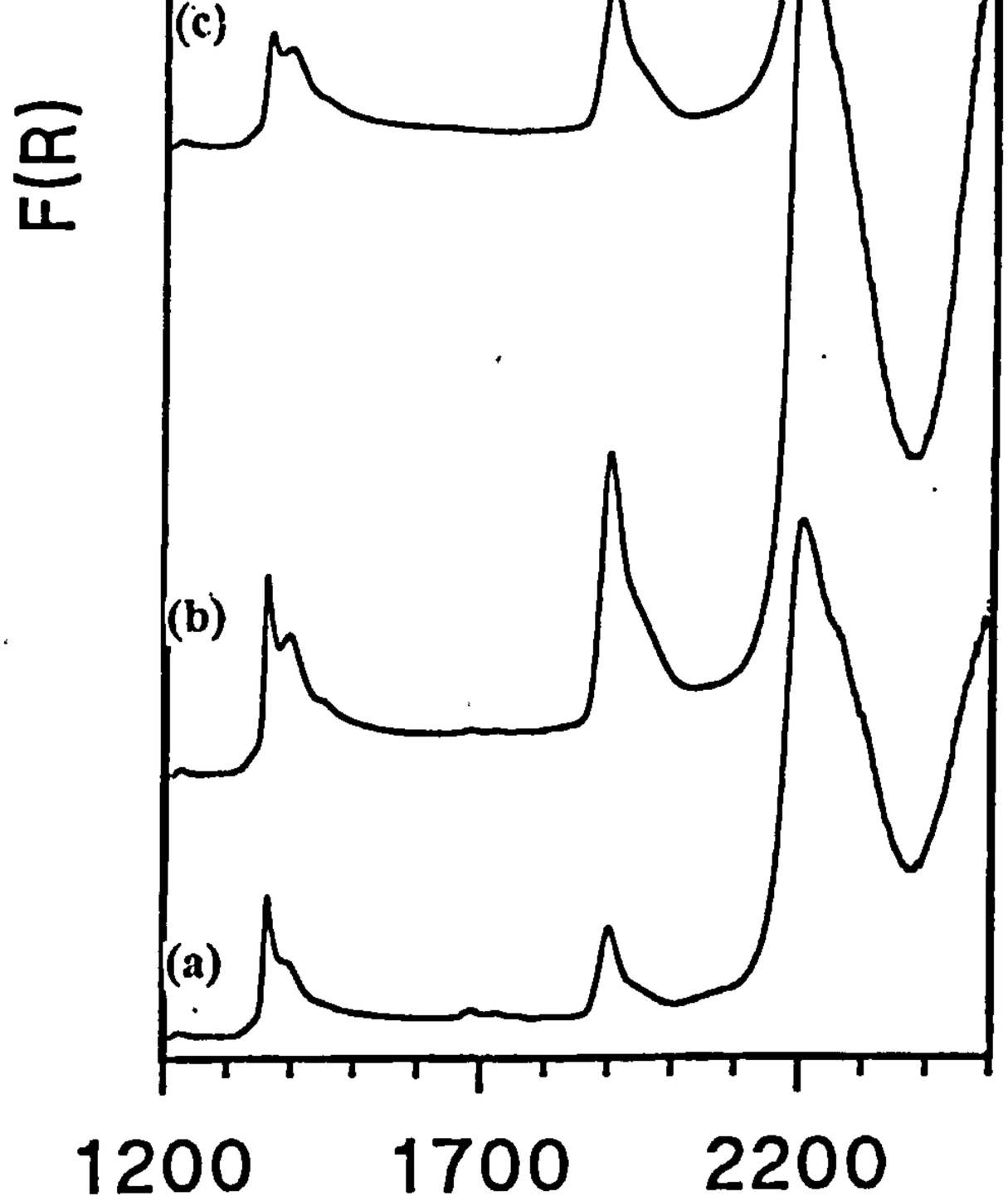

* All spectra plotted on the same reflectance scale.

As the treatment temperature of the gel was increased above 700°C then the peak at 2200nm began to decrease in intensity (like the band at 1375nm) until at 1100°C it was no longer detectable. Heating also resulted in a decrease in the asymmetry of the peak on the high wavelength side, corresponding to the observed loss of hydrogen bonded species at 1400nm.

From these results it appears that very little dehydroxylation occurs at temperatures up to 500°C and only becomes significant at temperatures greater than 700°C.

4.4.2.2 Variation of Titania Content

As the amount of titania (weight %) in the sample was increased then comparatively fewer free SiOH groups (1375nm) were observed with respect to hydrogen bonded species (1400nm). The spectrum of a silica only gel was found to contain much narrower peaks and compared to the silica-titania gels a more intense band due to free SiOH groups at 1375nm. This is indicative of there being fewer hydrogen bonded species and therefore more free SiOH groups on the surface of the gel.

The corresponding band near 2200nm which is attributable to silanol groups, is stronger and broader than the corresponding first overtone band at 1375nm. However, the high wavelength asymmetry due to perturbed species on the surface is still present. This combination band increases in intensity and develops a more apparent shoulder on the high wavelength side of the band as the amount of titania in the sample increases. This is indicative of an overall decrease in free -SiOH groups and a corresponding increase in hydrogen bonded species. Comparison of spectra arising from TiO_2 with those from mixed Si/Ti oxides have peaks in the same positions; although those due to TiO_2 *i.e.* Ti-OH are very weak due to the small change in dipole moment of the Ti-O bond (see section 4.3.1.2). Hence, at these levels it is not possible to determine the overall effect due to Ti-OH.

4.4.2.3 Variation of the Amount of Acid used in Hydrolysis

As the amount of hydrochloric acid used for the hydrolysis decreases, there was a corresponding decrease in the number of free -SiOH groups (1375nm), and hence an increase in the number of hydrogen bonded species(1400nm), see figure 4.8.

The band near 2200nm which is attributable to silanol groups, is stronger and broader than the corresponding first overtone band at 1375nm. However, high wavelength asymmetry due to perturbed species on the surface is still observed. This combination band increases in intensity and develops a more apparent shoulder on the high wavelength side of the band as the amount of acid used in the hydrolysis reaction decreases. This is indicative of an overall decrease in free -SiOH groups and a corresponding increase in hydrogen bonded species. (see figure 4.8)

For silica only gels, decreasing the amount of acid used in the hydrolysis reaction resulted in a similar increase in hydrogen bonded species. On comparison of silica and silica-titania gels the observed increase in hydrogen bonded species was greater in the samples with titania

present than for silica only. This confirms previous conclusions that the presence of titanium as oxides and mixed oxides results in there being more hydrogen bonded silicon containing species on the surface of the gel.

Figure 4.8: Effect of Varying the Amount of Acid used in the Hydrolysis Reaction on the Near Infrared Spectra of a Sample Containing TiO_2=6·34 weight % (a) 0·045 mole; (b) 0·030 mole; (c) 0·015 mole; (d) 7·5 x10^{-3} mole; (e) 5 x10^{-3} mole; (f) 2·5 x10^{-3} mole

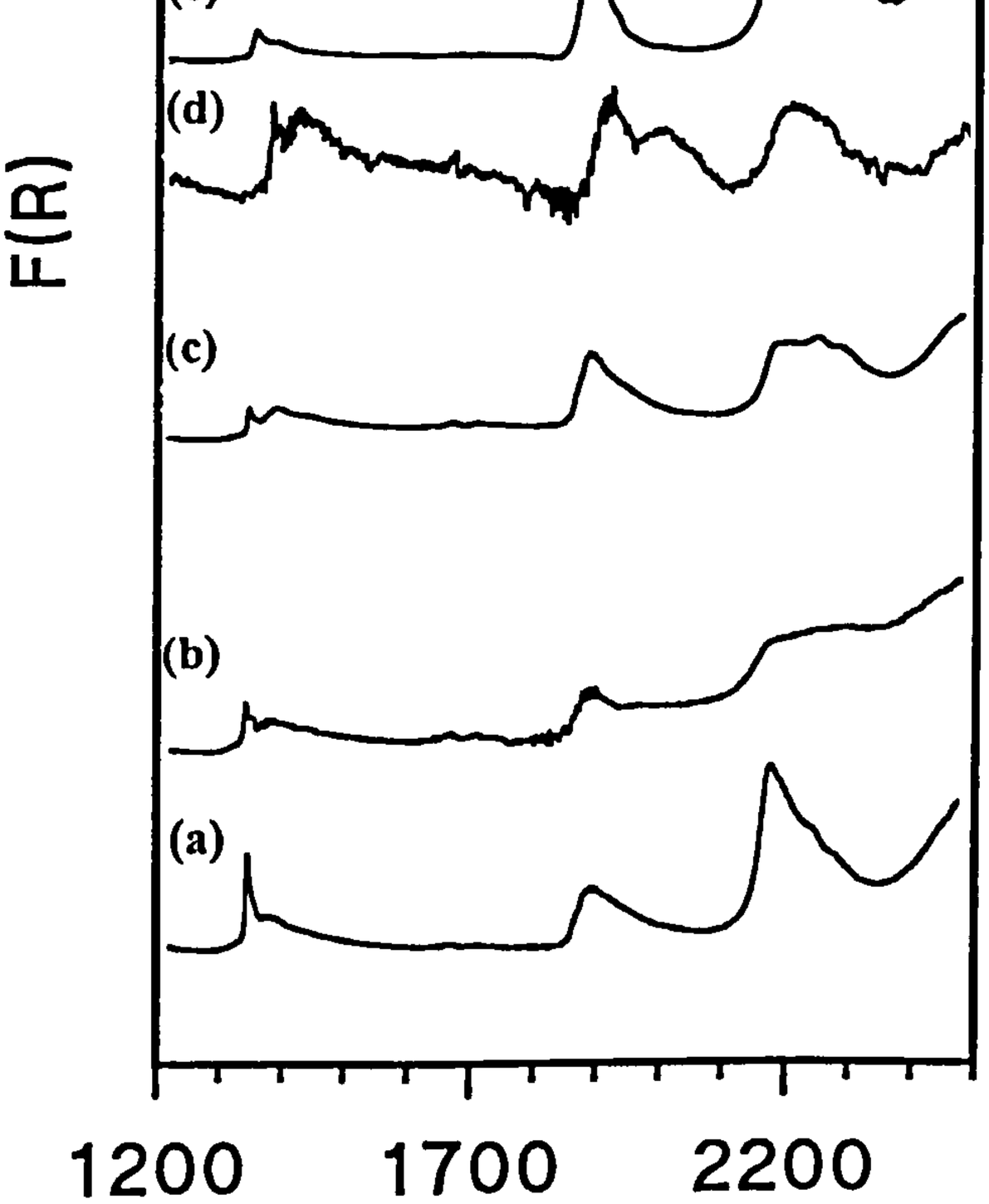

4.5 A NIR Investigation of the Interaction of Water with Silica/Titania Powders

4.5.1 Introduction

This section contains information on a series of reflectance studies that have been performed in the near-infrared region from 900-2500nm. The results obtained have been used to determine how water molecules interact with the surfaces of gels and the effect of thermal treatment on the activity of silanol groups in promoting surface hydration. The samples investigated contained varying amounts of titania and had been treated at temperatures of 120°C and 900°C.

Samples were prepared and scanned over the region detailed in section 2.2.5. Rehydration experiments were performed by leaving the sample in the instrument and scanning once every fifteen minutes. It was found that the instrument had to be kept in completely artificial light as sunlight warming the instrument stimulated the loss of water from the surface of the gel.

Reflectance spectra were obtained from a variety of silica/titania samples with different titania contents and varying thermal treatment, under conditions of increasing hydration. The wavelength region 1200-2500nm contains three principal groups of absorption bands at *ca* 2200nm, 1900nm and 1400nm. The second wavelength region of study, 900-1350nm, is a reduced replica of the first, with variations in anharmonicity constants for the vibrations involved, and also contains three groups of bands at *ca* 1200nm, 1100nm and 900nm.

Table 4.7: NIR Assignments for Water and SiOH Species on Gel Surface[18]

Adsorbed H_2O species on gel	**Ice**	**Liquid H_2O**		**Assignment**	**-SiOH species on gel surface**	**Assignment**
		ambient	**near b.p.**			
λ/nm	**λ/nm**	**λ/nm**	**λ/nm**		**λ/nm**	
1950				$\nu_{OH}+\delta_{HOH}(S'_1,S'_2)$	2270	$\nu_{OH}+\nu(SiOSi)(H)$
1892				$\nu_{OH}+\delta_{HOH}(S'_0)''$	2192	$\nu_{OH}+\nu_s(SiOSi)(F)$
1455				$2\nu_{OH}(S'_1, S'_2)$	1400	$2\nu_{OH}(H)^a$
1400				$2\nu_{OH}(S'_0)$	1365	$2\nu_{OH}(F)^a$
1245	1250[b]			$2\nu_{OH}+\delta_{HOH}(S'_2)$	1245	$2\nu_{OH}+\nu_s(SiOSi)(H)$
1188		1200[b]		$2\nu_{OH}+\delta_{HOH}(S'_1)$	1230	$2\nu_{OH}+\nu_s(SiOSi)(F)$
1142			1160[b]	$2\nu_{OH}+\delta_{HOH}(S'_0)$	950	$3\nu_{OH}(H)$
958	1025[c]	980[c]	967[b]	$3\nu_{OH}(S'_1, S'_2)$	930	$3\nu_{OH}(F)$
950				$3\nu_{OH}(S'_0)$		

$S'_0(S_0)$= monomeric; $S'_1(S_1)$= partially hydrogen bonded; $S'_2(S_2)$= fully hydrogen bonded; F= free; H= hydrogen bonded. [a] Ref. 15; [b] Ref. 13; [c] Ref. 25.

4.5.2 Results and Discussion

4.5.2.1 Mixed Silica/Titania Gels at 120°C

4.5.2.1.1 The Effect of Hydration on Silanol Derived Bands

After prolonged dehydration *in vacuo* at room temperature the reflectance spectra at t=0 over the regions 900-1350 and 1200-2500nm contain seven well-defined bands (see figures 4.9 to 4.12). At t=0 the bands due to free -SiOH groups are sharp, but they rapidly reduce in intensity as hydration proceeds; this is especially noticeable for the peak at 1370nm, the combination band at *ca* 2200nm reducing a much lower amount by comparison. Although this band remains unresolved, it shifts by approximately 40nm after 16 hours exposure to the atmosphere for all the titania contents studied. This shift towards a higher wavelength is indicative of a decrease in free -SiOH groups and a corresponding increase in hydrogen bonded species. A range of such surface monohydroxylated hydrogen bonded species are detailed in figure 4.13.

Figure 4.9: First Overtone and Combination Region (1200-2500nm) Near Infrared Spectra of a Dehydrated Sample Containing TiO_2=4·1 wt% Heated to 120°C and Exposed to the Atmosphere for Various Times.
(a) 0; (b) 0·5 hour; (c) 1 hour; (d) 2 hours; (e) 14 hours.

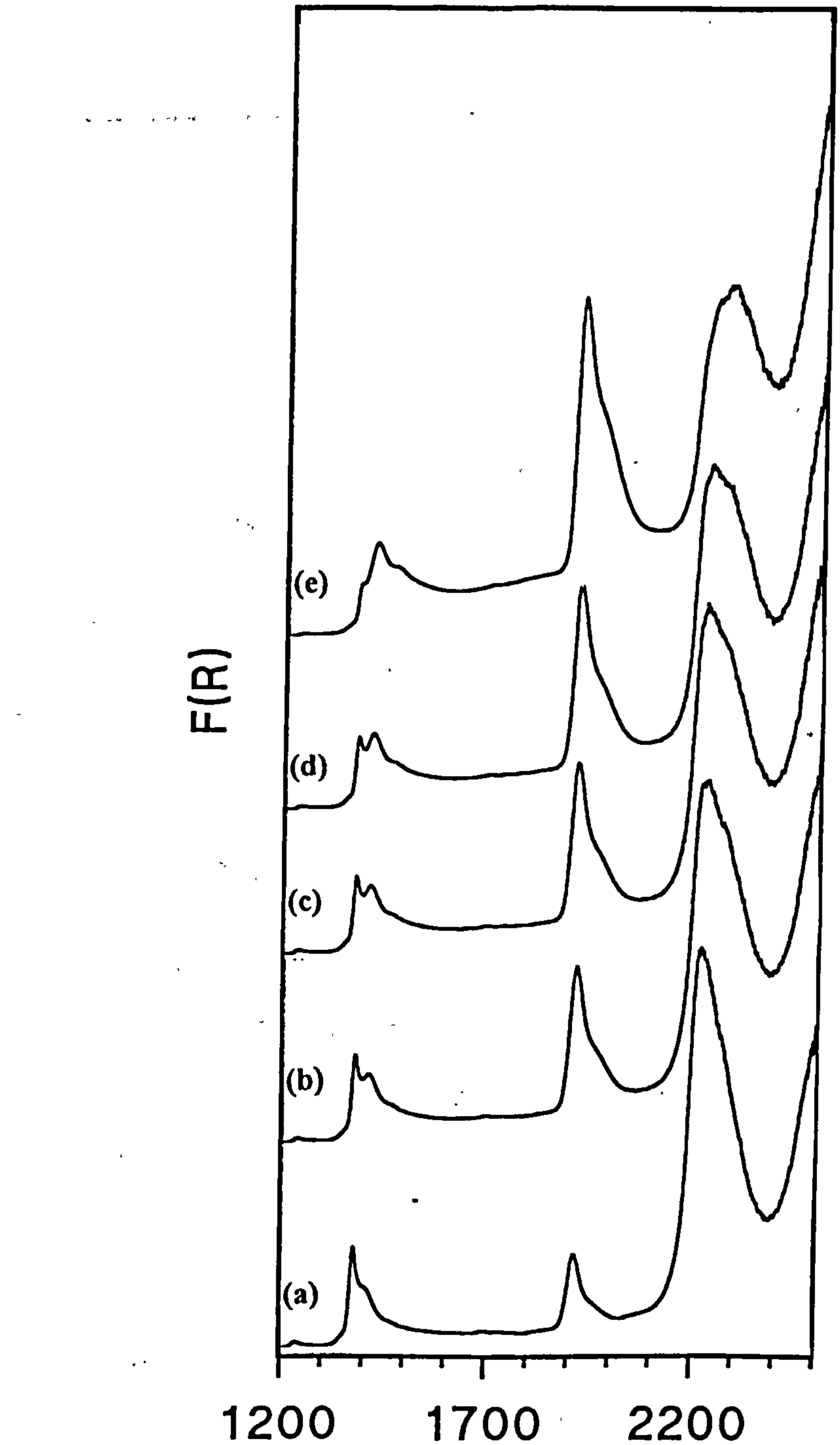

Figure 4.10: Second Overtone Region (900-1350nm) Near Infrared Spectra of a Dehydrated Sample Containing TiO_2=4·1 wt% Heated to 120°C and Exposed to the Atmosphere for Various Times.
(a) 0; (b) 0·5 hour; (c) 1 hour; (d) 2 hours; (e) 14 hours.

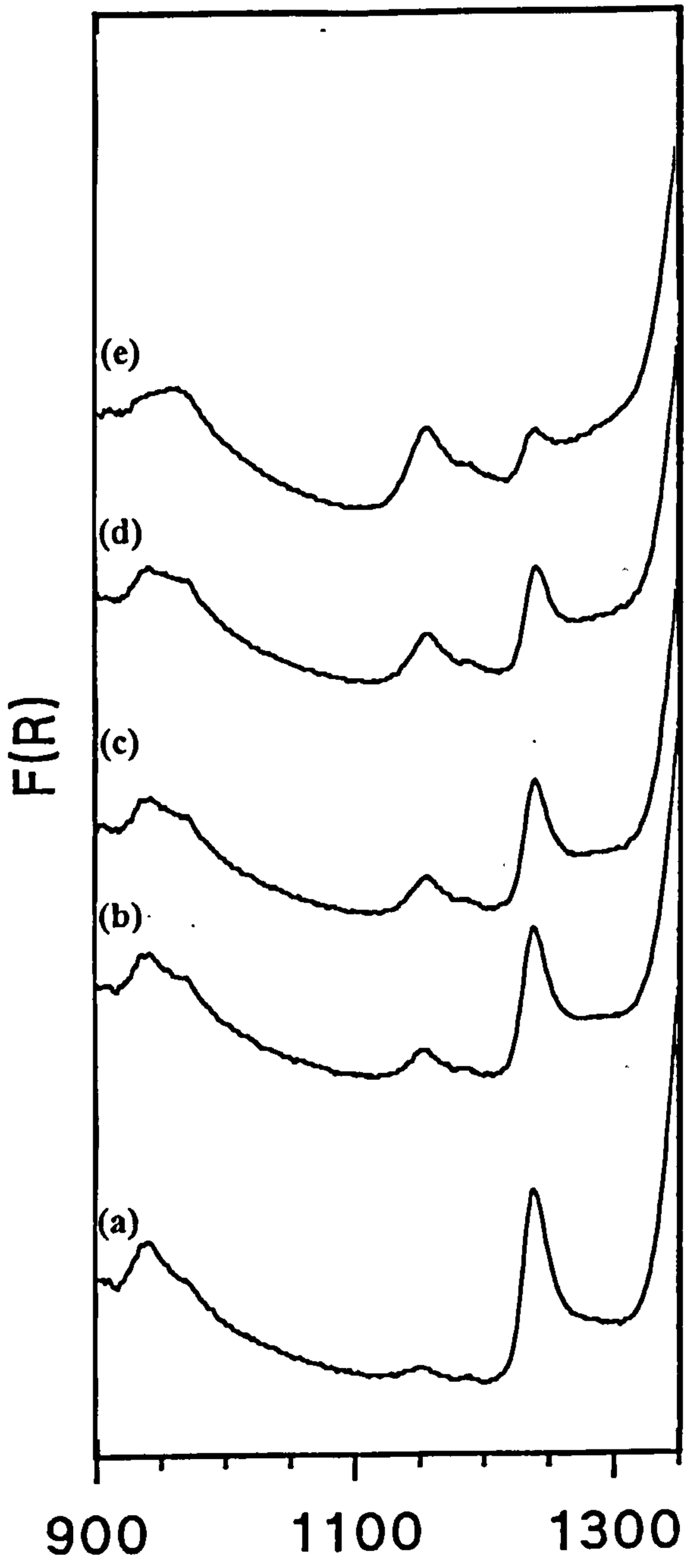

Figure 4.11: First Overtone and Combination Region (1200-2500nm) Near Infrared Spectra of a Dehydrated Sample Containing TiO_2=21·9 wt% Heated to 120°C and Exposed to the Atmosphere for Various Times.
(a) 0; (b) 0·5 hour; (c) 1 hour; (d) 2 hours; (e) 14 hours.

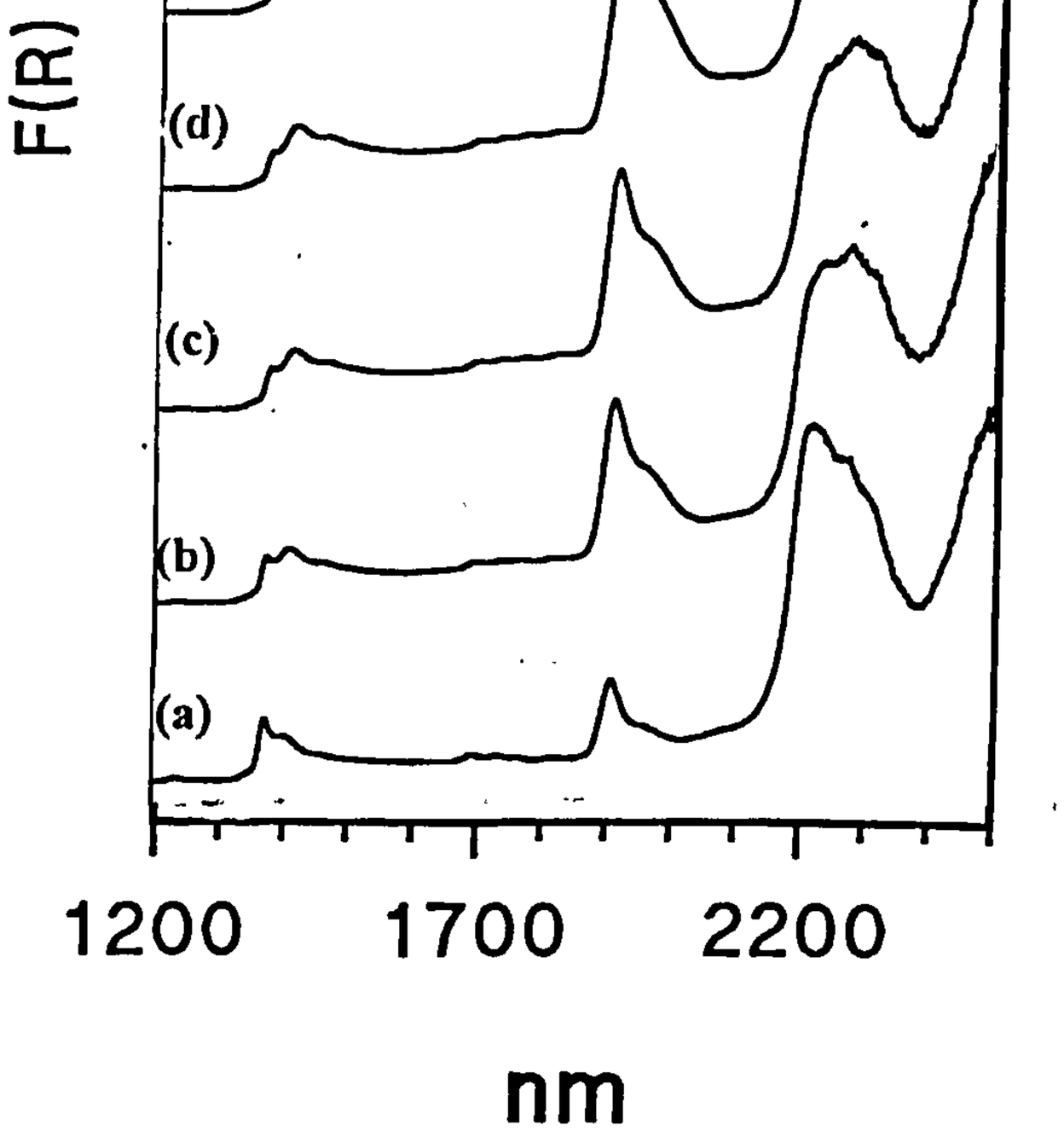

Figure 4.12: Second Overtone Region (900-1350nm) Near Infrared Spectra of a Dehydrated Sample Containing TiO_2=21·9 wt% Heated to 120°C and Exposed to the Atmosphere for Various Times.
(a) 0; (b) 0·5 hour; (c) 1 hour; (d) 2 hours; (e) 14 hours.

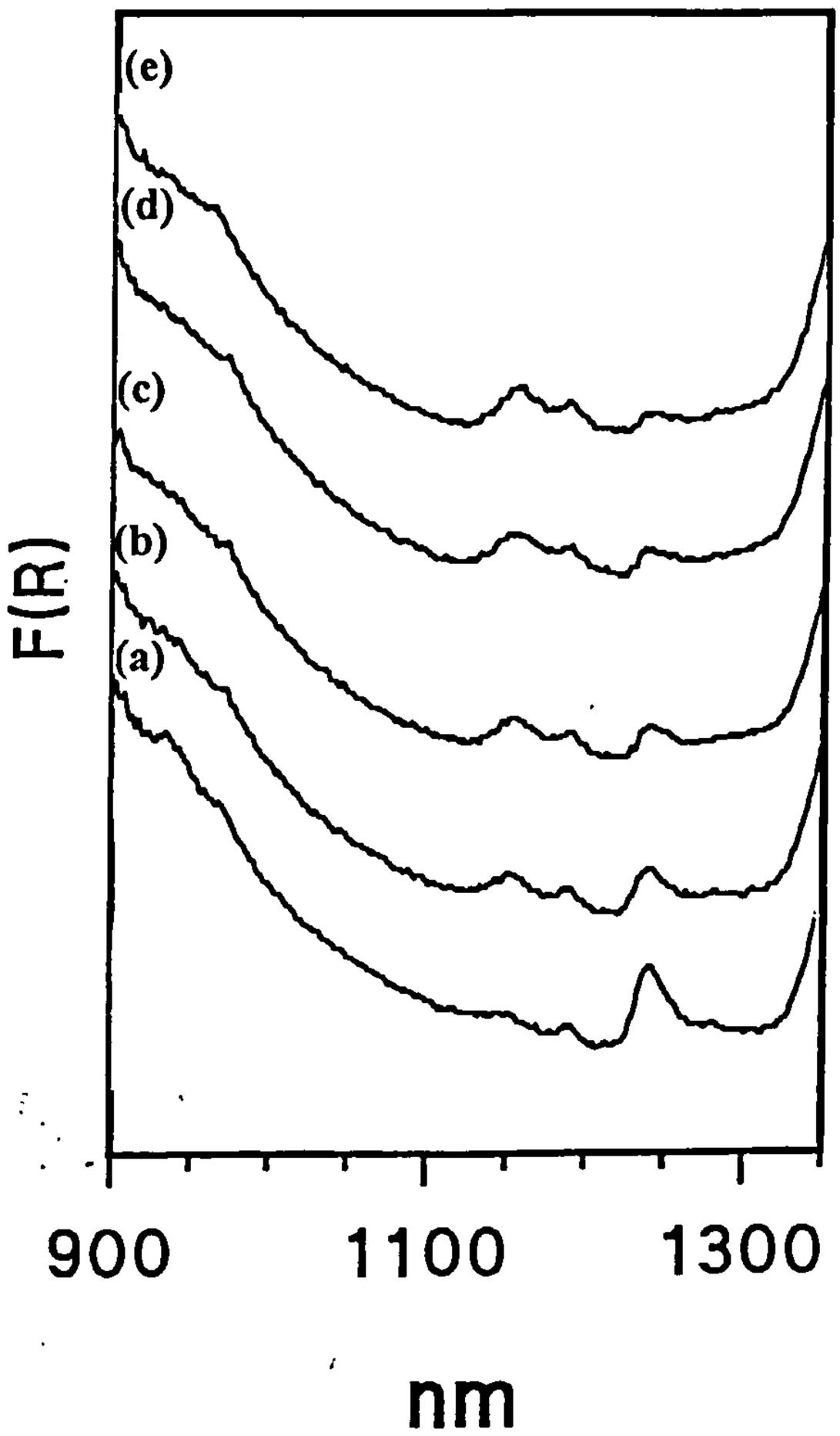

Figure 4.13 : Types of Surface Silanol Species and their Interactions with H_2O molecules[18]

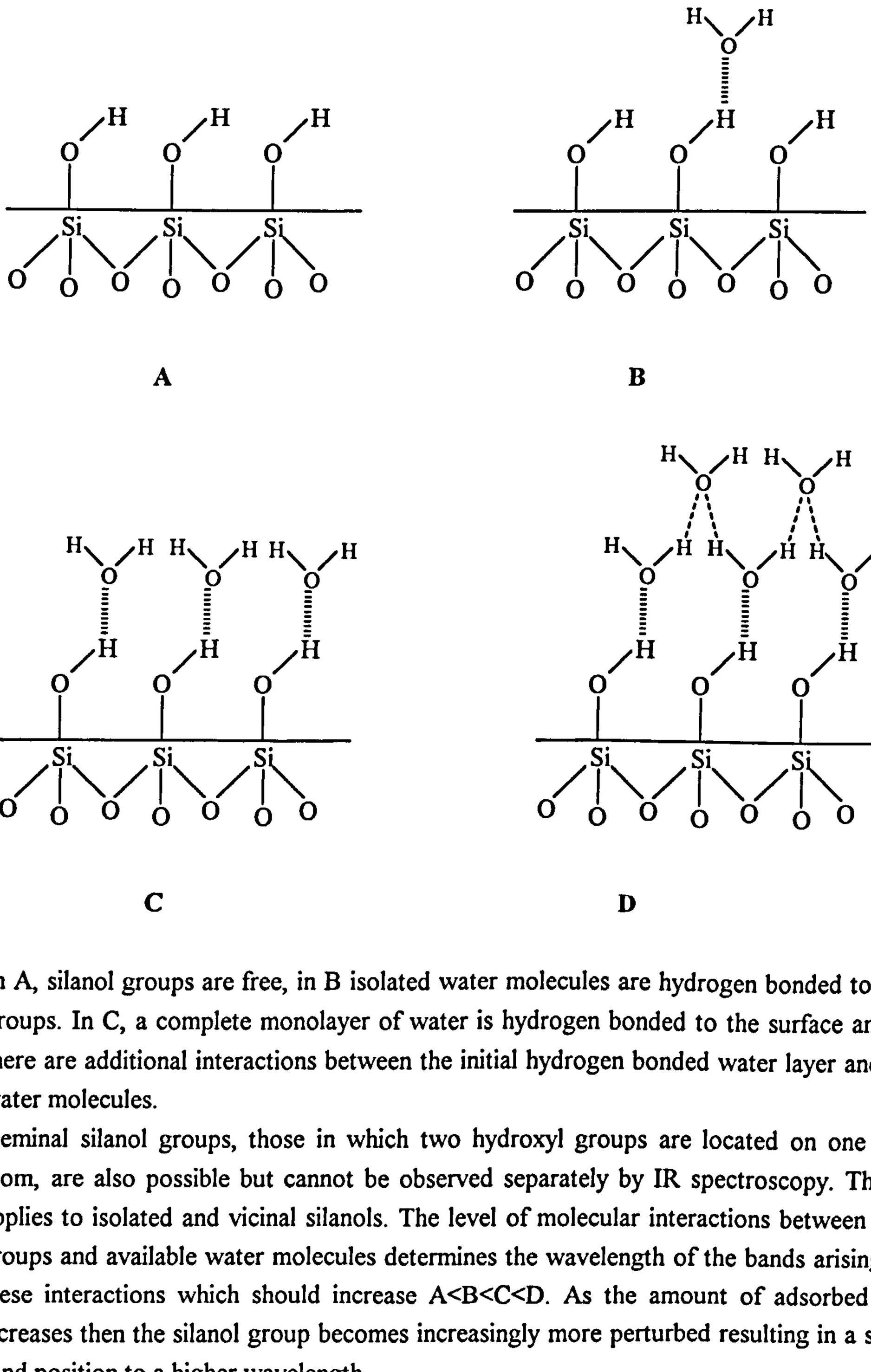

A

B

C

D

In A, silanol groups are free, in B isolated water molecules are hydrogen bonded to silanol groups. In C, a complete monolayer of water is hydrogen bonded to the surface and in D there are additional interactions between the initial hydrogen bonded water layer and other water molecules.

Geminal silanol groups, those in which two hydroxyl groups are located on one silicon atom, are also possible but cannot be observed separately by IR spectroscopy. This also applies to isolated and vicinal silanols. The level of molecular interactions between silanol groups and available water molecules determines the wavelength of the bands arising from these interactions which should increase A<B<C<D. As the amount of adsorbed water increases then the silanol group becomes increasingly more perturbed resulting in a shift of band position to a higher wavelength.

In the 1400nm region, the sharp peak between 1368-1373nm for all samples can be

assigned as a type A silanol group. The almost complete loss of this band with time, for all the samples at 120°C, implies that very few free silanol groups remain in the hydrated sample and are thus hydrogen bonded to water.

Similarly, in the second overtone and combination region the peak at 1230nm decreases in intensity with time but does not shift during hydration and is thus comparable to type A silanol groups. The higher baseline on the high wavelength side indicates the presence of types B to D hydrogen bonded species. The peak at approximately 930nm also follows the pattern of the first overtone region but cannot be assigned as individual perturbed -SiOH species because of the broad spectral envelope containing water bands.

4.5.2.1.2 Water Bands in the First Overtone and Combination Region

Even at t=0 the reflectance spectra obtained for titania contents of 4·1 to 21·9 weight %, show the presence of water on the surface (figures 4.9, 4.11 and appendix I). It was observed that the greater the amount of titania present in the sample then a greater amount of water bound to the surface at t=0 was observed, and the more extensive the hydration process.

Figure 4.9 shows that as the extent of hydration increases, then the combination band at *ca* 2200nm, and the band at 1900nm increase in intensity and new bands centred at 1400nm and 1450nm appear. A shoulder appears on the band at 1900nm at *ca* 1930nm. Both this band and the one at 1450nm behave in a similar manner and increase in intensity relative to the bands at 1400nm and 1900nm as exposure time increases. This implies that each set of bands (1400,1900 and 1450,1930nm) arise from the same molecular species.

By assuming that silanol groups provide a donor atom to adsorbing water molecules, the first monolayer adsorbed on the surface can include three different adsorbed species which are detailed in figure 4.14[18].

Figure 4.14: Types of Adsorbed Water on a Silica Surface[18]

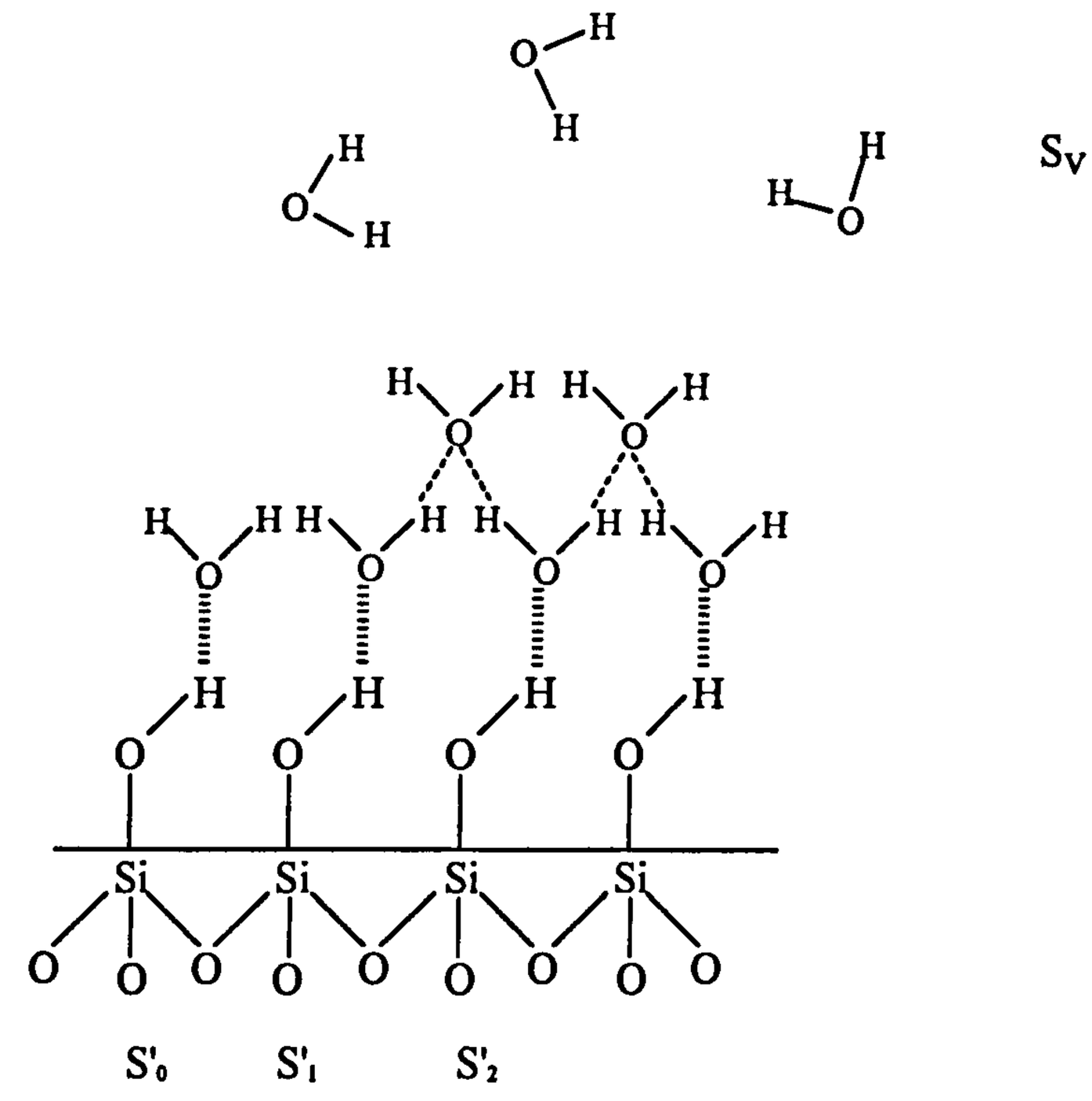

- S'_0 - water bonded to -SiOH *via* an oxygen atom. No hydrogen-bonding occurs between water molecules because of the separation of silanol groups on the surface *ie* monomerically bonded.
- S'_1 - water bound to -SiOH *via* oxygen and hydrogen bonded to one other water molecule *ie* partially hydrogen bonded.
- S'_2 - water bound to -SiOH *via* oxygen and hydrogen bonded to two other water molecules *ie* fully hydrogen bonded.
- S_v - vapour phase molecular water.

The increased hydrogen bonding of SiOH enables more interaction between surface groups. Consequently as interaction between the surface groups becomes increasingly more common then bands become broader, $S'_0 < S'_1 < S'_2$.

Similarly, as surface hydration progresses, layers of water build up resulting in some areas behaving like condensed phases. Also, water molecules can exist above the bound layers (S_v).

For the samples investigated, the 1900nm band has been assigned as arising from S'_0 species because apart from increasing in intensity the band remains essentially unchanged on increasing hydration. Anderson *et al* [15] found that at low levels of hydration, further adsorption of water can occur at either -SiOH or water groups with equal probability. If a water layer was formed sequentially then no S'_0 species would be observed on the surface of a fully hydrated sample. However, the presence of a shoulder at *ca* 1950nm and a raised

baseline on the high wavelength side of the band can be attributed to the overlap of peaks due to S'_1 and S'_2 species indicating that the water layer is not formed sequentially.
The overlap of perturbed -SiOH and H_2O bands makes precise assignment of the 1400nm band a complicated task. Since the intensity change of this band is comparable to that of the band at 1900nm, this has therefore been assigned as S'_0 type water with a contribution from hydrogen bonded silanol/water species. As the hydration of the surface proceeded, the peak maximum shifted to a higher wavelength by approximately 10nm. This may be attributed to the gradual formation of hydrogen bonded silanol groups which have a peak at about the same wavelength. The maximum at 1450nm arises because of a spectral envelope due to S'_1 and S'_2 water species which are partly and fully hydrogen bonded to other water molecules respectively. This evidence again indicates that the water layer on the surface does not form sequentially.

4.5.2.1.3 Water bands in the Second Overtone Region

Reflectance spectra at t=0 in the 900-1350nm region, show four absorption bands even after prolonged dehydration *in vacuo* at room temperature (see figures 4.10, 4.12 and appendix I).
Studies of water both by itself, in ionic solutions and in mixed solvents at varying temperatures have been made[13,25-28], on comparison with the first overtone region these weak bands have been assigned. The most intense bands were observed at approximately 930nm and 1230nm and were assigned as arising from SiOH groups. A further two weak bands were observed around 1150nm, which increased in intensity as the extent of hydration increased. The lower wavelength band was assigned as arising due to S'_0 species, and the higher one due to S'_1 species[18]. These bands were very well defined even at high levels of hydration suggesting that there was little interaction between adsorbed water molecules and that more than one type of water molecule can exist on the surface.
For a sample containing 4·1 weight % titania (figure 4.10) the sharp peak around 1230nm, assigned to the higher combination band of free -SiOH groups[18], was observed to decrease in intensity as hydration progressed. As the surface became increasingly more hydrated, the contribution from the baseline increased because of the presence of a broad band due to S'_2 water species. The simultaneous observation of S'_0, S'_1 and S'_2 water species at *ca* 1200nm suggests that water forms local clusters rather than complete molecular layers.
In the 900nm region, the band at 930nm has been assigned as the second overtone of the OH stretching of free SiOH groups. As hydration increases, this band not only decreases in intensity but broadens and shifts towards a higher wavelength. This arise due to the $3\nu_{OH}$ of adsorbed water as well as the second overtone of hydrogen bonded -SiOH groups. Asymmetry of this band towards higher wavelengths indicates the presence of the hydrogen bonded species, S'_1 and S'_2.

4.5.2.1.4 Effect of the Amount of TiO_2 (weight %) in the Sample

In the first overtone region (1200-2500nm) of the near-infrared spectra, it was found that increasing the amount of titanium present in the sample, as TiO_2 (weight %); resulted in an increase in hydrogen bonded silanols and water associated with the surface, and a decrease in free silanol groups even after extended evacuation (see appendix I).

From the spectra at t=2 hours, it was observed that increasing the amount of TiO_2 (weight %) in the sample, decreased the relative intensity of the peak at 1370nm on comparison with that at 1400nm, thus implying that as titania content increases there are fewer free silanols and more hydrogen bonded silanols on the surface. As the amount of titania in the sample was increased there was a corresponding increase in the intensity of the peak at 1940nm, due to polymeric hydrogen bonded water species. Comparing the spectra obtained after 2 hours exposure, the combination band at *ca* 2200nm was found to have shifted towards a higher wavelength as the levels of titania were increased. This is indicative of a decrease in free -SiOH groups and a corresponding increase in hydrogen bonded species.

These results are in good agreement with the results of Perry and Li[28] who found that the relative proportion of hydrogen bonded silanol groups and associated water molecules were marginally higher for silica-titania glasses than for silica-only glasses.

4.5.2.2 Mixed Silica-Titania Powders at 900°C

Comparison with the spectra at 120°C, for a sample containing 4·1 weight % (see figure 4.9 and 4.15), revealed an increase in the sharpness of the free SiOH bands at t=0, and a big reduction in the intensity of both the water and silanol bands. This has been attributed to the thermal treatment removing the majority of the surface silanol groups, which are the main adsorption sites on the surface of the gel. The surface of the high temperature gel is therefore less hydrophilic.

Thermal treatment resulted in the band due to free -SiOH species shifting to a slightly lower wavenumber. Exposure of the sample to the atmosphere resulted in changes due to hydration similar to those observed for the samples treated at a lower temperature.

After extended hydration free silanol groups (1370nm) were observed on the surface of the thermally treated sample (see figure 4.15). In section 4.4.2.1, thermal treatment was observed to reduce the number of free silanol groups present on the surface. The observed free silanol groups remaining on the surface are therefore susceptible to hydration. However extended exposure to the atmosphere resulted in an extremely weak peak at 1450nm due to the formation of S'_1 and S'_2 species. This and the presence of a broad shoulder at 1940nm also confirmed the presence of S'_1 and S'_2 species on the surface are shown in figure 4.15. After the same exposure time, the combination band at 2200nm was found to consist predominantly of free silanol groups. A shoulder was observed on the high wavelength side of the band (figure 4.15) due to hydrogen bonded species. This shoulder became more prominent as the hydration proceeded. However, it was observed that free silanol species

Figure 4.15: First Overtone and Combination Region (1200-2500nm) Near Infrared Spectra of a Dehydrated Sample Containing TiO_2=4·1 wt% Heated to 900°C and Exposed to the Atmosphere for Various Times.
(a) 0; (b) 0·5 hour; (c) 1 hour; (d) 2 hours; (e) 14 hours.

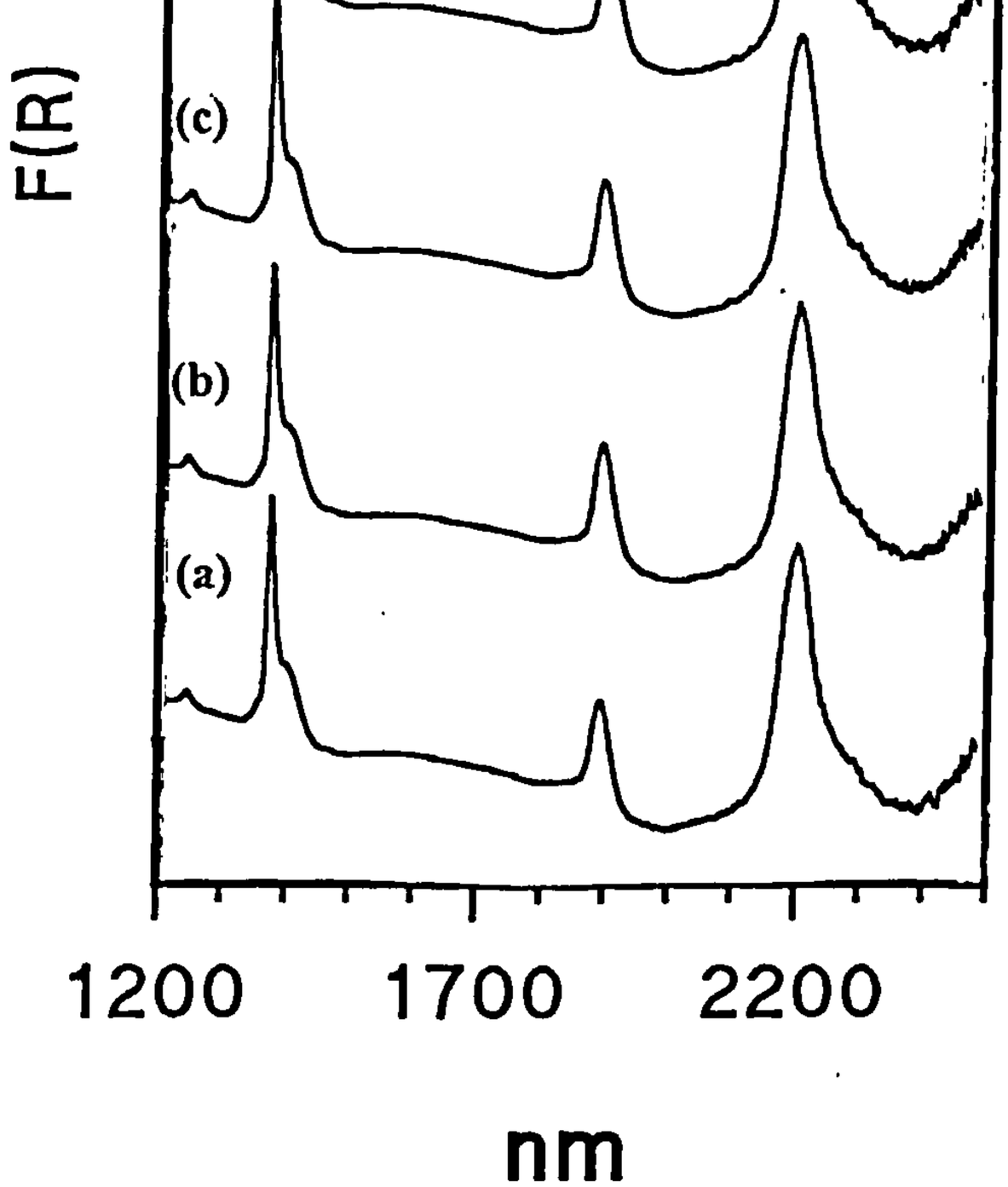

Figure 4.16: First Overtone and Combination Region (1200-2500nm) Near Infrared Spectra of a Dehydrated Sample Containing TiO_2=21·9 wt% Heated to 900°C and Exposed to the Atmosphere for Various Times.
(a) 0; (b) 0·5 hour; (c) 1 hour; (d) 2 hours; (e) 14 hours.

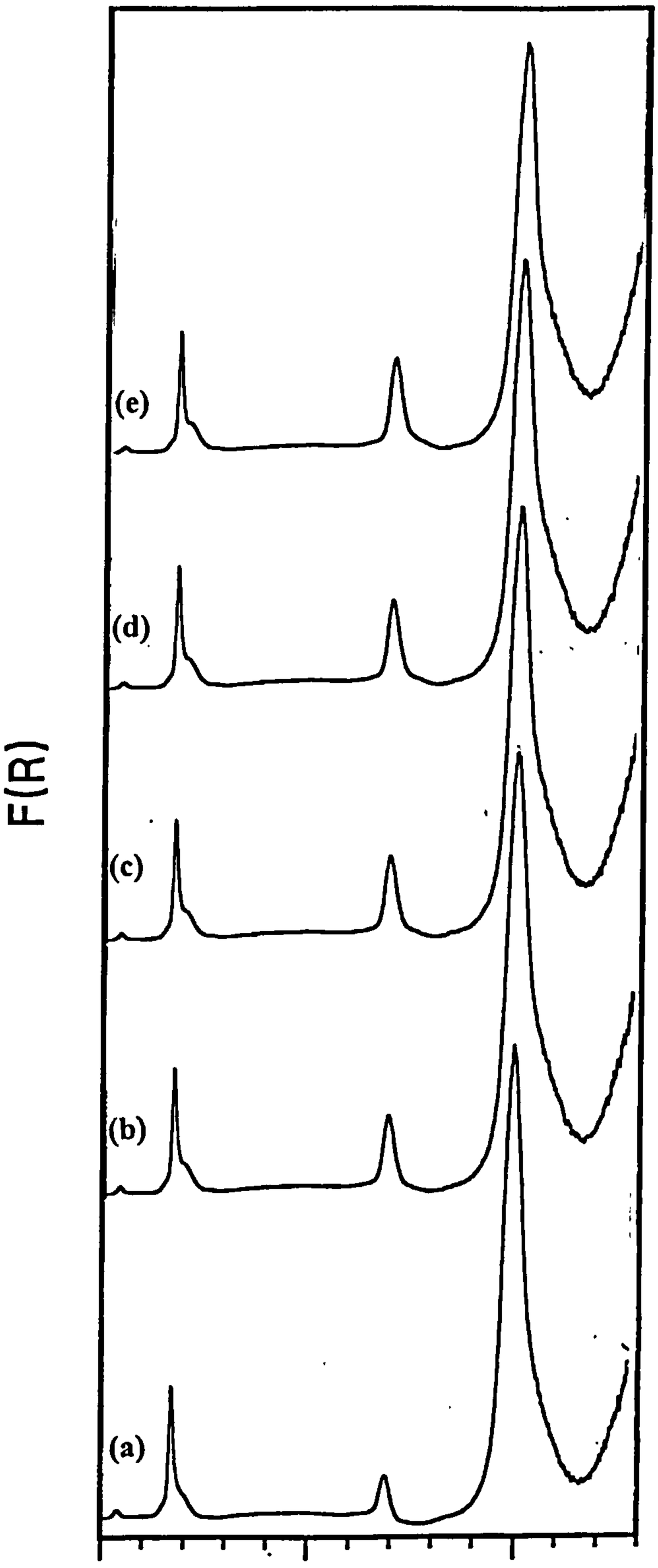

were still the predominant species after extended hydration. After extensive hydration, the peaks observed for a sample containing 4·1 weight % titania and treated at 900°C, were much sharper than for the corresponding low temperature sample. The weak bands arising due to hydrogen bonded species are consistent with there being little or no interaction between surface silanol groups. Therefore, the condensation of silanol groups is not complete since isolated silanol groups still remain within the sample.

As for the low temperature samples, increasing the amount of titania in the gel resulted in a greater relative number of hydrogen bonded species (*ca* 1400nm) on comparison with free silanol species (*ca* 1370nm) (see figure 4.16 and appendix I).

4.6 Thermal Analysis

Gels with varying titanium dioxide contents (weight %), as in table 4.4, were investigated using synchronous differential thermal (DTA) and thermogravimetric (TGA) analysis methods, with the aim of identifying the temperatures at which phase transformations occur.

4.6.1 Results and Discussion

The DTA curves obtained, see figure 4.17, did not record any changes due to crystallisation under the applied heating regime. As such, the DTA curves indicate only the loss of water and organics at low temperatures.

Figure 4.17: Typical Differential Thermal (DTA) and Thermogravimetric (TGA) Curves Obtained for Mixed SiO_2-TiO_2 Gel (in this instance TiO_2=4·9wt%)

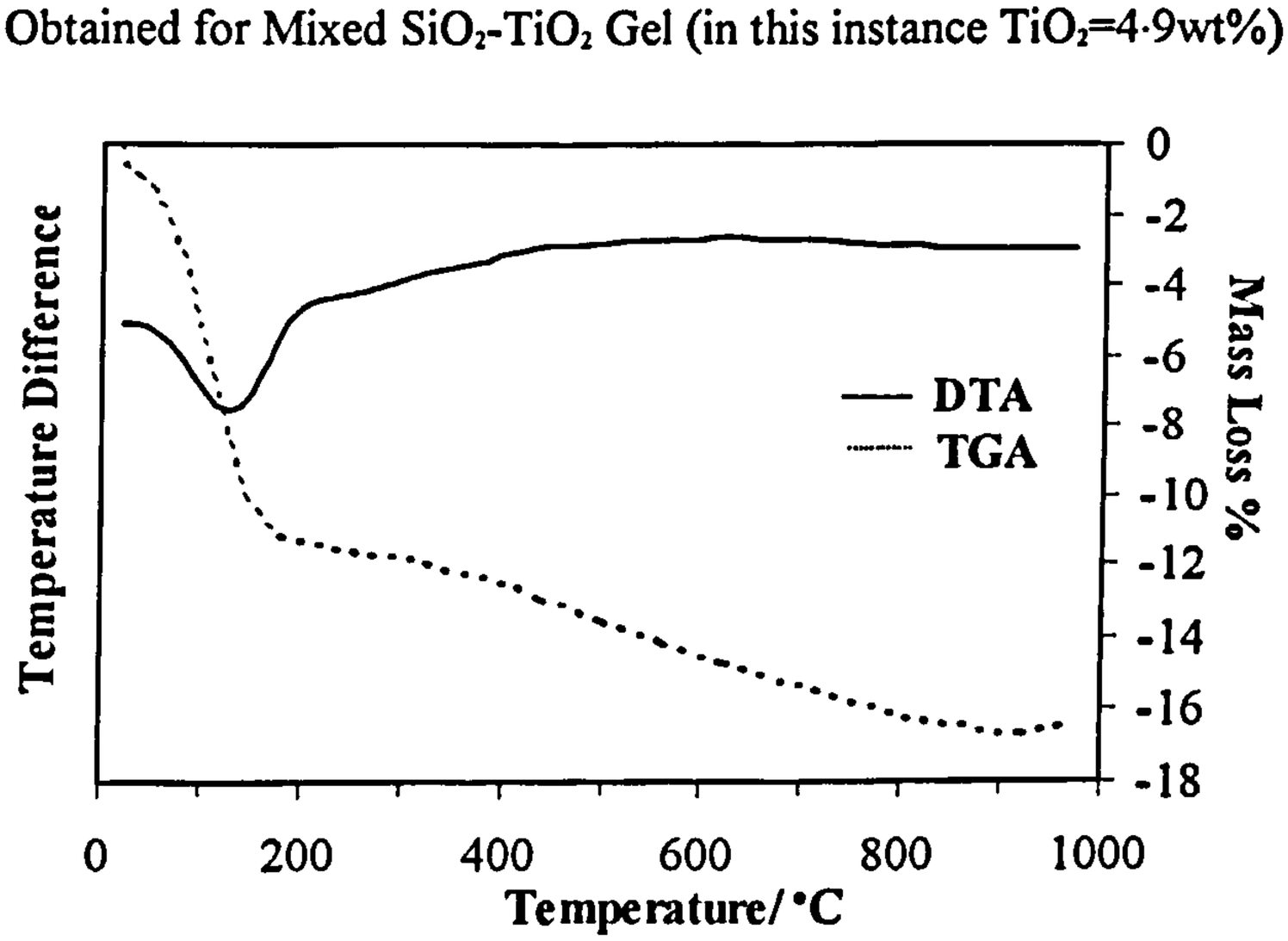

X-ray diffraction of samples containing TiO_2 (weight %) 4·1, 4·9, 6·1 and 6·34 (high and low acid), indicated that all remained amorphous after thermal analysis. However, the sample containing TiO_2=21·9 wt% was crystalline before thermal analysis took place, although the crystallinity observed may well be less than usually observed. Similarly, after heating and maintaining the samples at *ca* 970°C for 8 hours in the instrument, X-ray diffraction indicated that all remained amorphous. This implies that crystallisation occurs over a longer time period than that of the thermal analysis.

4.7 Gas Adsorption Investigation of Pore Structure

The titania contents of the powders under investigation are detailed in table 4.4. These samples have been subjected to temperatures of 120, 300, 500, 700, 900 and 1100°C for 12 hours. The aim was to study both the effect of temperature and titania content on the surface area and porosity of the sample. Similarly, the effect of variation of the amount of acid used in the hydrolysis reaction has also been investigated, see table 4.3.

4.7.1 Results and Discussion

4.7.1.1 Structural Evolution

4.7.1.1.1 Effect of the Amount of Acid used in the Hydrolysis Reaction for Monolithic Gels

For gels prepared using a large amount of acid in the hydrolysis reaction the resulting isotherms are type IV. Generally it can be seen that the greater the amount of acid used for the hydrolysis then the greater the extent of hysteresis observed and therefore the greater levels of mesoporosity shown by the material produced. Decreasing the amount of acid used in the hydrolysis reaction results in the elimination of hysteresis and the formation of type I isotherms which is characteristic of microporous solids.

For samples containing a high amount of acid the shape of the hysteresis loop observed in the adsorption/desorption isotherms suggests that the mesopores present are more slit shaped than cylindrical, see section 2.5.1.3. Reducing the amount of acid used in the hydrolysis reaction to $5x10^{-3}$ mole (and below), results in a decrease in the surface area, see figure 4.18 (also appendix I) and table 4.8. This is consistent with the elimination of hysteresis from the resulting isotherm and hence mesopores from the sample.

Both adsorption and desorption pore size distribution data confirm that decreasing the amount of acid used for hydrolysis reduces both the median pore diameter and the total pore volume of the materials. Therefore the mesoporosity is removed by decreasing the amount of acid.

Figure 4.18: Effect of Variation of the Amount of HCl used for the Hydrolysis of a Sample Containing TiO_2=6·34 weight % on the Resulting Adsorption/Desorption Isotherm

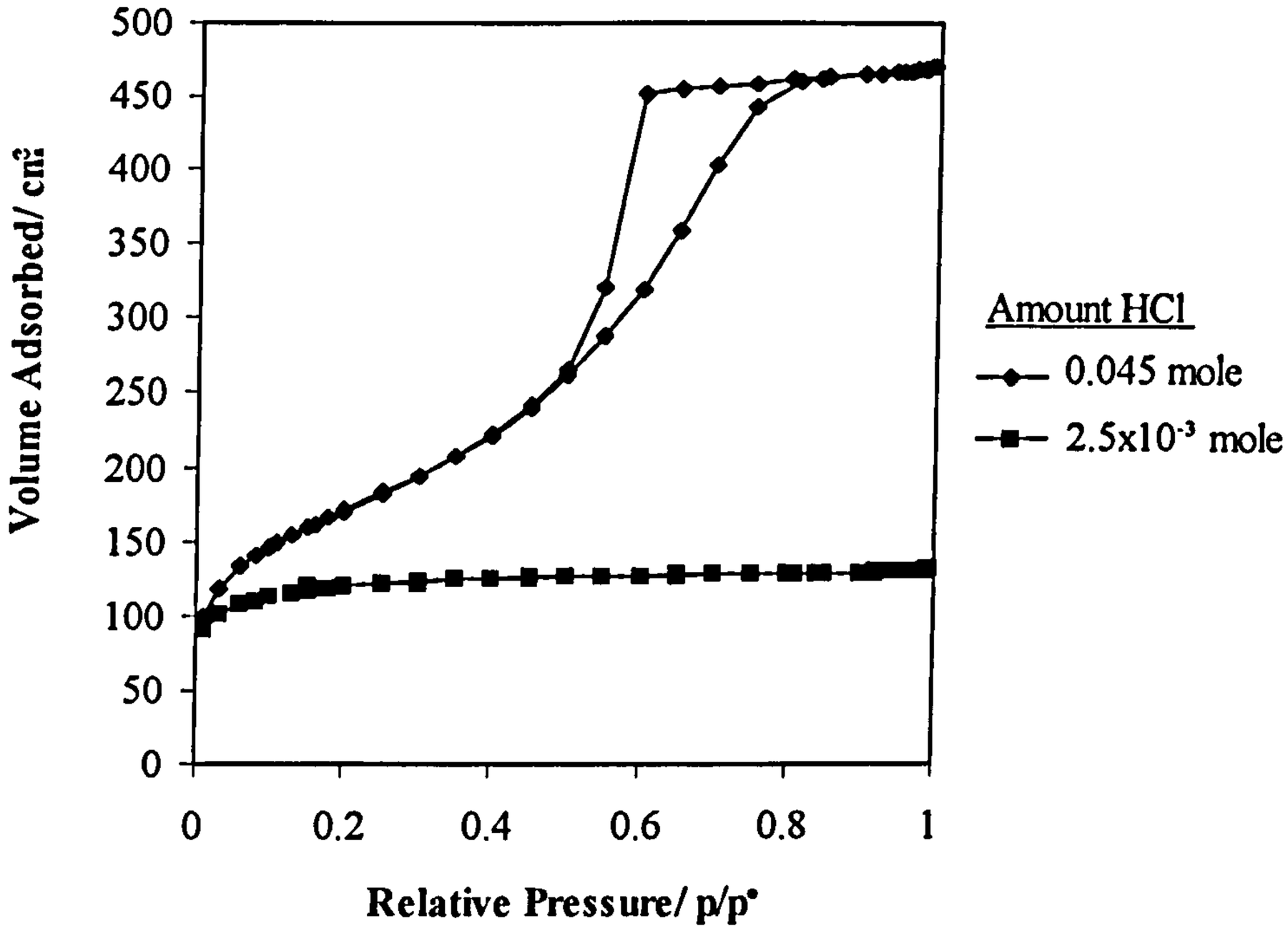

Table 4.8: Effect of Variation of the Amount of HCl used for the Hydrolysis of a Sample Containing TiO_2=6·34 weight % on the Pore Structure.

Amount of HCl (mole)	BET Surface Area (m^2g^{-1})		Pore Volume (cm^3g^{-1})		Average Pore Diameter (Å)	
		C	Adsorption	Desorption	Adsorption	Desorption
0·045	618	117·7	0·74	0·76	54·4	37·8
0·030	644	137	0·72	0·76	54·8	48·5
0·015	631	173·5	0·40	0·35	31·6	34·9
$7·5 \times 10^{-3}$	662	133	0·54	0·49	35·8	38·8
5×10^{-3}	558	-819	0·19	0·16	17·7	19·0
$2·5 \times 10^{-3}$	436	-120	0·08	0·13	17·3	19·2

The values for the BET parameter C, are indicative of the sample being mesoporous with probable contribution from some micropores. The microporosity is investigated by the α_s-method in section 4.7.2.3.

4.7.1.1.2 Effect of Temperature and Titania Content on Powdered Samples

On thermal treatment, all samples showed an overall decrease in surface area as the treatment temperature was increased (see for example table 4.9 and appendix I). However,

on heating of samples from 120 to 300°C there was a marked increase in surface area. This corresponds to the loss of water observed by thermal analysis, see section 4.6, in this region. Further heating to 1100°C results in the progressive decrease of surface area and pore volume, these changes being greatest between 900 and 1100°C. In comparison, conventionally prepared silicas[31] exhibit very little change in surface area or pore structure below 700°C, but at temperatures greater than 700°C these changes are larger. These observations are consistent with the densification of the gel and the progressive elimination of pores during thermal treatment.

Table 4.9: Effect of Temperature on the Pore Characteristics of a Sample Containing TiO_2=4·9 weight %

		Temperature/°C						
		120	**300**	**500**	**700**	**900**	**1100**	**1100 (Kr)**
BET Surface Area (m^2g^{-1})		513	538	473	472	314	0·355	0·42
C		98·4	118·7	95·5	71·9	63·9	1418	52·8
BJH Pore Volume (cm^3g^{-1})	**Adsorption**	0·56	0·57	0·43	0·48	0·30	0·001	
	Desorption	0·61	0·62	0·51	0·52	0·33	0·001	
BJH Average Pore Diameter (Å)	**Adsorption**	39·2	39·3	35·3	36·2	34·3	423·4	
	Desorption	38·4	38·6	34·8	35·8	33·7	282·4	

Heat treatment also results in the elimination of residual OH and OR groups by the following reactions, as H_2O and ROH which results in a further condensation of the system:

$$Si-OH+HO-Si \rightarrow Si-O-Si+H_2O$$

$$Si-OR+HO-Si \rightarrow Si-O-Si+ROH$$

$$Si-OH+HO-Ti \rightarrow Si-O-Ti+H_2O$$

Densification of the sample and the elimination of surface SiOH groups at 1100°C are indicative of surface and structural changes at high temperatures. This resulted in very low surface areas as detected by nitrogen adsorption.

Krypton vapour was used as the adsorptive to accurately measure low surface areas *via* the BET[32] method. Krypton adsorption at liquid nitrogen temperature for samples thermally treated at 1100°C resulted in measured surface areas of 1·35m^2g^{-1} or less. These results are consistent with sample densification totally eliminating the "accessible" pore surface making the once highly porous structure dense with low associated porosity.

Analysis of silicas prepared under the same conditions shows that the inclusion of titania results in pores becoming less cylindrical, a decrease in the overall surface area of up to 50%, an increase in average pore size and hence an increase in mesoporosity. Varying the amount of titania (weight %) present in the sample had no obvious effect on the surface area or pore volume, see table 4.10. However, comparison with studies on silica and silica-alumina[33-36] suggests that the presence of titania in the sample results in larger pores and hence a greater average pore diameter.

Table 4.10: Effect on Structural Characterisitics of Varying the Amount of Titania (wt%) for Samples Heated at 120°C.

TiO_2 (wt%)	**BET Surface Area (m^2g^{-1})**	**C**	**BJH Pore Volume (cm^3g^{-1})**		**BJH Average Pore Diameter (Å)**	
			Adsorption	**Desorption**	**Adsorption**	**Desorption**
0	812·5	137·1	0·33	0·47	25·1	25·3
4·1	441	93·9	0·48	0·55	40·5	39·5
4·9	513	98·4	0·56	0·61	39·2	38·4
6·1	551	113·9	0·66	0·72	43·7	43·2
6·34	394	65·6	0·54	0·57	44·6	43·1
21·9	477	58·5	0·51	0·55	37·4	37·1

The effect of thermal treatment of the samples on average pore diameter has also been studied. Heating the samples to 900°C resulted in very little change in average pore diameter. But heating to temperatures of greater than 900°C resulted in an increase in the average pore diameter. This is in contrast with both surface area and pore volume data which both decrease significantly with increasing temperature. Between 120 and 900°C the average pore diameters obtained *via* the BET method were between 39 and 76Å (mesopores)[37].

Van Nordstrand, Kreger and Ries[33] and Bastick[34] have found that in commercial silica gel with a pore diameter of about 20Å, as well as silica-alumina xerogel having a pore diameter of about 40Å, there is no change in average pore size as sintering progresses. Teichner[35] *et al* observed that on sintering a voluminous aerogel where shrinkage was 83% by volume,

the average pore diameter changed by only a small amount.

It is well documented that when silica gel is sintered it shrinks; the pore volume decreases in proportion to the decrease in surface area and the pores that remain do not change in size. It appears that pores are destroyed as the silica is converted from the porous to the nonporous state without the size of any remaining pores undergoing change[36].

Average pore diameters obtained for pore size distributions (PSDs) calculated from the adsorption branch of the isotherm (BJH method[29]) are compatible with those from the BET method. Typical PSD plots for samples at 120°C and 900°C are shown in figure 4.19. Both plots have the maximum pore volume at a pore diameter around 40Å, and contain few pores of diameter greater than 100Å.

Figure 4.19: dV/dlog(D) Adsorption Pore Size Distribution Plots of a Sample Containing TiO_2=4.9wt% Thermally Treated at 120 and 900°C

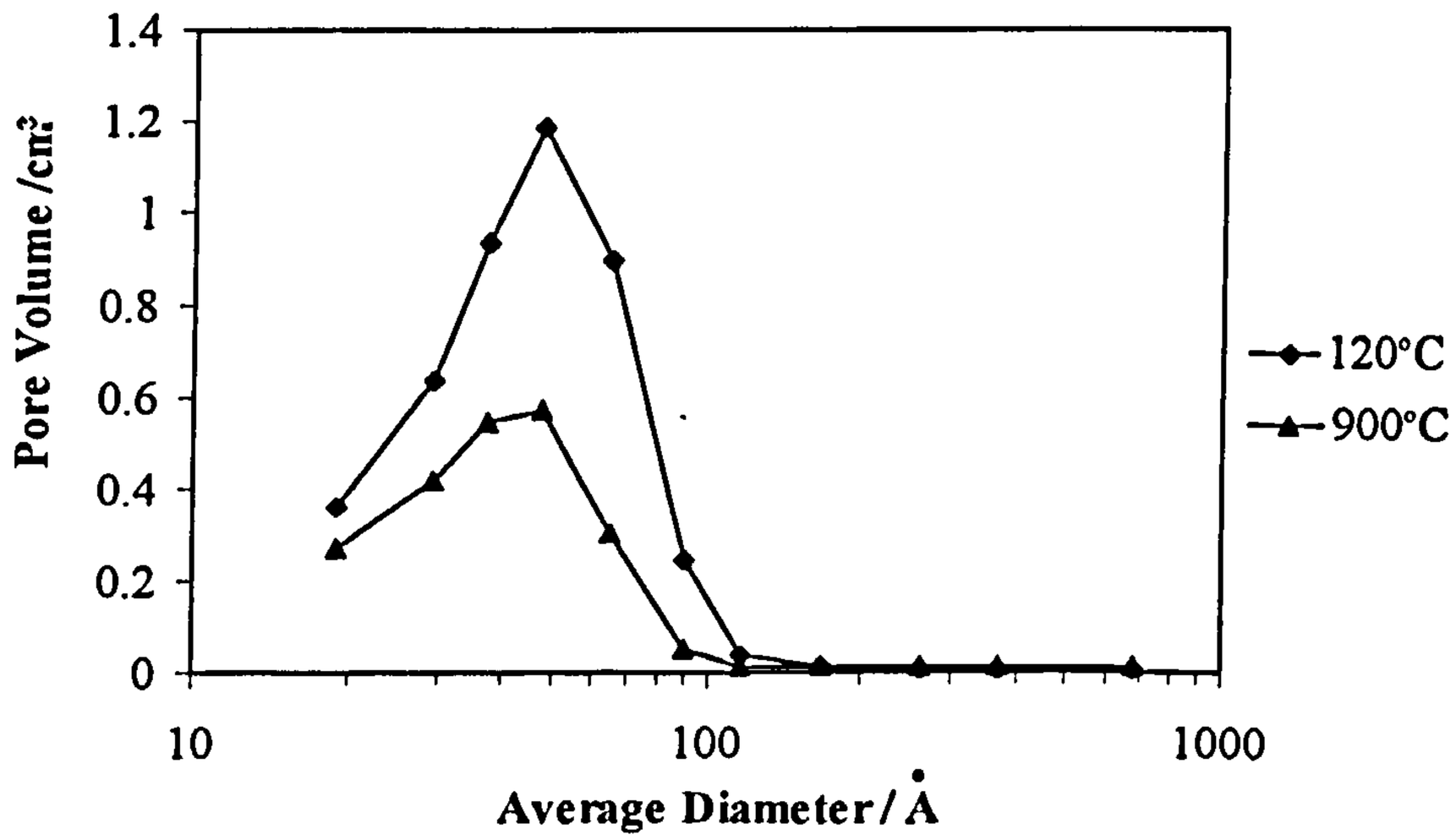

The relative symmetry of these plots about the maxima suggests that the pore diameter is uniformly distributed around 40Å. Sintering results in a decrease in the pore volume attributed to pores at the maxima and results in an overall decrease in the pore volume. Comparison of the PSD plots for a sample at 120 and 900°C (figure 4.19) reveals that although the average pore diameter remains constant the volume due to larger pores decreases.

As the thermal treatment temperature of the sample is increased the shape of the hysteresis loop changes slightly in that at 900°C, the desorption branch is much steeper than previously observed (see figure 4.20). A similar increase in the steepness of the desorption branch on sintering of a silica aerogel, due to a change in average pore geometry, was observed by Van Nordstrand *et al*[33]. This has been attributed to the preferential sintering of the larger pores. This change in shape of the hysteresis loop with temperature supports the theory that pores are destroyed and hence change shape as sintering progresses[36].

Figure 4.20: Comparison of Isotherms for a Sample Containing TiO_2=6·34 weight % after a Range of Thermal Treatment Temperatures (HCl =0·045 mole)

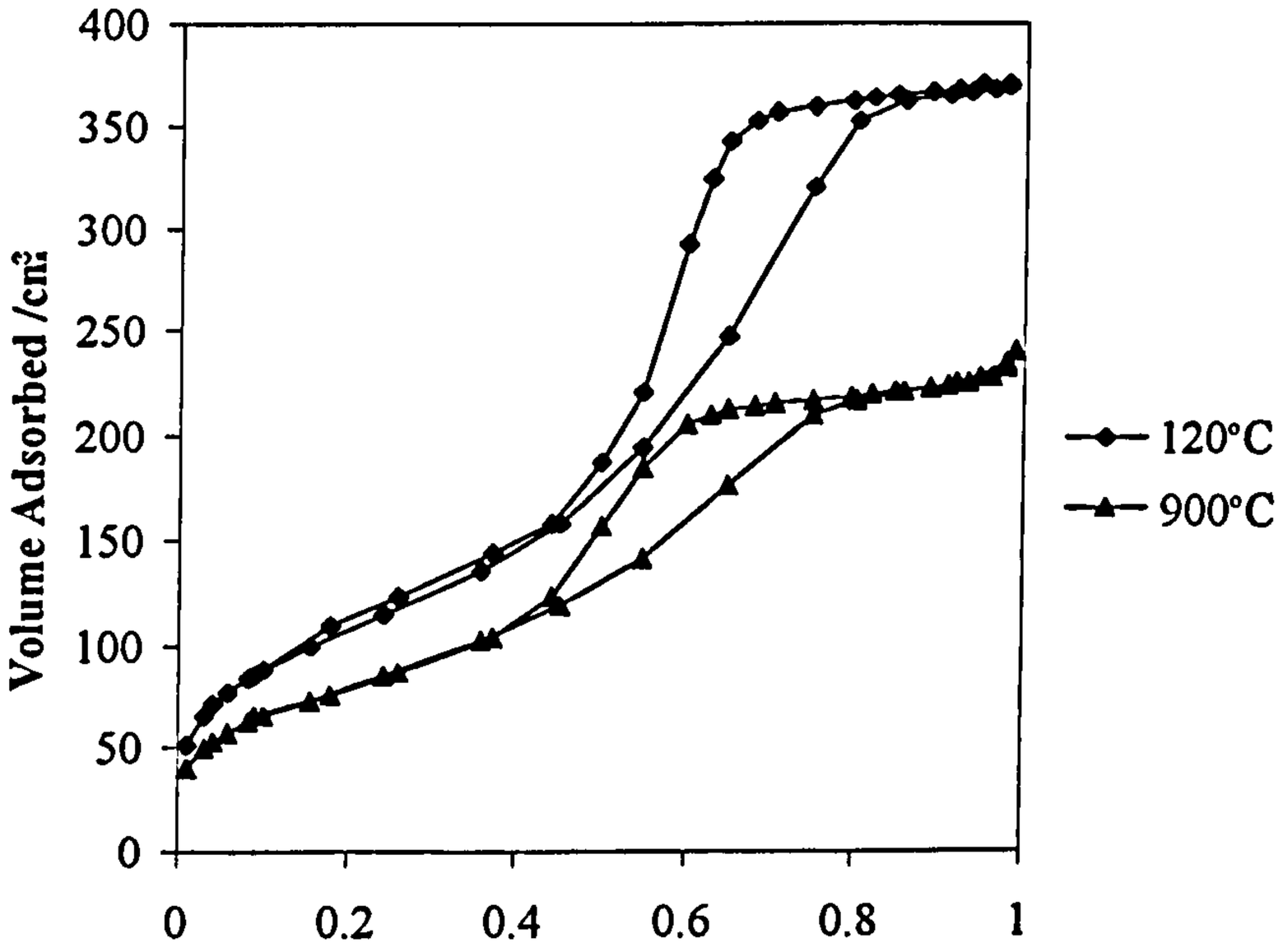

Therefore from the data presented in table 4.10, it is not possible to arrive at any conclusions about a relationship between the amount of titania present in a sample and the surface area and pore volume. However, comparison with studies on silica and silica-alumina[33-36] suggests that the presence of titania in the sample results in larger pores and hence a greater average pore diameter.

The structural changes observed in gels treated at 1100°C are large reductions in both surface area and pore volume and a large increase in mean pore size. Changes in the samples at 1100°C are also observed in mid-infrared spectroscopy where the band arising from the antisymmetric stretching vibrations of O-Si-O bonds shifts to a higher frequency. This and the appearance of vibrations due to Si-O-Ti have been attributed to the strengthening of the sample structure, which is a direct result of pore elimination.

4.7.2.2 Effect of Thermal Treatment on Monolithic Gels

After thermal treatment, a series of monolithic gels containing 6·34 weight % titania (HCl =0·045 mole) exhibited a progressive decrease in both surface area and pore volume as the treatment temperature was increased, see table 4.11. Increasing the temperature to 900°C or above, reduced the entire pore structure of the material until at 1100°C the pore structure had been virtually eliminated.

Table 4.11: Effect of Temperature on the Pore Characteristics of a Monolithic Gel Containing TiO_2=6·34 weight % (HCl =0·045 mole)

		Temperature/°C					
		120	300	500	700	900	1100
BET Surface Area (m^2g^{-1})		618	742	657	586	278	9
	C	117·7	119·0	111·0	106·7	8·9	47·5
BJH Pore Volume (cm^3g^{-1})	**Adsorption**	0·74	0·55	0·49	0·25	0·12	0·01
	Desorption	0·76	0·46	0·34	0·21	0·09	0·01
BJH Average Pore Diameter (Å)	**Adsorption**	54·4	29·3	30·5	23·0	21·0	----
	Desorption	47·8	34·8	34·7	32·1	19·6	----

The values for the BET parameter C, are indicative of the sample being mesoporous with a probable contribution from some micropores. The microporosity is investigated by the α_s-method in the following section, 4.7.2.3.

The isotherms obtained suggest that increasing the thermal treatment temperature reduces the mesoporosity of the sample and increasing the temperature to 900°C or above results in a material with virtually no pore structure, see figure 4.21 and appendix I. The shape of the adsorption/desorption hystersis loops observed suggest that the mesopores present are more slit shaped than cylindrical.

Figure 4.21: Comparison of Isotherms for a Monolithic Sample Containing TiO_2=6·34 weight % after a Range of Thermal Treatment Temperatures (HCl =0·045 mole)

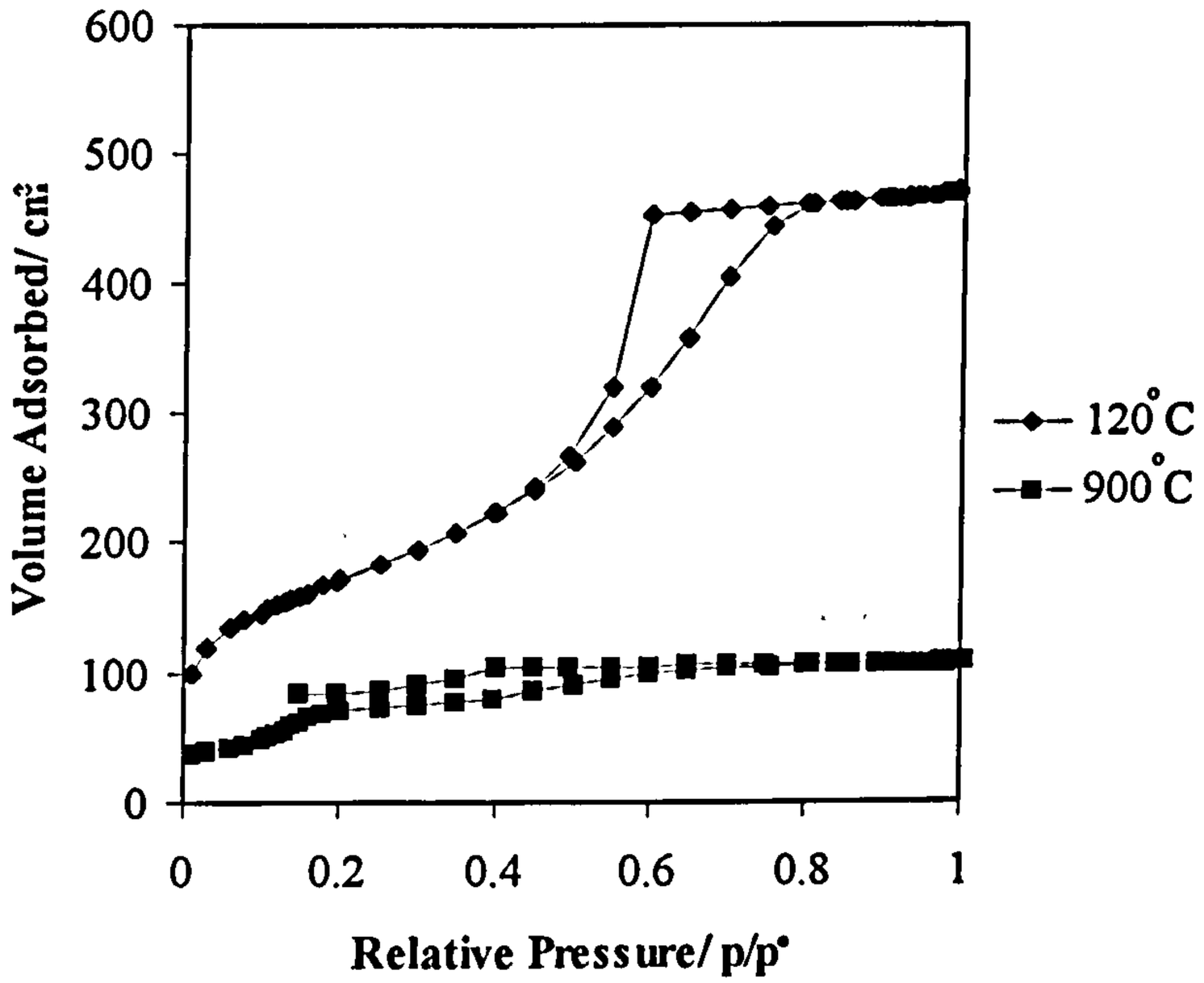

The effect of thermal treatment of the samples on average pore diameter has also been studied. Heating the samples to 900°C resulted in a progressive decrease in average pore diameter. Pore size distributions of monoliths heated at 120 and 900°C show this decrease in average pore diameter, see figure 4.22. It was not possible to obtain accurate values of average pore diameter for the monolith treated at 1100°C, although if the observed trend continued then the pore diameter would be expected to be smaller still.

Figure 4.22: dV/dlog(D) Adsorption Pore Size Distribution Plots of a Monolithic Sample Containing TiO_2=6·34wt% Thermally Treated at 120 and 900°C

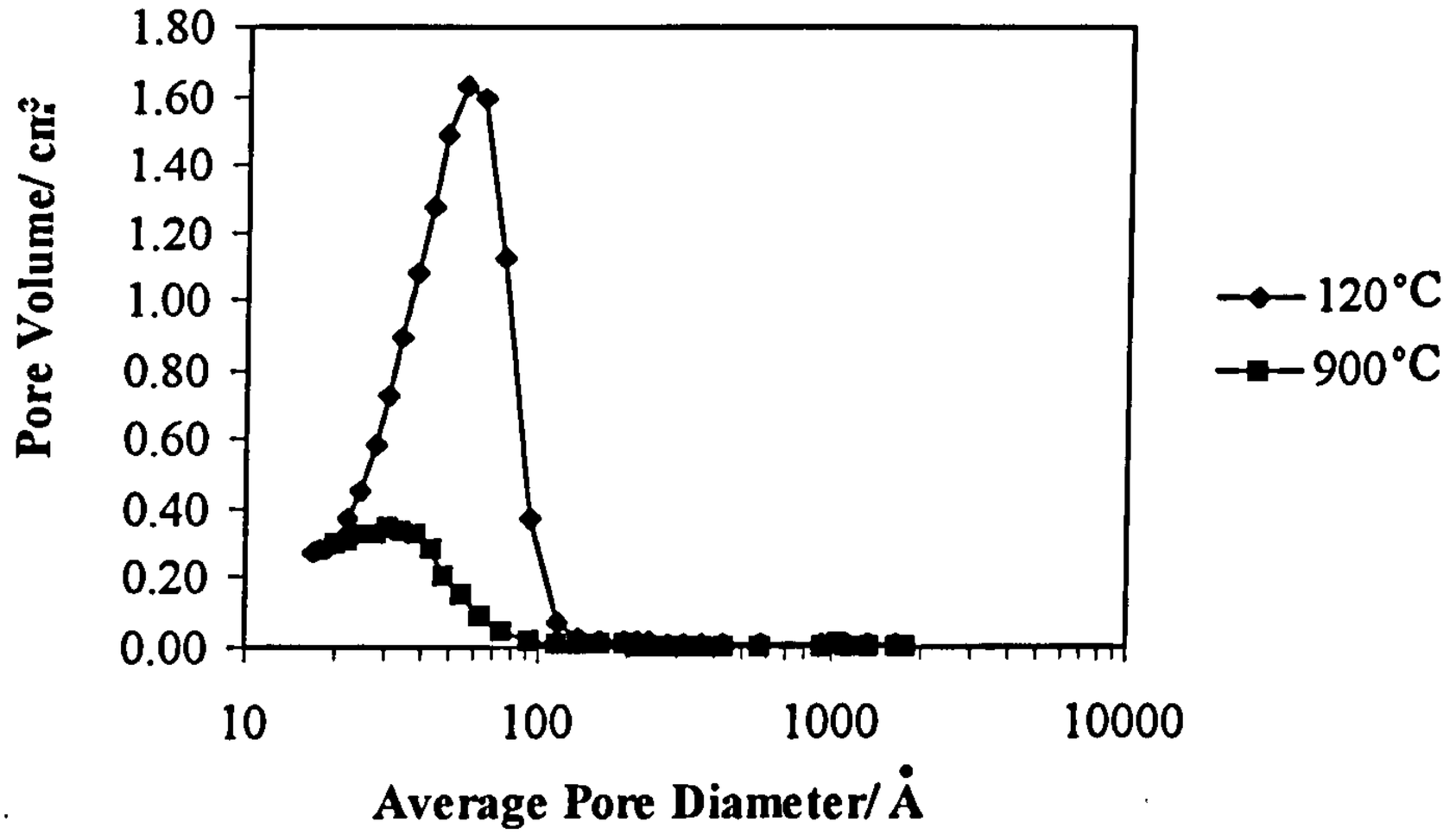

The observed effect of temperature on the average pore diameter of a monolith was in contrast to the results obtained for powdered samples, see section 4.7.1.1.2, where the average pore diameter remained constant at temperatures up to 900°C.

Sintering of a gel is a densification process driven by interfacial energy. Material within the sample moves *via* viscous flow or diffusion in a manner which eliminates porosity and hence reduces the solid/vapour interfacial area. In a monolith, the area is large and hence the driving force is large enough to produce sintering at low temperatures, where the transport processes are relatively slow. However, the kinetics of gel densification are complicated by dehydration and structural relaxation. This results in faster heating permitting complete densification at a lower temperature. In a crystalline gel, densification is hindered by grain growth and phase transformations[2].

The complete drying of gels as monoliths under normal conditions results in xerogels. Xerogels often contain significant amounts of residual organic groups and hydroxyl (OH) ions bound to the network. When very small pores are present in the gel then such groups can be difficult to remove. In the case of silica gel made from TEOS, the structure has been shown to depend on solution pH during both the hydrolysis and condensation reactions[3].

Base-catalysed systems produce gels that are granular in texture and retain less organic material. In this case, acid-catalysis has been used which generally results in a finer, denser structure that is not particulate. Acidic conditions promote the growth of comparatively linear, lightly cross-linked polymers. These polymers entangle early in the growth process, but a gel does not form until a sufficient density of cross-links forms[4,5]. The alkoxide completely hydrolyses[6] before condensation but because of re-esterification during drying, a large number of chemically bound alkoxy groups are found. On heating the gel, alkoxy and hydroxy groups are removed by condensation reactions which result in weight loss.

In a monolith, condensation reactions produce new cross-links and stiffen the structure. Further heating results in densification *via* viscous flow and structural relaxation.

When gels are broken up into pieces after gelation and subsequently to powders before being completely dried, some of the cross-links formed at the gel point are broken resulting in re-esterification. Drying in this manner probably results in the formation of regions of inhomogeneity which exist within a non-crystalline polymeric matrix containing chemically bound organics. On initial heating, material moves within these regions of inhomogeneity by diffusion processes from the convex surfaces of the particles to the concave surfaces and causes the filling of the necks between particles. This results in the region consisting of much larger particles, further heating results in particle growth.

The formation of crystalline regions within the bulk of the powder sample hinders densification since the primary processes occurring are those of grain growth and phase transformation. The densification of such powders only becomes the prevalent process at temperatures of 900°C, or greater, when the pore structure was observed to collapse.

4.7.2.3 Micropore Structure

The α_s-method can be used to calculate the micropore volume and the surface area of the samples. A typical α_s-plot for both the powdered and monolithic samples previously discussed is shown in figure 4.23. By drawing a line through the linear part of the plot and the origin the surface area can be calculated from the gradient:

$$A_s = \frac{2 \cdot 89V}{\alpha_s}$$

where 2·89 is a conversion factor obtained by calibration against the BET area of Fransil-I.

Figure 4.23: Typical α_s-plot for a Sample Containing TiO_2=6·34 wt% (HCl=0·045mole)

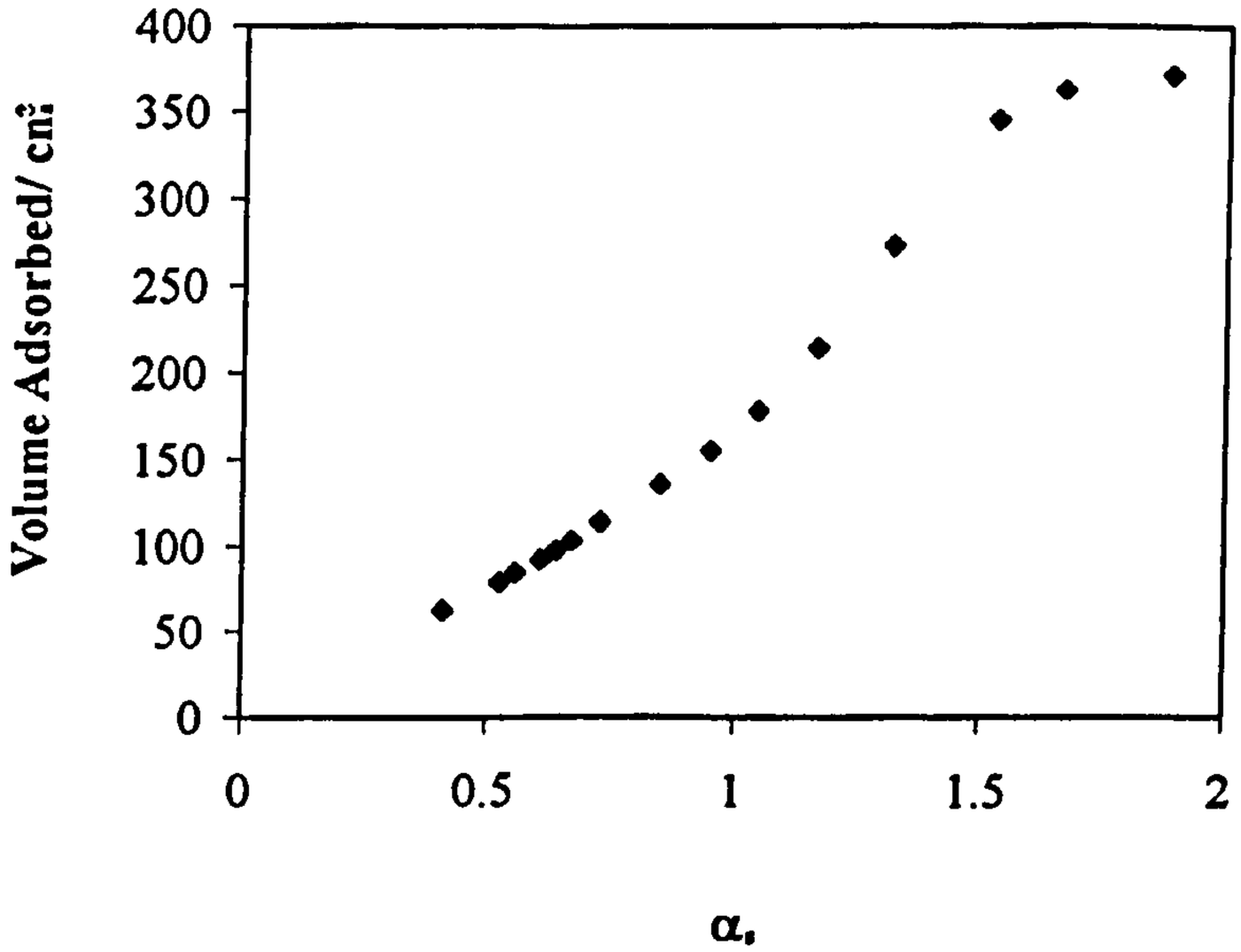

4.7.2.3.1 Effect of Temperature on the Micropore Structure of Powders and Monoliths

For both powders and monoliths there is little difference between the surface areeas calculated using either the BET or the α_s-methods suggesting that there is very little contribution to the overall surface area from micropores. From table 4.12 it can be seen that increasing the temperature results in a decrease in the micropore volume of both powders and monoliths as small pores are destroyed during the heating process.

The micropore volumes obtained for monolithic samples are greater than those of the corresponding powder samples. This suggests that the process of powdering destroys the smaller pores within the bulk.

Table 4.12: Comparison of BET and α_s-data Obtained for Powdered and Monolithic Samples Containing 6·34 weight % Titania

Temperature (°C)	Powders			Monoliths		
	Surface Area (m^2g^{-1})		Micropore Volume (cm^3g^{-1})	Surface Area (m^2g^{-1})		Micropore Volume (cm^3g^{-1})
	BET	α_s		BET	α_s	
120	394	371·9	≈0·000	618	633·1	0·037
300	475	477·6	0·015	742	742·9	0·029
500	439	450·5	0·022	657	661·7	0·033
700	455	439·6	≈0·000	586	587·1	0·010
900	293	284·1	0·008	278	269·6	≈0·000
1100	1·35	1·09	0·000	9	8·34	≈0·000

4.7.2.3.2 Effect on the Micropore Structure of Monolithic Gels of Varying the Amount of Acid used in the Hydrolysis Reaction

From table 4.13 it can be seen that there is little difference between the BET and α_s-derived surface areas suggesting that there is very little contribution to the overall surface area from micropores. Decreasing the amount of acid used in the hydrolysis reaction results in an increase in the micropore volume of the monoliths. This is consistent with the change from type IV (mesoporous solids) to type I (microporous solids) isotherms previously observed.

Table 4.13: Comparison of BET and α_s-data Obtained for Monolithic Samples Containing 6·34 weight % Titania and Prepared using Varying Amounts of Acid in the Hydrolysis Reaction

Amount of HCl (mole)	Surface Area (m^2g^{-1})		Micropore Volume (cm^3g^{-1})
	BET	α_s	
0·045	618	633·1	0·037
0·030	644	651·7	0·034
0·015	631	642·6	0·041
$7·5x10^{-3}$	662	671·9	0·034
$5x10^{-3}$	558	576·8	0·078
$2·5x10^{-3}$	436	479·2	0·099

4.7.2.3.3 Effect of Varying the Amount of Titania (weight %) in the Sample on the Micropore Structure of Powders

For a titania contents of 4·1 weight % the value obtained for the surface area by the α_s-method are significantly larger than those obtained from the BET method, see table 4.14. For a silica only gel prepared in the same way, the micropore volume was greater than for gels containing titania. Increasing the titania content eliminates virtually all microporosity, although as before (see section 4.7.1.1.2) there is no obvious relationship between the amount of titania present in the gel and the surface area and microporosity. Therefore inclusion of titania in the sample eliminates microporosity.

Table 4.14: Comparison of BET and α_s-data Obtained for Powder Samples Containing Varying Amounts of Titania [HCl=0·045 mole]

TiO_2 (wt %)	Surface Area (m^2g^{-1})		Micropore Volume (cm^3g^{-1})
	BET	α_s	
0	812	842·9	0·041
4·1	441	514·7	0·017
4·91	513	514·7	0·017
6·1	551	562·1	0·02
6·34	394	371·9	≈0·000
21·9	477	442·2	≈0·000

4.8 Cobalt(II) Doping

4.8.1 Introduction

Mixed Si/Ti oxide gels were doped with cobalt(II) ions by the pre-doping method and the visible spectra of the gels investigated. The cobalt(II) ion, has the electronic configuration $3d^7$. The splitting of the originally degenerate d-orbitals of the cobalt(II) ion by the attached ligands, enables cobalt(II) to form both tetrahedrally and octahedrally coordinated complexes[38].

The coordination symmetry of cobalt(II) ions has been related to the basicity of glass[39]. Generally, cobalt(II) ions in glass change from octahedral to tetrahedral symmetry as basicity increases, *eg.* by the addition of alkali metal ions. All sodium silicate glasses containing cobalt(II) are blue with the cobalt in tetrahedral coordination. Schultz[40] has shown that 4 and 6 coordinated cobalt(II) ions co-exist in fused silica glass which is acidic compared to other silicate glasses.

Analysis of the visible spectra of the doped gels provides evidence for the coordination environment of the cobalt(II) ions. The most likely donor atoms, surrounding the metal ion, being oxygen atoms in the gel matrix.

Table 4.15: Cobalt(II) Doped Gels Investigated at both 120°C and 900°C.

Titania Content (weight %)	Amount of HCl used in Hydrolysis (mole)
4·1	0·045
4·9	0·045
6·1	0·045
6·34	0·045
6·34	0·030
6·34	0·015
6·34	$7{\cdot}5 \times 10^{-3}$
6·34	5×10^{-3}
6·34	$2{\cdot}5 \times 10^{-3}$
21·9	0·045

4.8.2 Results

4.8.2.1 Visible Spectroscopy

The dehydrated self-supporting discs of the cobalt(II) doped samples were green in colour. Visible spectra of the samples contained a band at approximately 700nm which has been assigned to cobalt(II) ions in a tetrahedral environment (figure 4.24a).

On exposure to the atmosphere for 2 hours the band around 700nm due to the tetrahedral cobalt(II) ion decreases in intensity and a very weak band at approximately 550nm due to

octahedral cobalt(II) appears. This change in coordination of the cobalt(II) ion is accompanied by a colour change to yellow of the sample (figure 4.24b). On exposure to the atmosphere the bulk gels exhibit the same colour change (green→yellow), as the coordination of the cobalt changes from tetrahedral to octahedral.

Dehydrated self-supporting discs of cobalt(II) samples that had been subjected to thermal treatment at 900°C were green in colour. Visible spectra of the samples contained a band at approximately 700nm. After prolonged exposure to the atmosphere the samples remained green in colour and no changes were observed in the visible spectrum. The band remained at 700nm suggesting that the cobalt(II) ion remains tetrahedrally coordinated.

The results were identical for all titania contents and all amounts of acid used in the hydrolysis reaction, hence in the visible region the cobalt(II) is tetrahedrally coordinated. Therefore, the coordination of cobalt(II) is independent of both the amount of titania present in the gel and the reaction conditions.

Figure 4.24: Effect of Exposure to the Atmosphere on the Visible Spectra (400-800nm) of a Cobalt(II) Doped Gel Containing TiO_2=6·34 wt% (HCl=0·045 mole) after: (a) 0 hours; (b) 2 hours

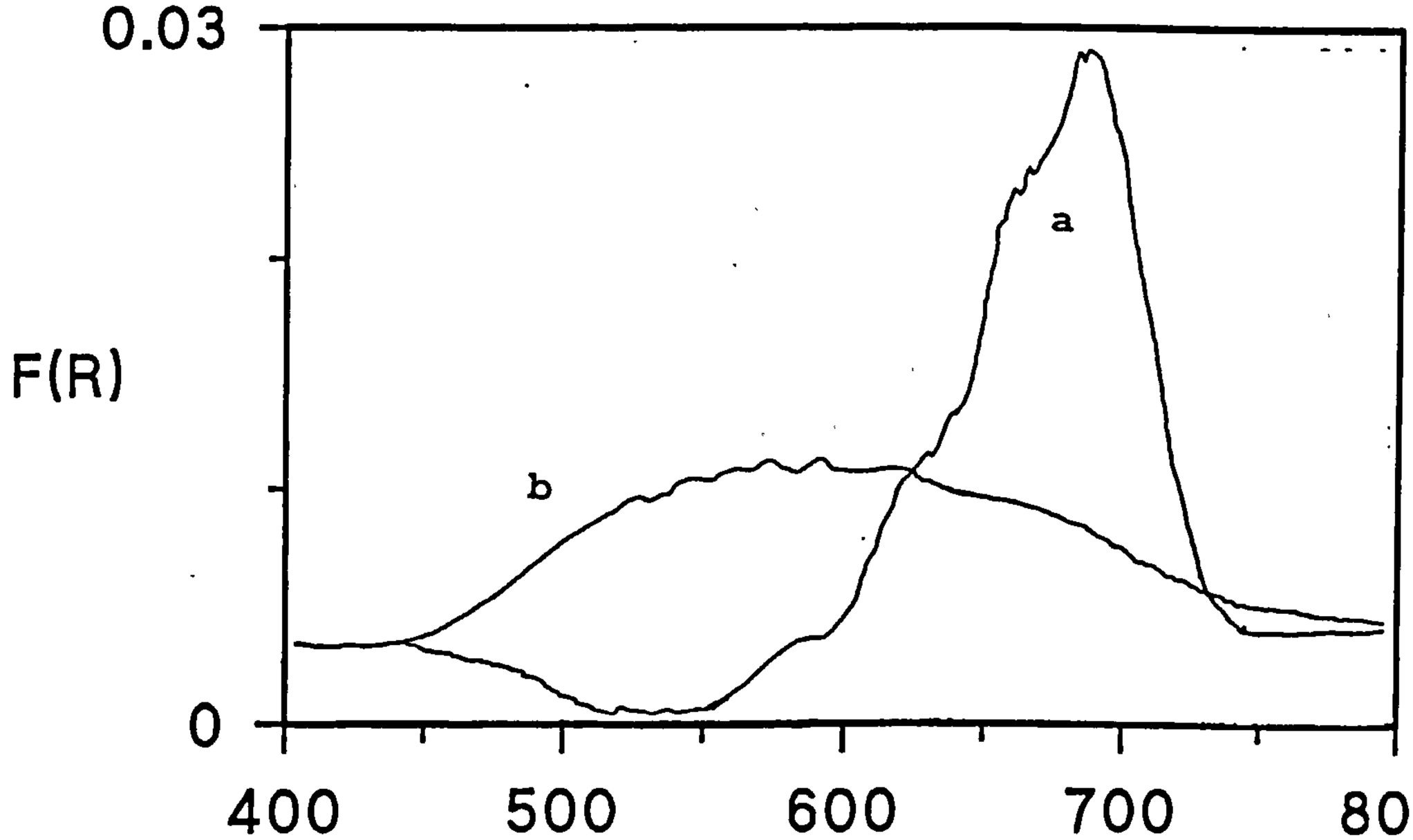

On sintering, cobalt(II) becomes trapped within the gel, in a position surrounded by four oxygen atoms from the gel matrix that is no longer exposed to the external environment.

4.8.2.2 Near-Infrared Spectroscopy

The near-infrared spectra of dehydrated Co(II) doped samples show bands arising from the overtone and combination bands of Si-OH and H-OH[7,8]. As mentioned previously, section 4.4.2, the region 1200-2500nm contains three sets of bands at *ca* 2200, 1900 and 1400nm, see figure 4.25. These bands have respectively been assigned as combination stretching vibrations for water, and the first overtones of the stretching modes of Si-OH and water. In addition to the bands usually observed a broad band from about 1400 to 1800nm was observed in the doped samples. This band has been assigned by Schultz[40] as the transition $^4A_2 \rightarrow {}^4T_1(F)$, arising from tetrahedrally coordinated cobalt.

The similarity of blank and doped gels in the 2200nm region implies that the band arises wholly from the effects of hydrogen bonding between silanol groups and residual water molecules. The presence of cobalt cations and chloride anions in the gel complicates the adsorption model by introducing additional interactions with the water molecules

The NIR spectra of samples that had been heated to 900°C indicate that the sample is not fully densified. Therefore some silanol groups remain as internal species, trapped within pores that are closed to the external environment. As before the additional broad band due to the $^4A_2 \rightarrow {}^4T_1(F)$ transition of tetrahedrally coordinated cobalt was observed from 1400 to 1800nm.

4.8.3 Discussion

The colour and spectroscopic features, suggest that the coordination geometry of cobalt(II) within the samples studied was tetrahedral, although octahedral and tetrahedral species may coexist. Due to the significant decrease in the intensity of the visible spectra of octahedral cobalt complexes compared to tetrahedral complexes it is possible that spectral contributions from octahedrally coordinated cobalt would not be observed in a sample containing some tetrahedrally coordinated cobalt(II).

Thermal treatment at 900°C implies that cobalt is tetrahedrally coordinated within the silica matrix. On sintering, cobalt(II) becomes trapped within the gel, in a position surrounded by four oxygen atoms from the gel matrix. The samples studied were not affected by rehydration suggesting that the cobalt is not accessible to the external environment.

The results were identical for all titania contents and all amounts of acid used in the hydrolysis reaction, hence in the visible region the cobalt(II) is tetrahedrally coordinated. Therefore, the coordination of cobalt(II) is independent of both the amount of titania present in the gel and the reaction conditions used to generate the gel.

Figure 4.25: Near-infrared Spectra of Dehydrated cobalt(II) doped Gels in the First Overtone and Combination Region (1200-2500nm) (a) blank ; (b) 120°C; (c) 900°C

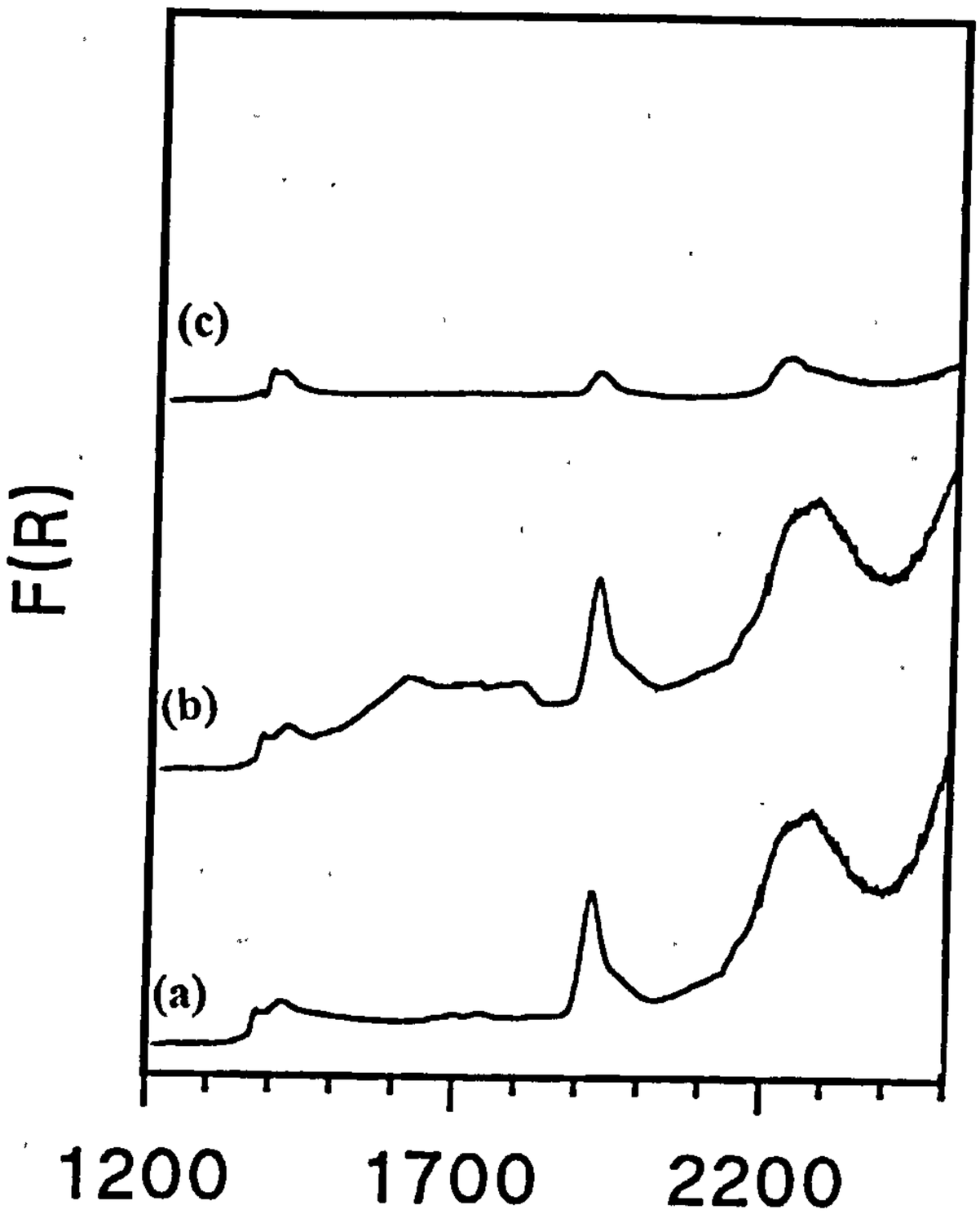

4.9 Conclusions

Reflectance NIR spectroscopic studies of these gels indicate that both decreasing the amount of acid used in the hydrolysis reaction and increasing the amount of TiO_2 in the sample resulted in higher relative levels of hydrogen bonded silanol species being present within the samples. On hydration, the presence of increased levels of titania result in no observable free silanols on the surface. Increasing the treatment temperature of the sample and the subsequent rehydration of the surface results in sharper and less intense peaks. This is consistent with the bulk of the silanol groups being removed and isolated silanol groups remaining on the surfaces and within the sample. The sharper peaks observed are consistent with there being little or no interaction between surface silanol groups. The presence of bands due to free silanol groups in samples treated at high temperatures, even after extended rehydration is indicative of the surface being less hydrophilic and free silanol groups remaining within the bulk of the sample.

Increasing the thermal treatment temperature of the sample to 900°C has been shown by both mid- and near-infrared spectroscopy to reduce the intensity of peaks due to both free and hydrogen bonded Si-OH. The shift of the band at *ca* 1100cm^{-1} to a higher wavenumber at temperatures greater than 900°C, corresponds to a strengthening of the gel matrix by shortening the Si-O bonds *via* the condensation processes detailed below.

$$Si-OH+HO-Si \rightarrow Si-O-Si+H_2O$$

$$Si-OH+HO-Ti \rightarrow Si-O-Ti+H_2O$$

At temperatures of 900 and 1100°C, mid-infrared spectroscopy has revealed the formation of Si-O-Ti bonds and the incorporation of titanium atoms into the silica framework.

However, the incorporation of titanium atoms into the framework is not complete. This is evidenced by the appearance of X-ray diffraction patterns due to both the rutile and anatase forms of titanium dioxide in samples dried as powders. The existence of increasingly more intense bands due to Ti-O in the mid-infrared may be attributed to the formation of crystals of titanium dioxide within the bulk sample exhibited at elevated temperatures.

Samples of high titania content were found to exhibit rutile crystallinity at low temperatures (120°C) suggesting that there may be an upper limit to the amount of titanium that can be fully incorporated into the silica framework.

For both powders and monoliths, increasing the thermal treatment temperature of the samples results in the progressive decrease in both surface area and pore volume. Changes in surface area and pore structure are only significant at temperatures greater than 700°C which is consistent with the removal of surface hydroxyl groups as observed by NIR spectroscopy.

Heating the samples to 900°C resulted in a decrease in pore volume but very little change in average pore diameter. This is supported by the changes observed in the shape of the hysteresis loop which suggest that pores are destroyed and their shapes change on sintering.

However, heating to temperatures of greater than 900°C resulted in an increase in the average pore diameter as the remaining pores collapsed and densification resulted.
Decreasing the amount of acid used in the hydrolysis reaction results in an increase in the micropore volume of the monoliths. Similarly, in the case of both powders and monoliths increasing the temperature results in a lower micropore volume.
Pre-doping with cobalt(II) chloride and dehydrating results in gels which possess cobalt(II) ions in a tetrahedral coordination environment. Visible spectroscopy of the gel treated at 120°C, revealed that on exposure to the atmosphere a band due to octahedral cobalt(II) replaced that arising from tetrahedral cobalt(II). However rehydration of the gels treated at 900°C had no effect on the environment of the cobalt(II) ions which remained tetrahedral. This suggests that each cobalt(II) ion is surrounded by four oxygen atoms from the gel matrix and is trapped within the matrix in sites which are inaccessible to the atmosphere.

4.10 References

1 P.P. Lottici, D. Bersani, M. Braghini and A. Montenero, *J. Mat. Sci.* **28**(1993) 177-183

2 C.J. Brinker and G.W. Scherer, *Sol-Gel Science* p 675 (Academic Press, New York, 1990)

3 M. Nogami and Y. Moriya, *J. Non Crystalline Solids* **37**(1980) 191-201

4 C.J. Brinker, W.D. Drotning and G.W. Scherer, in *Better Ceramics Through Chemistry,* eds C.J. Brinker, D.E. Clark and D.R. Ulrich p. 25-32 (North-Holland, New York, 1984)

5 C.J. Brinker and G.W.Scherer, *J. Non Crystalline Solids* **70** (1985) 301-322

6 R.A. Assink and B.D. Kay, in *Better Ceramics Through Chemistry,* eds C.J. Brinker, D.E. Clark and D.R. Ulrich p. 301-306 (North-Holland, New York, 1984)

7 A. Duran, C. Serna, V. Fornes & J.M. Fernandez-Navarro, *J. Non Crystalline Solids* **82**(1986) 69-77

8 M. Decottognies, J. Phalippou & J. Zarzycki, *J. Mat. Sci.* **13**(1978) 2605-2618

9 C.J.R. Gonzalez-Oliver, P.F. James & H. Rawson, *J. Non Crystalline Solids* **48**(1982) 129-152

10 M.F. Best and R.A. Condrate Sr., *J. Mat. Sci. Lett.* **4**(1985) 994-998

11 A. Bertoluzza, C.Fagnano, M.A. Morelli, V. Gottardi & M.Guglielmi, *J. Non Crystalline Solids* **48**(1982) 117-128

12 T. Isobe and M. Senna, *J. Solid St. Chem.* **93**(1991) 358-367

13 K. Buijs and G.R. Choppin, *J. Chem. Phys.* **39** (1963) 2035-2041; 2042-2050

14 C.C. Perry and X. Li, *J. Chem. Soc. Faraday Trans.* **87**(5) (1991) 761-766

15 J.H. Anderson and K.A. Wickersheim, *Surface Sci.* **2** (1964) 252-260

16 F. Orgaz and H. Rawson, *J. Non Crystalline Solids* **82** (1986) 57-68

17 M.R. Basila, *App. Spec. Rev.* **1** (1968) 289-372

18 C.C. Perry and X. Li, *J. Chem. Soc. Faraday Trans.* **87**(24) (1991) 3857-3862

19 A.V. Kiselev, *Disc. Faraday Soc.* **52** (1971) 14-32

20 D. Mifel, V.B. Kazarsky and V.M. Andreev, *Surface Sci.* **72** (1978) 342-356

21 E. Lippmaa, M. Mägi, A. Samosan, G. Engelhardt and A -R. Grimmer, *J. Am. Chem. Soc.* **102**(1980) 4889-4893

22 D.W. Sindorf and G. Maciel, *J. Am. Chem. Soc.* **105**(1983) 1487-1493

23 A -R. Grimmer, H. Rosenberger, H. Bürger and W. Vogel, *J.Non Crystalline Solids* **99** (1988) 371-378

24 D.L. Wood, E.M. Rabinovich, D.W. Johnson Jr, J.B. MacChesney and E.M. Vogel, *J. Am. Ceram. Soc.* **66**(1983) 693-699

25 H. Yametra, B. Fitzpatrick and G. Gordon, *J. Mol. Spec.* **14**(1964) 268-278

26 G.R. Choppin and H.R. Violante, *J. Chem. Phys.* **56**(1972) 5890-5898

27 G.R. Choppin and J.R. Downey, *J. Chem. Phys.* **56**(1972) 5899-5903

28 C.C. Perry and X. Li, in *Chemical Processing of Advanced Materials* p.131, eds. L.L. Hench and J.K. West Wiley, 1992)

29 S. Brunauer, P.H. Emmett and E. Teller, *J. Am. Chem. Soc.* **60** (1938) 309-319

30 E.P. Barrett, L.G. Joyner and P.P. Halenda, *J. Am.Chem. Soc.* **73** (1951) 373-380

31 M.R. Bhambhani, P.A. Cutting, K.S.W. Sing and D.H. Turk, *J. Colloid Interface Sci.* **38** (1) (1972) 109-117

32 R.K. Iler, in *The Chemistry of Silica* p.496 (Wiley, New York, 1979)

33 R.A. Beebe, J.B. Beckwith and J.M. Honig, *J. Am. Chem. Soc.* **67** (1945) 1554-1558.

34 R.A. Van Nordstrand, W.E. Kreger and H.E. Ries Jr., *J. Phys. Colloid Chem.* **55** (1951) 621-638

35 J. Bastick, *Bull. Soc. Chim. Fr.* **20** (1953) 437-440

36 S.J. Teichner, G.A. Nicolaon, M.A. Vicarini and G.E.E. Gardes, *Adv. Colloid Interface Sci.* **5** (1976) 245-273

37 R.K.Iler, in *The Chemistry of Silica* p.545-546 (Wiley, New York, 1979)

38 K.S.W. Sing, D.H. Everett, R.A.W. Haul, L. Moscou, R.A. Pierotti, J. Rouquérol and T. Siemieniewska, *Pure Appl. Chem.* **57** (1985) 603-619

39 C.J. Brinker, K.D. Keefer, D.W. Schaefer, R.A. Assink, B.D. Kay and C.S. Ashley, *J. Non Crystalline Solids* **63** (1984) 45-59

40 R.A. Assink and B.D. Kay, in *Better Ceramics Through Chemistry* p. 301-306 (North-Holland, New York, 1984)

Chapter 5: Mixed SiO_2-TiO_2 Gels from a Double Alkoxide Precursor

5.1 Introduction

The results of an investigation into the effects of reaction conditions and thermal treatment on the bulk structure and pore structure adopted by monolithic gels prepared using the double alkoxide prepared in section 3.4.1 are presented in this chapter. The nominal constitutions of the gels studied in this chapter are detailed in table 5.1.

Table 5.1: Silicon/Titanium Oxide Gels Investigated.

Nominal Amount of TiO_2 (weight %)	Amount of Acid used in Hydrolysis (mole)
6·34	0·045
6·34	0·030
6·34	0·015
6·34	$7{\cdot}5 \times 10^{-3}$
6·34	5×10^{-3}
6·34	$2{\cdot}5 \times 10^{-3}$

5.2 X-Ray Diffraction

5.2.1 Introduction

X-ray diffraction has been performed to determine the crystalline nature of mixed silicon-titanium oxides at a number of temperatures (see section 2.4.3). Once crystallinity was observed then the size of the crystallites was calculated using the Scherrer equation (equation 2.12).

5.2.2 Results

5.2.2.1 Effect of Varying both the Amount of Acid used in the Hydrolysis and Temperature on the Crystalline Nature of a Gel Nominally Containing TiO_2=6·34 weight%

From the X-ray diffraction pattern of a physical mixture of anatase:rutile (1:1), it was found that the height of the anatase peak at 24-25° was 1·5 times greater than the height of the corresponding rutile peak at 26-27°, see figure 4.1. Taking this into account it is possible to compare peak heights for the mixed silica-titania gels and determine whether anatase or rutile is the predominant crystalline phase.

Table 5.2: Effect of Varying both the Amount of Acid used in the Hydrolysis and Temperature on the Crystalline Nature of a Gel Nominally Containing TiO_2=6·34 weight %

Amount of HCl (mole)	Temperature/ °C					
	120	300	500	700	900	1100
0·045	X	X	X	X	X	X
0·030	X	X	X	X	X	X
0·015	X	X	X	X	X	A
$7·5x10^{-3}$	X	X	X	X	X	X
$5x10^{-3}$	X	X	X	X	X	A
$2·5x10^{-3}$	X	X	X	X	X	A

X=amorphous; A=anatase; R=rutile.

All the samples investigated were amorphous after treatment at temperatures up to and including 900°C. Increasing the treatment temperature to 1100°C resulted in the formation of anatase in samples prepared using 0·015, $5x10^{-3}$ and $2·5x10^{-3}$ mole HCl in the hydrolysis reaction, see figures 5.1 to 5.3.

5.2.2.2 Particle Sizes

Particle sizes have been calculated using the Scherrer equation from the major anatase peak at 24-25°. These are shown in table 5.3.

Table 5.3: Calculated Average Anatase Crystal Sizes at 1100°C Calculated from the Major Anatase Peak at 2θ=24-25°

Amount HCl /mole	Average Particle Size / nm
0·045	X
0·030	X
0·015	16·3
$7·5x10^{-3}$	X
$5x10^{-3}$	10·8
$2·5x10^{-3}$	10·8

Figure 5.1: X-ray Diffraction Patterns Obtained for a Powder Nominally Containing TiO_2=6·34 wt%; HCl=0·015 mole heated at (a) 900°C; (b) 1100°C
[A=anatase]

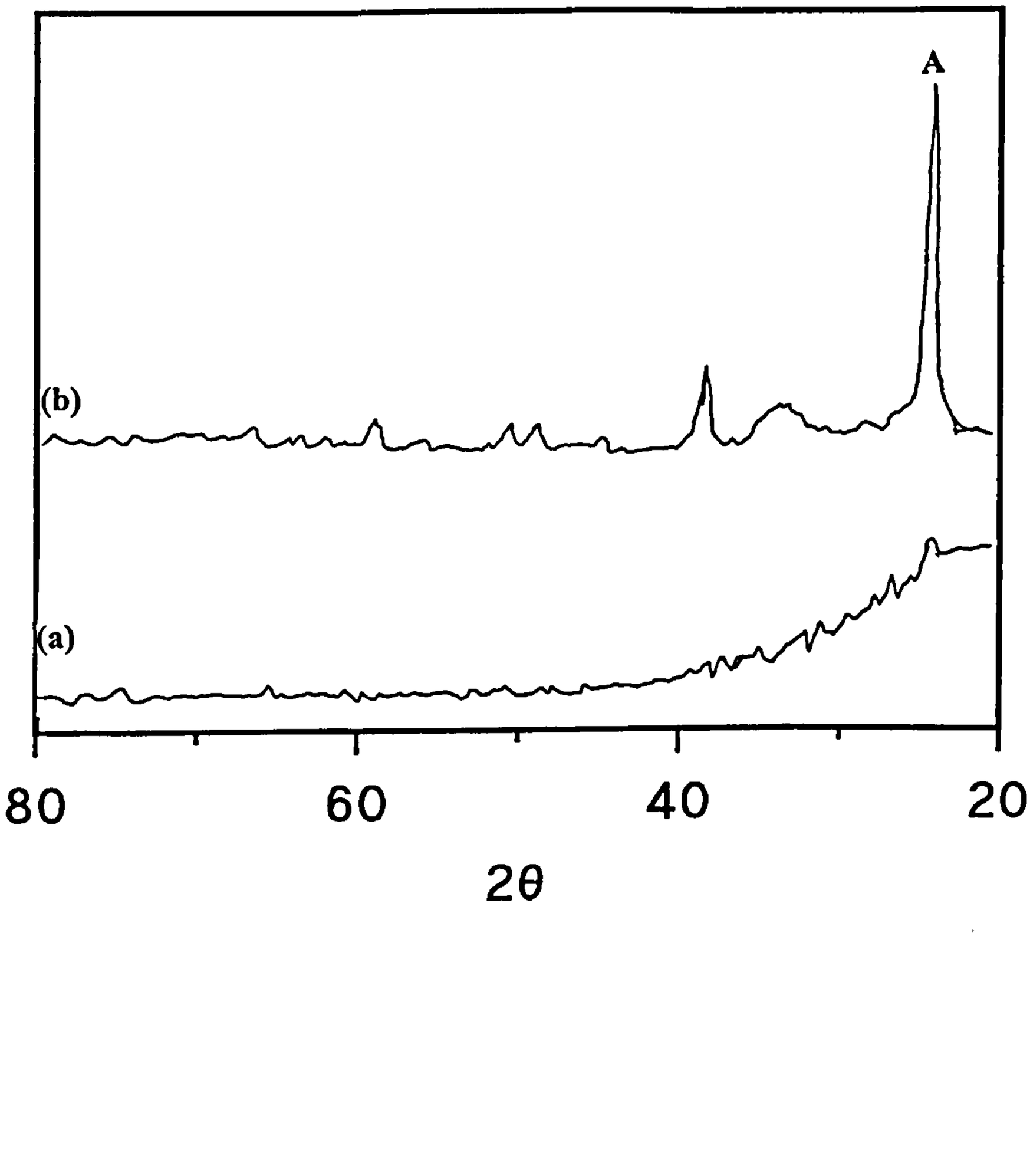

Figure 5.2: X-ray Diffraction Patterns Obtained for a Powder Nominally Containing TiO_2=6·34 wt%; HCl=$5x10^{-3}$ mole heated at (a) 900°C; (b) 1100°C
[A=anatase]

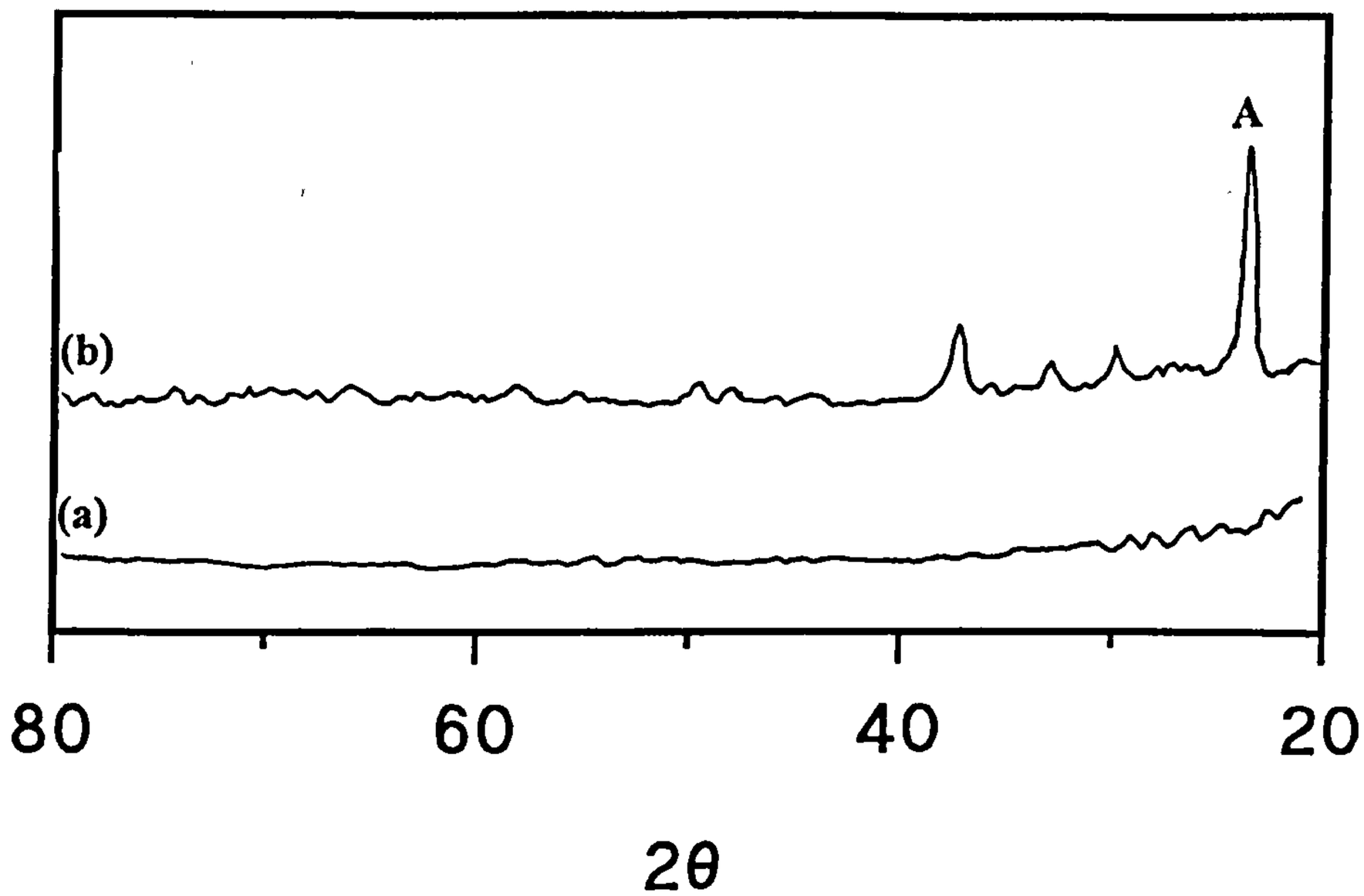

Figure 5.3: X-ray Diffraction Patterns Obtained for a Powder Nominally Containing TiO_2=6·34 wt%; HCl=$2·5x10^{-3}$ mole heated at (a) 900°C; (b) 1100°C
[A=anatase]

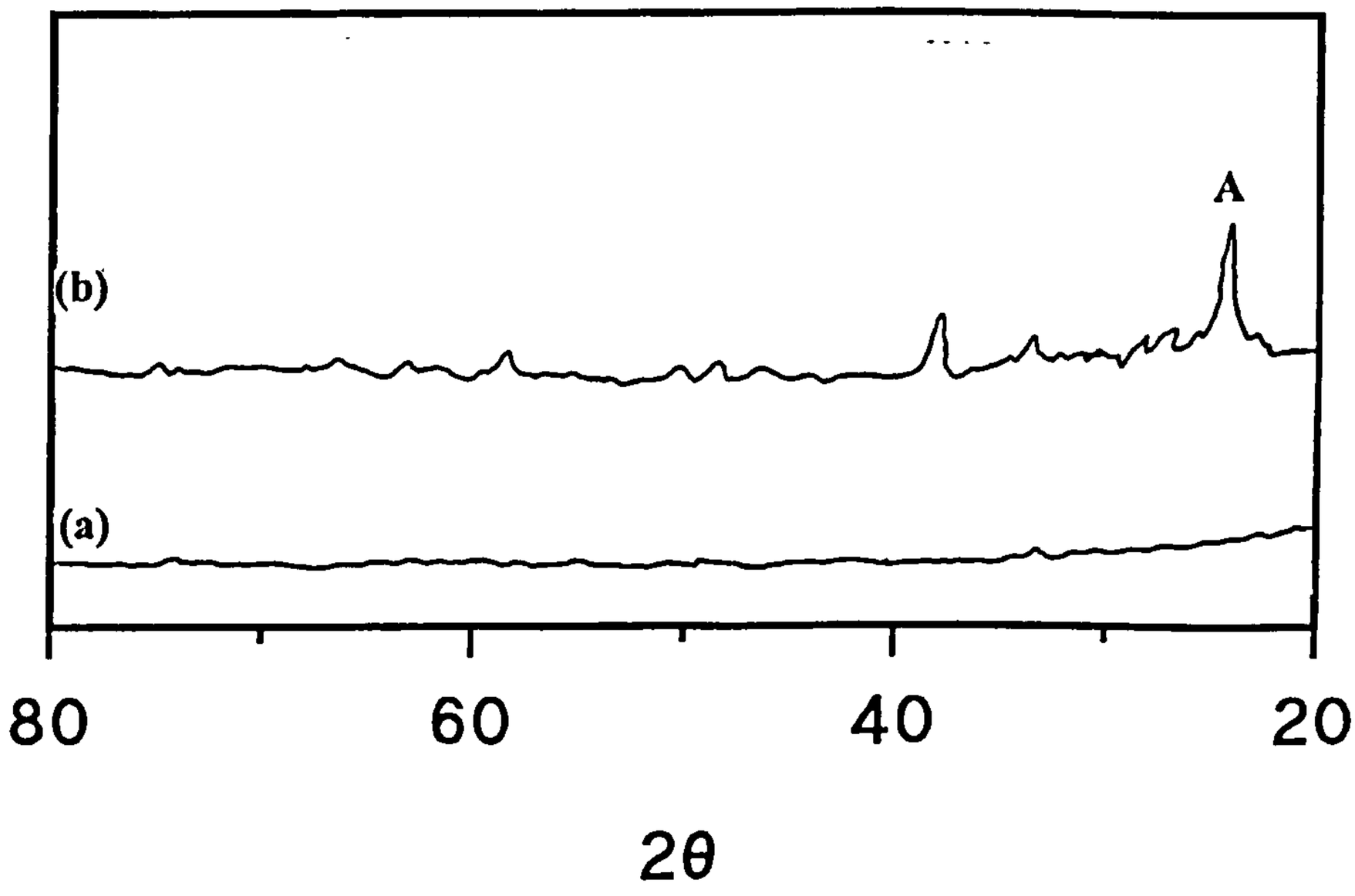

As the amount of acid used for the hydrolysis reaction decreases, the average size of the particles formed at 1100°C decreases. Therefore as the peak intensity decreases the smaller the crystals formed.

5.2.3 Discussion

On sintering, condensation reactions produce new cross-links which stiffen the structure and lead ultimately to densification, see section 4.2.3 for further details. Further heating to 900°C results in complete densification *via* viscous flow and structural relaxation, as no crystallinity has been detected by X-ray diffraction. Further heating to 1100°C results in the formation of crystalline regions of anatase. Since the gel has already shrunk during densification there are more points of contact through which diffusion and growth of a second phase can occur. The input of thermal energy results in the formation of crystalline regions by the diffusion of material either from the convex surfaces of the particles to the concave surfaces or through the lattice and causes the filling of the necks between the particles. This results in larger crystallites which can be detected by X-ray diffraction.

5.3 Effect of Temperature on the Infrared Spectra of Silica-Titania Gels Nominally Containing 6-34 weight % Titania

5.3.1 Introduction

The IR fundamental region (4000-400 cm^{-1}) has been used to investigate any structural changes that may occur within the bulk of the mixed silica-titania gel as a function of temperature. The gels investigated are detailed in table 5.1.

There are six main vibrational bands of interest in the region studied, the assignments of which are detailed in table 5.4.

Table 5.4: Mid-infrared Absorbance Spectral Assignments

Assignment	Wavenumber/cm^{-1}
ν_{as}(Si-O-Si), LO[1]	1200-1250
ν_{as}(Si-O-Si), TO[1] ν_{as}(Si-O-Ti)*[4]	1024-1100
[a]ν(SiOH, Si-O^-)[2] [b]ν(TiOH, Ti-O^-)[3,6] ν_{as}(Si-O-Ti)**[4]	931-964
ν_s(Si-O-Si)[2]	790-800
ν_s(Ti-O)[3]	550-600
δ(Si-O-Si), o.p[5]	451-468

* Partial contribution to observed band at > 1000°C.

** Major contribution to band at > 1000°C.

[a] ν(SiOH, Si-O^-)=960cm^{-1}; [b] ν(TiOH, Ti-O^-)=970cm^{-1}

5.3.1 Results and Discussion

The spectra obtained for a sample containing 6·34 weight % at an acid concentration of 0·030 mole, after treatment at various temperatures are shown in figure 5.4 (spectra of other acid contents are shown in appendix II).

The most intense band at *ca* 1100cm^{-1} is asymmetric and possesses a weak shoulder at *ca* 1200cm^{-1} that is present at all temperatures (see figure 5.4). The two bands are associated with the transverse optical (TO) and longitudinal optical (LO) modes of the antisymmetric Si-O-Si stretching vibration respectively[1]. At temperatures of 900°C and above, the band at *ca* 1100cm^{-1} shifts to a higher wavenumber indicating a strengthening of the Si-O bonds. This shift is shown in figure 5.5.

Figure 5.4: Mid-infrared Spectra of a Sample Containing 6·34 weight % Titania, HCl=0·030 mole Treated at Different Temperatures. (a) 120°C; (b) 300°C; (c) 500°C; (d) 700°C; (e) 900°C; (f) 1100°C.

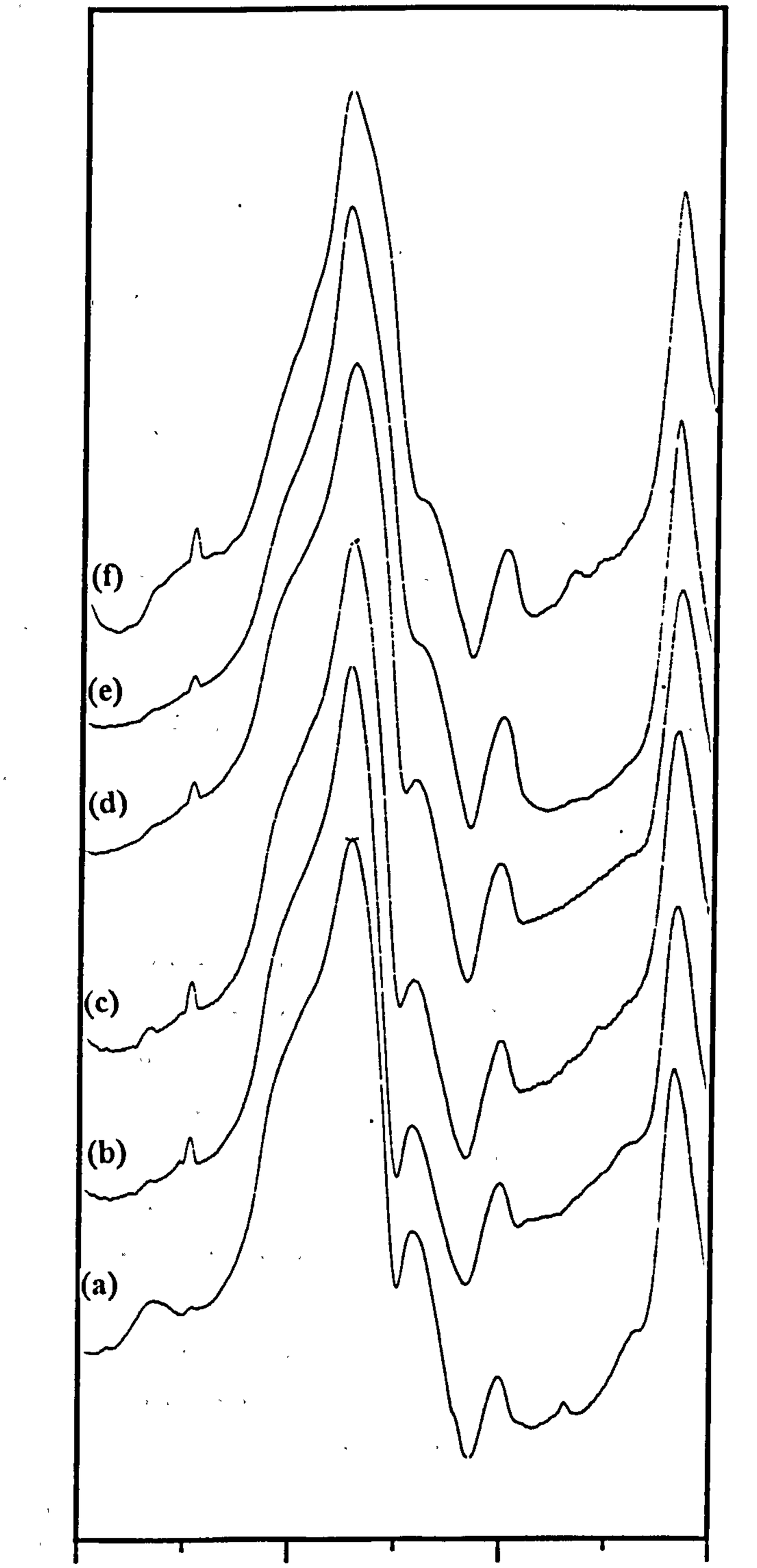

Figure 5.5: Position of the Antisymmetric O-Si-O Stretching Vibration Near 1100cm^{-1} at Different Temperatures for a Sample Containing HCl=0·015 mole

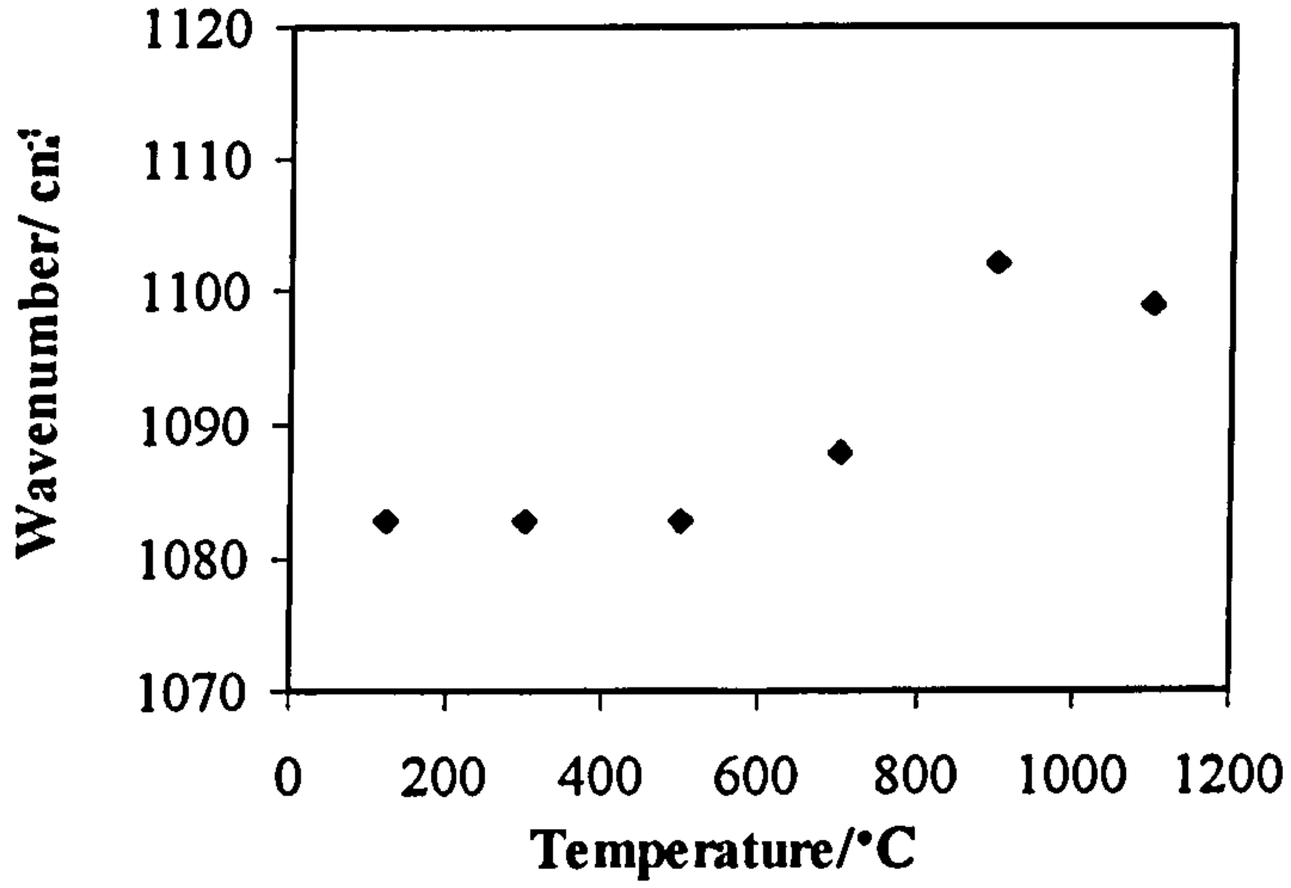

The band at *ca* 960cm^{-1} is mainly associated with Si-OH stretching with an appreciable contribution from TiOH stretching vibrations[2,3,6]. The relative intensity of the peak decreases as the treatment temperature is increased to 900°C, see figure 5.4. This is consistent with the removal of SiOH/TiOH from the surface. However, increasing the temperature above 900°C results in an increase in the relative intensity of the observed band due to an increase in the concentration of Si-O-Ti bonds in the sample. This is indicative of the incorporation of titanium into the network at elevated temperatures.

From figure 5.4 it is observed that the network Si-O-Si symmetric bond stretching vibration at *ca* 800cm^{-1} [2] does not shift appreciably or change in intensity relative to the band at *ca* 1100cm^{-1} with increasing treatment temperature. Similarly, varying the amount of acid used in the hydrolysis reaction had no effect on either the intensity or position of the peak. Therefore, the inclusion of titanium in the sample has no effect on the silica matrix.

At all temperatures there is evidence in the spectra (figure 5.4) of a shoulder appearing at *ca* 600cm^{-1}. At temperatures of 900°C and above, the intensity of this shoulder relative to the 800cm^{-1} band was observed to increase in intensity. This band has been attributed to the symmetric stretching vibrations of the Ti-O bond[3] and arises due to the formation of titanium dioxide in the bulk gel.

The peak at *ca* 460cm^{-1} has been assigned to the out-of-plane bending vibrations of network Si-O-Si[5]. This band remains unchanged in both intensity and position at temperatures up to and including 900°C. Increasing the treatment temperature to 1100°C resulted in an increase in the peak intensity relative to the band at 1100cm^{-1} and a shift to 470cm^{-1}. This is due to the strengthening of the silica network at elevated temperatures.

5.3.1.1 Fourier Self-Deconvolution

The spectra acquired were manipulated using Fourier self-deconvolution (OMNIC software) to separate peaks and their shoulders and derivative methods to determine

Figure 5.6: Spectra Resulting from Fourier Self-Deconvolution for a Sample Containing TiO_2=6·34 weight % and Treated at 300°C (a) second derivative; (b) first derivative; (c) Fourier self-deconvolution; (d) original spectrum

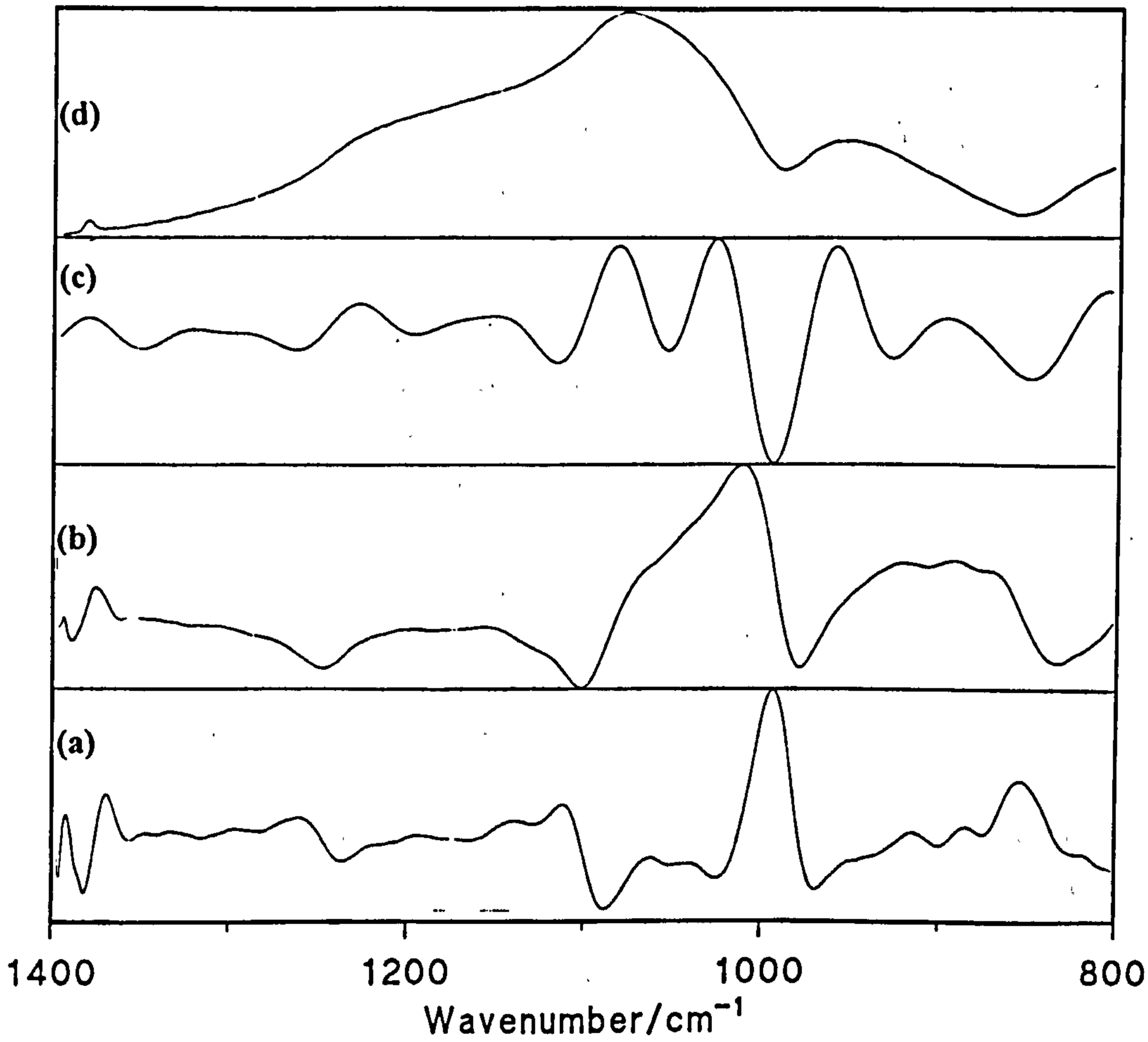

whether the peaks observed were 'real'. It is obvious that the original spectra usually contain more than one peak within the spectral envelope encompassing 920 and 1250cm^{-1} and this has been confirmed by spectral deconvolution.

On deconvolution, the band at *ca* 1200cm^{-1} previously assigned to the longitudinal optical mode of the antisymmetric Si-O-Si stretching vibration, split into three peaks at *ca* 1230cm^{-1} *ca* 1207cm^{-1} and *ca* 1170cm^{-1}. The peak at *ca* 1230cm^{-1} can be attributed as the longitudinal optical mode of antisymmetric Si-O-Si stretching vibrations and that at 1170cm^{-1} to antisymmetric stretching vibrations of Si-O within a slightly different environment. In the instances where splitting into three bands was observed, comparison of the deconvoluted spectra with the first and second derivative spectra implied that the peak at *ca* 1207cm^{-1} was not real and arose due to excessive spectral enhancement.

The peak at approximately 1100cm^{-1} split into a further two peaks centred at *ca* 1090cm^{-1} and *ca* 1040cm^{-1}. The higher wavenumber peak has been assigned as the transverse optical mode of antisymmetric Si-O-Si stretching vibrations and the peak at *ca* 1040cm^{-1} to the antisymmetric stretching vibrations of Si-O-Ti bonds.

At thermal treatment temperatures of 1100°C or less, the spectra of all the samples (see for example figure 5.6) show that the relative intensity of the band at *ca* 1230cm^{-1} was about the same as that of the band at *ca* 1170cm^{-1}. Varying the amount of acid used for the hydrolysis reaction had no effect on the resulting spectra.

At temperatures less than or equal to 500°C, the band at *ca* 1090cm^{-1}, assigned to the transverse optical mode of antisymmetric Si-O-Si stretching vibrations was approximately the same intensity as the band at *ca* 1040cm^{-1}. Any small variation in the intensity of the bands is difficult to quantify since differences may occur as a result of the data manipulation process. At increased treatment temperatures the band at *ca* 1090cm^{-1} became the more intense of the two bands. Increasing the treatment temperature to 1100°C resulted in the band at *ca* 1090cm^{-1} shifting to a higher wavenumber *ca* 1106cm^{-1}, this has been attributed to a strengthening of the Si-O bonds.

No variation in the behaviour or splitting of the remaining bands on deconvolution was observed.

5.4 The Effect Of Temperature and the Amount of Acid used in Hydrolysis on the Near Infrared (NIR) Spectra of Silica-Titania Gels in the First Overtone Region (1200-2500nm)

5.4.1 Introduction

This section contains data obtained for a series of spectroscopic studies in the first overtone region of the near-infrared (1200-2500nm). Samples were prepared and reflectance spectra recorded as detailed in section 2.2.5. The results obtained have been used to determine how the surface changes with heat treatment.

The spectral region contains three sets of bands at *ca* 2200, 1900 and 1400nm. These have respectively been assigned as combination stretching vibrations for SiOH with a contribution from the bulk matrix, the combination of stretching and deformation vibrations for water, and the first overtones of the stretching modes of SiOH and H_2O. These are detailed more extensively in table 4.6 (page 110).

5.4.2 Results and Discussion

The most prominent absorptions occur at 1370 and 2200nm. For samples treated at 120°C, the sharp peak at 1370nm has been assigned to the first overtone of the fundamental OH stretch of free silanol groups[7]. However, the peak at 2200nm is more perturbed and has a greater intensity. This has been attributed[8,10] to a combination of the fundamental OH stretching of free silanol groups with the fundamental symmetric stretching of the silica framework at 800cm^{-1}. The band at 1900nm arises from the combination of stretching and deformation modes of water, and the shoulder at 1400nm from a combination of symmetric and antisymmetric stretching vibrations. Absorptions like these arise from isolated water molecules hydrogen bonded to silanol groups. The presence of shoulders on the major peaks at 1940 and 1450nm is indicative of water molecules hydrogen bonded to one another. A more detailed description of spectral assignments can be found in section 4.4.2.

5.4.2.1 Effect of Thermal Treatment

As previously observed for silica-titania gels (see section 4.4.2.1), the overall effect of increasing the thermal treatment temperature of the sample is a systematic reduction in the intensity of all three bands, see figure 5.7. This is consistent with the dehydroxylation processes:

$$Si-OH+HO-Si \rightarrow Si-O-Si+H_2O$$
$$Si-OH+HO-Ti \rightarrow Si-O-Ti+H_2O$$

Surface dehydroxylation occurs across a wide temperature range with the removal of monomerically bound water (1400nm) at low temperatures. However, from figure 5.7 it can be seen that the most significant reduction in the number of free silanols is only visible in the NIR at temperatures greater than 700°C.

The sharp peak at 1374nm attributable to both vicinal free OH groups and isolated free OH groups, is only visible in the sample treated at 120°C. Increasing the treatment temperature to 300°C and above, results in the band shifting to 1413nm. Although the band remains sharp there is an asymmetry on the high wavelength side at *ca* 1450nm. Both of these bands are attributable to the presence of perturbed or hydrogen bonded silanol groups. Progressively increasing the treatment temperature to 900°C results in the elimination of these bands, see figure 5.7.

As the treatment temperature of the gel was increased from 120°C, then the peak at 2200nm began to decrease in intensity (like the band at 1400nm) until at 900°C it was no longer detectable.

From these results it appears that even after extended dehydration, the surface of gels prepared from the double alkoxide consist of water hydrogen bonded to silanol groups. The elimination of silanol groups with temperature is more regular than previously observed for silica/titania gels (see section 4.4.2.1). In contrast to the results obtained for silica[8] and the silica/titania gels described previously (4.4.2.1) the elimination of surface silanol groups is completed at a much lower temperature (900°C).

Figure 5.7: Effect of Thermal Treatment Temperature on the Near Infrared (NIR) Spectra of a Sample Containing TiO_2=6·34 weight % [Hydrolysis Acid =0·045 mole]
(a) 120°C; (b) 300°C; (c) 500°C; (d) 700°C; (e) 900°C.

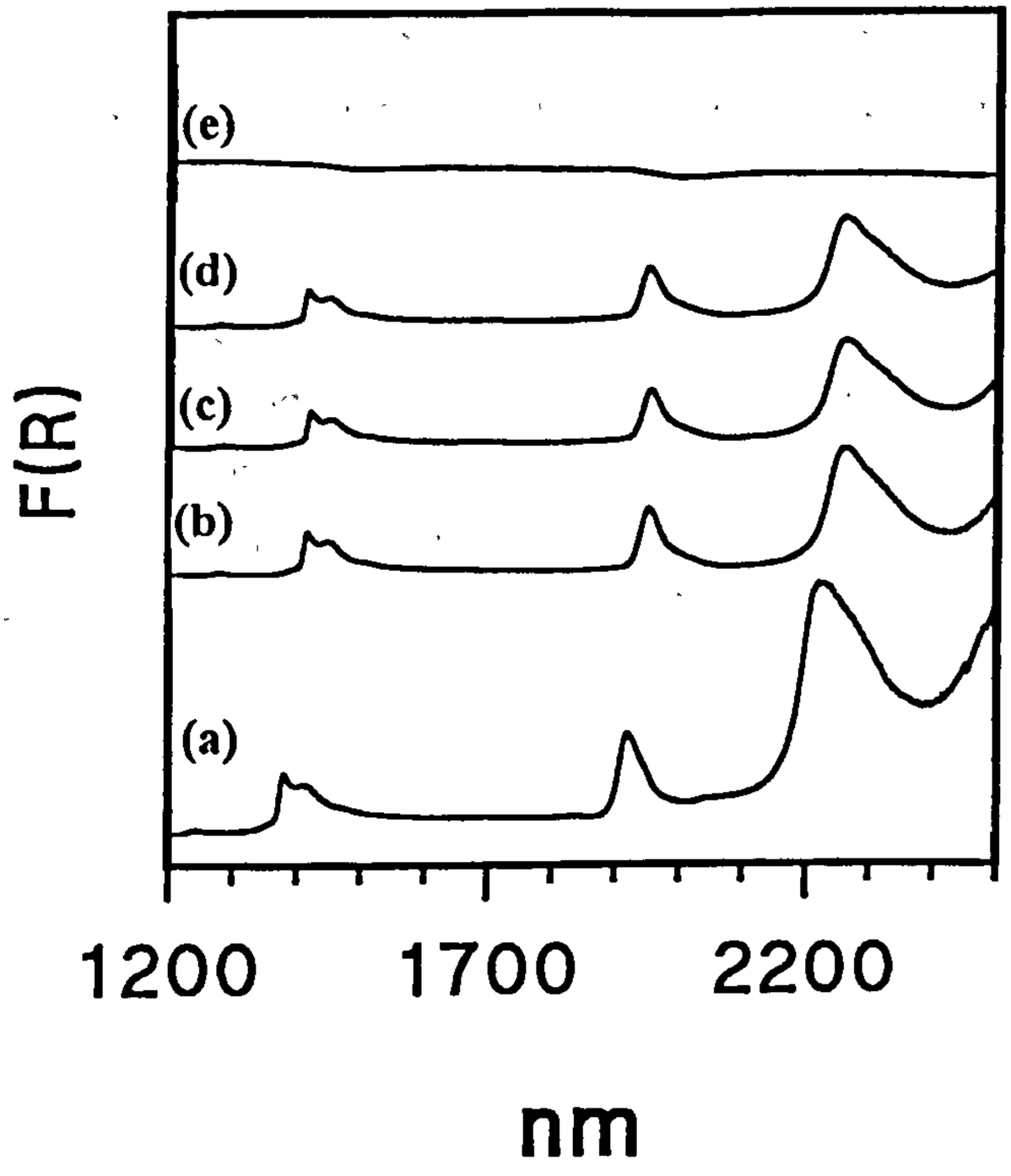

* All spectra on same reflectance scale.

5.4.2.2 Variation of the Amount of Acid used in the Hydrolysis Reaction

As the amount of acid used in the hydrolysis reaction was decreased, there was a corresponding decrease in the number of free -SiOH groups (1375nm), and an increase in the number of hydrogen bonded species (1400nm), see figure 5.8.

The band near 2200nm which is attributable to silanol groups, is stronger and broader than the corresponding first overtone band at 1375nm. However, high wavelength asymmetry due to perturbed species on the surface is still observed. This combination band increases in intensity and develops a more apparent shoulder on the high wavelength side of the band as the amount of acid used in the hydrolysis reaction decreases, see figure 5.8. This is indicative of an overall decrease in free -SiOH groups and an increase in hydrogen bonded species.

For silica only gels, decreasing the amount of acid used in the hydrolysis reaction resulted in a similar increase in hydrogen bonded species. On comparison of silica and silica-titania gels the observed increase in hydrogen bonded species was greater in the samples with titania present than for silica only. This confirms previous conclusions that the presence of titania results in there being more hydrogen bonded silanol species on the surface of the gel.

Figure 5.8: Effect of Varying the Amount of Acid used in the Hydrolysis Reaction on the Near Infrared Spectra of a Sample Containing TiO_2=6·34 weight %. (a) 0·045mole; (b) 0·030mole; (c) 0·015mole; (d) $7{\cdot}5x10^{-3}$mole; (e) $5x10^{-3}$mole; (f) $2{\cdot}5x10^{-3}$mole.

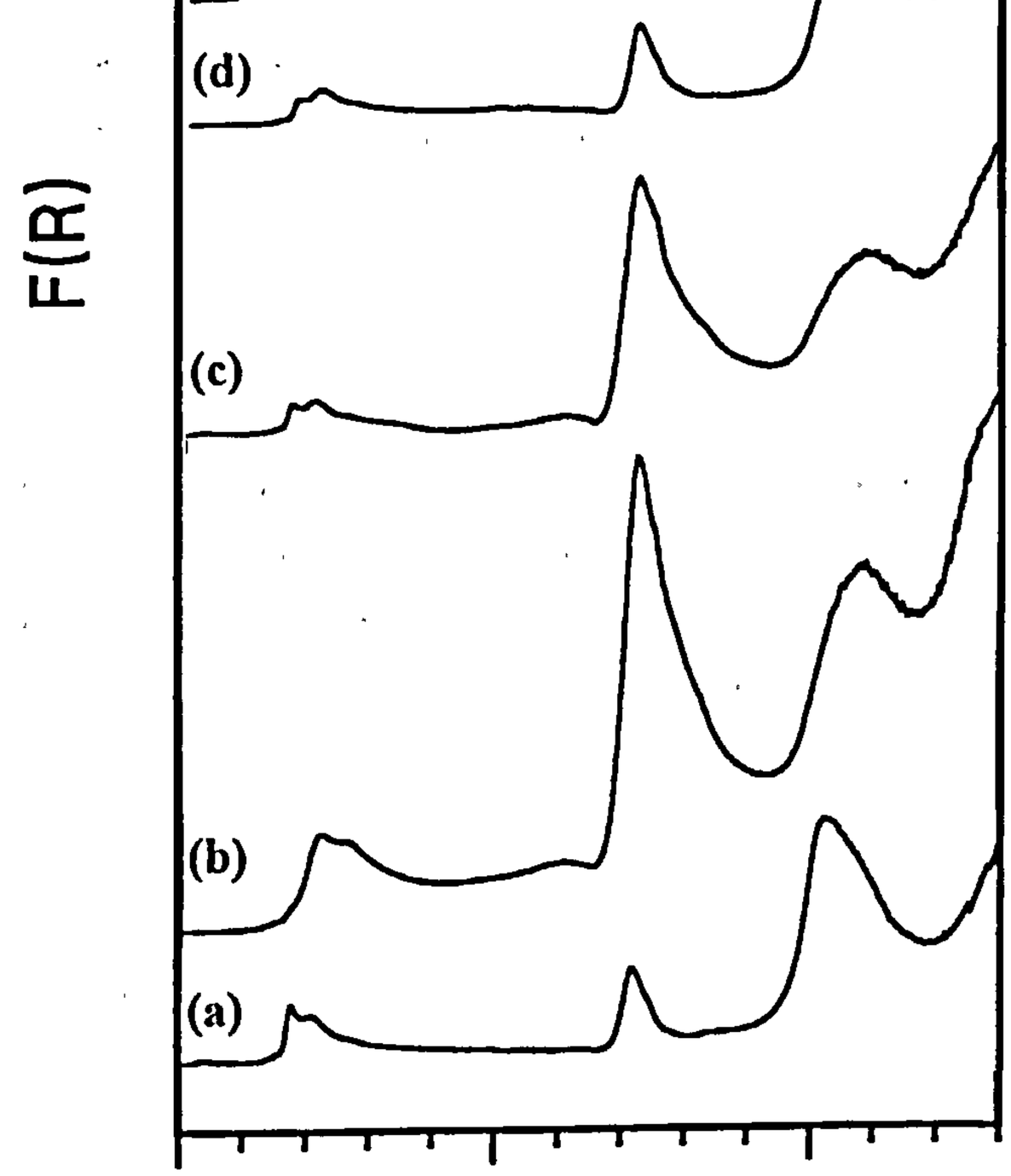

5.5 A NIR Investigation of the Interaction of Water with Silica/Titania Gels prepared from Double Alkoxide Precursors

5.5.1 Introduction

This section contains information on a series of reflectance studies that have been performed in the near-infrared region from 900-2500nm. The results obtained have been used to determine how water molecules interact with the surfaces of mixed silica/titania gels and the effect of thermal treatment on the activity of silanol groups in promoting surface hydration. The sample investigated nominally contained 6·34 weight % titania and had been treated at a temperature of 120°C.

Reflectance spectra were obtained under conditions of increasing hydration, see section 4.5.1.

The wavelength region 1200-2500nm contains three principal groups of absorption bands at *ca* 2200, 1900 and 1400nm. The second wavelength region of study, 900-1350nm, is a reduced replica of the first, with variations in anharmonicity constants for the vibrations involved, and also contains three groups of bands at *ca* 1200,1100 and 900nm. Full assignments are detailed in table 4.7 (page 117).

5.5.2 Results and Discussion

5.5.2.1 The Effect of Hydration on Silanol Derived Bands

After prolonged dehydration *in vacuo* at room temperature the reflectance spectra at t=0 over the regions 900-1350 and 1200-2500nm contain seven well-defined bands (see figures 5.9, 5.10 and appendix II). At t=0 the bands due to free -SiOH groups are sharp, but they rapidly reduce in intensity as hydration proceeds; this is especially noticeable for the peak at 1370nm, the combination band at *ca* 2200nm reducing a much lower amount by comparison, see figure 5.9. Although this band remains unresolved, it shifts by approximately 40nm after 14 hours exposure to the atmosphere. This shift towards a higher wavelength is indicative of a decrease in free SiOH groups and a corresponding increase in hydrogen bonded species. A range of such surface monohydroxylated hydrogen bonded species are fully described in section 4.5.2.

In the 1400nm region, the sharp peak at 1374nm for all samples can be assigned as a type A silanol group. The complete loss of this band with time, for all the samples at 120°C, implies that no free silanol groups remain in the hydrated sample and are thus hydrogen bonded to water.

Similarly, in the second overtone and combination region the peak at 1230nm decreases in intensity with time but does not shift during hydration and is thus comparable to type A silanol groups. The higher baseline on the high wavelength side indicates the presence of types B to D hydrogen bonded species, see figure 5.10.

Figure 5.9: First Overtone and Combination Region (1200-2500nm) Near Infrared Spectra of a Dehydrated Sample Containing TiO_2=6·34 wt% (HCl=7·5x10^{-3} mole) Heated to 120°C and Exposed to the Atmosphere for Various Times.
(a) 0; (b) 0·5 hour; (c) 1 hour; (d) 2 hours; (e) 14 hours.

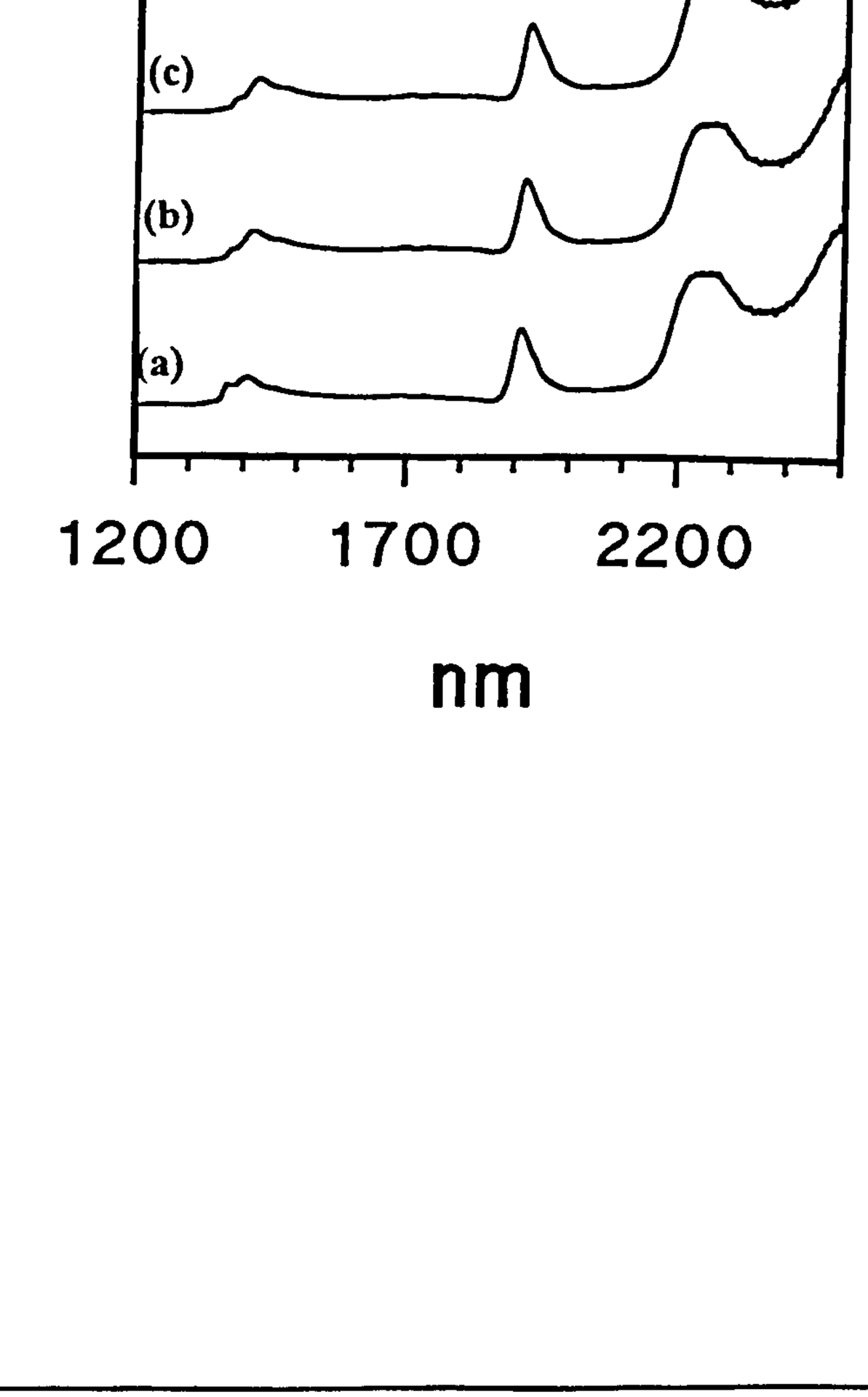

Figure 5.10: Second Overtone Region (900-1350nm) Near Infrared Spectra of a Dehydrated Sample Containing TiO_2=6·34 wt% (HCl=7·5x10^{-3} mole) Heated to 120°C and Exposed to the Atmosphere for Various Times.
(a) 0; (b) 0·5 hour; (c) 1 hour; (d) 2 hours; (e) 14 hours.

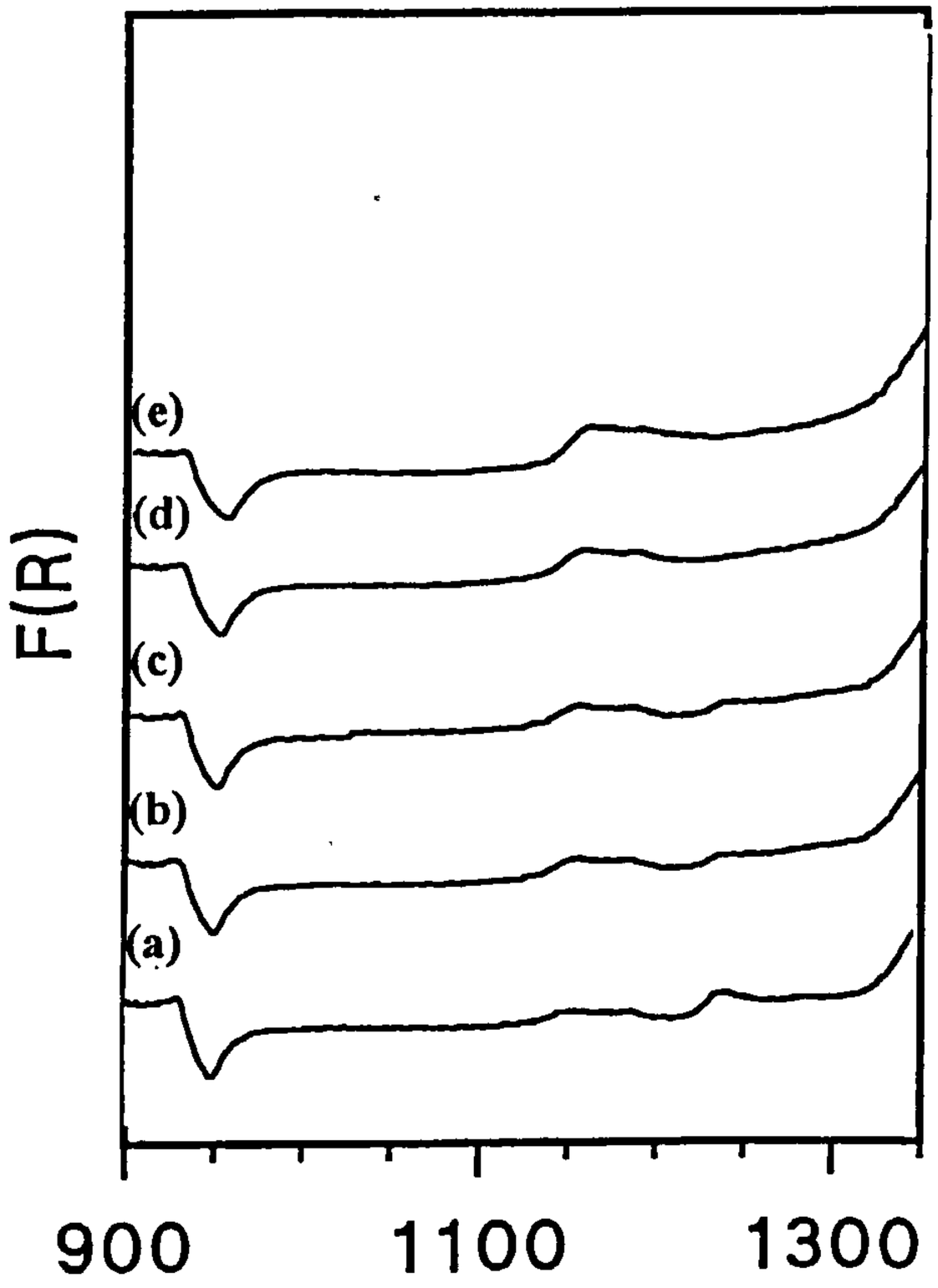

5.5.2.2 Water Bands in the First Overtone and Combination Region

The reflectance spectra obtained at t=0, see figure 5.9, indicate the presence of water on the surface of the sample. From figure 5.9, it is obvious that as the extent of hydration increases, then the combination band at *ca* 2200nm, and the band at 1900nm increase in intensity and new bands centred at 1400nm and 1450nm appear. A shoulder also appears on the band at 1900nm at *ca* 1930nm. Both this band and the one at 1450nm behave in a similar manner and increase in intensity relative to the bands at 1900 and 1400nm as exposure time increases. Therefore the sets of bands at 1400, 1900 and 1450, 1930nm arise from the same molecular species.

The 1900nm band has been assigned as arising from S'_0 species[10] because apart from increasing in intensity the band remains essentially unchanged on increasing hydration. Anderson *et al*[9] found that at low levels of hydration, further adsorption of water can occur at either -SiOH or water groups with equal probability. If a water layer was formed sequentially then no S'_0 species would be observed on the surface of a fully hydrated sample. However, the presence of a shoulder at *ca* 1950nm and a raised baseline on the high wavelength side of the band can be attributed to the overlap of peaks due to S'_1 and S'_2 species indicating that the water layer is not formed sequentially.

The overlap of perturbed -SiOH and H_2O bands makes precise assignment of the 1400nm band a complicated task. Since the intensity change of this band is comparable to that of the band at 1900nm, this has therefore been assigned as S'_0 type water with a contribution from hydrogen bonded silanol/water species. As the hydration of the surface proceeded, the peak maximum shifted to a higher wavelength by approximately 10nm. This may be attributed to the gradual formation of hydrogen bonded silanol groups which have a peak at about the same wavelength. The maximum at 1450nm arises because of a spectral envelope due to S'_1 and S'_2 water species which are partly and fully hydrogen bonded to other water molecules respectively. This evidence again indicates that the water layer on the surface does not form sequentially.

5.5.2.3 Water Bands in the Second Overtone Region

Reflectance spectra at t=0 in the 900-1350nm region, show two distinct bands even after prolonged dehydration *in vacuo* at room temperature, see figure 5.10.

Studies of water both by itself, in ionic solutions and in mixed solvents at varying temperatures have been made[7,11-14], on comparison with the first overtone region these weak bands have been assigned. The most intense band was observed at approximately 1230nm and was assigned as arising from SiOH groups. A further two weak bands were observed around 1150nm, which increased in intensity as the extent of hydration increased. These were assigned as arising due to S'_0 species, and at higher wavelengths to S'_1 species[10]. These bands were very well defined even at high levels of hydration suggesting that there was

little interaction between adsorbed water molecules and that more than one type of water molecule can exist on the surface.

For a sample containing 6·34 weight % titania (figure 5.10) the sharp peak around 1230nm, assigned to the higher combination band of free -SiOH groups[10], was observed to decrease in intensity as hydration progressed. As the surface became increasingly more hydrated, the contribution from the baseline increased because of the presence of a broad band due to S'_2 water species. The simultaneous observation of S'_0, S'_1 and S'_2 water species at *ca* 1200nm suggests that water forms local clusters rather than complete molecular layers.

5.6 Thermal Analysis

A series of gels with varying amounts of acid used for the hydrolysis reaction, as in table 5.1, was investigated using synchronous differential thermal (DTA) and thermogravimetric (TGA) analysis methods. The aim of these studies was to identify the temperatures at which phase transformations occur.

5.6.1 Results and Discussion

A typical DTA and TGA curve is shown in figure 5.11. The curves obtained did not record any changes due to crystallisation under the applied heating regime. As such, the DTA curves indicate only the loss of water and organics at low temperatures.

Figure 5.11: Typical Differential Thermal (DTA) and Thermogravimetric (TGA) Curves Obtained for Mixed SiO_2-TiO_2 Gel

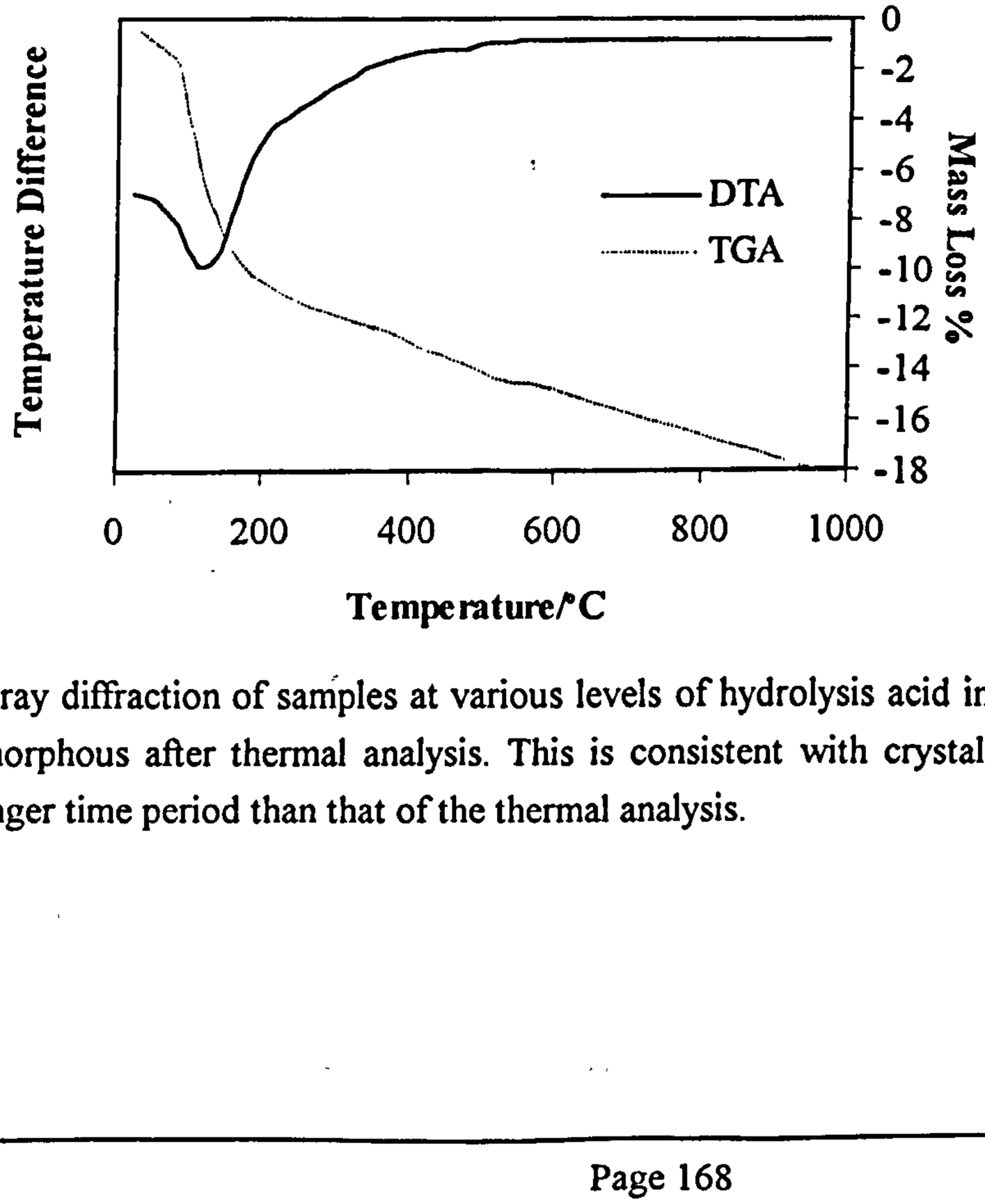

X-ray diffraction of samples at various levels of hydrolysis acid indicated that all remained amorphous after thermal analysis. This is consistent with crystallisation occurring over a longer time period than that of the thermal analysis.

5.7 Gas Adsorption Investigation of Pore Structure

5.7.1 Introduction

Gels containing titanium oxide 6·34 weight %, as in table 5.1, was investigated after treatment at 120, 300, 500, 700, 900 and 1100°C. The aim was to study the effect of temperature on the surface area and porosity of the samples. Similarly, the effect of varying of the amount of acid used in the hydrolysis reaction has also been investigated, see table 5.1.

5.7.2 Results and Discussion

5.7.2.1 Structural Evolution

5.7.2.1.1 Effect of the Amount of Acid used in the Hydrolysis Reaction

For the series of samples, surface areas from 570-112m^2g^{-1}, pore volumes between 0·5-0·006cm^3g^{-1} and average pore diameters in the region of 22-28Å were obtained. Generally decreasing the amount of acid used for the hydrolysis reaction decreased both the overall surface area and pore volume of the resulting material. The isotherms of the higher acid content samples exhibited a small amount of hysteresis (type IV isotherms). On comparison, the resulting adsorption and desorption average pore diameters are virtually identical implying that the pores are cylindrical in shape. Decreasing the amount of acid used in the hydrolysis reaction results in the elimination of hysteresis and the formation of type I isotherms, this is characteristic of microporous solids. However, neither adsorption or desorption average pore diameters changed significantly as the amount of acid used in the hydrolysis reaction was decreased. This implies that the pore structure is a mixture of mesopores and micropores.

From figure 5.12 (and appendix II) and table 5.5, it can be seen that decreasing the amount of acid to $2·5x10^{-3}$ mole eliminates pore structure. Therefore, decreasing the amount of acid used in the hydrolysis reaction removes mesoporosity.

Table 5.5: Effect of Variation of the Amount of HCl used for the Hydrolysis of a Sample Nominally Containing TiO_2=6·34 weight % on the Pore Structure of Gels Treated at 120°C.

Sample HCl (mole)	BET Surface Area (m^2g^{-1})	C	BJH Pore Volume (cm^3g^{-1}) Adsorption	Desorption	BJH Average Pore Diameter (Å) Adsorption	Desorption
0·045	479·1	-295·3	0·18	0·15	21·96	23·72
0·030	569·7	89·3	0·37	0·49	27·79	28·56
0·015	491·8	-1293	0·14	0·20	25·54	23·28
$7·5x10^{-3}$	398·1	-96·1	0·11	0·06	24·43	22·41
$5x10^{-3}$	304·4	-60·6	0·038	0·023	23·18	25·52
$2·5x10^{-3}$	112·3	-84·5	0·037	0·006	26·85	26·05

The values for the BET parameter C, are indicative of the samples being predominantly mesoporous with a contribution from micropores. The results of an investigation into the presence of microporosity by the α_s-method are presented in section 5.7.3.

Figure 5.12: Effect of Variation of the Amount of HCl used for the Hydrolysis of a Sample Nominally Containing TiO_2=6·34 weight % on the Resulting Adsorption/Desorption Isotherm

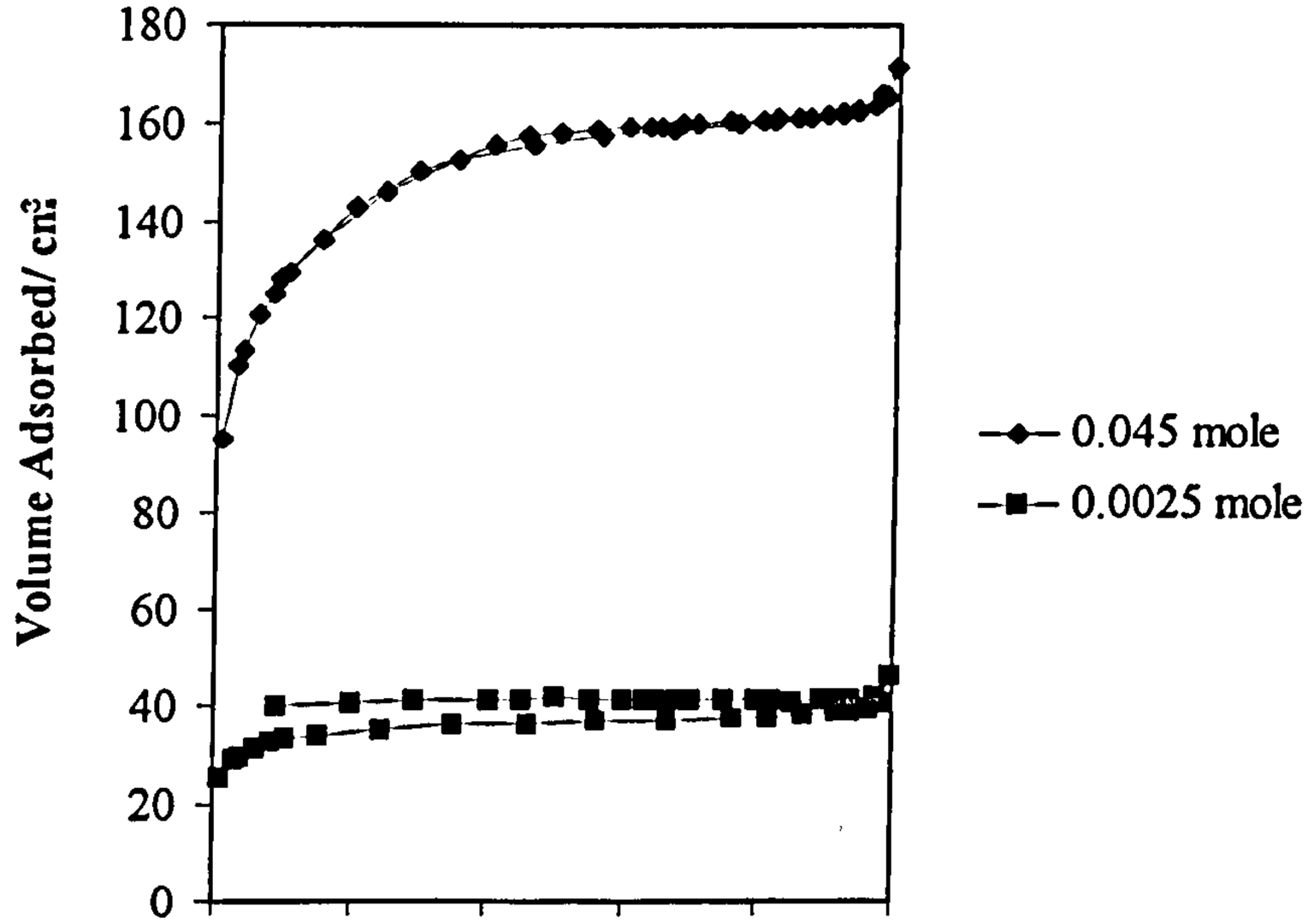

Low pressure hysteresis was observed for the gel prepared using 0·0025 mole for the hydrolysis reaction. This has been associated with a distortion of the adsorbent which is difficult to reverse and leads to an increase in the saturation uptake. The mechanism was proposed by Everett *et al*[15] as an irreversible intercalation of molecules of adsorbate within micropores.

5.7.2.1.2 Effect of Thermal Treatment on Structural Evolution

The samples investigated exhibited a range of surface areas between 533-6m^2g^{-1} and pore volumes between 0·18-0·002cm^3g^{-1} . Between 120 and 700°C, the average pore diameter was 22-27Å. On heating to 900°C and above the average pore diameter increased to over 90Å.

After thermal treatment, a monolithic gel prepared using 0·045mole acid in the hydrolysis reaction and containing 6·34 weight % titania exhibited a progressive decrease in both surface area and pore volume as the treatment temperature was increased, see table 5.6. Increasing the temperature to 900°C results in the virtual elimination of pore structure.

Table 5.6: Effect of Temperature on the Pore Characteristics of a Monolithic Gel Nominally Containing TiO_2=6·34 weight % (HCl=0·045 mole)

		Temperature (°C)					
		120	300	500	700	900	1100
BET Surface Area (m^2g^{-1})		479·1	532·7	444·2	304·3	2·99	6·4
	C	-295	-1017	-246	-386	77·9	-194
BJH Pore Volume (cm^3g^{-1})	**Adsorption**	0·18	0·12	0·093	0·066	0·005	0·003
	Desorption	0·15	0·17	0·135	0·099	0·005	0·002
BJH Average Pore Diameter (Å)	**Adsorption**	21·96	24·93	25·24	26·93	91·59	460
	Desorption	23·72	23·39	22·75	23·31	94·76	307

The values for the BET parameter C, are indicative of the sample being predominantly mesoporous with a contribution from micropores. Further details of the micropore structure investigated by the α_s-method are presented in section 5.7.3.

Figure 5.13: Effect of Temperature on the Pore Characteristics of a Monolithic Gel Nominally Containing TiO_2=6·34 weight % (HCl=0·045 mole)

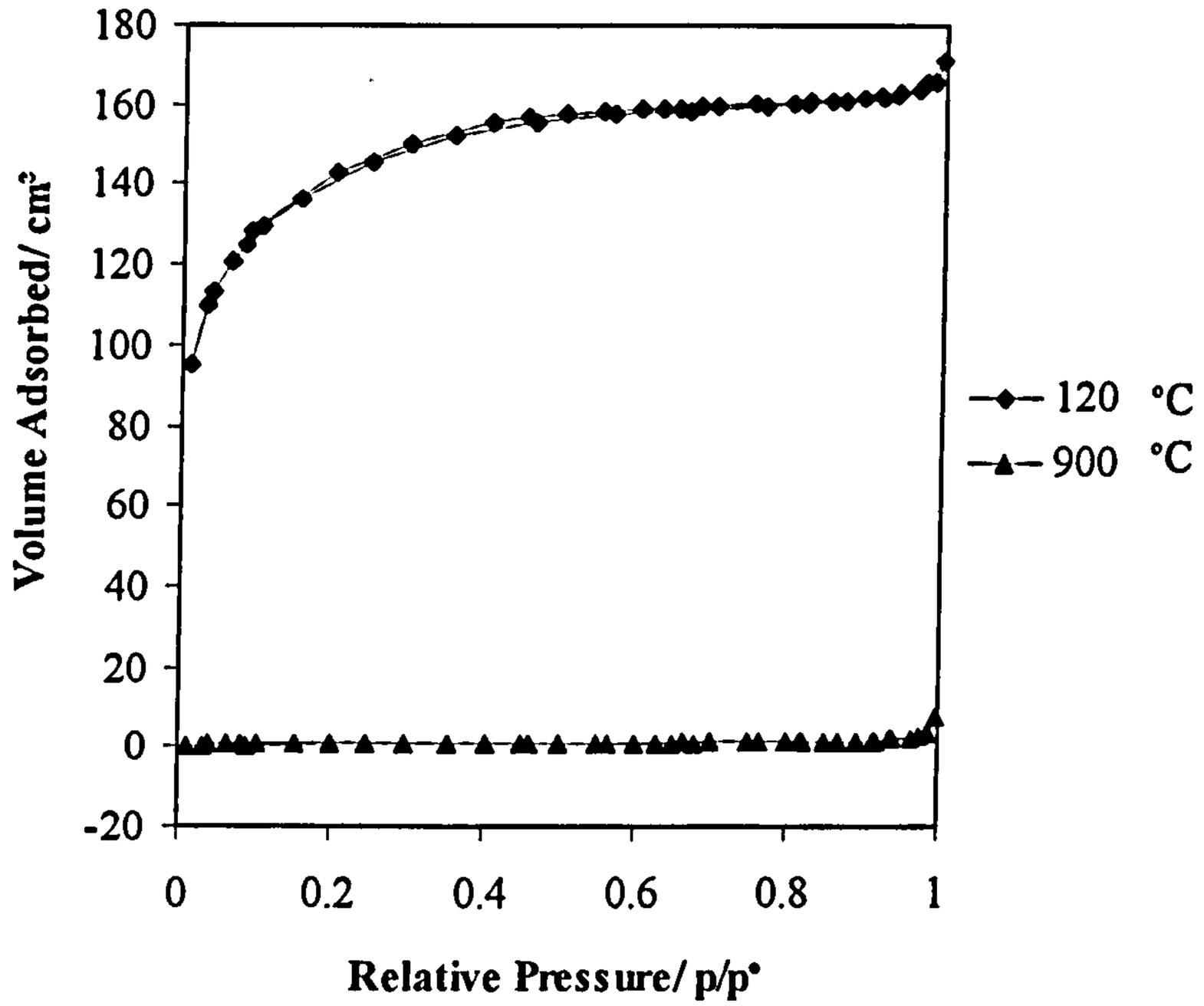

The isotherms obtained suggest that increasing the treatment temperature reduces the mesoporosity of the sample and increasing the temperature to 900°C results in the elimination of the pore structure, see figure 5.13* .

The effect of thermal treatment of the samples on average pore diameter has also been studied. Heating the sample at temperatures up to 700°C has no effect on average pore diameter. Further heating to 900°C results in an increase in average pore diameter as the smaller pores within the sample collapse. This is in contrast with both surface area and pore volume data which both decrease significantly with increasing temperature. Pore size distribution plots of the monolithic sample heated at 120, 700 and 900°C are shown in figure 5.14.

Typical PSD plots for samples at 120°C and 900°C are shown in figure 5.14. Both plots have the maximum pore volume at a pore diameter around 25Å, and contain few pores of diameter greater than 100Å. Sintering results in a decrease in the pore volume attributed to pores of average diameter and hence a decrease in the overall pore volume.

* Additional nitrogen adsorption /desorption isotherms are shown in appendix II.

Figure 5.14: dV/dlog(D) Adsorption Pore Size Distribution Plots of a Monolithic Sample Nominally Containing TiO_2=6.34 wt% After Thermal Treatment at 120, 700 and 900°C

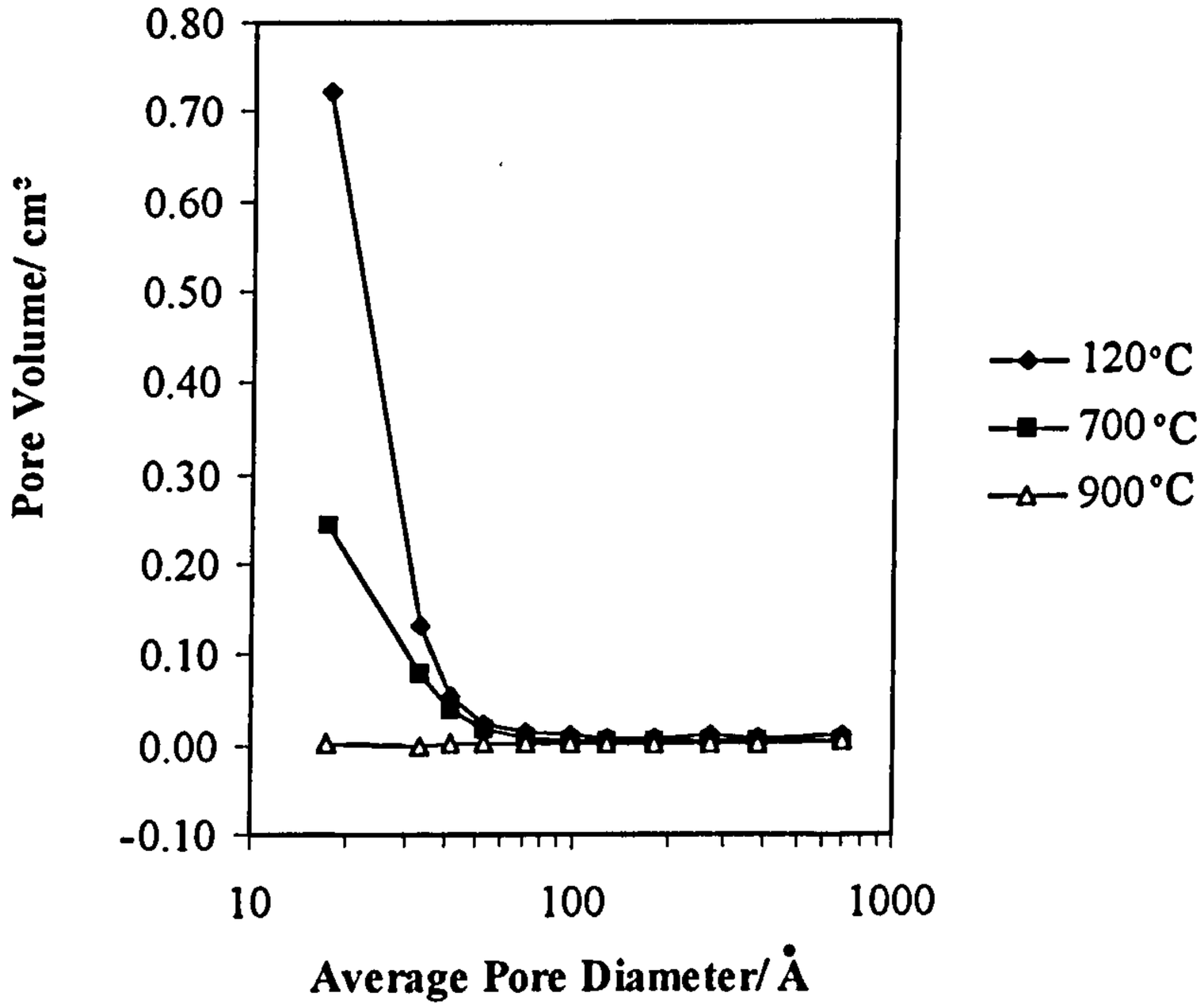

Van Nordstrand, Kreger and Ries[16] and Bastick[17] have found that in commercial silica gel with a pore diameter of about 20Å, as well as a silica-alumina xerogel having a pore diameter of about 40Å, there is no change in average pore size as sintering progresses. Teichner[18] *et al* observed that on sintering a voluminous aerogel where shrinkage was 83% by volume, the average pore diameter changed by only a small amount.

It is well documented that when silica gel is sintered it shrinks; the pore volume decreases in proportion to the decrease in surface area and the pores that remain do not change in size. It appears that pores are destroyed as the silica is converted from the porous to the nonporous state without the size of any remaining pores undergoing any change[18].

5.7.3 Micropore Structure

The α_s-method[19] can be used to calculate the micropore volume and the surface area of the samples, see section 4.7.2.3. A typical α_s-plot for the samples previously discussed is shown in figure 5.15.

Figure 5.15: Typical α_s-plot for Samples Nominally Containing TiO_2=6·34 wt% (HCl=0·015mole)

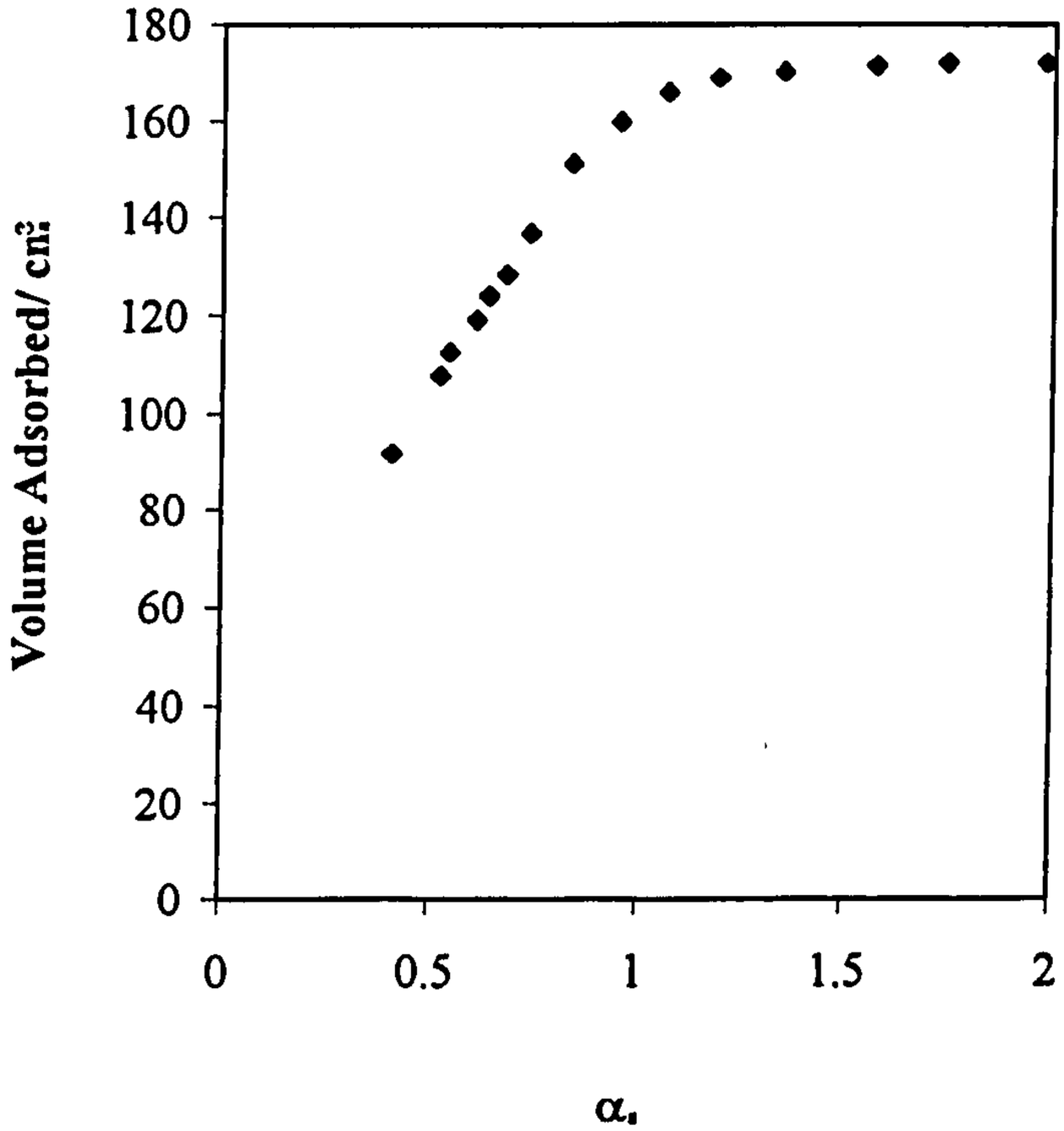

5.7.3.1 Effect of Amount of Hydrolysis Acid

For the samples prepared using 0·030 and $2{\cdot}5x10^{-3}$ mole of acid in the hydrolysis reaction there is little difference between the derived BET and α_s-surface areas. This suggests that in these samples there are few micropores. For the remaining samples, the values for the surface area obtained from the α_s-method are significantly larger than those obtained from the BET method, see table 5.7. Therefore there must be a contribution to the overall measured surface area from micropores. The total micropore volume of the sample may be calculated by extrapolating the linear portion of the curve back to the volume adsorbed axis, see table 5.7. Therefore the samples are predominantly mesoporous but also contain some micropores.

Table 5.7: Comparison of BET and α_s-data Obtained for Varying the Amount of Acid in the Hydrolysis Reaction

Amount of HCl (mole)	Surface Area (m^2g^{-1})		Micropore Volume (cm^3g^{-1})
	BET	α_s	
0·045	479·1	577·9	0·07
0·030	569·7	565·4	0·03
0·015	491·8	570·1	0·06
$7·5x10^{-3}$	398·1	529·3	0·08
$5x10^{-3}$	304·4	449·7	0·10
$2·5x10^{-3}$	112·3	152·0	0·02

5.7.3.2 Effect of Temperature on the Micropore Structure

At temperatures up to 500°C the values for the surface area obtained from the α_s-method are significantly larger than those obtained from the BET method, see table 5.8. Therefore there must be a significant contribution to the overall surface area from micropores. The total micropore volume of the sample may be calculated by extrapolating the linear portion of the curve back to the volume adsorbed axis, see table 5.8. Increasing the temperature to 700°C and above results in little difference between the BET and α_s-surface areas. This suggests that on heating the very small micropores are destroyed in preference to larger pores.

Table 5.8: Comparison of BET and α_s-data for a Sample Nominally Containing 6·34 weight % Titania After Thermal Treatment (HCl=0·045 mole)

Temperature (°C)	Surface Area (m^2g^{-1})		Micropore Volume (cm^3g^{-1})
	BET	α_s	
120	479	577·9	0·070
300	533	609·0	0·059
500	444	526·1	0·057
700	304	344·7	0·034
900	3·00	3·0	0·000

5.8 Conclusions

The effect of thermal treatment on the bulk and pore structures of a series of monolithic gels nominally containing 6·34 weight % titania and prepared using varying amounts of acid in the hydrolysis reaction has been investigated.

Increasing the temperature used for thermal treatment of the samples resulted in a progressive decrease in surface area, pore volume and micropore volume. However, the average pore diameter remained constant at temperatures up to 700°C. Changes in pore volume, surface area and average pore diameter were largest between 700 and 900°C; being the temperatures between which full densification occurred. In comparison, monolithic gels prepared using the precursor bis(acetylacetonato) titanium diisopropoxide, did not undergo complete densification until treatment at 1100°C. On comparison, the resulting adsorption and desorption average pore diameters were virtually identical implying that the pores are cylindrical in shape. This is in contrast to both powdered and monolithic gels prepared from bis(acetylacetonato) titanium diisopropoxide in which the desorption average pore diameters were greater than the corresponding adsorption values, this and the shape of the resulting isotherm led to the conclusion that the pores were slit shaped.

For gels prepared from the double alkoxide the surface area, pore volume and average pore diameters observed were significantly lower than those of monolithic gels prepared from bis(acetylacetonato) titanium diisopropoxide, see table 5.9.

Table 5.9: Comparison of the Pore Structures of Gels Prepared from the Double Alkoxide and bis(acetylacetonato) titanium diisopropoxide Nominally Containing TiO_2=6·34 weight% and HCl=0·045 mole

		Double Alkoxide	$Ti(acac)_2(O^iPr)_2$
BET Surface Area (m^2g^{-1})		479	618
BJH Pore Volume (cm^3g^{-1})		0·18	0·74
BJH Average Pore	**Adsorption**	22	54
Diameter (Å)	**Desorption**	24	38

Generally, decreasing the amount of acid used for the hydrolysis reaction decreases both the overall surface area and pore volume of the resulting material. However, the average pore diameter remained constant as the amount of acid used for the hydrolysis reaction was decreased. This is in contrast to gels prepared from bis(acetylacetonato) titanium diisopropoxide in which the average pore diameters decreased as the amount of acid used was decreased.

Although the amount of acid used for the hydrolysis reaction was decreased, the amount of water was increased. Since the solvent:silicate ratio remained constant, the silicate concentration was reduced. Increasing the amount of water generally promotes hydrolysis,

however in this case the reduction of the silicate ratio reduces both the hydrolysis and condensation rates, causing an increase in the gel time. Increasing the gel time results in more weakly branched gels. Since the condensation rate is low and the branching is weak, the gel structure can freely interpenetrate and shrink in response to solvent removal. This results in a decrease in surface area, pore volume and average pore diameters. For gels prepared from either a large amount of acid (low water) or a double alkoxide there is an increase in branching on gelation. This can be attributed to an increase in the condensation rate for the former and an increase in branching in the precursor for the latter. On drying, not as much shrinkage occurred since branching prevents the structures form interpenetrating. This resulted in larger more rigid pores.

After heating at temperatures up to 900°C, the samples prepared using the double alkoxide remained amorphous as determined by X-ray diffraction. However, increasing the temperature to 1100°C resulted in the detection of some crystalline anatase. In contrast, gels prepared from bis(acetylacetonato) titanium diisopropoxide remained amorphous after treatment at 1100°C. These differences may be explained by the input of thermal energy, in excess of that required for densification being used to form crystalline regions. These crystalline regions can be formed by the diffusion of particles either from the convex surfaces of the particles to the concave surfaces or through the lattice, this causes the filling of the necks between particles and results in particle growth.

Reflectance NIR spectroscopic studies of double alkoxide gels indicate that decreasing the amount of acid used in the hydrolysis reaction resulted in higher relative levels of hydrogen bonded silanol species. This is consistent with the results obtained for gels prepared from bis(acetylacetonato) titanium diisopropoxide.

Increasing the thermal treatment temperature to 900°C has been shown to reduce the level of Si-OH functionality within the gel. At 900°C no silanol groups were observed by NIR spectroscopy, which is consistent with complete sample densification. This is in contrast to gels prepared from bis(acetylacetonato) titanium diisopropoxide which underwent complete sample densification at 1100°C. At 900 and 1100°C, mid-infrared spectroscopy has revealed the formation of Si-O-Ti bonds and the further incorporation of titanium atoms into the silica framework. This is consistent with the results obtained for gels prepared from bis(acetylacetonato) titanium diisopropoxide.

Therefore the preparation of gels from a double alkoxide precursor results in lower surface areas, pore volumes and average pore diameters than for corresponding gels prepared from bis(acetylacetonato) titanium diisopropoxide. Gas adsorption has revealed that the double alkoxide gels contain cylindrical pores, are less mesoporous and have a greater micropore volume than gels prepared from bis(acetylacetonato) titanium diisopropoxide. These differences can be explained by the presence of Si-O-Ti bonds in gels prepared from the double alkoxide, even at low temperatures. On heating above 700°C, the infrared band at *ca*

1100cm^{-1} shifted to a higher wavenumber as these Si-O-Ti bonds shorten and strengthen. The highly branched gel structure results in more rigid pores which are unable to shrink during heating. This resulted in more compact structures with lower surface areas, pore volumes and average pore diameters than observed for gels prepared from bis(acetylacetonato) titanium diisopropoxide. After thermal treatment, densification has been found by both gas adsorption and near infrared spectroscopy to occur at a temperature *ca* 200°C lower than for gels prepared from bis(acetylacetonato) titanium diisopropoxide.

5.9 References

1 A. Duran, C. Serna, V. Fornes & J.M. Fernandez-Navarro, *J. Non Crystalline Solids* **82**(1986) 69-77

2 M. Decottognies, J. Phalippou & J. Zarzycki, *J. Mat. Sci.* **13**(1978) 2605-2618

3 C.J.R. Gonzalez-Oliver, P.F. James & H. Rawson, *J. Non Crystalline Solids* **48**(1982) 129-152

4 M.F. Best and R.A. Condrate Sr., *J. Mat. Sci. Lett.* **4**(1985) 994-998

5 A. Bertoluzza, C.Fagnano, M.A. Morelli, V. Gottardi & M.Guglielmi, *J. Non Crystalline Solids* **48**(1982) 117-128

6 T. Isobe and M. Senna, *J. Solid St. Chem.* **93**(1991) 358-367

7 K. Buijs and G.R. Choppin, *J. Chem. Phys.* **39** (1963) 2035-2041; 2042-2050

8 C.C. Perry and X. Li, *J. Chem. Soc. Faraday Trans.* **87**(5) (1991) 761-766

9 J.H. Anderson and K.A. Wickersheim, *Surface Sci.* **2** (1964) 252-260

10 C.C. Perry and X. Li, J. Chem. Soc. Faraday Trans. 87(24) (1991) 3857-3862

11 H. Yametra, B. Fitzpatrick and G. Gordon, *J. Mol. Spec.* **14**(1964) 268-278

12 G.R. Choppin and H.R. Violante, *J. Chem. Phys.* **56**(1972) 5890-5898

13 G.R. Choppin and J.R. Downey, *J. Chem. Phys.* **56**(1972) 5899-5903

14 C.C. Perry and X. Li, in *Chemical Processing of Advanced Materials* p.131, eds. L.L. Hench and J.K. West Wiley, 1992)

15 A. Bailey, D.A. Cadenhead, D.H. Davis, D.H. Everett and A.J. Miles, *Trans. Faraday Soc.* **67** (1971) 231-243

16 R.A. Van Nordstrand, W.E. Kreger and H.E. Ries Jr., *J. Phys. Colloid Chem.* **55** (1951) 621-638

17 J. Bastick, *Bull. Soc. Chim. Fr.* **20** (1953) 437-440

18 S.J. Teichner, G.A. Nicolaon, M.A. Vicarini and G.E.E. Gardes, *Adv. Colloid Interface Sci.* **5** (1976) 245-273

19 M.R. Bhambhani, P.A. Cutting, K.S.W. Sing and D.H. Turk, *J. Colloid Interface Sci.* **38** (1) (1972) 109-117

Chapter 6: Monolithic Mixed SiO_2/ZrO_2 Gels

6.1 Introduction

The results of an investigation into the effects of reaction conditions, the amount of zirconia (weight %) present in the gel, and thermal treatment on the structure adopted by monolithic gels are presented in this chapter. The gels studied in this chapter are listed in table 6.1.

Table 6.1: Silicon/Zirconium Oxide Gels Investigated.

Amount of ZrO_2 (weight %)	Amount of Acid used in Hydrolysis (mole)
6·4	0·045
6·4	0·030
6·4	0·015
6·4	$7{\cdot}5 \times 10^{-3}$
6·4	5×10^{-3}
6·4	$2{\cdot}5 \times 10^{-3}$
4·1	0·045
4·97	0·045
22·1	0·045

Overall the aim of this investigation was to compare the properties of monolithic silicon/titanium and silicon/zirconium oxide gels prepared by the same method.

6.2 X-ray Diffraction

6.2.1 Introduction

X-ray diffraction has been performed to determine the crystalline nature of mixed silicon-zirconium oxides at a number of temperatures (see section 2.4.3). Once crystallinity was observed then the size of the crystallites was calculated using the Scherrer equation (equation 2.12).

6.2.2 Results

6.2.2.1 Effect of Varying both Zirconia Content (weight %) and Temperature on the Crystalline Nature of the Gel

Gels containing 4·1 and 4·97 weight % zirconia were found to be amorphous at temperatures up to 1100°C. Increasing the level of zirconia to 6·4 weight % resulted in a gel that was amorphous up to 900°C. At 1100°C broad peaks due to cristobalite and tetragonal zirconia were observed by X-ray diffraction, see figure 6.1.

An increase in the zirconia level to 22·1 weight% resulted in a gel that was amorphous up to 900°C. Thermal treatment at 1100°C resulted in the formation of broad diffraction peaks due to tetragonal zirconia, see figure 6.2. These results are detailed in table 6.2.

Figure 6.1: X-ray Diffractograms for Sample Containing 6·4 weight % Zirconia heated at: (a) 900°C; (b) 1100°C ; (c) tetragonal zirconia. [HCl=0·045 mole] [T=ZrO_2 tetragonal; C=cristobalite]

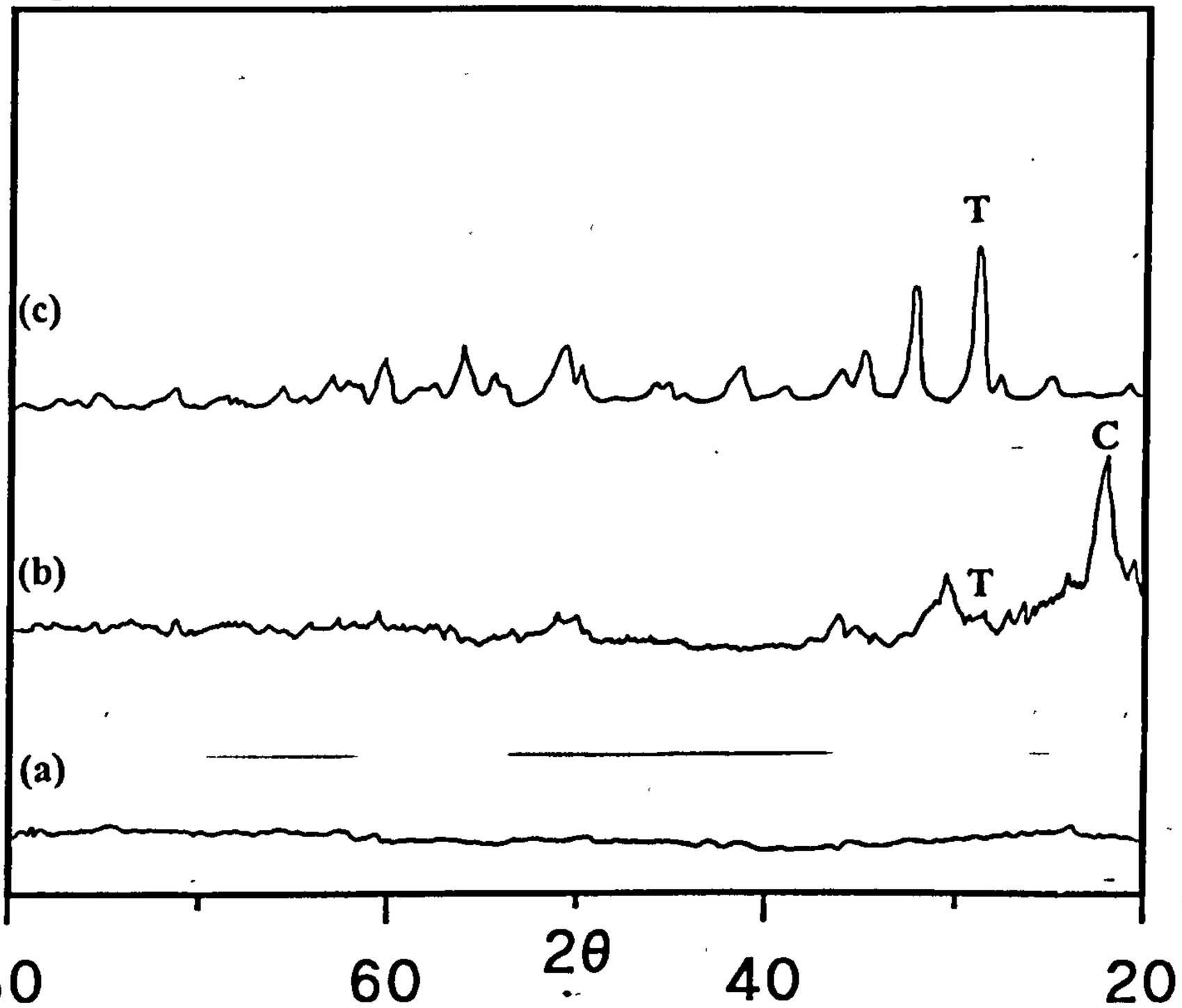

Figure 6.2: X-ray Diffractograms for Sample Containing 22·1 weight % Zirconia heated at: (a) 900°C; (b) 1100°C. [HCl=0·045 mole] [T=ZrO_2 tetragonal; C=cristobalite]

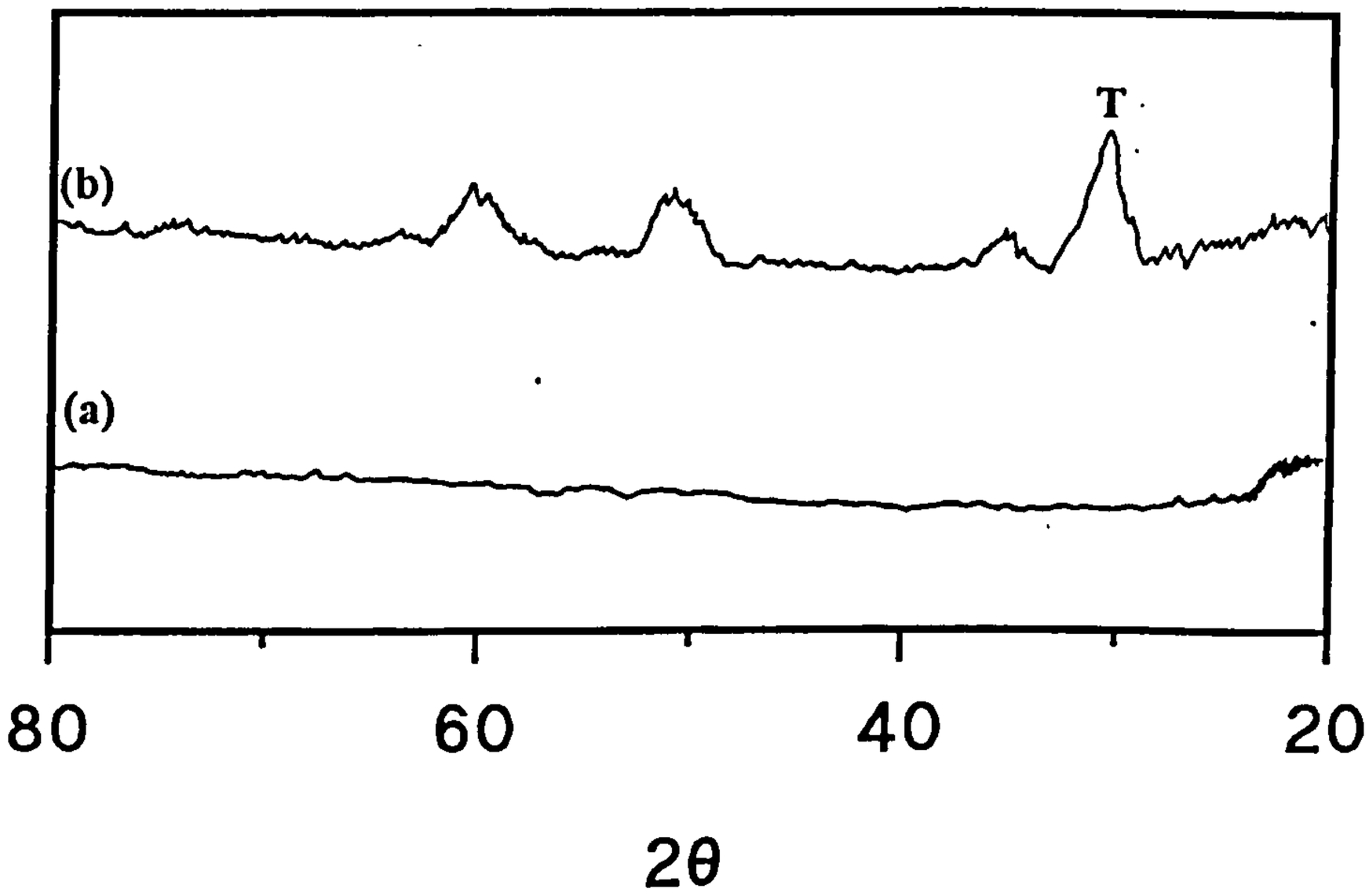

Table 6.2: Effect of Varying both Zirconia Content (weight %) and Temperature on the Crystalline Nature of the Gel

ZrO_2 (weight %)	Temperature/ °C					
	120	300	500	700	900	1100
4·1	X	X	X	X	X	X
4·97	X	X	X	X	X	X
6·4	X	X	X	X	X	C/T
22·1	X	X	X	X	X	T

X=amorphous; T= ZrO_2 tetragonal; C=cristobalite

6.2.2.2 Effect of Varying both the Amount of Acid used in the Hydrolysis and Temperature on the Crystalline Nature of a Gel Containing ZrO_2=6·4 weight%

Decreasing the amount of hydrochloric acid used in the hydrolysis reaction had no effect on the temperature above which crystallinity was observed by X-ray diffraction (section 6.2.2.1). On heating to 1100°C, gels containing 0·045 and 0·030 mole acid possessed diffraction patterns containing broad peaks due to cristobalite and tetragonal zirconia, see figure 6.3 and appendix III.

Figure 6.3: X-ray Diffractograms for Sample Containing 6·4 weight % Zirconia heated at: (a) 900°C; (b) 1100°C [HCl=0·030 mole].

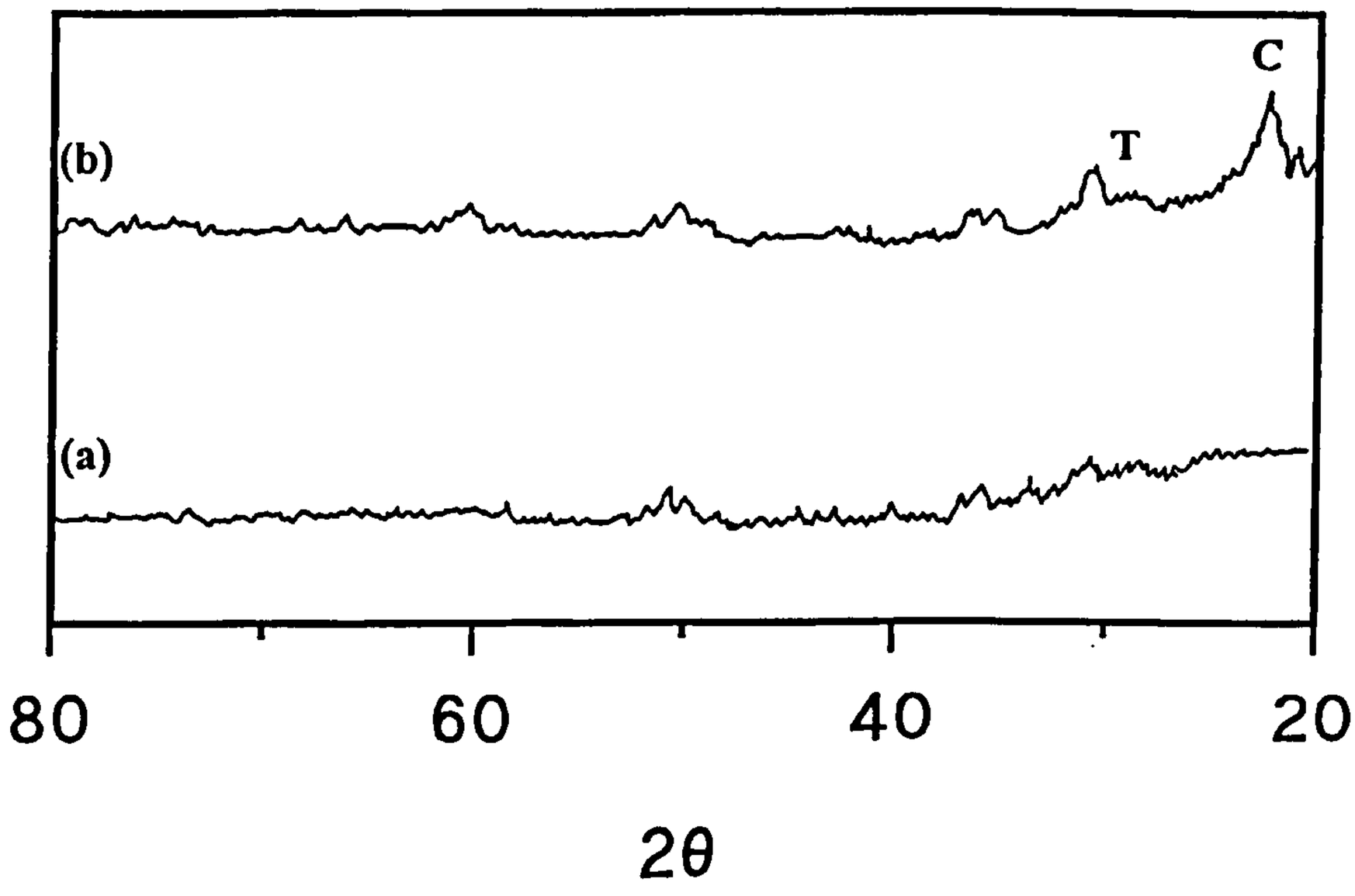

The samples containing less than 0·015 mole acid and heated to 1100°C exhibited crystallinity due to tetragonal zirconia only, see appendix III. The progressive decrease in the amount of acid used resulted in a corresponding decrease in the intensity of the diffraction peaks observed.

Table 6.3: Effect of Varying both the Amount of Acid used in the Hydrolysis and Temperature on the Crystalline Nature of a Gel Containing ZrO_2=6·4 weight %

Amount of HCl (mole)	Temperature/ °C					
	120	300	500	700	900	1100
0·045	X	X	X	X	X	C/T
0·030	X	X	X	X	X	C/T
0·015	X	X	X	X	X	T
$7·5x10^{-3}$	X	X	X	X	X	T
$5x10^{-3}$	X	X	X	X	X	T
$2·5x10^{-3}$	X	X	X	X	X	T

X=amorphous; T= ZrO_2 tetragonal; C=cristobalite

6.2.2.3 Particle Sizes

Particle sizes have been calculated using the Scherrer equation from the major cristobalite peak at 22-23° and the major tetragonal zirconia peak at 30°. These are shown in table 6.4.

As the amount of acid used for the hydrolysis reaction decreases, the average size of the particles formed at 1100°C decreases.

From the results obtained there appears to be no relationship between the amount of zirconia present in the initial reaction mixture and the crystal sizes observed at 1100°C.

Table 6.4: Average Particle Sizes at 1100°C

ZrO_2 /weight %	Amount HCl /mole	Average Particle Size /nm	
		SiO_2 Cristobalite	ZrO_2 Tetragonal
6·4	0·045	4·1	2·7
6·4	0·030	2·8	2·7
6·4	0·015	X	2·7
6·4	$7·5x10^{-3}$	X	2·0
6·4	$5x10^{-3}$	X	1·6
6·4	$2·5x10^{-3}$	X	1·6
22·1	0·045	X	2·7

6.2.3 Discussion

Monolithic gels containing 4·1 and 4·97 weight % zirconia remained amorphous at temperatures up to 1100°C. Increasing the zirconia content initially to 6·4 weight % and then 22·1 weight % and heating to 1100°C resulted in the formation of crystals of tetragonal zirconia.

After thermal treatment the structure of a series of monolithic gels with decreasing acid content was investigated by X-ray diffraction. The X-ray diffraction results showed that all the samples were amorphous after heating at 900°C. Increasing the treatment temperature to 1100°C resulted in crystallinity due to tetragonal zirconia being observed for all acid contents. Diffraction patterns due to cristobalite were only observed for the highest acid contents of 0·045 and 0·030 mole.

In a monolith, condensation reactions produce new cross-links and stiffen the structure. The processes involved in sintering and densification are described in section 4.2.3. Heating to 900°C results in densification *via* viscous flow and structural relaxation, as no crystallinity was detected by X-ray diffraction. Increasing the treatment temperature to 1100°C resulted in the observation of crystalline tetragonal zirconia and cristobalite in two instances.

However, the heating process must cause the formation of some regions of inhomogeneity which exist within a non-crystalline polymeric matrix. At temperatures up to 900°C material moves within these regions by diffusion processes from the convex surfaces of the particles to the concave surfaces and causes the filling of the necks between particles. This results in the region consisting of much larger particles. Heating to 1100°C causes more growth, the larger particles formed are more likely to be detected by X-ray diffraction.

From table 6.4, it can be concluded that increasing the concentration of zirconia in the gel from 6·4 to 22·1 weight %, had no effect on the size of the resulting crystals. However,

decreasing the amount of acid used in the hydrolysis reaction results in the formation of smaller crystals at 1100°C. Similar results were obtained by Miranda Salvado[1] who concluded that hydrolysis in a strong acid medium favoured the segregation of zirconia and lowering the amount of acid stabilised the crystalline zirconia formed. Hence, the greater the amount of acid used for the hydrolysis reaction the greater the crystal growth observed on heating.

The stability of silica against nucleation and eventual crystallisation can be increased by the incorporation of a less soluble oxide such as SnO_2, TiO_2 and Al_2O_3. Even if phase separation of this insoluble oxide occurs, the nucleation of the silica is retarded. The segregation of zirconia during hydrolysis in a strong acid medium results in regions of zirconia within the gel. On heating the gel shrinks due to a combination of condensation reactions and structural relaxation. When structural relaxation occurs, excess free volume is removed allowing the structure to approach the configuration characteristics of a metastable liquid. This occurs by the diffusion of particles through the network either through the lattice, over the surface or along the boundary. This results in the growth of necks between particles and nucleation. Therefore heating a gel results in competition between sintering and nucleation processes.

Increasing the treatment temperature of the gel to 1100°C, causes shrinkage of the gel structure, sintering, particle growth through nucleation and eventually crystallisation of both tetragonal zirconia and cristobalite.

6.3 The Effect of Temperature on the IR Spectra of Silica/Zirconia Gels of Different Zirconia Contents

6.3.1 Introduction

The IR fundamental region (4000-400cm^{-1}) has been used to investigate any structural changes that may occur as a function of temperature in the bulk of the mixed silica/zirconia gel.

There are six main vibrational bands of interest in the region studied, the assignments of which are detailed in table 6.5.

Table 6.5: Infrared Band Assignments for Silica/Zirconia Gels

Assignment	Wavenumber/cm^{-1}
ν_{as}(Si-O-Si), LO[2]	1200-1250
ν_{as}(Si-O-Si), TO[2]	1024-1100
ν(SiOH, Si-O^-)[3] ν(ZrOH, Zr-O^-)[6] ν_{as}(Si-O-Zr)[6]	931-964
ν_s(Si-O-Si)[3]	790-800
ZrO_2 (m)[5]	740
ZrO_2 (t)[5]	600
ZrO_2 (t)[5]	485
δ(Si-O-Si), o.p[4] ZrO_2 (c)[5]	451-468
ZrO_2 (m)[5]	418

m=monoclinic; c=cubic; t=tetragonal

• ν(SiOH, Si-O^-)=960cm^{-1};

6.3.2 Results and Discussion

6.3.2.1 Mixed SiO_2-ZrO_2 Gels

The spectra obtained for a sample containing a zirconia concentration of 4·1 weight %, treated at various temperatures (see section 3.3.2) are shown in figure 6.4 (spectra of other zirconia contents are shown in appendix III). The most intense band in the mid-infrared spectra, at *ca* 1100cm^{-1} is asymmetric with a weak shoulder at 1200cm^{-1} which is present for all thermal treatment temperatures. These two bands are associated with the transverse optical (TO) and longitudinal optical (LO) modes of the antisymmetric Si-O-Si stretching vibration respectively[4]. The band at *ca* 1100cm^{-1} shifts to a higher wavenumber as the temperature increases above 900°C suggesting that the Si-O bonds are strengthened at these elevated temperatures. Variation of the amount of zirconia present in the samples has no effect on the temperature at which the shift occurs, see figure 6.5.

Figure 6.4: Mid-infrared Spectra of a Sample Containing 4·1 weight % Zirconia Treated at Different Temperatures. (a) 120°C; (b) 300°C; (c) 500°C; (d) 700°C; (e) 900°C; (f) 1100°C.

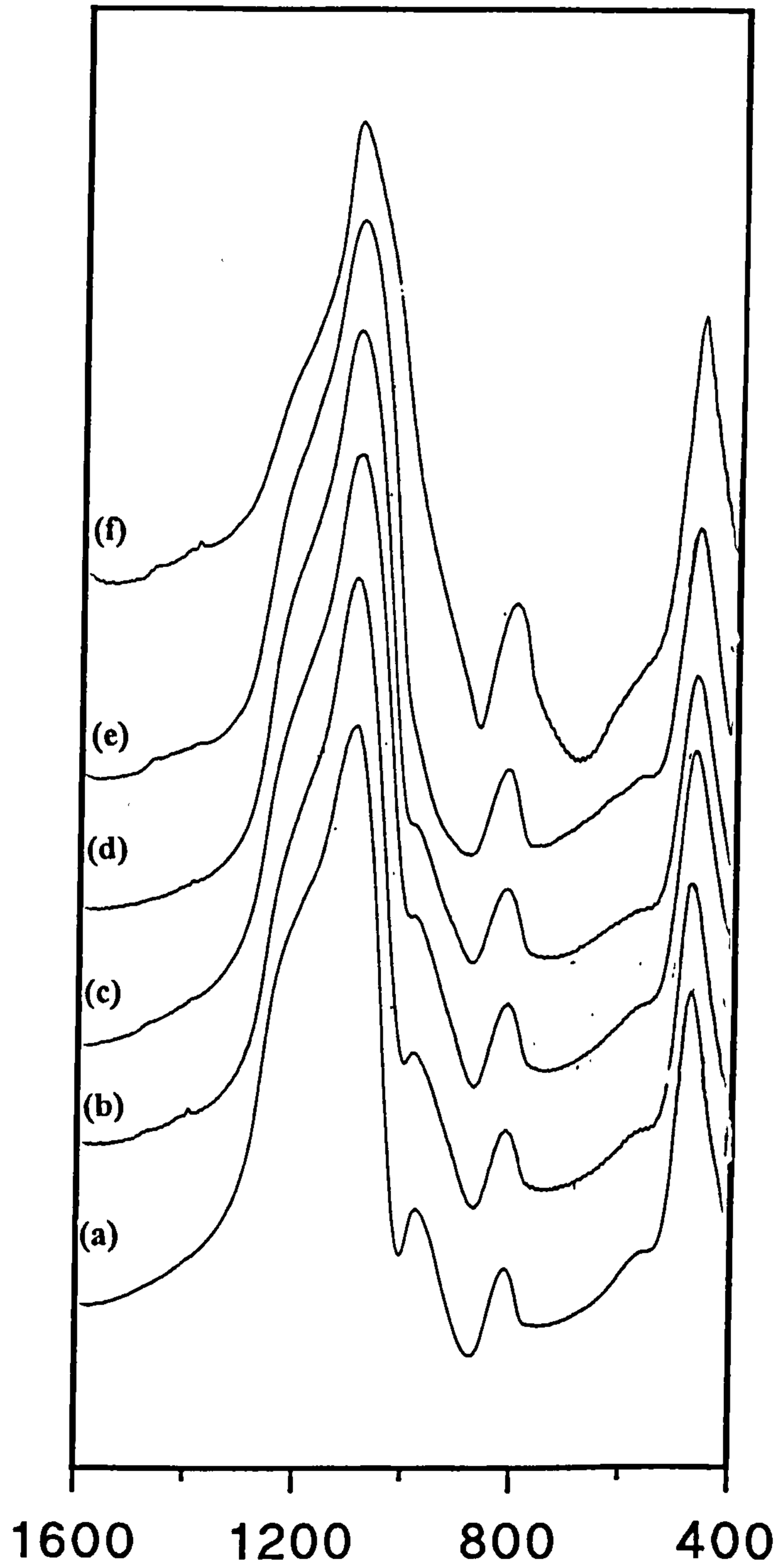

Figure 6.5: Position of the Antisymmetric O-Si-O Stretching Vibration Near 1100cm^{-1} of Gels Containing Varying Amounts of Zirconia.

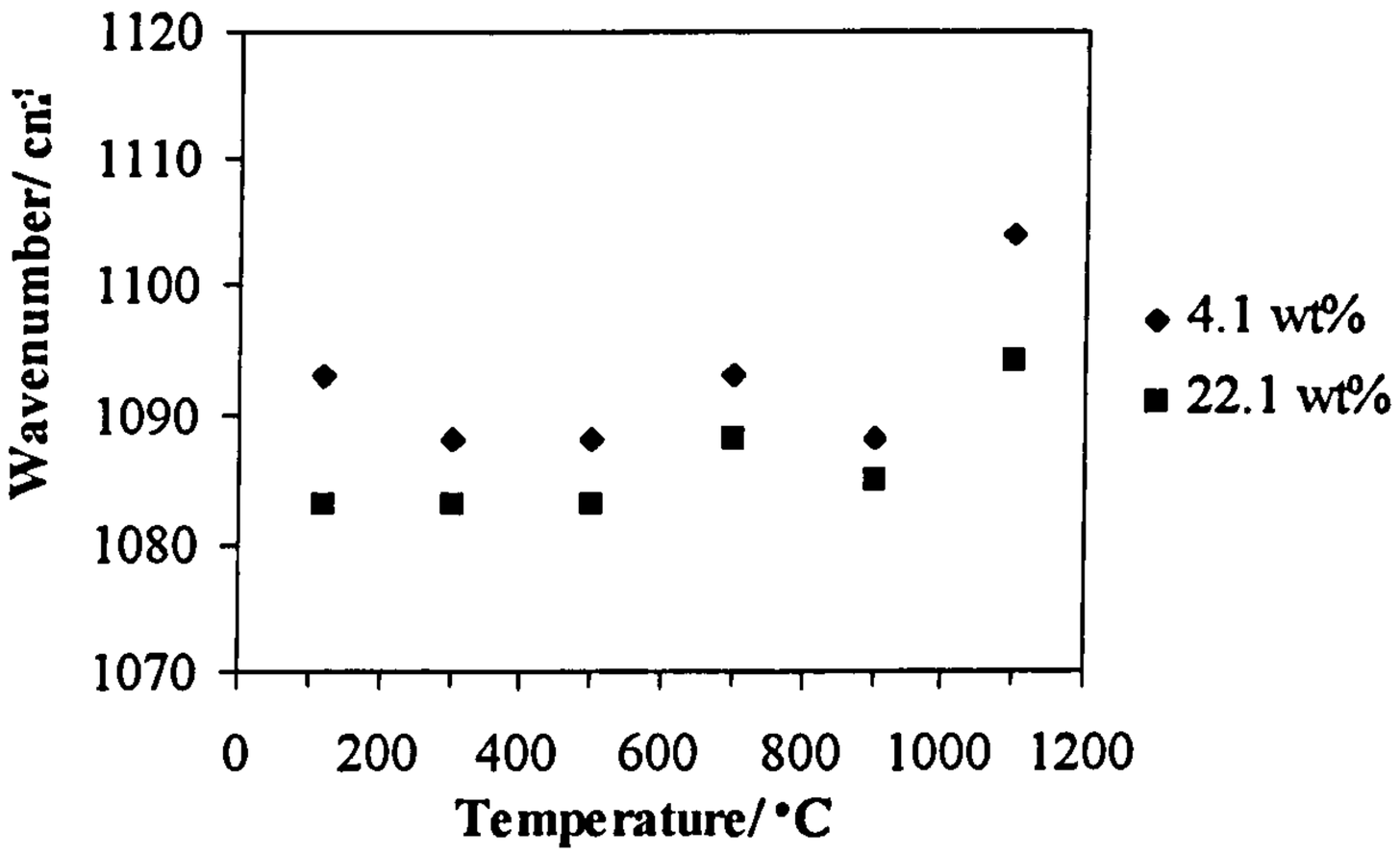

The band at *ca* 960cm^{-1} is mainly associated with Si-OH stretching and probably a contribution from Zr-OH and Si-O-Zr stretching vibrations. The relative intensity of the peak decreases as the treatment is increased up to 900°C (see figure 6.4) which is consistent with the removal of SiOH/ZrOH from the surface. In sharp contrast to the results obtained for silica/titania gels, further increasing the temperature to 1100°C has no effect on the intensity of the peak. Increasing the amount of zirconia present in the gel results in a decrease in the intensity of the band. Therefore, since the intensity of the band decreases with both increasing temperature and zirconia content, it must be generated predominantly by a vibrational mode involving Si-OH stretching motions.

The band at *ca* 800cm^{-1} has been assigned to a network Si-O-Si symmetric bond stretching vibration that does not shift appreciably nor change in intensity with treatment temperatures up to 900°C. Increasing the treatment temperature to 1100°C results in an increase in the relative intensity of the band (see figure 6.4 and appendix III). This intensity increase occurs because of the formation of new Si-O-Si bonds due to phase separation and the formation of crystalline zirconia, see section 6.2.2.

At temperatures below 700°C a broad shoulder at *ca* 550cm^{-1} was observed on the peak at *ca* 460cm^{-1}, see figure 6.4 and appendix III. After thermal treatment above 700°C, the shoulder at *ca* 550cm^{-1} was observed to broaden and increase in intensity. Although no X-ray diffraction pattern was observed for samples treated at less than 1100°C, see section 6.2.2, the band has been assigned as tetragonal zirconia. The lack of X-ray diffraction pattern can be explained by the regions of crystallinity being too small to be detected.

The band at *ca* 470cm^{-1} has been assigned to the out-of-plane bending vibrations of network Si-O-Si[4]. For all zirconia contents, this band remains unchanged in both position and intensity at temperatures up to and including 900°C (see figure 6.4 and appendix III). However, treatment at 1100°C resulted in an increase in intensity of the peak relative to the

peak at 1100cm^{-1}, but there is no appreciable shift in the band position as the Si-O bonds strengthen. This intensity increase occurs because of the formation of new Si-O-Si bonds due to phase segregation and the formation of crystalline zirconia, see section 6.2.2.

6.3.2.2 Fourier Self-Deconvolution

The spectra discussed in section 6.3.2.1, were manipulated using Fourier self-deconvolution and derivative methods (Nicolet OMNIC software). The deconvolution results obtained suggested that the main region of interest was that between 920 and 1250cm^{-1}, from table 6.5 it is obvious that the original spectra usually contain more than one peak within this spectral envelope.

After deconvolution the band at *ca* 1200cm^{-1} previously assigned to the longitudinal optical mode of the antisymmetric Si-O-Si stretching vibration, divided into two peaks at *ca* 1230cm^{-1} and *ca* 1170cm^{-1}. The peaks can be assigned as follows, the peak at *ca* 1230cm^{-1} to the longitudinal optical mode of the antisymmetric Si-O-Si stretching vibrations and that at *ca* 1170cm^{-1} to the antisymmetric stretching vibrations of Si-O in a slightly different environment.

The peak at approximately 1100cm^{-1} split into a further two peaks centred at *ca* 1090cm^{-1} and *ca* 1040cm^{-1}. The higher wavenumber peak has been assigned as the transverse optical mode of antisymmetric Si-O-Si stretching vibrations and the peak at *ca* 1040cm^{-1} to the antisymmetric stretching vibrations of Si-O-Zr bonds.

At thermal treatment temperatures of 900°C or less, the spectra of the sample containing 4·1 weight % zirconia show that the relative intensity of the band at *ca* 1230cm^{-1} was greater than the band at 1170cm^{-1} (see figure 6.6). Further heating of the sample to 1100°C resulted in the relative intensity of the band at *ca* 1170cm^{-1} being greater than that of the band at *ca* 1230cm^{-1}. Varying the amount of acid used in the hydrolysis reaction and the amount of zirconia in the samples has no effect on the deconvoluted spectra.

The band at *ca* 1090cm^{-1}, assigned to the transverse optical mode of antisymmetric Si-O-Si stretching vibrations was of an equal relative intensity on comparison with the band at *ca* 1040cm^{-1}. Increasing the temperature to 1100°C resulted in the band at *ca* 1090cm^{-1} shifting to a higher wavenumber (1110cm^{-1}), this has been attributed to a strengthening of the Si-O bonds. As well as this shift the band at *ca* 1110cm^{-1} increased in intensity relative to the band at 1040cm^{-1}. This intensity increase occurs because of the formation of new Si-O-Si bonds due to phase separation and the formation of crystalline zirconia. Increasing the concentration of zirconia in the sample has no effect on the position of the transverse optical mode of the antisymmetric stretching band of Si-O-Si. Any small variation in the intensity of the bands is difficult to quantify since differences may occur as a result of the data manipulation process.

Figure 6.6: Spectra Resulting from Fourier Self-Deconvolution for a Sample Containing ZrO_2=4·1 weight % and Treated at 500°C (a) second derivative; (b) first derivative; (c) Fourier self-deconvolution; (d) original spectrum

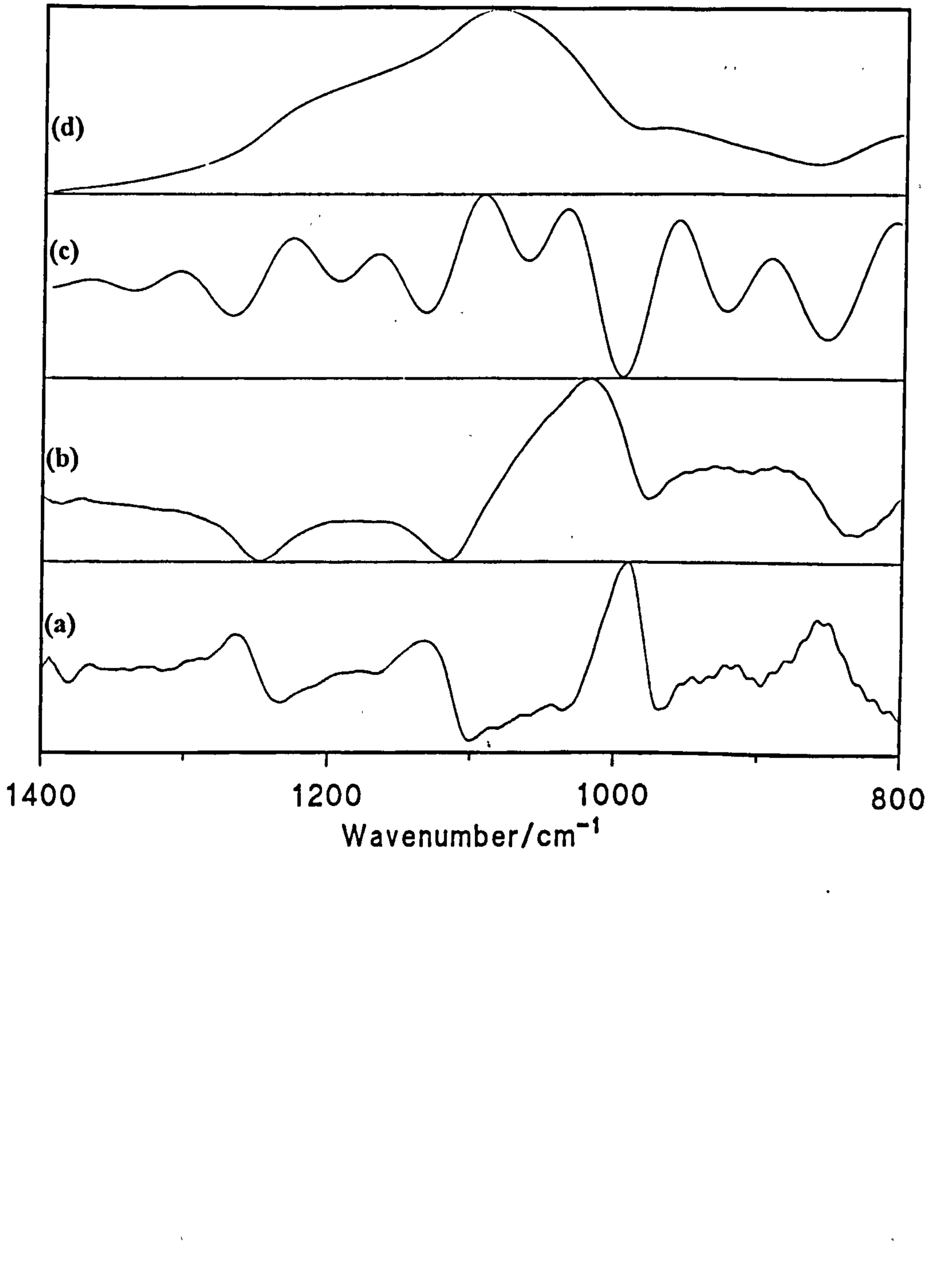

6.4 The Effect of Temperature and the Amount of Acid used in Hydrolysis on the Near Infrared (NIR) Spectra of Silica-Zirconia Gels of Varying Zirconia Content in the First Overtone Region (1200-2500nm)

6.4.1 Introduction

This section contains data obtained for a series of spectroscopic studies in the first overtone region of the near-infrared (1200-2500nm). Samples were prepared and reflectance spectra recorded as detailed in section 2.2.5. The results obtained have been used to determine how the surface changes with heat treatment.

The spectral region contains three sets of bands at *ca* 2200, 1900 and 1400nm. These have respectively been assigned as combination stretching vibrations for SiOH with a contribution from the bulk matrix, the combination of stretching and deformation vibrations for water, and the first overtones of the stretching modes of SiOH and H_2O, see table 4.6.

6.4.2 Results and Discussion

The most prominent absorptions occur at 1370 and 2200nm. For samples treated at 120°C, the sharp peak at 1370nm has been assigned to the first overtone of the fundamental OH stretch of free silanol groups[7]. However, the peak at 2200nm is more perturbed and has a greater intensity. This has been attributed[8,10] to a combination of the fundamental OH stretching of free silanol groups with the fundamental symmetric stretching of the silica framework at $800cm^{-1}$. The band at 1900nm arises from the combination of stretching and deformation modes of water, and the shoulder at 1400nm from a combination of symmetric and antisymmetric stretching vibrations. Absorptions like these arise from isolated water molecules hydrogen bonded to silanol groups. The presence of shoulders on the major peaks at 1940 and 1450nm is indicative of water molecules hydrogen bonded to one another. A more detailed description of spectral assignments can be found in section 4.4.2.

6.4.2.1 Effect of Thermal Treatment

As previously observed for silica-titania gels (see section 4.4.2.1), the overall effect of increasing the thermal treatment temperature of the sample is a systematic reduction in the intensity of all three bands, see figure 6.7 and appendix III. This is consistent with the dehydroxylation processes:

$$Si-OH+HO-Si \rightarrow Si-O-Si+H_2O$$

$$Si-OH+Zr-OH \rightarrow Si-O-Zr+H_2O$$

Surface dehydroxylation occurs across a wide temperature range with the removal of monomerically bound water (1400nm) at low temperatures. However, from figure 6.7 it can be seen that a significant reduction in the number of free silanols is only visible in the NIR at temperatures greater than or equal to 700°C.

A sharp peak is visible at 1375nm, which is attributable to both vicinal free OH groups and isolated free OH groups. The free SiOH band, at 1370nm, moves progressively to a lower wavelength by approximately 4nm as the temperature increases. At 1100°C no peaks due

to surface silanol species are observed, see figure 6.7. This is consistent with the results obtained for silica[8,10] and silica-titania gels (see section 4.4.2.1) of a shift to shorter wavelengths at 1000°C. This has been attributed to the consolidation of the silica network and the strengthening and/or shortening of the O-H bond of the silanol group.

Since these vicinal and free silanol groups are unable to interact, the vibrations of the atoms in these groups are unperturbed. Although this band is sharp, there is an asymmetry observed on the high wavelength side that appears as a shoulder at approximately 1400nm. Such asymmetry is attributed to the presence of perturbed or hydrogen bonded silanol groups. Both vicinal and geminal silanol groups are possible but cannot be observed separately by infrared spectroscopy unlike ^{29}Si NMR spectroscopy[11-13]. However, Wood *et al*[14] assigned a peak at 1362nm to vicinal free OH groups and a shoulder at 1369nm due to isolated free OH groups. Isolated free OH groups should be much less susceptible to dehydroxylation at low treatment temperatures than vicinal OH groups in which new siloxane bonds are formed inside particles instead of between particles. If Wood *et al*[14] are correct then in the early stages of dehydroxylation, the absorption arising from isolated OH groups should become more pronounced and increase in relative intensity with respect to the band arising from vicinal OH groups. In this case, a shoulder at 1369nm is not observed on the peak at 1373nm at low temperatures, although at 700°C a peak is observed at this wavelength (see figure 6.7). Hence the surface of the low temperature gel consists of vicinal OH groups, whereas that of the high temperature gel consists of free silanol groups.

The band at 2200nm, which is attributable to the combination of stretching and deformation vibrations of silanol groups, is stronger and much broader than the first overtone band at 1375nm. As the treatment temperature of the sample was increased above 700°C, the band at 2200nm began to decrease in intensity until at 1100°C it was no longer detectable. Heating of the sample also resulted in a decrease in the asymmetry of the peak on the high wavelength side, corresponding to the loss of hydrogen bonded species as seen at 1400nm. From these results it appears that very little dehydroxylation occurs at temperatures up to 500°C and only becomes significant at temperatures greater than 700°C.

Figure 6.7: Effect of Temperature on the Near-Infrared (NIR) Spectra in the First Overtone Region (1200-2500nm) of a Sample Containing ZrO_2=4.97 weight %. (a) 120°C; (b) 300°C; (c) 500°C; (d) 700°C; (e) 900°C; (f) 1100°C.

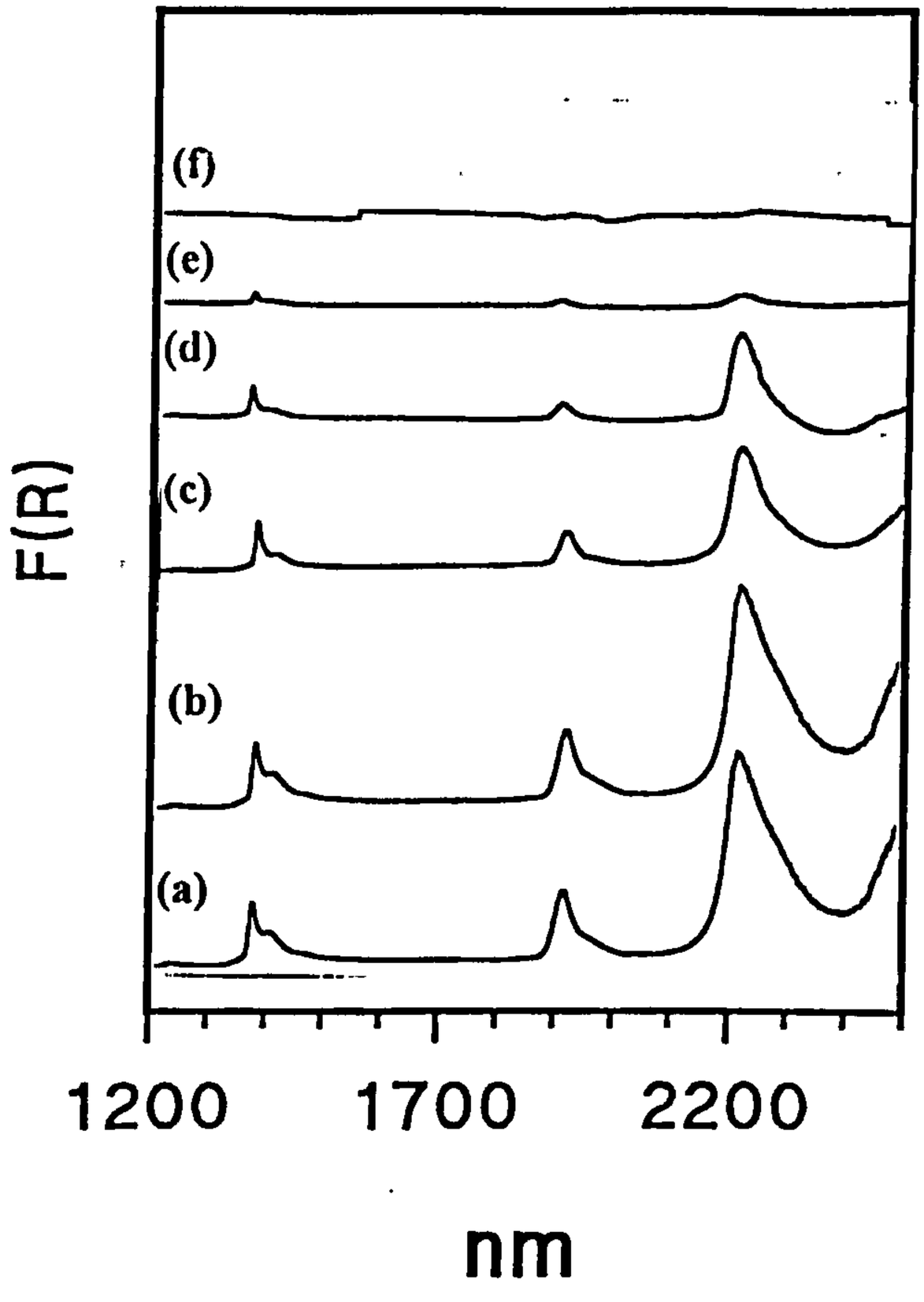

6.4.2.2 Variation of Zirconia Content

Increasing the amount of zirconia (weight %) present in the sample resulted in the observation of fewer free silanol groups at 1375nm compared to hydrogen bonded species at 1400nm (see appendix III). The spectrum of a silica only gel was found to contain much narrower peaks and compared to the silica-zirconia gels the peaks at 1375nm due to free SiOH groups were more intense. This is indicative of there being fewer free SiOH groups at 1375nm and therefore more hydrogen bonded SiOH groups on the surface of a silica-zirconia gel.

As the amount of zirconia present in the sample increases, the combination band at 2200nm increases in intensity and develops a more apparent shoulder on the high wavelength side of the band. This is indicative of an overall decrease in free SiOH groups and a corresponding increase in hydrogen bonded species. Because of the low levels of zirconia present in the gels and the small change in dipole moment of the Zr-O bond any contributions to the peaks will be negligible. Hence at these levels it is not possible to determine the overall effect due to Zr-OH.

6.4.2.3 Variation of the Amount of Acid used in Hydrolysis

Similarly as the amount of hydrochloric acid used for the hydrolysis reaction decreases, there is a corresponding decrease in the number of free silanol groups (1375nm), and hence an increase in the number of hydrogen bonded species (1400nm), see figure 6.8.

The band near 2200nm which is attributable to silanol groups, is stronger and broader than the corresponding first overtone band at 1375nm. However, high wavelength asymmetry due to perturbed species on the surface is still observed. This combination band increases in intensity and develops a more apparent shoulder on the high wavelength side of the band as the amount of acid used in the hydrolysis reaction decreases. This is indicative of an overall decrease in free -SiOH groups and a corresponding increase in hydrogen bonded species. (see figure 6.8)

For silica only gels, decreasing the amount of acid used in the hydrolysis reaction resulted in a similar increase in hydrogen bonded species. On comparison of silica and silica-zirconia gels the observed increase in hydrogen bonded species was greater in the samples with zirconia present than for silica only. This confirms previous conclusions that the presence of zirconia results in there being more hydrogen bonded species on the surface of the gel.

Figure 6.8: Effect of Varying the Amount of Acid used in the Hydrolysis Reaction on the Near-Infrared Spectra (1200-2500nm) of a Sample Containing ZrO_2=6·4 weight % and Treated at 120°C (a) 0·045 mole; (b) 0·030 mole; (c) 0·015 mole; (d) $7{\cdot}5x10^{-3}$ mole; (e) $5x10^{-3}$ mole; (f) $2{\cdot}5x10^{-3}$ mole

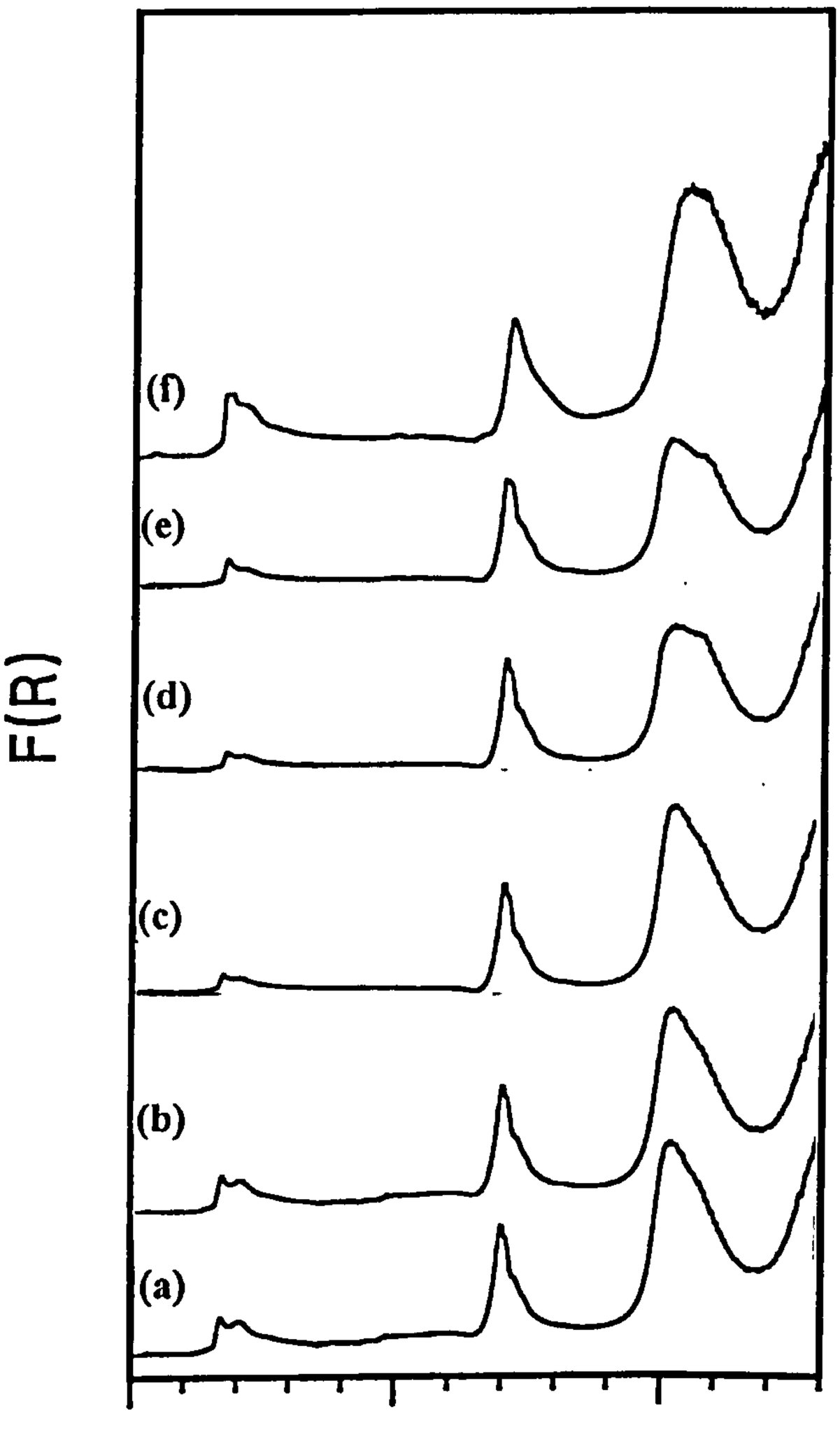

6.5 A NIR Investigation of the Interaction of Water with Silica/Zirconia Gels

6.5.1 Introduction

This section contains information on a series of reflectance studies that have been performed in the near-infrared region from 900-2500nm. The results obtained have been used to determine how water molecules interact with the surfaces of mixed silica/zirconia gels and the effect of thermal treatment on the activity of silanol groups in promoting surface hydration. The sample investigated contained 6·4 weight % zirconia and had been treated at temperatures of 120 and 900°C. Reflectance spectra were obtained under conditions of increasing hydration, see section 4.5.1.

The wavelength region 1200-2500nm contains three principal groups of absorption bands at *ca* 2200, 1900 and 1400nm. The second wavelength region of study, 900-1350nm, is a reduced replica of the first, with variations in anharmonicity constants for the vibrations involved, and also contains three groups of bands at *ca* 1200,1100 and 900nm. Full assignments are detailed in table 4.7.

6.5.2 Results and Discussion

6.5.2.1 Mixed Silica/Zirconia Gels at 120°C

6.5.2.1.1 The Effect of Hydration on Silanol Derived Bands

After prolonged dehydration *in vacuo* at room temperature the reflectance spectra at t=0 over the regions 900-1350 and 1200-2500nm contain seven well-defined bands (see figures 6.8 and 6.9). At t=0 the bands due to free -SiOH groups are sharp, but they rapidly reduce in intensity as hydration proceeds; this is especially noticeable for the peak at 1370nm, the combination band at *ca* 2200nm reducing a much lower amount by comparison. Although this band remains unresolved, it shifts by approximately 40nm after 14 hours exposure to the atmosphere. This shift towards a higher wavelength is indicative of a decrease in free -SiOH groups and a corresponding increase in hydrogen bonded species. A range of such surface monohydroxylated hydrogen bonded species are fully described in section 4.5.2.

In the 1400nm region, the sharp peak between 1368-1373nm for all samples can be assigned as a type A silanol group. The almost complete loss of this band with time, for all the samples at 120°C, implies that very few free silanol groups remain in the hydrated sample and are thus hydrogen bonded to water.

Figure 6.9: First Overtone and Combination Region (1200-2500nm) Near Infrared Spectra of a Dehydrated Sample Containing ZrO_2=6·4 wt% Heated to 120°C and Exposed to the Atmosphere for Various Times.
(a) 0; (b) 0·5 hour; (c) 1 hour; (d) 2 hours; (e) 14 hours.

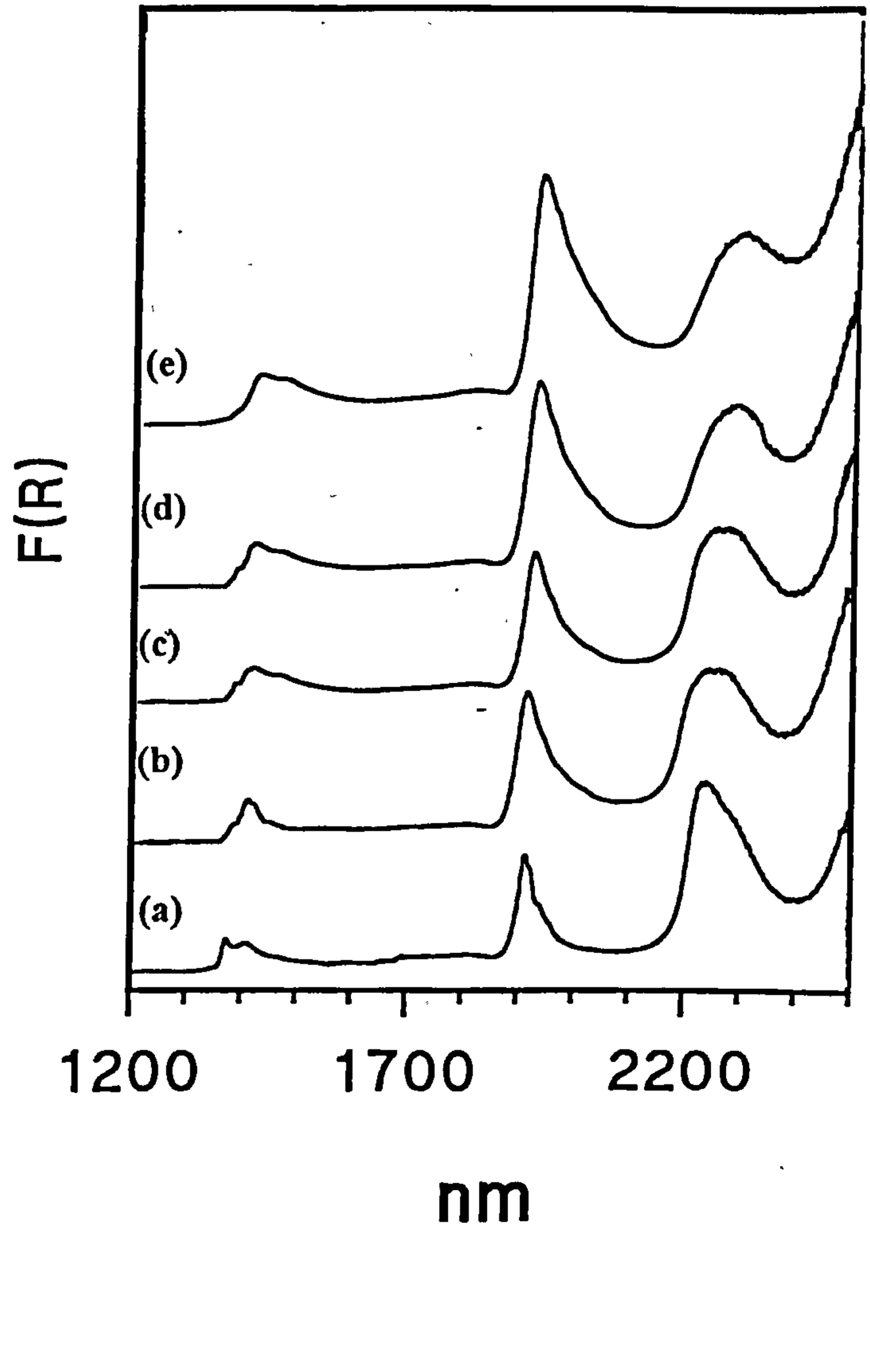

Figure 6.10: Second Overtone Region (900-1350nm) Near Infrared Spectra of a Dehydrated Sample Containing ZrO_2=6·4 wt% Heated to 120°C and Exposed to the Atmosphere for Various Times.
(a) 0; (b) 0·5 hour; (c) 1 hour; (d) 2 hours; (e) 14 hours.

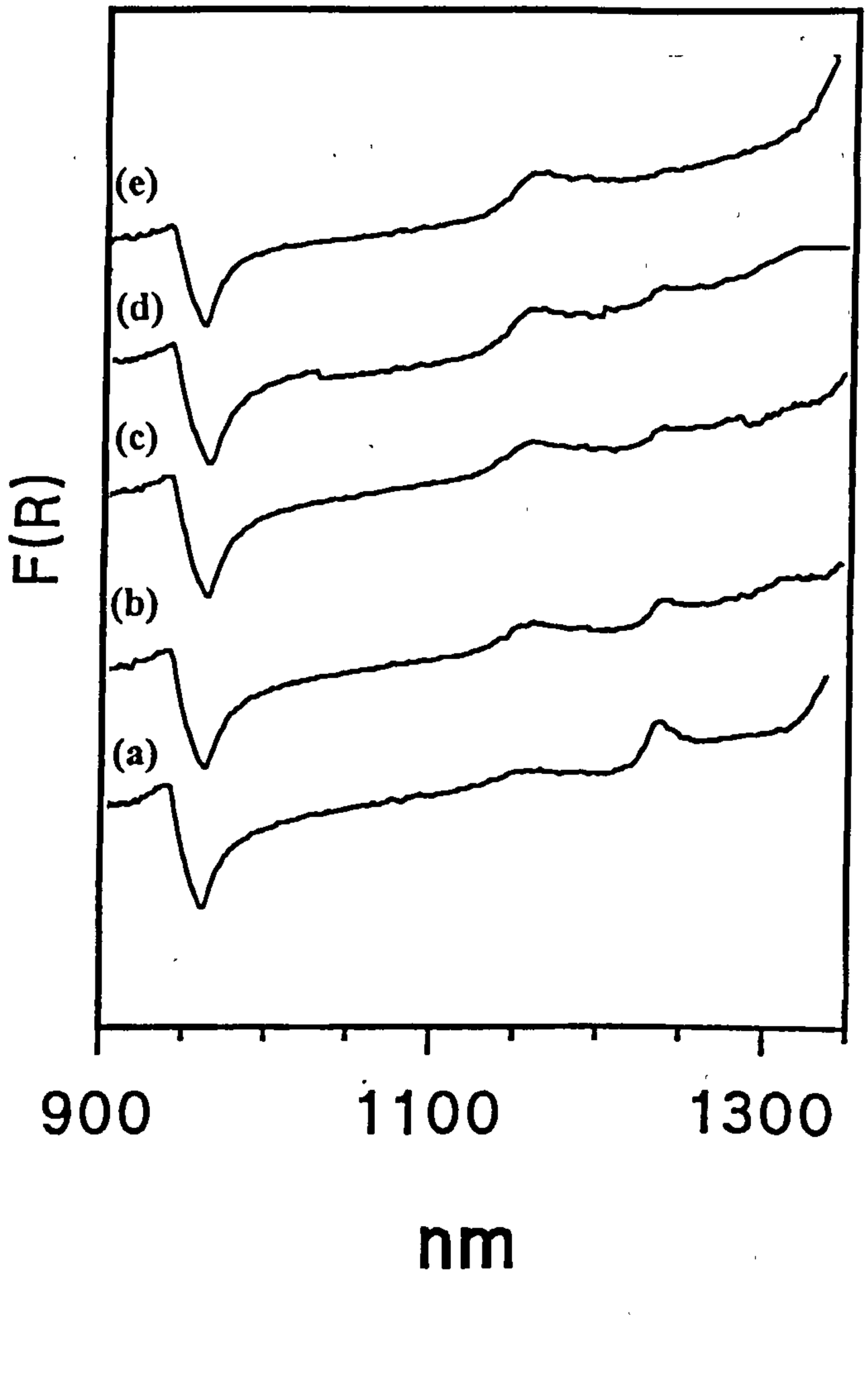

Similarly, in the second overtone and combination region the peak at 1230nm decreases in intensity with time but does not shift during hydration and is thus comparable to type A silanol groups. The higher baseline on the high wavelength side indicates the presence of types B to D hydrogen bonded species.

6.5.2.1.2 Water Bands in the First Overtone and Combination Region

The reflectance spectra obtained at t=0, see figure 6.9, indicate the presence of water on the surface of the sample. From figure 6.9, it is obvious that as the extent of hydration increases, then the combination band at *ca* 2200nm, and the band at 1900nm increase in intensity and new bands centred at 1400nm and 1450nm appear. A shoulder also appears on the band at 1900nm at *ca* 1930nm. Both this band and the one at 1450nm behave in a similar manner and increase in intensity relative to the bands at 1900 and 1400nm as exposure time increases. Therefore the sets of bands at 1400, 1900 and 1450, 1930nm arise from the same molecular species.

The 1900nm band has been assigned as arising from S'_0 species[10] because apart from increasing in intensity the band remains essentially unchanged on increasing hydration. Anderson *et al*[9] found that at low levels of hydration, further adsorption of water can occur at either -SiOH or water groups with equal probability. If a water layer was formed sequentially then no S'_0 species would be observed on the surface of a fully hydrated sample. However, the presence of a shoulder at *ca* 1950nm and a raised baseline on the high wavelength side of the band can be attributed to the overlap of peaks due to S'_1 and S'_2 species indicating that the water layer is not formed sequentially.

The overlap of perturbed -SiOH and H_2O bands makes precise assignment of the 1400nm band a complicated task. Since the intensity change of this band is comparable to that of the band at 1900nm, this has therefore been assigned as S'_0 type water with a contribution from hydrogen bonded silanol/water species. As the hydration of the surface proceeded, the peak maximum shifted to a higher wavelength by approximately 10nm. This may be attributed to the gradual formation of hydrogen bonded silanol groups which have a peak at about the same wavelength. The maximum at 1450nm arises because of a spectral envelope due to S'_1 and S'_2 water species which are partly and fully hydrogen bonded to other water molecules respectively. This evidence again indicates that the water layer on the surface does not form sequentially.

6.5.2.1.3 Water Bands in the Second Overtone Region

Reflectance spectra at t=0 in the 900-1350nm region, show two distinct bands even after prolonged dehydration *in vacuo* at room temperature, see figure 6.10.

Studies of water both by itself, in ionic solutions and in mixed solvents at varying temperatures have been made[7,15-18], on comparison with the first overtone region these weak bands have been assigned. The most intense band was observed at approximately 1230nm and was assigned as arising from SiOH groups. A further two weak bands were observed

around 1150nm, which increased in intensity as the extent of hydration increased. These were assigned as arising due to S'_0 species, and at higher wavelengths to S'_1 species[10]. These bands were very well defined even at high levels of hydration suggesting that there was little interaction between adsorbed water molecules and that more than one type of water molecule can exist on the surface.

For a sample containing 6·4 weight % zirconia (figure 6.10) the sharp peak around 1230nm, assigned to the higher combination band of free -SiOH groups[10], was observed to decrease in intensity as hydration progressed. As the surface became increasingly more hydrated, the contribution from the baseline increased because of the presence of a broad band due to S'_2 water species. The simultaneous observation of S'_0, S'_1 and S'_2 water species at *ca* 1200nm suggests that water forms local clusters rather than complete molecular layers.

6.5.2.2 Mixed Silica/Zirconia Gels at 900°C

Comparison with the spectra at 120°C, see figures 6.9 and 6.11, revealed an increase in the sharpness of the free SiOH bands at t=0, and a big reduction in the intensity of both the water and silanol bands. This has been attributed to the thermal treatment removing the majority of the surface silanol groups, which are the main adsorption sites on the surface of the gel. The surface of the high temperature gel is therefore less hydrophilic.

Thermal treatment resulted in the band due to free -SiOH species shifting to a slightly lower wavenumber. Exposure of the sample to the atmosphere resulted in changes due to hydration similar to those observed for the samples treated at a lower temperature.

After extended hydration free silanol groups (1370nm) were observed on the surface of the thermally treated sample (see figure 6.11). In section 6.4.2.1, thermal treatment was observed to reduce the number of free silanol groups present on the surface. The observed free silanol groups remaining on the surface are therefore susceptible to hydration. However extended exposure to the atmosphere resulted in an extremely weak peak at 1450nm due to the formation of S'_1 and S'_2 species. This and the presence of a broad shoulder at 1940nm also confirmed the presence of S'_1 and S'_2 species on the surface are shown in figure 6.11.

After the same exposure time, the combination band at 2200nm was found to consist predominantly of free silanol groups. A shoulder was observed on the high wavelength side of the band (figure 6.11) due to hydrogen bonded species. This shoulder became more prominent as the hydration proceeded. However, it was observed that free silanol species were still the predominant species after extended hydration.

Figure 6.11: First Overtone and Combination Region (1200-2500nm) Near Infrared Spectra of a Dehydrated Sample Containing ZrO_2=6·4 wt% Heated to 900°C and Exposed to the Atmosphere for Various Times.
(a) 0; (b) 0·5 hour; (c) 1 hour; (d) 2 hours; (e) 14 hours.

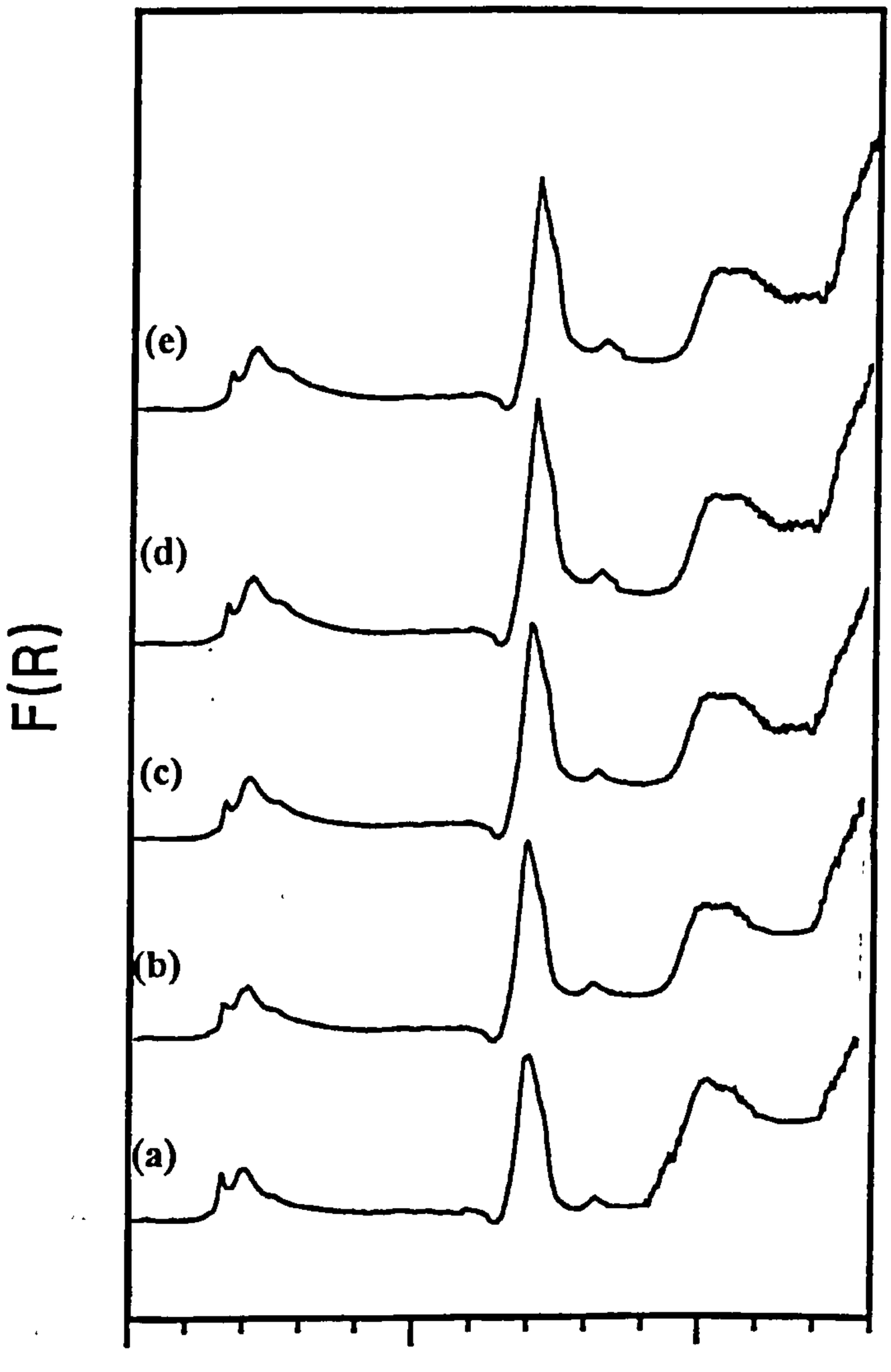

6.6 Thermal Analysis

A series of gels with varying zirconium oxide contents (weight %), as in table 6.1, were investigated using synchronous differential thermal (DTA) and thermogravimetric (TGA) analysis methods. The aim of these studies was to identify the temperatures at which phase transformations occur.

6.6.1 Results and Discussion

A typical DTA and TGA curve is shown in figure 6.12. The curves obtained did not record any changes due to crystallisation under the applied heating regime. As such, the DTA curves indicate only the loss of water and organics at low temperatures.

Figure 6.12: Typical Differential Thermal (DTA) and Thermogravimetric (TGA) Curves Obtained for Mixed SiO_2-ZrO_2 Gel (in this instance ZrO_2=6·4wt%)

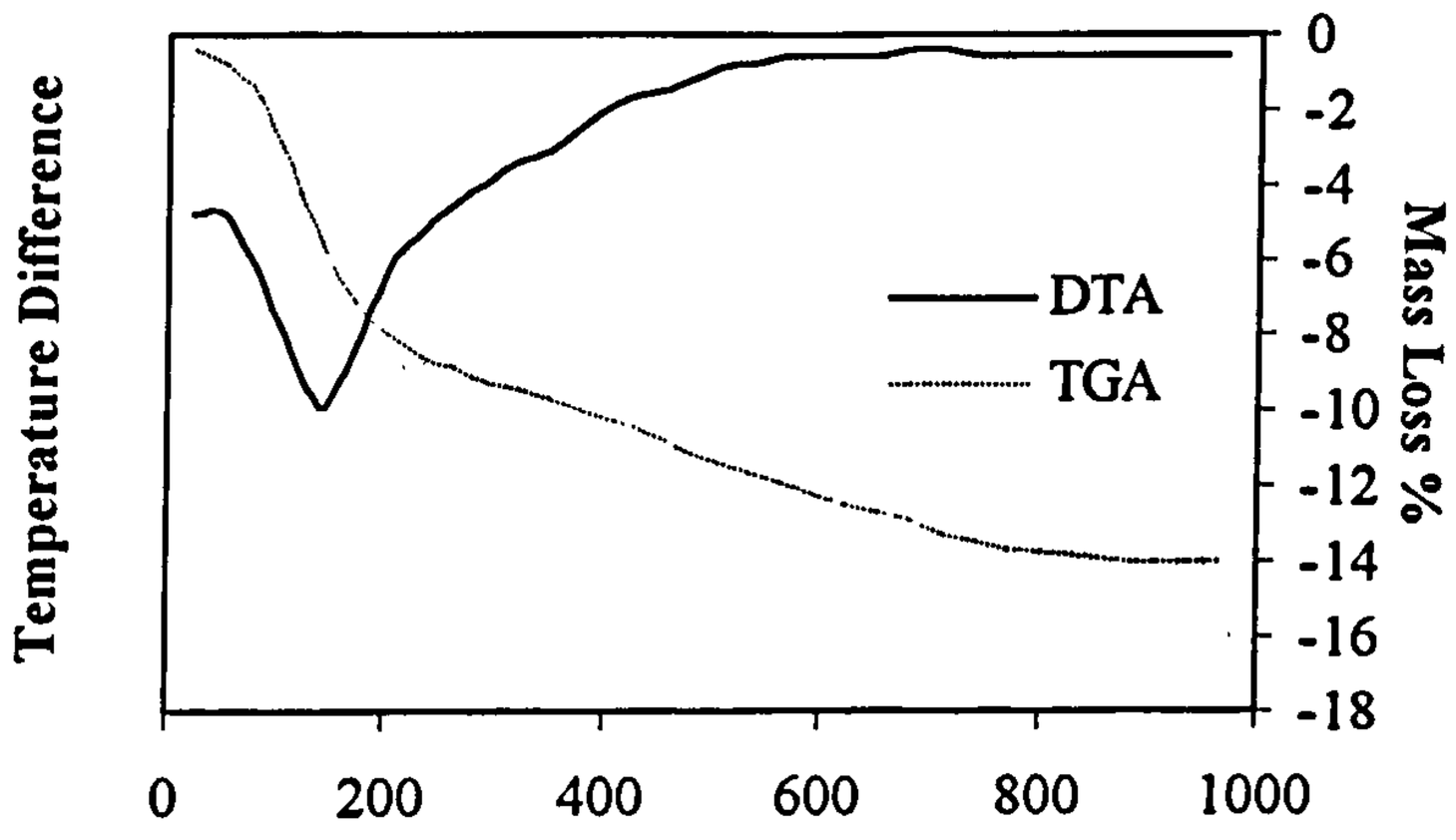

X-ray diffraction of samples containing ZrO_2 of 4·1, 4·97, 6·4 (at various levels of hydrolysis acid) and 22·1 weight %, all remained amorphous after thermal analysis. This is consistent with crystallisation occurring over a longer time period than that of the thermal analysis.

6.7 Gas Adsorption Investigation of Pore Structure

6.7.1 Introduction

Gels with varying zirconium oxide contents (weight %), as in table 6.1, were investigated after treatment at 120, 300, 500, 700, 900 and 1100°C. The aim was to study the effect of temperature and zirconia content on the surface area and porosity of the samples. Similarly, the effect of variation of the amount of acid used in the hydrolysis reaction has also been investigated, see table 6.6.

Table 6.6: Hydrolysis Acid and Water Contents for Investigated Mixed SiO_2-ZrO_2 Gels Containing 6·4 weight % Zirconia.

ZrO_2 /weight %	Amount HCl /mole
6·4	0·045
6·4	0·030
6·4	0·015
6·4	$7{\cdot}5x10^{-3}$
6·4	$5x10^{-3}$
6·4	$2{\cdot}5x10^{-3}$
4·1	0·045
4·97	0·045
22·1	0·045

6.7.1 Results and Discussion

6.7.1 Structural Evolution

6.7.1.1 Effect of the Amount of Acid used in the Hydrolysis Reaction

For gels prepared using a large amount of acid in the hydrolysis reaction the resulting isotherms are type IV. Generally it can be seen that the greater the amount of acid used for the hydrolysis then the greater the mesoporosity exhibited by the resulting material as evidenced by the hysteresis effects observed. Decreasing the amount of acid used in the hydrolysis reaction results in the elimination of hysteresis and the formation of type I isotherms, this is characteristic of microporous solids. As the amount of acid used in the hydrolysis reaction is decreased both the surface area and pore volume decrease; the surface area from 640 to $156m^2g^{-1}$ and the pore volume from 0·33 to $0{\cdot}04cm^3g^{-1}$. Varying the amount of acid used in the hydrolysis reaction resulted in a slight decrease in the average pore diameter from *ca* 27-24Å.

For samples containing a high amount of acid, 0·030 and 0·045 mole, the isotherms exhibited hysteresis. The shape of the observed hysteresis loop suggests that the mesopores present are more slit shaped than cylindrical, see section 2.5.1.3. Both adsorption and desorption pore size distribution data verify that there is a reduction in total pore volume and median pore diameter as the amount of acid used for hydrolysis decreases. Therefore the mesoporosity is removed by decreasing the amount of acid.

From figure 6.13 (also see appendix III) and table 6.7, it is observed that decreasing the amount of acid to 0·015mole (and below) removes the hysteresis observed in the isotherm and decreases the surface area and pore volume of the samples.

Figure 6.13: Effect of Variation of the Amount of HCl used for the Hydrolysis of a Sample Containing ZrO_2=6·4 weight % on the Resulting Adsorption/Desorption Isotherm

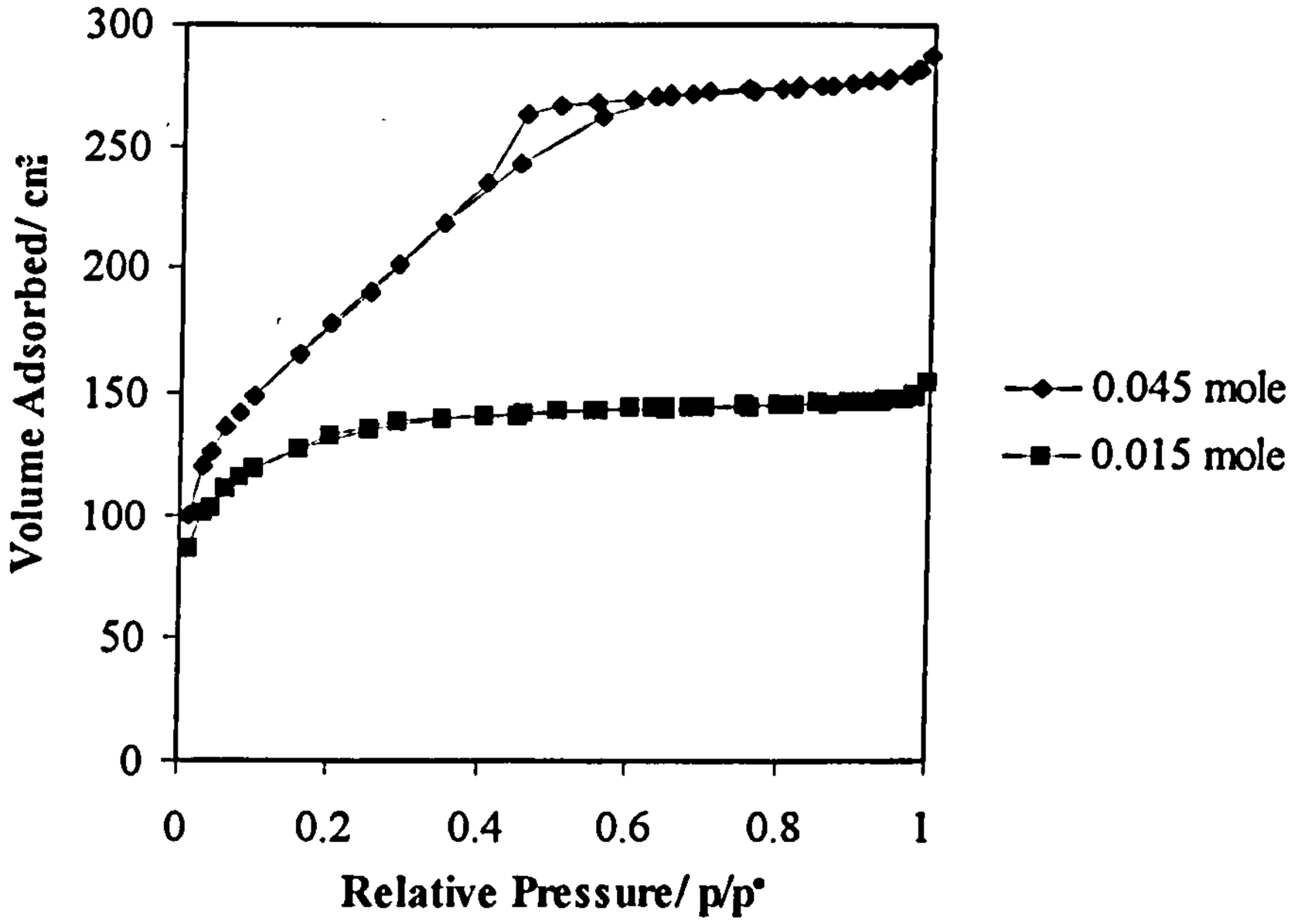

Table 6.7: Effect of Variation of the Amount of HCl used for the Hydrolysis of a Sample Containing ZrO_2=6·4 weight % on the Pore Structure of Gels Treated at 120°C.

Sample HCl (mole)	BET Surface Area (m^2g^{-1})		BJH Pore Volume (cm^3g^{-1})		BJH Average Pore Diameter (Å)	
		C	Adsorption	Desorption	Adsorption	Desorption
0·045	639·6	101·3	0·33	0·52	26·1	28·9
0·030	608·7	93·6	0·27	0·46	25·2	26·6
0·015	442·4	-310·5	0·08	0·12	27·3	23·0
$7·5x10^{-3}$	484·0	-190·5	0·17	0·12	21·9	23·3
$5x10^{-3}$	593·6	-2769	0·15	0·21	24·3	22·8
$2·5x10^{-3}$	156·0	-78·9	0·04	0·01	24·3	23·5

The high values for the BET parameter C for acid contents of 0·045 and 0·030mole, are indicative of the knee at point B (see figure 2.11, section 2.5.1.2) in the isotherm being sharp and hence easy to find. When C is small, the knee becomes difficult to locate and point B can not be used to estimate the monolayer capacity. The high values for the BET parameter C (≈100), are typical of the sample being mesoporous with a probable contribution from some micropores. The results of an investigation into the microporosity of the samples by the α_s-method are presented in section 6.7.1.4.

6.7.1.2 Effect of Varying the Amount of Zirconia

Comparison of the structural characteristics of silica and silica-zirconia gels prepared under the same conditions shows that the inclusion of zirconia results in pores that are less cylindrical, a decrease in the overall surface area of up to 50% and an increase in average pore diameter, see table 6.8. Varying the amount of zirconia (weight %) present in the sample had no obvious effect on the surface area or pore volume, see table 6.8. However, comparison with studies on silica and silica-alumina[21-24] gels suggests that the presence of zirconia in the sample results in larger pores and hence an increased average pore diameter.*

Table 6.8: Effect on Structural Characteristics of Variation of the Amount of Zirconia (weight %) for Samples Heated at 120°C [HCl=0·045mole].

ZrO_2 (wt %)	BET Surface Area (m^2g^{-1})		BJH Pore Volume (cm^3g^{-1})		BJH Average Pore Diameter (Å)	
		C	Adsorption	Desorption	Adsorption	Desorption
0	812·5	137·1	0·33	0·47	25·1	25·3
4·1	440·8	101·9	0·38	0·42	35·3	37·2
4·97	520·6	95·4	0·59	0·64	41·0	40·9
6·4	639·6	101·3	0·33	0·52	26·1	28·9
22·1	413·1	97·8	0·44	0·48	37·6	36·4

The high values for the BET parameter C (≈100), are typical of the sample being mesoporous with a probable contribution from some micropores. The results of an investigation into the presence of microporosity by the α_s-method is presented in section 6.7.1.4.

6.7.1.3 Effect of Varying the Treatment Temperature

On thermal treatment, a decrease in both surface area and pore volume was observed as the treatment temperature was increased, see table 6.9. On heating to 700°C both surface area and pore volume decreased by a small amount. On heating to 900 and 1100°C, the observed decrease in surface area and pore volume was larger than that observed at lower temperatures. Similarly, conventionally prepared silicas[19] exhibit very little change in surface area or pore structure below 700°C, but at temperatures greater than 700°C these changes are larger. These results are consistent with the densification of the gel and the progressive elimination of pores during thermal treatment.

* Nitrogen adsorption/desorption isotherms can be found in appendix III.

Table 6.9: Effect of Temperature on the Pore Characteristics of a Sample Containing ZrO_2=6·4 weight %.

		Temperature (°C)					
		120	**300**	**500**	**700**	**900**	**1100**
BET Surface Area (m^2g^{-1})		639·6	607·5	599·5	550·4	303·9	2·1
	C	101·3	113·0	88·3	74·3	69·8	20·5
BJH Pore Volume (cm^3g^{-1})	**Adsorption**	0·33	0·30	0·32	0·30	0·17	0·002
	Desorption	0·52	0·48	0·48	0·44	0·24	0·002
BJH Average Pore Diameter (Å)	**Adsorption**	26·1	25·5	24·9	25·1	25·8	129·6
	Desorption	28·9	27·3	27·4	26·0	26·0	67·8

The high values for the BET parameter C (≈100), are typical of the sample being mesoporous with a probable contribution from some micropores. The results of an investigation into the presence of microporosity by the α_s-method is presented in section 6.7.1.4.

Densification of the sample and the elimination of surface SiOH groups at 1100°C are indicative of surface and structural changes at high temperatures. This resulted in very low surface areas as detected by nitrogen adsorption.

On increasing the treatment temperature of the sample to 900°C, the isotherms exhibit hysteresis indicating a degree of mesoporosity. The shape of the hysteresis loop and the average pore diameters obtained from BJH theory both indicate that the pores are slit shaped (see figure 6.14 and appendix III). At 1100°C the isotherm exhibited no hysteresis and the resulting material had virtually no pore structure.

Figure 6.14: Comparison of Isotherms for a Sample Containing ZrO_2=6.4 weight % after a Range of Thermal Treatment Temperatures (HCl =0·045mole).

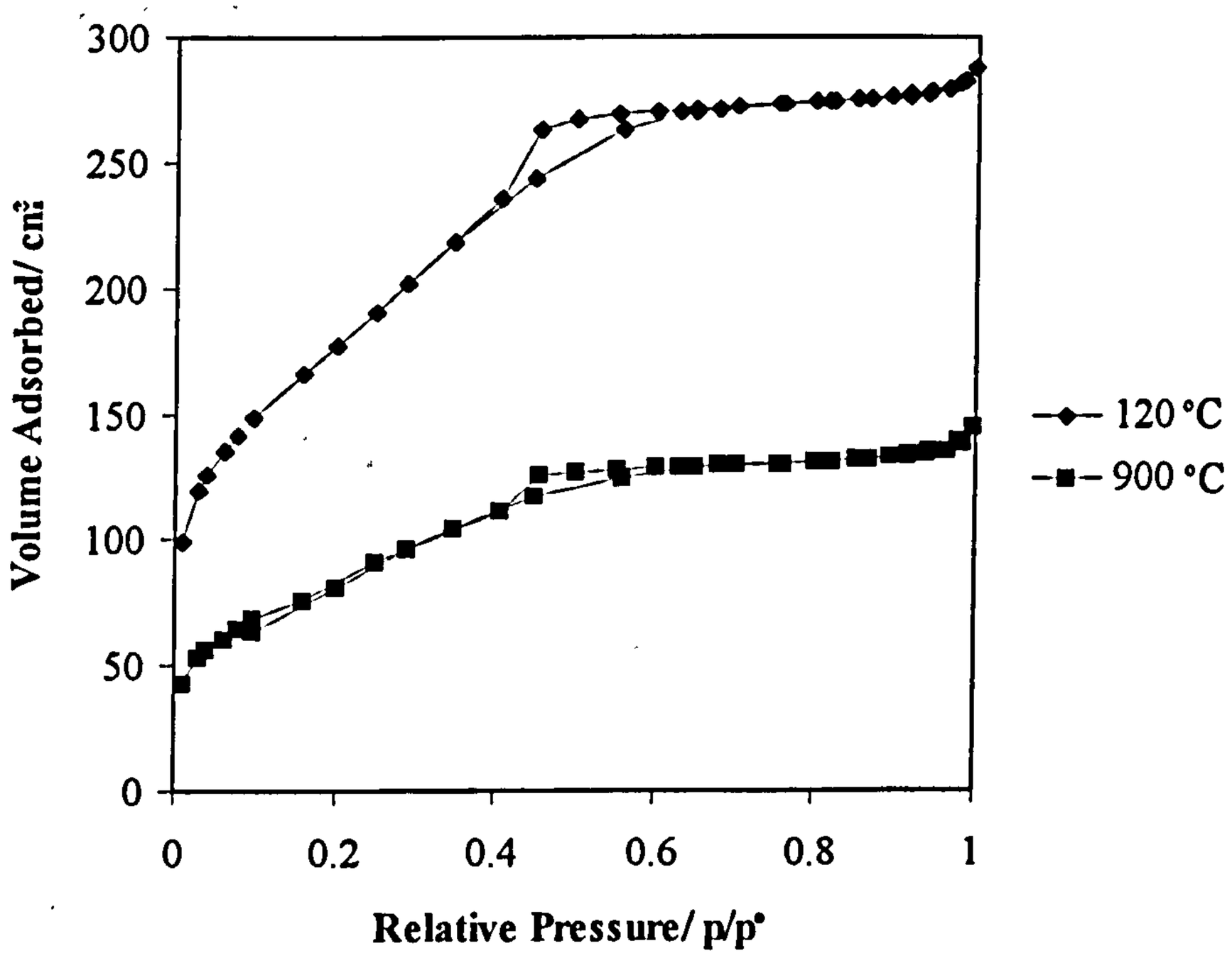

The effect of thermal treatment of the samples on average pore diameter has also been studied. Heating the samples to 900°C resulted in very little change in average pore diameter. The destruction of small pores during treatment at temperatures of greater than 900°C, resulted in an increase in an increase in the average pore diameter. This is in contrast with both surface area and pore volume data which both decrease significantly with increasing temperature. These results are consistent with the destruction of smaller pores during sintering and the resulting structure comprising of fewer, much larger pores.

Van Nordstrand, Kreger and Ries[22] and Bastick[23] have found that in commercial silica gel with a pore diameter of about 20Å, as well as a silica-alumina xerogel having a pore diameter of about 40Å, there is no change in average pore size as sintering progresses. Teichner[24] *et al* observed that on sintering a voluminous aerogel where shrinkage was 83% by volume, the average pore diameter changed by only a small amount.

It is well documented that when silica gel is sintered it shrinks; the pore volume decreases in proportion to the decrease in surface area and the pores that remain do not change in size. It appears that pores are destroyed as the silica is converted from the porous to the nonporous state without the size of any remaining pores undergoing any change[24].

Average pore diameters obtained for pore size distributions (PSDs) calculated from the adsorption branch of the isotherm (BJH method[20]) are compatible with those from the BET method. Typical PSD plots for samples at 120°C and 900°C are shown in figure 6.15. Both

plots have the maximum pore volume at a pore diameter around 26Å, and contain few pores of diameter greater than 100Å.

Figure 6.15: dV/dlog(D) Adsorption Pore Size Distribution Plots of a Sample Containing ZrO_2=6·4wt% Thermally Treated at 120 and 900°C.

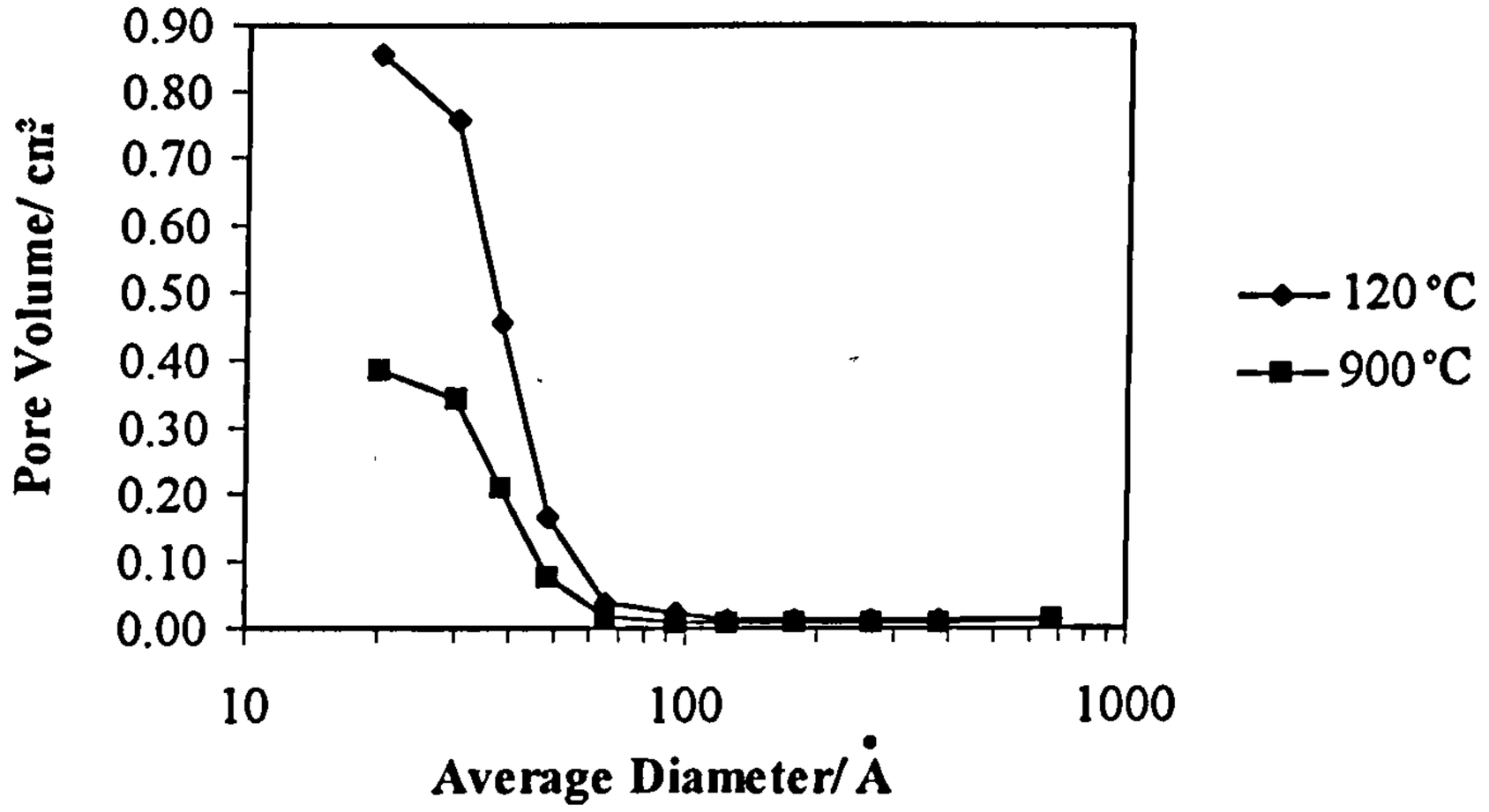

Therefore from the data presented in table 6.8, it is not possible to arrive at any conclusions about a relationship between the amount of zirconia present in a sample and the surface area and pore volume. However, comparison with studies on silica and silica-alumina[21-24] suggests that the presence of zirconia in the sample results in larger pores and hence a greater average pore diameter. The structural changes observed in gels treated at 1100°C are large reductions in both surface area and pore volume and a large increase in mean pore size.

6.7.1.4 Micropore Structure

The α_s-method[19] can be used to calculate the micropore volume and the surface area of the samples. A typical α_s-plot for monolithic samples previously discussed is shown in figure 6.16 (also see appendix III).

Figure 6.16: Effect of Variation of the Amount of HCl used for the Hydrolysis of a Sample Containing ZrO_2=6·4 weight % on the Resulting α_s-plots.

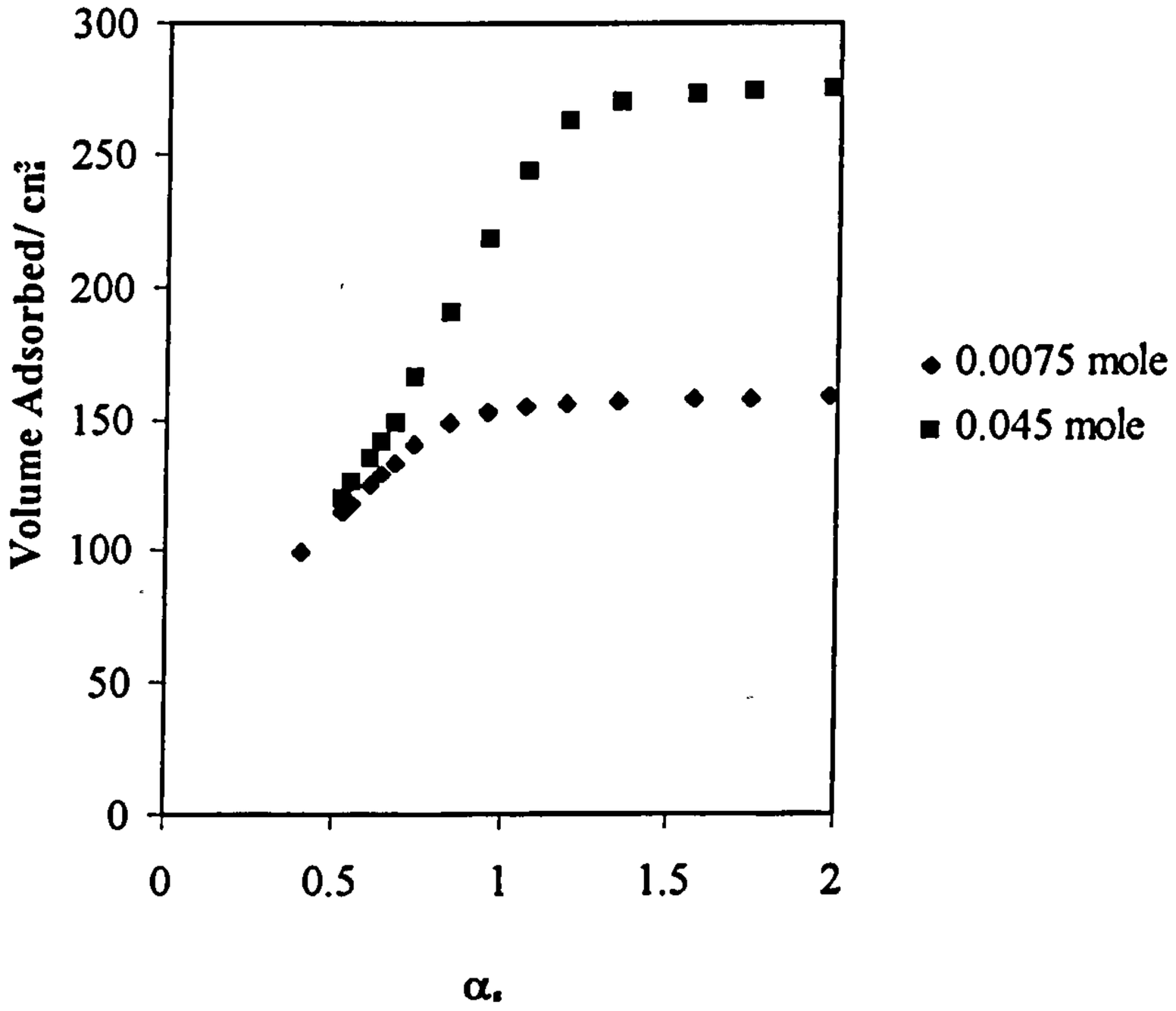

6.7.1.4.1 Effect on the Micropore Structure of Varying the Amount of Zirconia (weight %) in the Sample

Samples of all zirconia contents, prepared using 0·045mole of acid in the hydrolysis reaction all exhibited typical type IV isotherms. The values for the surface area presented in table 6.10 show that there is very little difference between the values obtained from the BET and α_s-methods. Increasing the zirconia content of the gel eliminates vitually all microporosity, although there is no obvious relationship between the amount of zirconia present in the gel and the surface area and microporosity (see section 6.7.1.2).

These results are typical of predominantly mesoporous solids and support the conclusions drawn previously, although there may be a small contribution from micropores.

Table 6.10: Comparison of BET and α_s-data Obtained for Powder Samples Containing Varying Amounts of Zirconia [HCl=0·045 mole]

ZrO_2 (wt %)	Surface Area (m^2g^{-1})		Micropore Volume (cm^3g^{-1})
	BET	α_s	
0	813	842·9	0·041
4·1	441	443·9	0·014
4·97	521	521·0	0·015
6·4	640	646·6	0·030
22·1	413	414·4	0·012

6.7.1.4.2 Effect on the Micropore Structure of Varying the Amount of Acid used in the Hydrolysis Reaction

For samples containing a high amount of acid, 0·030 and 0·045 mole, there is little difference between the BET and α_s- surface areas. This is indicative of there being few micropores. The results presented in table 6.11, show that for amounts of acid lower than 0·015 mole the values for the surface area obtained from the α_s-method are significantly larger than those obtained from the BET method. Therefore there must be a contribution to the overall surface area from micropores. Typically, decreasing the amount of acid removes mesoporosity and hence increases the microporous nature of the sample.

Table 6.11: Comparison of BET and α_s-data Obtained for Monolithic Samples Containing 6·4 weight % Zirconia and Prepared using Varying Amounts of Acid in the Hydrolysis Reaction

Amount of HCl (mole)	Surface Area (m^2g^{-1})		Micropore Volume (cm^3g^{-1})
	BET	α_s	
0·045	640	646·6	0·036
0·030	609	611·2	0·029
0·015	442	530·0	0·056
$7·5x10^{-3}$	484	597·9	0·076
$5x10^{-3}$	594	685·3	0·063
$2·5x10^{-3}$	156	211·3	0·037

6.7.1.4.3 Effect of Temperature on the Micropore Structure

On heating, there is little difference between the BET and α_s-surface areas obtained for the gels, see table 6.12. this is consistent with there being few micropores present within the bulk gel. The calculated micropore volumes decrease with increasing temperature, as small pores are preferentially destroyed by the sintering process.

Table 6.12: Comparison of BET and α_s-data for a Sample Containing 6·4 weight % Zirconia After Thermal Treatment

Temperature (°C)	Surface Area (m^2g^{-1})		Micropore Volume (cm^3g^{-1})
	BET	α_s	
120	640	646·6	0·036
300	608	620·9	0·033
500	442	594·8	0·020
700	484	532·0	0·013
900	156	290·9	≈0·000

6.8 Conclusions

The results of an investigation into the effects of reaction conditions, the amount of zirconia (weight %) present in the gel, and thermal treatment on the structure adopted by monolithic gels have been investigated.

Increasing the treatment temperature of the samples resulted in the progressive decrease of surface area, pore volume and micropore volume. The shape of the resulting hysteresis loop suggested that the pores are slit shaped. Heating to 900°C resulted in a decrease in pore volume but little change in average pore diameter. This is supported by changes in the hysteresis loop that suggests that small pores are destroyed and the shapes of other pores change on sintering. Changes in surface area and pore volume are only significant at temperatures greater than 700°C which is consistent with the removal of surface hydroxyl groups. Futher heating to 1100°C resulted in the complete densification of the gel.

On comparison with monolithic silica-titania gels there is a difference in overall surface areas of around $20m^2g^{-1}$ for gels made using 0·045 mole of acid for the hydrolysis reaction and treated at 120°C. The major difference was observed in the values obtained for pore volumes and average pore diameters, zirconia gels had average pore diameters around 5Å less than the corresponding titania gels and pore volumes about $0·2cm^3g^{-1}$ less than the corresponding titania gels. Such differences in surface area, average pore diameter and pore volume may be due to inhomogeneity in the silica/zirconia gel resulting in the segregation of

regions of amorphous zirconia and silica phases. In contrast no phase segragation of crystalline titania was observed on heating the corresponding silica/titania monolith.

Generally, decreasing the amount of acid used for the hydrolysis reaction decreases both the overall surface area and pore volume of the resulting material. However, the average pore diameter remains constant as the amount of acid used for the hydrolysis reaction was decreased. Typically, decreasing the amount of acid removes mesoporosity and hence increases the microporous nature of the sample.

After treatment at temperatures up to 1100°C gels containing 4·1 and 4·9 weight % zirconia were found to be amorphous by X-ray diffraction. Increasing the zirconia content to 6·4 and 22·1 weight % resulted in gels that were amorphous at temperatures up to 900°C. Further treatment at 1100°C resulted in diffraction patterns arising from tetragonal zirconia and some cristobalite. Similar results were obtained by Miranda Salvado[1] who concluded that hydrolysis in a strong acid medium favoured the segregation of zirconia and lowering the amount of acid stabilized the crystalline zirconia formed. Hence, the greater the amount of acid used for the hydrolysis reaction the greater the extent of crystal growth observed on heating. Since zirconia is more soluble than silica, the stability of silica against nucleation is reduced and the separation of zirconia allows the phase separation of cristobalite by nucleation processes. These nucleation processes are typically the diffusion of particles either through the lattice, over the surface or along the boundary. Therefore heating a gel results in competition between sintering and nucleation processes. In titania containing gels prepared under the same conditions no segregation of titania occurred in strong acid media. On heating to 1100°C titania gels remained amorphous implying that on heating no phase separation or nucleation occurred and the main process involved in densification was sintering.

Reflectance NIR spectroscopic studies of these gels indicate that both decreasing the amount of acid used in the hydrolysis reaction and increasing the amount of zirconia in the sample resulted in higher relative levels of hydrogen bonded silanol species. On hydration, the increased levels of zirconia resulted in no observable free silanol groups on the surface.

Increasing the treatment temperature of the sample to 900°C has been shown by both mid- and near-infrared spectroscopy results in a progressive decrease in the intensity of peaks due to Si-OH. In the mid-infrared the relative intensity of the peak at *ca* 960cm^{-1} due to SiOH, decreases as the treatment temperature is increased up to 900°C which is consistent with the removal of SiOH/ZrOH from the surface. In sharp contrast to the results obtained for silica/titania gels, further increasing the temperature to 1100°C has no effect on the intensity of the peak. The relative intensity of the band at *ca* 550cm^{-1} increased as the treatment was raised above 700°C. This band has been assigned to Zr-O vibrations in tetragonal zirconia and is consistent with phase separation occurring at these temperatures. These results imply that no new Si-O-Zr bonds are formed at elevated temperatures.

6.9 References

1 J.M. Miranda Salvado, C.J. Serna and J.M. Fernandez Navarro, *J. Non Crystalline Solids* **100** (1988) 330-338

2 A. Duran, C. Serna, V. Fornes and J.M. Fernandez-Navarro, *J. Non Crystalline Solids* **82**(1986) 69-77

3 M. Decottognies, J. Phalippou and J. Zarzycki. *J. Mat. Sci.* **13**(1978) 2605-2618

4 A. Bertoluzza, C. Fagnano, M.A. Morelli, V. Gottardi and M. Guglielmi, *J. Non Crystalline Solids* **48** (1982) 117-128

5 S.K. Saha and P. Pramanik, *J. Non Crystalline Solids* **159** (1993) 31-37

6 S.W. Lee and R.A. Condrate Sr., *J. Mat. Sci.* **23** (1988) 2951-2959

7 K. Buijs and G.R. Choppin, *J. Chem. Phys.* **39** (1963) 2035-2041; 2042-2050

8 C.C. Perry and X. Li, *J. Chem. Soc. Faraday Trans.* **87**(5) (1991) 761-766

9 J.H. Anderson and K.A. Wickersheim, *Surface Sci.* **2** (1964) 252-260

10 C.C. Perry and X. Li, *J. Chem. Soc. Faraday Trans.* **87**(24) (1991) 3857-3862

11 E. Lippmaa, M. Mägi, A. Samosan, G. Engelhardt and A -R. Grimmer, *J. Am. Chem. Soc.* **102** (1980) 4889-4893

12 D.W. Sindorf and G. Maciel, *J. Am. Chem. Soc.* **105** (1983) 1487-1493

13 A -R. Grimmer, H. Rosenberger, H. Bürger and W. Vogel, *J. Non Crystalline Solids* **99** (1988) 371-378

14 D.L. Wood, E.M. Rabinovich, D.W. Johnson Jr, J.B. MacChesney and E.M. Vogel, *J. Am. Ceram. Soc.* **66** (1983) 693-699

15 H. Yametra, B. Fitzpatrick and G. Gordon, *J. Mol. Spec.* **14**(1964) 268-278

16 G.R. Choppin and H.R. Violante, *J. Chem. Phys.* **56**(1972) 5890-5898

17 G.R. Choppin and J.R. Downey, *J. Chem. Phys.* **56**(1972) 5899-5903

18 C.C. Perry and X. Li, in *Chemical Processing of Advanced Materials* p.131, eds. L.L. Hench and J.K. West Wiley, 1992)

19 M.R. Bhambhani, P.A. Cutting, K.S.W. Sing and D.H. Turk, *J. Colloid Interface Sci.* **38** (1) (1972) 109-117

20 E.P. Barrett, L.G. Joyner and P.P. Halenda, *J. Am.Chem. Soc.* **73** (1951) 373-380

21 R.A. Beebe, J.B. Beckwith and J.M. Honig, *J. Am. Chem. Soc.* **67** (1945) 1554-1558

22 R.A. Van Nordstrand, W.E. Kreger and H.E. Ries Jr., *J. Phys. Colloid Chem.* **55** (1951) 621-638

23 J. Bastick, *Bull. Soc. Chim. Fr.* **20** (1953) 437-440

24 S.J. Teichner, G.A. Nicolaon, M.A. Vicarini and G.E.E. Gardes, *Adv. Colloid Interface Sci.* **5** (1976) 245-273

Chapter 7: Conclusions

7.1 Introduction

In this chapter, the structures of gels prepared by the acid hydrolysis of the following preparative systems:

(i) SiO_2-TiO_2 from bis(acetylacetonato) titanium diisopropoxide and TEOS

(ii) SiO_2-TiO_2 from the double alkoxide bis(acetylacetonato) titanium di(triethoxysilane) and TEOS

(iii) SiO_2-ZrO_2 from bis(acetylacetonato) zirconium dipropoxide and TEOS

are compared after heating at 120°C and then after treatment at temperatures up to 1100°C.

7.2 Samples Heated at 120°C

After treatment at 120°C samples from each of the three preparative systems investigated were amorphous by X-ray diffraction. The only exception was the sample containing TiO_2=21·9wt % which exhibited a diffraction pattern due to crystalline rutile, this suggests that there may be an upper limit to the amount of titania that may be incorporated into the silica matrix.

In the mid-infrared, the small change in dipole moment of the Ti-O and Zr-O bonds in comparison with that of the Si-O bond, results in weak bands. The mid-infrared spectra of the SiO_2-TiO_2 (both methods) and SiO_2-ZrO_2 gels arose principally from the strong vibrational bands of the silica matrix. Due to the selection rules, mid-infrared and Raman spectroscopic investigations are complementary in nature. Ideally Raman spectra should have been able to provide more information on the Ti-O and Zr-O bonds within the silica matrix. However, for these samples it was not possible to obtain detailed Raman spectra.

Reflectance NIR spectroscopic studies have revealed that for SiO_2-TiO_2 (both methods) and SiO_2-ZrO_2 gels, decreasing the amount of acid used in the hydrolysis reaction resulted in higher relative levels of hydrogen bonded SiOH species on the surface. Similarly, increasing the titania and zirconia contents of the gels also resulted in a decrease in free silanol species and an increase in hydrogen bonded SiOH species on the surface.

The effect of drying method, powder or monolith, on pore structure was investigated for gels prepared from bis(acetylacetonato) titanium diisopropoxide. Results presented in table 7.1 show that drying the samples as powders results in a decrease in the overall surface area, pore volume and micropore volume of the samples. For both powders and monoliths there is little difference between the surface areas calculated using either the BET or the α_s-methods suggesting that there are few micropores within the structure. But the greater micropore volumes obtained for monolithic samples compared to the corresponding powder samples implies that the process of powdering destroys the smaller pores within the bulk.

Table 7.1: Comparison of Pore Structures of SiO_2-TiO_2 Gels Containing TiO_2=6·34wt% dried as Powders and Monoliths at 120°C (HCl=0·045 mole)

		Powder	Monolith
BET Surface Area (m^2g^{-1})		394	618
α, Surface Area (m^2g^{-1})		372	633
BJH Pore	**Adsorption**	0·54	0·74
Volume (cm^3g^{-1})	**Desorption**	0·57	0·76
α, Micropore Volume (cm^3g^{-1})		≈0·000	0·037
BJH Average	**Adsorption**	44·6	54·4
Pore Diameter (Å)	**Desorption**	43·1	47·8

For materials prepared by the three different routes, as the amount of acid used in the hydrolysis reaction was decreased there was a decrease in overall surface area and pore volume. This was accompanied by a change in the isotherms obtained from type IV to type I, as mesoporosity was decreased and the micropore volume was increased. However, the average pore diameter of silica-zirconia gels, silica-titania powders (prepared from $Ti(acac)_2(O^iPr)_2$) and silica-titania gels prepared from the double alkoxide remained constant as the amount of acid used for the hydrolysis reaction was decreased. In the case of silica-titania monoliths, decreasing the amount of acid used for the hydrolysis reaction resulted in a decrease in the measured average pore diameter.

Increasing the amount of water (decreasing the amount of acid) generally promotes hydrolysis, however in this case the silicate ratio is reduced resulting in a decrease in both the hydrolysis and condensation rates. Such a decrease in the hydrolysis and condensation rates results in an increase in the gel time and more weakly branched gels. Since the condensation rate is low and the branching is weak, the gel structure can freely interpenetrate and shrink in response to solvent removal. This results in a decrease in surface area, pore volume and average pore diameters. For gels prepared from a large amount of acid (low water) there is an increase in branching on gelation which can be ascribed to an increase in the condensation rate. On drying, not as much shrinkage occurs since branching prevents the structures from entangling. This results in larger, more rigid pores.

From table 7.2, it can be seen that the preparation of SiO_2-TiO_2 gels using a double alkoxide precursor resulted in a decrease in the surface area, pore volume and average pore diameters compared to those prepared from bis(acetylacetonato) titanium diisopropoxide.

Table 7.2: Comparison of the Pore Structure of Monolithic Gels Prepared by Different Methods Containing *ca* 6·3-6·4 weight% of Titania or Zirconia Heated to 120°C (HCl=0·045 mole)

		$Ti(acac)_2(O^iPr)_2$	Double Alkoxide	$Zr(acac)_2(O^nPr)_2$
BET Surface Area (m^2g^{-1})		618	479	640
α, Surface Area (m^2g^{-1})		633	578	647
BJH Pore Volume (cm^3g^{-1})	**Adsorption**	0·74	0·18	0·33
	Desorption	0·76	0·15	0·52
α, Micropore Volume (cm^3g^{-1})		0·037	0·070	0·036
BJH Average Pore Diameter (Å)	**Adsorption**	54·4	22·0	26·1
	Desorption	47·8	23·7	28·9

In SiO_2-TiO_2 gels (prepared from $Ti(acac)_2(O^iPr)_2$), the formation of Si-O-Ti bonds is achieved by condensation reactions. The formation of these bonds as well as Si-O-Si bonds causes the gel matrix to shrink. However, the formation of Si-O-Si bonds is preferential to that of Si-O-Ti bonds and it is likely that the latter form after gelation, resulting in less shrinkage of the gel. Similarly, the use of large amounts of acid in the hydrolysis reaction results in an increase in branching on gelation. This prevents large amounts of shrinkage and results in larger more rigid pores.

For gels prepared from the double alkoxide precursor, the Si-O-Ti bonds are already present in the precursor. Hence the condensation reactions occurring in solution are predominantly due to Si-O-Si bond formation. After gelation the consolidation of the gel network results in a large amount of shrinkage as liquid is expelled from the pores rather than *via* the fomation of Si-O-Ti bonds as in SiO_2-TiO_2 gels (prepared from $Ti(acac)_2(O^iPr)_2$). On comparison, there is little difference between the pore volume and average pore diameters of the SiO_2-TiO_2 gels (double alkoxide) compared to silica gels prepared under the same conditions, see table 7.3. This can be explained by the similarity in reactions occurring in solution and on gelation of silica and gels prepared from the double alkoxide.

On comparison, the pore volume and average pore diameters of SiO_2-ZrO_2 gels are approximately equal to those of a silica gel prepared under the same conditions, see table 7.3. In SiO_2-ZrO_2 gels prepared using a large amount of acid for the hydrolysis reaction phase separation of zirconia within the silica matrix occurs. Hence the resulting gel contains regions of zirconia surrounded by silica. The lower surface area of SiO_2-ZrO_2 gels compared

to silica gels can be explained by regions of low porosity zirconia surrounded by higher porosity silica.

Table 7.3: Pore Structure of a Monolithic Silica Gel Heated to 120°C (HCl=0·045 mole)

		SiO_2
BET Surface Area (m^2g^{-1})		812
α_s Surface Area (m^2g^{-1})		845
BJH Pore	**Adsorption**	0·33
Volume (cm^3g^{-1})	**Desorption**	0·47
α_s Micropore Volume (cm^3g^{-1})		0·041
BJH Average	**Adsorption**	25·1
Pore Diameter (Å)	**Desorption**	25·3

7.3 The Effect of Thermal Treatment on the Resulting Gel Structure

On heating SiO_2-TiO_2 (both methods) and SiO_2-ZrO_2 gels to temperatures greater than 900°C there is a strengthening of the gel matrix by the shortening of Si-O bonds *via* the condensation reactions described previously. This is evidenced by the shifting of the mid-infrared band at *ca* 1100cm^{-1} (ascribed to antisymmetric Si-O-Si stretching vibrations) to a higher wavenumber. For SiO_2-TiO_2 gels (both methods), heating to temperatures greater than 900°C resulted in the formation of Si-O-Ti bonds and the incorporation of titanium atoms into the silica framework. This is shown as an increase in intensity of the band at *ca* 960cm^{-1} assigned as stretching vibrations of SiOH/TiOH and
ν_{as}(Si-O-Ti). Increasing the temperature of SiO_2-ZrO_2 gels to 1100°C results in the further segregation of zirconia from the silica matrix. Since increasing the treatment temperature to 1100°C has no effect on the intensity of the band at *ca* 960cm^{-1} relative to the band at *ca* 1100cm^{-1}, there can be no Si-O-Zr bond formation. However, the relative intensity of the band at *ca* 800cm^{-1} increased due to the formation of new Si-O-Si bonds as a result of phase separation and the separation of crystalline zirconia.

Reflectance NIR spectroscopic studies have revealed that increasing the treatment temperature of SiO_2-TiO_2 (both methods) and SiO_2-ZrO_2 gels to 900°C, results in a progressive decrease in the number of free and hydrogen bonded SiOH groups. This is only significant at temperatures greater than 700°C where dehydroxylation processes are more significant. On increasing the treatment temperature of the SiO_2-TiO_2 (prepared from $Ti(acac)_2(O^iPr)_2$) and SiO_2-ZrO_2 gels a progressive decrease in the number of SiOH groups was observed until at 1100°C no SiOH groups were observed by NIR spectroscopy. In contrast, the complete removal of SiOH groups from the surface of SiO_2-TiO_2 (double alkoxide) gels was achieved at 900°C.

The removal of SiOH groups from the surface of SiO_2-TiO_2 (double alkoxide) gels occurs at a temperature *ca* 200°C lower than for SiO_2-TiO_2 (prepared from $Ti(acac)_2(O^iPr)_2$) and SiO_2-ZrO_2 gels. On heating, the SiO_2-TiO_2 (double alkoxide) gel shrinks as pores within the gel are destroyed; this occurs by two processes condensation reactions and viscous sintering. Since Si-O-Ti bonds are already present in the structure few condensation reactions can occur on heating suggesting that shrinkage must occur due to sintering. The more compact structure of SiO_2-TiO_2 (double alkoxide) gels compared to SiO_2-TiO_2 (prepared from $Ti(acac)_2(O^iPr)_2$) and SiO_2-ZrO_2 gels has been discussed in section 7.2. The combination of a more compact structure, low pore volume and preferential sintering result in densification at lower temperatures.

At temperatures greater than 700°C, SiO_2-TiO_2 (prepared from $Ti(acac)_2(O^iPr)_2$) powders exhibited X-ray diffraction patterns due to both anatase and rutile, although the former was the predominant phase. On heating to 1100°C, monolithic SiO_2-TiO_2 (prepared from $Ti(acac)_2(O^iPr)_2$) gels remained amorphous implying that drying as powders results in phase separation. On heating any gel, alkoxy and hydroxy groups are removed by condensation reactions which result in weight loss. In a monolith, these reactions produce new cross-links and stiffen the structure. Further heating results in densification *via* viscous flow and structural relaxation, as no crystallinity was detected by X-ray diffraction.

When gels are broken up into pieces after gelation and subsequently to powders before being completely dried, some of the cross-links formed at the gel point are broken which may result in ester bonds being reformed. Drying in this manner probably results in the formation of regions of inhomogeneity which exist within a non-crystalline polymeric matrix containing chemically bound organics. On heating a powder, some of the alkoxy groups are removed by condensation and form new cross-links within the bulk and some form cross-links with the regions of inhomogeneity.

Monolithic SiO_2-TiO_2 (double alkoxide) gels remained amorphous by X-ray diffraction after heating to 900°C. Increasing the temperature to 1100°C resulted in the detection of some crystalline anatase. However, monolithic SiO_2-TiO_2 (prepared from $Ti(acac)_2(O^iPr)_2$) gels remained amorphous on heating to 1100°C. The more compact structure of SiO_2-TiO_2 (double alkoxide) gels results in preferential sintering and densification at a lower temperature, 900°C. Once densification has occurred the diffusion of particles through the network either through the lattice, over the surface or along a boundary results in nucleation. Nucleation causes particle growth *via* the growth of necks between particles and the formation of regions of crystalline anatase.

For zirconia contents of 4·1 and 4·9 wt%, SiO_2-ZrO_2 gels were found to be amorphous by X-ray diffraction after heating at 1100°C. Increasing the zirconia content to 6·4 and 22·1 wt% resulted in gels that were amorphous up to 900°C. Further treatment to 1100°C resulted in diffraction patterns arising from tetragonal zirconia and cristobalite. Increasing

the amount of acid used for the hydrolysis reaction resulted in the increased segregation of zirconia compared to lower acid levels where the crystalline zirconia formed is stabilised. Therefore, the greater the amount of acid used for the hydrolysis reaction the greater the extent of crystal growth observed on heating. The greater solubility of zirconia compared to silica reduces the stability of silica against nucleation. Heating a gel results in competition between sintering and nucleation processes. The phase separation of zirconia and the reduced stability of silica to nucleation results in the formation of cristobalite by the nucleation processes described above.

For SiO_2-TiO_2 (both methods) and SiO_2-ZrO_2 gels (see tables 7.4 to 7.6), increasing the treatment temperature results in a progressive decrease in both surface area and pore volume. In the case of SiO_2-TiO_2 (prepared from $Ti(acac)_2(O^iPr)_2$) and SiO_2-ZrO_2 gels, the shape of the hysteresis loops implied that the pores were slit shaped. The results of the BJH analyses suggested that the average pore diameter remained constant at temperatures up to 900°C. However, heating to temperatures greater than 900°C resulted in an increase in the average pore diameter. For SiO_2-TiO_2 (double alkoxide) gels, the experimental data suggests that the pores were cylindrical and the average pore diameter remained constant up to 700°C and increased on heating to 900°C. Such increases in average pore diameter have been attributed to the remaining pores collapsing and subsequent densification of the gels.

Table 7.4: Effect of Temperature on the Pore Structure of a SiO_2-TiO_2 (double alkoxide) Gel Nominally containing TiO_2=6·34wt% (HCl=0·045 mole)

		120°C	700°C	900°C
BET Surface Area (m^2g^{-1})		479	304	3
α, Surface Area (m^2g^{-1})		578	345	3
BJH Pore	**Adsorption**	0·18	0·066	0·005
Volume (cm^3g^{-1})	**Desorption**	0·15	0·099	0·005
α, Micropore Volume (cm^3g^{-1})		0·070	0·034	≈0·000
BJH Average	**Adsorption**	22·0	26·9	91·6
Pore Diameter (Å)	**Desorption**	23·7	23·3	94·8

Table 7.5: Effect of Temperature on the Pore Structure of a Monolithic SiO_2-TiO_2 (prepared from $Ti(acac)_2(O^iPr)_2$) Gel Containing TiO_2=6·34wt% (HCl=0·045 mole)

		120°C	700°C	900°C	1100°C
BET Surface Area (m^2g^{-1})		618	586	278	9
α, Surface Area (m^2g^{-1})		633	587	270	8
BJH Pore	**Adsorption**	0·74	0·25	0·12	0·01
Volume (cm^3g^{-1})	**Desorption**	0·76	0·21	0·09	0·01
α, Micropore Volume (cm^3g^{-1})		0·037	0·010	≈0·000	≈0·000
BJH Average	**Adsorption**	54·4	23·0	21·0	
Pore Diameter (Å)	**Desorption**	47·8	32·1	19·6	

Table 7.6: Effect of Temperature on the Pore Structure of a Monolithic SiO_2-ZrO_2 Gel Containing ZrO_2=6·4wt% (HCl=0·045 mole)

		120°C	700°C	900°C	1100°C
BET Surface Area (m^2g^{-1})		640	550	304	2
α, Surface Area (m^2g^{-1})		647	532	291	2
BJH Pore	**Adsorption**	0·33	0·30	0·17	0·002
Volume (cm^3g^{-1})	**Desorption**	0·52	0·44	0·24	0·002
α, Micropore Volume (cm^3g^{-1})		0·036	0·013	≈0·000	≈0·000
BJH Average	**Adsorption**	26·1	25·1	25·8	129·6
Pore Diameter (Å)	**Desorption**	28·9	26·0	26·0	67·8

On heating SiO_2-TiO_2 (both methods) and SiO_2-ZrO_2 gels were found to decrease in surface area as the treatment temperature was increased. The most significant decrease was between 700 and 900°C. Increasing the treatment temperature of the SiO_2-TiO_2 (prepared from $Ti(acac)_2(O^iPr)_2$) and SiO_2-ZrO_2 gels to 1100°C resulted in the complete densification of the gels. However at 900°C, gas adsorption data indicates that SiO_2-TiO_2 (double alkoxide) gels are completely dense. This has been attributed to a more compact gel structure undergoing viscous sintering at a lower temperature as discussed earlier in this section.

7.4 Summary

Drying SiO_2-TiO_2 (prepared from $Ti(acac)_2(O^iPr)_2$) gels as powders destroys smaller pores within the bulk as evidenced by the absence of a micropore volume. Breaking the gel down into a powder during drying leads to phase separation during thermal treatment. In contrast,

SiO_2-TiO_2 (prepared from $Ti(acac)_2(O^iPr)_2$) monoliths contain some micropore structure and are resistant to phase separation on heating.

For SiO_2-TiO_2 (double alkoxide) gels the increased branching of the precursor and the presence of Si-O-Ti bonds in solution resulted in a more compact structure. This structure resulted in densification at temperatures *ca* 200°C lower than for the other systems studied.

The SiO_2-ZrO_2 gels have a pore structure similar to that of SiO_2 gels prepared under the same conditions. This has been attributed to the instability of zirconia in acid which leads to the segregation and growth of regions of zirconia within the gel. The segregation of zirconia also decreases the stability of silica towards nucleation resulting in the formation of cristobalite at 1100°C.

7.5 Suggestions for Further Work

Due to the lack of sensitivity of X-ray diffraction to the formation of small regions of inhomogeneity transmission electron microscopy could prove to be a useful tool in determining structural evolution and phase separation. This should provide information on the effect of gel structure of precursors, temperature and the amount of acid used for the hydrolysis reaction. In the case of SiO_2-TiO_2 powders and SiO_2-ZrO_2 gels the phase separation observed by X-ray diffraction on heating should be detectable from the outset in the TEM. It should be possible to follow the growth and eventual crystallisation of such regions and draw more conclusions about the processes involved.

The presence of residual toluene in the double alkoxide may affect the structural characteristics of the resulting gels by becoming trapped within the pores and preventing the gel to shrink to its full extent. A more extensive investigation into the synthesis of $Ti(acac)_2(OSi(OEt)_3)_2$ with the aim of eliminating all toluene would be useful in determining its effect (if any) on the gel structure.

On the evidence presented within this thesis on SiO_2-TiO_2 (double alkoxide) gels the molecular structure of the double alkoxide appears to have a large effect on the eventual structure and sintering characteristics of the resulting gel. Further studies on the formation of gels from $Ti(acac)_2(OSi(OEt)_3)_2$ and from Si-O-Ti bond containing double alkoxides of different compositions should provide information on the effect of precursor structure on the ultimate structure of the resulting gel.

Appendices

For completeness, the appendices found in the following pages contain:

- X-ray diffraction patterns
- mid-infrared spectra of samples treated at different temperatures
- the effects of thermal treatment and rehydration on the near infrared spectra
- gas adsorption results

referred to but not included in the main body of this thesis.

Appendix I: Mixed SiO_2-TiO_2 Gels

X-Ray Diffraction

X-ray Diffraction Patterns Obtained for a Powder Containing TiO_2=4·1 weight % [HCl=0·045mole] Treated at: (a) 500°C; (b) 700°C; (c) 900°C; (d) 1100°C.

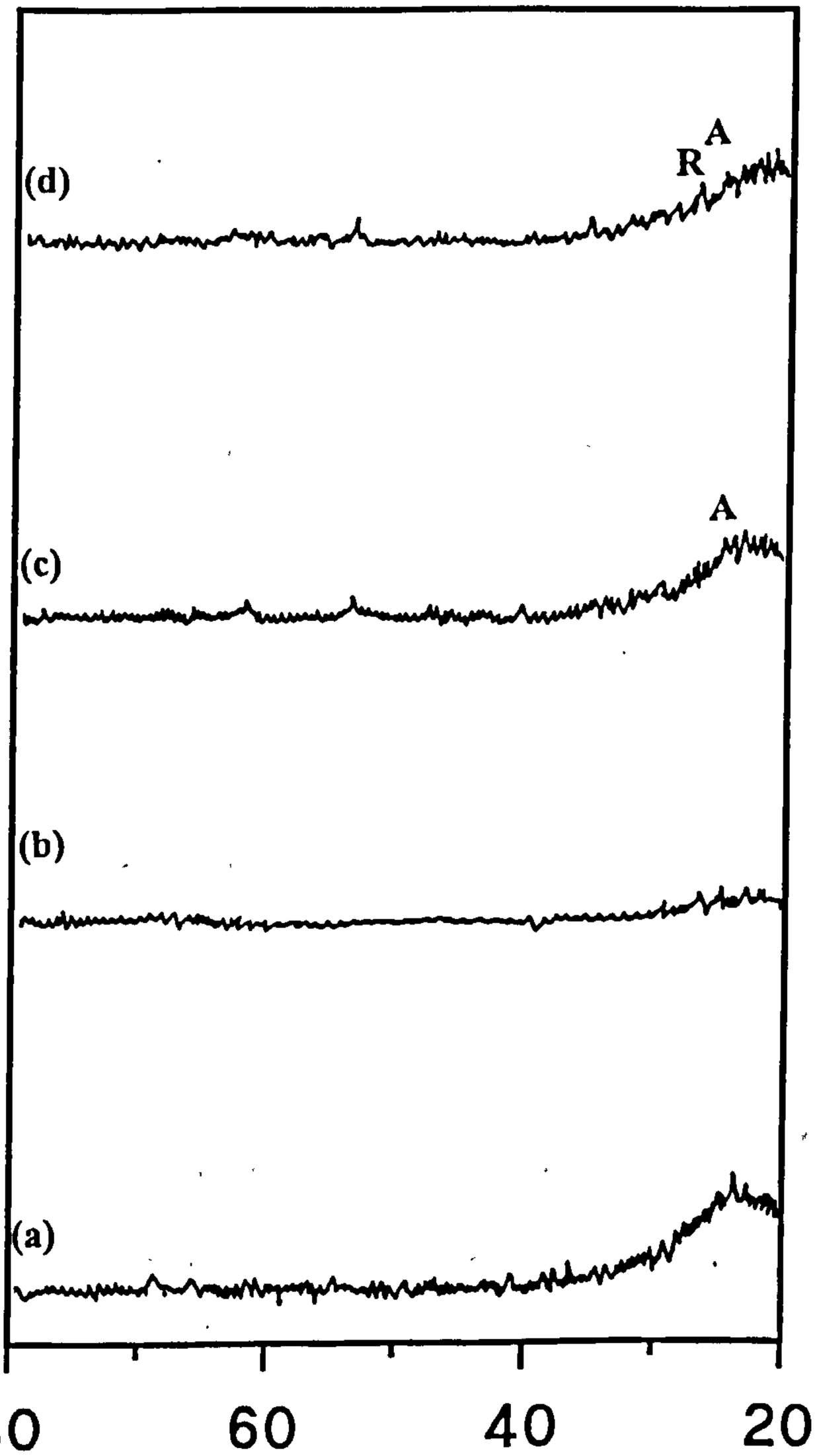

X-ray Diffraction Patterns Obtained for a Powder Containing TiO_2=4·9 weight % [HCl=0·045mole] Treated at: (a) 700°C; (b) 900°C; (c) 1100°C.

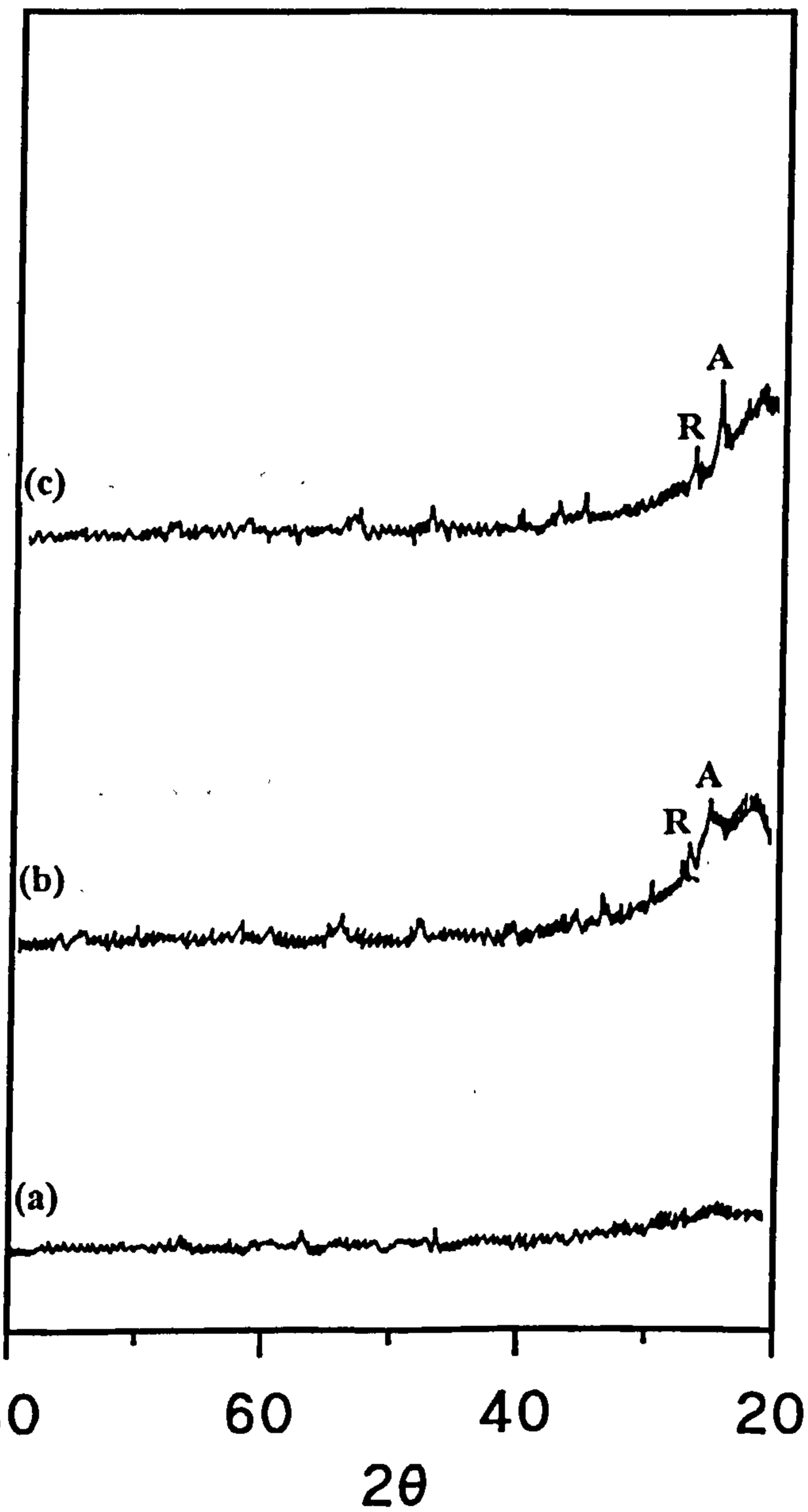

X-ray Diffraction Patterns Obtained for a Powder Containing TiO_2=6·1 weight % [HCl=0·045mole] Treated at: (a) 900°C; (b) 1100°C.

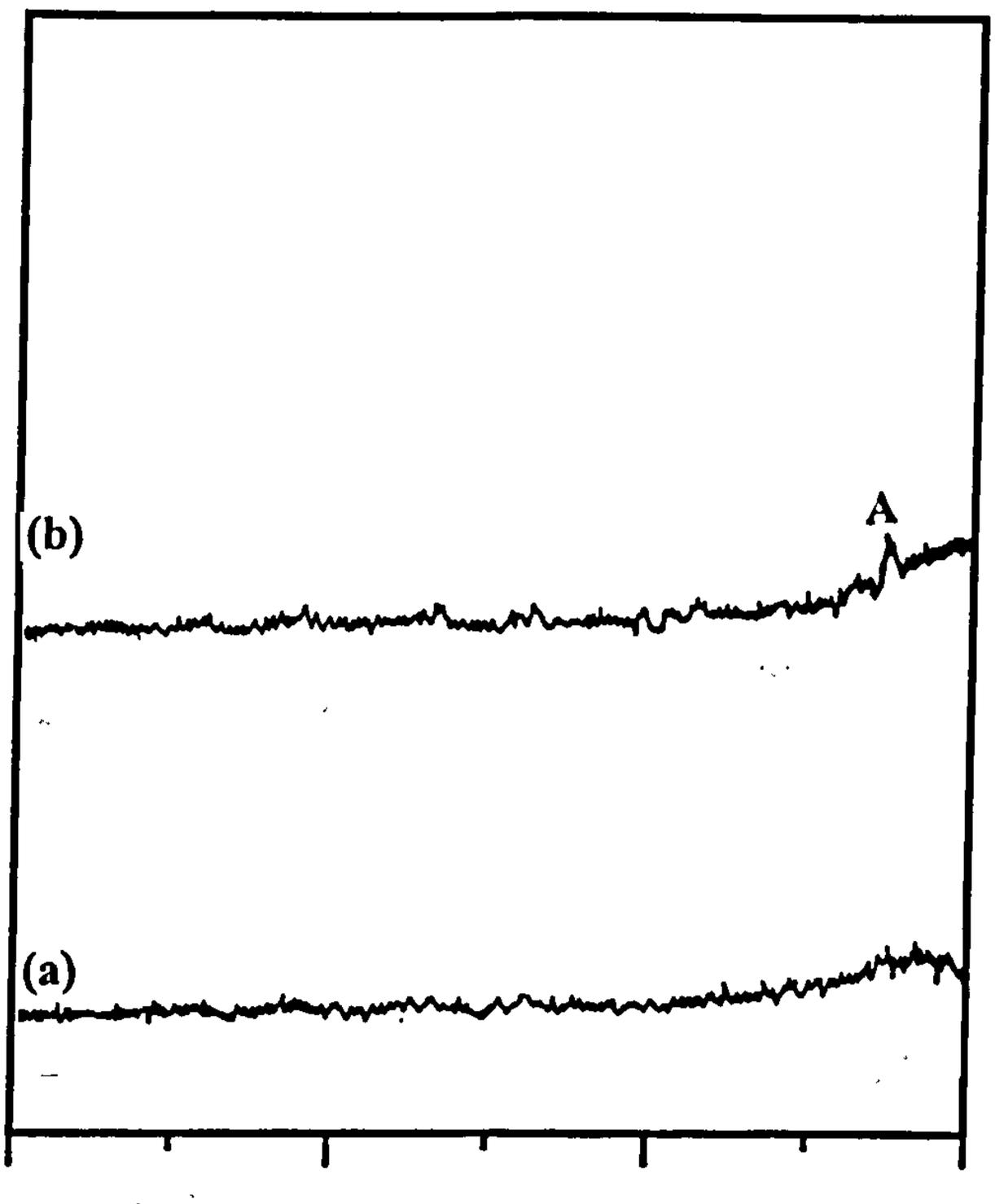

X-ray Diffraction Patterns Obtained for a Powder Containing TiO_2=21·9 weight % [HCl=0·045mole] Treated at: (a) 120°C; (b) 300°C; (c) 500°C; (d) 700°C; (e) 900°C; (f) 1100°C.

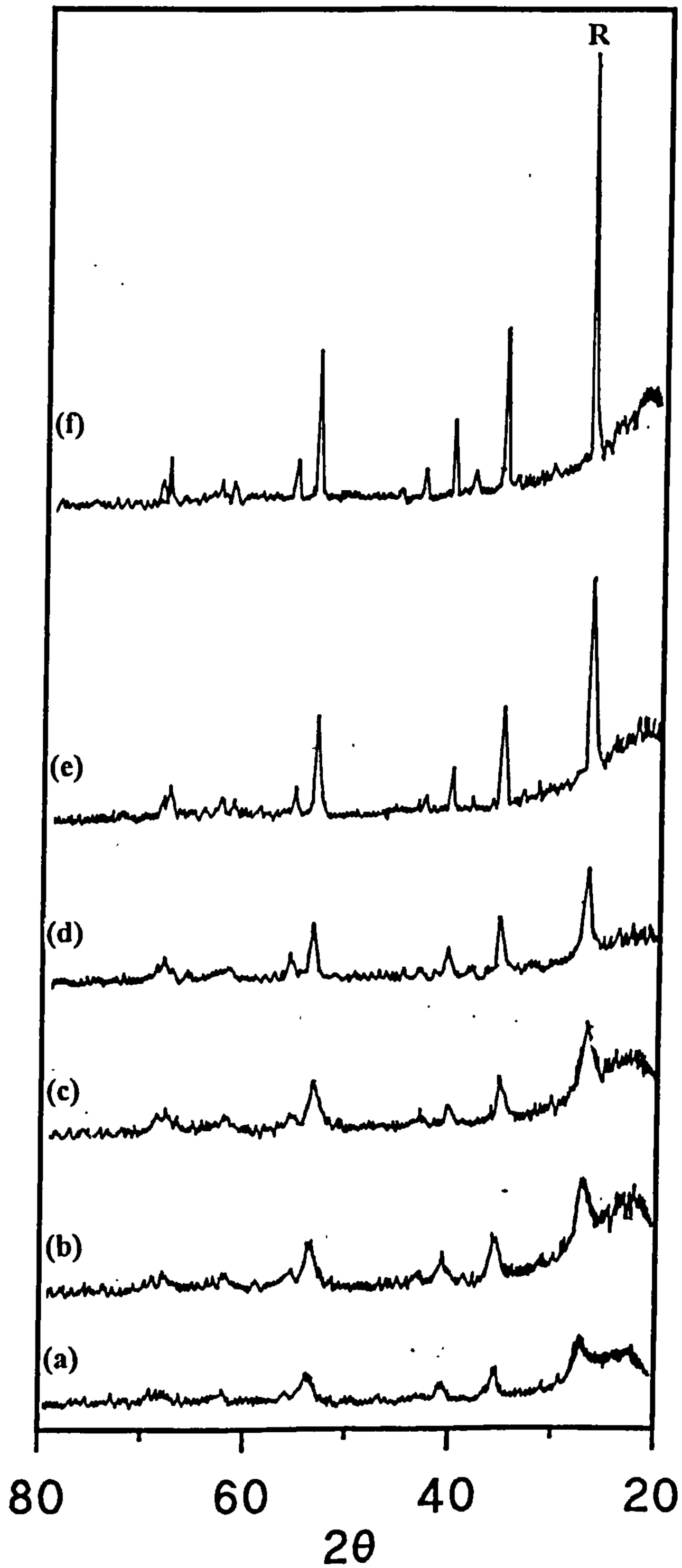

X-ray Diffraction Patterns Obtained for a Powder Containing TiO_2=6·34 weight % [HCl=0·030mole] Treated at: (a) 300°C; (b) 500°C; (c) 700°C; (d) 900°C; (e) 1100°C.

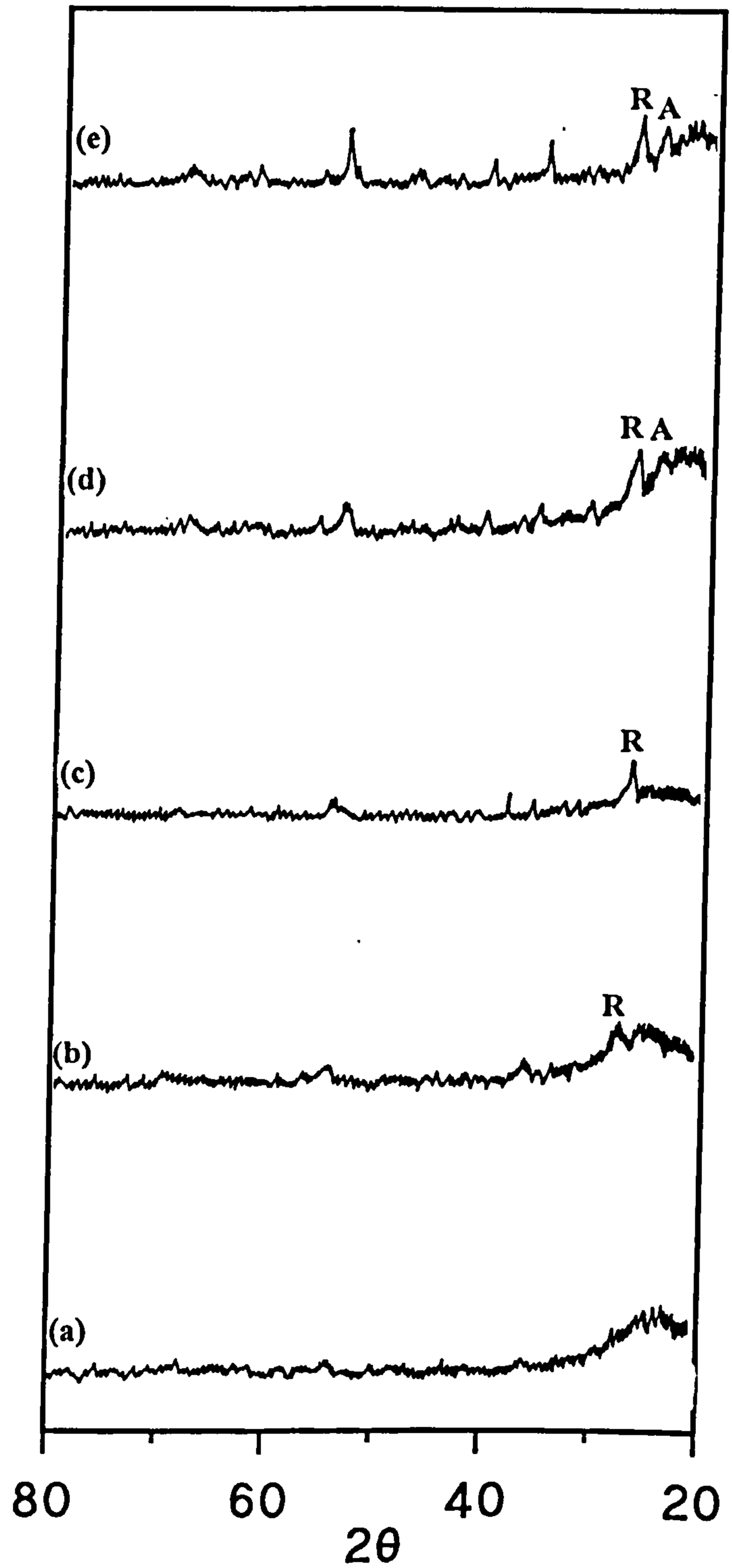

Mid-Infrared Spectra of Samples Treated at Different Temperatures

Mid-infrared Spectra of a Sample Containing 4·91 weight % Titania [HCl=0·045mole] Treated at: (a) 120°C; (b) 300°C; (c) 500°C; (d) 700°C; (e) 900°C; (f) 1100°C.

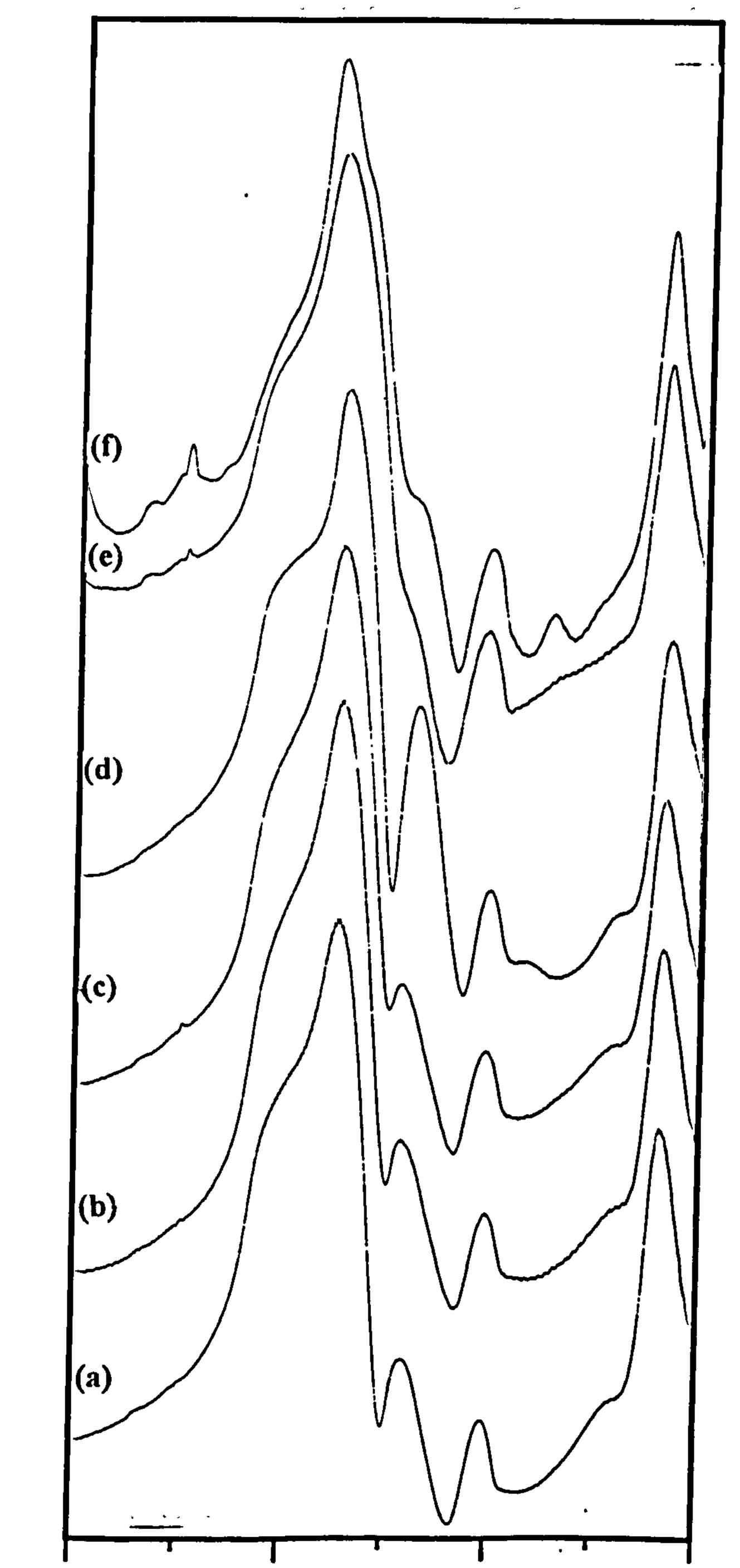

Mid-infrared Spectra of a Sample Containing 6·1 weight % Titania [HCl=0·045mole] Treated at: (a) 120°C; (b) 300°C; (c) 500°C; (d) 700°C; (e) 900°C; (f) 1100°C.

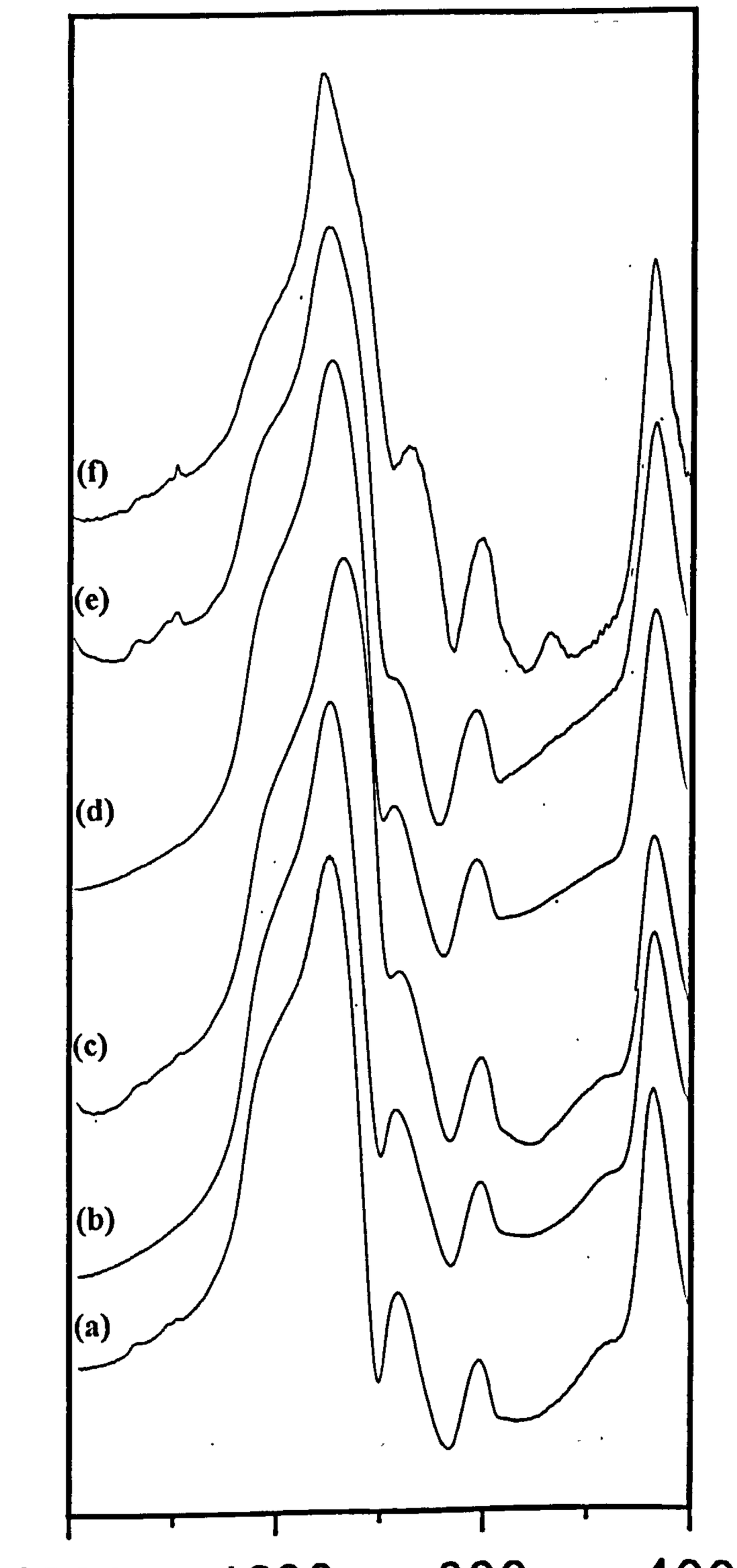

Mid-infrared Spectra of a Sample Containing 6·34 weight % Titania [HCl=0·045mole] Treated at: (a) 120°C; (b) 300°C; (c) 500°C; (d) 700°C; (e) 900°C; (f) 1100°C.

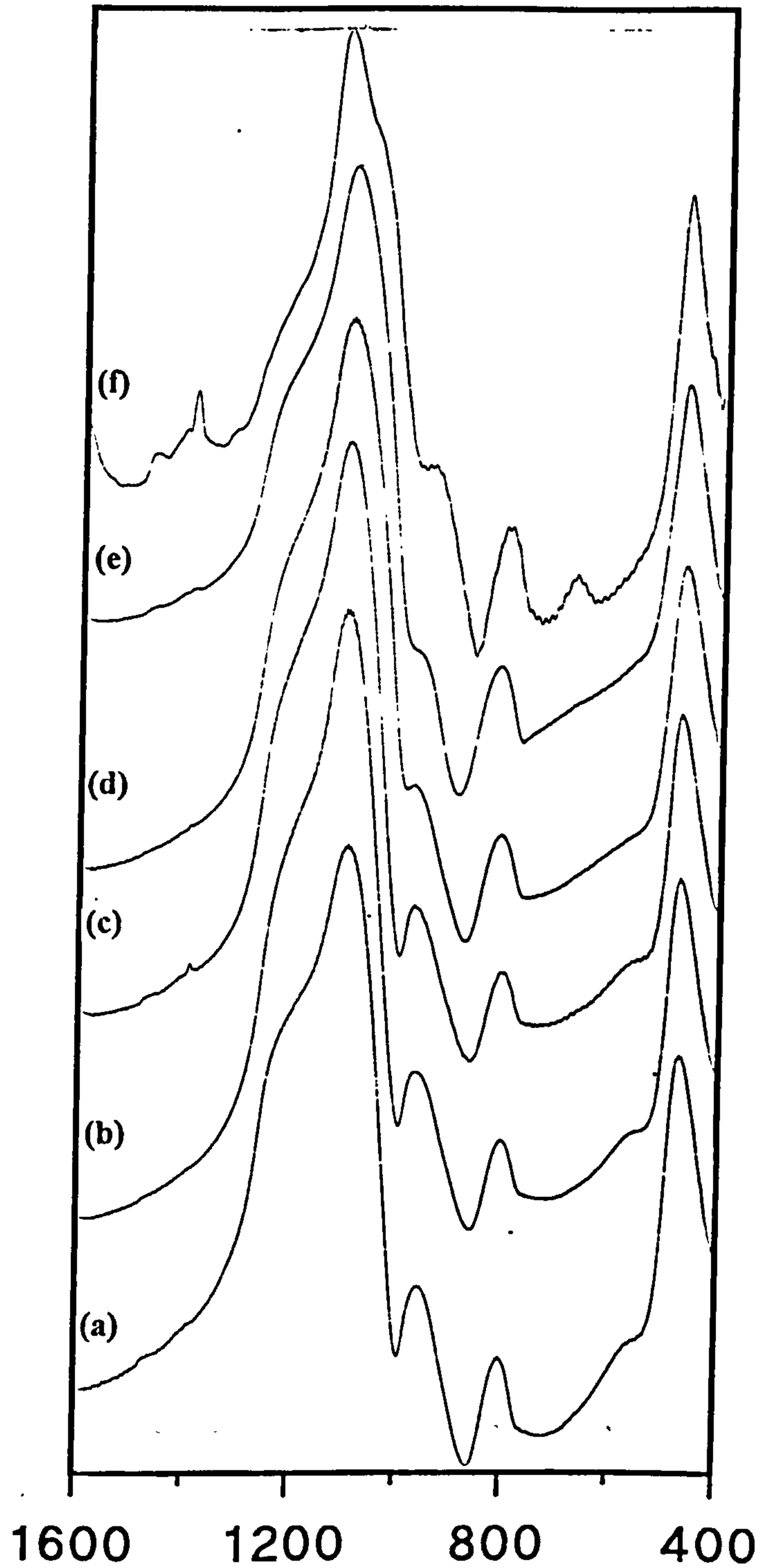

Mid-infrared Spectra of a Sample Containing 21·9 weight % Titania [HCl=0·045mole] Treated at: (a) 120°C; (b) 300°C; (c) 500°C; (d) 700°C; (e) 900°C; (f) 1100°C.

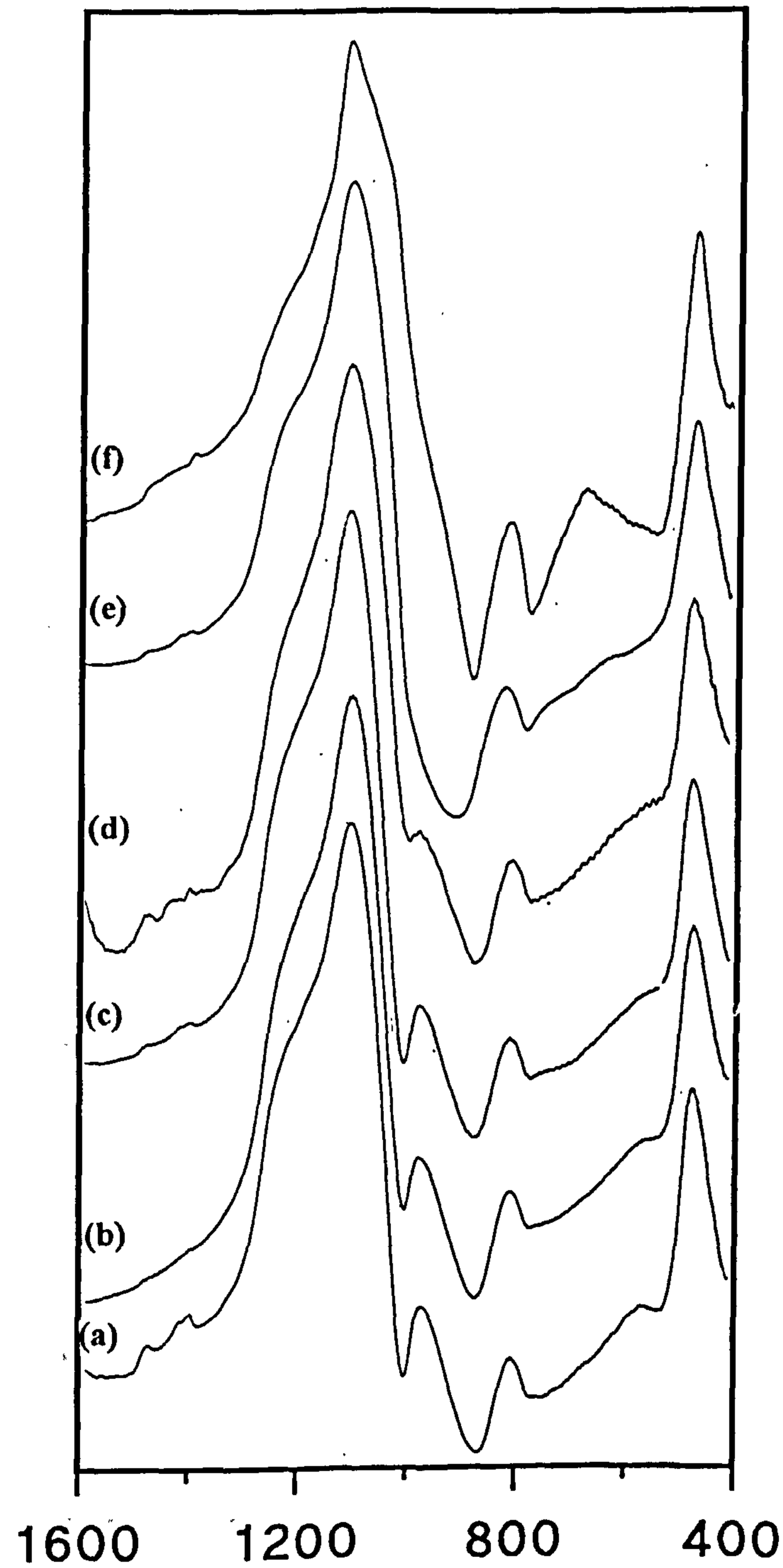

Mid-infrared Spectra of a Sample Containing 6·34 weight % Titania [HCl=0·030mole] Treated at: (a) 120°C; (b) 300°C; (c) 500°C; (d) 700°C; (e) 900°C; (f) 1100°C.

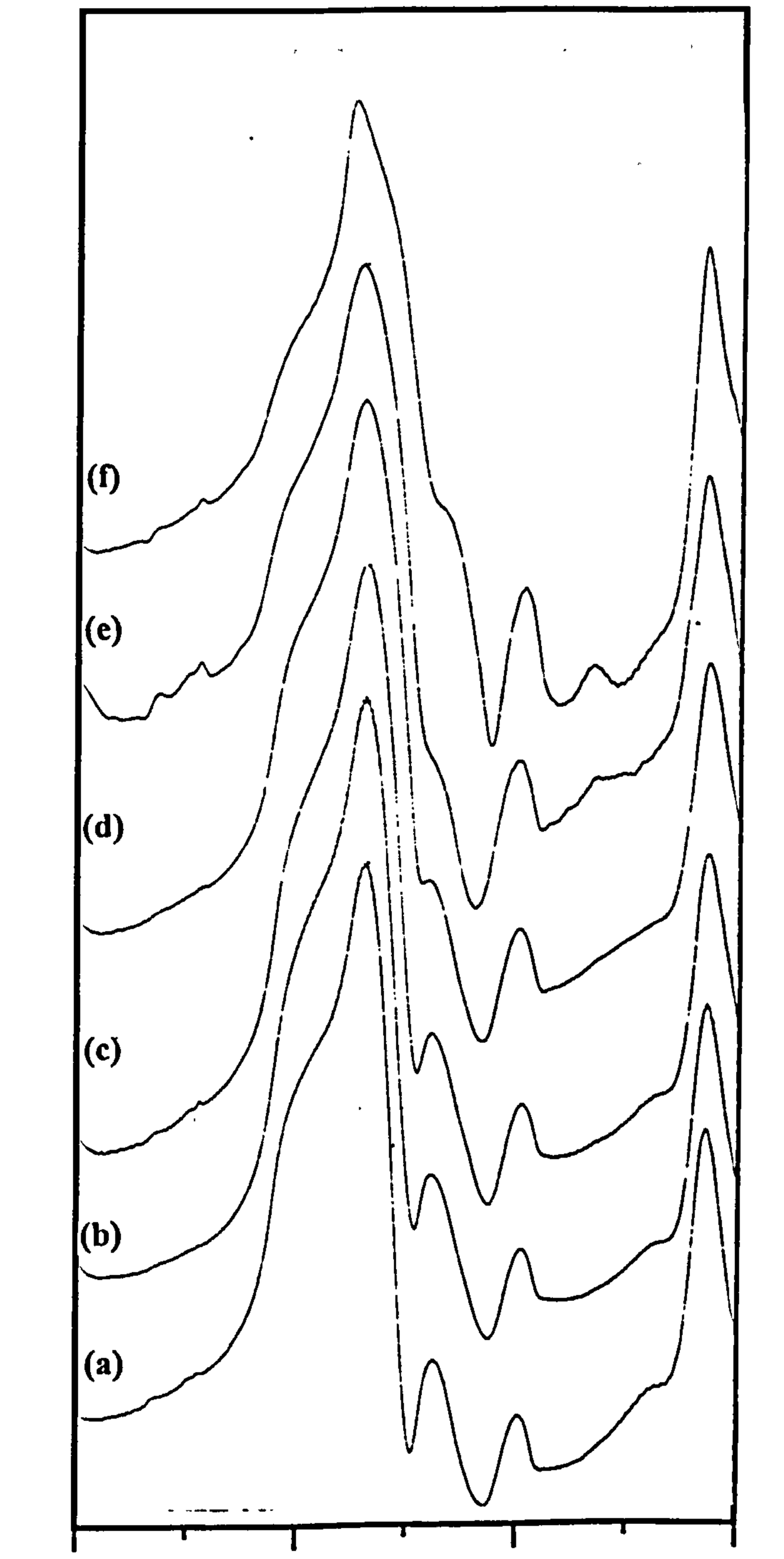

Near Infrared Spectra: Effect of Thermal Treatment

Effect of Thermal Treatment Temperature on the Near Infrared (NIR) Spectra of a Sample Containing TiO_2=4·1 weight % [HCl=0·045mole] (a) 120°C; (b) 300°C; (c) 500°C; (d) 700°C; (e) 900°C; (f) 1100°C

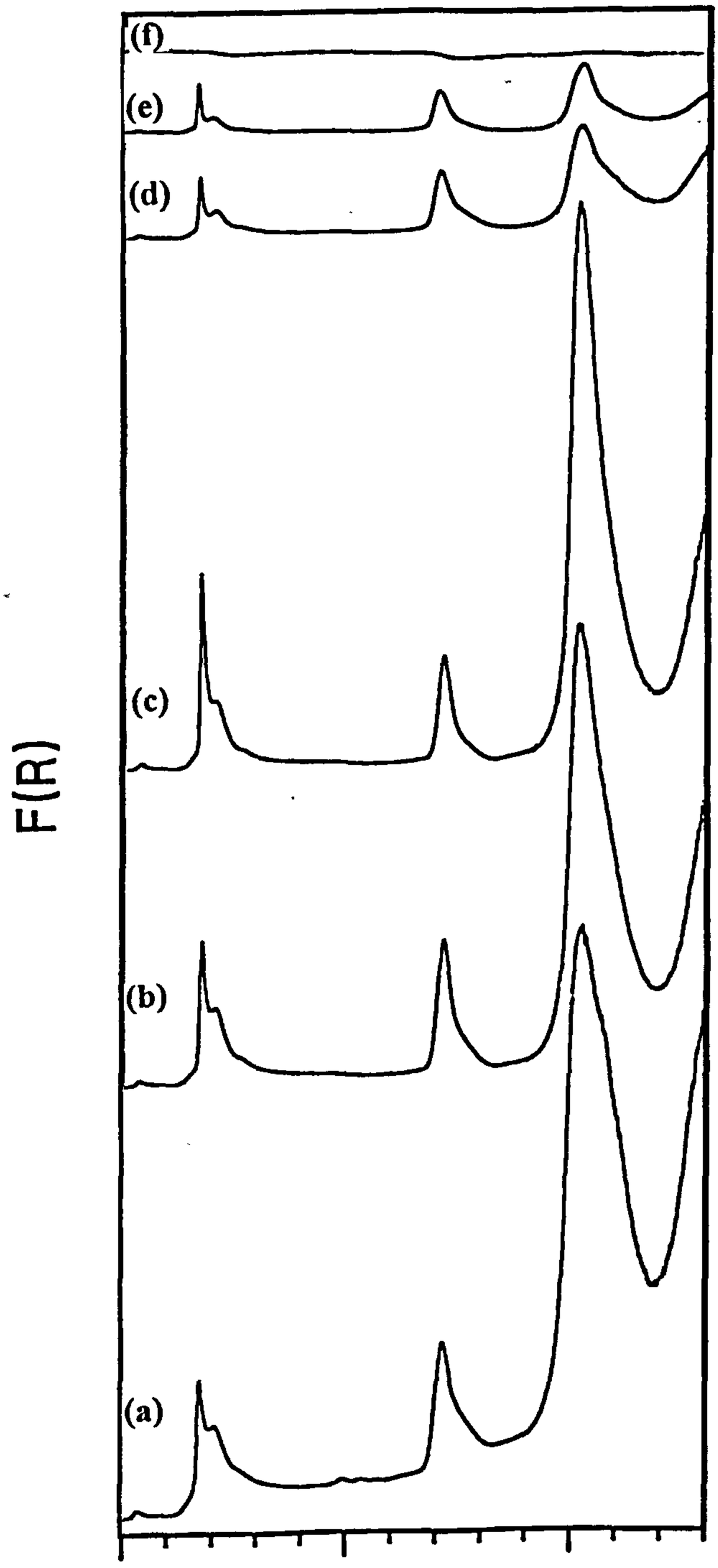

Effect of Thermal Treatment Temperature on the Near Infrared (NIR) Spectra of a Sample Containing TiO_2=4·9 weight % [HCl=0·045mole] (a) 120°C; (b) 300°C; (c) 500°C; (d) 700°C; (e) 900°C; (f) 1100°C

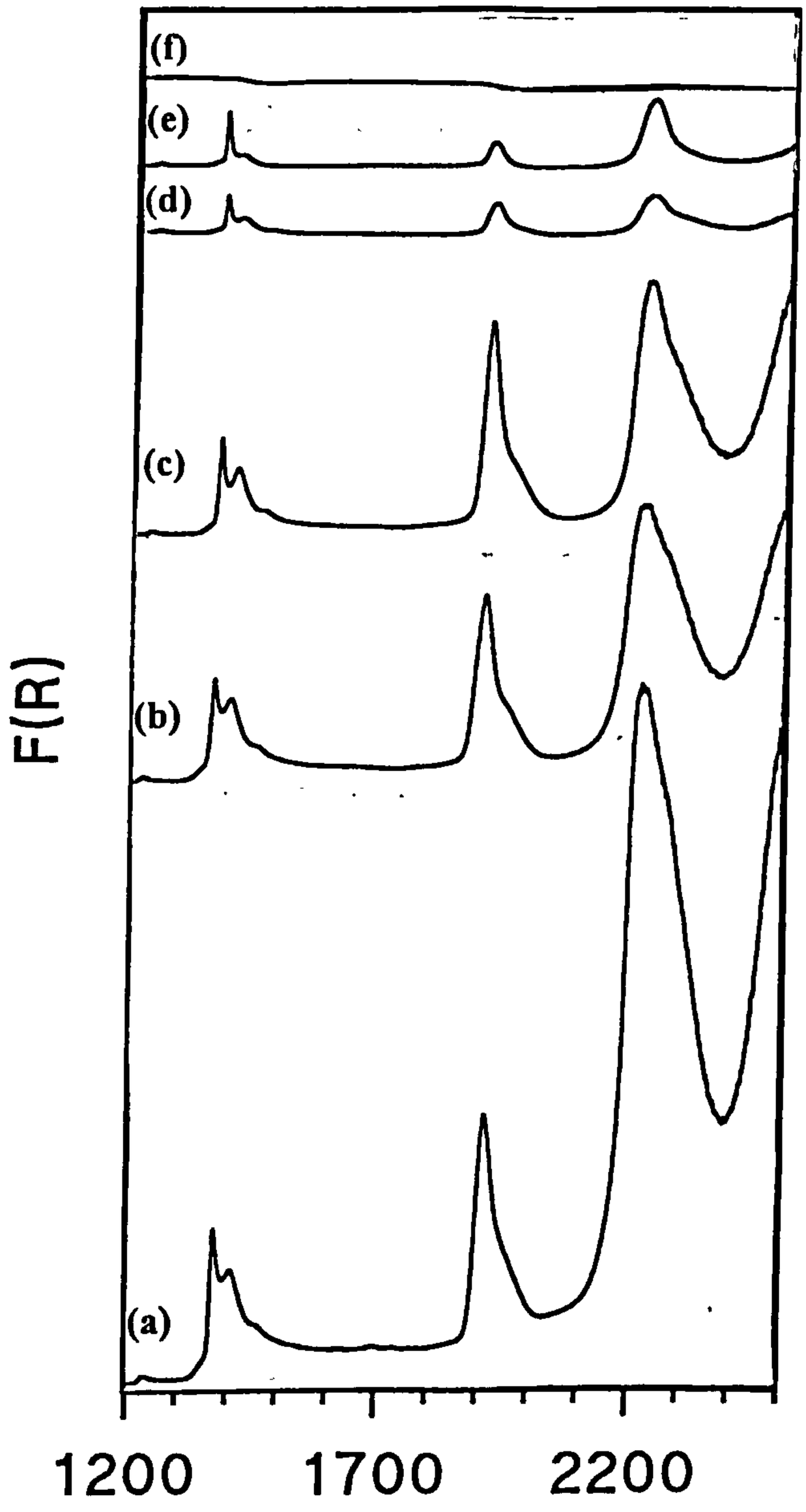

Effect of Thermal Treatment Temperature on the Near Infrared (NIR) Spectra of a Sample Containing TiO_2=6·1 weight % [HCl=0·045mole] (a) 120°C; (b) 300°C; (c) 500°C; (d) 700°C; (e) 900°C; (f) 1100°C

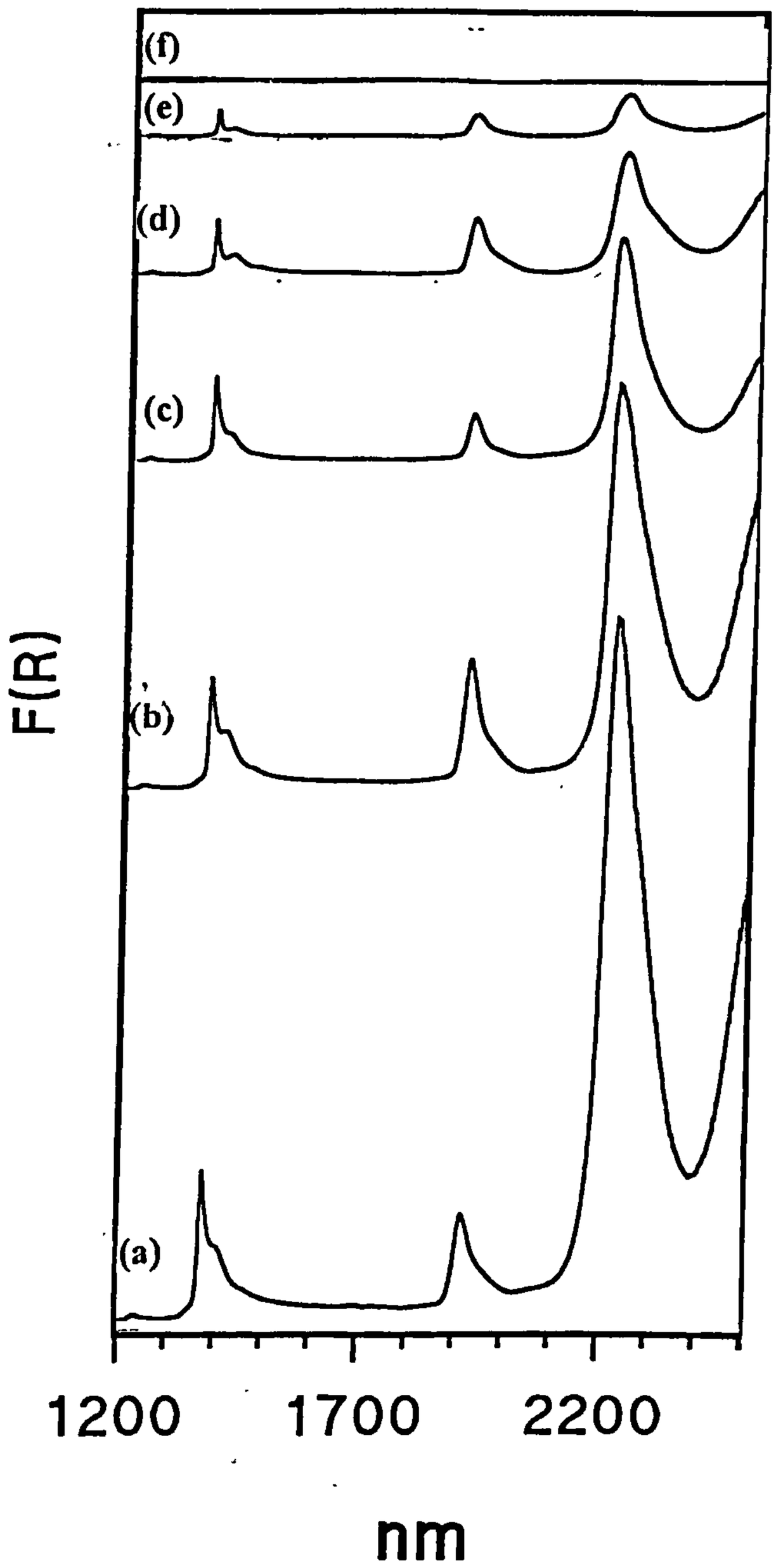

Effect of Thermal Treatment Temperature on the Near Infrared (NIR) Spectra of a Sample Containing TiO_2=21·9 weight % [HCl=0·045mole] (a) 120°C; (b) 300°C; (c) 500°C; (d) 700°C; (e) 900°C; (f) 1100°C

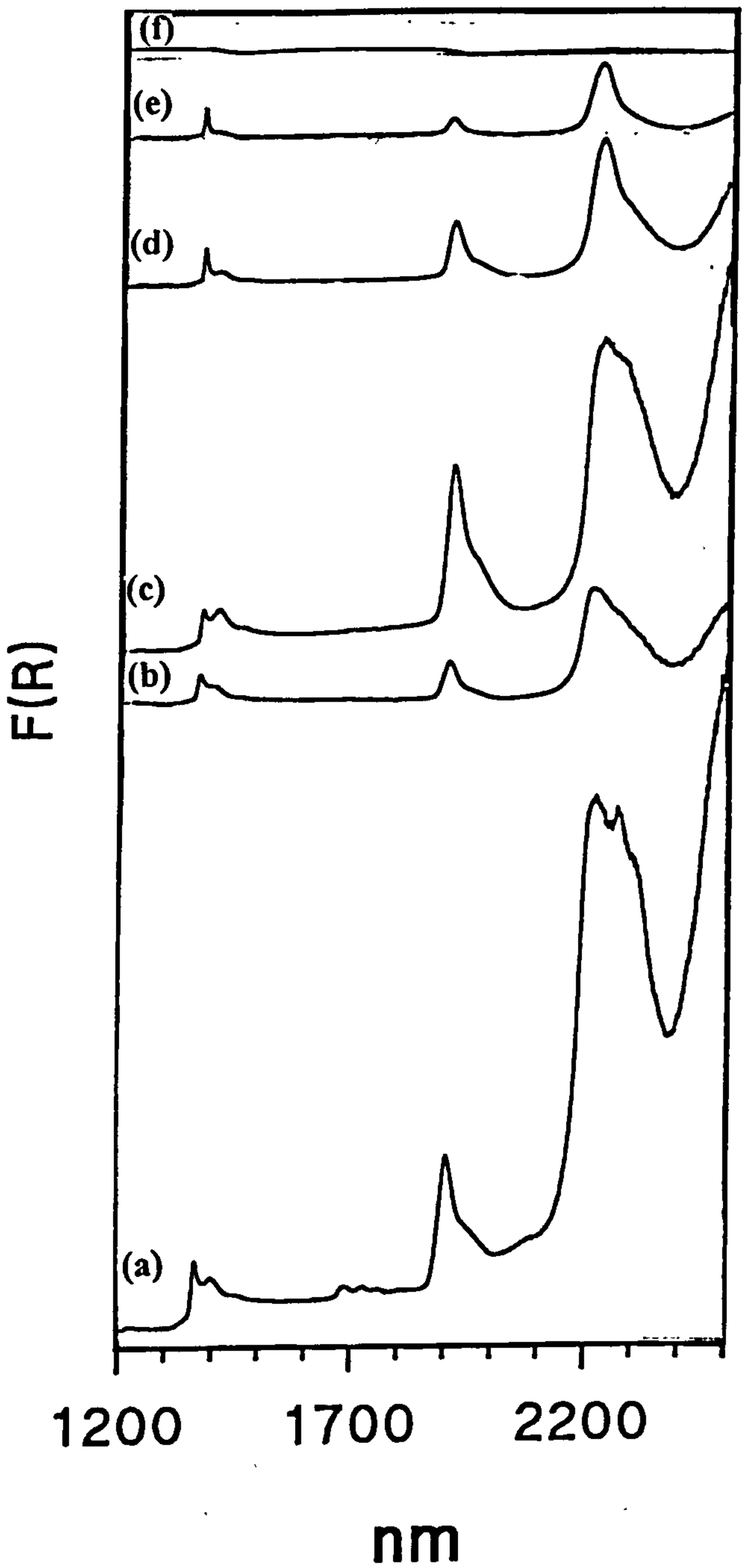

Effect of Thermal Treatment Temperature on the Near Infrared (NIR) Spectra of a Sample Containing TiO_2=6·34 weight % [HCl=0·030mole] (a) 120°C; (b) 300°C; (c) 500°C; (d) 700°C; (e) 900°C; (f) 1100°C

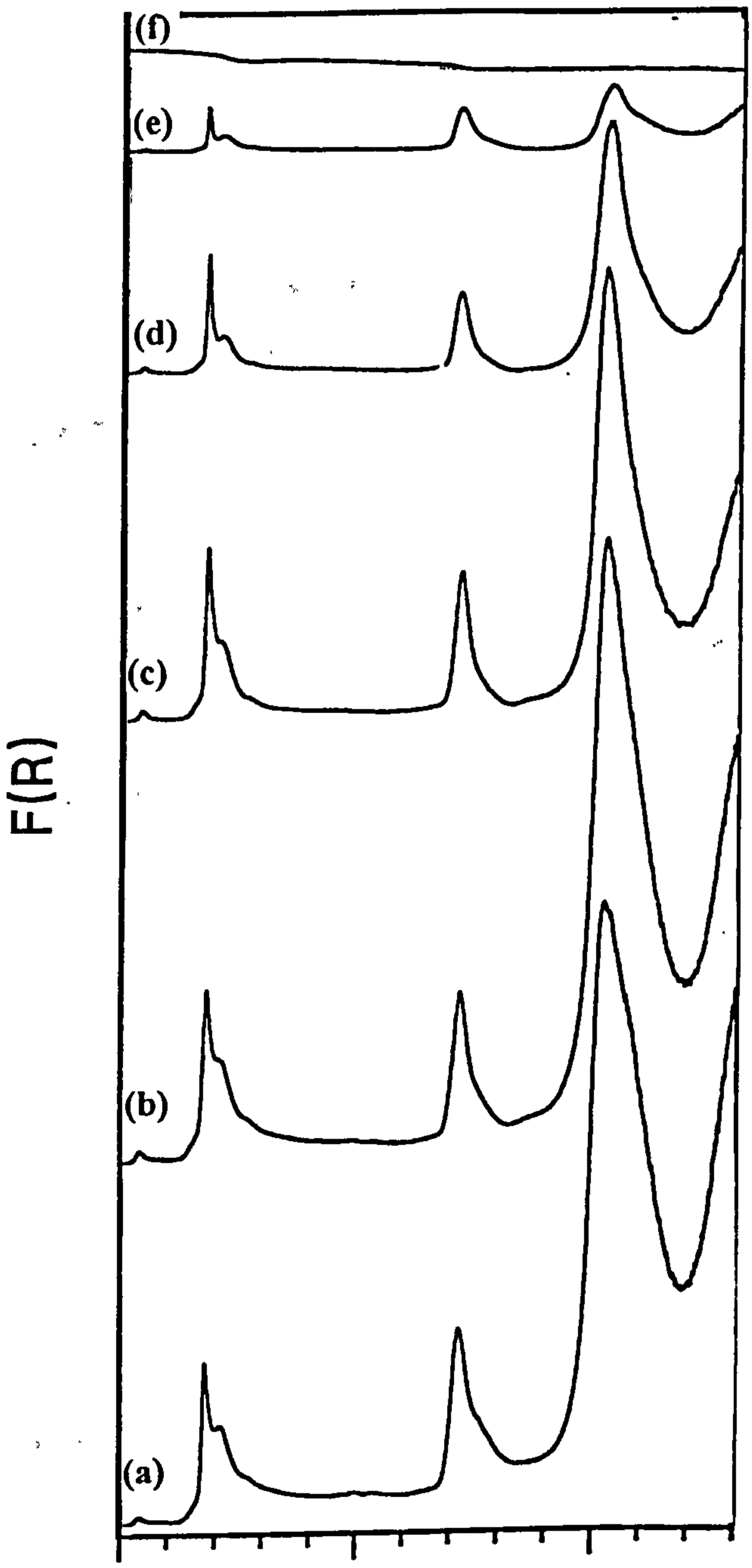

Gas Adsorption Investigation of Pore Structure

Effect of Varying the Amount of Acid used for the Hydrolysis Reaction on the Pore Characteristics of a Monolith Containing TiO_2=6·34 weight % and Heated at 120°C

HCl=0·045 mole (TiO_2=6·34 weight % ; Heated at 120°C)

(a) Adsorption/Desorption Isotherm (b) α_s-plot

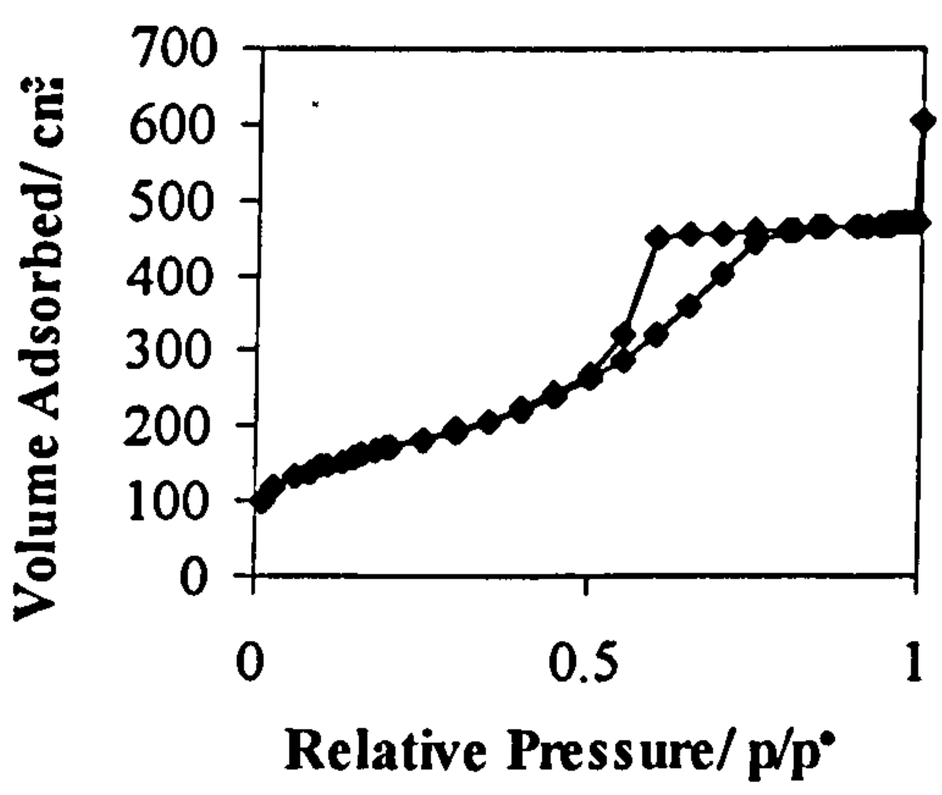

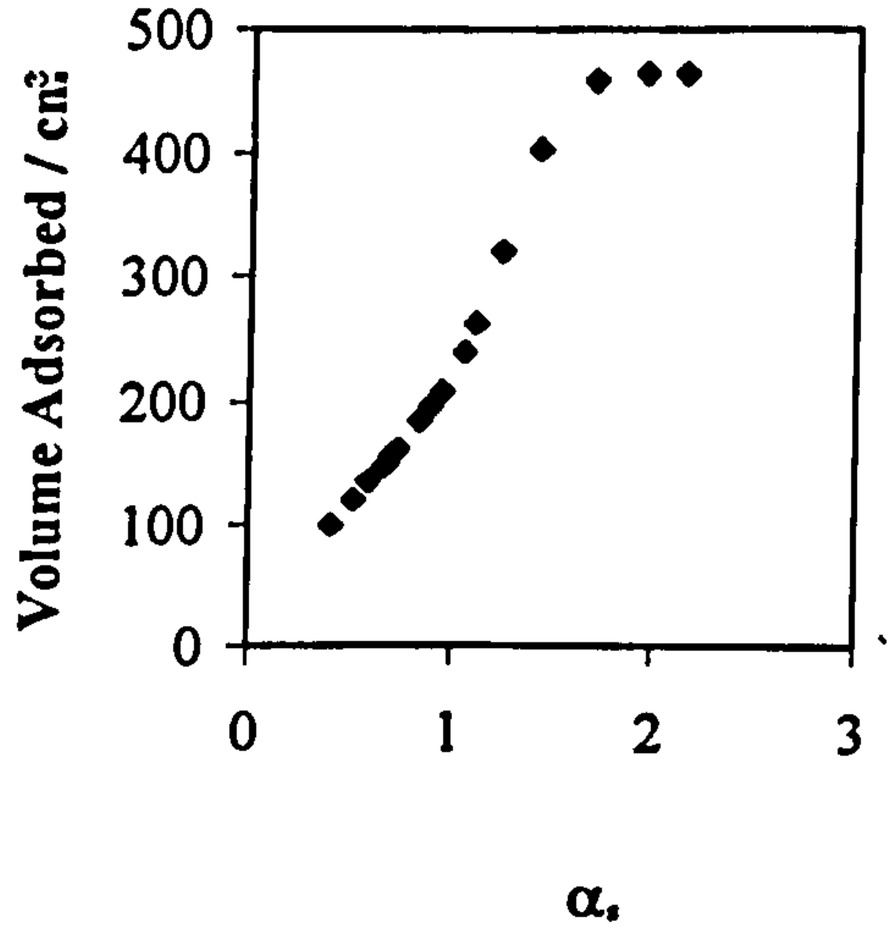

HCl=0·030 mole (TiO_2=6·34 weight % ; Heated at 120°C)

(a) Adsorption/Desorption Isotherm (b) α_s-plot

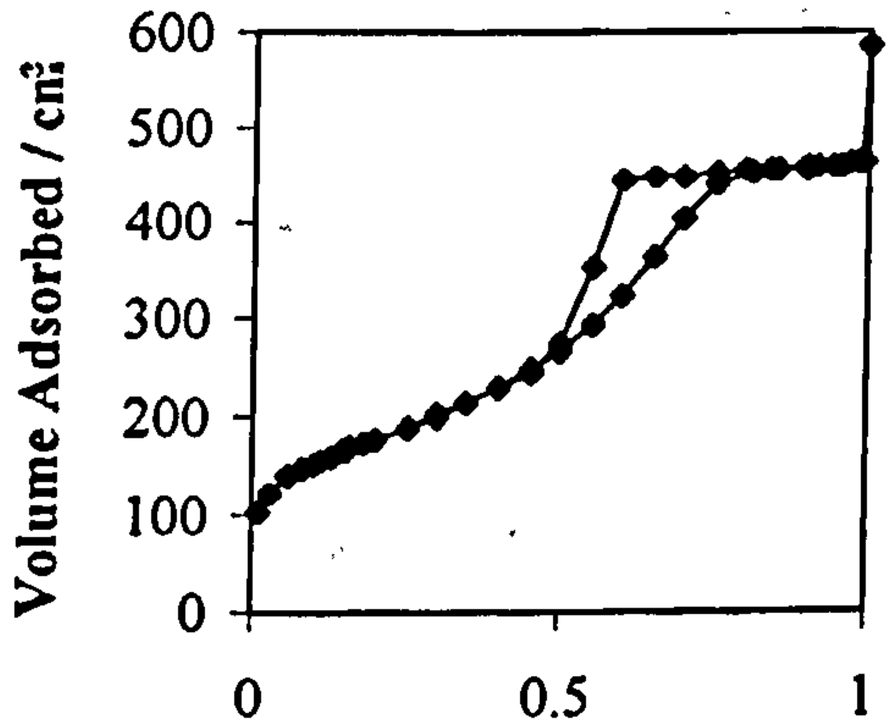

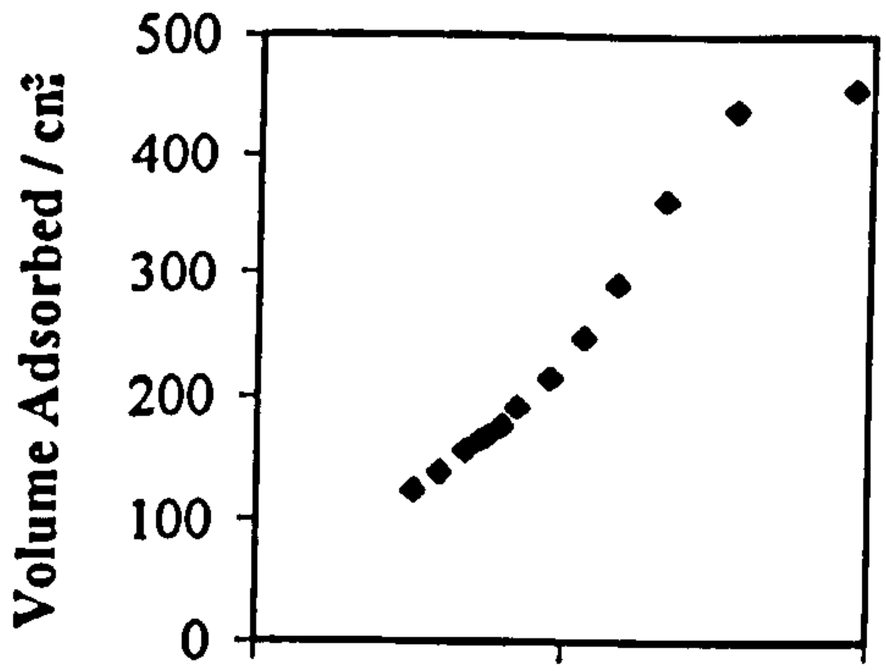

HCl=0·015 mole (TiO_2=6·34 weight % ; Heated at 120°C)

(a) Adsorption/Desorption Isotherm (b) α_s-plot

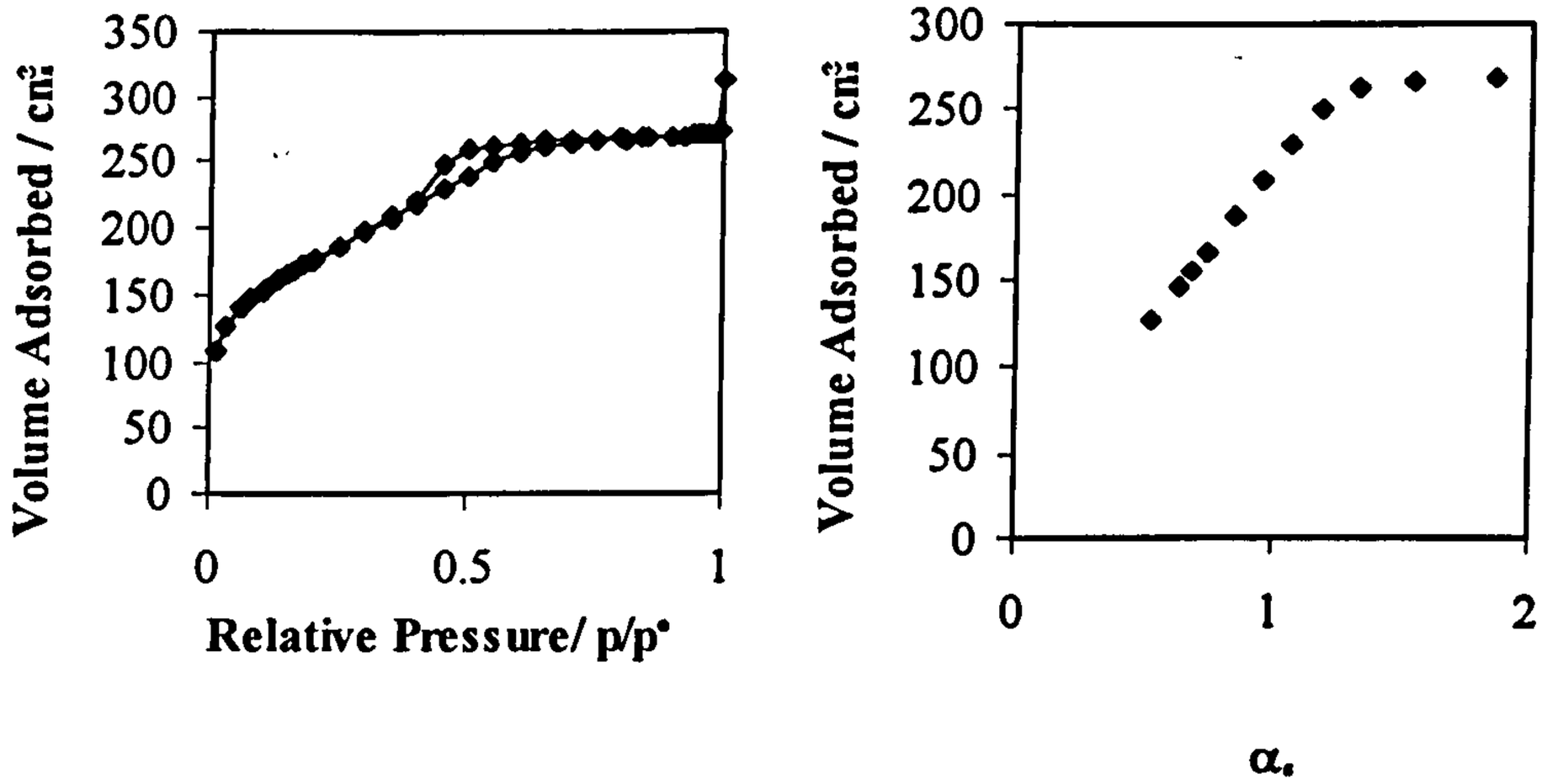

HCl=7·5x10^{-3} mole (TiO_2=6·34 weight % ; Heated at 120°C)

(a) Adsorption/Desorption Isotherm (b) α_s-plot

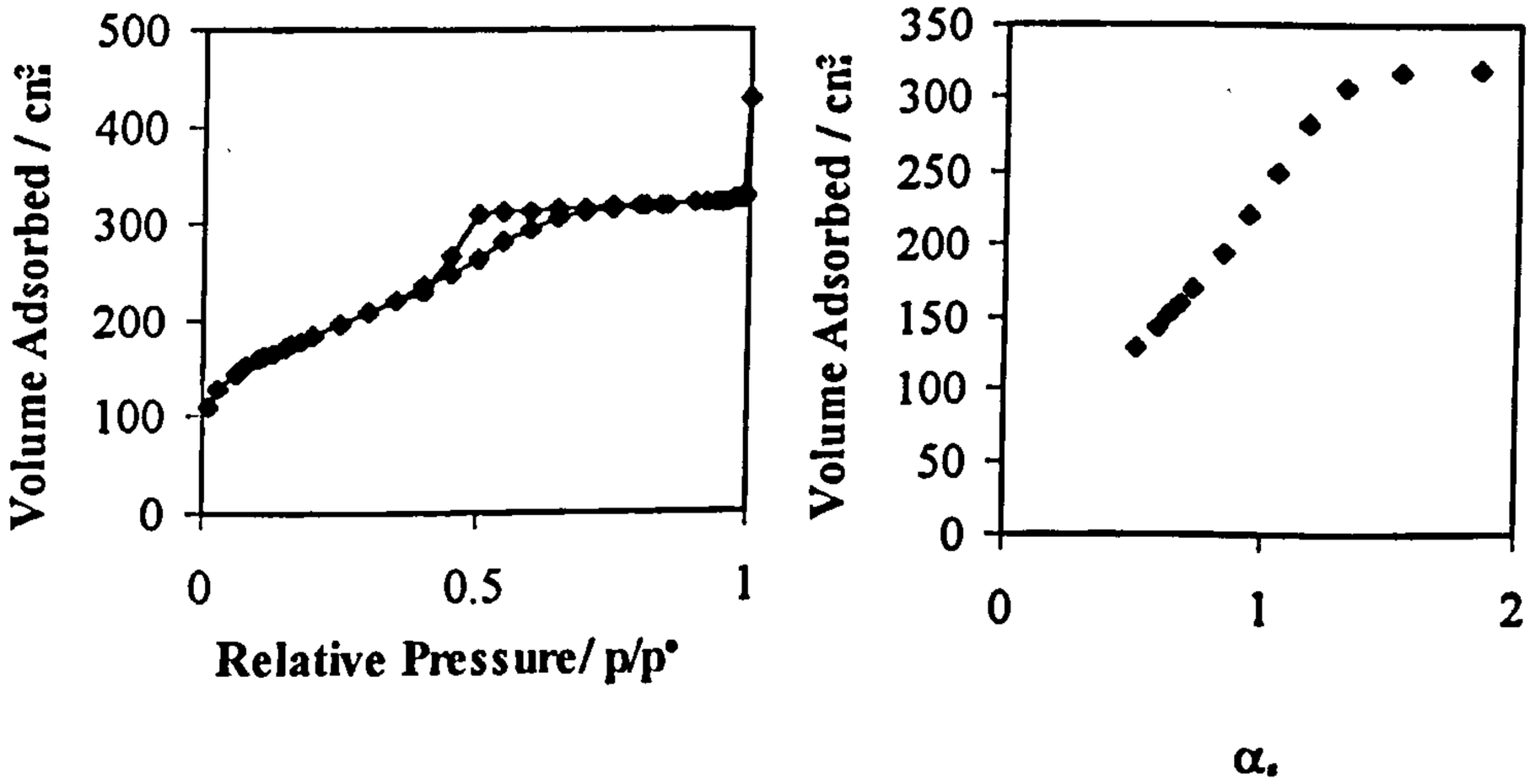

HCl=5x10^{-3} mole (TiO_2=6·34 weight % ; Heated at 120°C)

(a) Adsorption/Desorption Isotherm (b) α_s-plot

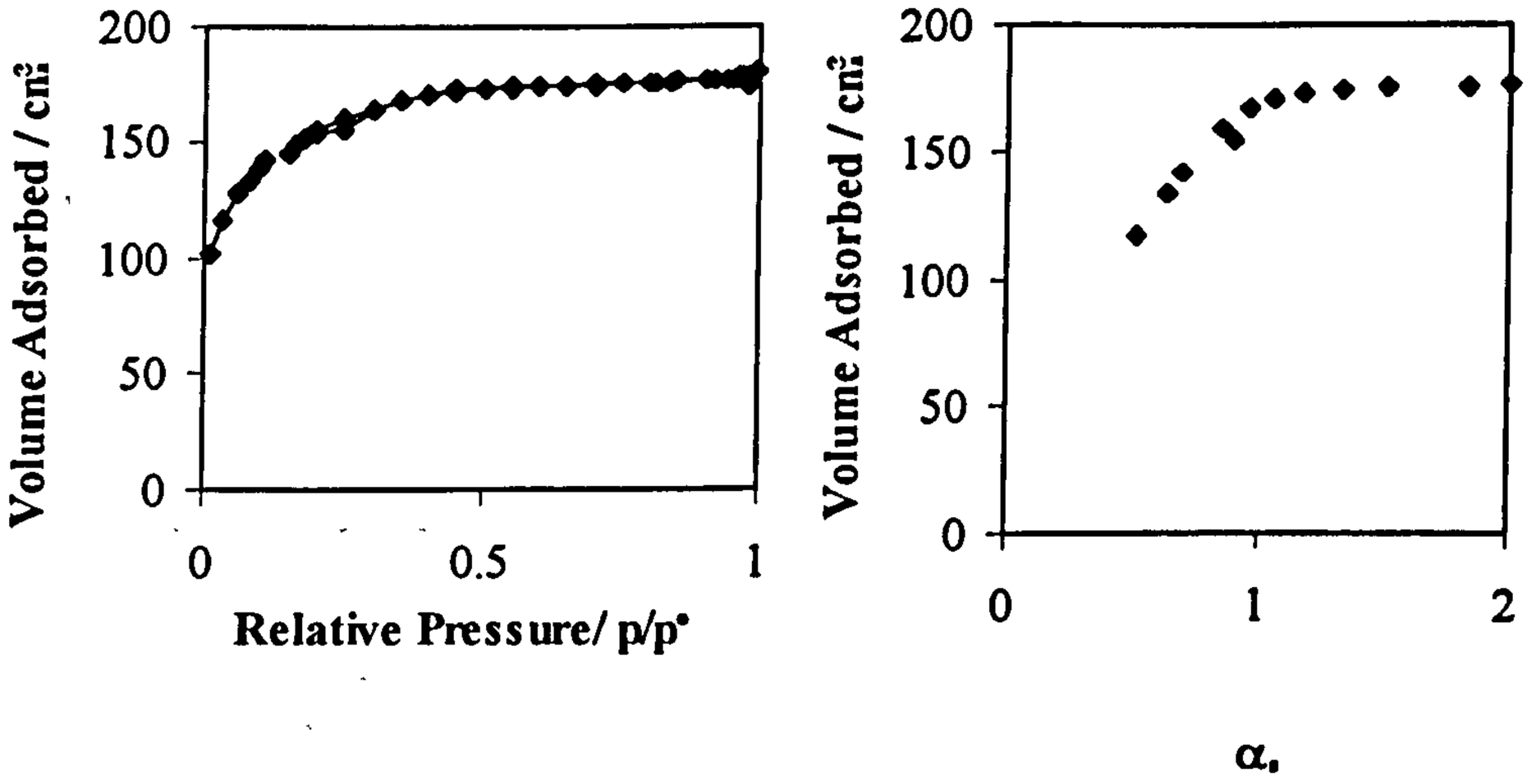

HCl=2·5x10^{-3} mole (TiO_2=6·34 weight % ; Heated at 120°C)

(a) Adsorption/Desorption Isotherm (b) α_s-plot

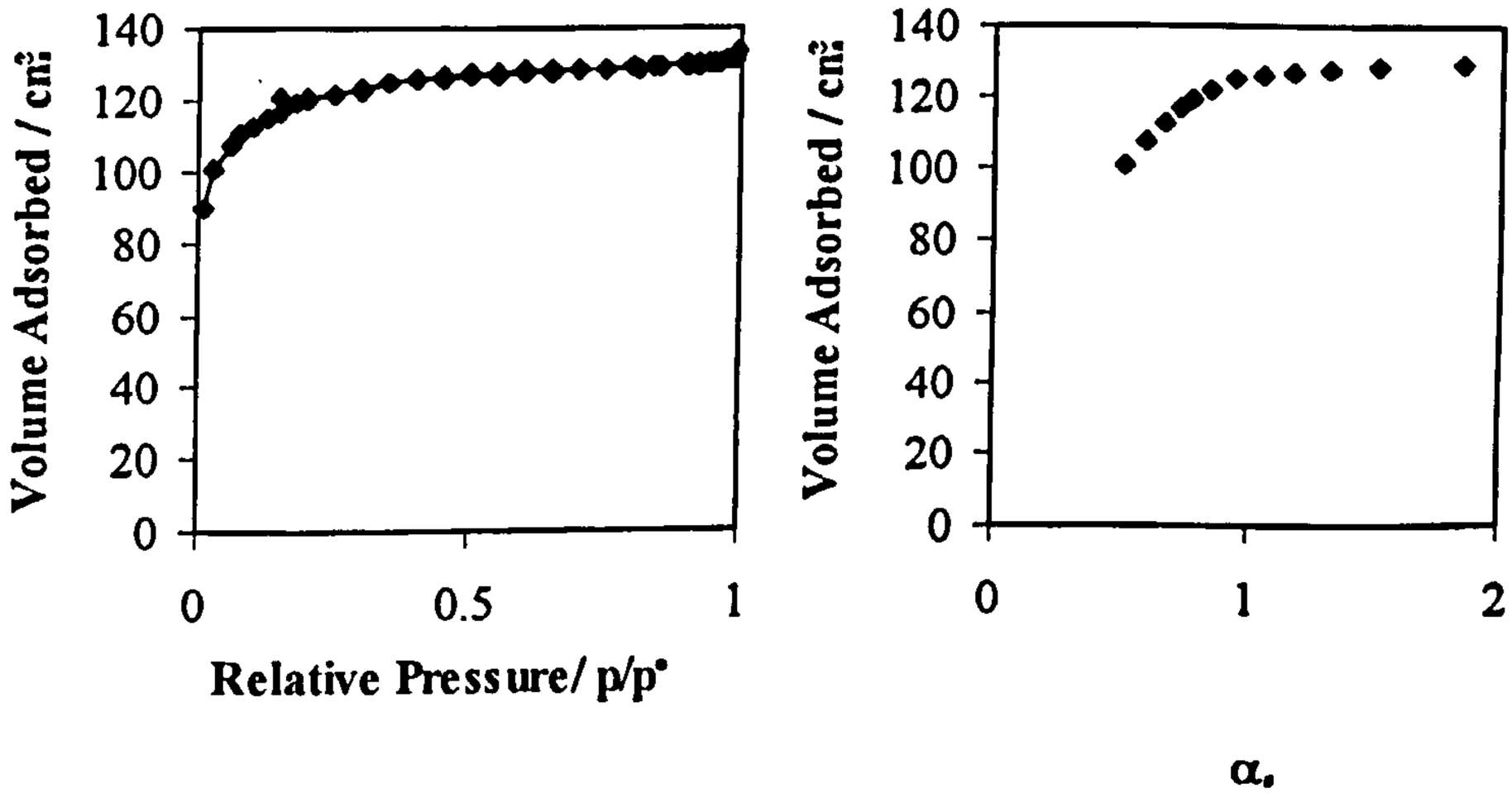

Effect of Temperature on the Pore Characteristics of a Sample Containing TiO_2=4·1 weight %; HCl=0·045 mole

		Temperature/°C						
		120	300	500	700	900	1100	1100 (Kr)
BET Surface Area (m^2g^{-1})		441	522	481	459	364	1·016	0·96
	C	93·9	117·9	122·4	76·9	65·7	1418	82
BJH Pore Volume (cm^3g^{-1})	Adsorption	0·48	0·76	0·44	0·63	0·49	0·006	
	Desorption	0·55	0·81	0·49	0·66	0·51	0·003	
BJH Average Pore Diameter (Å)	Adsorption	40·5	52·3	37·6	46·5	44·6	118·3	
	Desorption	39·5	49·8	38·9	45·0	42·8	147·3	

120°C: TiO_2=4·1 weight %; HCl=0·045 mole

(a) Adsorption/Desorption Isotherm

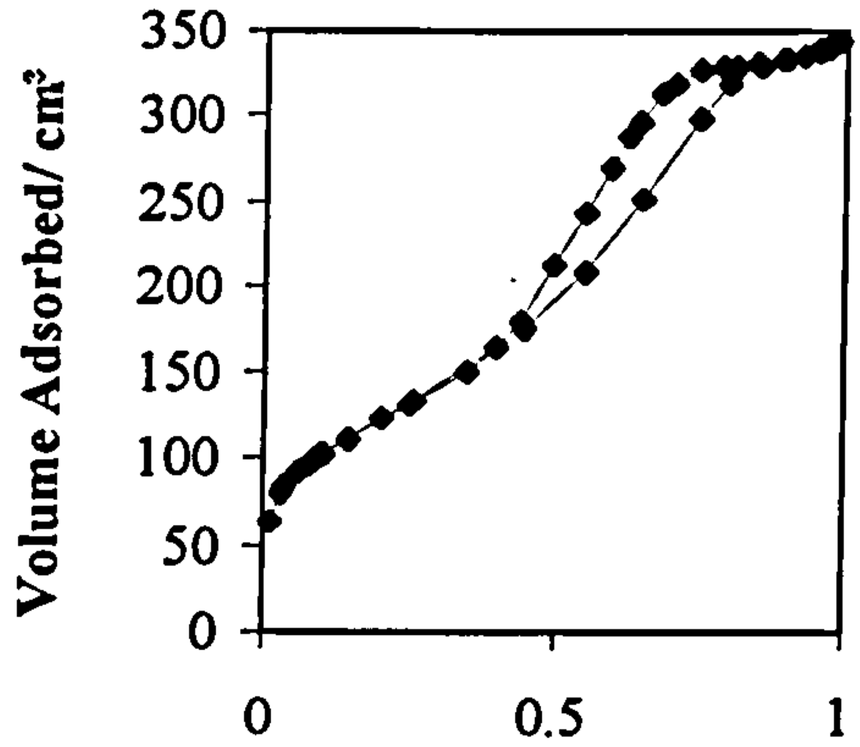

(b) α_s-plot

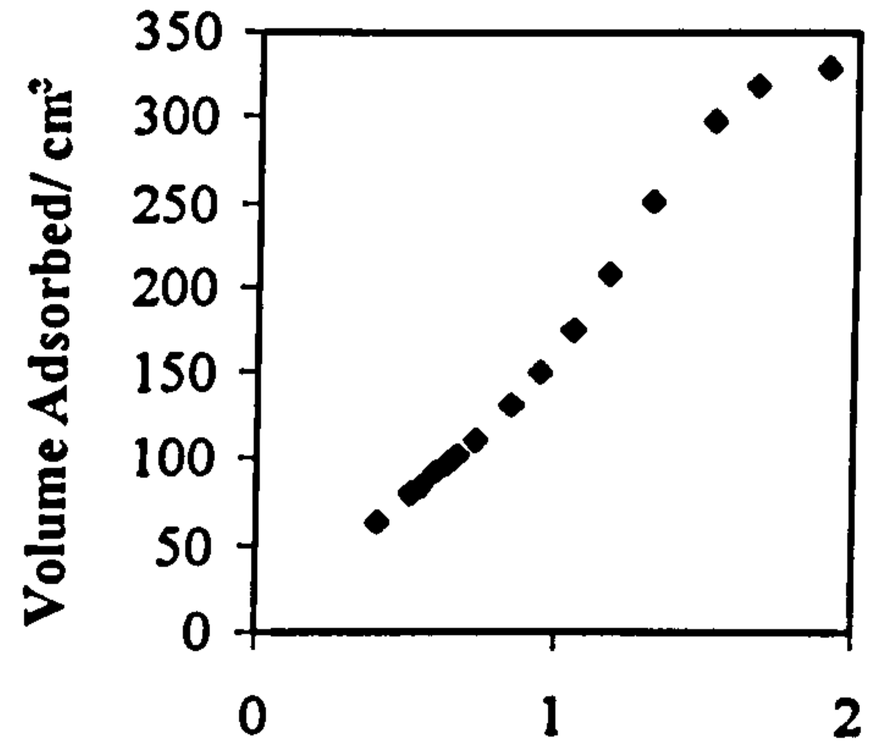

300°C: TiO_2=4·1 weight %; HCl=0·045 mole

(a) Adsorption/Desorption Isotherm

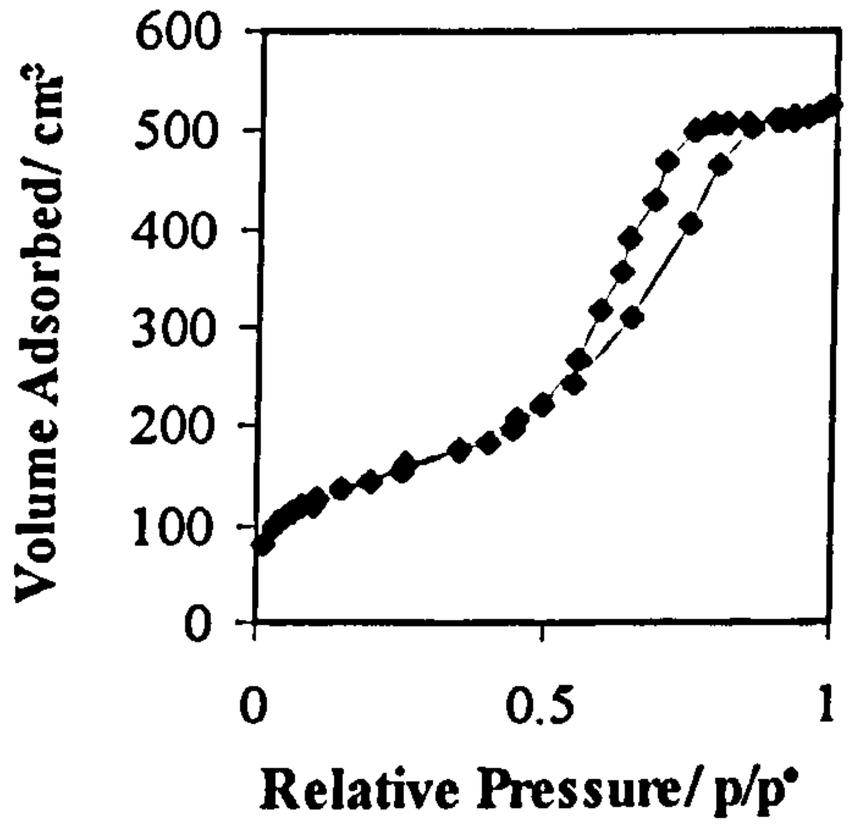

(b) α_s-plot

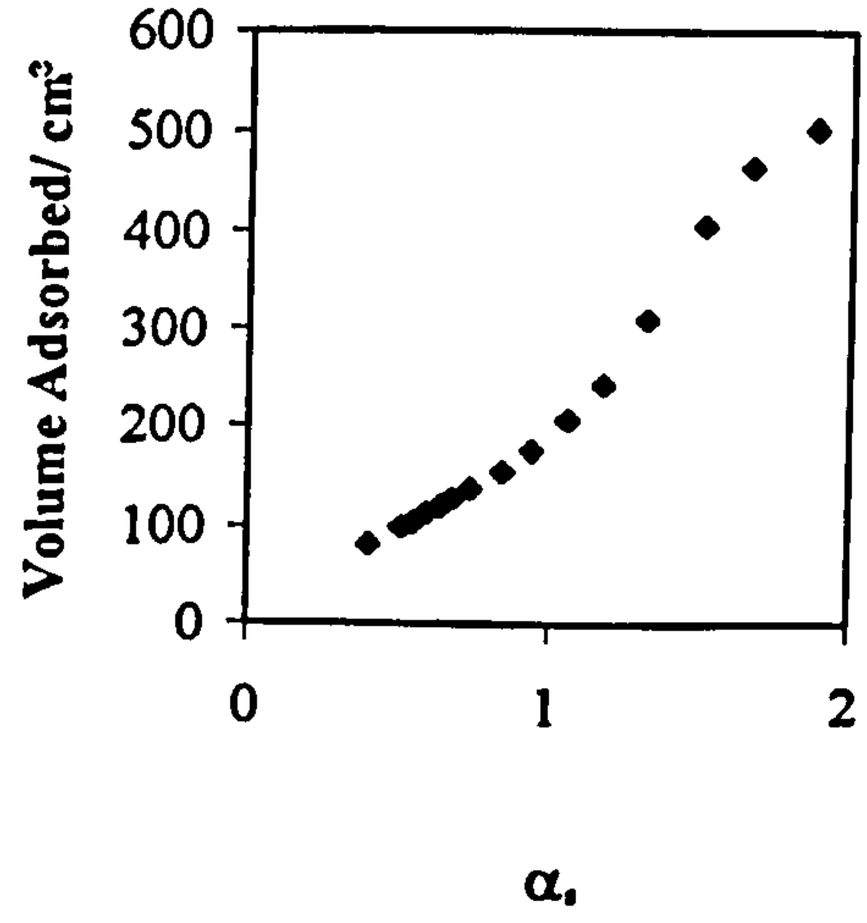

500°C: TiO_2=4·1 weight %; HCl=0·045 mole

(a) Adsorption/Desorption Isotherm

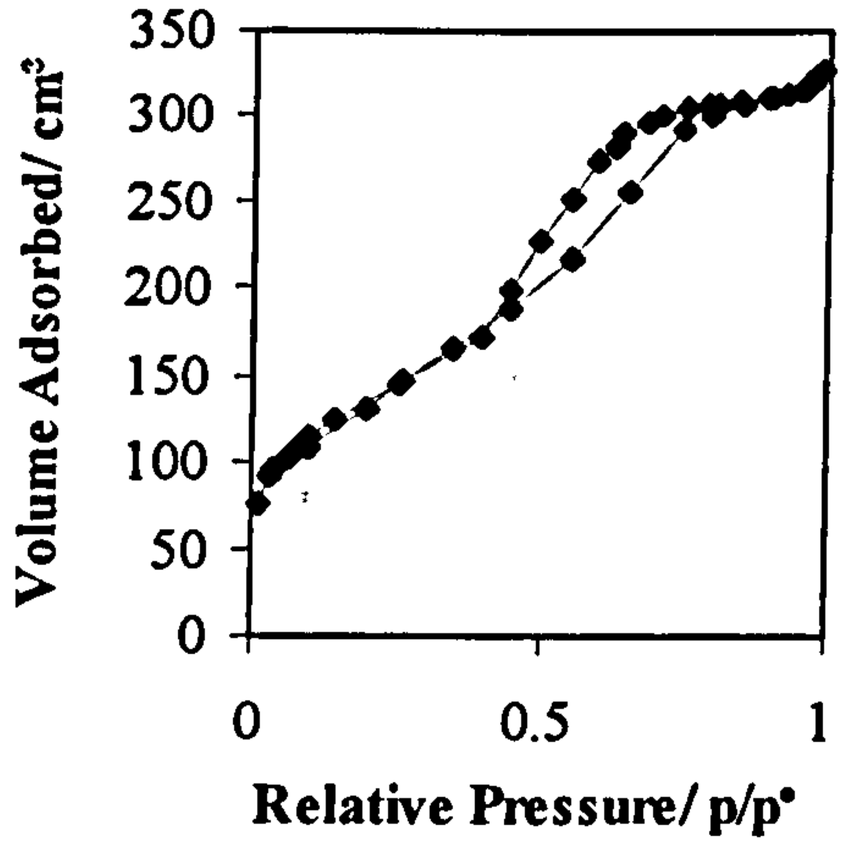

(b) α_s-plot

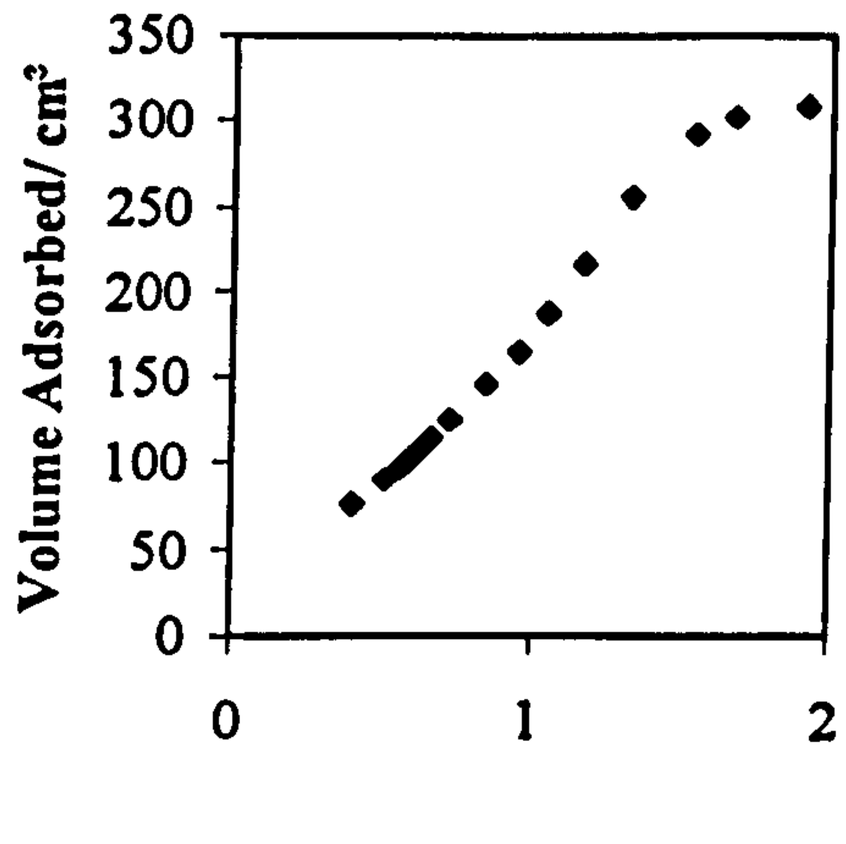

700°C: TiO_2=4·1 weight %; HCl=0·045 mole

(a) Adsorption/Desorption Isotherm

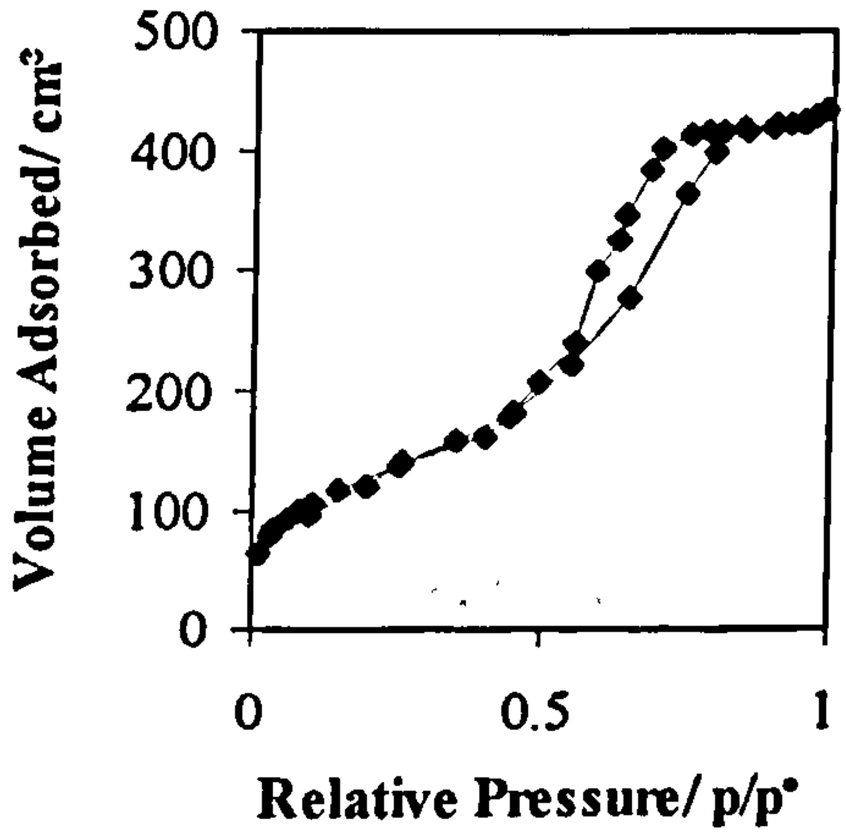

(b) α_s-plot

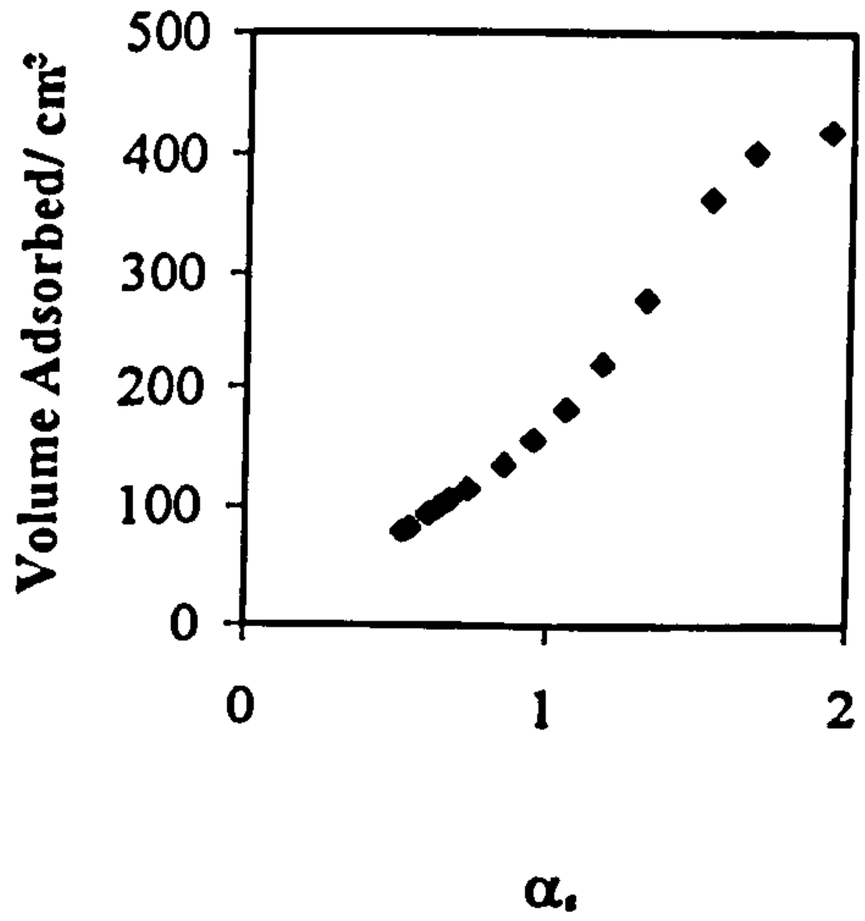

900°C: TiO_2=4·1 weight %; HCl=0·045 mole

(a) Adsorption/Desorption Isotherm

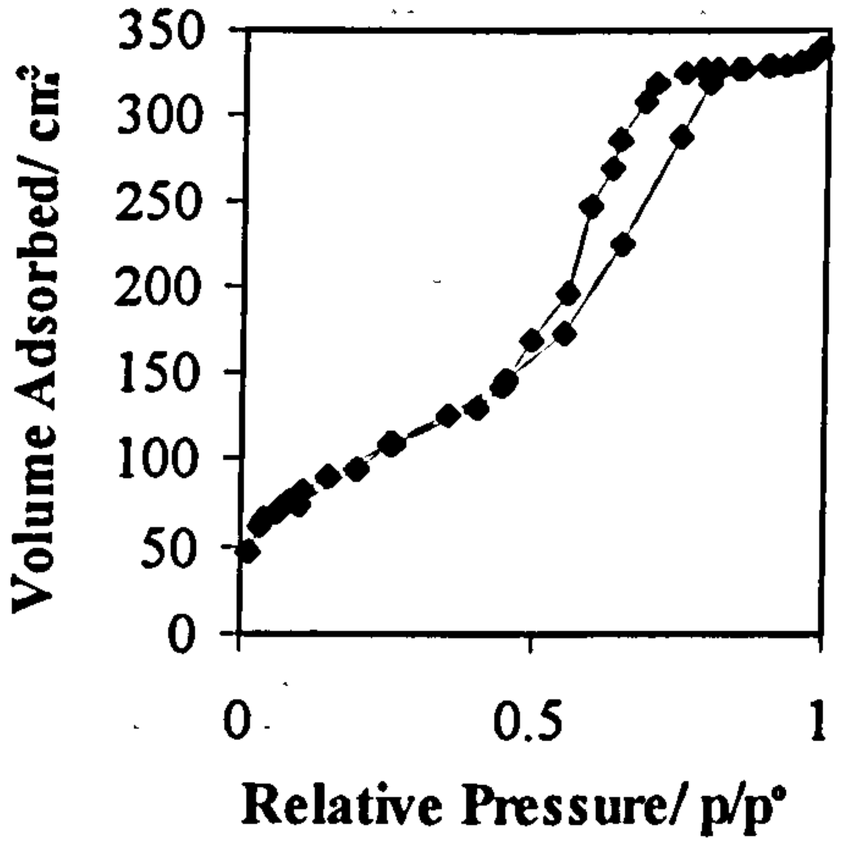

(b) α_s-plot

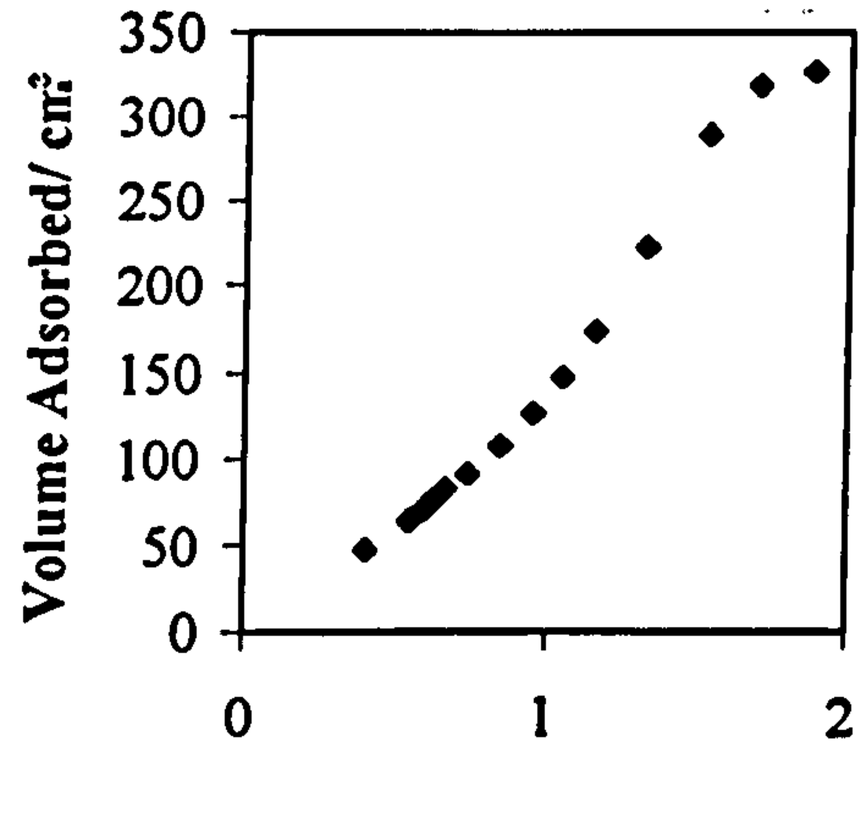

1100°C: TiO_2=4·1 weight %; HCl=0·045 mole

(a) Adsorption/Desorption Isotherm

(b) α_s-plot

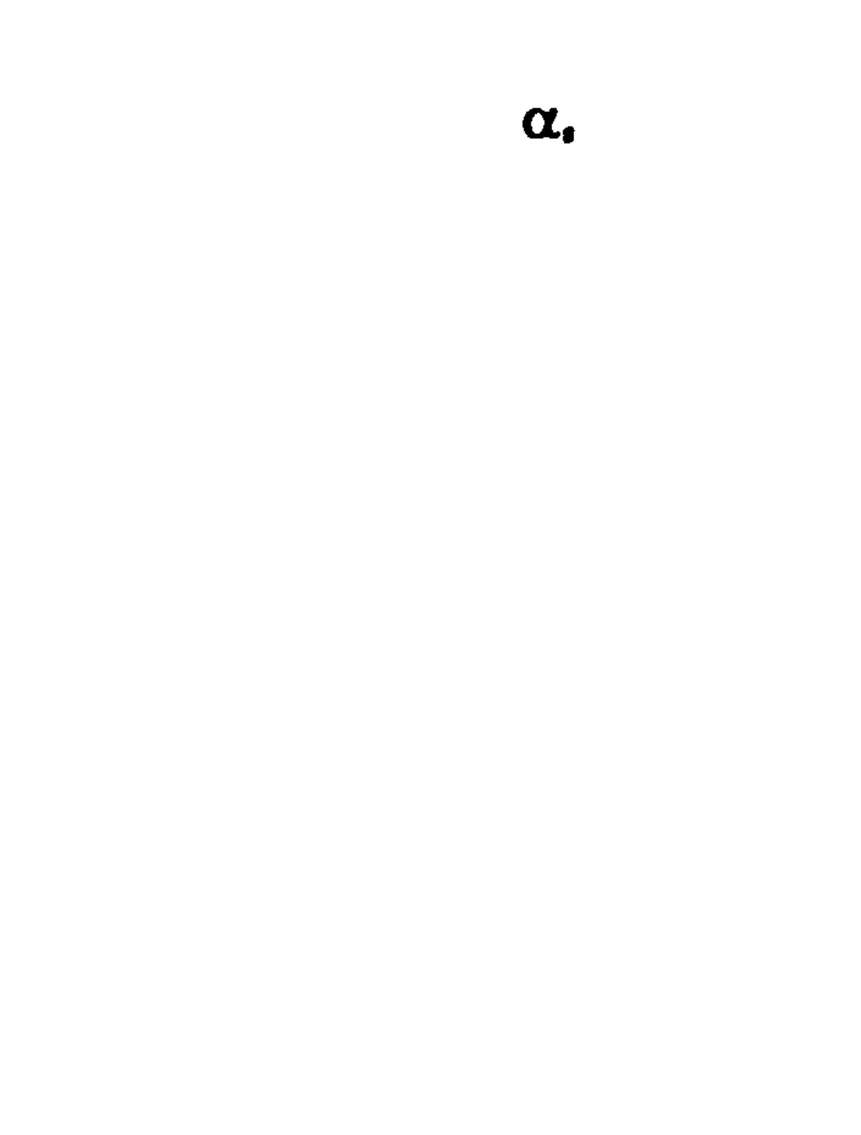

Effect of Temperature on the Pore Characteristics of a Sample Containing TiO_2=4·9 weight %; HCl=0·045 mole

		Temperature/°C						
		120	300	500	700	900	1100	1100 (Kr)
BET Surface Area (m^2g^{-1})		513	538	473	472	314	0·355	0·42
	C	98·4	118·7	95·5	71·9	63·9	1418	52·8
BJH Pore Volume (cm^3g^{-1})	Adsorption	0·56	0·57	0·43	0·48	0·30	0·001	
	Desorption	0·61	0·62	0·51	0·52	0·33	0·001	
BJH Average Pore Diameter (Å)	Adsorption	39·2	39·3	35·3	36·2	34·3	423·4	
	Desorption	38·4	38·6	34·8	35·8	33·7	282·4	

120°C: TiO_2=4·9 weight %; HCl=0·045 mole

(a) Adsorption/Desorption Isotherm

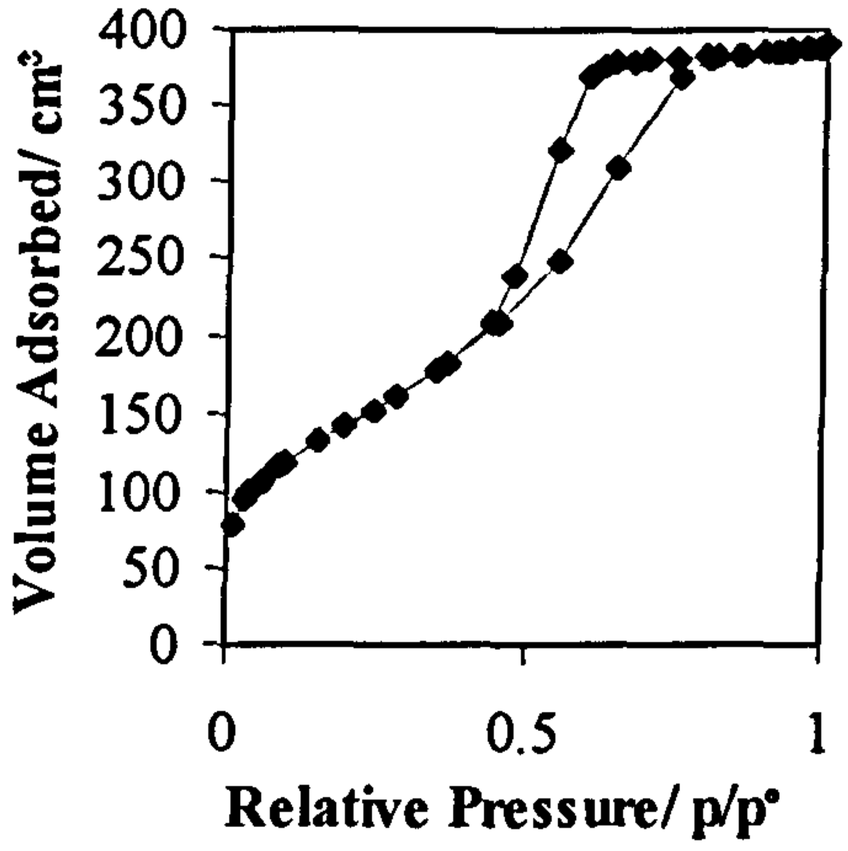

(b) α_s-plot

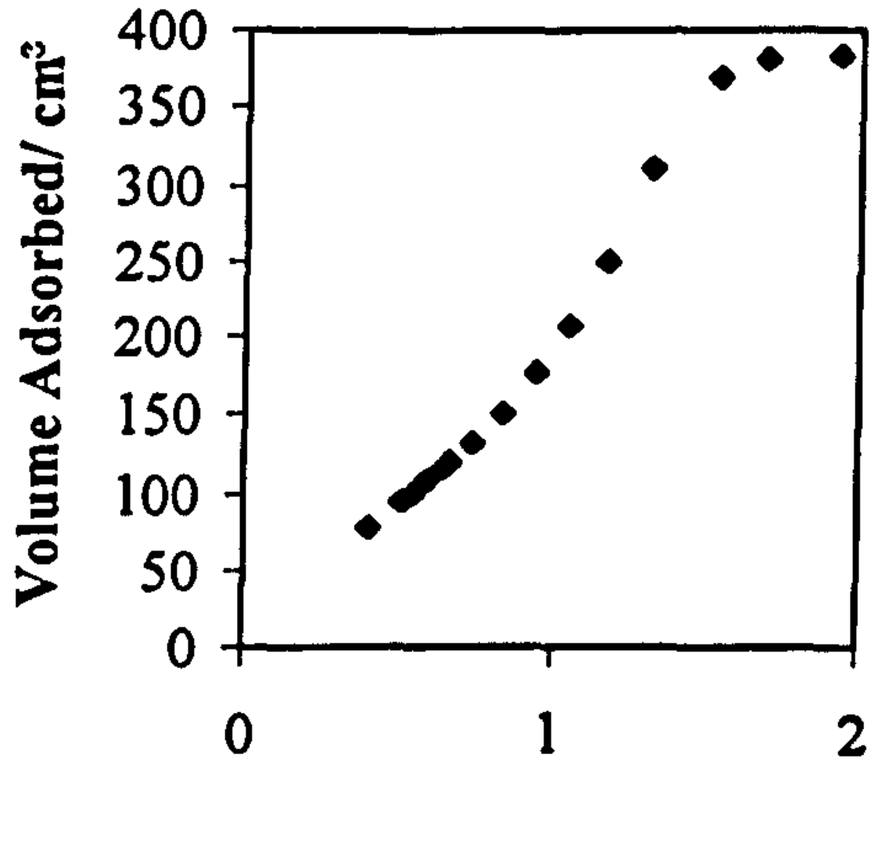

300°C: TiO_2=4·9 weight %; HCl=0·045 mole

(a) Adsorption/Desorption Isotherm

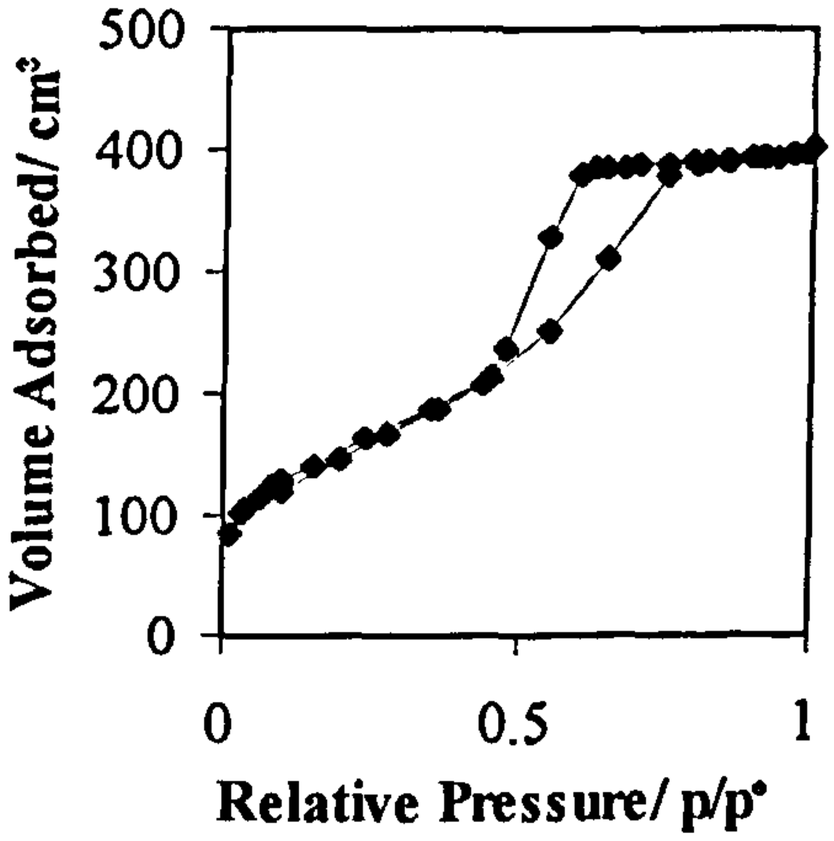

(b) α_s-plot

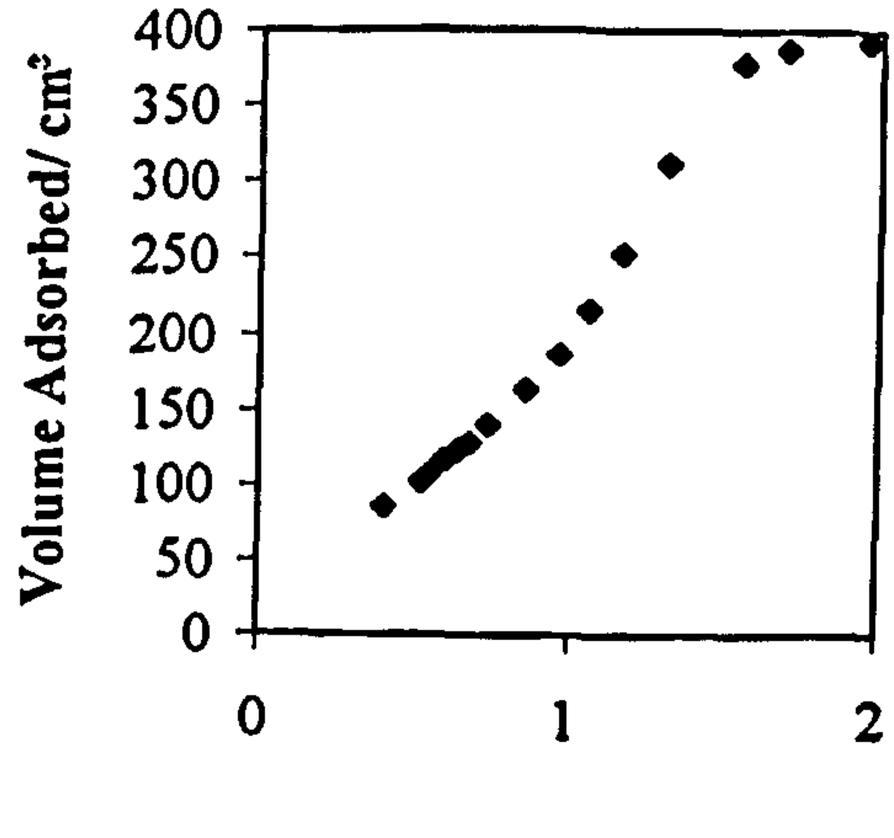

500°C: TiO_2=4·9 weight %; HCl=0·045 mole

(a) Adsorption/Desorption Isotherm

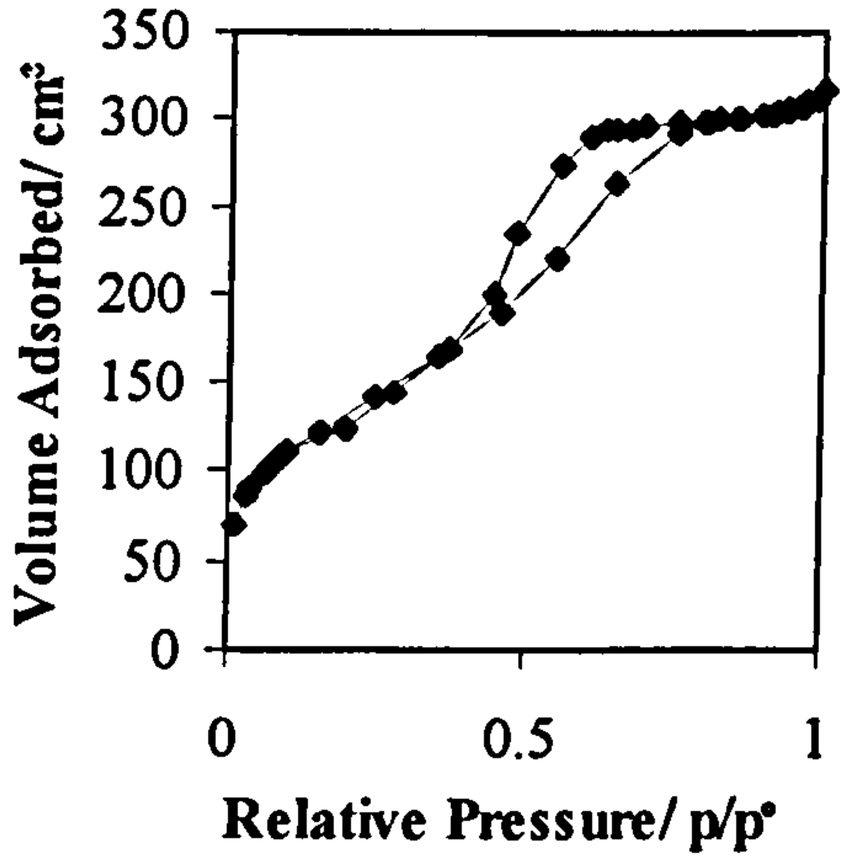

(b) α_s-plot

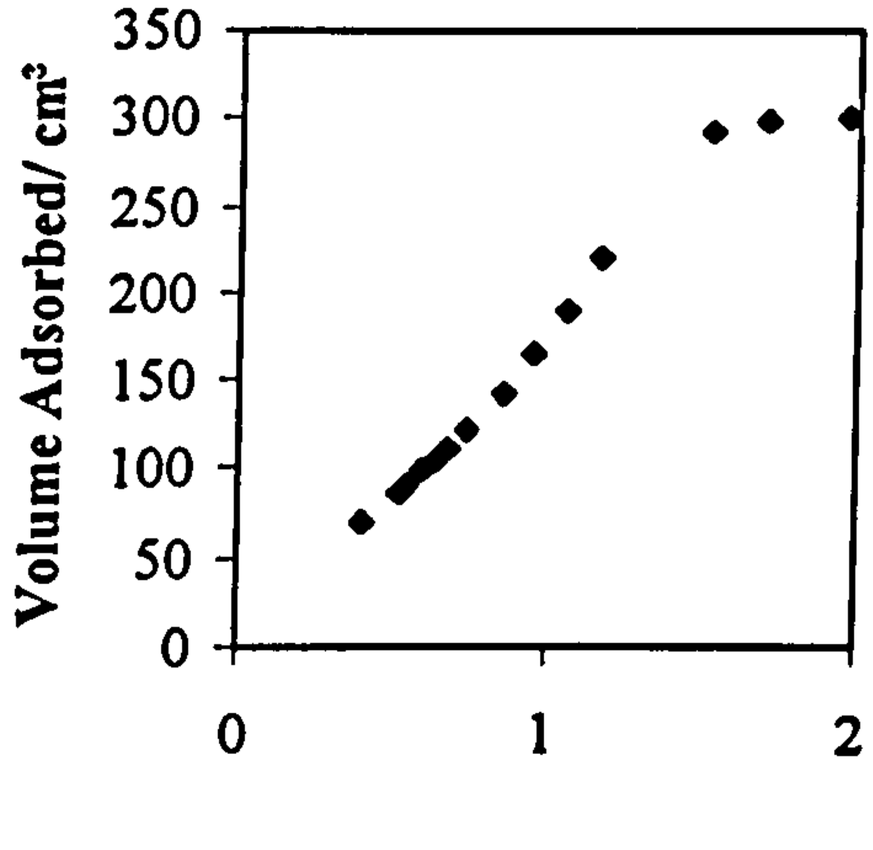

700°C: TiO_2=4·9 weight %; HCl=0·045 mole

(a) Adsorption/Desorption Isotherm

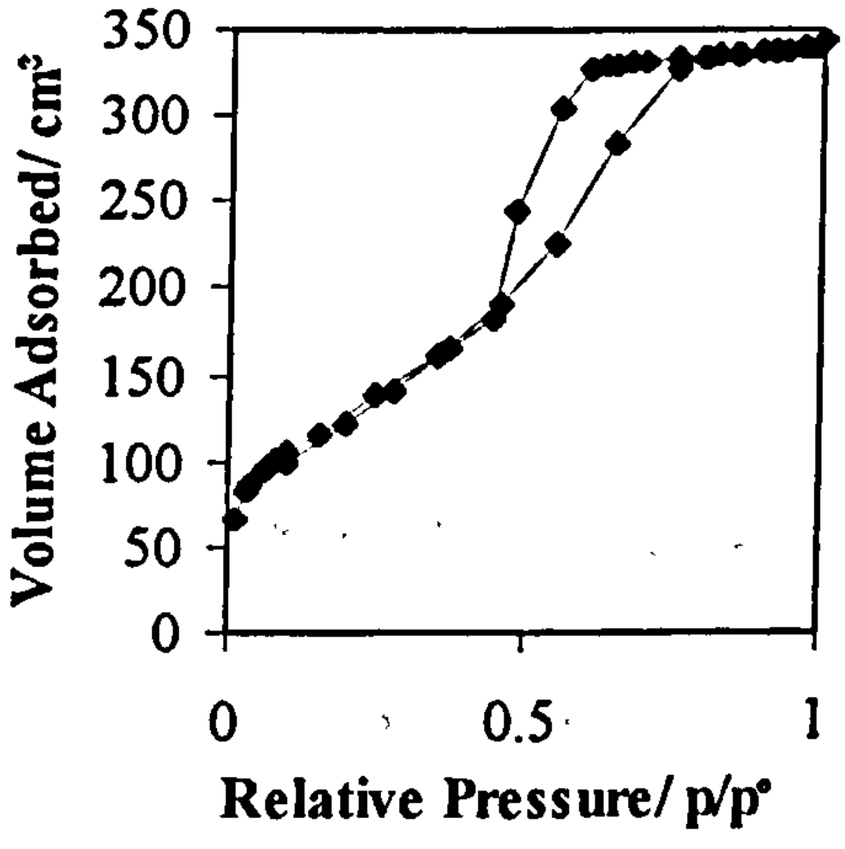

(b) α_s-plot

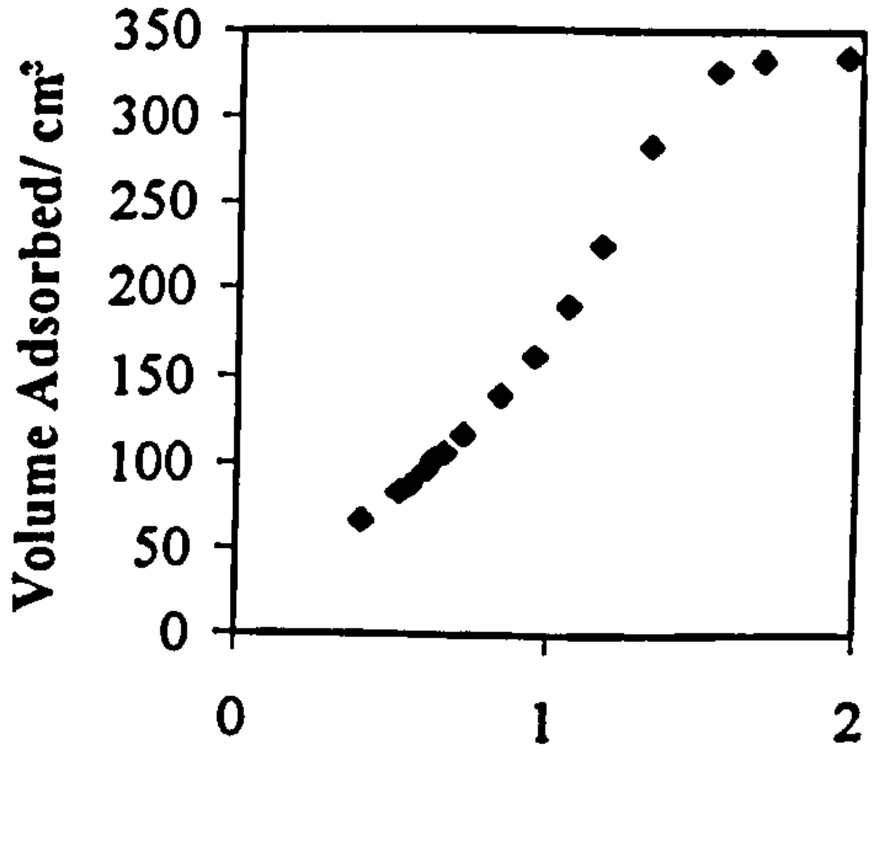

900°C: TiO_2=4·9 weight %; HCl=0·045 mole

(a) Adsorption/Desorption Isotherm

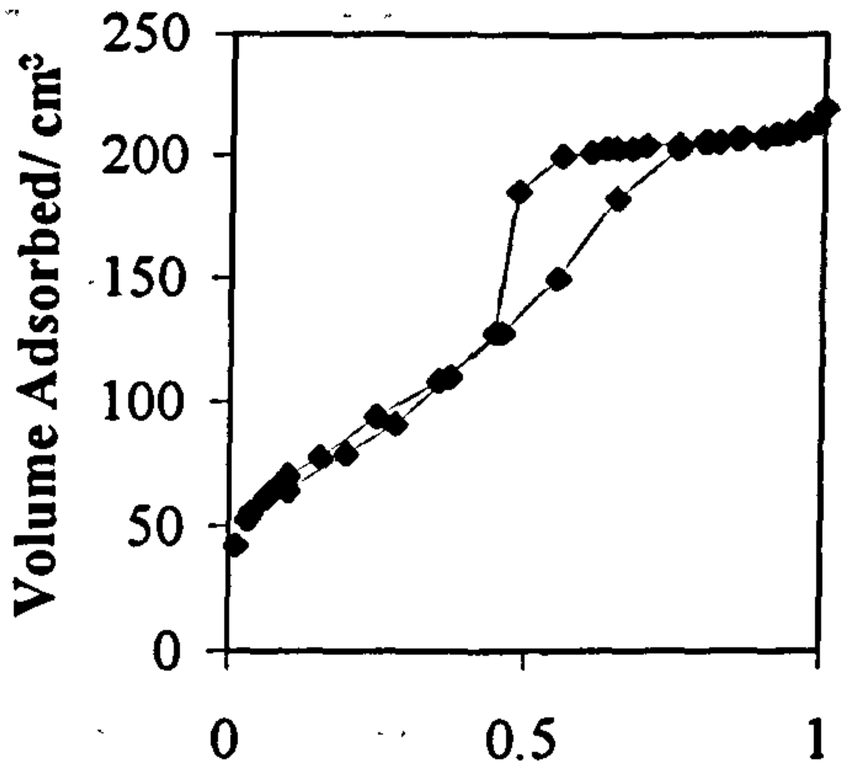

(b) α_s-plot

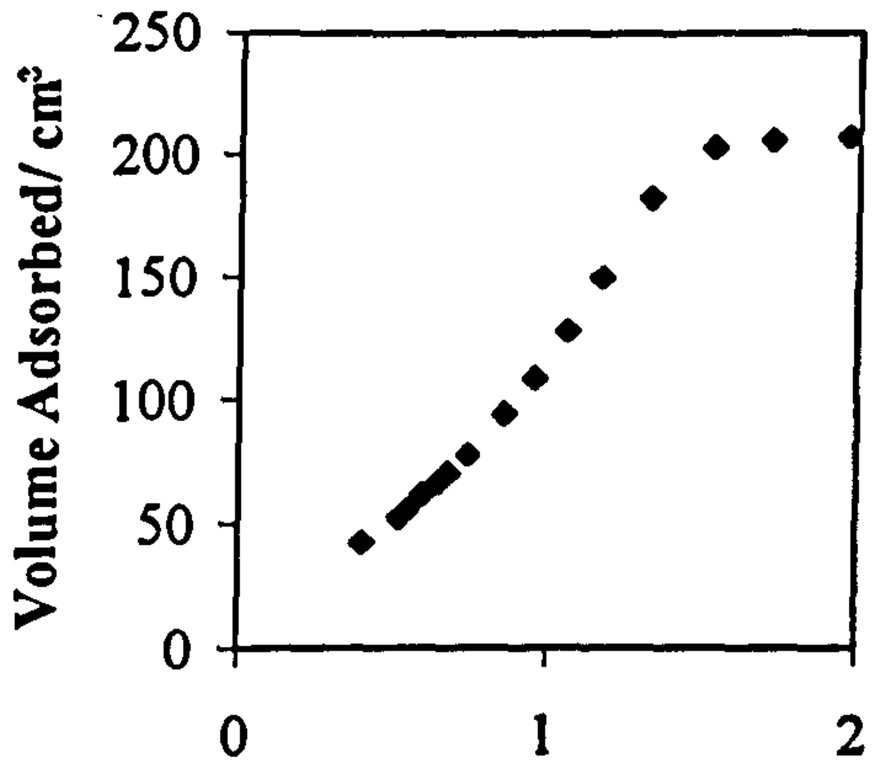

1100°C: TiO_2=4·9 weight %; HCl=0·045 mole

(a) Adsorption/Desorption Isotherm

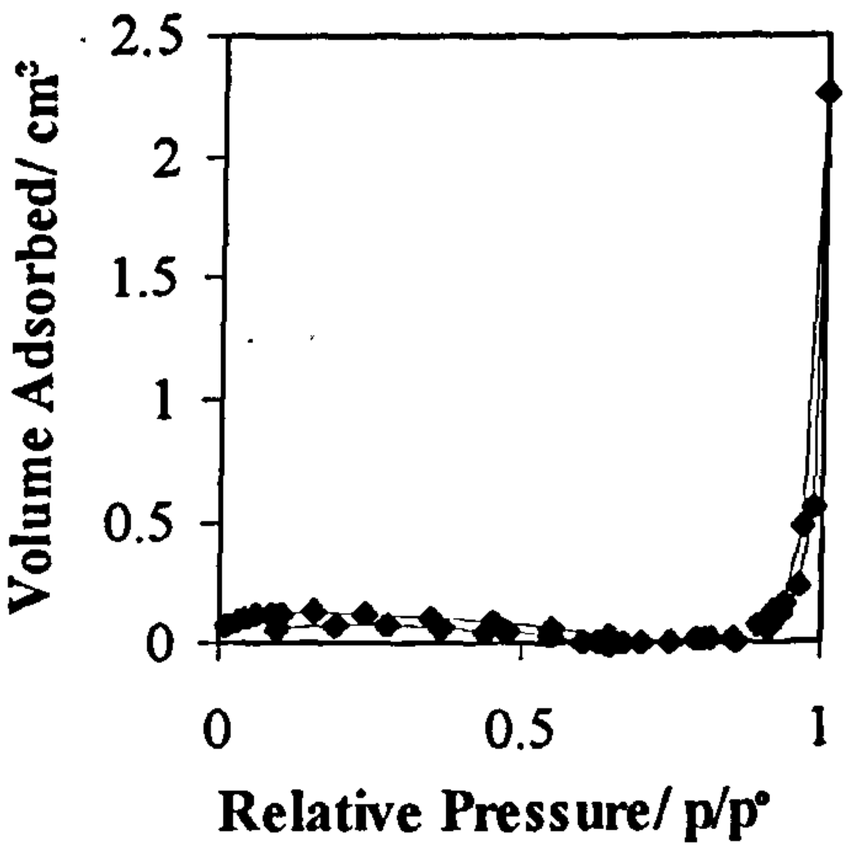

Effect of Temperature on the Pore Characteristics of a Sample Containing TiO_2=6·1 weight %; HCl=0·045 mole

		Temperature/°C						
		120	300	500	700	900	1100	1100 (Kr)
BET Surface Area (m^2g^{-1})		551	590	510	530	384	0·41	0·43
	C	113·9	124·1	107·6	83·9	73·7	-89·8	59·5
BJH Pore Volume (cm^3g^{-1})	Adsorption	0·66	0·69	0·44	0·60	0·42	0·001	
	Desorption	0·72	0·75	0·49	0·64	0·46	0·001	
BJH Average Pore Diameter (Å)	Adsorption	43·7	43·9	34·5	40·7	39·0	353	
	Desorption	43·2	43·3	36·2	40·6	37·9	247	

120°C: TiO_2=6·1 weight %; HCl=0·045 mole

(a) Adsorption/Desorption Isotherm

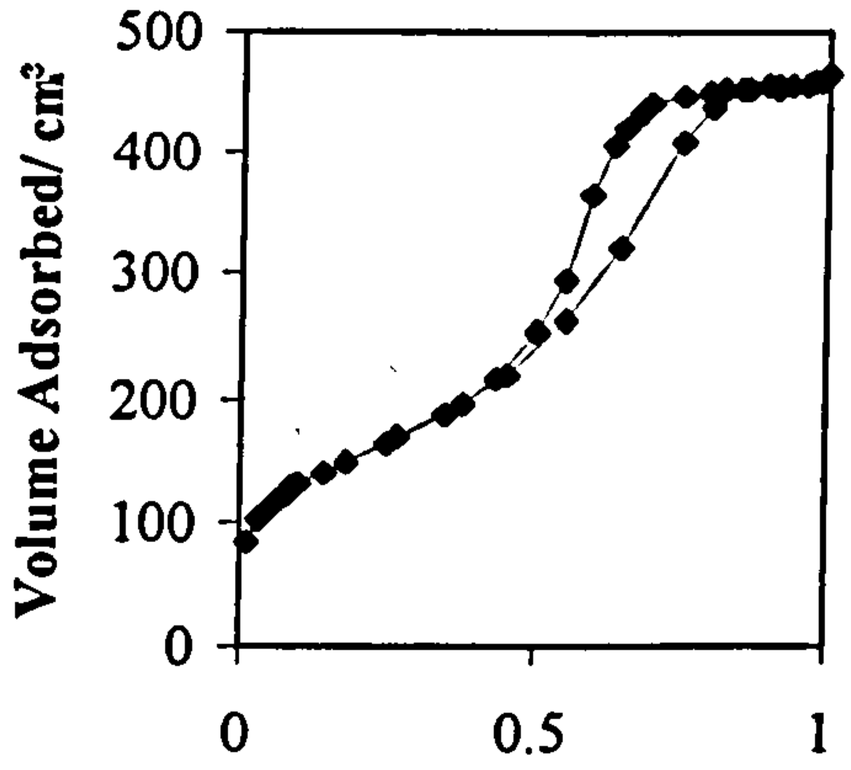

(b) α_s-plot

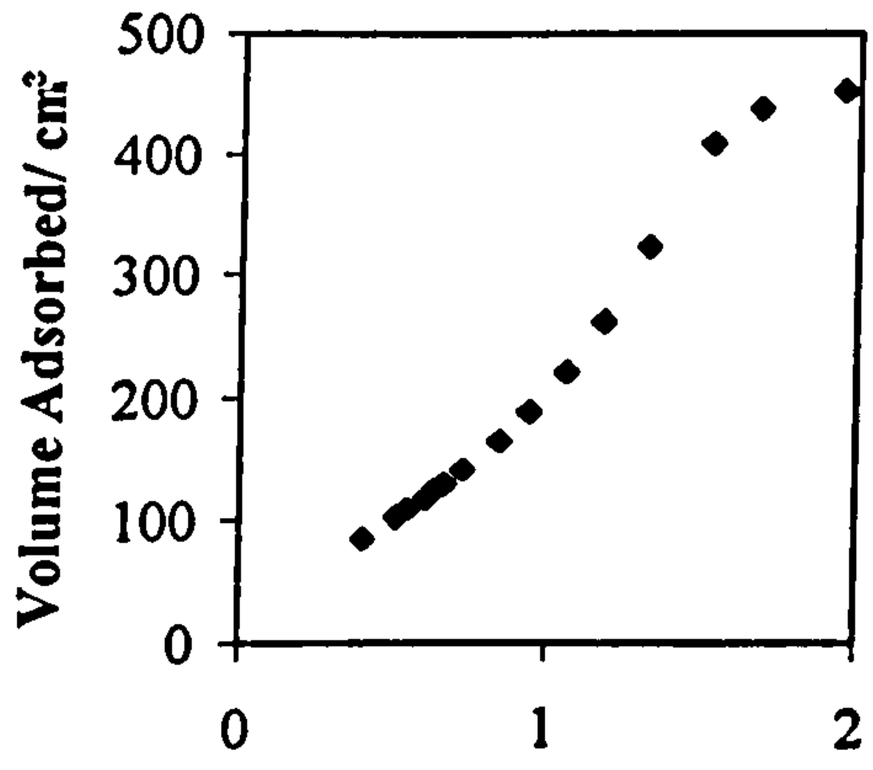

300°C: TiO_2=6·1 weight %; HCl=0·045 mole

(a) Adsorption/Desorption Isotherm

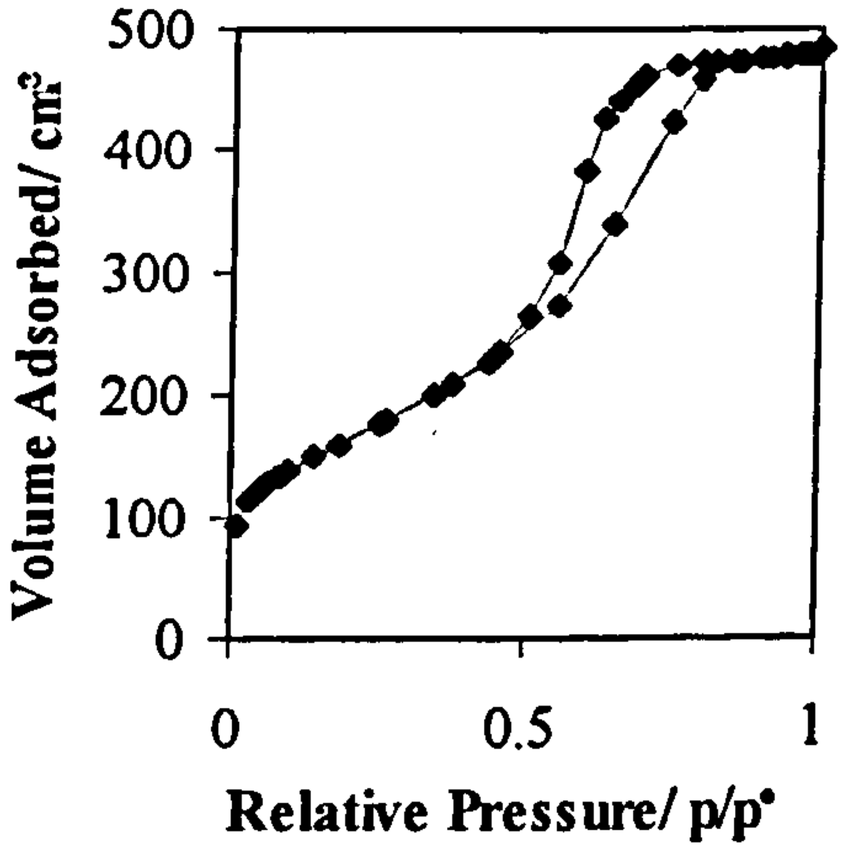

(b) α_s-plot

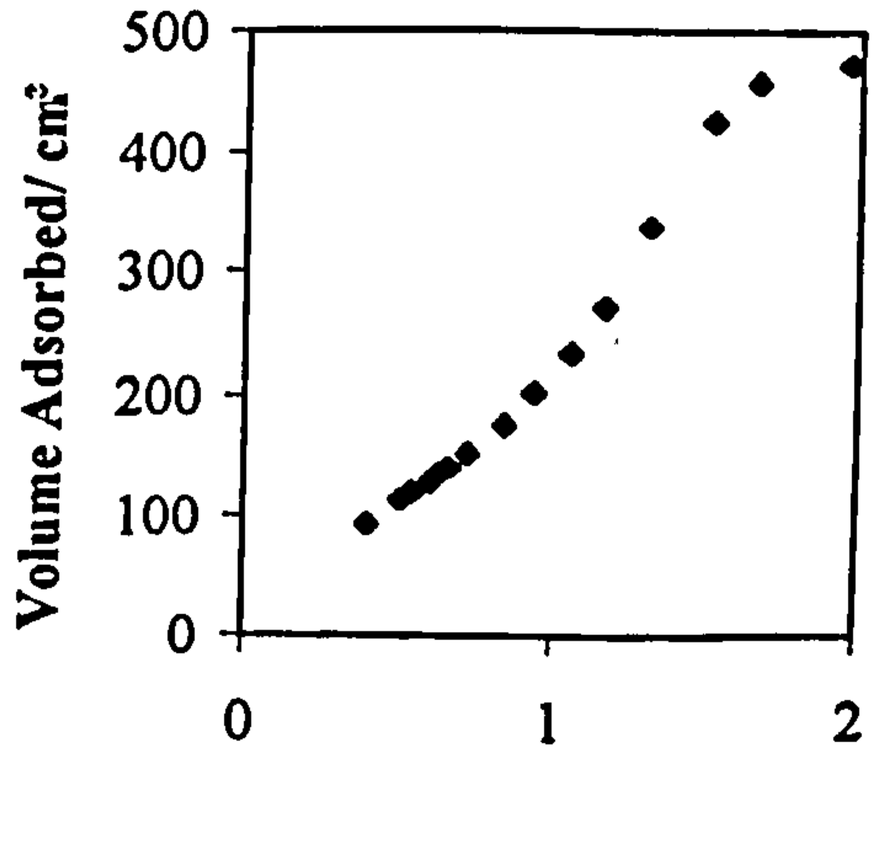

500°C: TiO_2=6·1 weight %; HCl=0·045 mole

(a) Adsorption/Desorption Isotherm

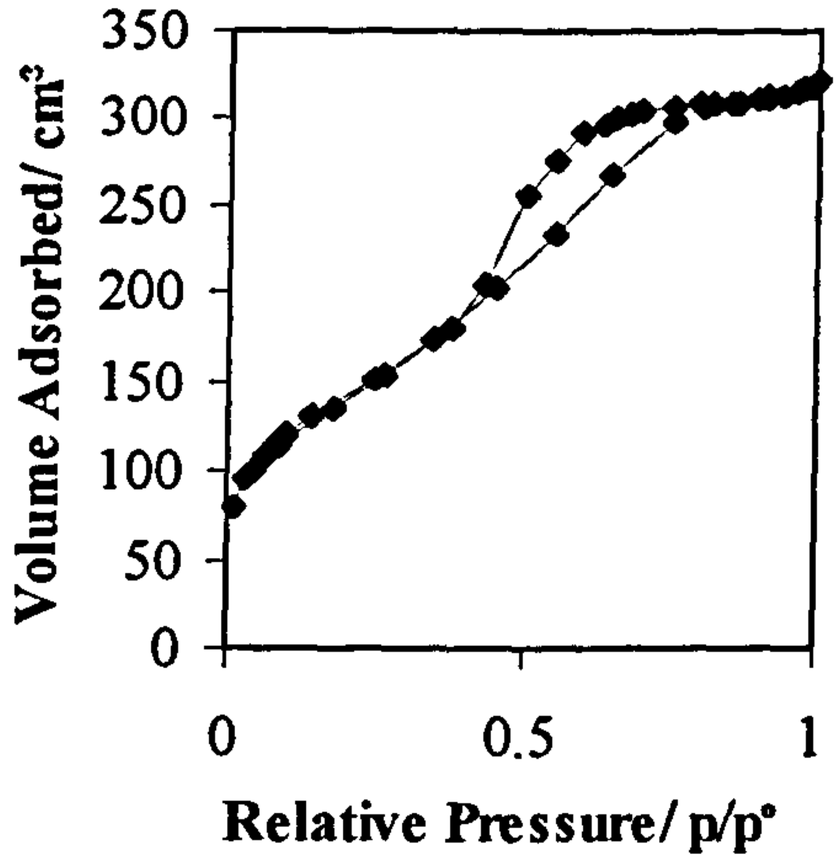

(b) α_s-plot

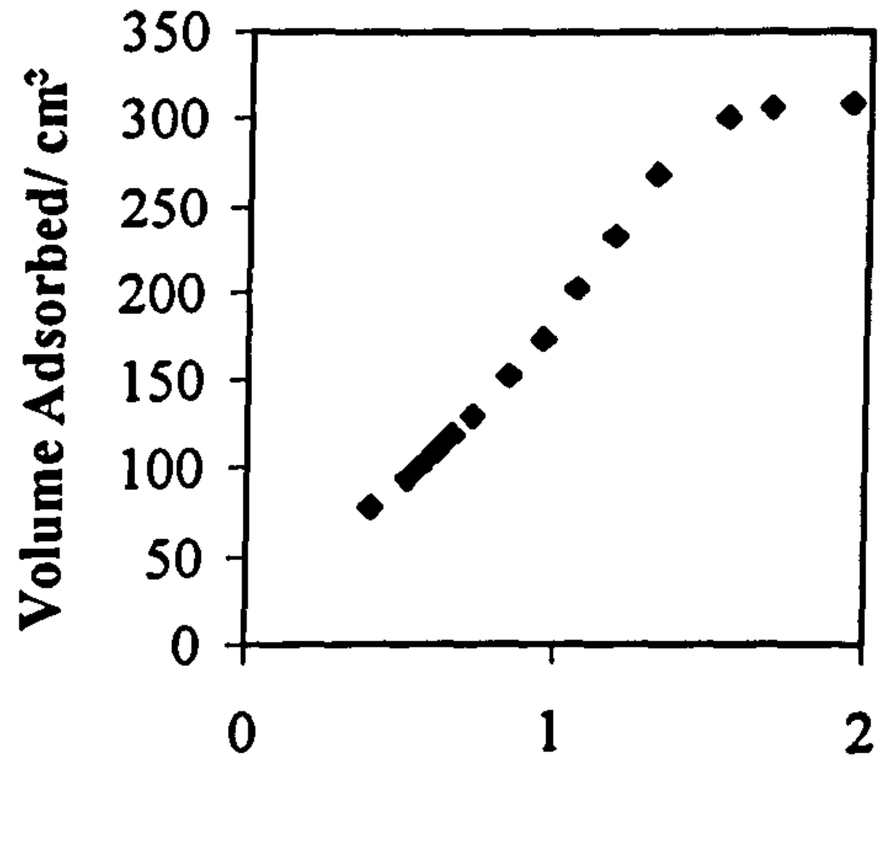

700°C: TiO_2=6·1 weight %; HCl=0·045 mole

(a) Adsorption/Desorption Isotherm

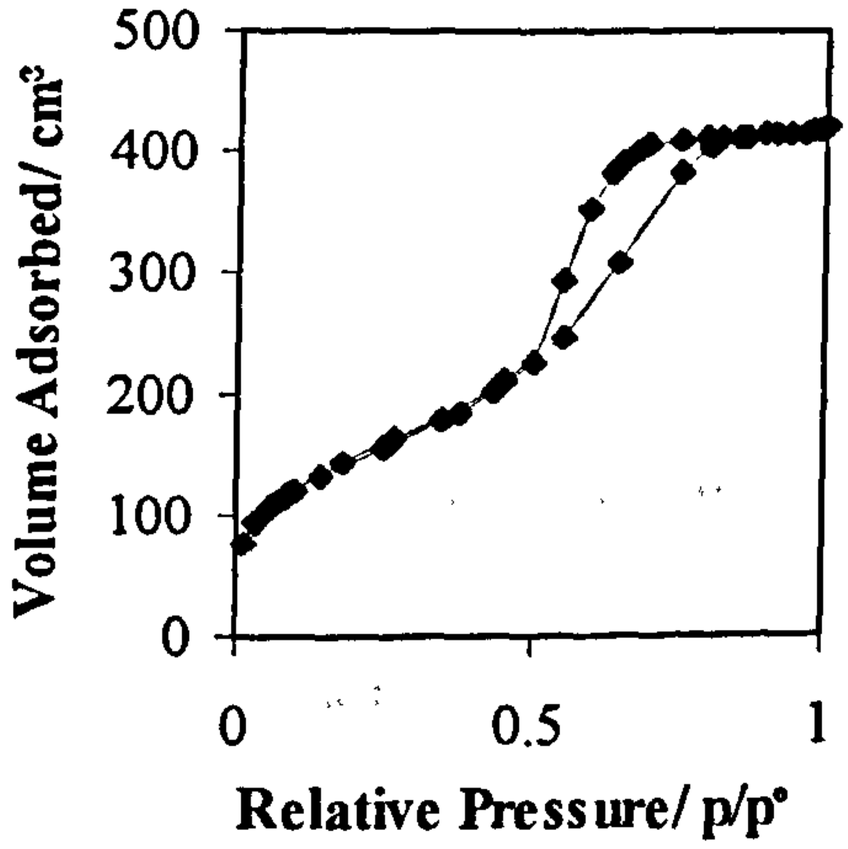

(b) α_s-plot

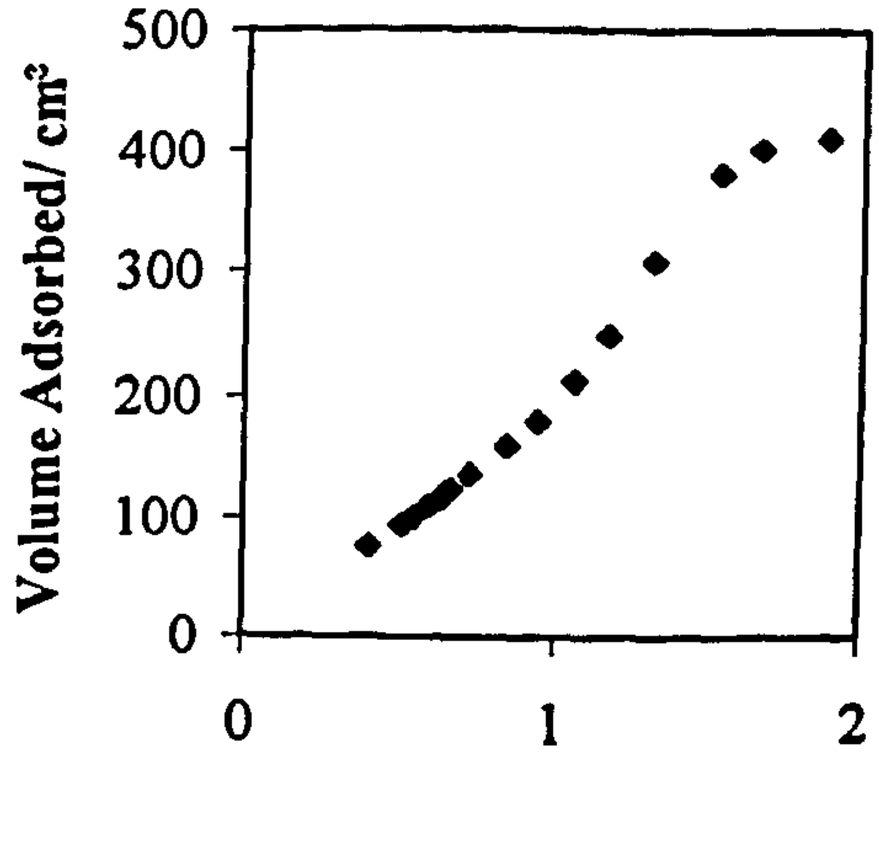

900°C: TiO_2=6·1 weight %; HCl=0·045 mole

(a) Adsorption/Desorption Isotherm

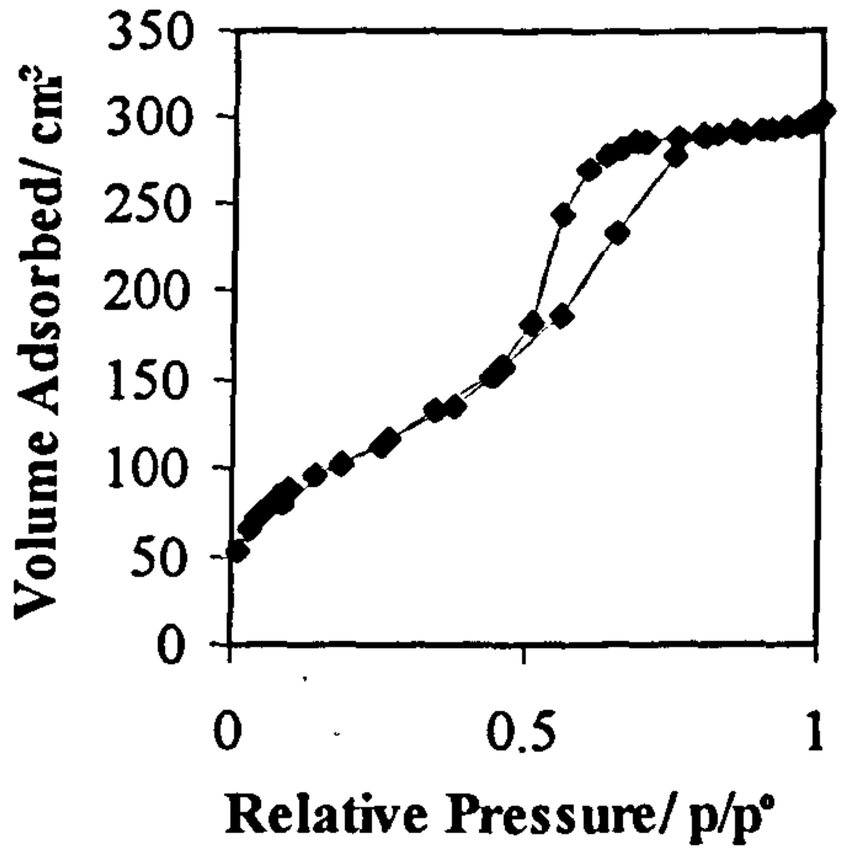

(b) α_s-plot

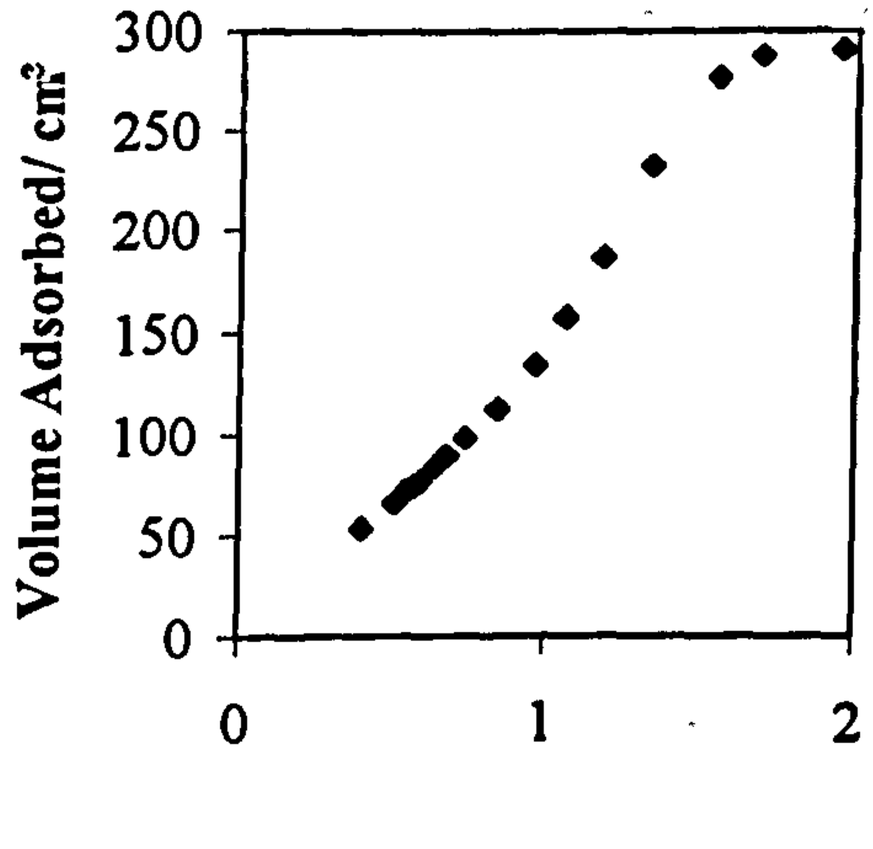

1100°C: TiO_2=6·1 weight %; HCl=0·045 mole

(a) Adsorption/Desorption Isotherm

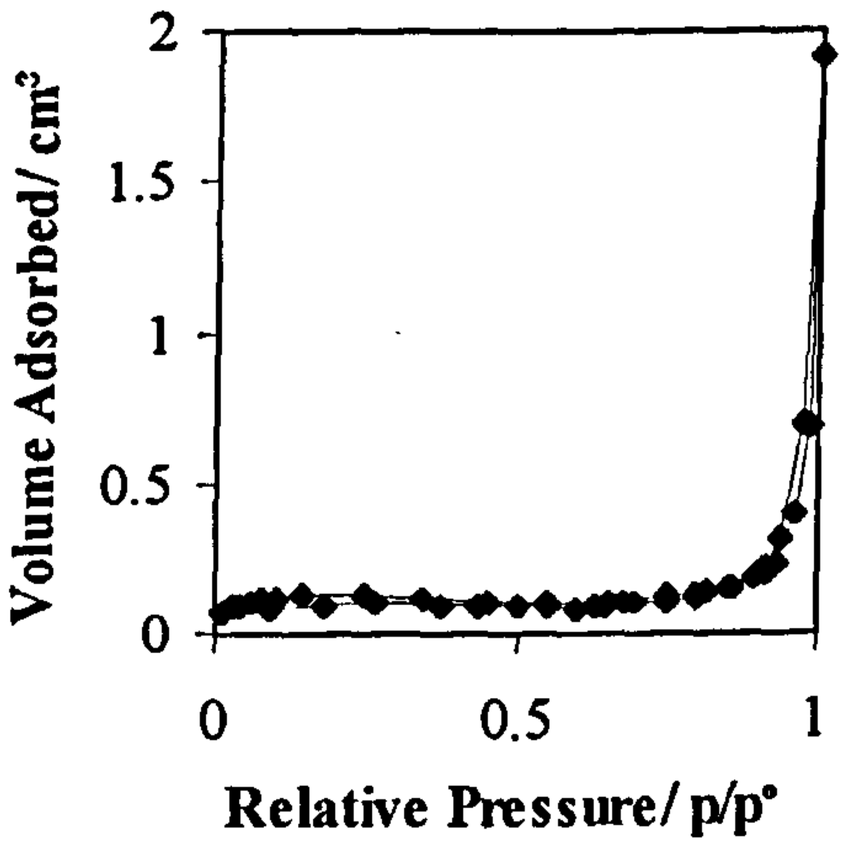

Effect of Temperature on the Pore Characteristics of a Sample Containing TiO_2=6·34 weight %; HCl=0·045 mole

		Temperature/°C						
		120	300	500	700	900	1100	1100 (Kr)
BET Surface Area (m^2g^{-1})		394	475	439	455	293	1·35	0·26
	C	65·6	99·9	79·9	74·5	67·5	44·1	88·2
BJH Pore Volume (cm^3g^{-1})	Adsorption	0·54	0·56	0·43	0·55	0·33	0·003	
	Desorption	0·57	0·60	0·50	0·58	0·37	0·003	
BJH Average Pore Diameter (Å)	Adsorption	44·6	42·2	38·7	41·8	39·9	108	
	Desorption	43·1	42·0	37·8	41·0	38·8	90	

120°C: TiO_2=6·34 weight %; HCl=0·045 mole

(a) Adsorption/Desorption Isotherm

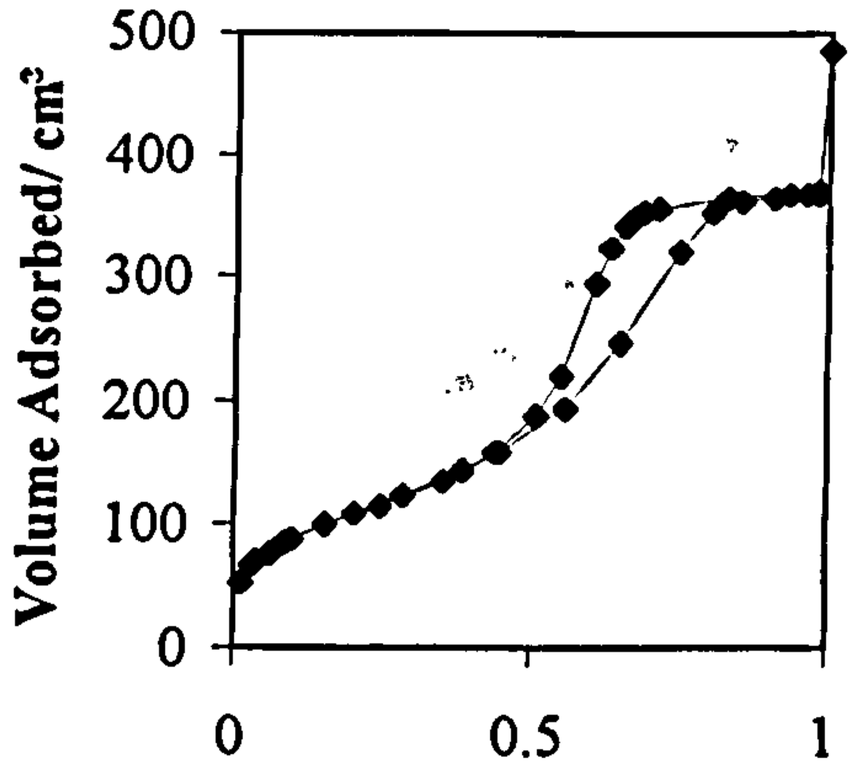

(b) α_s-plot

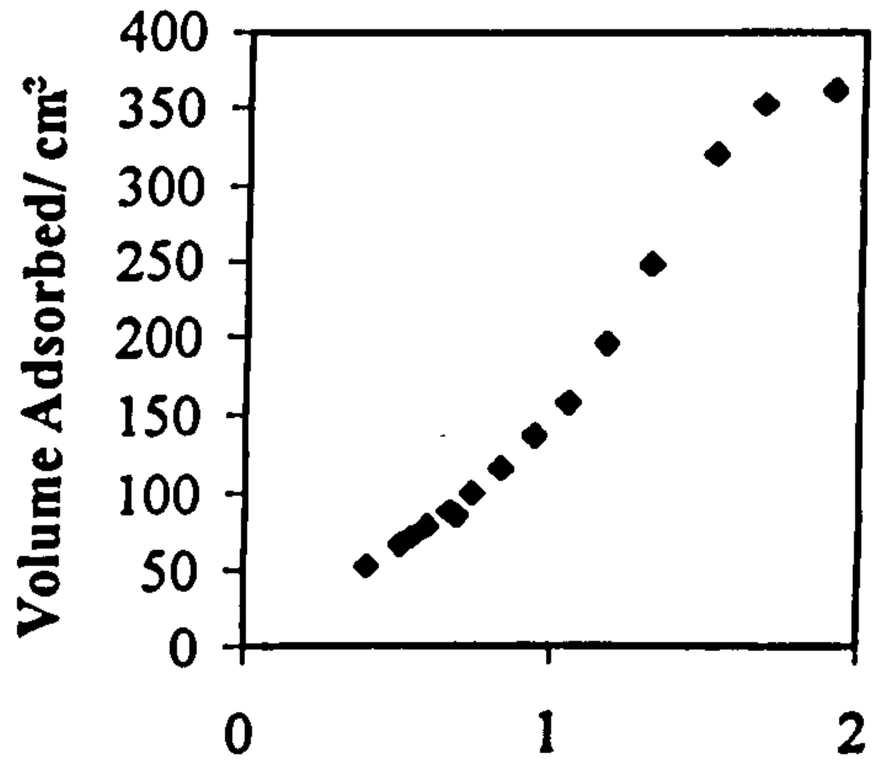

300°C: TiO_2=6·34 weight %; HCl=0·045 mole

(a) Adsorption/Desorption Isotherm

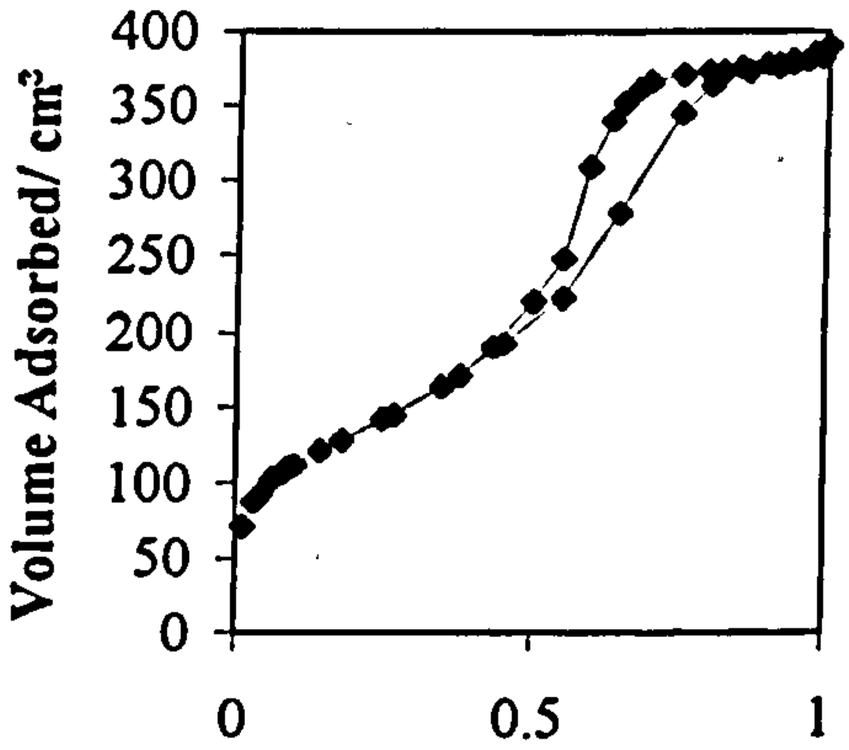

(b) α_s-plot

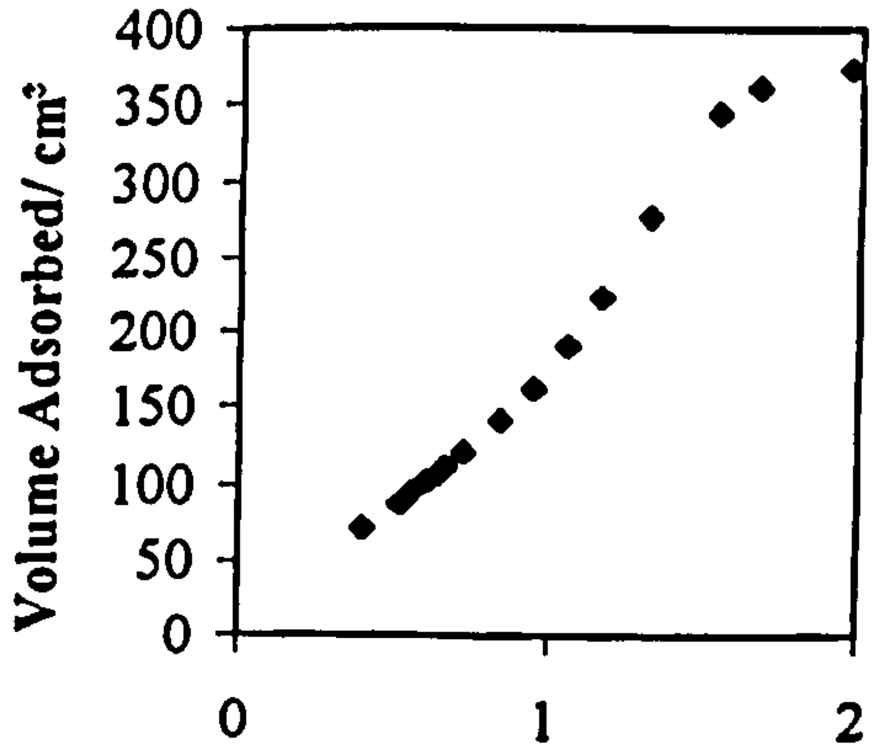

500°C: TiO_2=6·34 weight %; HCl=0·045 mole

(a) Adsorption/Desorption Isotherm

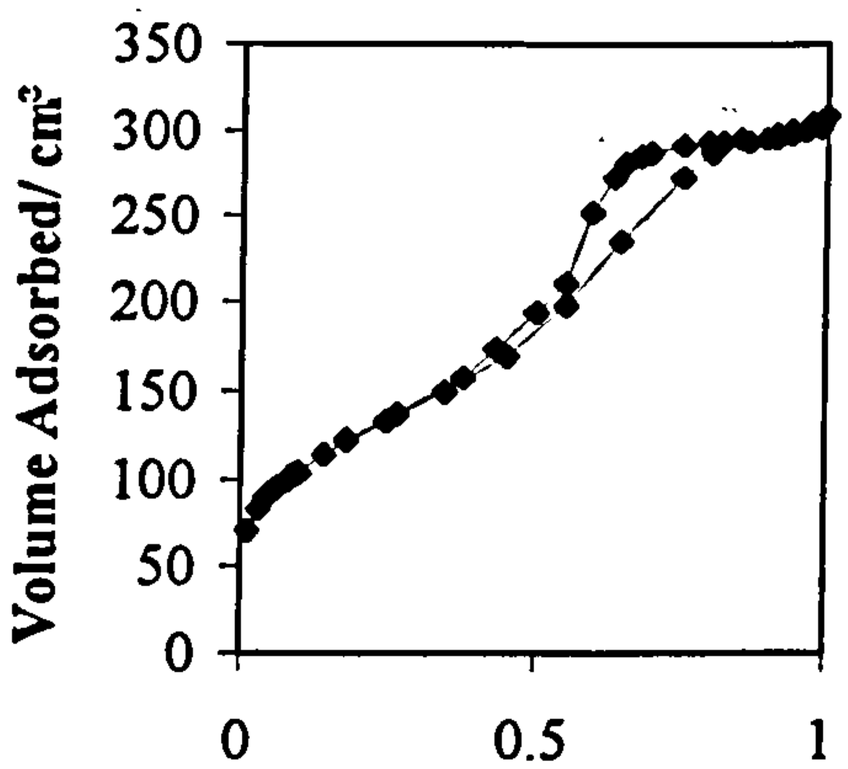

(b) α_s-plot

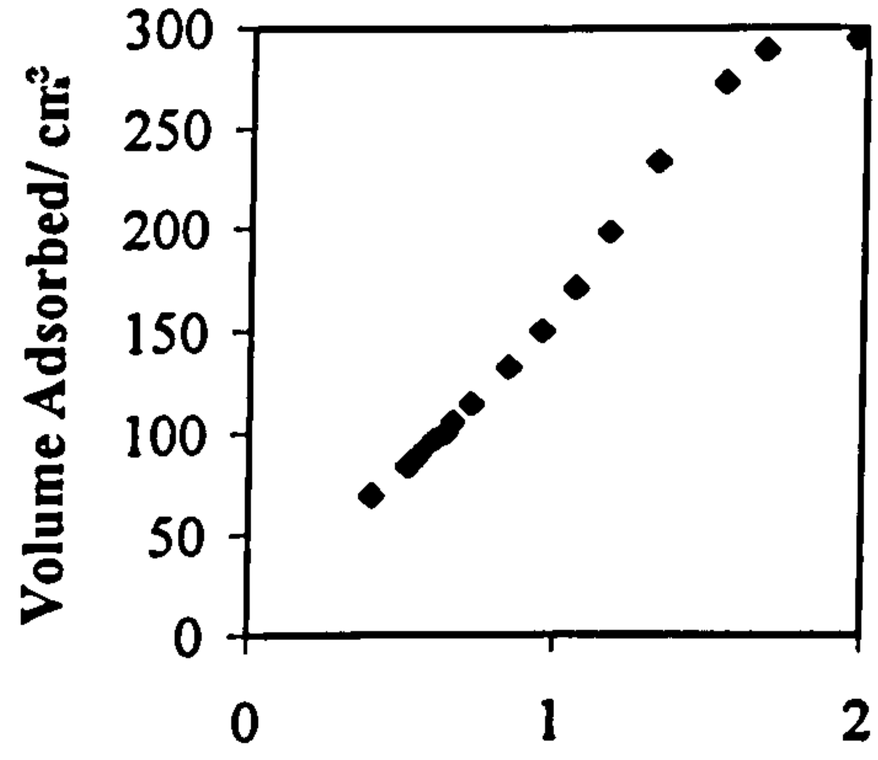

700°C: TiO_2=6·34 weight %; HCl=0·045 mole

(a) Adsorption/Desorption Isotherm

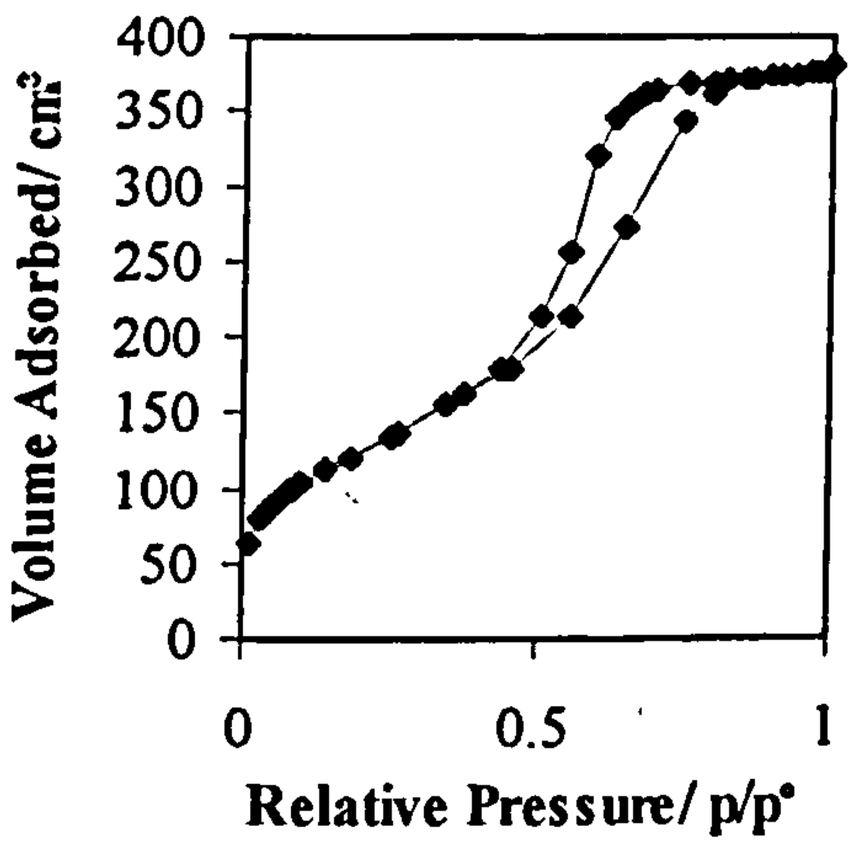

(b) α_s-plot

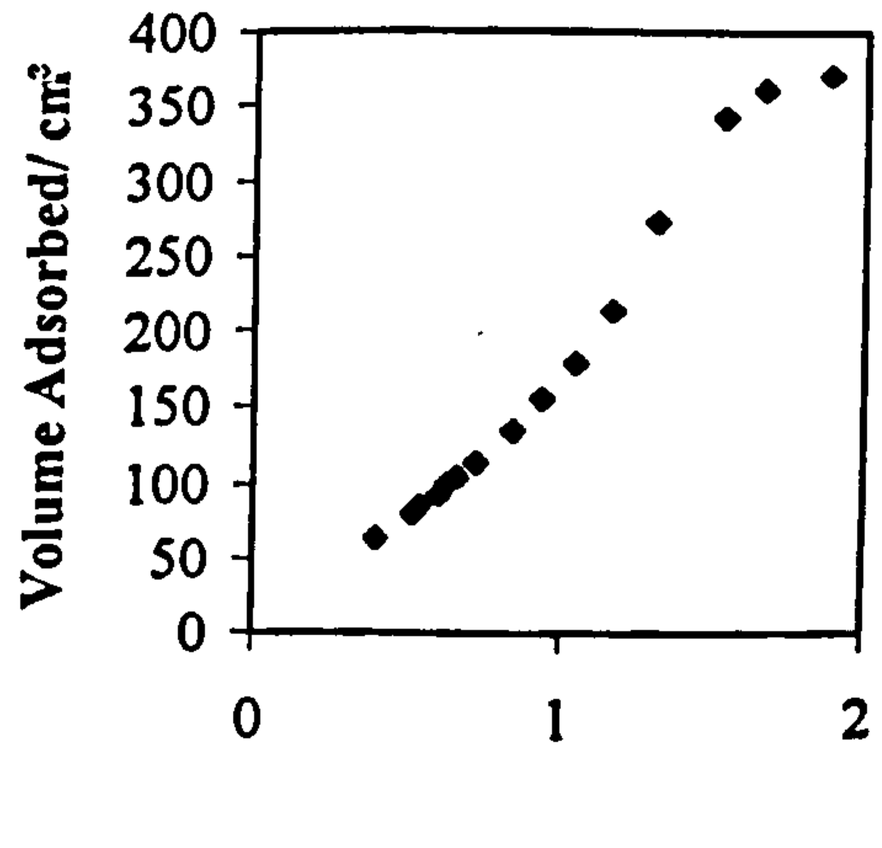

900°C: TiO_2=6·34 weight %; HCl=0·045 mole

(a) Adsorption/Desorption Isotherm

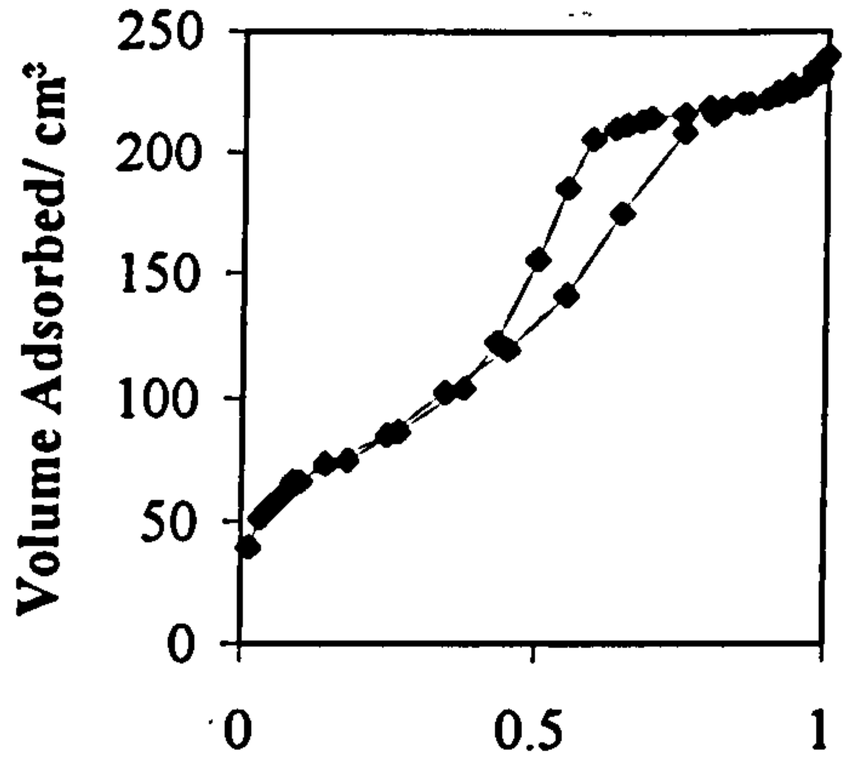

(b) α_s-plot

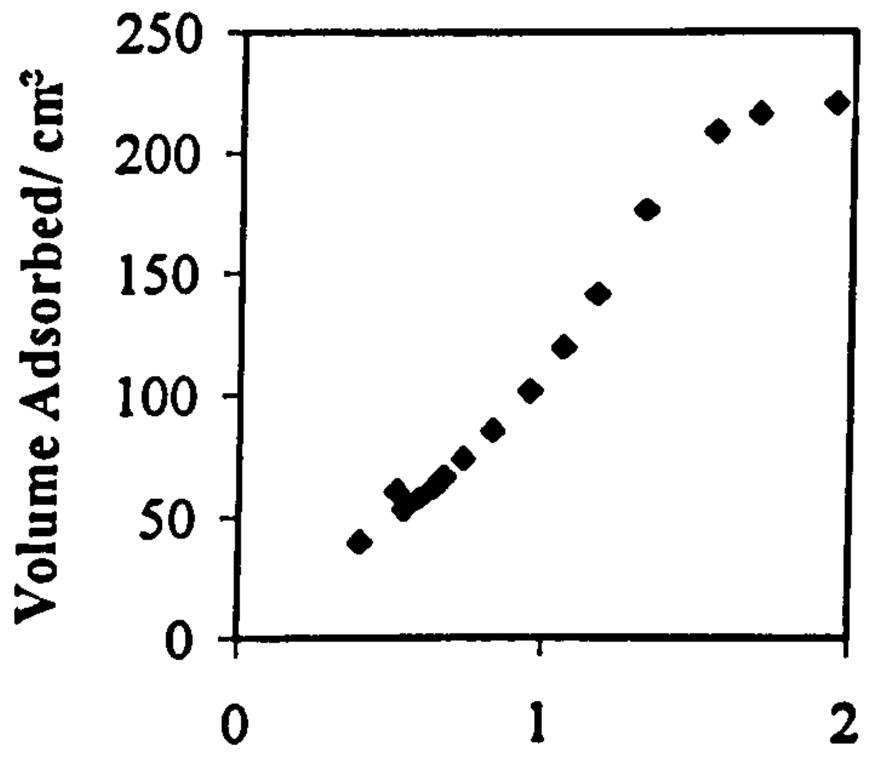

1100°C: TiO_2=6·34 weight %; HCl=0·045 mole

(a) Adsorption/Desorption Isotherm

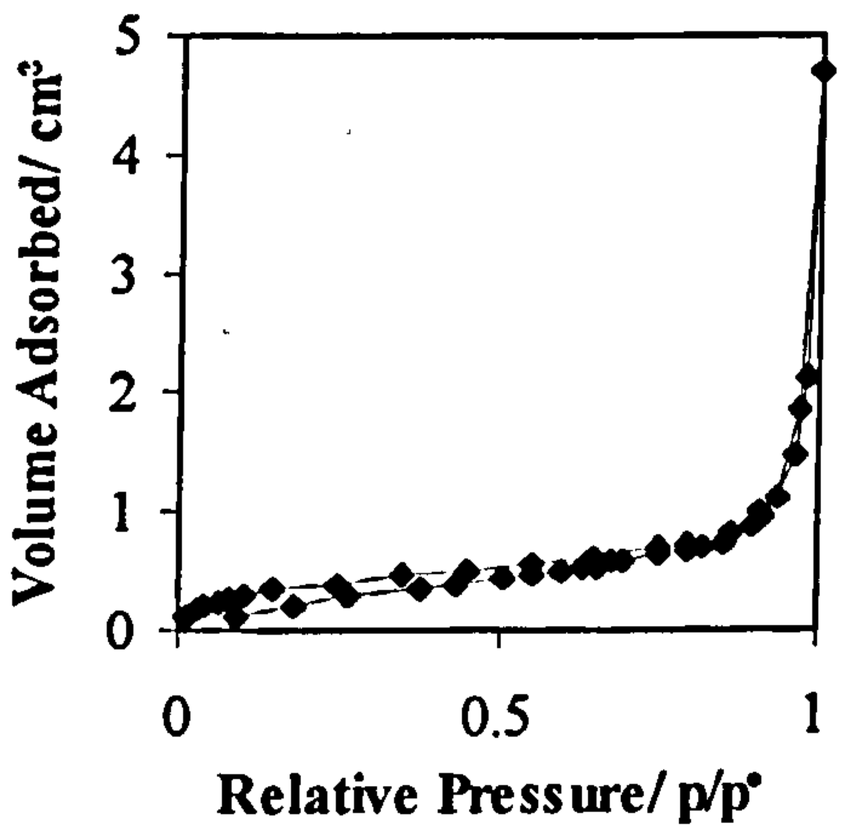

(b) α_s-plot

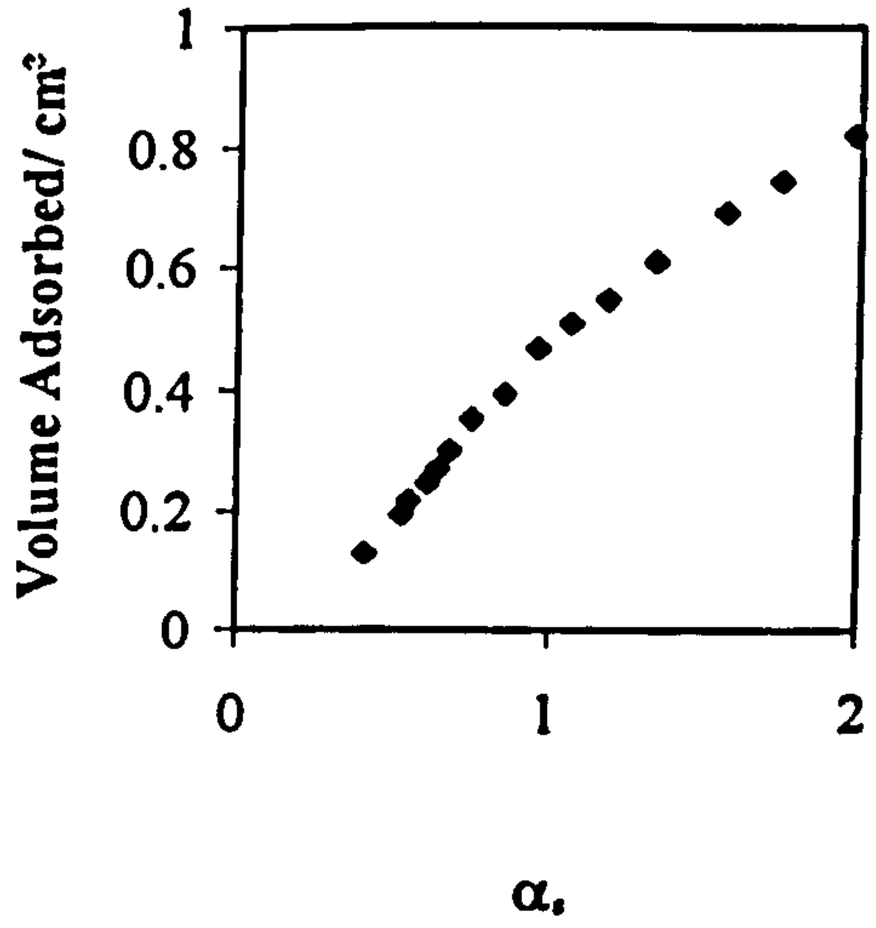

Effect of Temperature on the Pore Characteristics of a Sample Containing TiO_2=21·9 weight %; HCl=0·045 mole

		Temperature/°C						
		120	300	500	700	900	1100	1100 (Kr)
BET Surface Area (m^2g^{-1})		477	917	502	494	355	0·76	0·84
	C	60·4	106·3	93·1	77·0	69·1	114·2	59·5
BJH Pore Volume (cm^3g^{-1})	Adsorption	0·51	0·81	0·42	0·47	0·33	0·002	
	Desorption	0·55	0·97	0·47	0·51	0·36	----	
BJH Average Pore Diameter (Å)	Adsorption	43·7	43·9	34·5	40·7	39·0	499	
	Desorption	43·2	43·3	36·2	40·6	37·9	----	

120°C: TiO_2=21·9 weight %; HCl=0·045 mole

(a) Adsorption/Desorption Isotherm

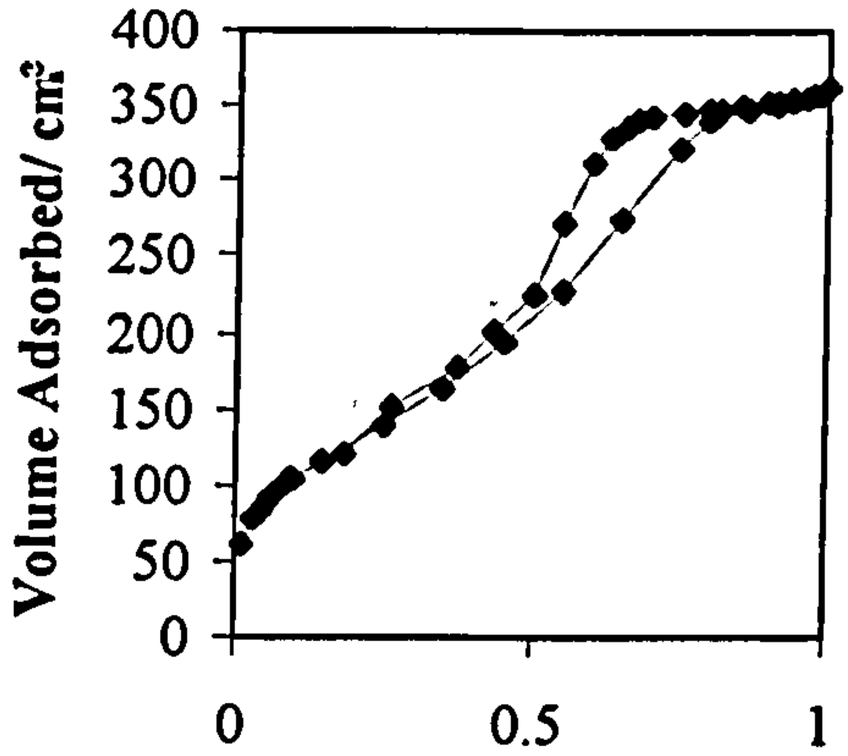

(b) α_s-plot

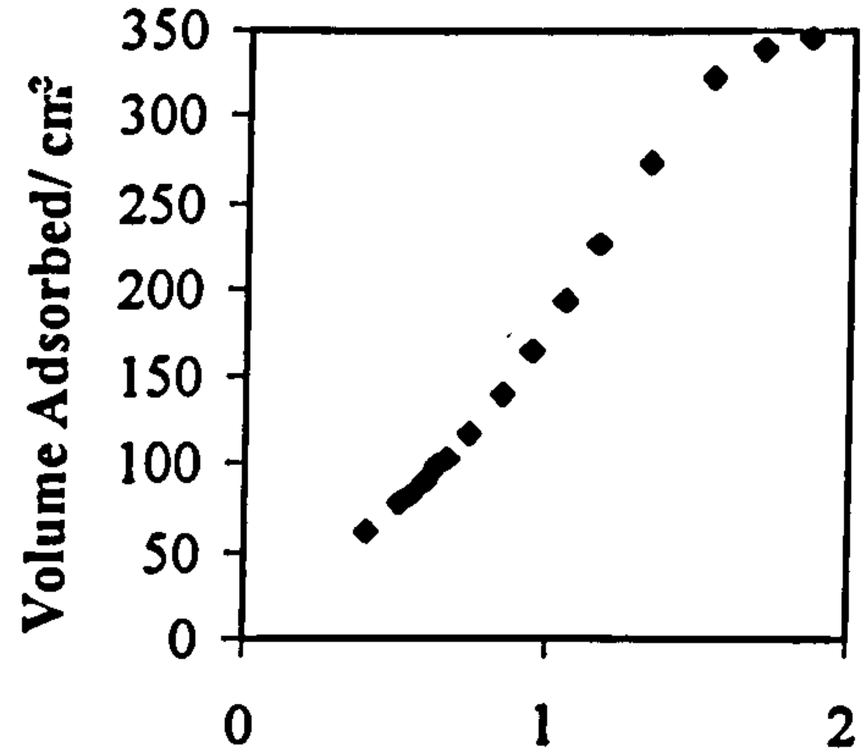

300°C: TiO_2=21·9 weight %; HCl=0·045 mole

(a) Adsorption/Desorption Isotherm

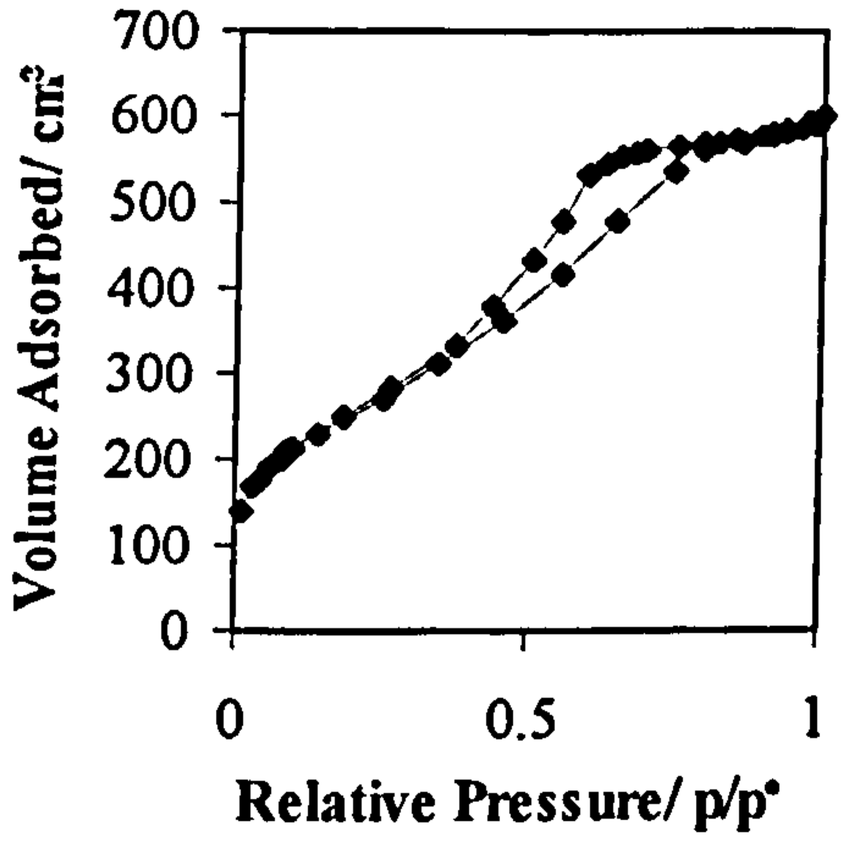

(b) α_s-plot

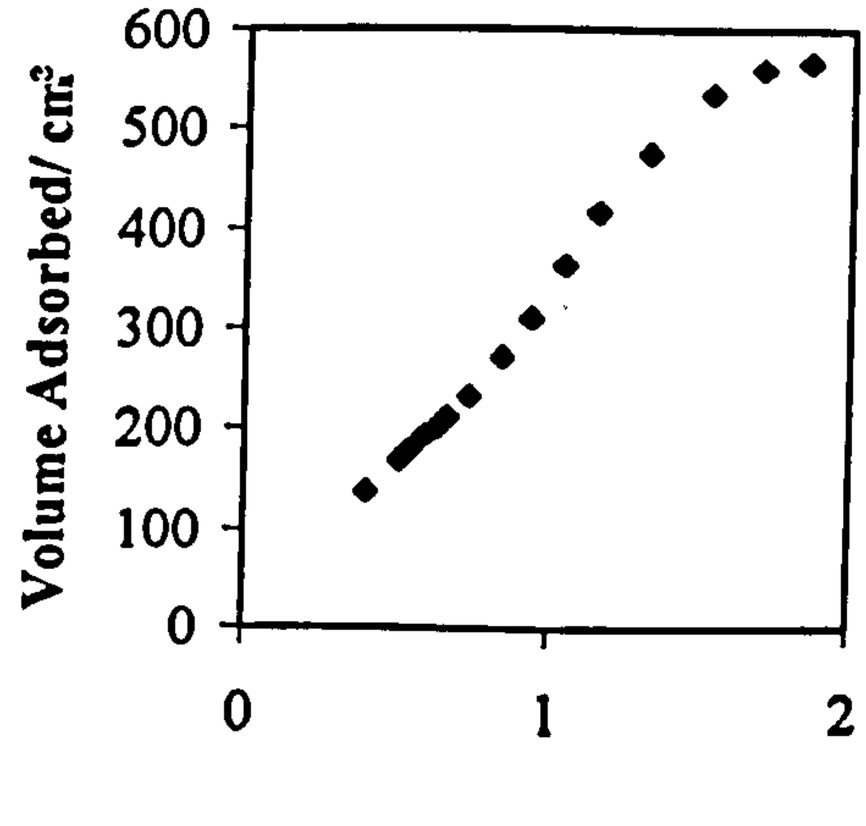

500°C: TiO_2=21·9 weight %; HCl=0·045 mole

(a) Adsorption/Desorption Isotherm

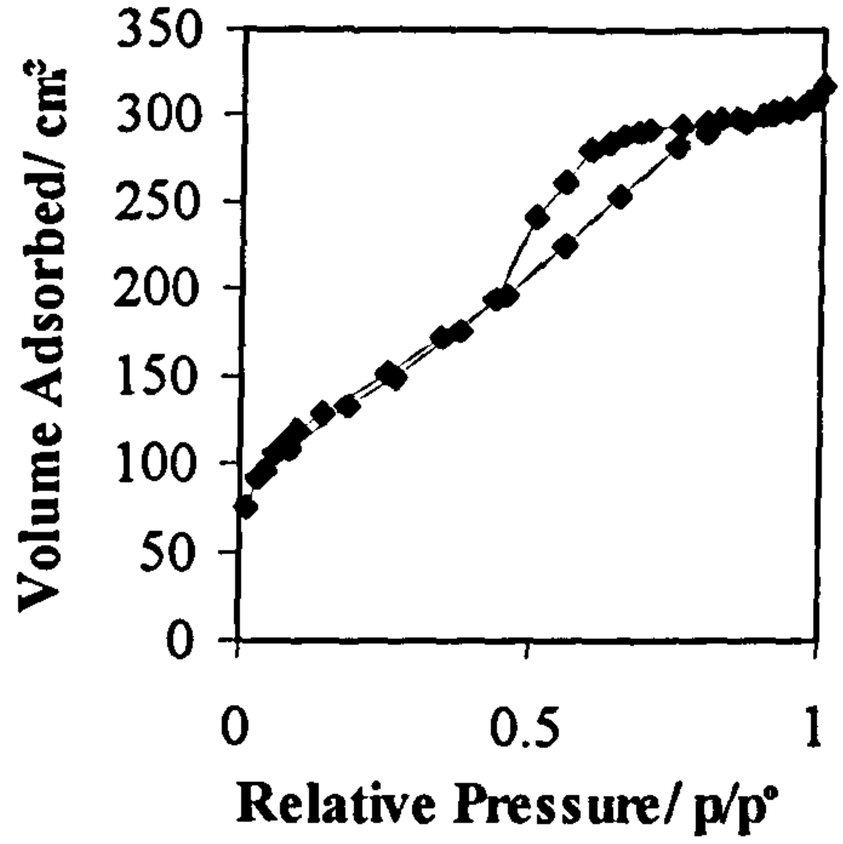

(b) α_s-plot

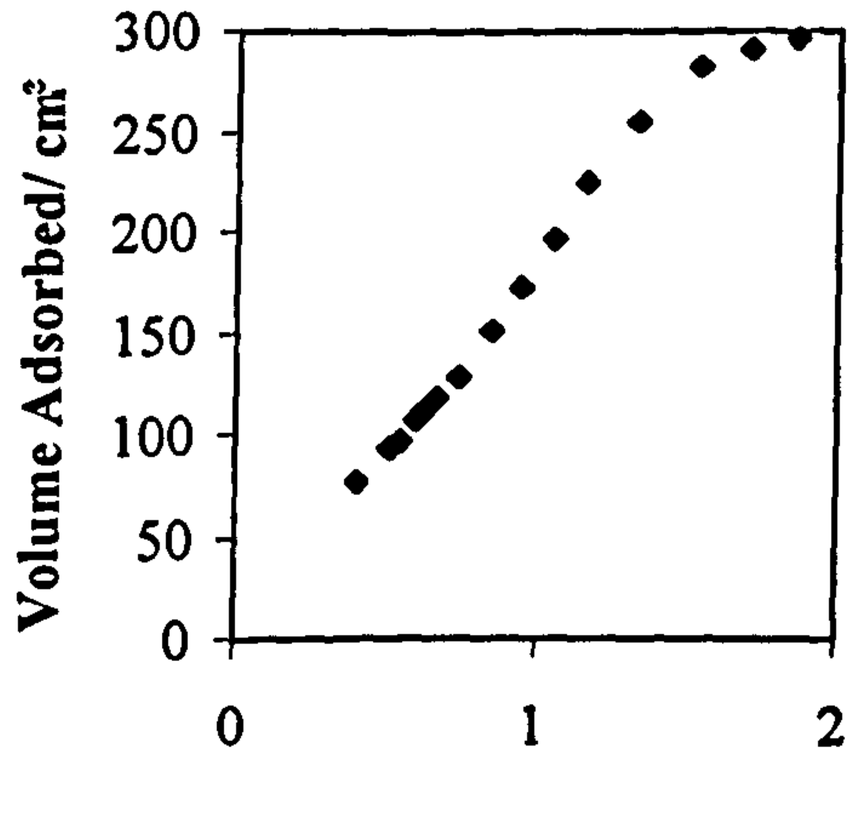

700°C: TiO_2=21·9 weight %; HCl=0·045 mole

(a) Adsorption/Desorption Isotherm

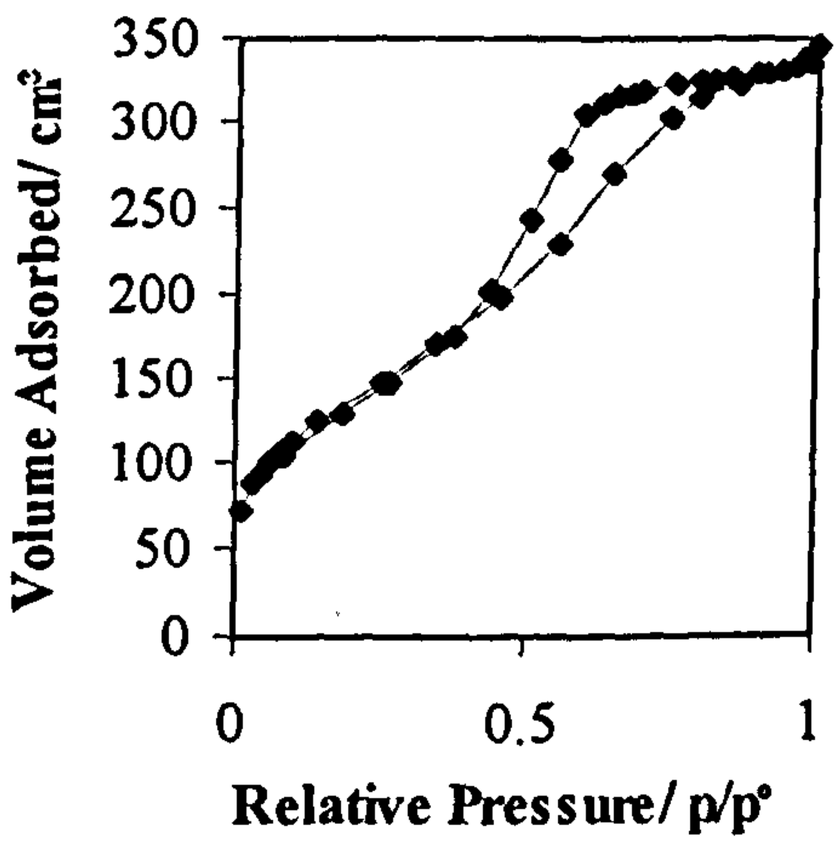

(b) α_s-plot

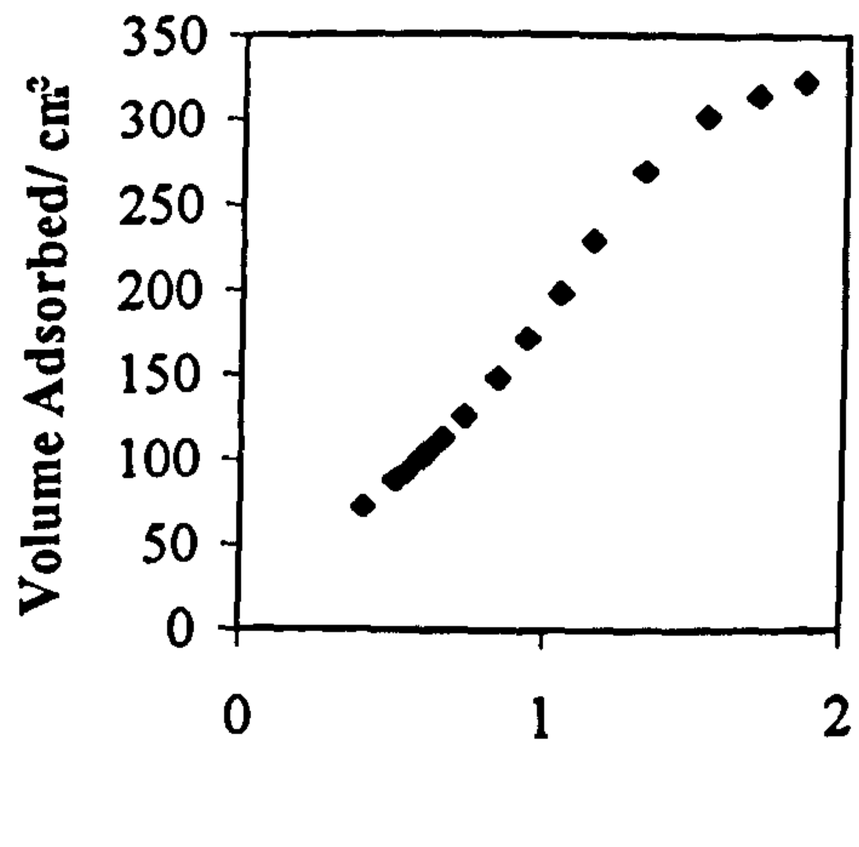

900°C: TiO_2=21·9 weight %; HCl=0·045 mole

(a) Adsorption/Desorption Isotherm

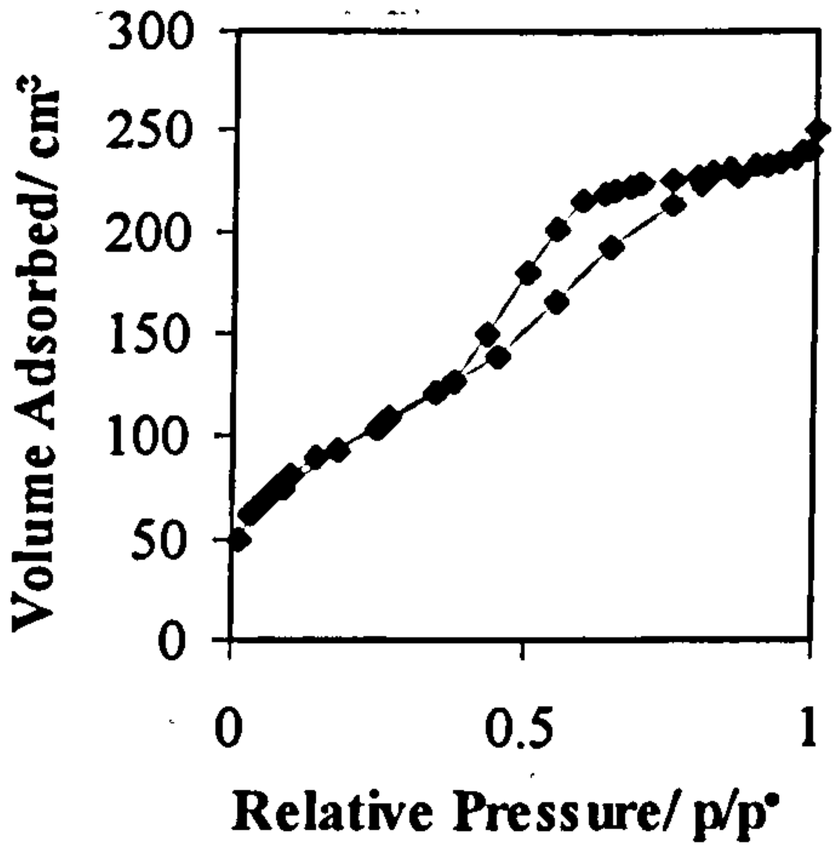

(b) α_s-plot

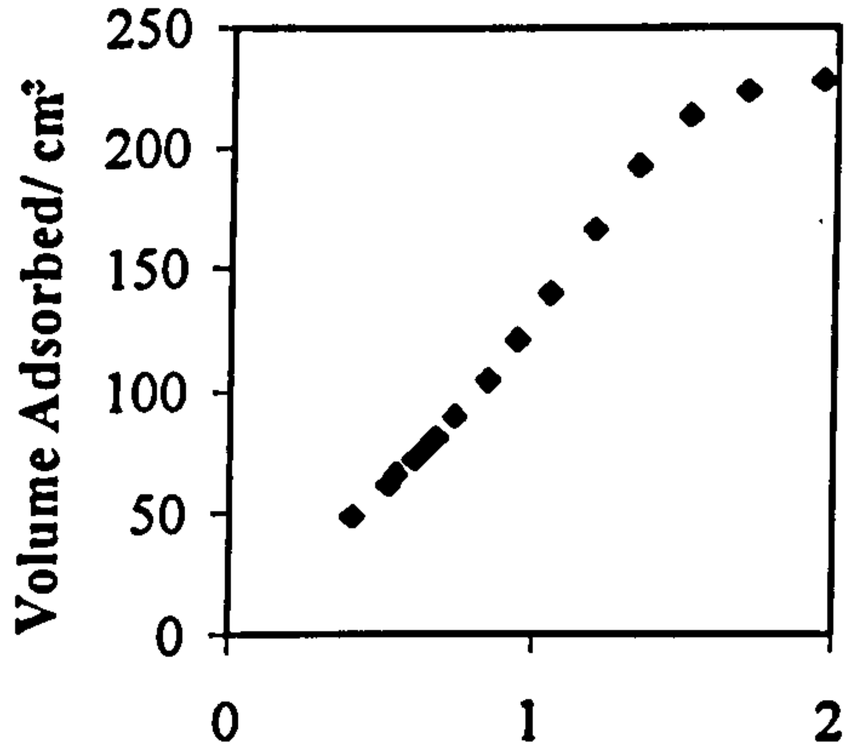

1100°C: TiO_2=21·9 weight %; HCl=0·045 mole

(a) Adsorption/Desorption Isotherm

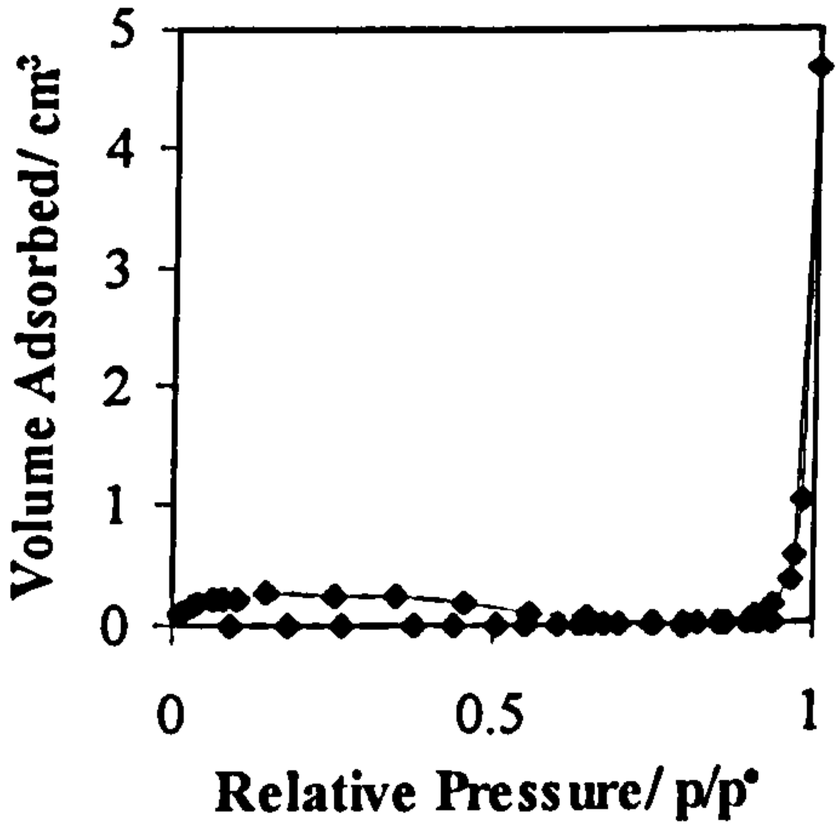

Effect of Temperature on the Pore Characteristics of a Sample Containing TiO_2=6·34 weight %; HCl=0·030 mole

		Temperature/°C						
		120	300	500	700	900	1100	1100 (Kr)
BET Surface Area (m^2g^{-1})		434	512	484	493	344	0·88	0·88
	C	60·4	106·2	93·0	77·0	69·1	114·2	30·9
BJH Pore Volume (cm^3g^{-1})	Adsorption	0·53	0·59	0·50	0·54	0·37	0·002	
	Desorption	0·57	0·63	0·55	0·58	0·41	0·002	
BJH Average Pore Diameter (Å)	Adsorption	40·6	41·5	38·5	39·1	39·1	163·7	
	Desorption	39·9	40·4	38·2	38·6	37·5	116·6	

120°C: TiO_2=6·34 weight %; HCl=0·030 mole

(a) Adsorption/Desorption Isotherm

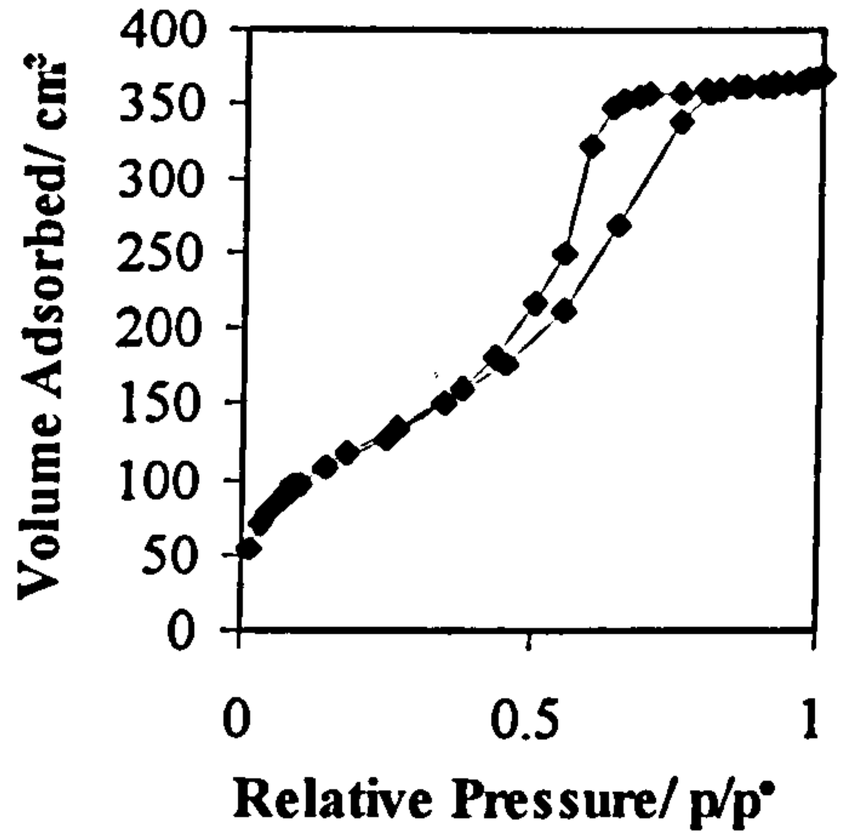

(b) α_s-plot

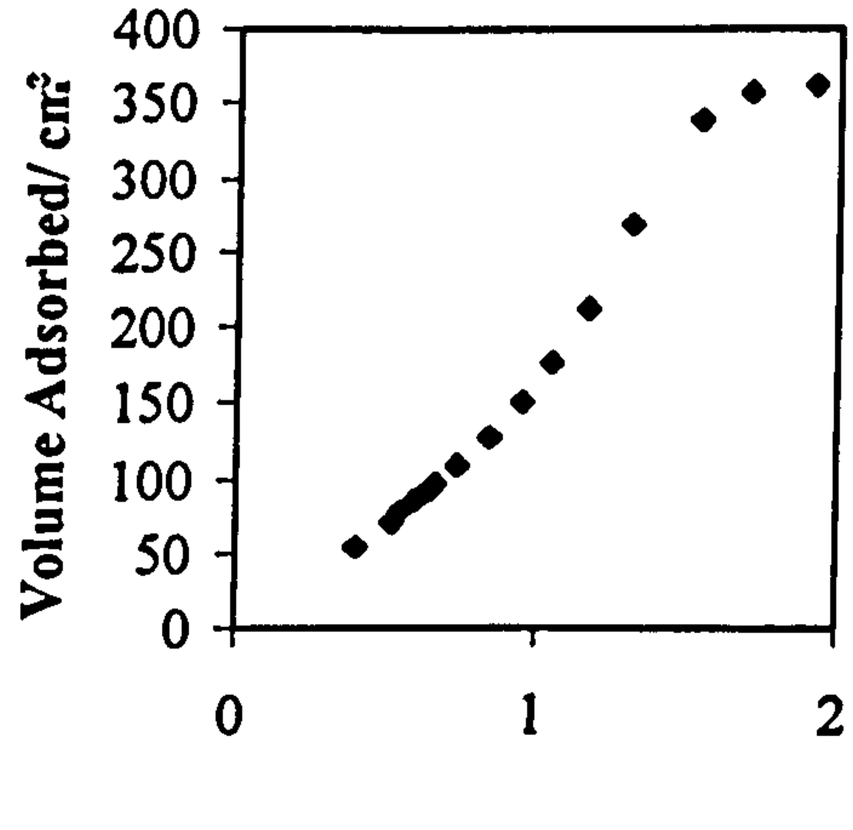

300°C: TiO_2=6·34 weight %; HCl=0·030 mole

(a) Adsorption/Desorption Isotherm

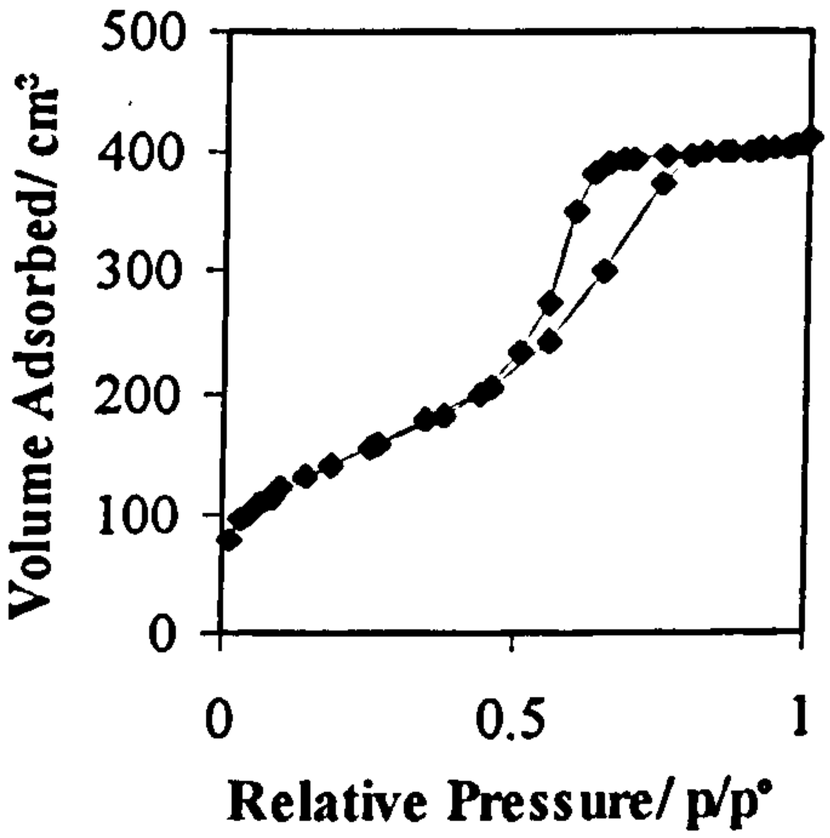

(b) α_s-plot

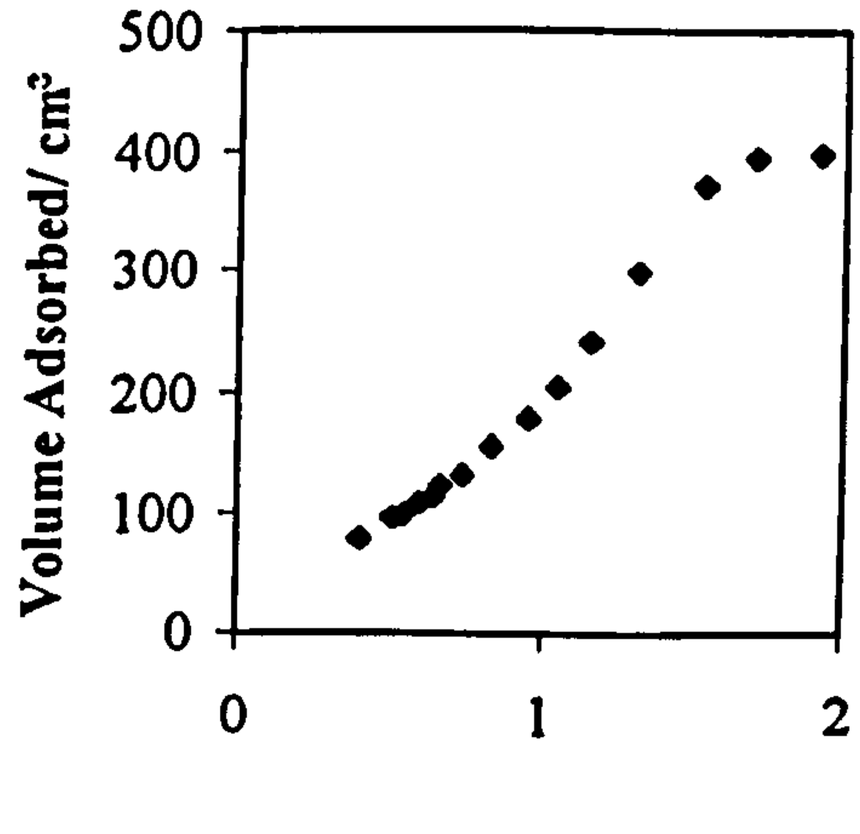

500°C: TiO_2=6·34 weight %; HCl=0·030 mole

(a) Adsorption/Desorption Isotherm

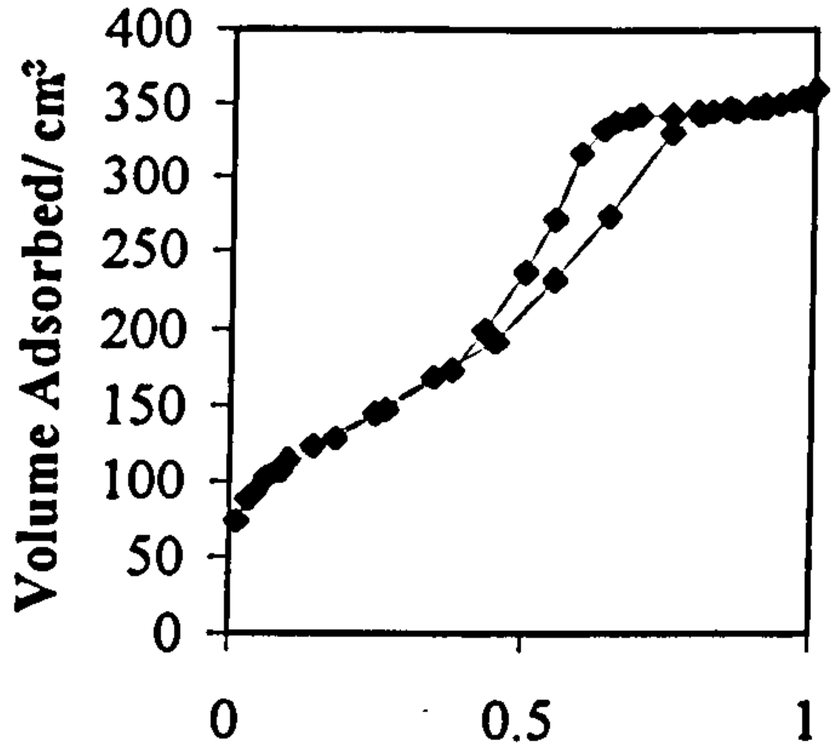

(b) α_s-plot

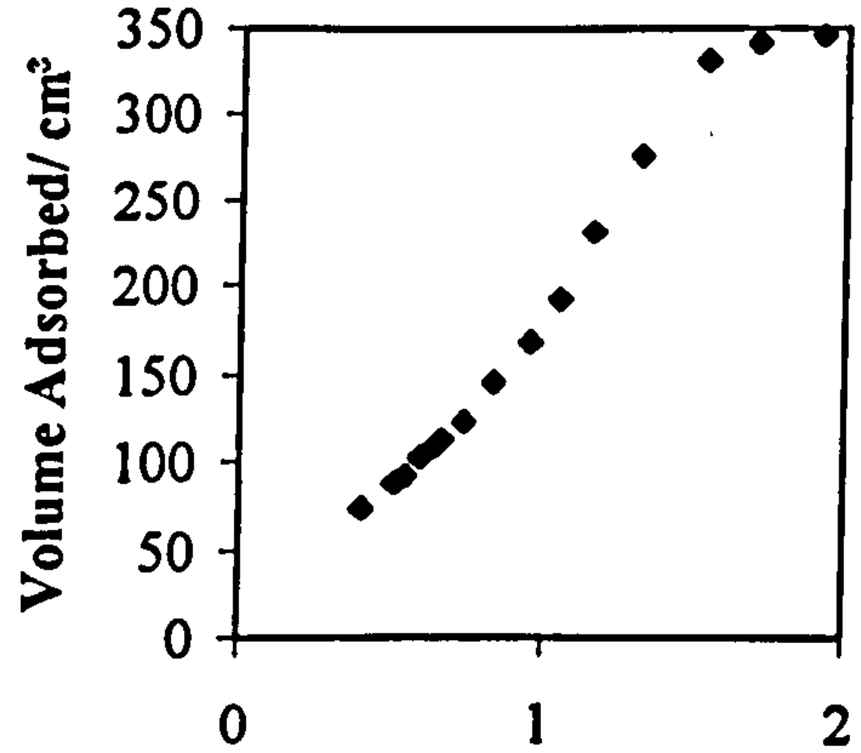

700°C: TiO_2=6·34 weight %; HCl=0·030 mole

(a) Adsorption/Desorption Isotherm

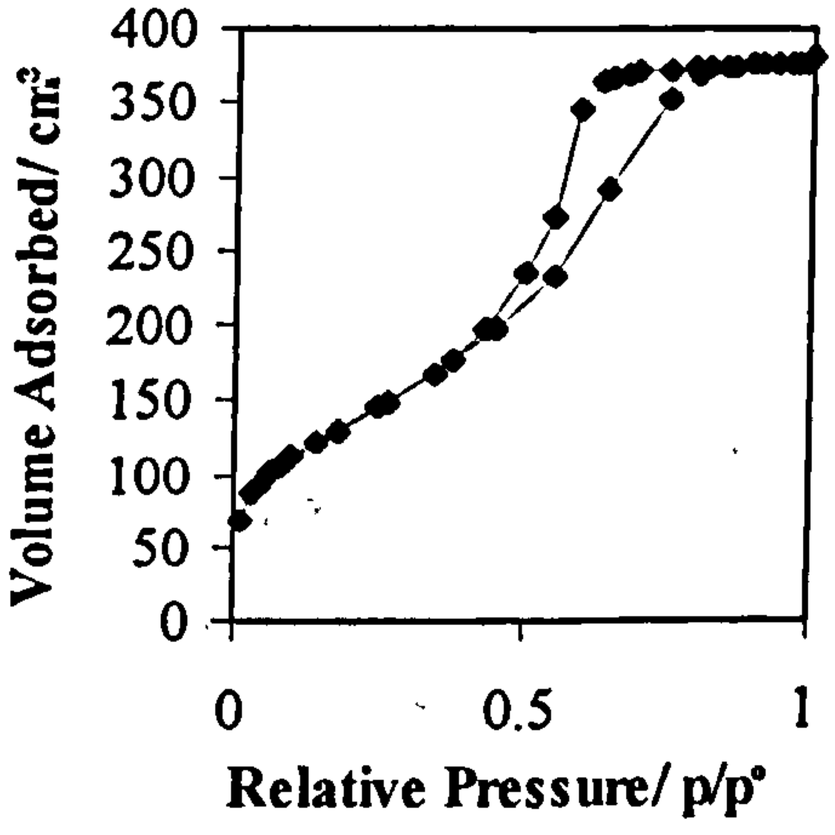

(b) α_s-plot

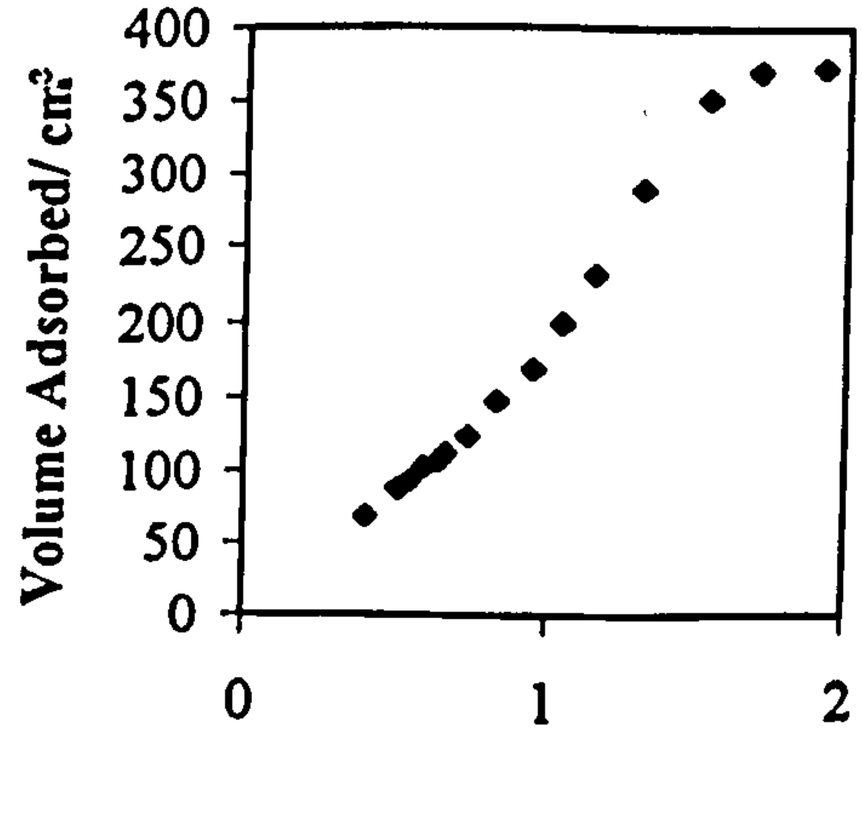

900°C: TiO_2=6·34 weight %; HCl=0·030 mole

(a) Adsorption/Desorption Isotherm

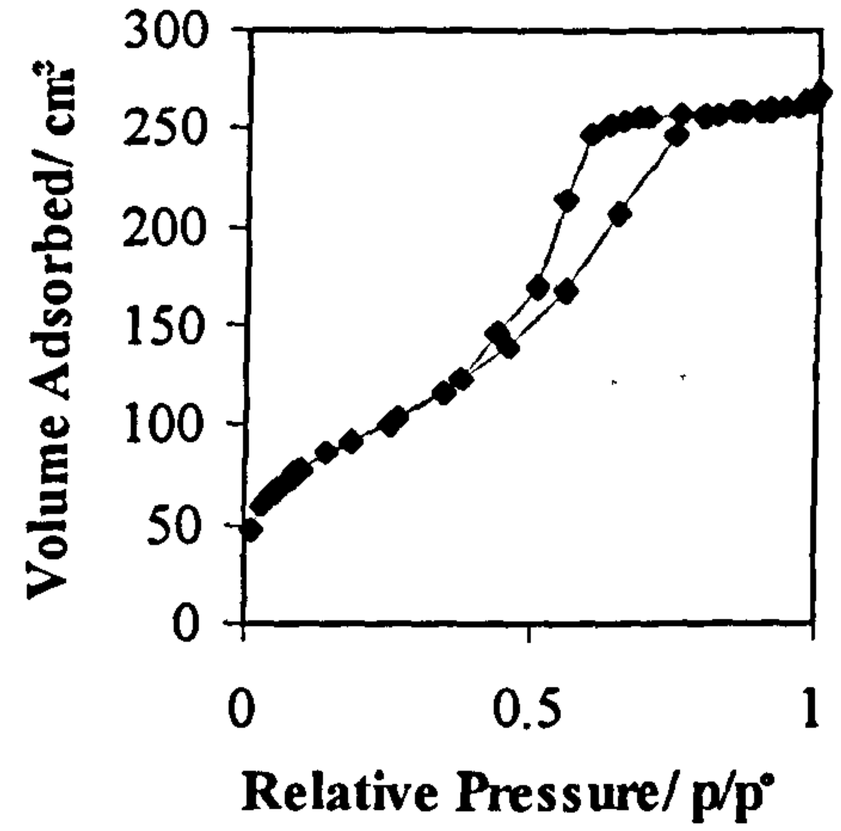

(b) α_s-plot

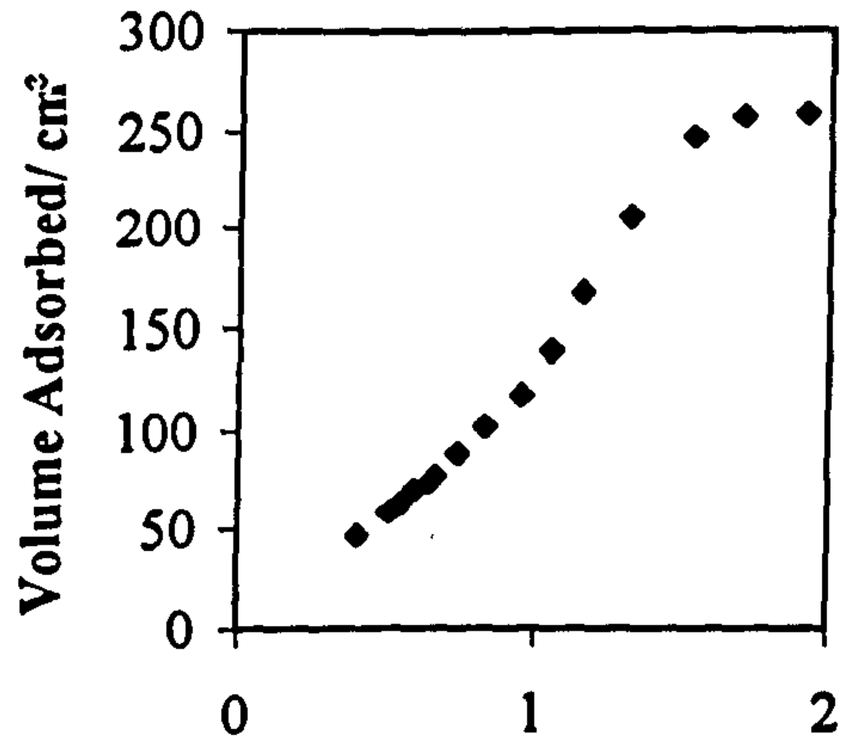

1100°C: TiO_2=6·34 weight %; HCl=0·030 mole

(a) Adsorption/Desorption Isotherm

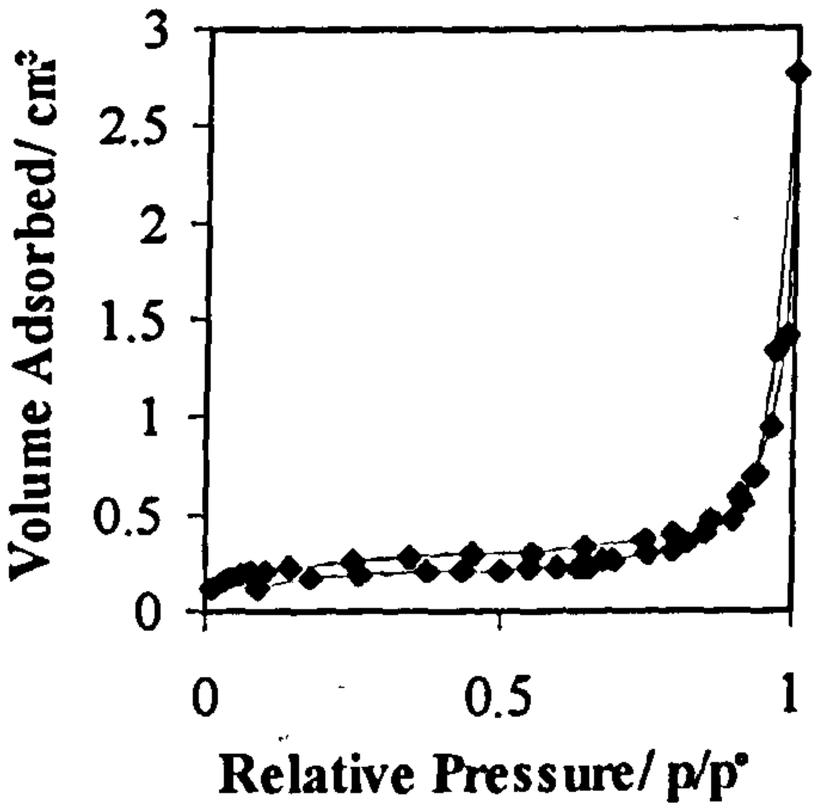

(b) α_s-plot

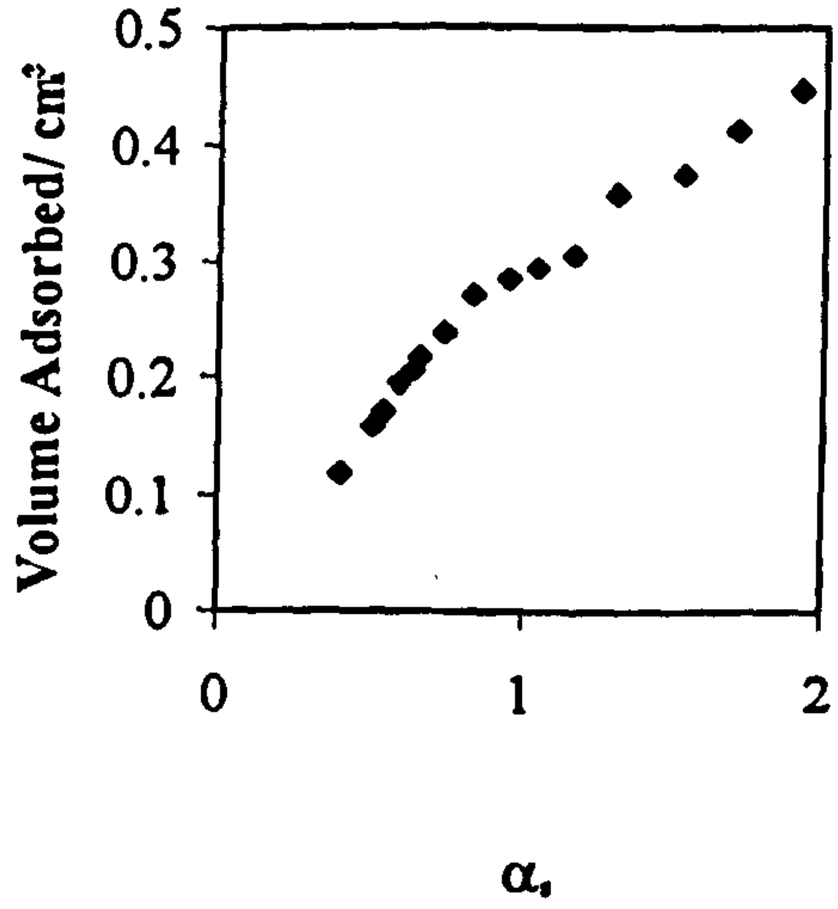

Effect of Temperature on the Pore Characteristics of a Monolith Containing TiO_2=6·34 weight %; HCl=0·045 mole*

300°C: TiO_2=6·34 weight %; HCl=0·045 mole

(a) Adsorption/Desorption Isotherm

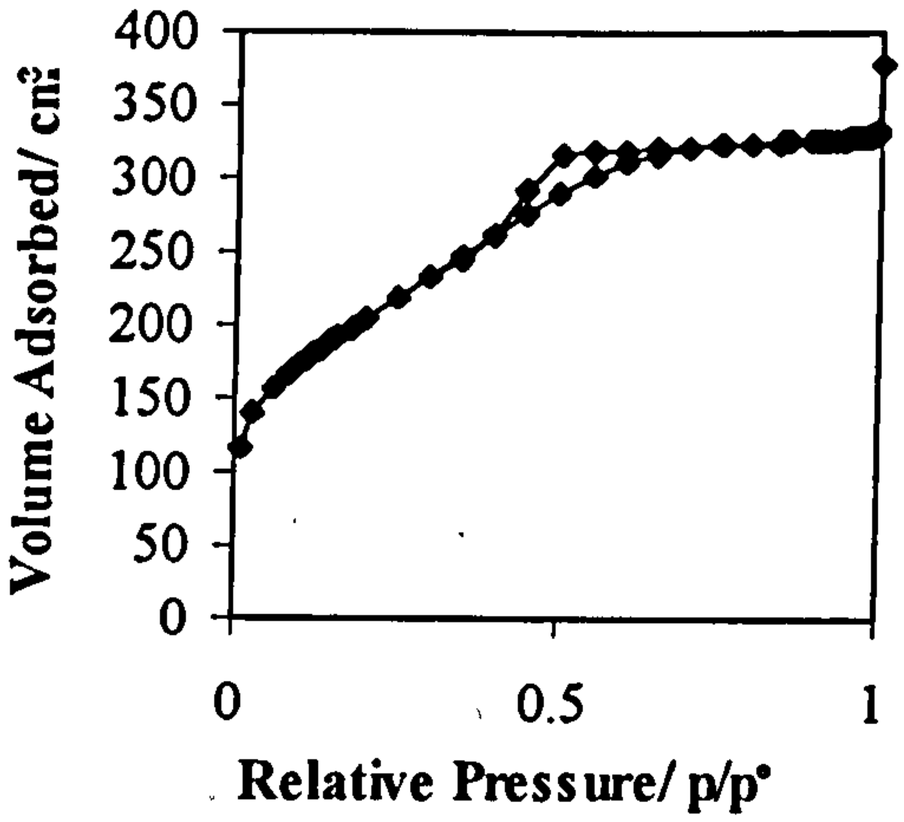

(b) α_s-plot

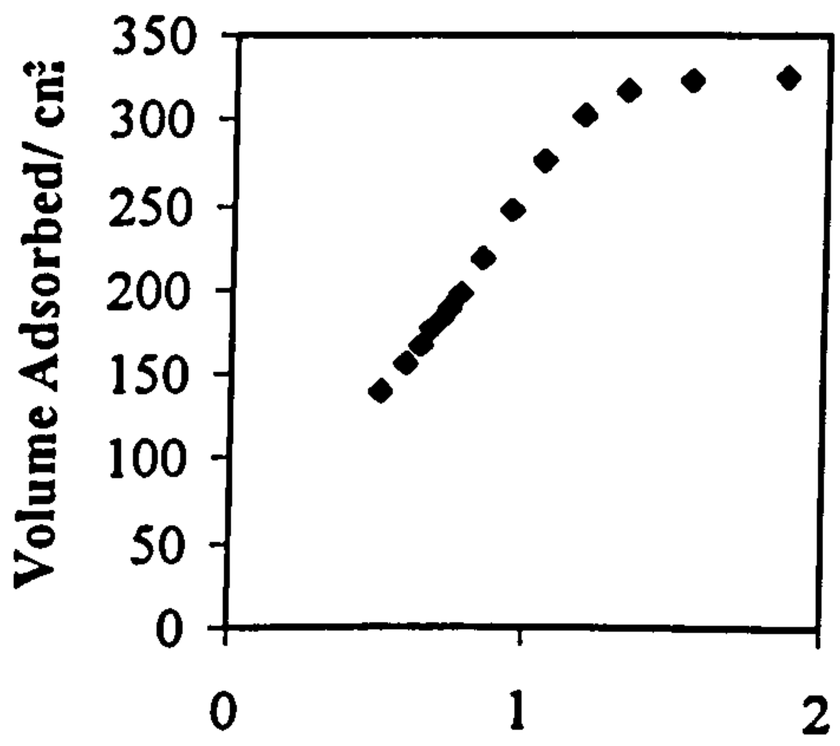

500°C: TiO_2=6·34 weight %; HCl=0·045 mole

(a) Adsorption/Desorption Isotherm

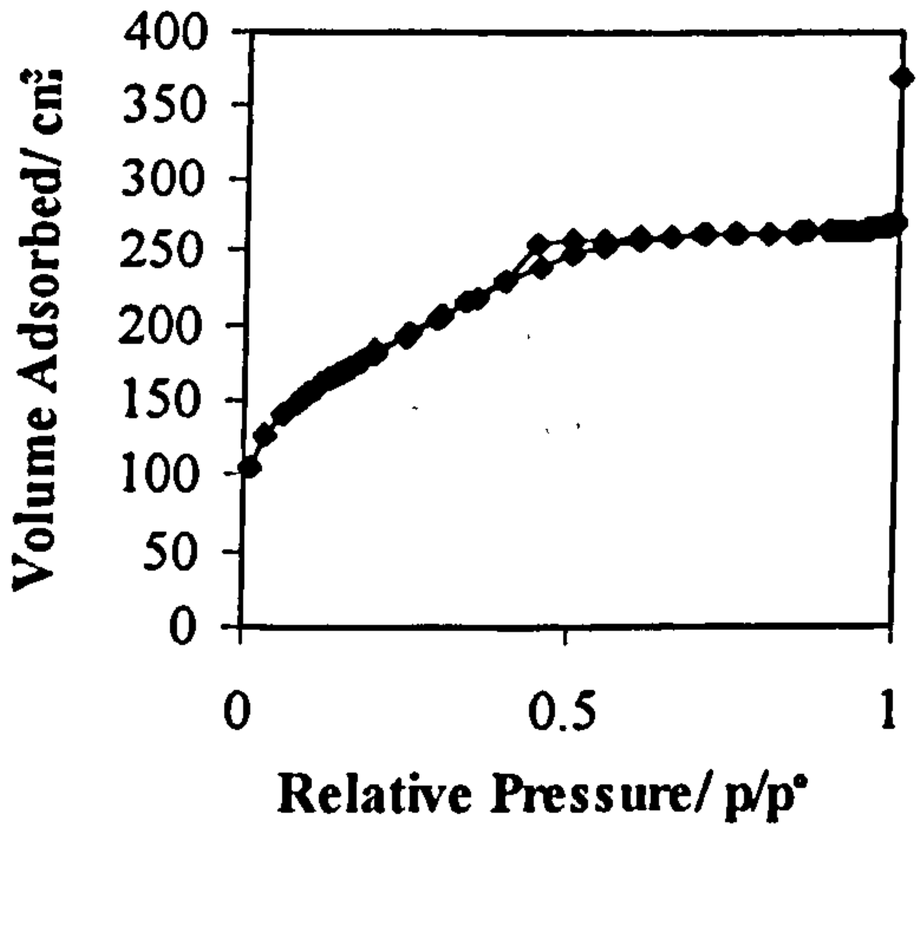

(b) α_s-plot

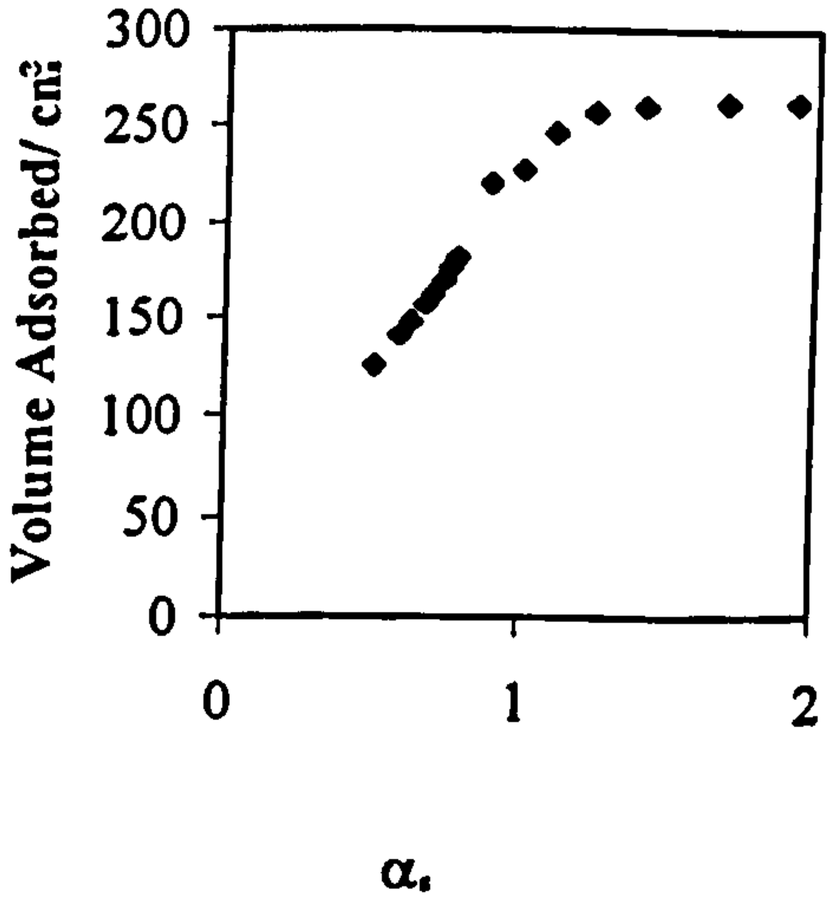

* Isotherm for the monolithic gel containing TiO_2=6·34 wt% at 120°C can be found with the isotherms for the effect of varying the amount of acid used for the hydrolysis reaction.

700°C: TiO_2=6·34 weight %; HCl=0·045 mole

(a) Adsorption/Desorption Isotherm

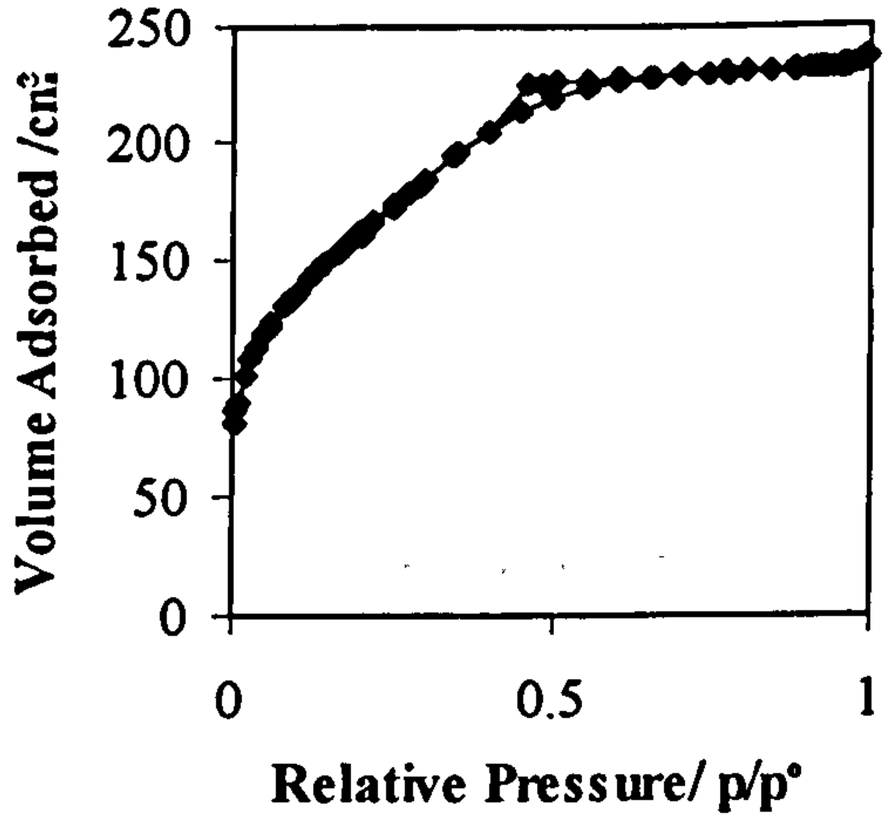

(b) α_s-plot

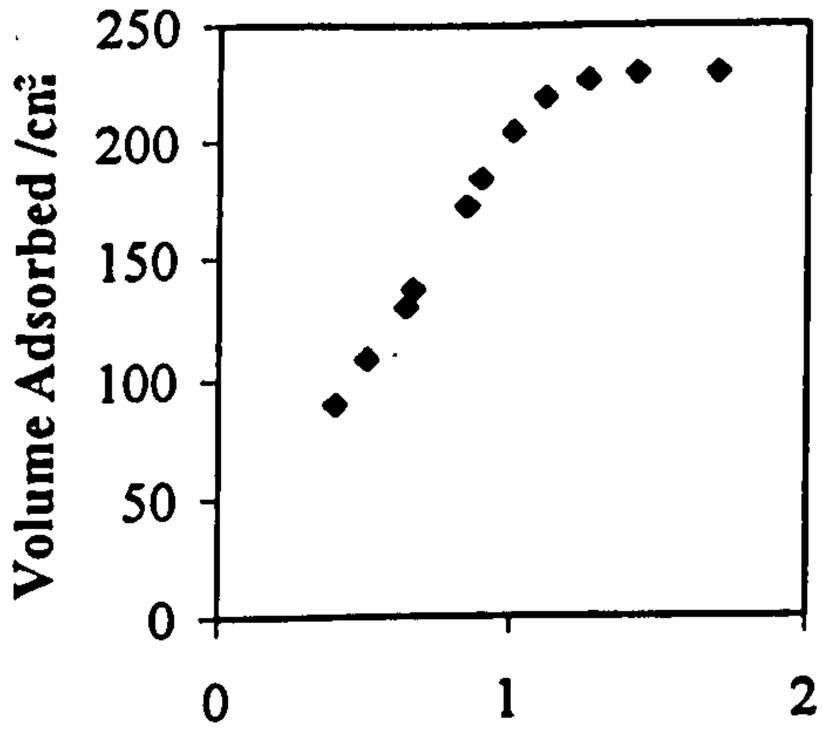

900°C: TiO_2=6·34 weight %; HCl=0·045 mole

(a) Adsorption/Desorption Isotherm

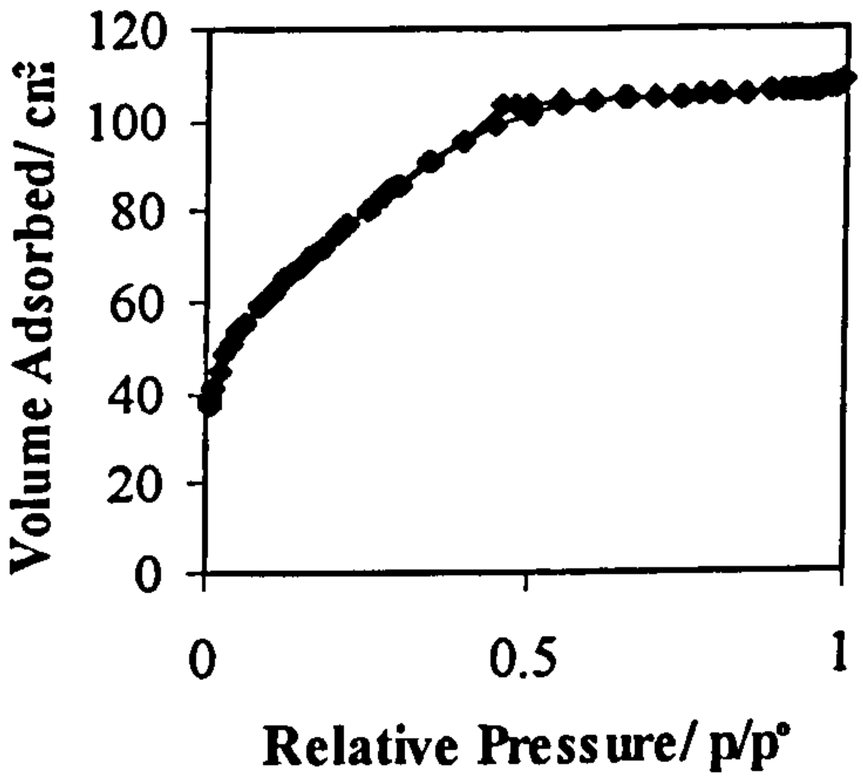

(b) α_s-plot

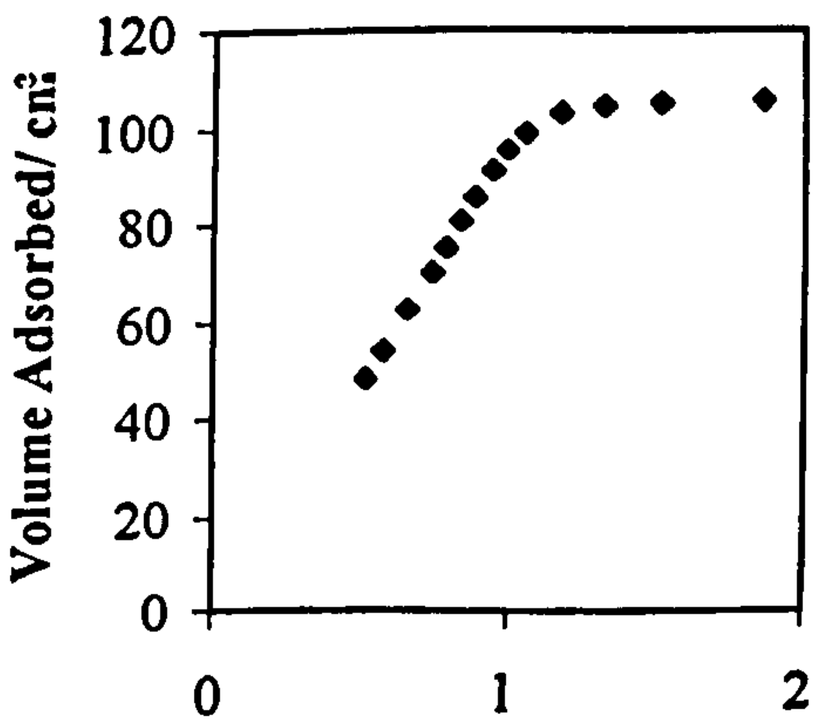

1100°C: TiO_2=6·34 weight %; HCl=0·045 mole

(a) Adsorption/Desorption Isotherm

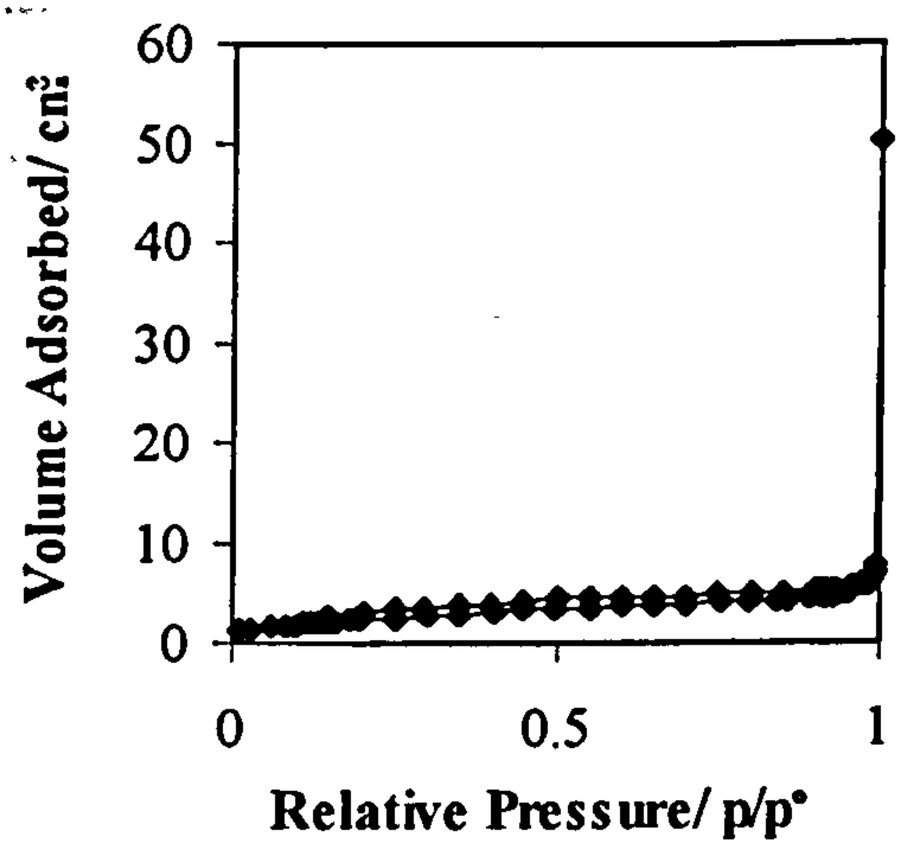

(b) α_s-plot

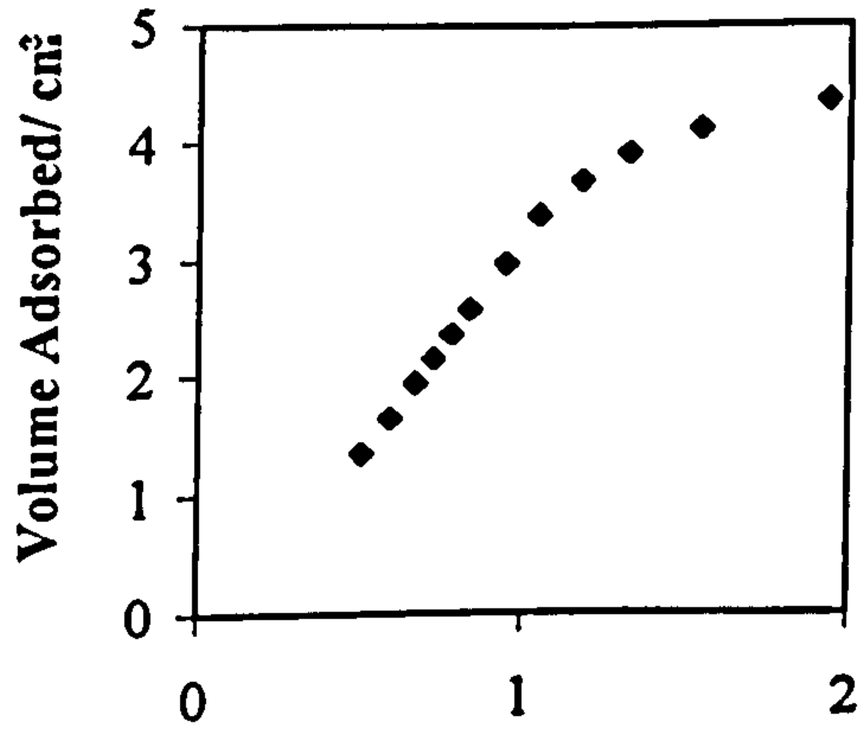

Appendix II: Mixed SiO_2-TiO_2 Gels Prepared from a Double Alkoxide Precursor

Mid-Infrared Spectra of Samples Treated at Different Temperatures

Mid-infrared Spectra of a Sample Nominally Containing 6·34 weight % Titania, HCl=0·045 mole Treated at Different Temperatures. (a) 120°C; (b) 300°C; (c) 500°C; (d) 700°C; (e) 900°C; (f) 1100°C.

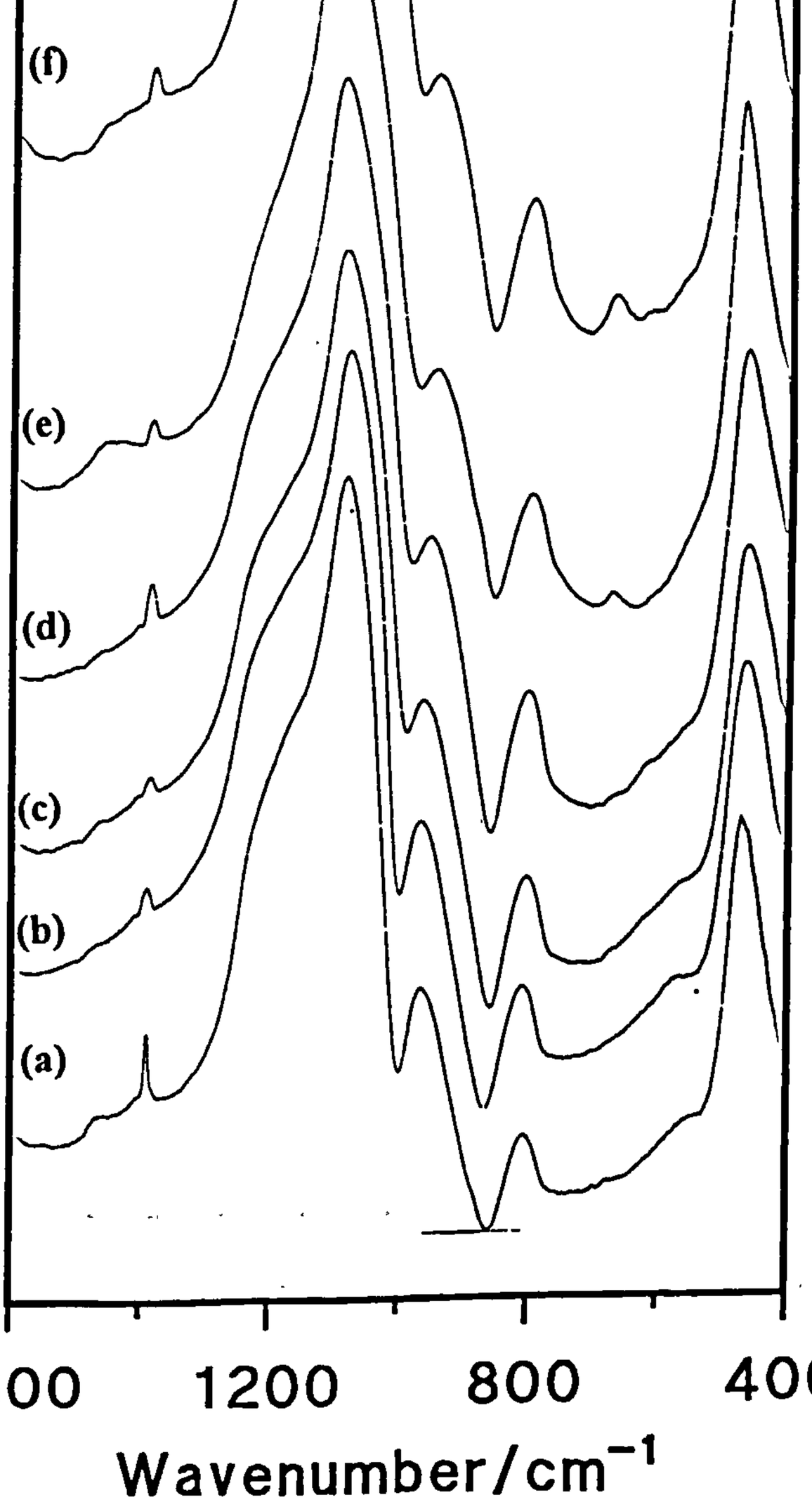

Mid-infrared Spectra of a Sample Nominally Containing 6·34 weight % Titania, HCl=0·015 mole Treated at Different Temperatures. (a) 120°C; (b) 300°C; (c) 500°C; (d) 700°C; (e) 900°C; (f) 1100°C.

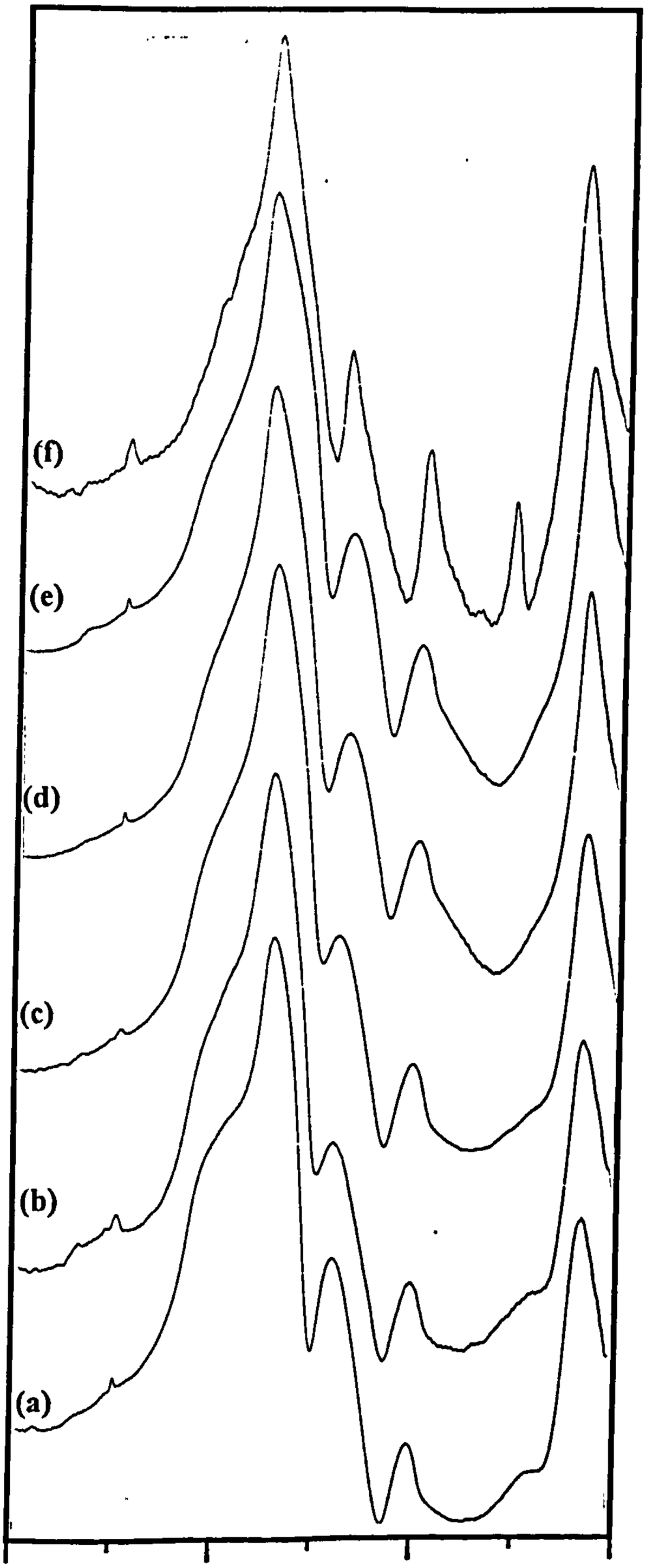

Mid-infrared Spectra of a Sample Nominally Containing 6·34 weight % Titania, HCl=$7{\cdot}5 \times 10^{-3}$ mole Treated at Different Temperatures. (a) 120°C; (b) 300°C; (c) 500°C; (d) 700°C; (e) 900°C; (f) 1100°C.

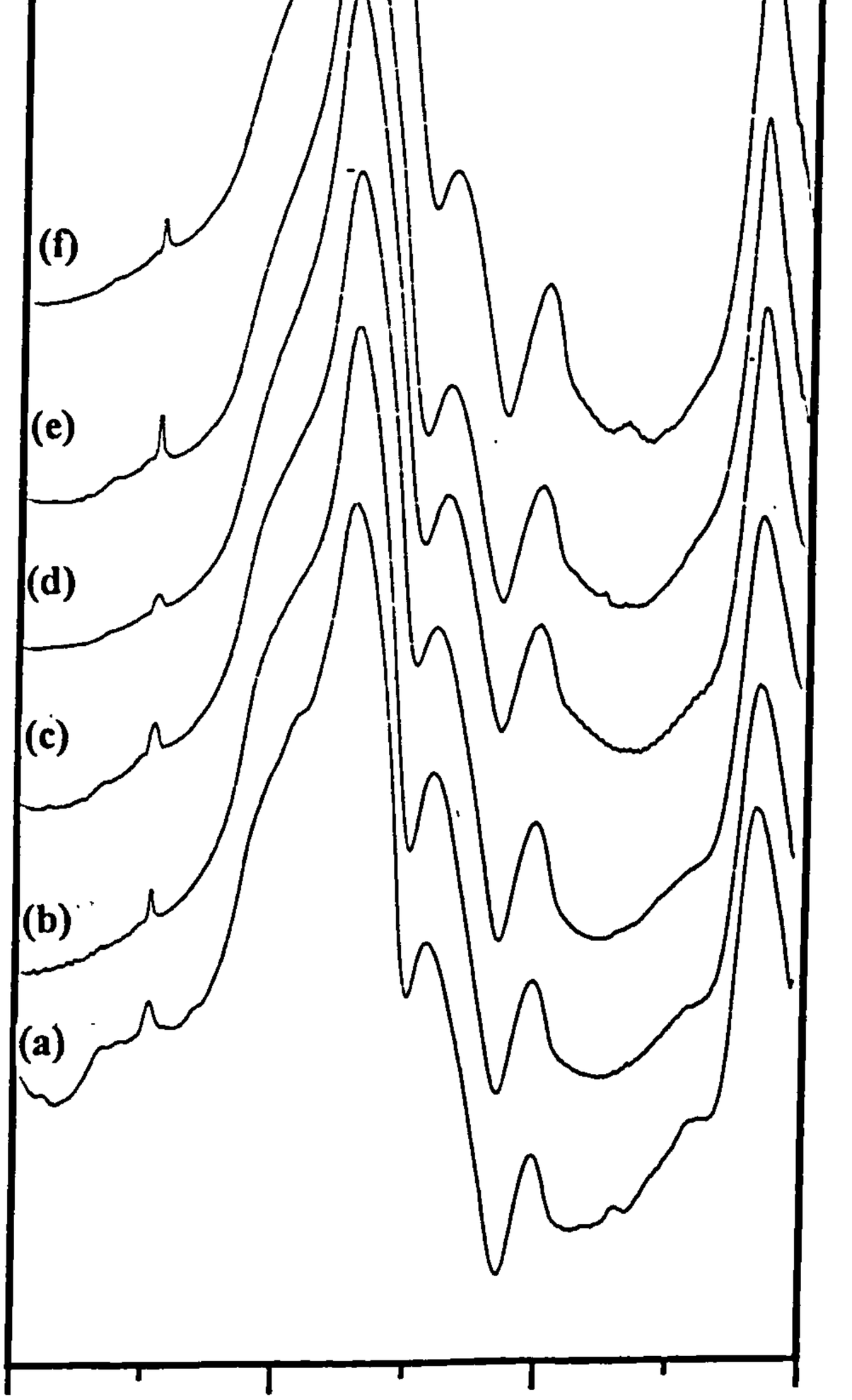

Mid-infrared Spectra of a Sample Nominally Containing 6·34 weight % Titania, HCl=$5x10^{-3}$ mole Treated at Different Temperatures. (a) 120°C; (b) 300°C; (c) 500°C; (d) 700°C; (e) 900°C; (f) 1100°C.

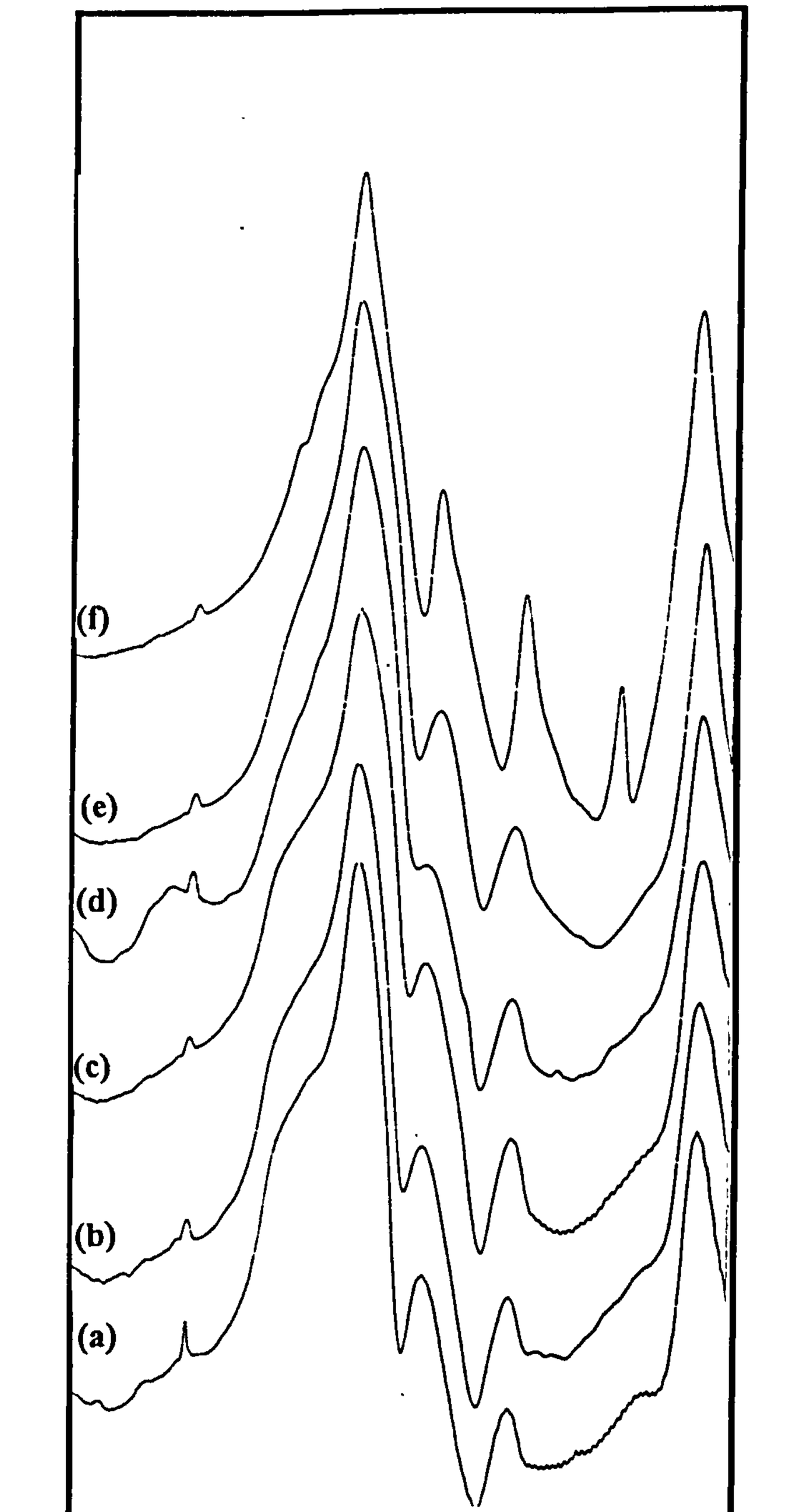

Mid-infrared Spectra of a Sample Nominally Containing 6·34 weight % Titania, HCl=$2{\cdot}5x10^{-3}$ mole Treated at Different Temperatures. (a) 120°C; (b) 300°C; (c) 500°C; (d) 700°C; (e) 900°C; (f) 1100°C.

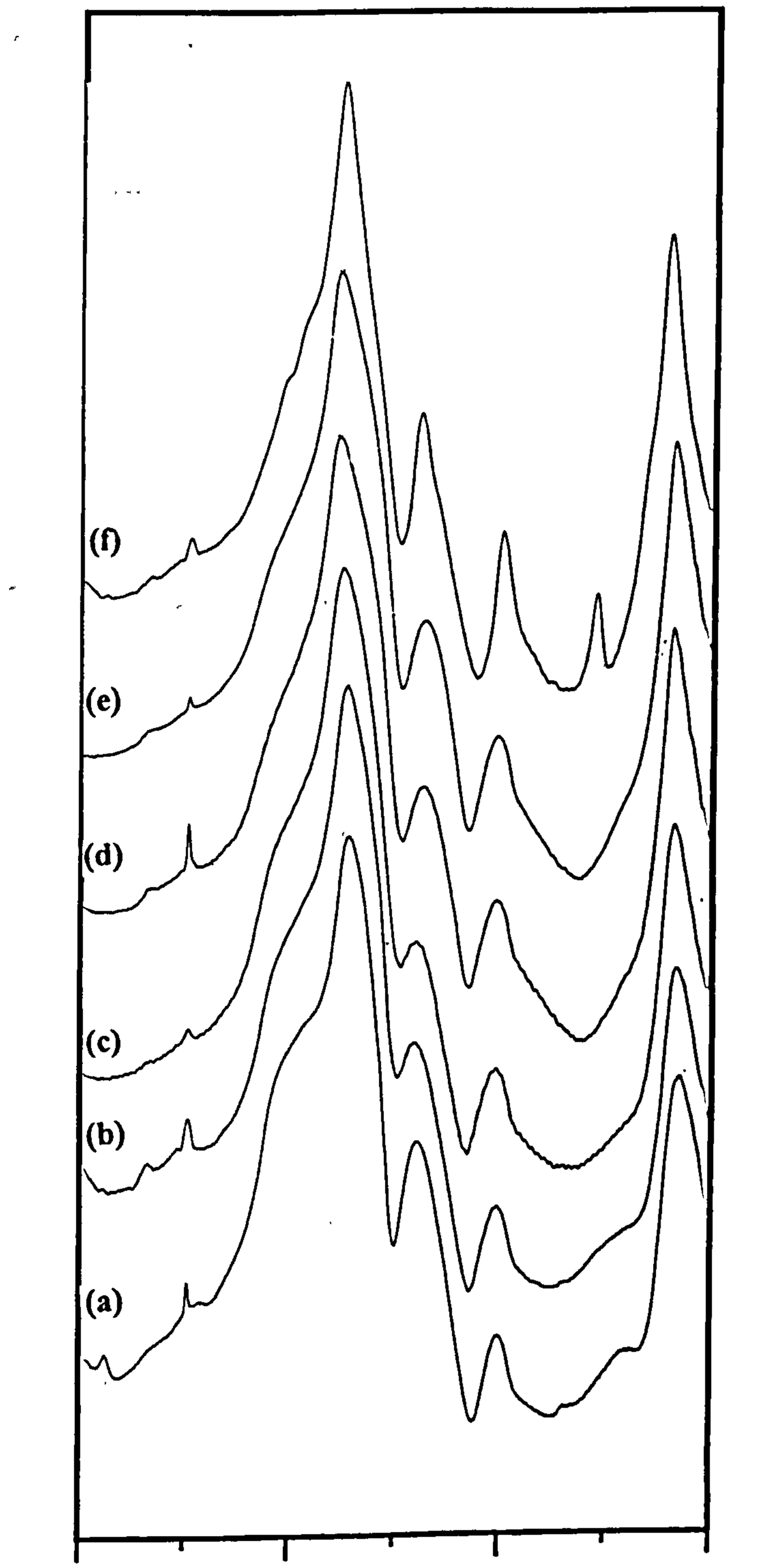

Near Infrared Spectra: Effect of Rehydration

First Overtone and Combination Region (1200-2500nm) Near Infrared Spectra of a Dehydrated Sample Containing TiO_2=6·34 wt% (HCl=0·045 mole) Heated to 120°C and Exposed to the Atmosphere for Various Times.

(a) 0; (b) 0·5 hour; (c) 1 hour; (d) 2 hours; (e) 14 hours.

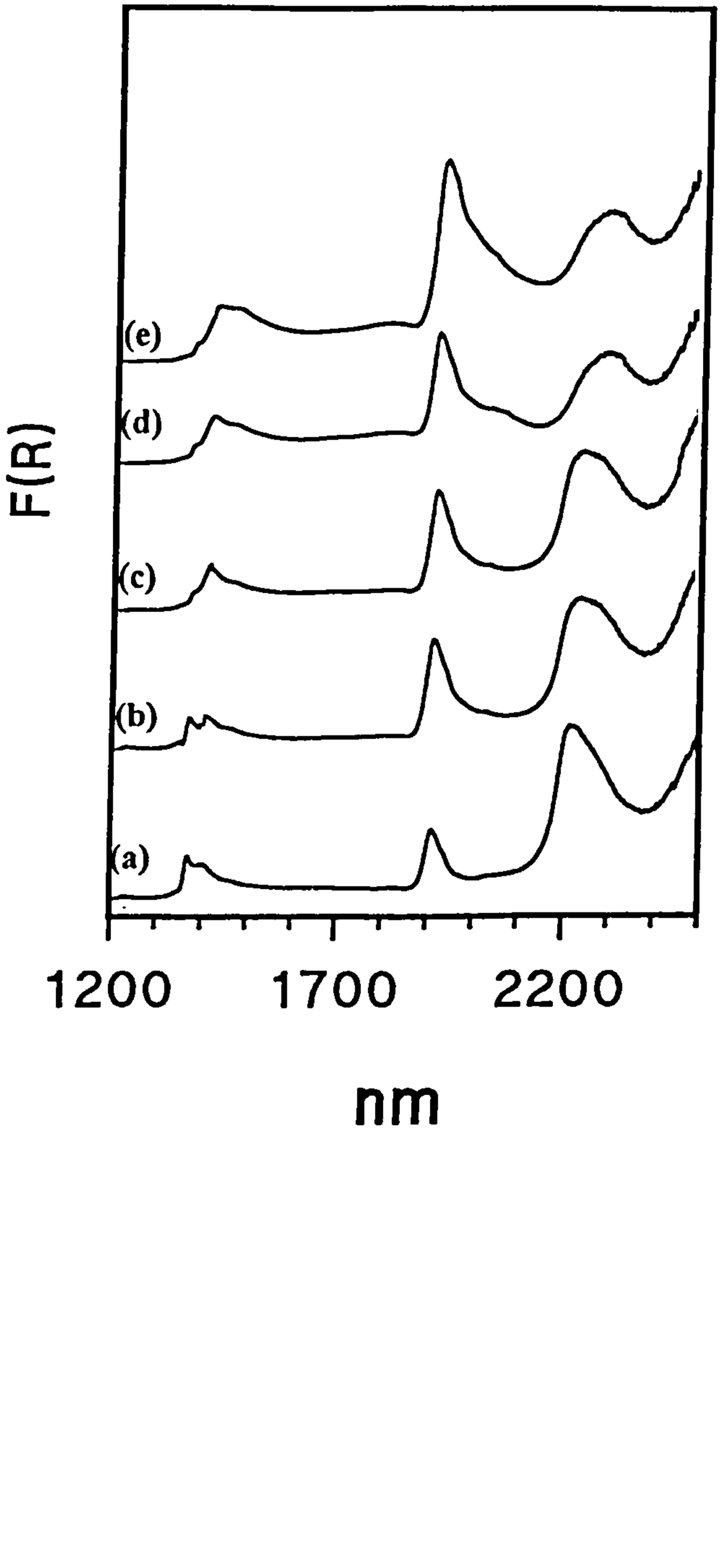

Second Overtone Region (900-1350nm) Near Infrared Spectra of a Dehydrated Sample Containing TiO_2=6·34 wt% (HCl=0·045 mole) Heated to 120°C and Exposed to the Atmosphere for Various Times.
(a) 0; (b) 0·5 hour; (c) 1 hour; (d) 2 hours; (e) 14 hours.

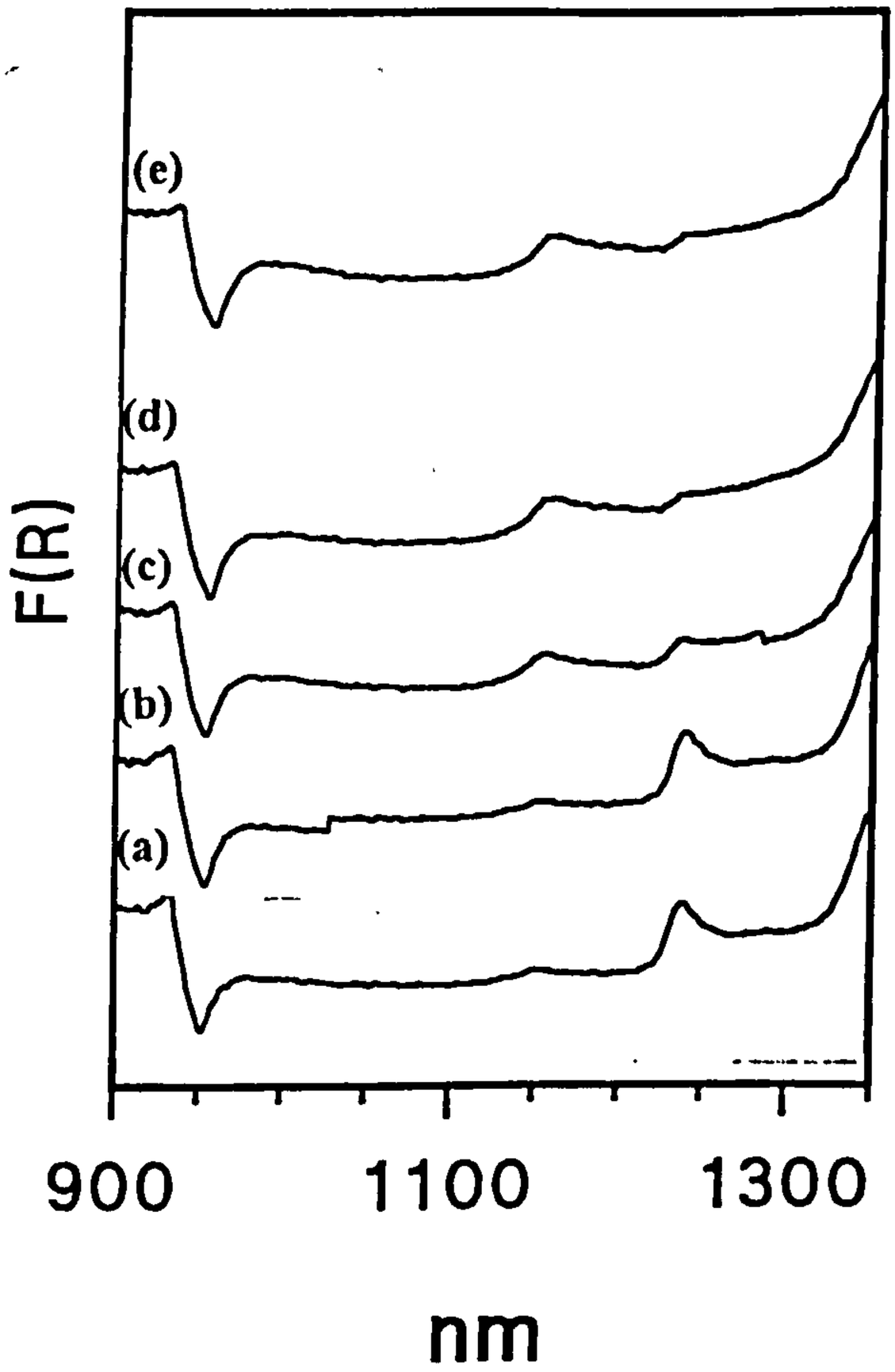

First Overtone and Combination Region (1200-2500nm) Near Infrared Spectra of a Dehydrated Sample Containing TiO_2=6·34 wt% (HCl=0·030 mole) Heated to 120°C and Exposed to the Atmosphere for Various Times.
(a) 0; (b) 0·5 hour; (c) 1 hour; (d) 2 hours; (e) 14 hours.

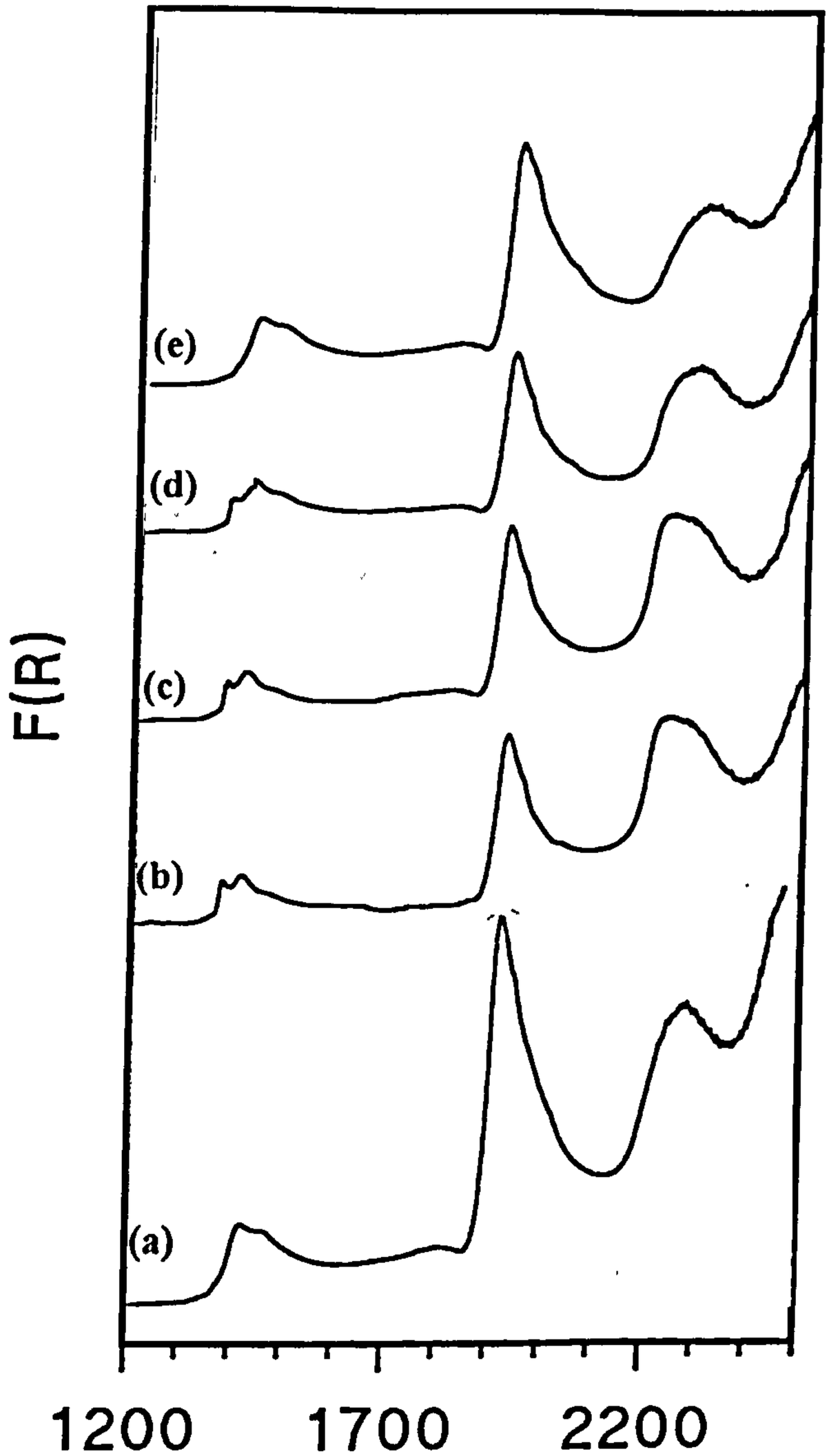

Second Overtone Region (900-1350nm) Near Infrared Spectra of a Dehydrated Sample Containing TiO_2=6·34 wt% (HCl=0·030 mole) Heated to 120°C and Exposed to the Atmosphere for Various Times.
(a) 0; (b) 0·5 hour; (c) 1 hour; (d) 2 hours; (e) 14 hours.

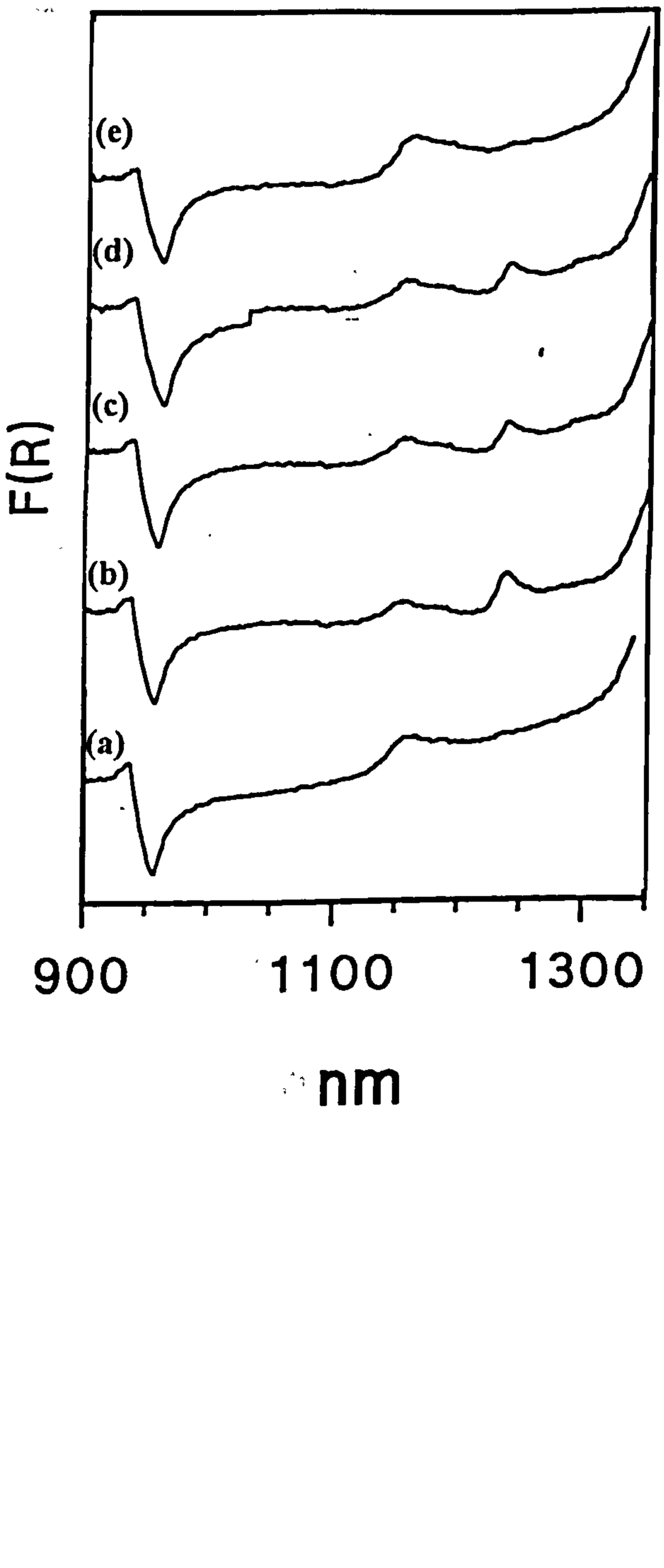

First Overtone and Combination Region (1200-2500nm) Near Infrared Spectra of a Dehydrated Sample Containing TiO_2=6·34 wt% (HCl=0·015 mole) Heated to 120°C and Exposed to the Atmosphere for Various Times.
(a) 0; (b) 0·5 hour; (c) 1 hour; (d) 2 hours; (e) 14 hours.

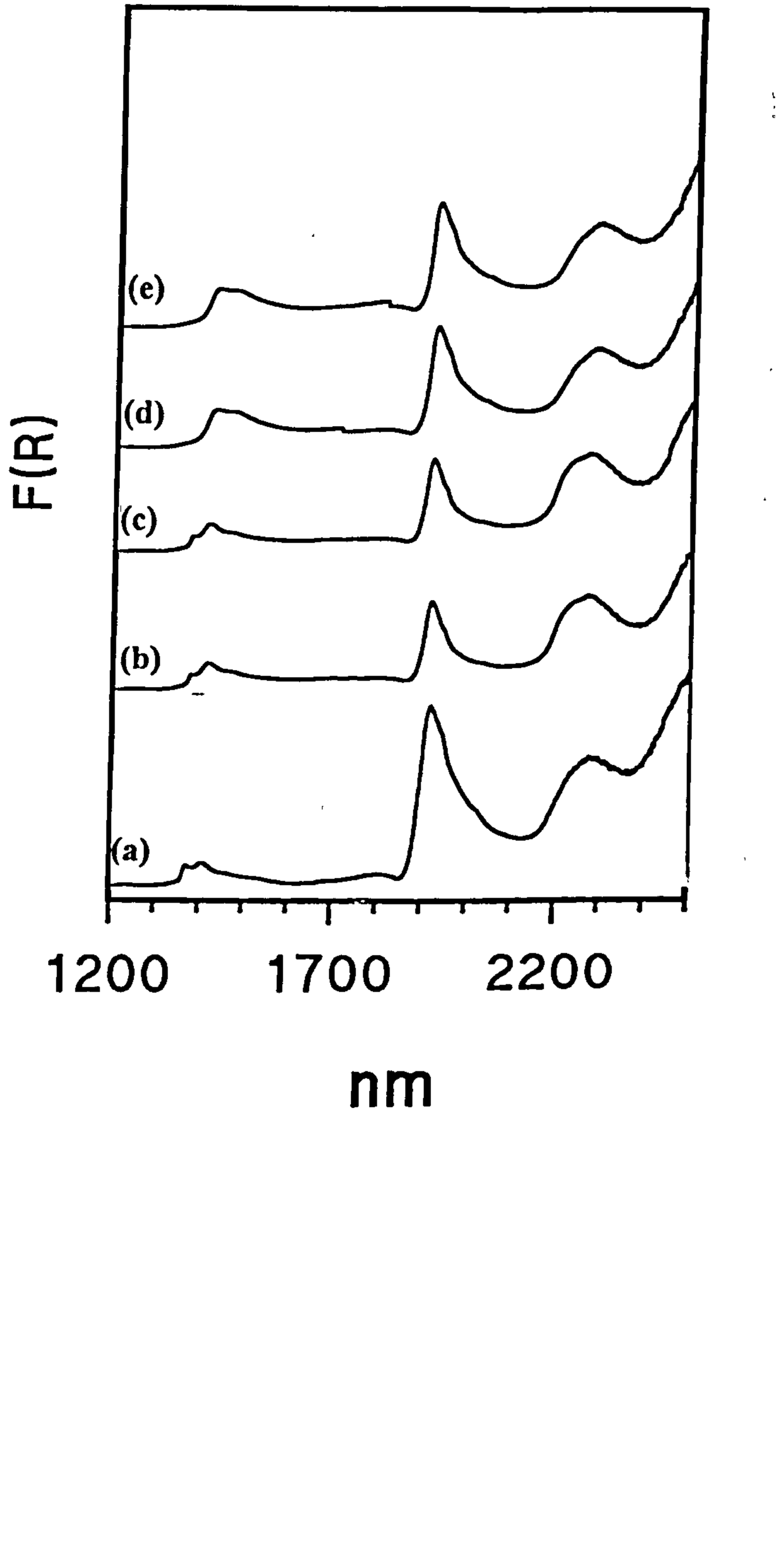

Second Overtone Region (900-1350nm) Near Infrared Spectra of a Dehydrated Sample Containing TiO_2=6·34 wt% (HCl=0·015 mole) Heated to 120°C and Exposed to the Atmosphere for Various Times.
(a) 0; (b) 0·5 hour; (c) 1 hour; (d) 2 hours; (e) 14 hours.

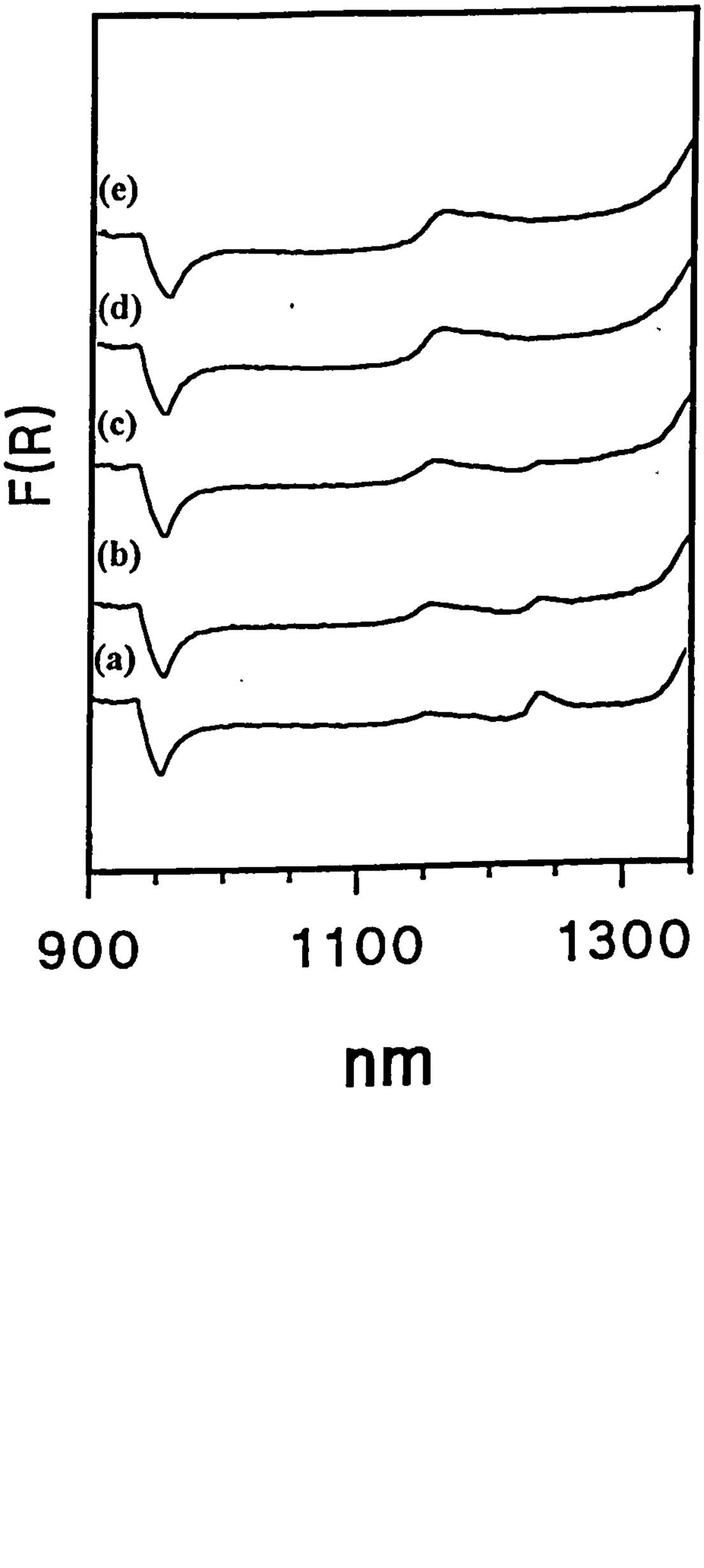

First Overtone and Combination Region (1200-2500nm) Near Infrared Spectra of a Dehydrated Sample Containing TiO_2=6·34 wt% (HCl=$5x10^{-3}$ mole) Heated to 120°C and Exposed to the Atmosphere for Various Times.
(a) 0; (b) 0·5 hour; (c) 1 hour; (d) 2 hours; (e) 14 hours.

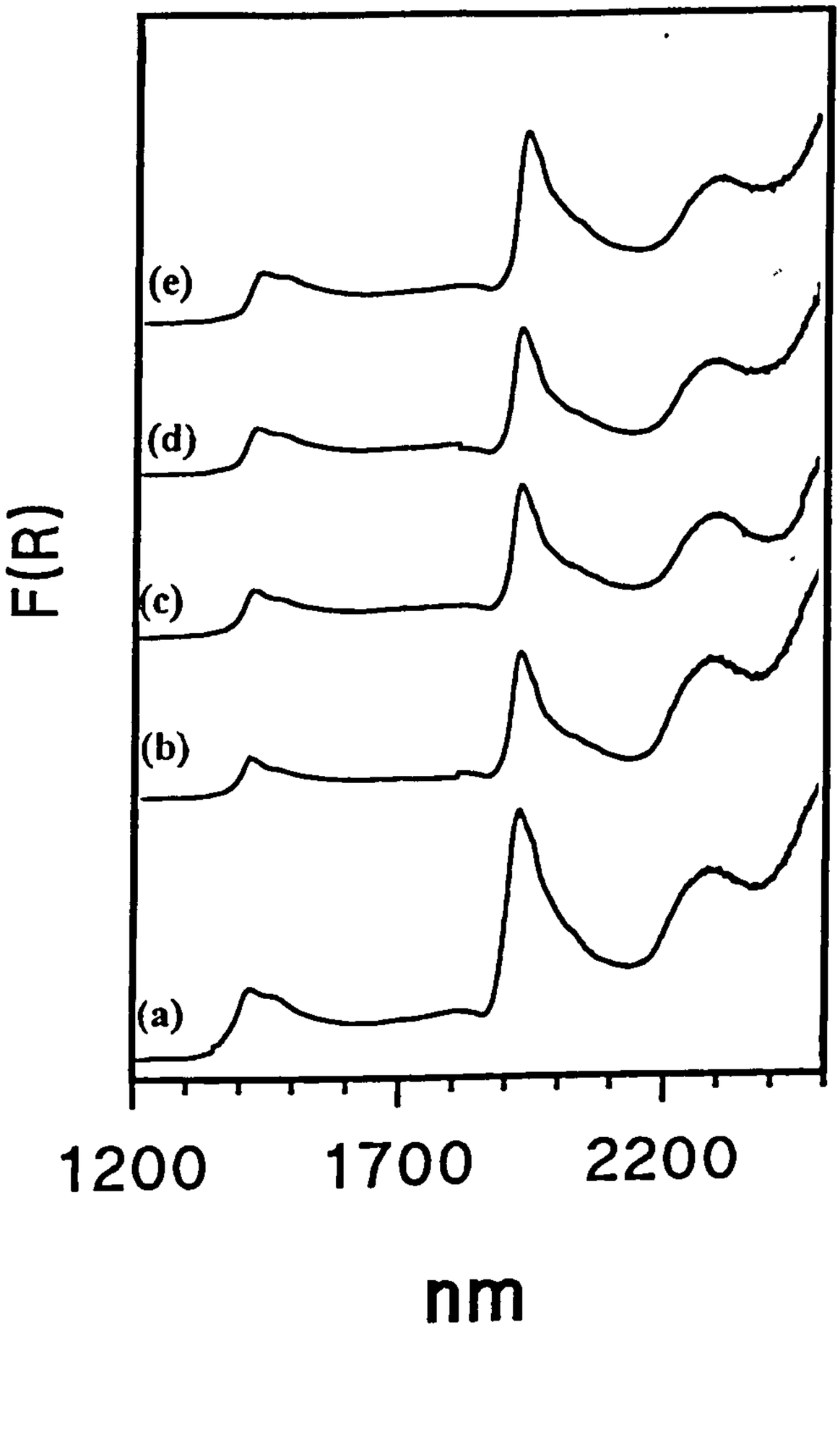

Second Overtone Region (900-1350nm) Near Infrared Spectra of a Dehydrated Sample Containing TiO_2=6·34 wt% (HCl=$5x10^{-3}$ mole) Heated to 120°C and Exposed to the Atmosphere for Various Times.

(a) 0; (b) 0·5 hour; (c) 1 hour; (d) 2 hours; (e) 14 hours.

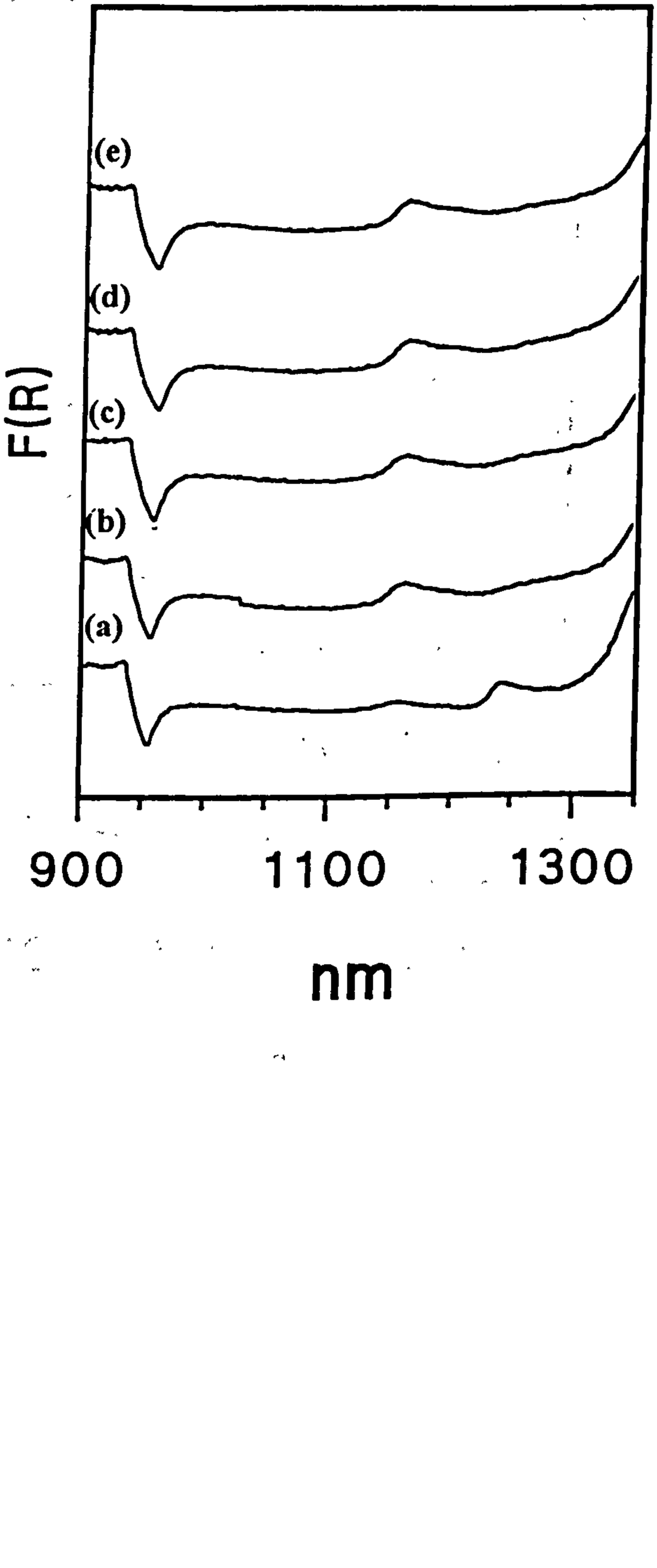

First Overtone and Combination Region (1200-2500nm) Near Infrared Spectra of a Dehydrated Sample Containing TiO_2=6·34 wt% (HCl=2·5x10^{-3} mole) Heated to 120°C and Exposed to the Atmosphere for Various Times.
(a) 0; (b) 0·5 hour; (c) 1 hour; (d) 2 hours; (e) 14 hours.

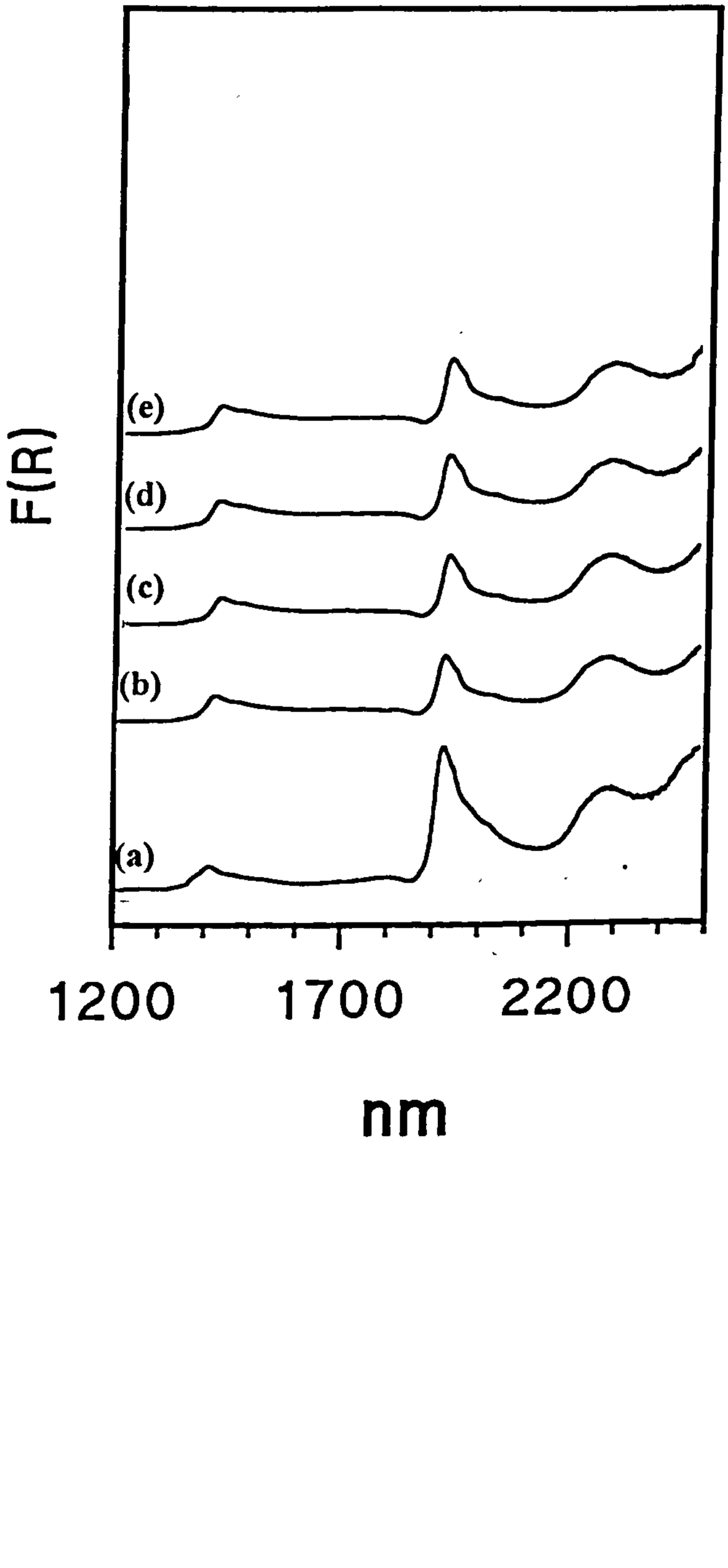

Second Overtone Region (900-1350nm) Near Infrared Spectra of a Dehydrated Sample Containing TiO_2=6·34 wt% (HCl=2·5x10^{-3} mole) Heated to 120°C and Exposed to the Atmosphere for Various Times.

(a) 0; (b) 0·5 hour; (c) 1 hour; (d) 2 hours; (e) 14 hours.

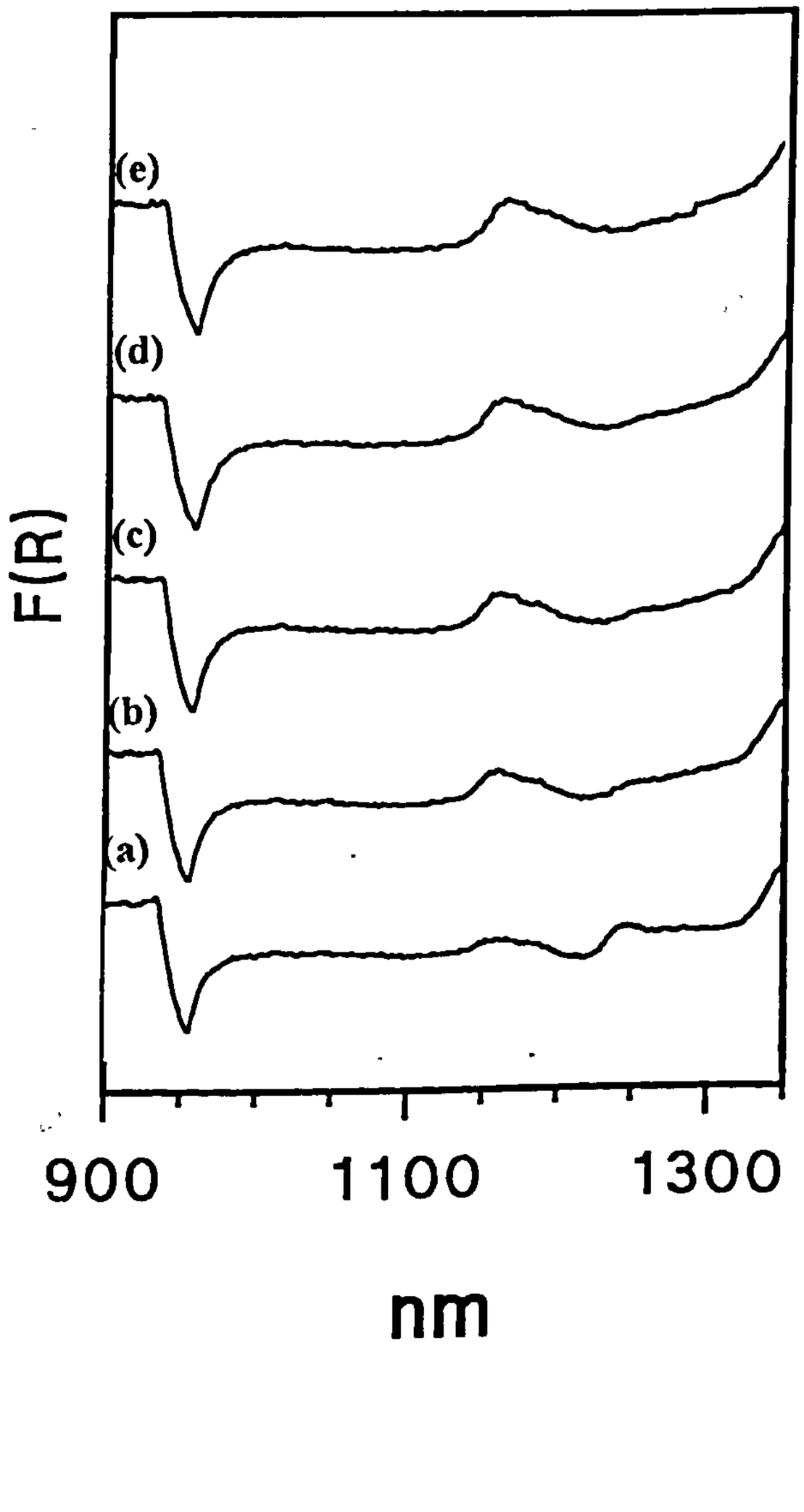

Gas Adsorption Investigation of Pore Structure

Effects of Varying the Amount of Acid used for the Hydrolysis Reaction on the Pore Characteristics of a Monolith Nominally Containing TiO_2=6·34 weight % and Heated at 120°C

HCl=0·045 mole (TiO_2=6·34 nominally weight %; Heated at 120°C)

(a) Adsorption/Desorption Isotherm

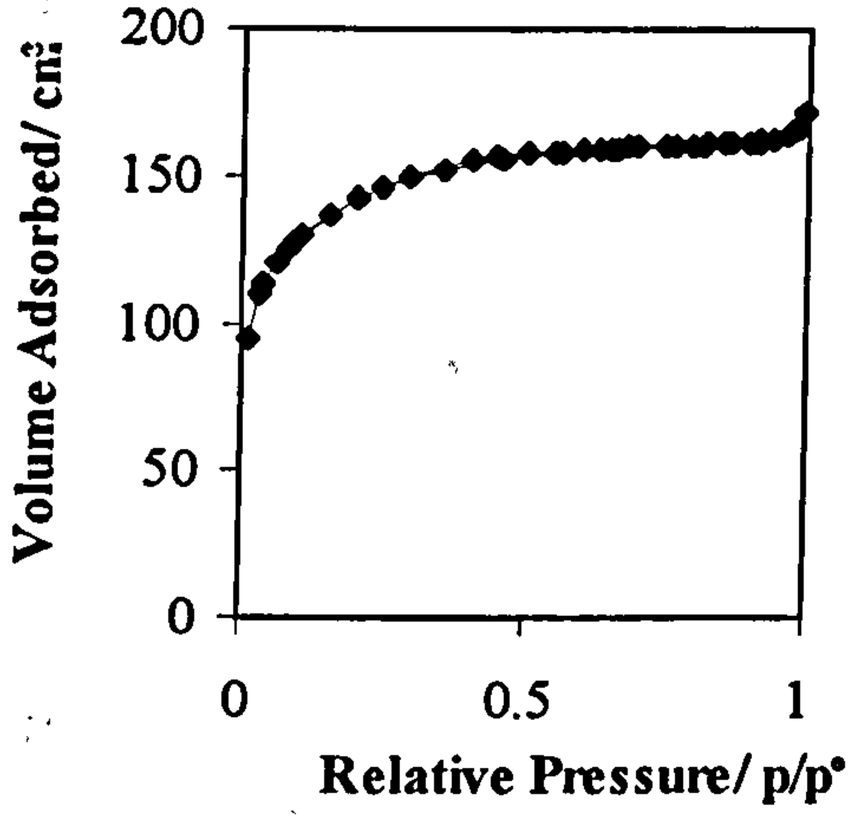

(b) α_s-plot

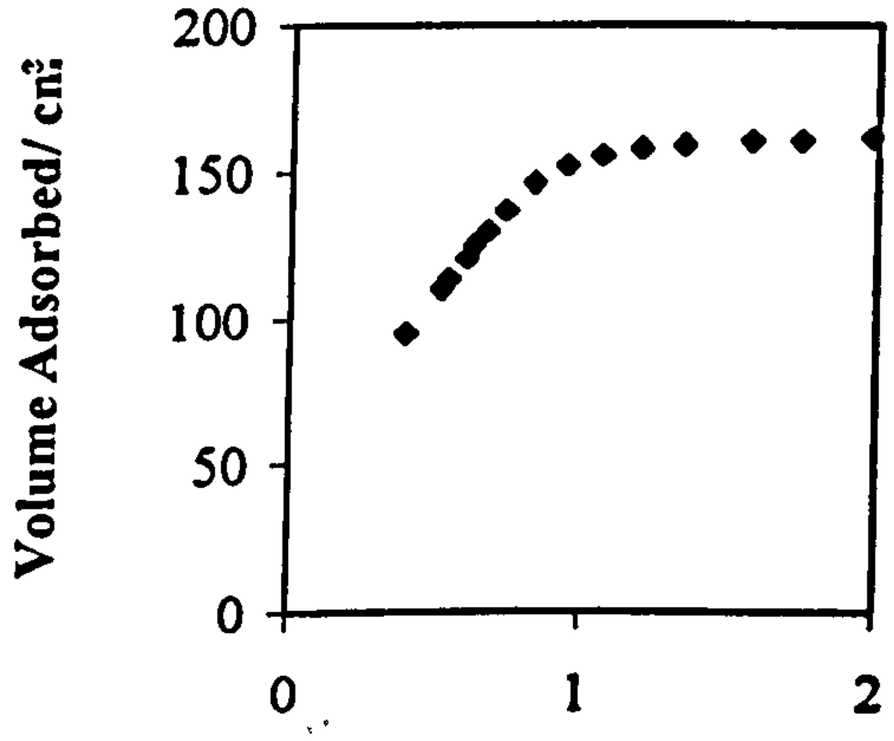

HCl=0·030 mole (TiO_2=6·34 nominally weight %; Heated at 120°C)

(a) Adsorption/Desorption Isotherm

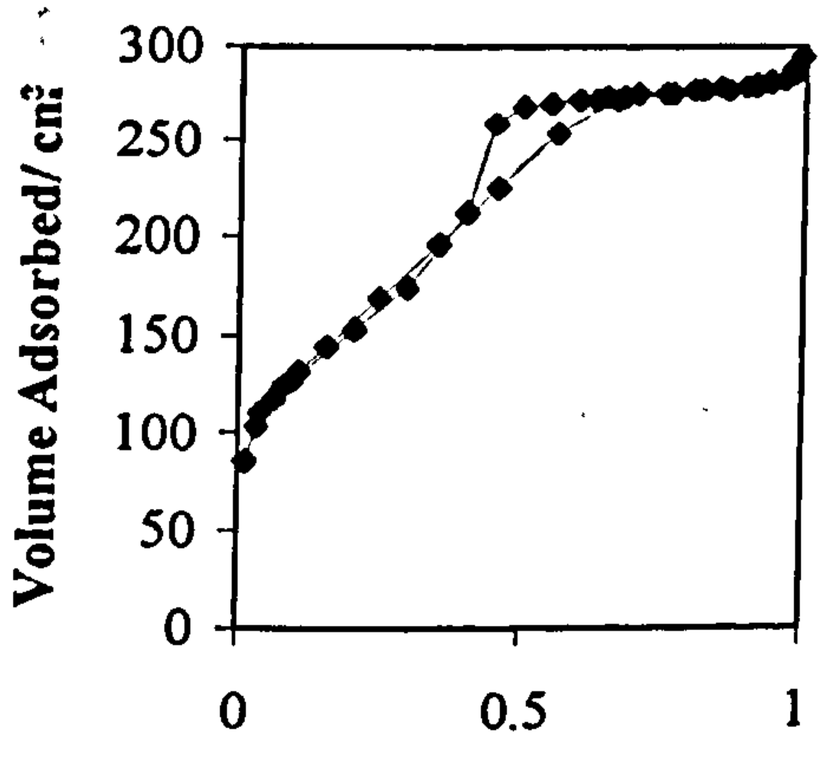

(b) α_s-plot

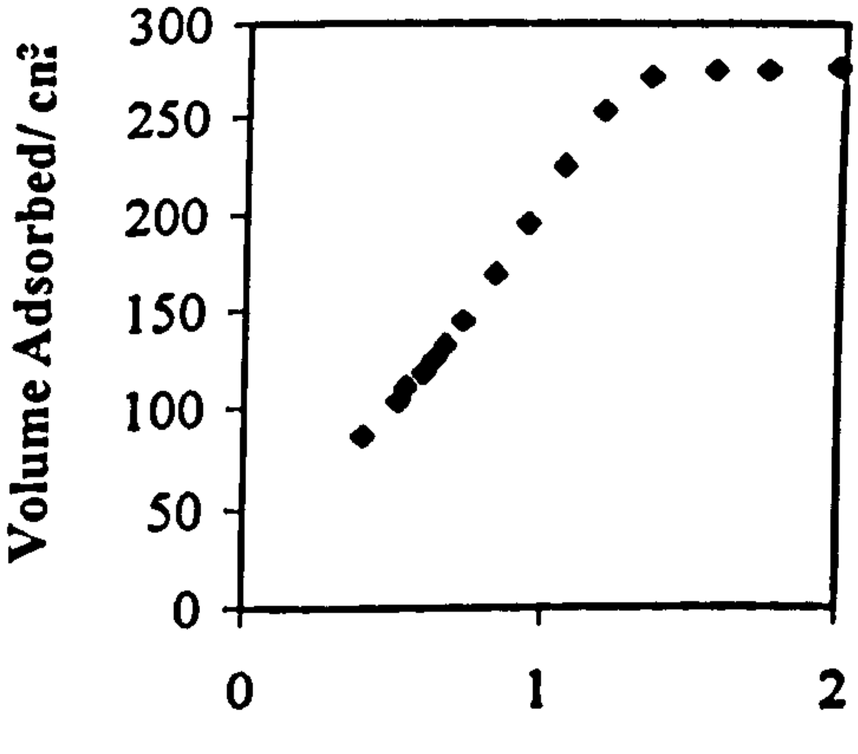

HCl=0·015 mole (TiO_2=6·34 nominally weight %; Heated at 120°C)

(a) Adsorption/Desorption Isotherm

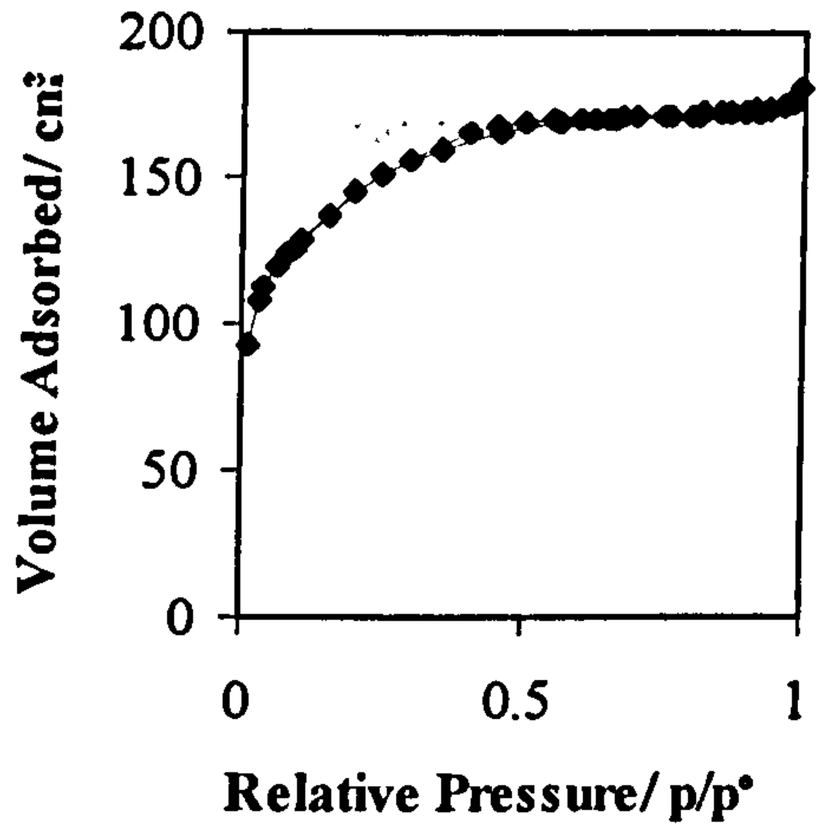

(b) α_s-plot

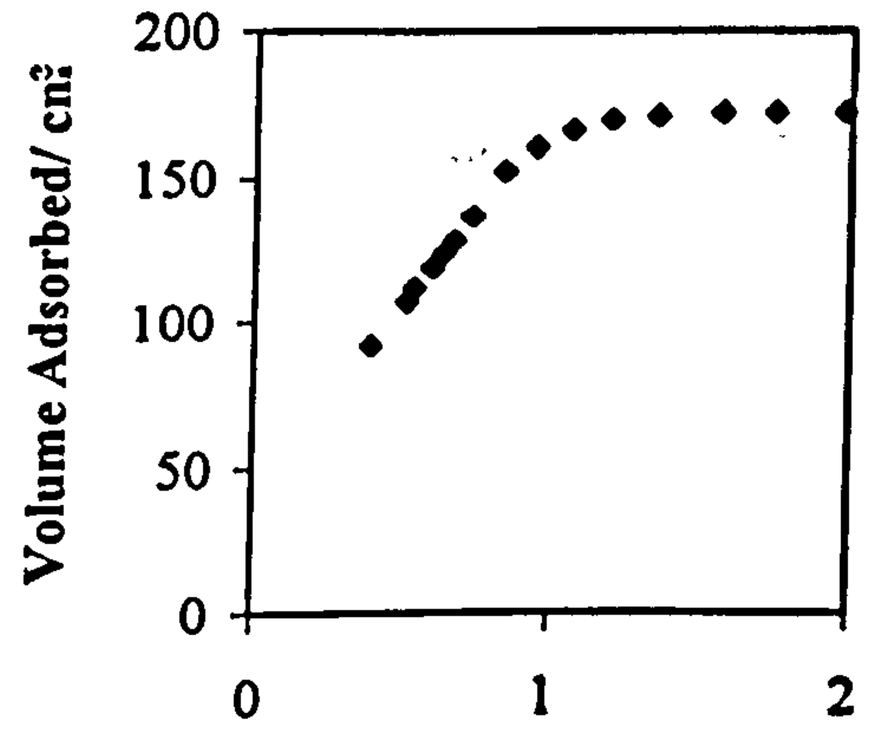

HCl=7·5x10^{-3} mole (TiO_2=6·34 nominally weight %; Heated at 120°C)

(a) Adsorption/Desorption Isotherm

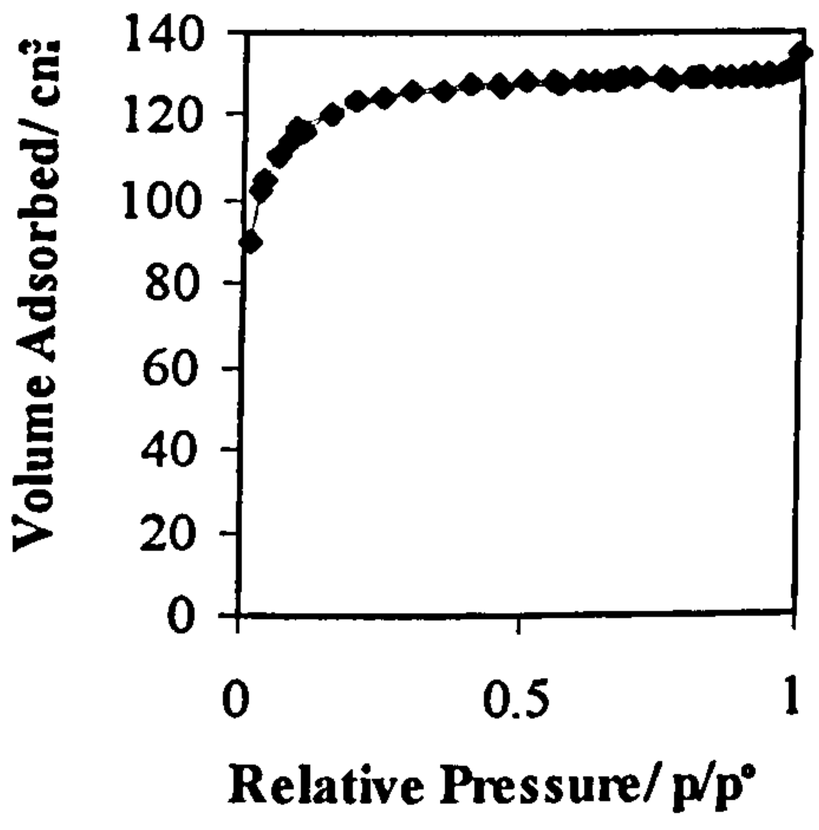

(b) α_s-plot

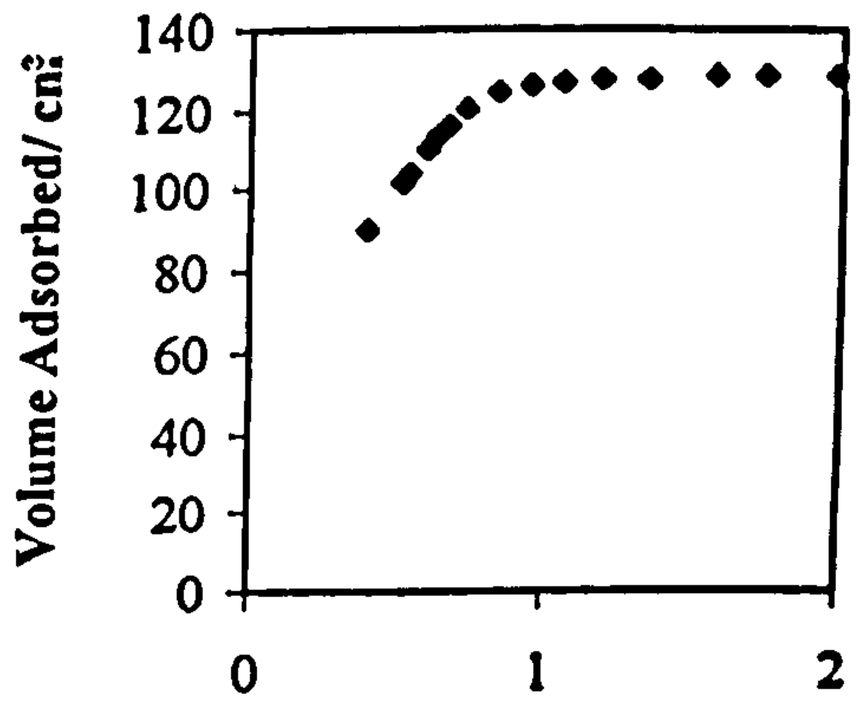

HCl=5x10^{-3} mole (TiO_2=6·34 nominally weight %; Heated at 120°C)

(a) Adsorption/Desorption Isotherm

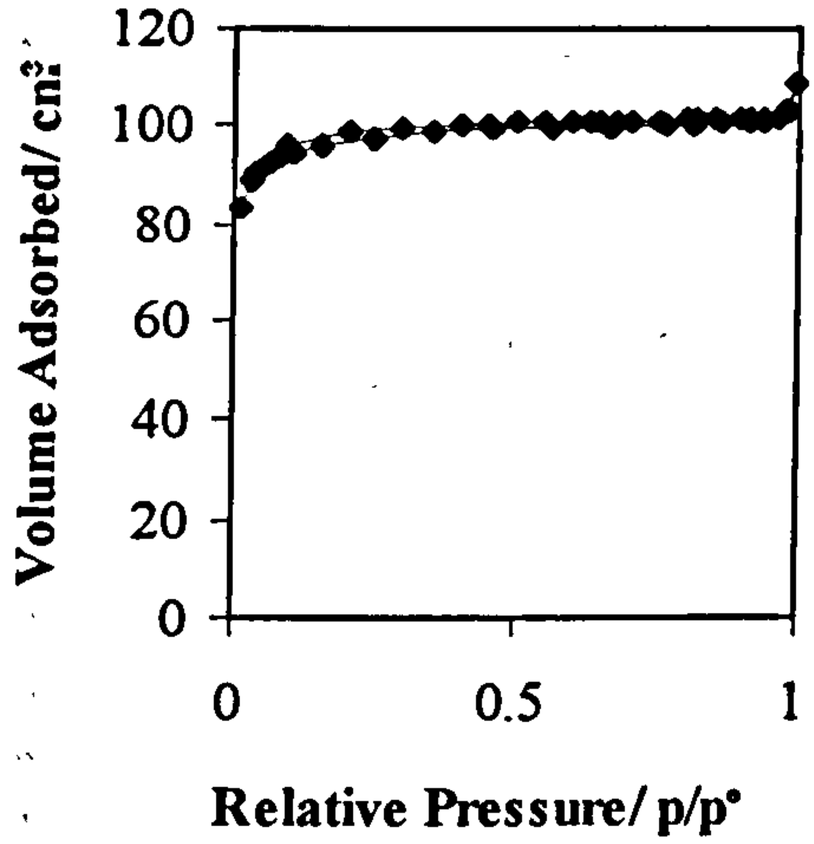

(b) α_s-plot

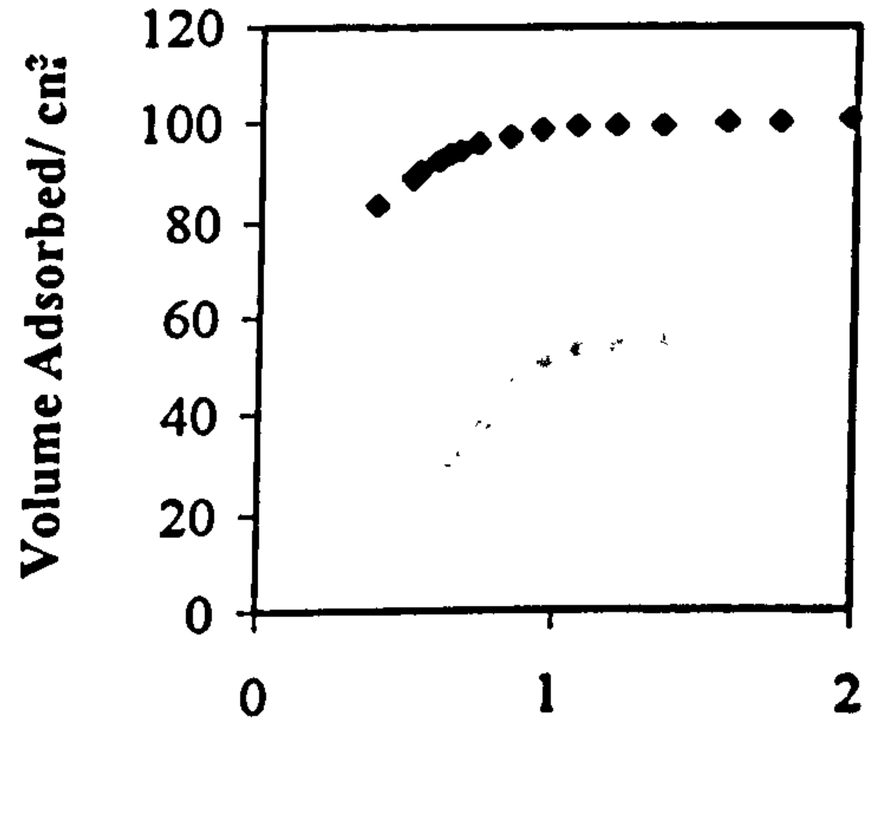

HCl=2·5x10^{-3} mole (TiO_2=6·34 nominally weight %; Heated at 120°C)

(a) Adsorption/Desorption Isotherm

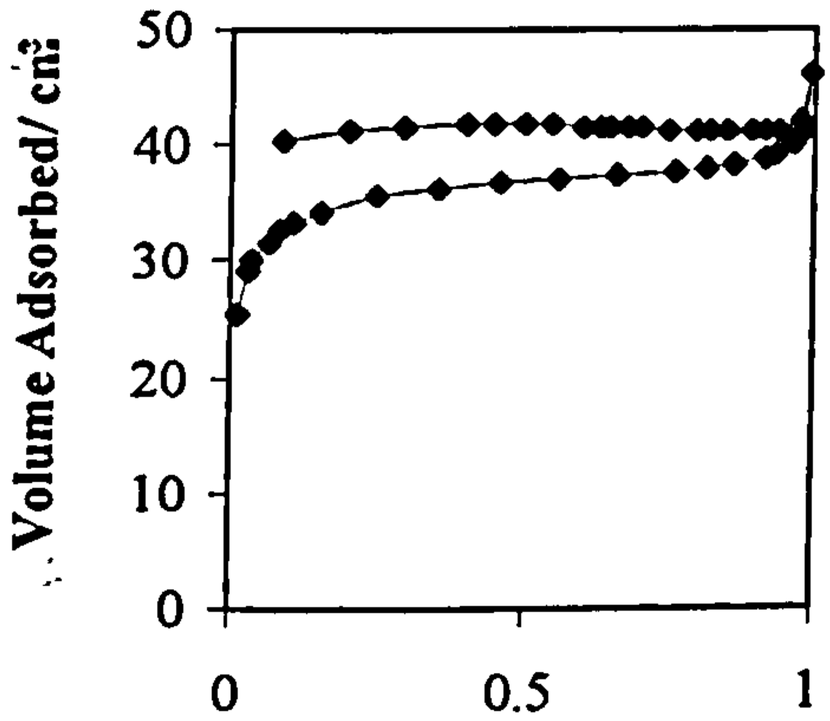

(b) α_s-plot

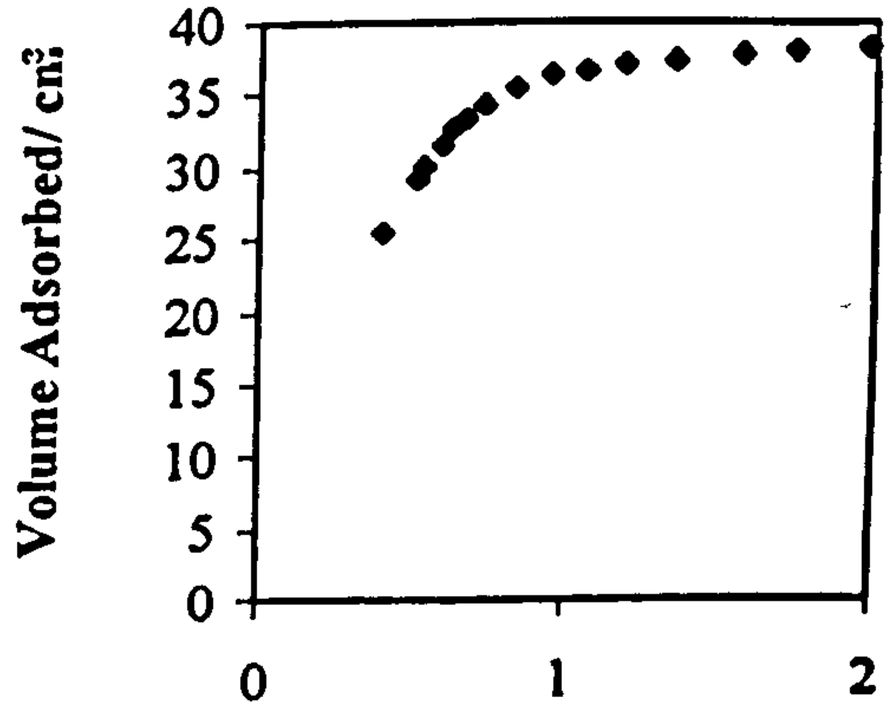

Effect of Temperature on the Pore Characteristics of a Monolith Nominally Containing TiO_2=6·34 weight % ; HCl=0·045 mole *

300°C: TiO_2=6·34 weight % ; HCl=0·045 mole

(a) Adsorption/Desorption Isotherm

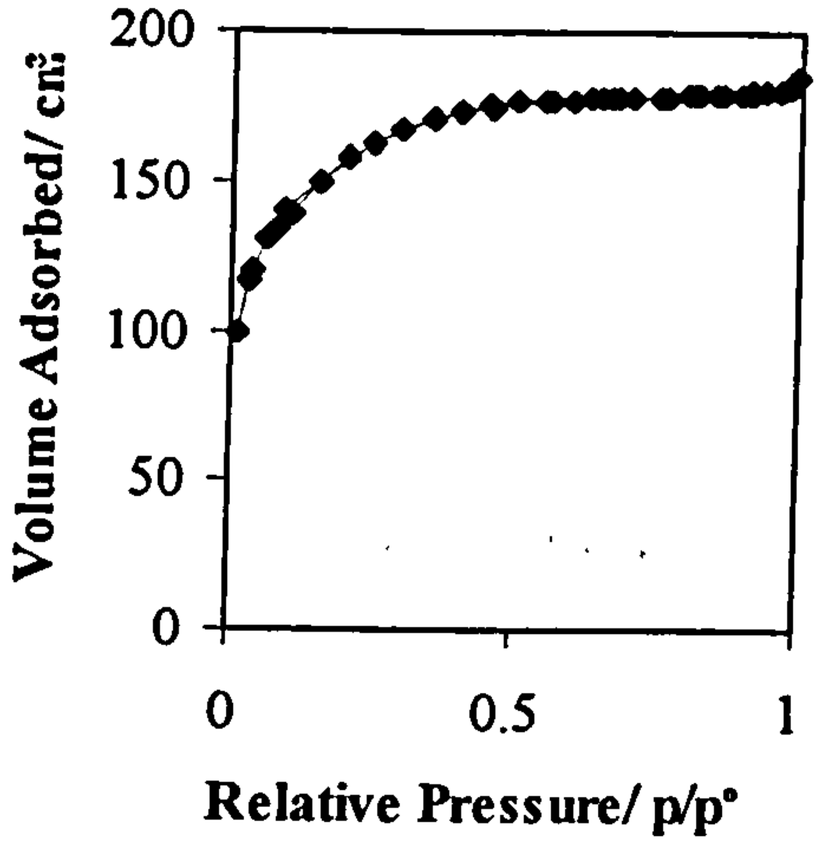

(b) α_s-plot

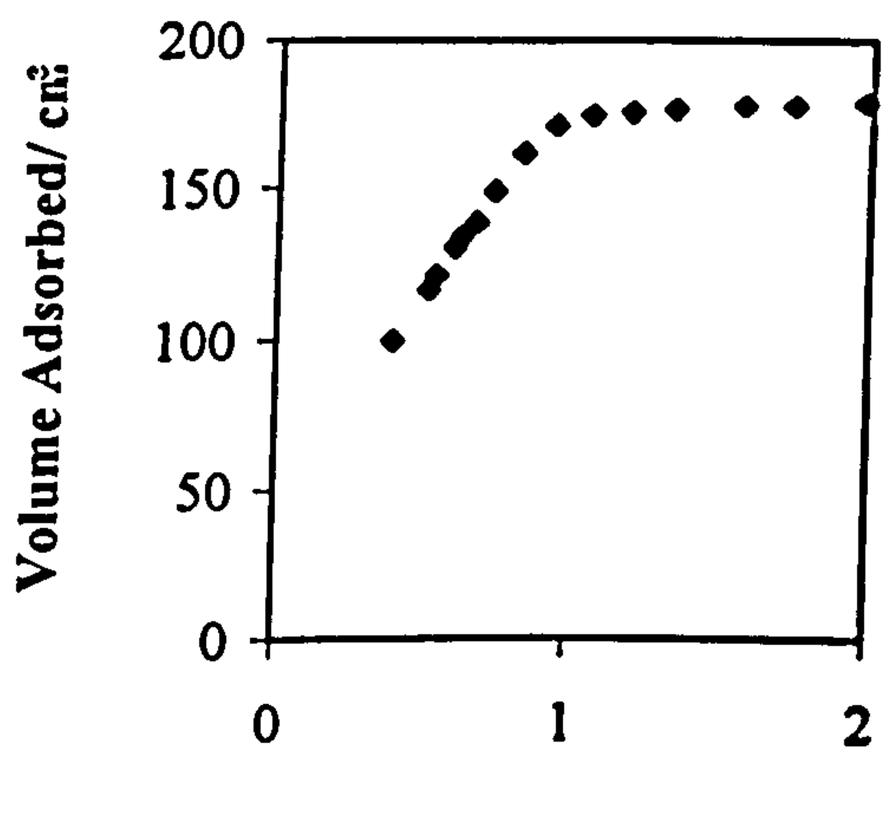

500°C: TiO_2=6·34 weight % ; HCl=0·045 mole

(a) Adsorption/Desorption Isotherm

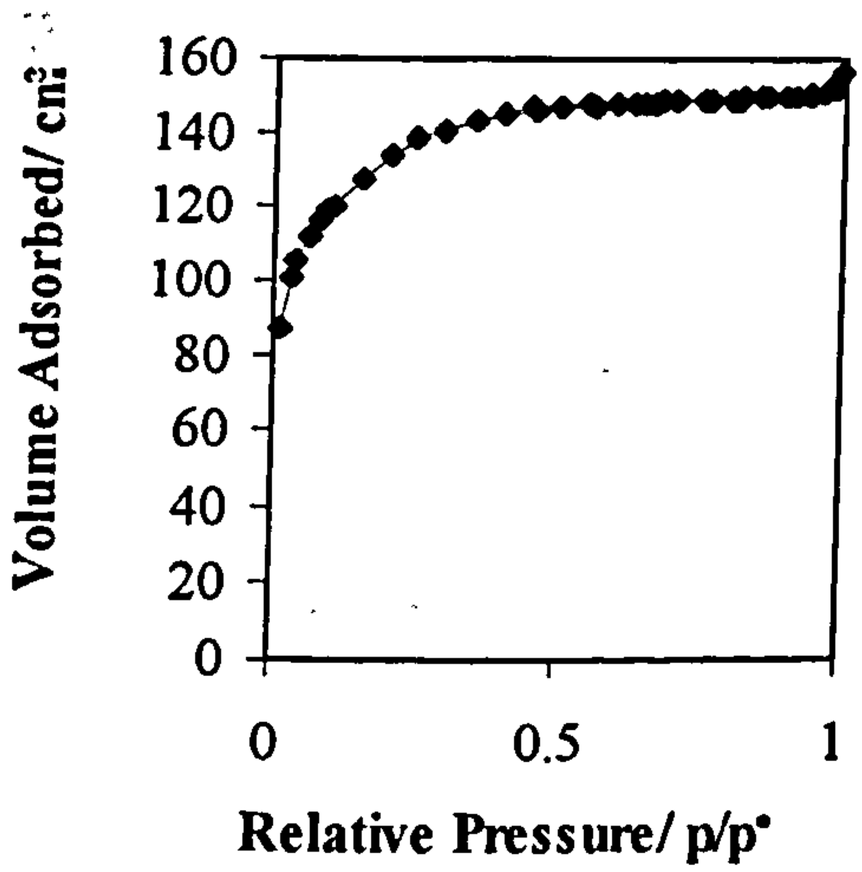

(b) α_s-plot

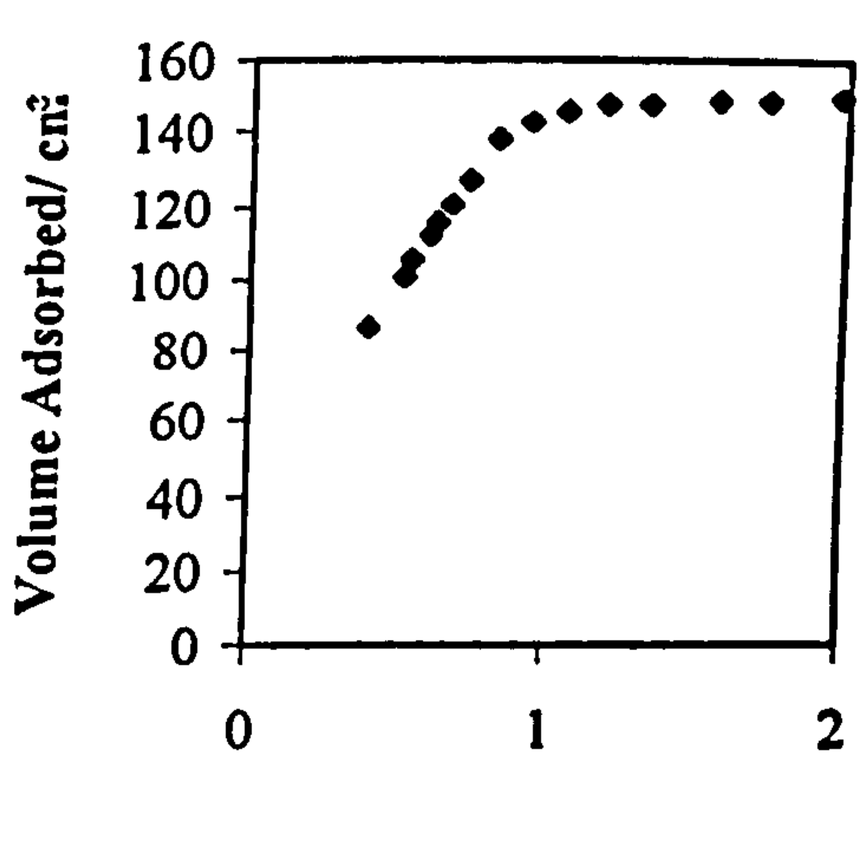

* Isotherm for TiO_2=6·34 wt% at 120°C can be found with the isotherms for effect of varying the amount of acid used for the hydrolysis reaction.

700°C: TiO_2=6·34 weight % ; HCl=0·045 mole

(a) Adsorption/Desorption Isotherm

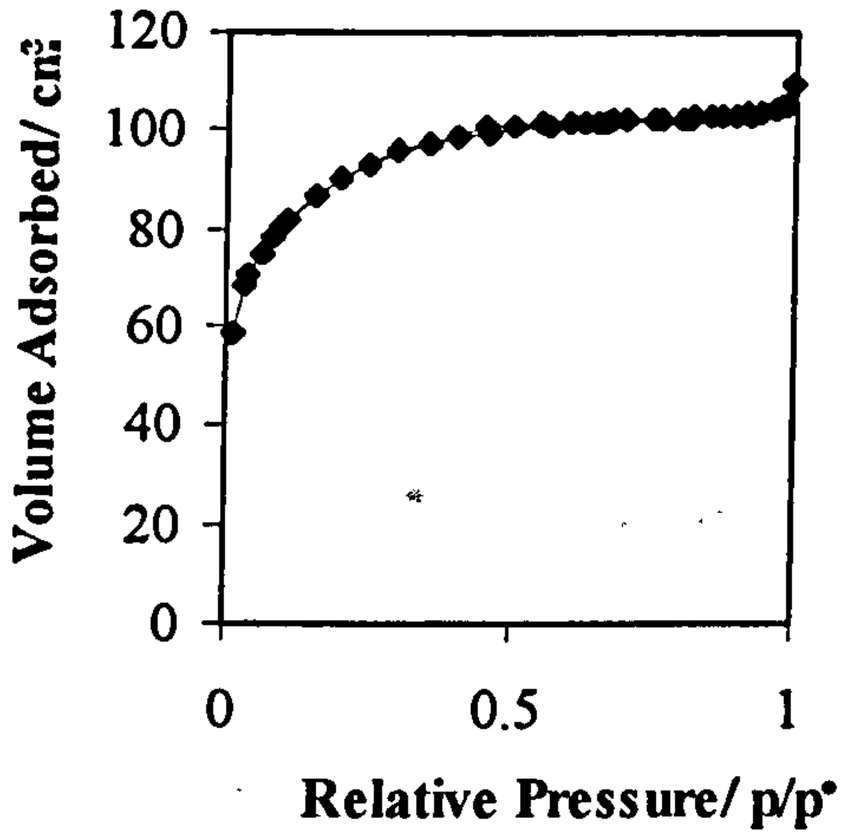

(b) α_s-plot

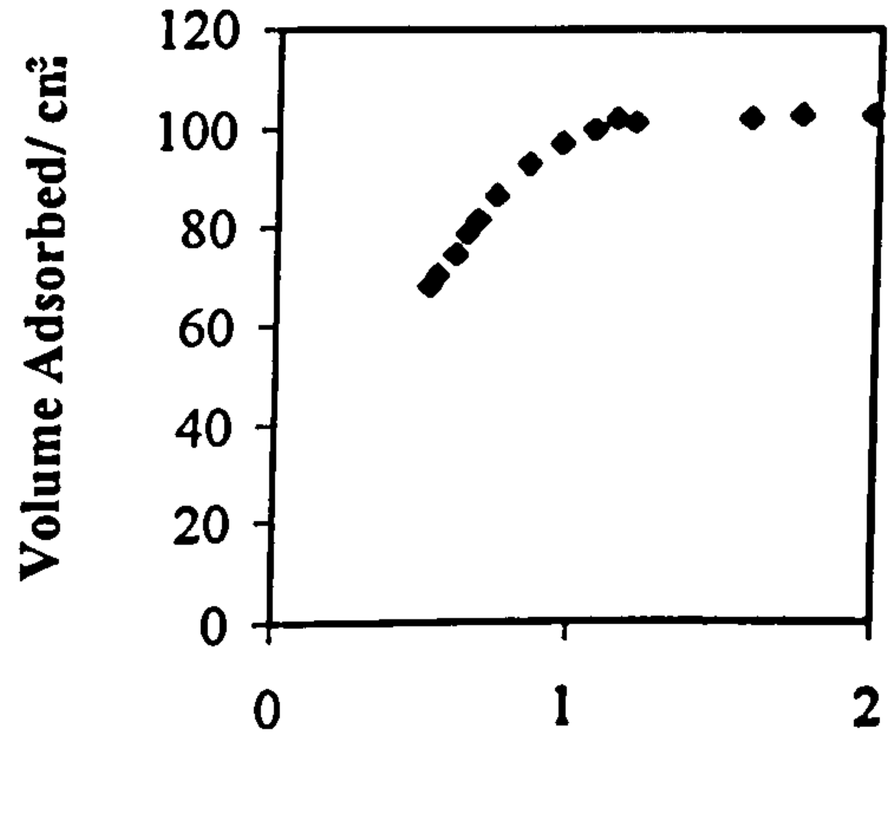

900°C: TiO_2=6·34 weight % ; HCl=0·045 mole

(a) Adsorption/Desorption Isotherm

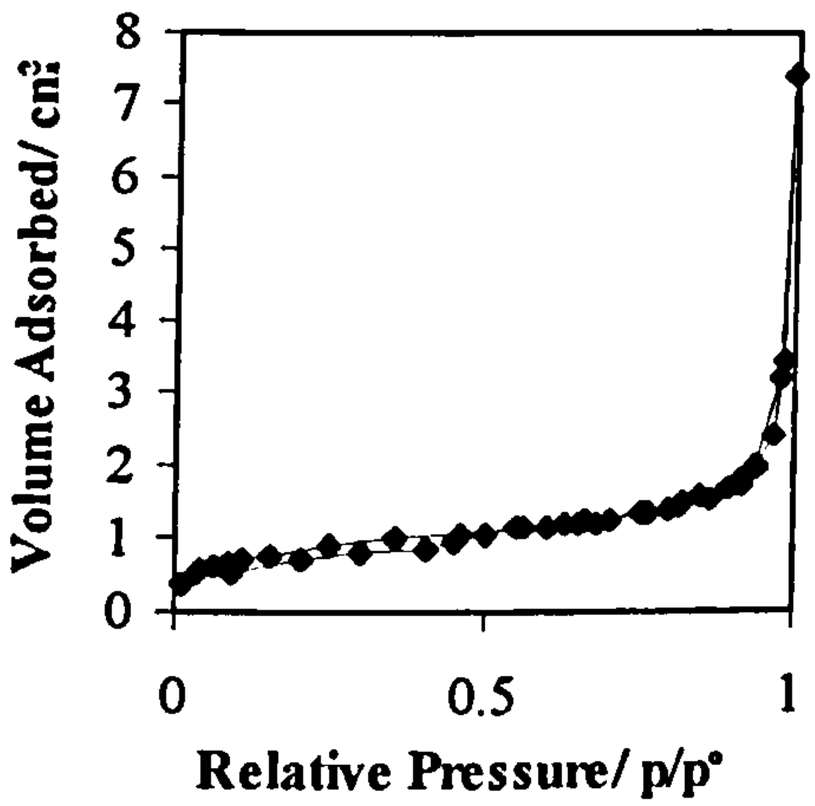

(b) α_s-plot

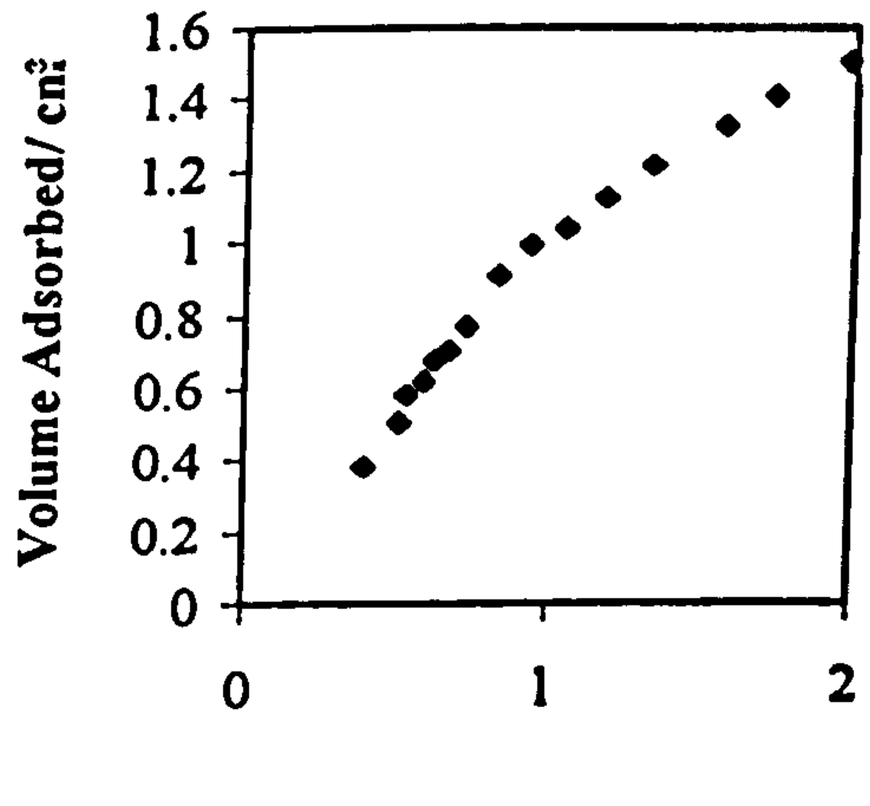

1100°C: TiO_2=6·34 weight % ; HCl=0·045 mole

(a) Adsorption/Desorption Isotherm

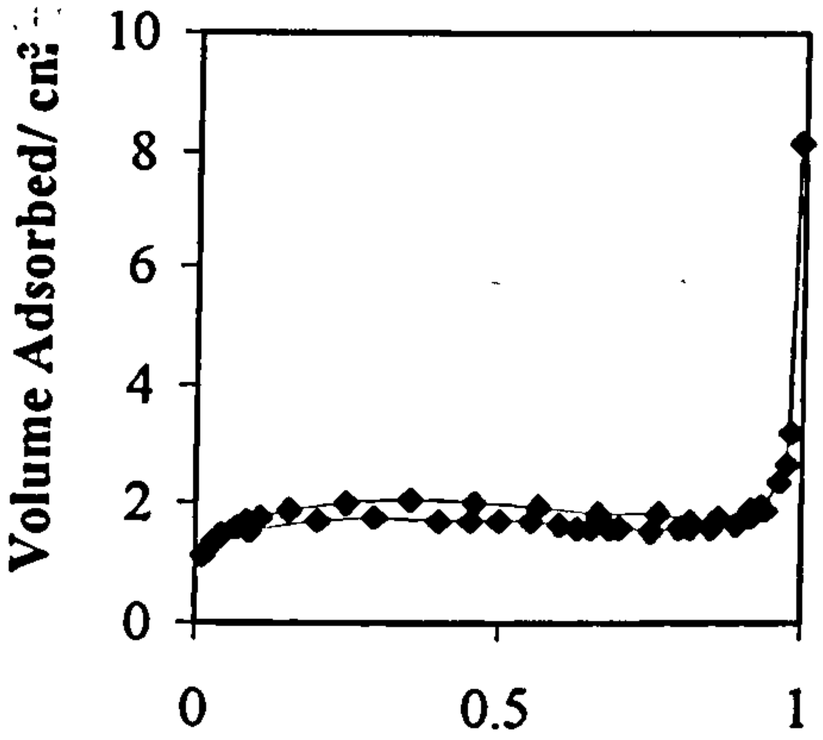

Appendix III: Monolithic Mixed SiO_2-ZrO_2 Gels

X-Ray Diffraction

X-ray Diffraction Patterns Obtained for a Sample Containing ZrO_2=6·4 weight % [HCl=0·015mole] Treated at: (a) 900°C; (b) 1100°C.

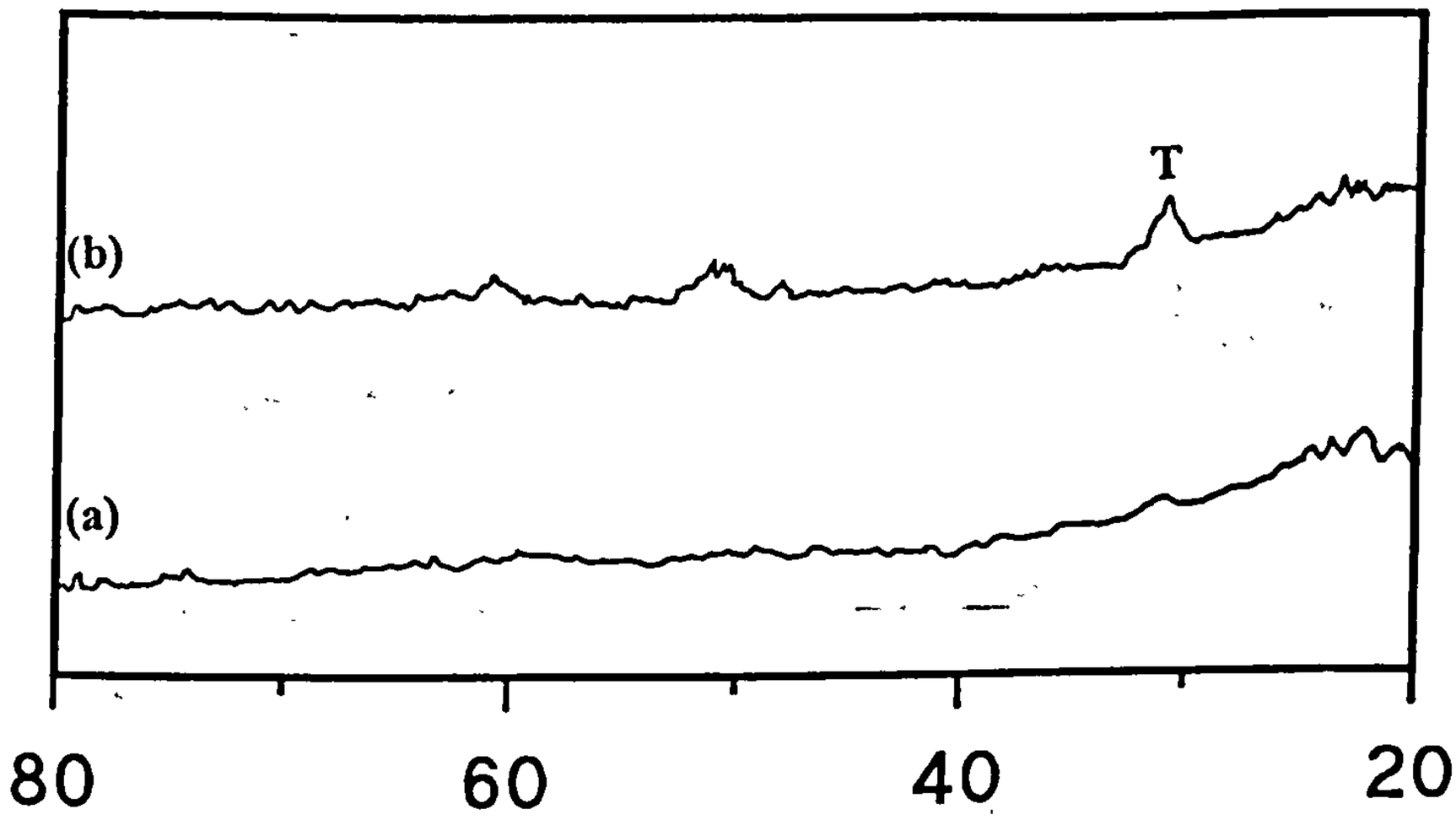

X-ray Diffraction Patterns Obtained for a Sample Containing ZrO_2=6·4 weight % [HCl=$7{\cdot}5x10^{-3}$ mole] Treated at: (a) 900°C; (b) 1100°C.

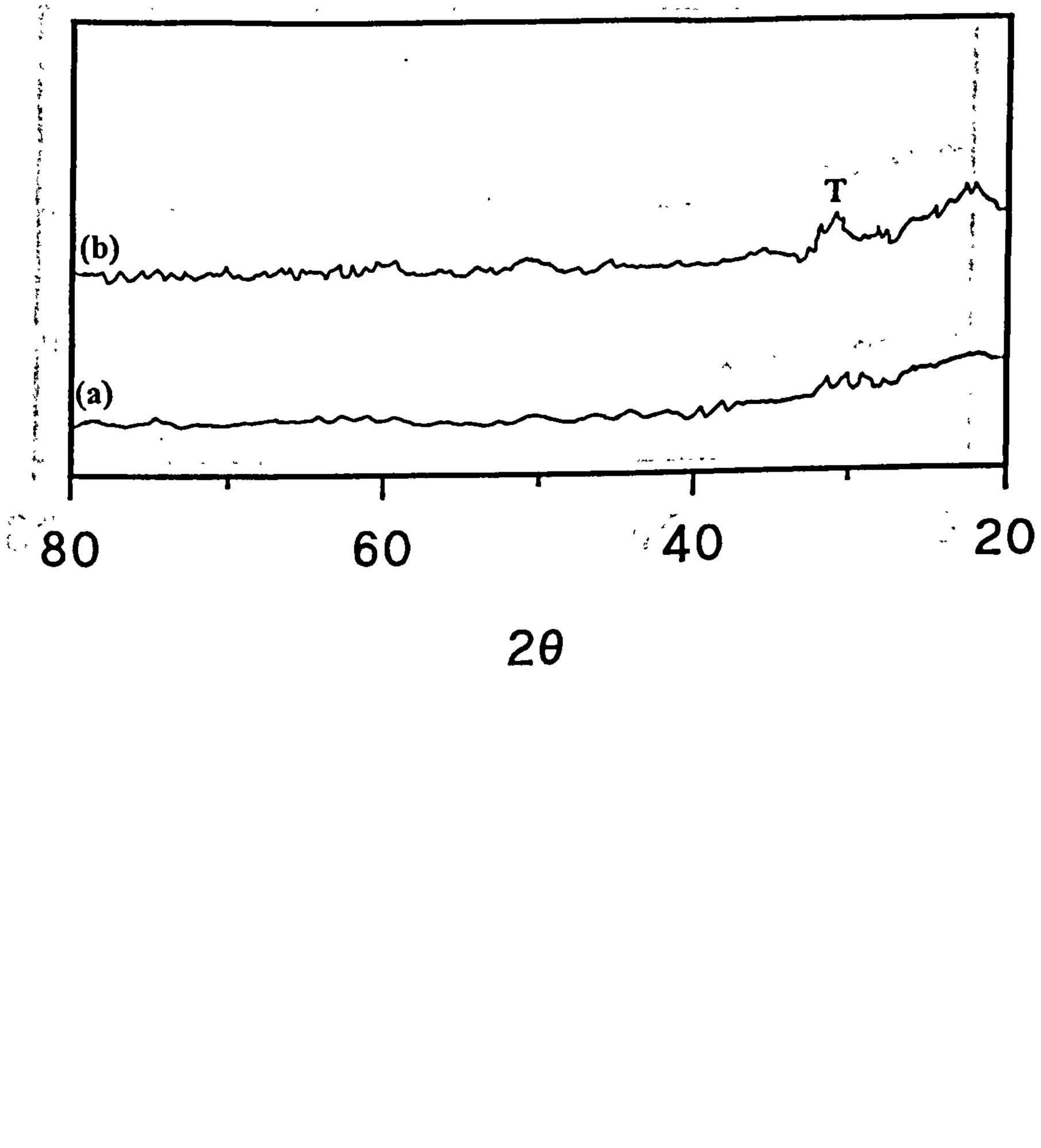

X-ray Diffraction Patterns Obtained for a Sample Containing ZrO_2=6·4 weight % [HCl=$5x10^{-3}$ mole] Treated at: (a) 900°C; (b) 1100°C.

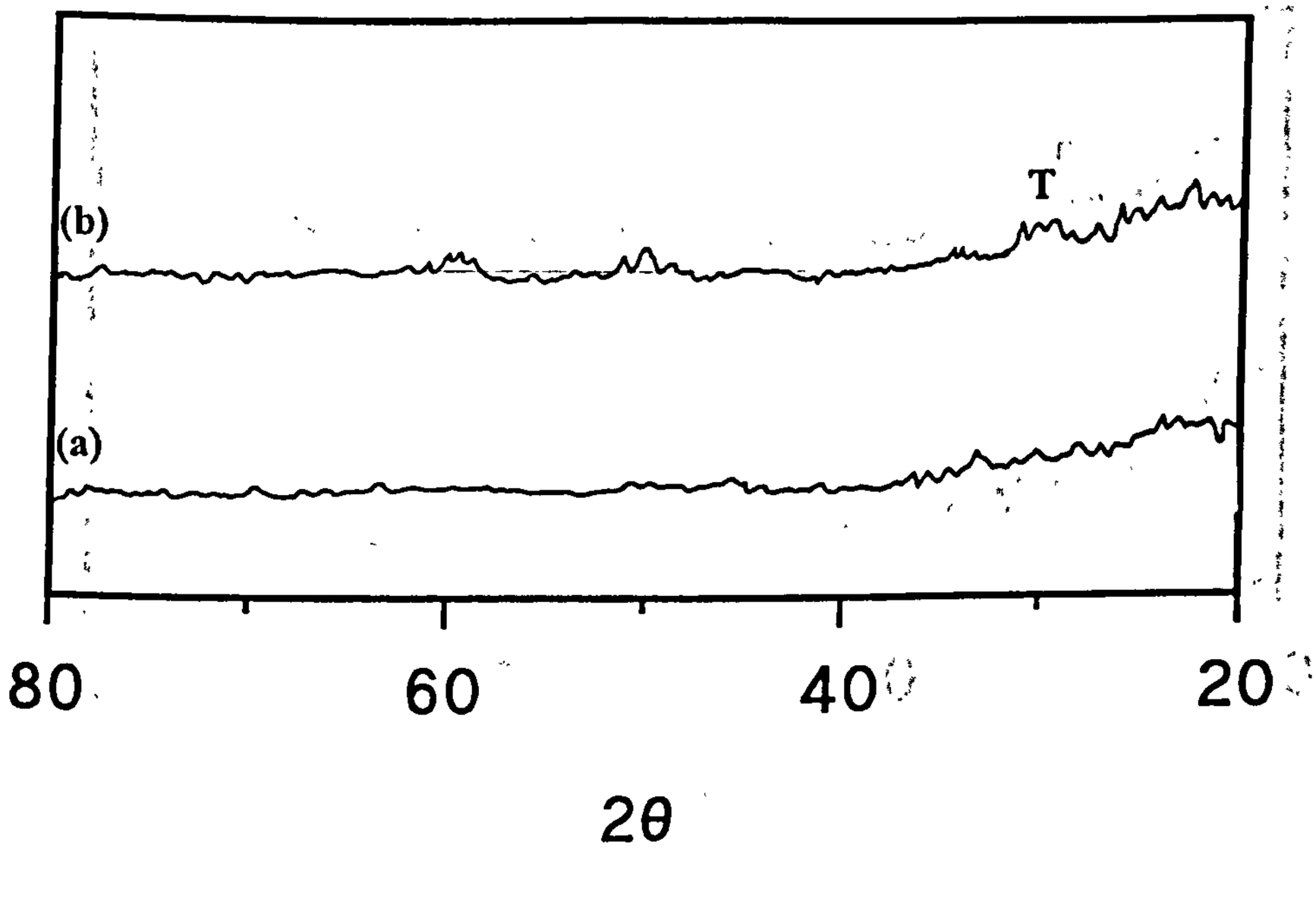

X-ray Diffraction Patterns Obtained for a Sample Containing ZrO_2=6·4 weight % [HCl=$2{\cdot}5x10^{-3}$ mole] Treated at: (a) 900°C; (b) 1100°C.

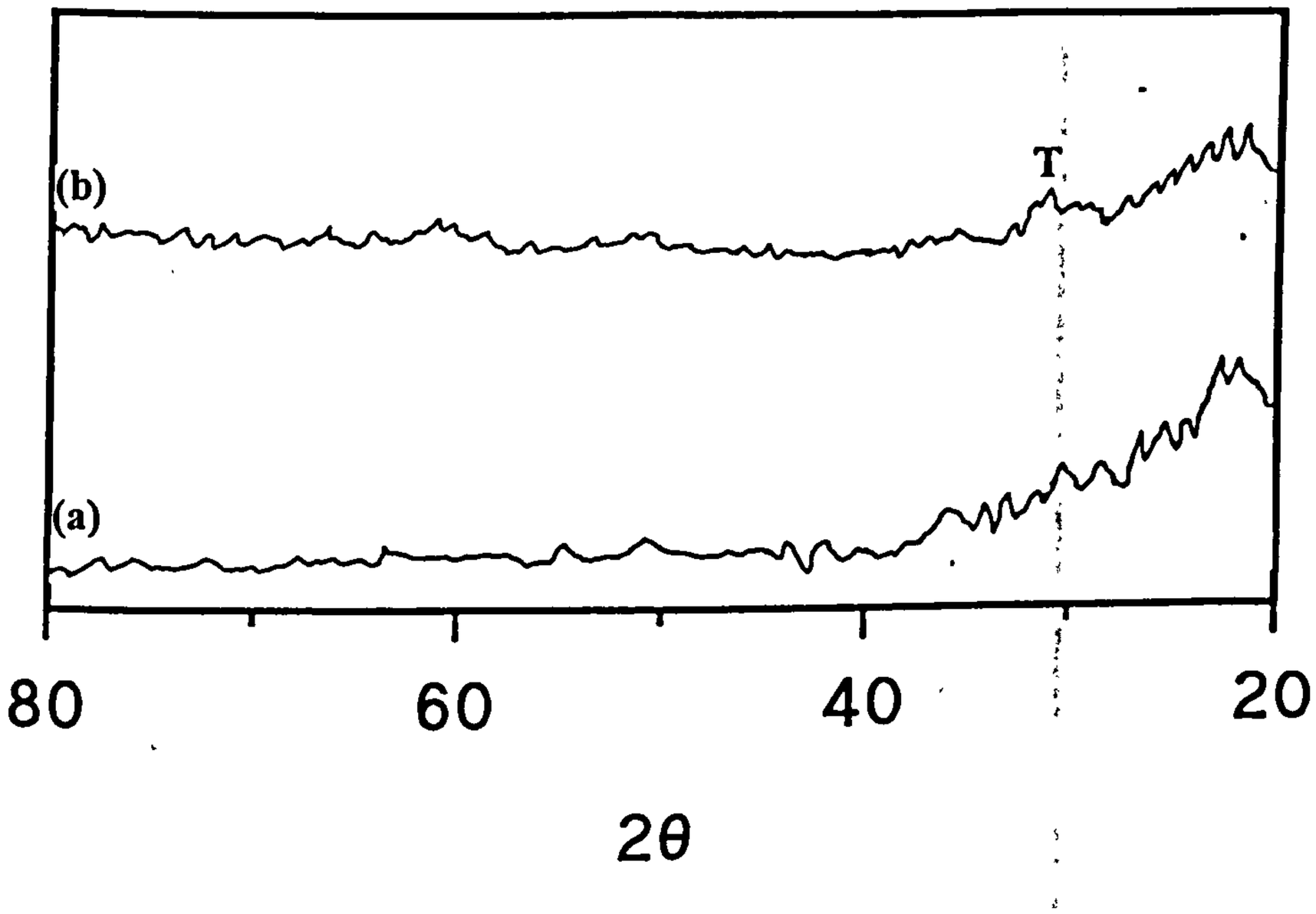

Mid-Infrared Spectra of Samples Treated at Different Temperatures

Mid-infrared Spectra of a Sample Containing 4·97 weight % Zirconia [HCl=0·045mole] Treated at: (a) 120°C; (b) 300°C; (c) 500°C; (d) 700°C; (e) 900°C; (f) 1100°C.

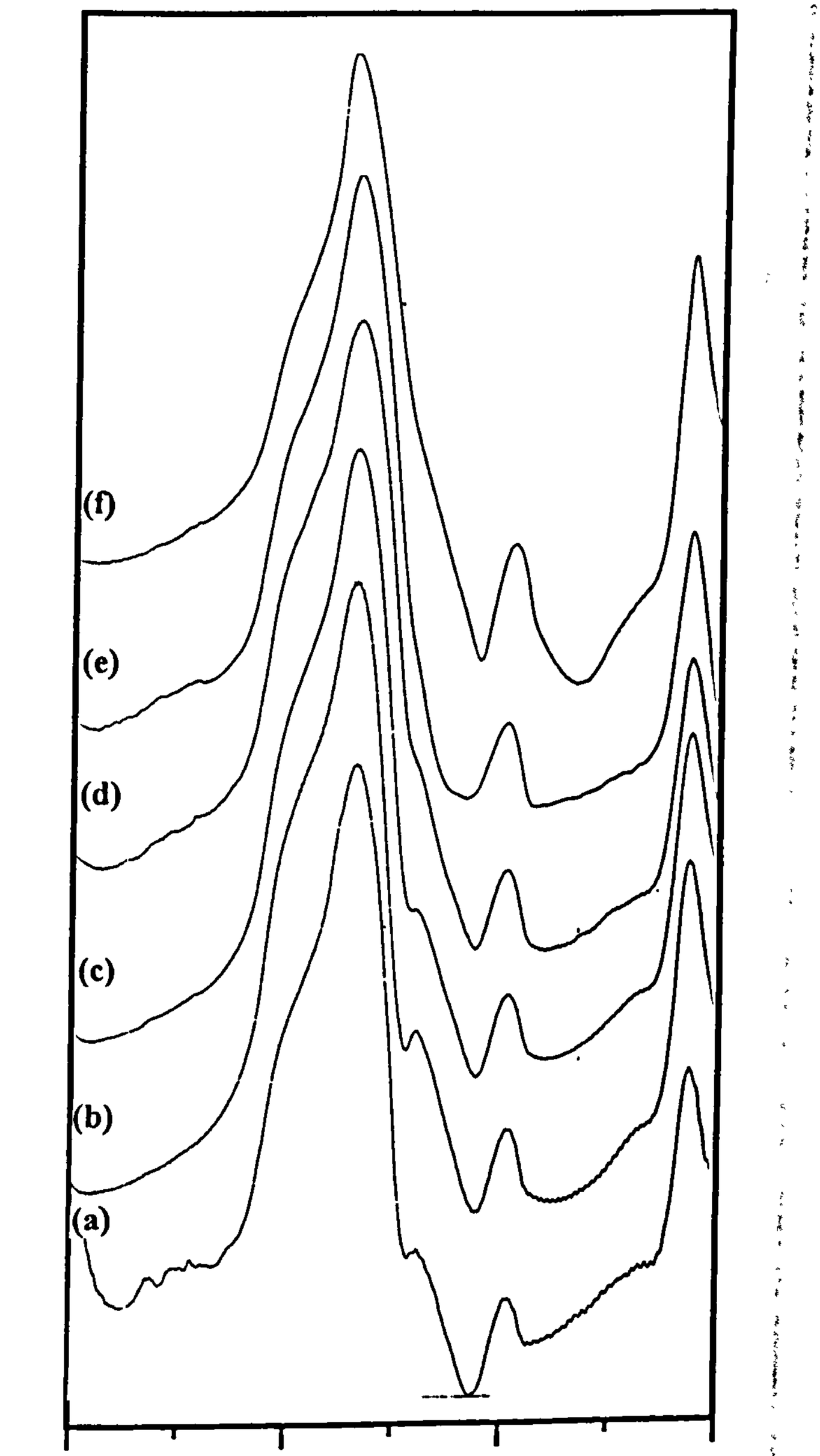

Mid-infrared Spectra of a Sample Containing 6·4 weight % Zirconia [HCl=0·045mole] Treated at: (a) 120°C; (b) 300°C; (c) 500°C; (d) 700°C; (e) 900°C; (f) 1100°C.

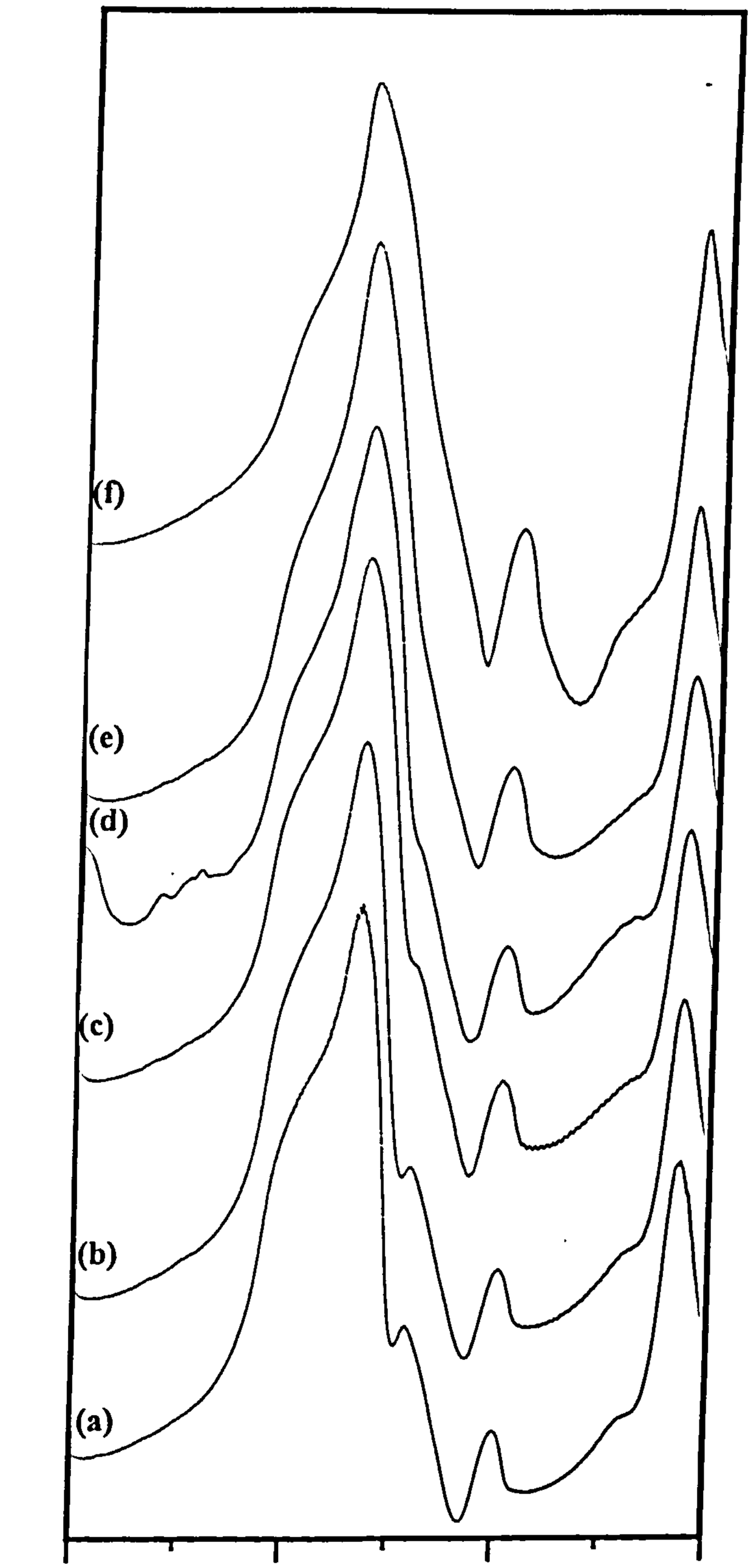

Mid-infrared Spectra of a Sample Containing 22·1 weight % Zirconia [HCl=0·045mole] Treated at: (a) 120°C; (b) 300°C; (c) 500°C; (d) 700°C; (e) 900°C; (f) 1100°C.

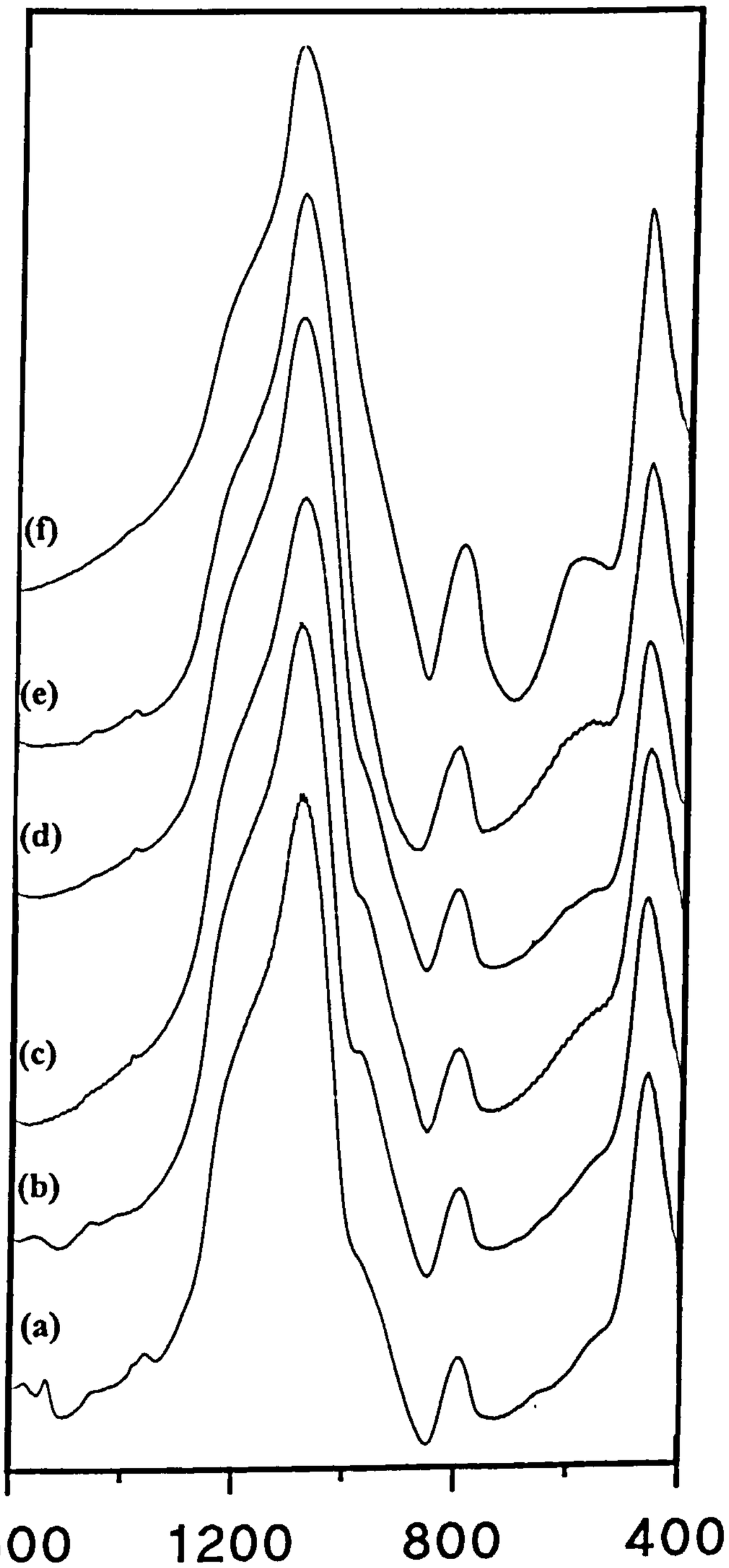

Near Infrared Spectra: Effect of Thermal Treatment

Effect of Thermal Treatment Temperature on the Near Infrared (NIR) Spectra of a Sample Containing ZrO_2=4·1 weight % [HCl=0·045mole]

(a) 120°C; (b) 300°C; (c) 500°C; (d) 700°C; (e) 900°C; (f) 1100°C

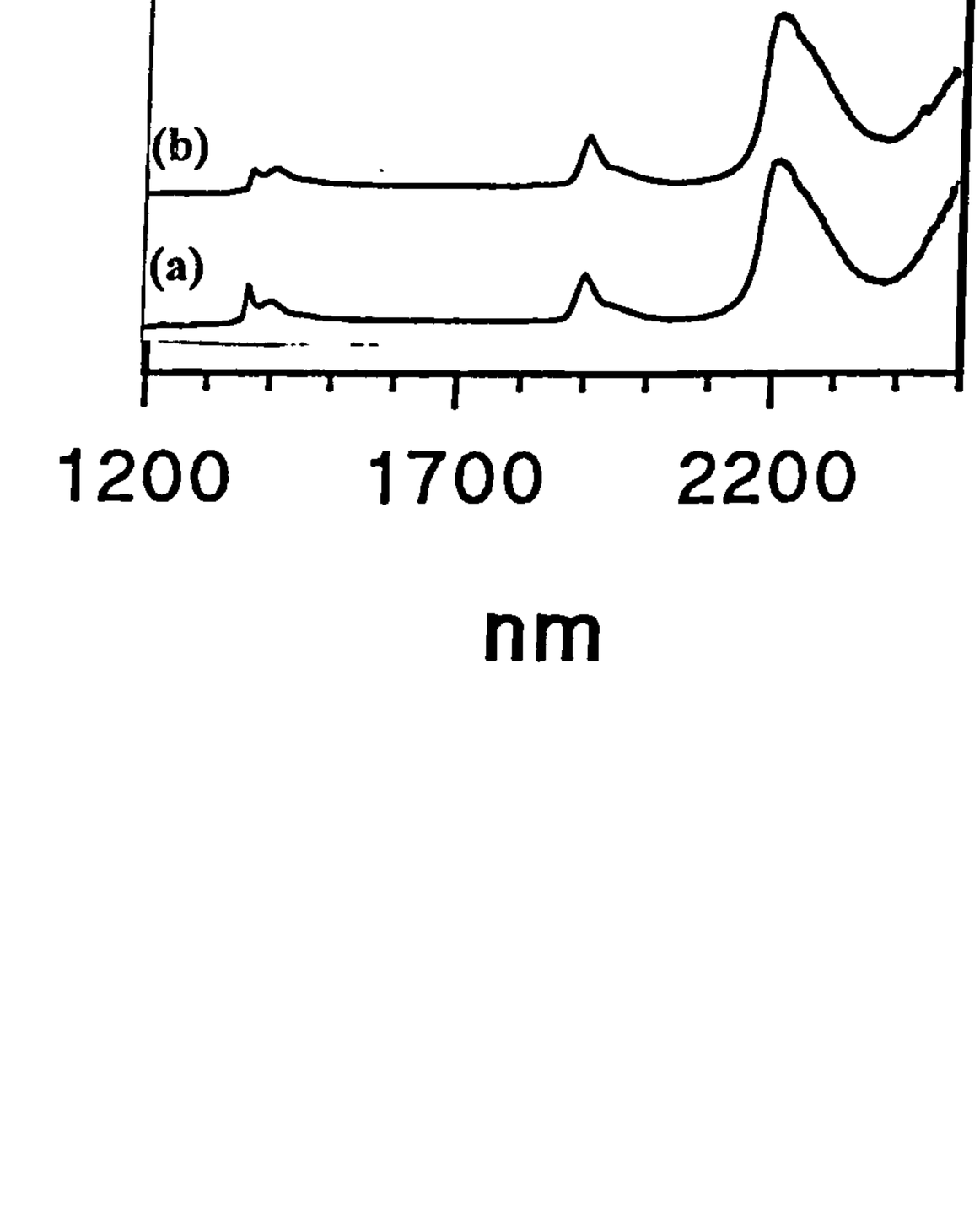

Effect of Thermal Treatment Temperature on the Near Infrared (NIR) Spectra of a Sample Containing ZrO_2=6·4 weight % [HCl=0·045mole]
(a) 120°C; (b) 300°C; (c) 500°C; (d) 700°C; (e) 900°C; (f) 1100°C

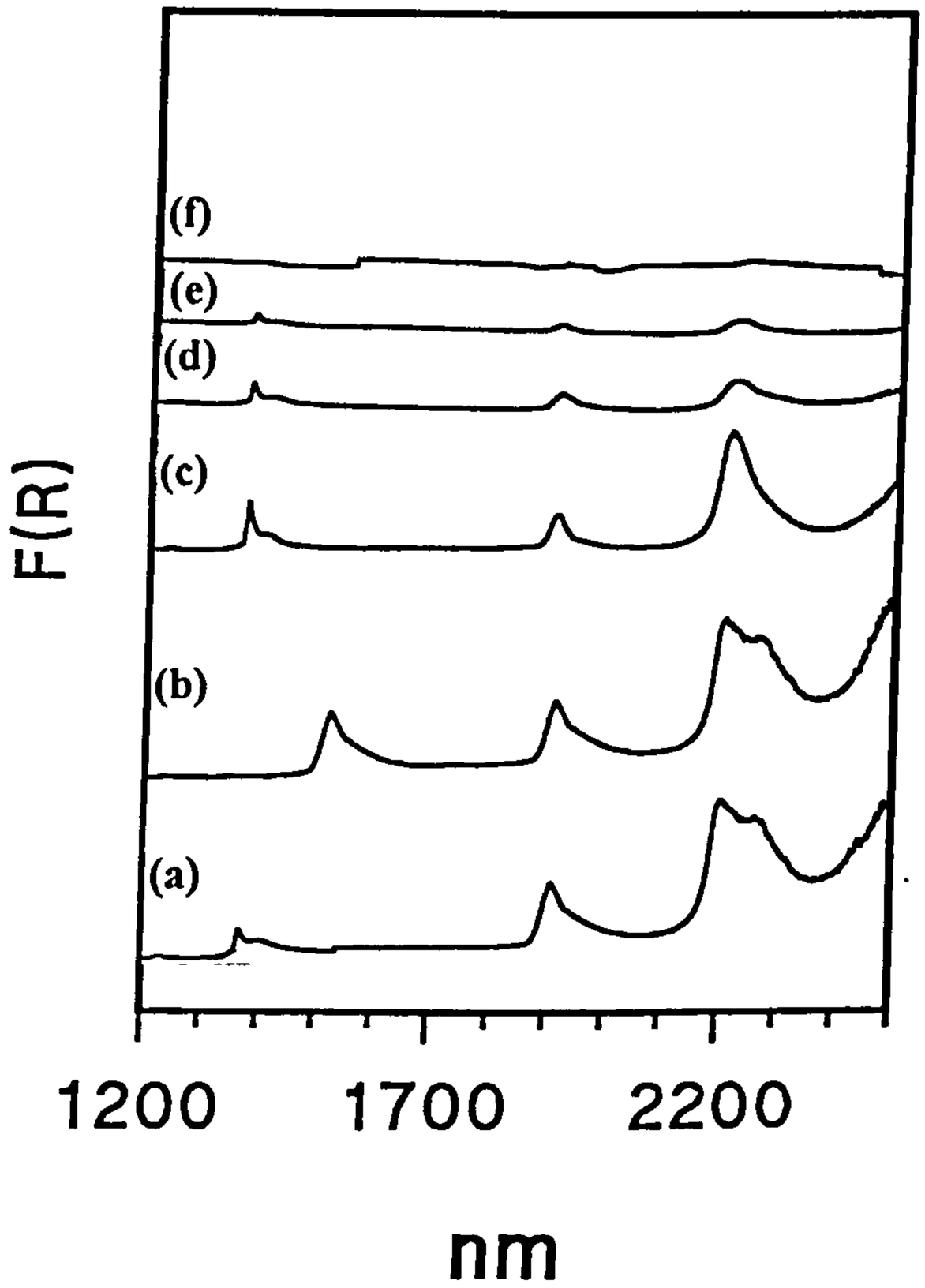

Effect of Thermal Treatment Temperature on the Near Infrared (NIR) Spectra of a Sample Containing ZrO_2=22·1 weight % [HCl=0·045mole]
(a) 120°C; (b) 300°C; (c) 500°C; (d) 700°C; (e) 900°C; (f) 1100°C

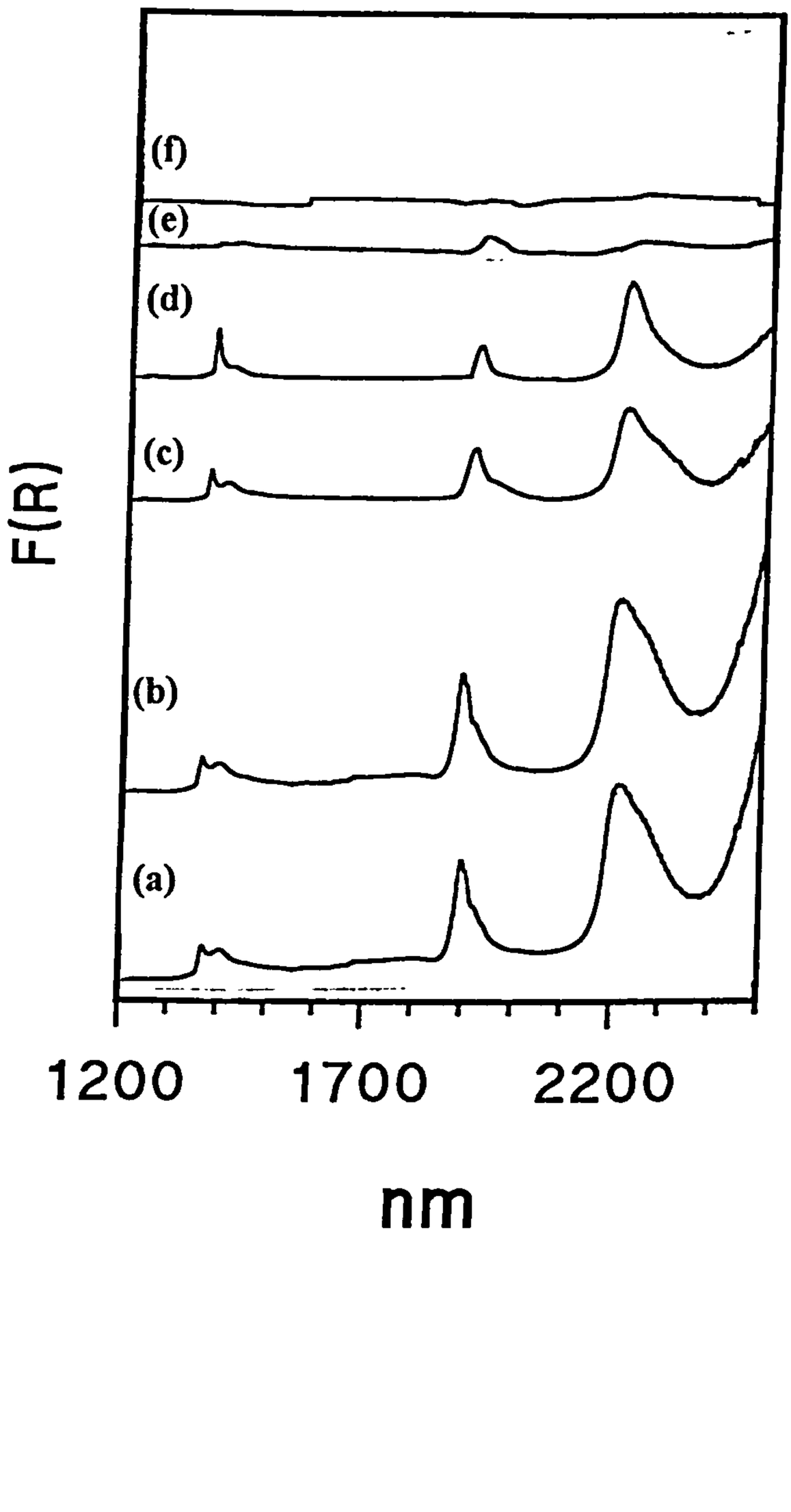

Gas Adsorption Investigation of Pore Structure

Effects of Varying the Amount of Acid used for the Hydrolysis Reaction on the Pore Characteristics of a Monolith Containing ZrO_2=6·4 weight % and Heated at 120°C

HCl=0·045 mole (ZrO_2=6·4 weight %; Heated at 120°C)

(a) Adsorption/Desorption Isotherm (b) α_s-plot

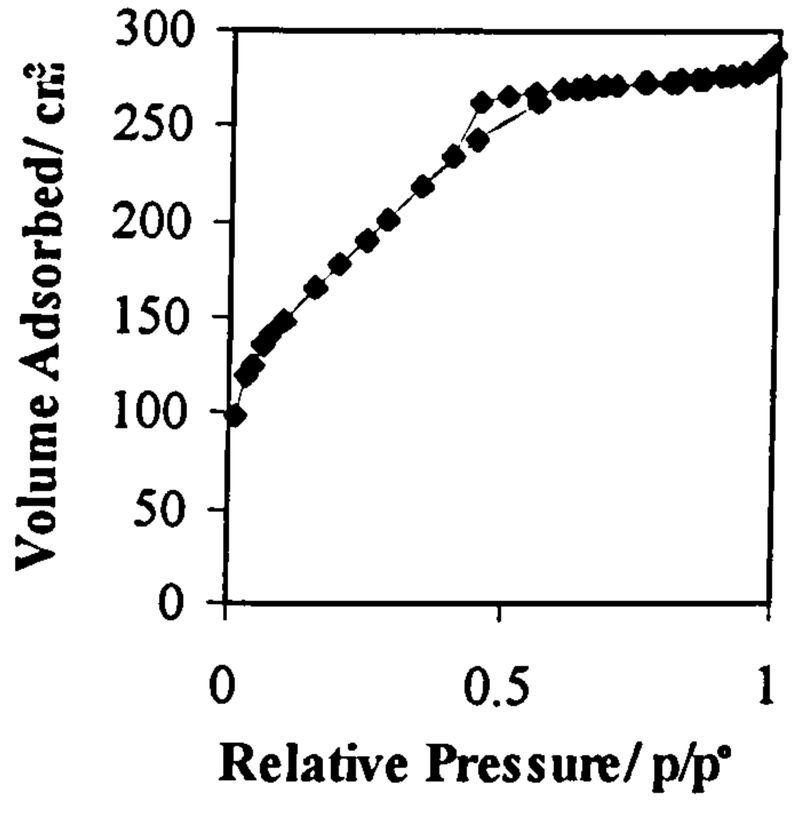

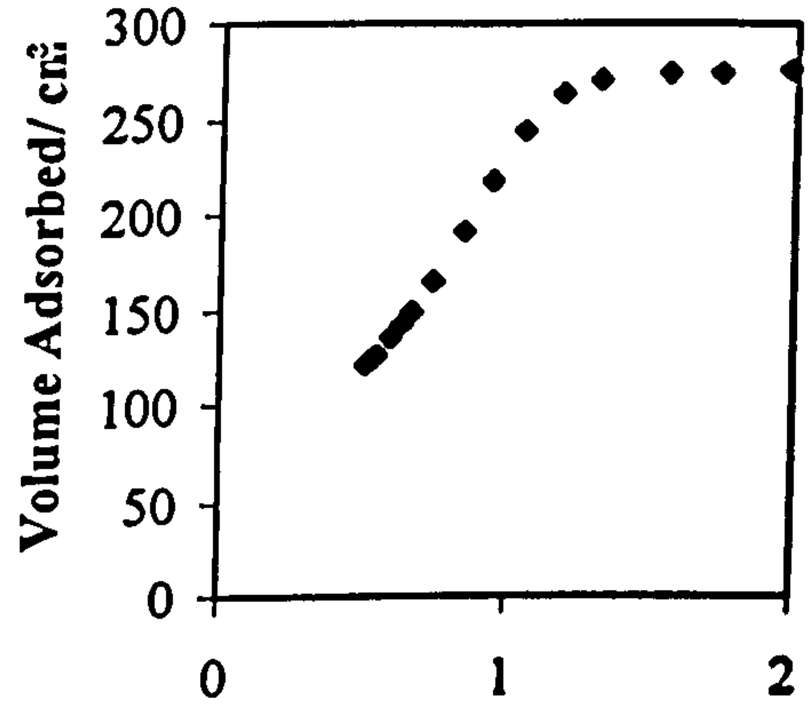

HCl=0·030 mole (ZrO_2=6·4 weight %; Heated at 120°C)

(a) Adsorption/Desorption Isotherm (b) α_s-plot

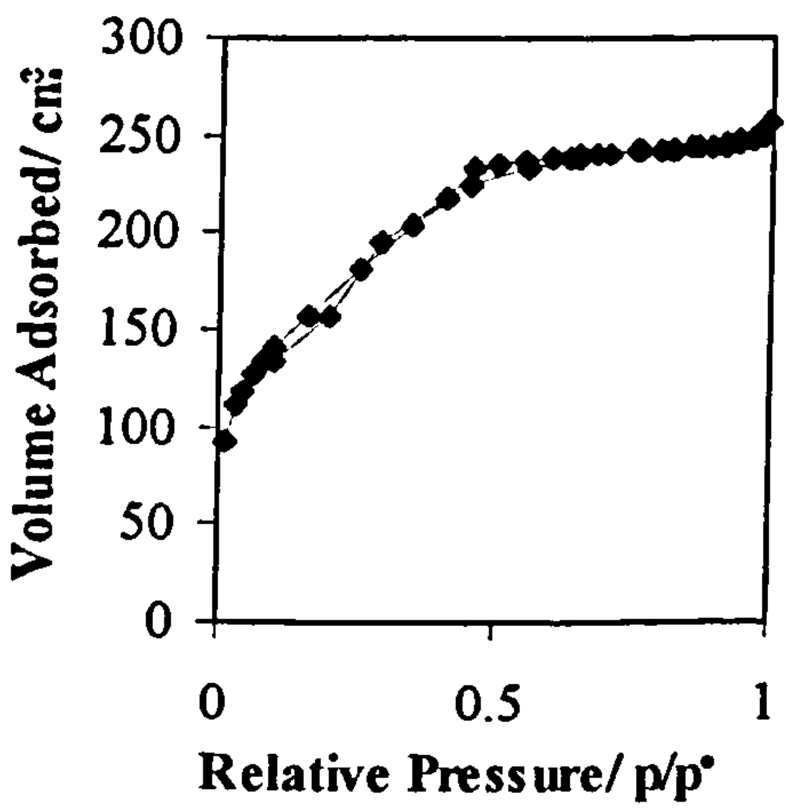

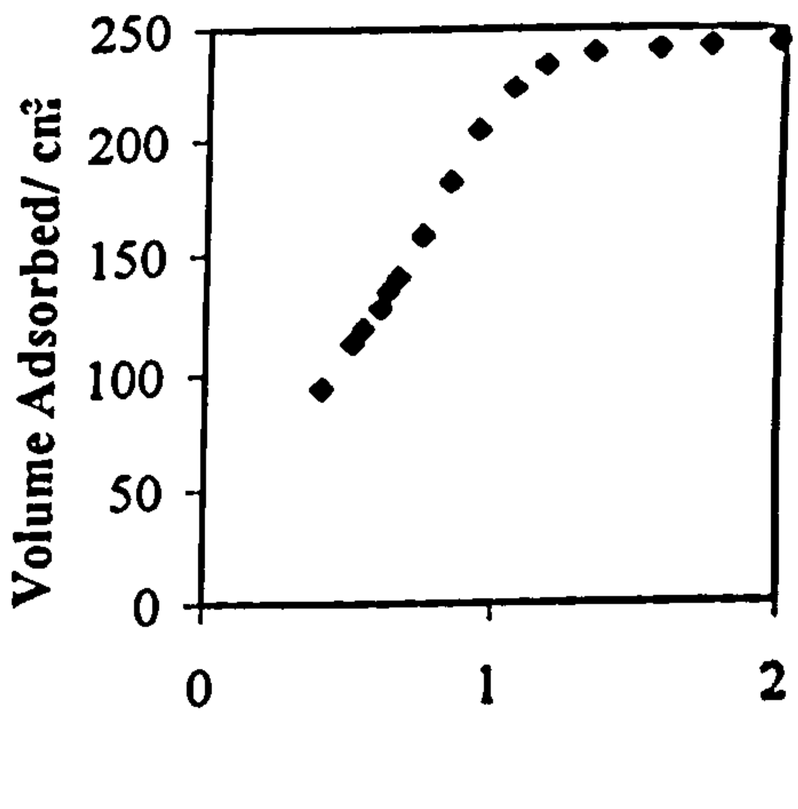

HCl=0·015 mole (ZrO_2=6·4 weight %; Heated at 120°C)

(a) Adsorption/Desorption Isotherm (b) α_s-plot

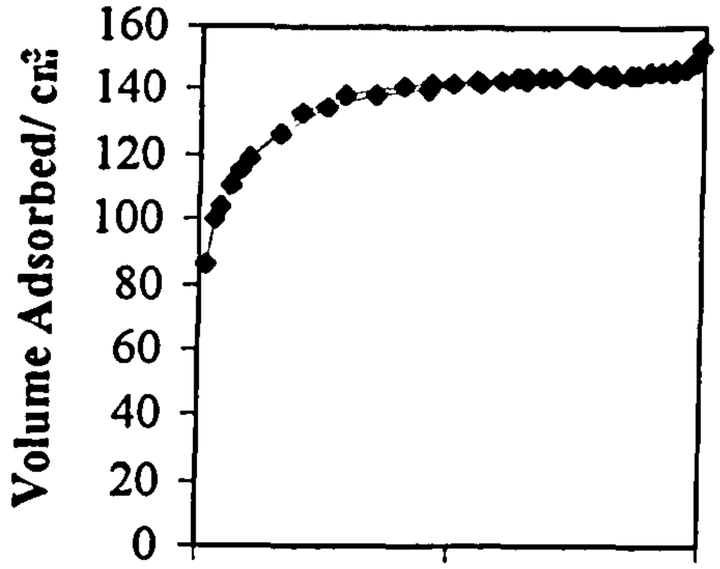

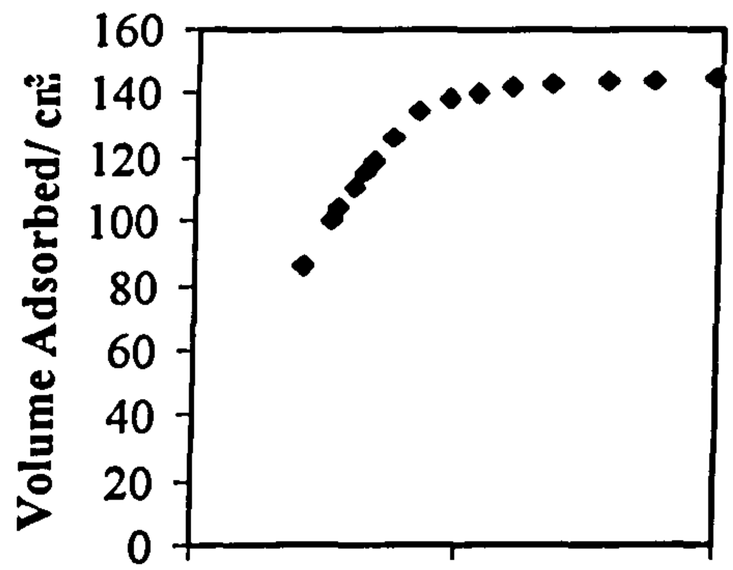

HCl=7·5x10^{-3} mole (ZrO_2=6·4 weight %; Heated at 120°C)

(a) Adsorption/Desorption Isotherm (b) α_s-plot

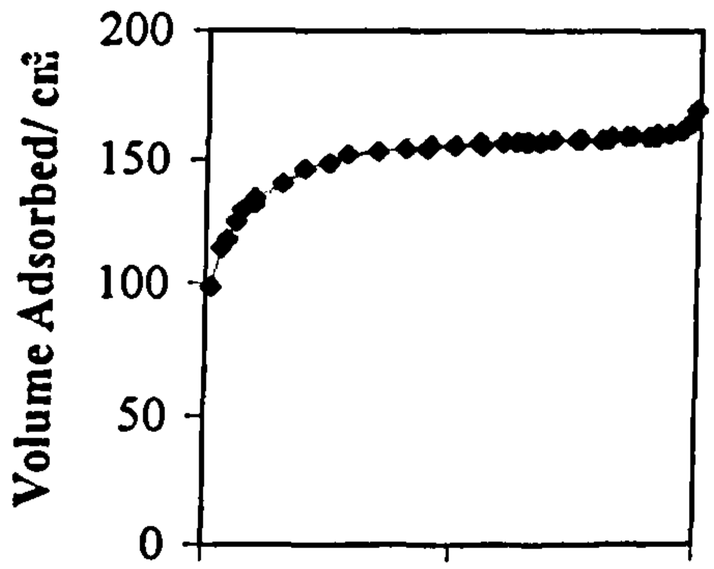

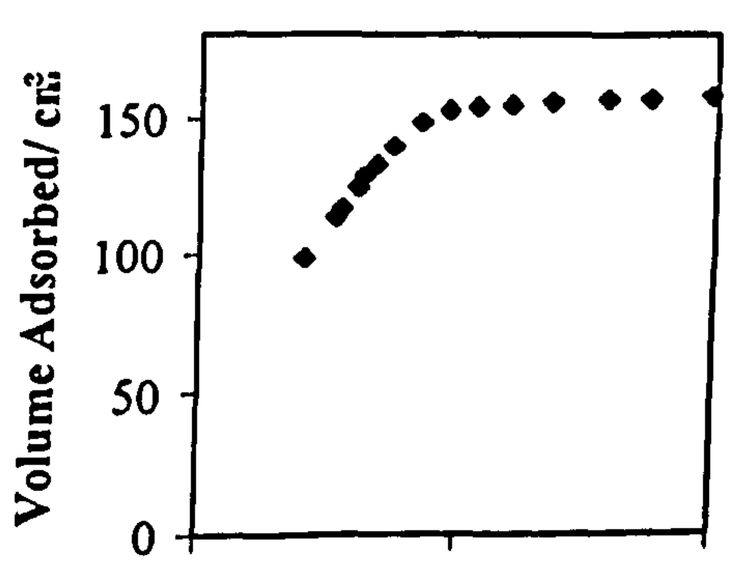

HCl=5x10^{-3} mole (ZrO_2=6·4 weight %; Heated at 120°C)

(a) Adsorption/Desorption Isotherm (b) α_s-plot

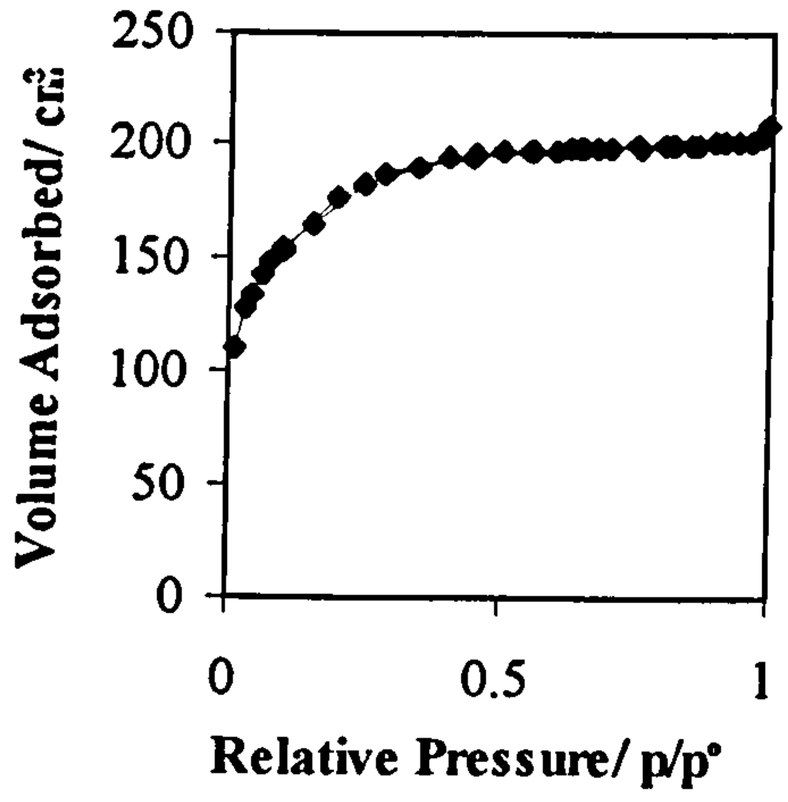

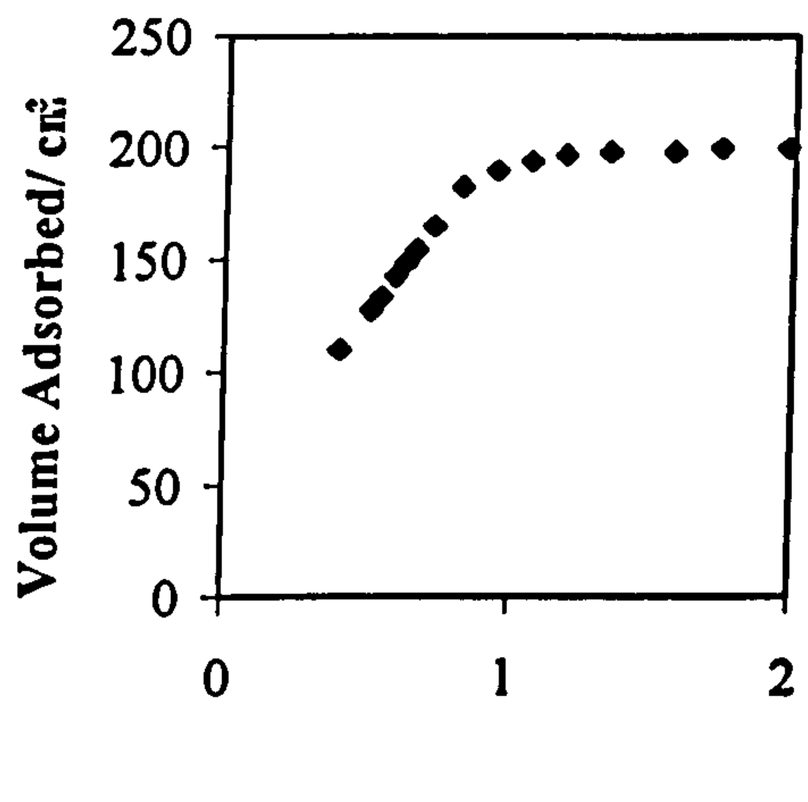

HCl=2·5x10^{-3} mole (ZrO_2=6·4 weight %; Heated at 120°C)

(a) Adsorption/Desorption Isotherm (b) α_s-plot

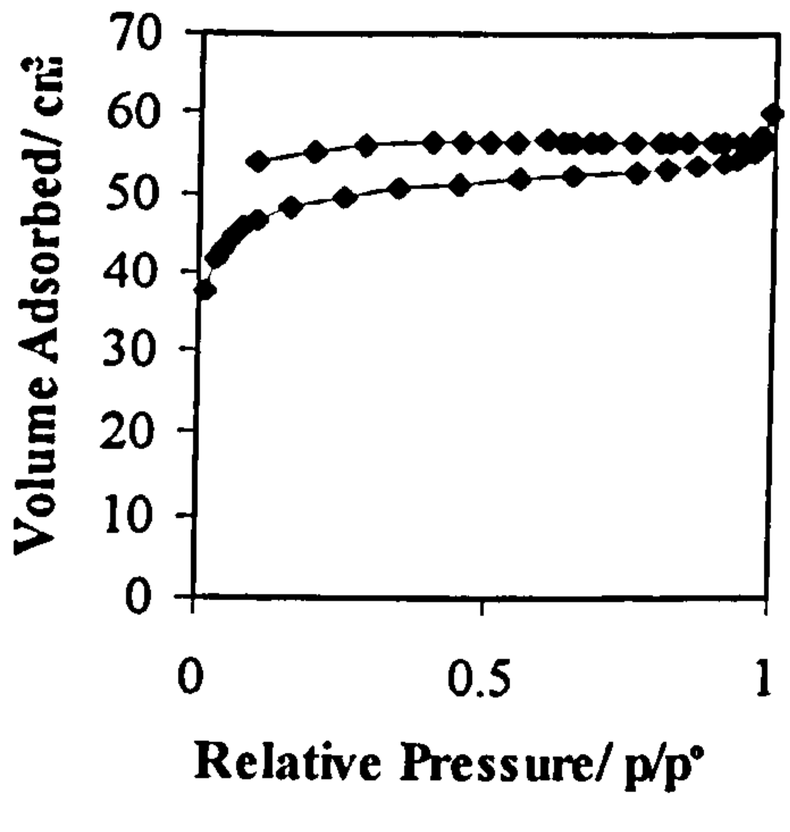

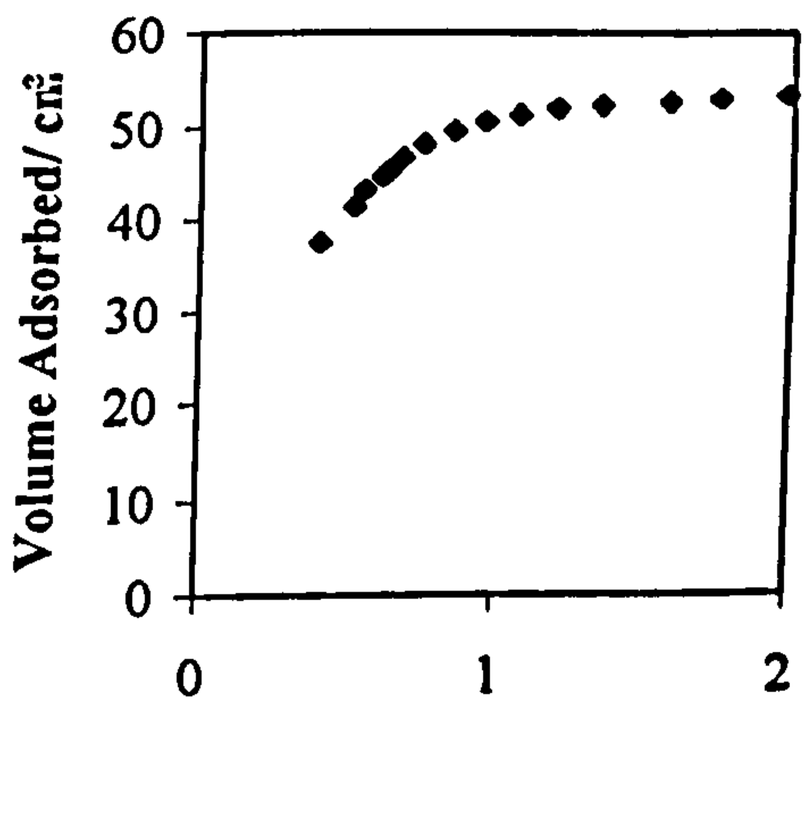

Effect of Temperature on the Pore Characteristics of a Monolith Containing ZrO_2=6·4 weight % ; HCl=0·045 mole *

300°C: ZrO_2=6·4 weight % ; HCl=0·045 mole

(a) Adsorption/Desorption Isotherm (b) α_s-plot

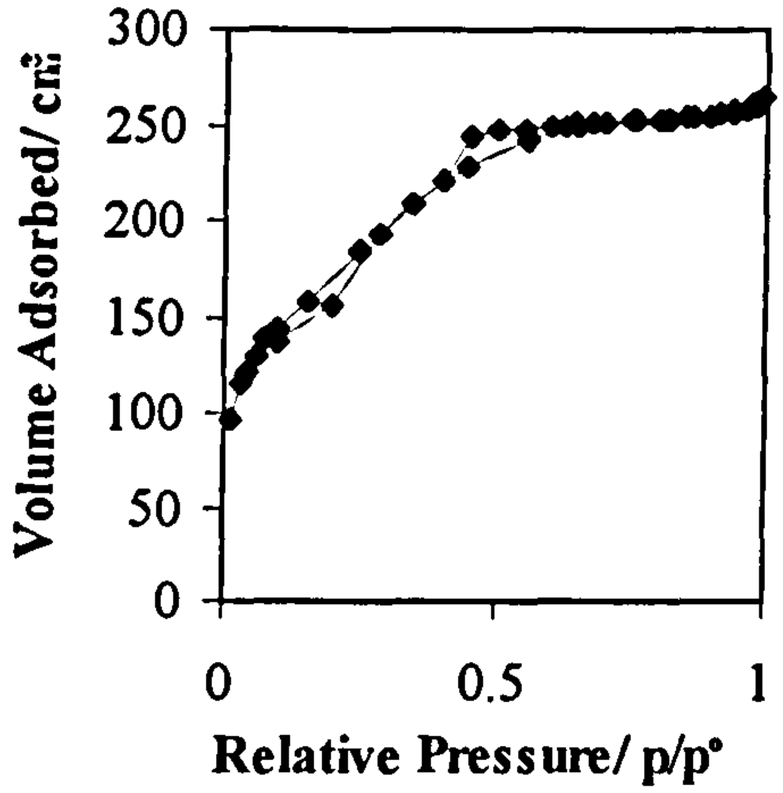

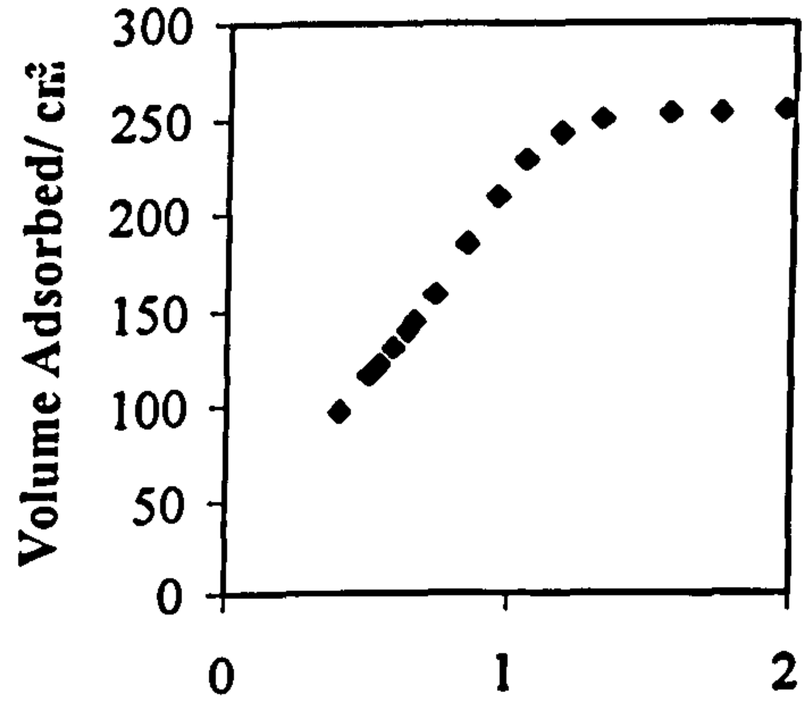

500°C: ZrO_2=6·4 weight % ; HCl=0·045 mole

(a) Adsorption/Desorption Isotherm (b) α_s-plot

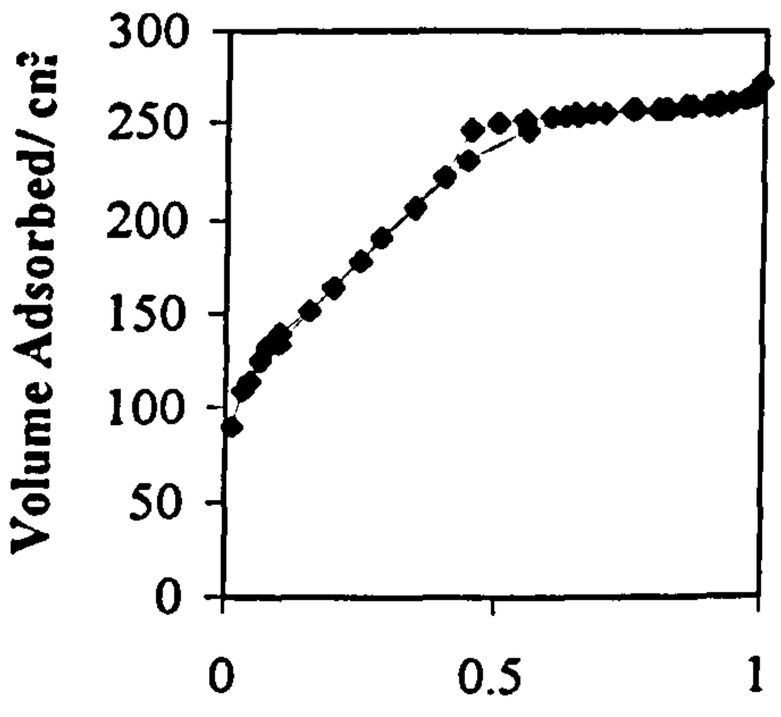

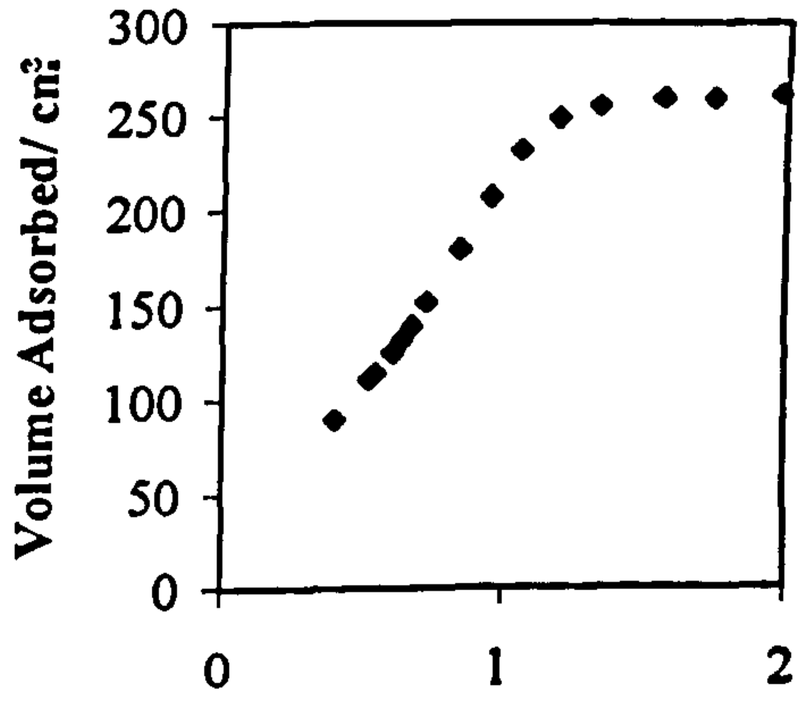

* Isotherm for the monolithic gel containing ZrO_2=6·4 wt% at 120°C can be found with the isotherms for the effect of varying the amount of acid used for the hydrolysis reaction.

700°C: ZrO_2=6·4 weight % ; HCl=0·045 mole

(a) Adsorption/Desorption Isotherm (b) α_s-plot

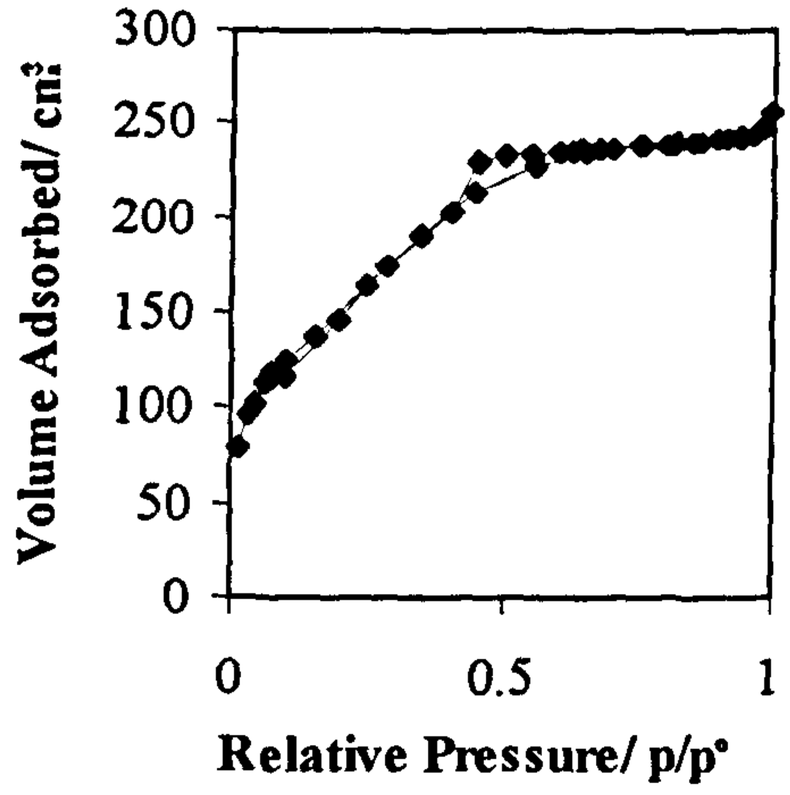

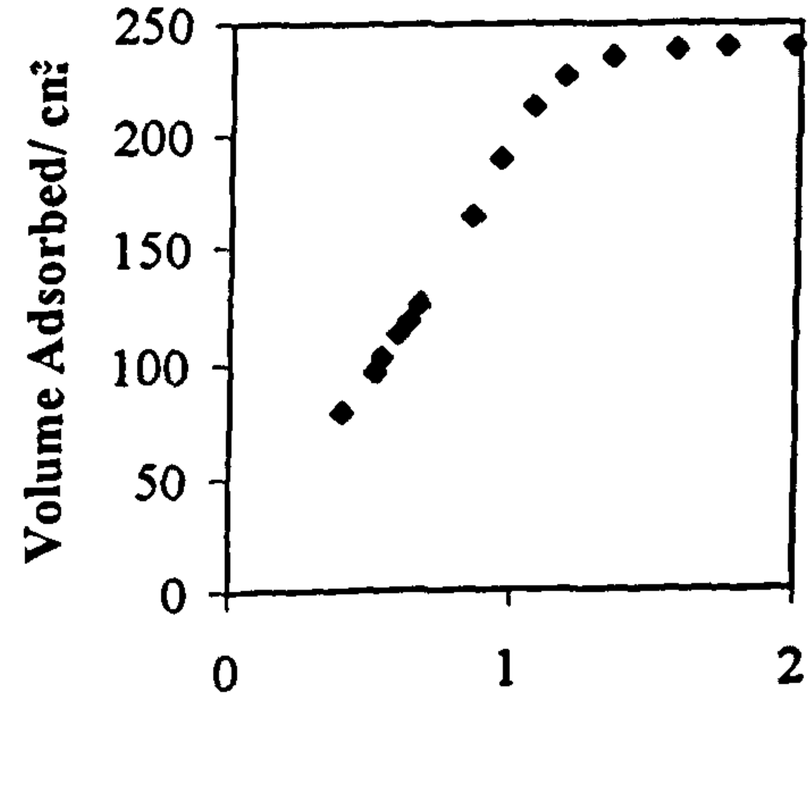

900°C: ZrO_2=6·4 weight % ; HCl=0·045 mole

(a) Adsorption/Desorption Isotherm (b) α_s-plot

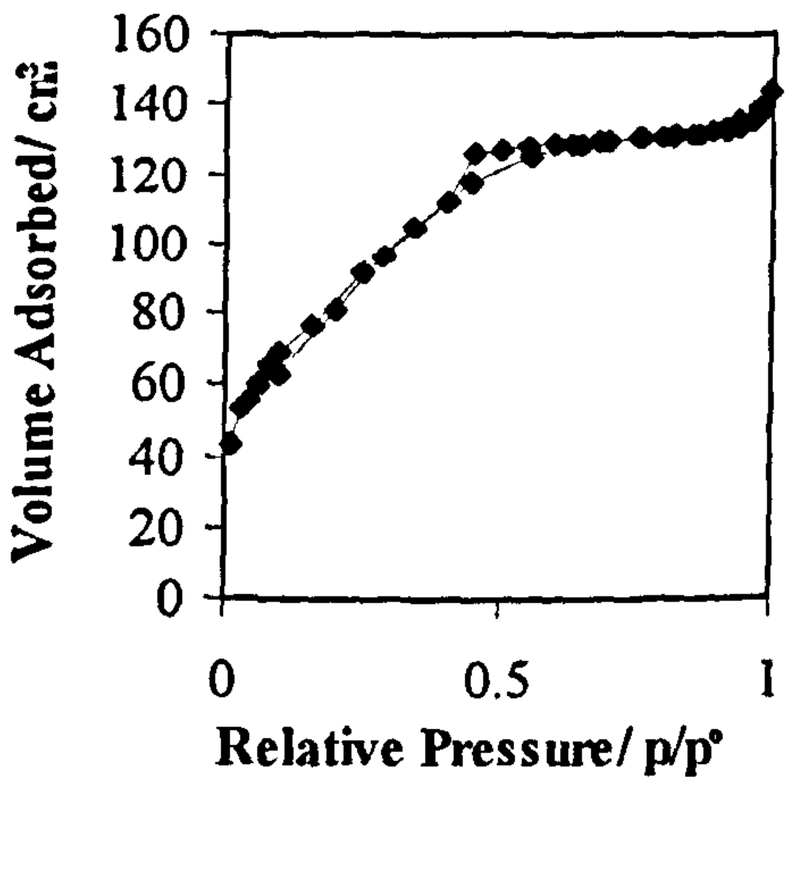

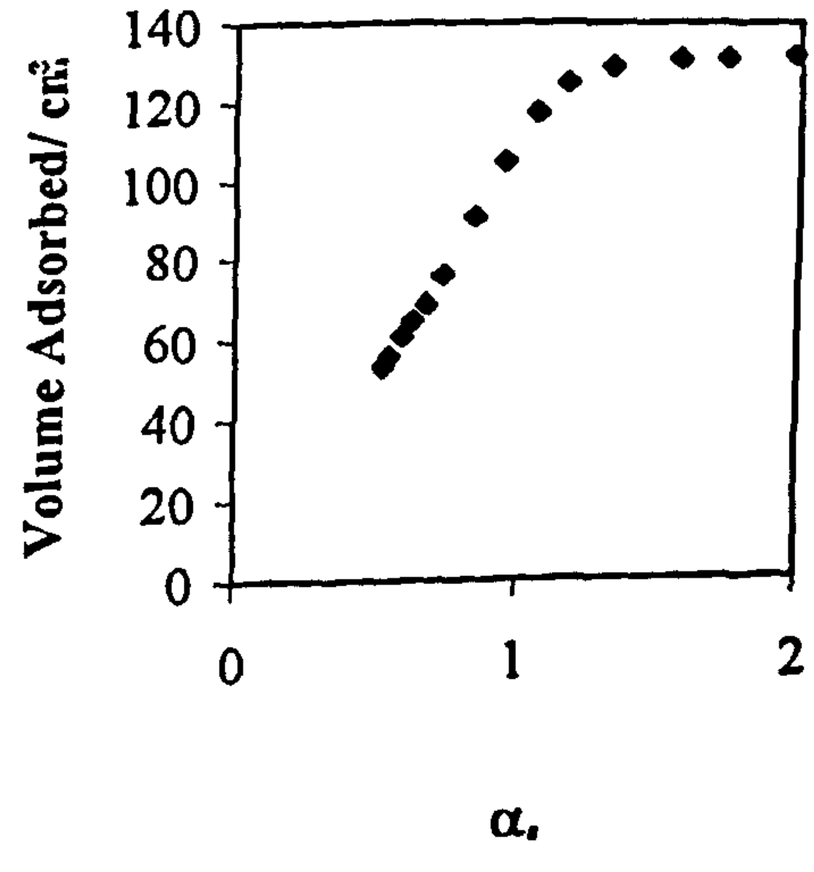

1100°C: ZrO_2=6·4 weight % ; HCl=0·045 mole

(a) Adsorption/Desorption Isotherm (b) α_s-plot

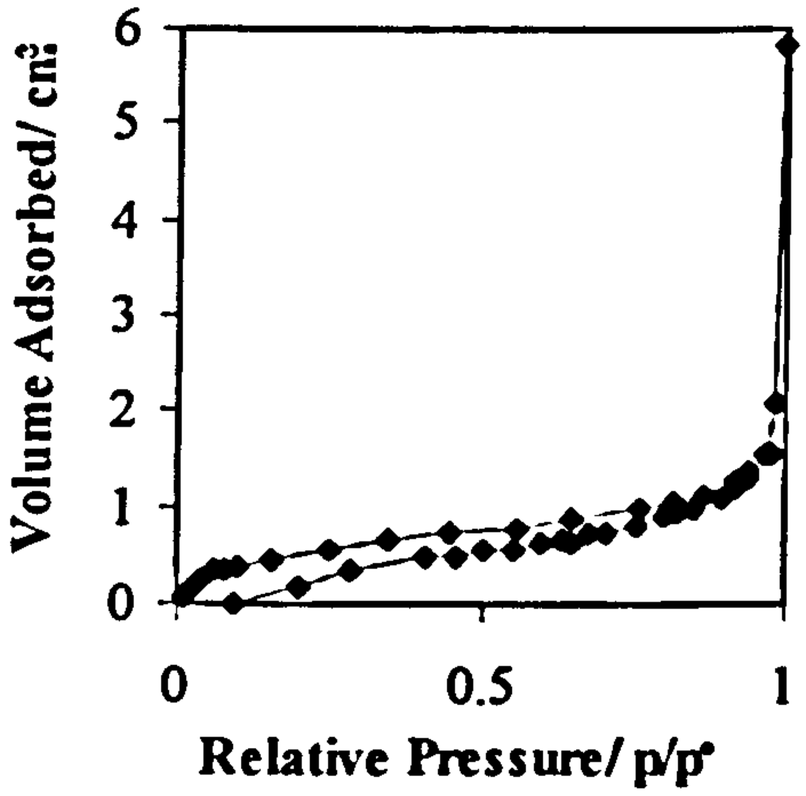

Effects of Varying the Amount of Zirconia (weight %) on the Pore Characteristics of a Monolith Containing HCl=0·045 mole and Heated at 120°C

ZrO_2=4·1 weight % (HCl=0·045 mole; Temperature=120°C)

(a) Adsorption/Desorption Isotherm (b) α_s-plot

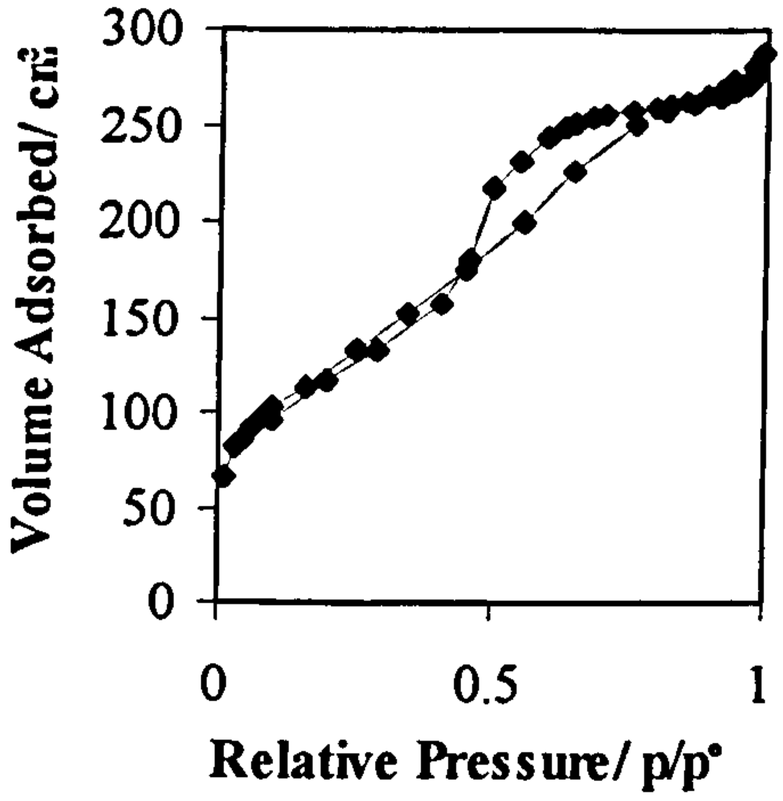

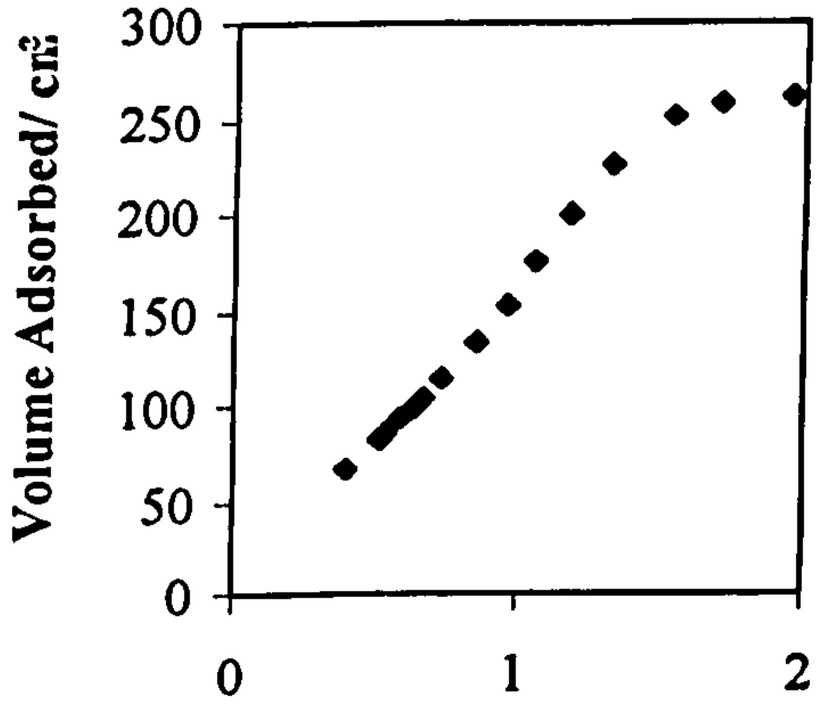

ZrO_2=4·9 weight % (HCl=0·045 mole; Temperature=120°C)

(a) Adsorption/Desorption Isotherm (b) α_s-plot

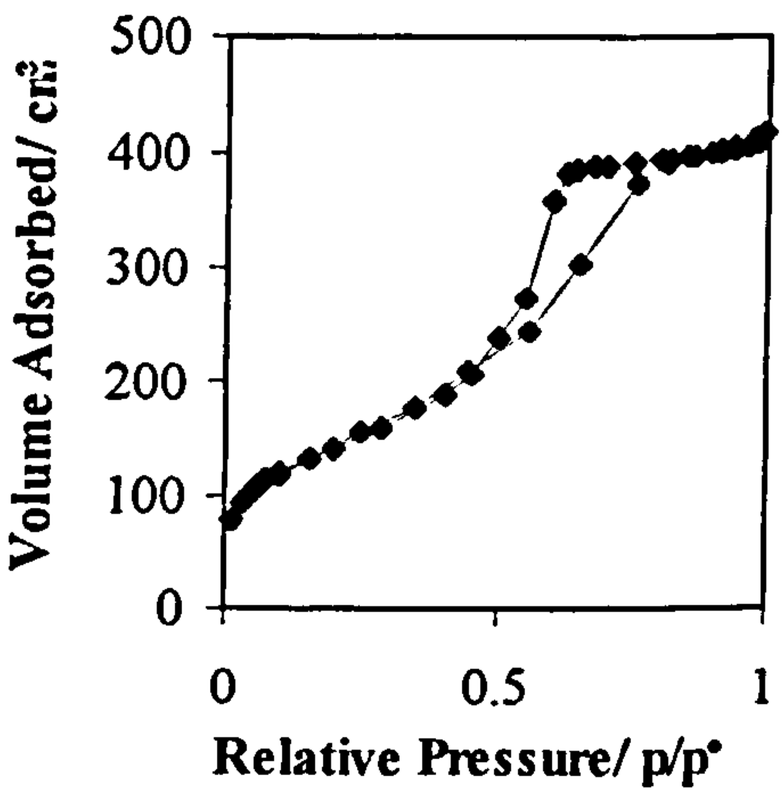

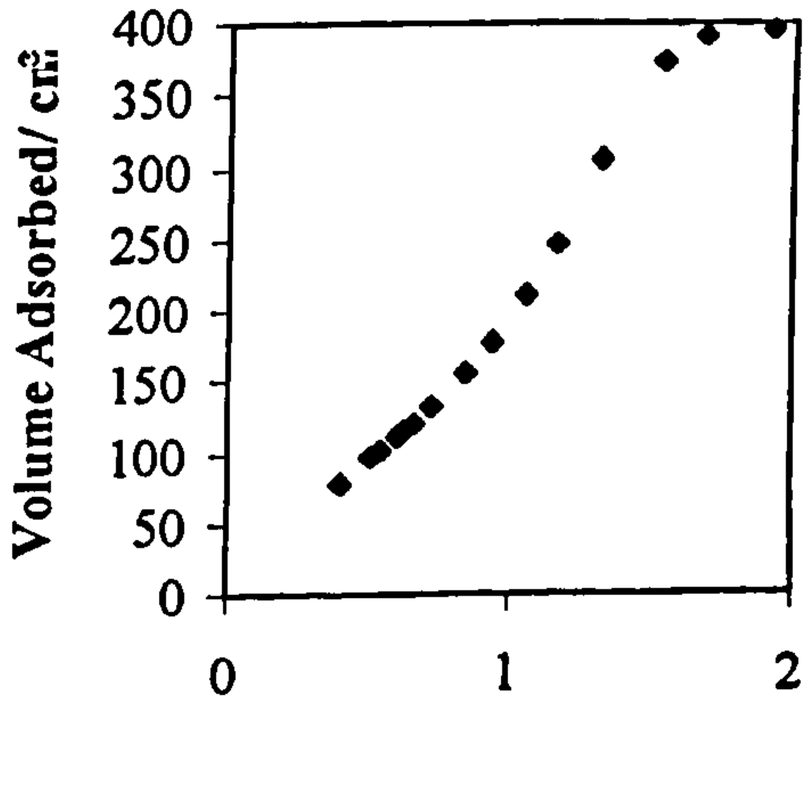

ZrO_2=22·1 weight % (HCl=0·045 mole; Temperature=120°C)

(a) Adsorption/Desorption Isotherm (b) α_s-plot